

## Myocardial Imaging: Tissue Doppler and Speckle Tracking

To my three Muses – Rosey, Victoria and Tess

*Thomas H. Marwick*

My respected parents, Tit-ngan and Chan-siu Yu,  
My beloved wife, Joan,  
My dear sons, Yannick and Ryan,  
for their love and support

*C.M. Yu*

To my husband, Dr. Xing Sheng Yang,  
for continued support of my efforts

*Jing-Ping Sun*

# Myocardial Imaging: Tissue Doppler and Speckle Tracking

EDITED BY

**Thomas H. Marwick, MBBS, PhD**

Professor of Medicine, University of Queensland  
Princess Alexandra Hospital  
Brisbane, Australia

**Cheuk-Man Yu, MBChB**

Head, Division of Cardiology  
Department of Medicine and Therapeutics  
The Chinese University of Hong Kong  
Prince of Wales Hospital, Shatin, N.T.  
Hong Kong

**Jing Ping Sun, MD**

Associate Professor of Medicine  
The Carlyle Fraser Heart Center  
Cardiology Department  
Atlanta, GA  
USA



**Blackwell**  
Publishing

© 2007 by Blackwell Publishing  
Blackwell Futura is an imprint of Blackwell Publishing

Blackwell Publishing, Inc., 350 Main Street, Malden, Massachusetts 02148-5020, USA

Blackwell Publishing Ltd, 9600 Garsington Road, Oxford OX4 2DQ, UK

Blackwell Science Asia Pty Ltd, 550 Swanston Street, Carlton, Victoria 3053, Australia

All rights reserved. No part of this publication may be reproduced in any form or by any electronic or mechanical means, including information storage and retrieval systems, without permission in writing from the publisher, except by a reviewer who may quote brief passages in a review.

First published 2007

1 2007

ISBN: 978-1-4051-6113-8

Library of Congress Cataloging-In-Publication/Data

Myocardial imaging / edited by Thomas H. Marwick, Cheuk-Man Yu, Jing Ping Sun.  
p. ; cm.

Includes bibliographical references and index.

ISBN 978-1-4051-6113-8 (alk. paper)

1. Echocardiography. 2. Myocardium — Ultrasonic imaging. I. Marwick, Thomas H. II. Yu, Cheuk-Man. III. Sun, Jingping.

[DNLM: 1. Heart — radionuclide imaging. 2. Angiocardiography. WG 141.5.R2 M9966 2007]  
RC683.5.U5M97 2007  
616.1'207543 — dc22

2007000374

A catalogue record for this title is available from the British Library

Commissioning Editor: Gina Almond

Development Editor: Fiona Pattison

Editorial Assistant: Victoria Pitman

CD produced by: Meg Barton and Nathan Harris

Set in 9.5/12pt Minion by Newgen Imaging Systems (P) Ltd, Chennai, India

Printed and bound in Singapore by Fabulous Printers Pte Ltd

For further information on Blackwell Publishing, visit our website:

[www.blackwellcardiology.com](http://www.blackwellcardiology.com)

The publisher's policy is to use permanent paper from mills that operate a sustainable forestry policy, and which has been manufactured from pulp processed using acid-free and elementary chlorine-free practices. Furthermore, the publisher ensures that the text paper and cover board used have met acceptable environmental accreditation standards.

Blackwell Publishing makes no representation, express or implied, that the drug dosages in this book are correct. Readers must therefore always check that any product mentioned in this publication is used in accordance with the prescribing information prepared by the manufacturers. The author and the publishers do not accept responsibility or legal liability for any errors in the text or for the misuse or misapplication of material in this book.

# Contents

Contributors, vii

Foreword, xi

## Part 1 Methodology, 1

- 1 Technical principles of tissue velocity and strain imaging methods, 3  
*Andreas Heimdal*
- 2 Principles and different techniques for speckle tracking, 17  
*Jan D'hooge*
- 3 Physiologic and magnetic resonance imaging validation of strain techniques, 26  
*Thor Edvardsen and Otto A. Smiseth*
- 4 Designation of tissue Doppler normal range, 36  
*Jing Ping Sun, Zoran B. Popović, Neil L. Greenberg, Xiao-Fang Xu, Craig R. Asher, William J. Stewart and James D. Thomas*

## Part 2 Application to hemodynamic evaluation, 53

- 5 Assessment of filling pressure at rest, 55  
*Jianwen Wang and Sherif F. Nagueh*
- 6 Assessment of left ventricular filling pressure with stress, 72  
*Jong-Won Ha*

## Part 3 Application in heart failure, 79

- 7 Assessment of systolic heart failure, 81  
*John E. Sanderson*
- 8 Assessment of diastolic heart failure, 89  
*Gabriel W. Yip and Cheuk-Man Yu*

- 9 Assessment of dyssynchrony and its application, 102  
*Cheuk-Man Yu, Qing Zhang and Jeffrey Wing-Hong Fung*

## Part 4 Ischemic heart disease, 129

- 10 Experimental studies on myocardial ischemia and viability using tissue Doppler and deformation, 131  
*Geneviève Derumeaux*
- 11 Assessment of viability, 141  
*Rainer Hoffmann*
- 12 Use of tissue velocity imaging during stress echocardiography, 150  
*Thomas H. Marwick*
- 13 Strain and strain rate imaging in ischemia, 162  
*Hsin-Yueh Liang, Jeroen J. Bax and Theodore P. Abraham*

## Part 5 Noncoronary heart disease, 173

- 14 Tissue Doppler echocardiography in the assessment of hypertensive heart disease, 175  
*John D. Merlino and Patrick E. BeDell*
- 15 Using myocardial imaging to identify and manage subclinical heart disease in diabetes mellitus and obesity, 185  
*Niels Holmark Andersen*
- 16 Constrictive pericarditis versus restrictive cardiomyopathy, 198  
*Sunil V. Mankad, Seong-Mi Park and Jae K. Oh*

- 17 Use of myocardial imaging to identify and manage subclinical heart disease in thyroid and other endocrine diseases, 209  
*Vitantonio Di Bello*
- 18 Myocardial imaging in valvular heart disease, 223  
*Sudhir Wahi and Thomas H. Marwick*
- 19 Use of myocardial imaging to identify and manage systemic diseases, 233  
*Frank Weidemann and Joerg M. Strotmann*
- 20 Tissue Doppler imaging and strain rate imaging to evaluate right ventricular function, 243  
*Gabe B. Bleeker, Eduard R. Holman, Theodore P. Abraham and Jeroen J. Bax*
- 22 Three-dimensional reconstruction of strain measurement and measurement of strain in three-dimensions, 265  
*Asbjorn Stoylen*
- 23 Ventricular torsion, 273  
*Jing Ping Sun*
- 24 Automated strain and strain rate, 278  
*Charlotte Bjork-Ingul and Svein A. Aase*
- 25 Use of tissue characterization in relation to arterial function, 288  
*Brian A. Haluska and James E. Sharman*
- 26 Future application of speckle tracking echocardiography, 301  
*Jing Ping Sun*

Index, 315

**Part 6 Coming developments and applications, 253**

- 21 Atrial function, 255  
*Qing Zhang and Cheuk-Man Yu*

*A companion CD-ROM with 32 videoclips and a figure database is included at the back of the book*

# Contributors

## **Svein A. Aase**

Master of Science in Computer Science  
Medinsk Teknisk Forskningssenter  
NO-7489  
Norway

## **Theodore P. Abraham, MD, FACC, FASE**

Johns Hopkins University  
Baltimore, MD, USA

## **Niels Holmark Andersen, PhD**

Medical Department M (Diabetes & Endocrinology)  
Aarhus University Hospital  
Norrebrogade 44  
DK-8000 Aarhus C  
Denmark

## **Craig R. Asher, MD, FACC**

The Department of Cardiovascular Imaging  
The Cleveland Clinic Foundation  
Cleveland, Ohio, USA

## **Jeroen J. Bax, MD**

Department of Cardiology  
Leiden University Medical Center  
Leiden  
The Netherlands

## **Patrick E. BeDell, BBA, RDCS, FASE**

Technical Director/Core Lab Manager  
The Emory Clinic  
Crawford Long Hospital, USA

## **Charlotte Bjork-Ingul, MD**

Department of Cardiology  
Norwegian Technical University  
Trondheim  
Norway

## **Gabe B. Bleeker, MD**

Department of Cardiology  
Leiden University Medical Center  
Leiden  
The Netherlands

## **Jan D'hooge, PhD**

Medical Image Computing  
Department of Cardiology  
Catholic University Leuven  
Leuven  
Belgium

## **Geneviève Derumeaux**

Department of Cardiology  
CHU de Lyon  
Hôpital Cardio-vasculaire et Pneumologique  
Louis PRADEL  
28 Avenue Doyen Lépine  
69500 Bron  
France

## **Vitantonio Di Bello**

Associate Professor of Cardiology  
Cardiac Ultrasound Laboratory  
Cardiac and Thoracic Department  
University of Pisa  
Italy

## **Thor Edvardsen, MD, PhD**

Director of Cardiovascular Imaging Research  
Department of Cardiology  
Rikshospitalet University Hospital  
University of Oslo, Oslo  
Norway

## **Neil L. Greenberg, PhD**

The Department of Cardiovascular Imaging  
The Cleveland Clinic Foundation  
Cleveland, Ohio, USA

## **Jeffrey Wing-Hong Fung MBChB,**

## **MRCP, FHKCP, FHKAM, FRCP**

Director of Pacing and Electrophysiology Services  
Division of Cardiology  
Department of Medicine and Therapeutics  
Prince of Wales Hospital  
The Chinese University of Hong Kong  
Hong Kong

**Jong-Won Ha, MD, PhD**

Associate Professor  
Cardiology Division  
Yonsei University College of Medicine  
Seoul  
South Korea

**Brian A. Haluska, MSc, RDCS, AMS,****FASE**

UQ Department of Medicine  
Princess Alexandra Hospital  
Brisbane, Q4102  
Australia

**Andreas Heimdal, MSc, PhD**

Research and Development Engineer  
GE Vingmed Ultrasound  
Forskningsparken  
Gaustadalléen 21  
0349 Oslo  
Norway

**Rainer Hoffmann, MD, FESC**

Senior Staff Cardiologist  
Medical Clinic I  
University Aachen  
Lamwelsstrasse  
52097 Aachen  
Germany

**Eduard R. Holman**

Department of Cardiology  
Leiden University Medical Center  
Leiden  
The Netherlands

**Hsin-Yueh Liang**

Johns Hopkins University  
Baltimore, MD, USA

**Sunil V. Mankad, MD, FACC, FASE**

Assistant Professor, Internal Medicine and Cardiovascular Disease  
Senior Associate Consultant, Cardiovascular Diseases  
Echocardiography Laboratory  
Mayo Clinic College of Medicine  
Rochester, MN, USA

**Thomas H. Marwick, MBBS, PhD**

Professor of Medicine, University of Queensland,  
Princess Alexandra Hospital, Brisbane,  
Q4102, Australia

**John D. Merlino, MD, FACC**

Division of Cardiology  
Emory Crawford Long Campus  
Atlanta, GA, USA

**Sherif F. Nagueh, MD, FACC**

Professor of Medicine, Weill Medical College  
Cornell University  
6550 Fannin SM-677  
The Methodist Hospital  
Houston, TX 77030-2717  
United States

**Jae K. Oh, MD, FACC, FAHA**

Professor, Internal Medicine and Cardiovascular Disease  
Co-director, Echocardiography Laboratory  
Director, Echocardiography Core Lab  
Consultant, Cardiovascular Diseases  
Mayo Clinic College of Medicine  
Rochester, MN, USA

**Seong-Mi Park, MD, PhD**

Assistant Professor, Internal Medicine and Cardiology  
Cardiovascular Center, Anam Hospital  
College of medicine, Korea University  
Seoul, Korea

**Zoran B. Popović, MD**

The Department of Cardiovascular Imaging  
The Cleveland Clinic Foundation  
Cleveland, Ohio, USA

**John E. Sanderson, MA, MD, FRCP, FACC**

Professor of Cardiology & Consultant Cardiologist  
Keele University Medical School, University Hospital of  
North Staffordshire; Department of Cardiology,  
City General Hospital, Stoke On Trent, UK

**James E. Sharman, PhD**

Department of Medicine  
University of Queensland  
Princess Alexandra Hospital  
Brisbane, Australia

**Otto A. Smiseth, MD, PhD**

Department of Cardiology  
Rikshospitalet University Hospital  
University of Oslo, Norway

**William J. Steward, MD, FACC**

The Department of Cardiovascular Imaging  
The Cleveland Clinic Foundation  
Cleveland, Ohio, USA

**Asbjørn Stoylen, MD**

Associate Professor  
Department of Circulation and Medical Imaging  
Faculty of Medicine  
Norwegian University of Science and Technology  
Medisinsk teknisk forskningssenter  
N-7489 Trondheim  
Norway

**Joerg M. Strotmann, MD**

Department of Internal Medicine I/Center of  
Cardiovascular Disease  
University of Wuerzburg  
Germany

**Jing Ping Sun, MD, FACC, FAHA**

Associate Professor of Medicine  
The Carlyle Fraser Heart Center  
Cardiology Department, 6th Floor  
Atlanta, Georgia  
USA

**James D. Thomas, MD, FACC**

The Department of Cardiovascular Imaging  
The Cleveland Clinic Foundation  
Cleveland, Ohio, USA

**Sudhir Wahi, MD, FRCR, FCSANZ**

Department of Cardiology  
Princess Alexandra Hospital  
Ipswich Road, Brisbane  
Queensland  
Australia

**Jianwen Wang, PhD, MD**

The Echocardiography laboratory of the Methodist  
DeBakey Heart Center  
The Methodist Hospital, Houston  
Texas, USA

**Frank Weidemann, MD**

Department of Internal Medicine I/Center of  
Cardiovascular Disease  
University of Wuerzburg  
Germany

**Gabriel W. Yip, MD, MRCP, FACC, FASE**

Department of Medicine and Therapeutics  
Prince of Wales Hospital  
Shatin, NT  
Hong Kong  
China

**Cheuk-Man Yu MBChB, MRCP, MD,  
FHKCP, FHKAM, FRACP, FRCP**

Professor  
Head of Division of Cardiology  
Department of Medicine and Therapeutics  
Prince of Wales Hospital  
The Chinese University of Hong Kong  
Hong Kong

**Qing Zhang, BM, MM, PhD**

Research Assistant Professor  
Division of Cardiology  
Department of Medicine and Therapeutics  
Prince of Wales Hospital  
The Chinese University of Hong Kong  
Hong Kong

**Xiao-Fang Xu, MD, PhD**

The Department of Cardiovascular Imaging  
The Cleveland Clinic Foundation  
Cleveland, Ohio, USA



# Foreword

It has been barely 50 years since Inge Edler and Helmut Hertz first used an ultrasound transducer—purloined from a Malmo shipyard where it was used to examine the hulls of ships—to record the motion of structures in their hearts, not knowing whether the ultrasonic energy might rupture their ventricles. In the relatively brief interim, we have seen staggering technical progress: A-mode, M-mode, B-mode, PW, CW, color Doppler, TEE, digital echo, stress echo, contrast perfusion, tissue harmonics, 3D, and on and on. Over the past 10 years, however, perhaps the most important advance has been the development of techniques to quantify tissue motion and deformation. These techniques—tissue Doppler and speckle tracking imaging—have fundamentally altered the way echocardiography approaches the characterization of global and regional myocardial function. The notion that tissue motion—as opposed to endocardial excursion—is useful in the assessment of ventricular function is hardly new: Derek Gibson utilized M-mode over 30 years ago to relate myocardial velocity to ventricular function. What these new methods provide is an unprecedented view of tissue motion on a region-by-region basis. Exploiting the revolution in image quality, parallel processing, and digital storage and analysis that has also occurred in this time period, giving us 2D and color Doppler frame rates exceeding 100 Hz, these methods have literally launched a thousand (at least) research papers describing applications in ventricular physiology, heart failure management, ischemia and viability assessment, ventricular synchrony, and valvular heart disease.

What has been lacking in much of this work has been practical instruction in how to apply these new methods in routine clinical practice.

So many times I have been addressing audiences of advanced echocardiographers in the United States and abroad only to find that TDI and speckle tracking, while unquestioned in their utility, are rarely used in routine clinical assessment. This is the gap that I believe this book will help fill. Drawing on the expertise of many of the individuals who developed and validated these techniques in the first place, these chapters describe not just the technical background and research validation of these methods but also provide practical outlines of how to integrate them into routine clinical practice in a busy echo lab. All the brilliant research in the world is of little value if a new technique is rarely used.

On a personal level, I am especially pleased to see this book coming from these particular editors. Not only has CM Yu combined his renaissance-man skills in heart failure management, electrophysiology, and echocardiography to define the tissue Doppler criteria for LV synchrony, but he is also a dear friend with whom I fondly remember sharing oysters at the top of the Hong Kong Sheraton among many other good times. Jing Ping Sun worked with me at the Cleveland Clinic for over a decade, validating the clinical utility of many of the new technologies to emerge during this period. Calling herself my “Chinese mother” she has taught me much about the role of dedication and perseverance in succeeding, which in her case included overcoming two years of “reeducation” during the Cultural Revolution in China, completely separated from her family and work. I’ve likened her tenacity on any project to a “pit-bull on a porkchop”, and I have no doubt that this book reflects this same determination. Finally, Tom Marwick is simply one of the most focused and organized researchers in the world, investigating the role of new imaging

technologies in real-world problems like ischemia, viability, cardiomyopathies, and the impact of systemic diseases like diabetes on the heart. Beyond this he is also a close friend who spent several years with me in Cleveland where his brilliance, dry wit, and remarkable ability to cut through excreta won me over forever. Most of all, though, I owe Tom an unending debt of gratitude: you see, it was he who first introduced me to my wife, Yngvild. It just doesn't get better than that!

In closing I wish to commend the authors for their brilliant work and clear, practical writing, and the editors for their organizational talents and foresight. Finally, to you, the reader, I highly recommend this book. Drink deeply of it, read and reread the chapters, and you will come away with the practical knowledge you need to apply these

important new techniques for the betterment of your patients.

**James D. Thomas, MD, FACC, FAHA, FESC**

Charles and Lorraine Moore Chair of  
Cardiovascular Imaging  
Department of Cardiovascular Medicine  
Cleveland Clinic Foundation

Professor of Medicine and Biomedical

Engineering  
The Ohio State University  
and  
Case Western Research University

Lead Scientist for Ultrasound

National Aeronautics and Space Administration

# 1

## PART 1

# Methodology



# Technical principles of tissue velocity and strain imaging methods

*Andreas Heimdal*

## Introduction

Tissue velocity imaging (TVI) is an ultrasound technique that provides quantitative information on the velocity of the tissue. Traditionally, Doppler techniques have mainly been used to measure blood flow, and the signal component from tissue was considered noise that needed to be removed. There were early studies in the 1960s and 1970s using the pulsed-wave (PW) Doppler method to detect myocardial motion [1,2]. However, the method has had widespread use only since the late 1980s [3]. In the 1990s, color-coded TVI was introduced, allowing simultaneous velocity samples from an entire field of view [4–6]. This color TVI provides the possibility of extracting other parameters through spatial and temporal processing of the velocity data. Displacement, strain, and strain rate are examples of such parameters [7–9].

This chapter describes the technical aspects of TVI, including the acquisition technique, how the velocity is estimated, and how it may be presented and analyzed. The chapter also defines the parameters *displacement*, *strain*, and *strain rate* and explains how they can be derived from the tissue velocity data.

## Tissue velocity imaging

TVI is a technique where the velocity of the myocardium toward or away from the transducer is measured and displayed. The velocities can be calculated and displayed as a PW spectrogram or as a color coding of the image. Both methods calculate the velocity based on the echoes of several ultrasound pulses fired in the same direction. The pulses are

fired at a certain pulse repetition frequency (PRF). Each echo is sampled at a fixed depth, and the samples are collected into a new signal representing a certain position in the image. This signal is called the Doppler signal. The frequency of the Doppler signal is related to the velocity of the tissue in the sample region through the Doppler equation:

$$f_d = \frac{2f_0v}{c}$$

In this equation,  $f_0$  is the central frequency of the transmitted ultrasound pulse,  $c$  is the speed of sound, and  $v$  is the tissue velocity component in the ultrasound beam direction\*.

Note that the Doppler equation also describes the frequency shift in a received pulse relative to the transmitted pulse. However, due to the short pulse length or, equivalently, the large bandwidth normally used for TVI, it is not feasible to estimate the frequency shift from one pulse only.

A consequence of using pulsed imaging is that there is a limit on the maximum velocity that can be measured. This limit is called the Nyquist velocity:

$$v_{Nyq} = \frac{c \cdot PRF}{4f_0}$$

If the actual velocity is higher than this limit, there will be frequency aliasing, resulting in misrepresentation of the velocity. The Nyquist velocity can be

---

\*If second-harmonic Doppler imaging is used, the Doppler equations is  $f_d = (4f_0v)/c$ .

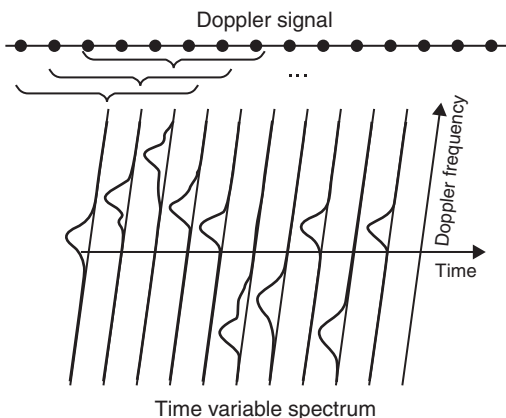


**Figure 1.1** Generation of PW TVI. The Doppler signal is split into overlapping windows, and the frequency content of each window is calculated. Each circle in the illustration of the Doppler signal represents a sampled value.

modified by adjusting the PRF or the ultrasound frequency  $f_0$ .

The combination of frequency, pulse length, and beam width that gives the optimal Doppler acquisition is not the same as that which gives good gray-scale image quality. Typically, lower frequencies, longer pulses, and wider beams are used for the Doppler acquisition. Therefore, the gray-scale image and the Doppler data are usually based on different acquisitions and may have different frame rates and spatial resolutions.

### Pulsed-wave tissue velocity imaging

In PW TVI, the Doppler signal from only one sample region is collected. The signal is first split into overlapping windows, and then the frequency content of each window is calculated using the Fourier transform. Other, more advanced processing methods involving data from several sample regions may also be used. The result is a signal spectrum for each window, representing the frequency content at a certain time, as illustrated in Figure 1.1.

The spectral amplitude is next coded as gray-scale intensity, and the collection of signal spectra is visualized with Doppler frequency on the vertical axis and time on the horizontal axis. Because the Doppler frequency is linearly related to the tissue velocity, the vertical axis can also be a velocity axis. An example of PW TVI from the basal segment of a healthy interventricular septum is shown in Figure 1.2.

Note that the peak of each spectrum, representing the tissue velocity, is typically found in the *middle*

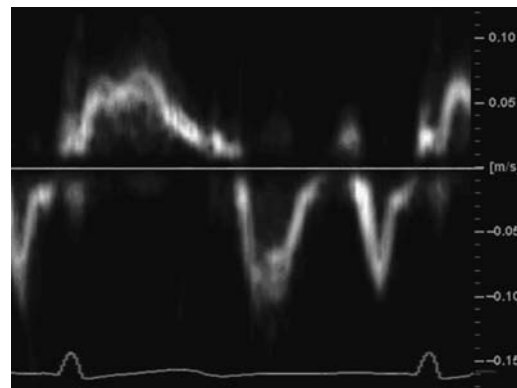


**Figure 1.2** Example of PW TVI from the basal part of a healthy interventricular septum. The velocity variations over one full cardiac cycle are shown, as indicated by the electrocardiogram trace below the spectrum.

of the spectral signal. The spectrum bandwidth, represented as the vertical thickness of the spectral signal, is related to the duration of the estimation windows. Using longer windows will typically give a smaller bandwidth, but at the same time, the temporal resolution will be reduced; therefore, there is a trade-off between accuracy and temporal resolution. Other factors that influence the bandwidth are acceleration in the tissue and acoustical noise.

### Color tissue velocity imaging

In color TVI, a Doppler signal is collected for each depth and each ultrasound beam. This process normally requires more time, so each Doppler signal consists of fewer samples per time unit than in the PW case. This requirement normally limits the ability to calculate full-signal spectra for each position in the image. Instead, only the mean Doppler frequency is estimated for each position.

The most common way to estimate this mean frequency is to calculate the phase shift relative to the transmitted ultrasound pulse for each sample in the Doppler signal\*. If the tissue is not moving, the phase shift is the same for all the samples. If the tissue is moving relative to the transducer, the phase shift increases or decreases from sample to sample according to the velocity of the tissue, as illustrated in Figure 1.3. The difference in phase shift from sample to sample in the Doppler signal can thus be

\*A common way to calculate the phase shift is through the autocorrelation technique [10].

used to calculate the velocity. The sign of the phase corresponds to the sign of the estimated velocity.

When the velocity has been estimated for all parts of the ultrasound image, each pixel is color coded according to the velocity. As mentioned earlier, the Doppler acquisition is usually separate from the image acquisition; therefore, for each gray-scale image, there is at least one corresponding velocity image. The velocity image may have a lower resolution than the gray-scale image, but is normally interpolated to match the resolution of the gray-scale image. This finding means that neighboring pixels in the color-coded image may represent strongly correlated velocity values. The color code ranges from dark red for low velocities to bright yellow for high velocities toward the transducer, and from

dark blue for low velocities to bright cyan for high velocities away from the transducer.

## Quantitative analysis

One of the major advantages of TVI is that it allows quantitative analysis of the motion pattern of the cardiac walls. In PW TVI, accurate timing and velocity measurements may be performed from the spectrogram. In color TVI, each pixel in the image represents a velocity measurement, and the quantitative value can be presented in various ways, as described in the following sections. The quantitative velocity values have been validated *in vitro* [11] and *in vivo* [12].

### Time-traces

By picking one region of interest (ROI) in each frame of a color TVI cine-loop, the corresponding velocities can be presented as a time-trace, as illustrated in Figure 1.4. The time-trace represents the velocity pattern of the tissue within the ROI, similar to PW TVI. One of the differences between the two methods is that the PW TVI only can be acquired from one position at a time, whereas with color TVI, multiple time-traces from various regions can be generated from a single cine-loop. The PW TVI usually allows higher temporal resolution. The PW TVI in Figure 1.2 is taken from the same position and the same heart as the TVI time-trace in Figure 1.4.

The ROI used to generate the time-trace can be fixed to the same position in all the frames, or it can be moved to follow a certain anatomical structure.

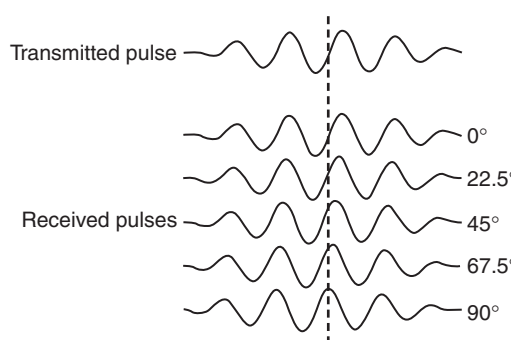


**Figure 1.3** Illustration of echo pulses with increasing phase shifts relative to the transmitted pulse. A phase shift of 90° corresponds to half the Nyquist velocity.

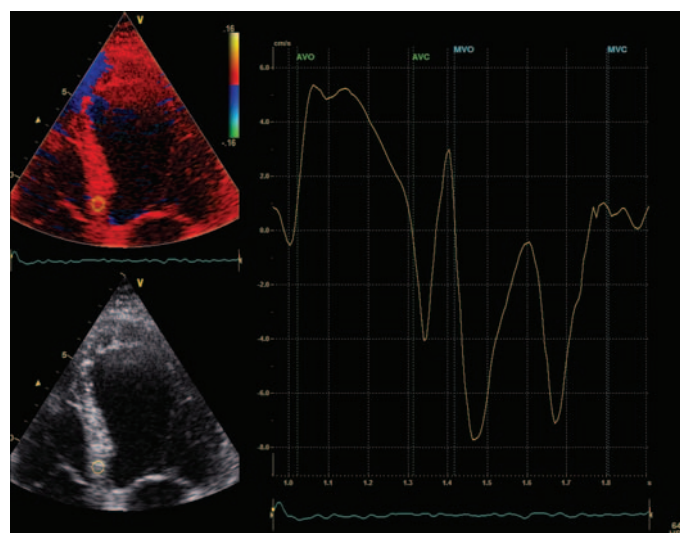


**Figure 1.4** Example of a TVI time-trace from an ROI in the basal part of the interventricular septum of a healthy volunteer. The ROI is shown as a yellow circle in each of the left panels. An electrocardiogram trace is shown below the velocity trace. AVO, aortic valve opening; AVC, aortic valve closure; MVO, mitral valve opening; MVC, mitral valve closure.

To avoid having to adjust the position of the ROI in every single frame, it is recommended to reposition the ROI only in the extreme positions, and let the software perform a linear translation between these positions for the intervening frames. For a cardiac cycle, it is usually enough to anchor the ROI at three time instances: the onset of systole, the end of systole, and at the end of the early filling period.

### Curved anatomical M-mode

Another way to visualize the color TVI data is to make an anatomical M-mode. The M-mode line may be a straight line in any direction through the two-dimensional (2-D) image. Alternatively, a curve may be manually drawn to an arbitrary shape, usually along the mid-myocardium. The resulting image is then called a curved anatomical M-mode (CAMM). Figure 1.5 shows an example of a TVI CAMM from the left ventricle of a healthy volunteer.

For apical views, the CAMM curve may be drawn separately in the two visible walls, or, as illustrated in Figure 1.5, the curve may be drawn from the base of one wall to the apex and down to the base of the other wall in one operation. The latter method produces a still CAMM image that represents the velocities of all the segments in all the 2-D frames.

### Displacement imaging

When the velocity of the tissue is known, several other parameters can be derived. One of the simplest

to calculate is displacement, which is the integral of the velocity over time:

$$d = \int_{T_0}^T v(t) dt$$

In this equation,  $T_0$  and  $T$  are the start and end integration times, respectively, and  $v(t)$  is the velocity at a given position at the time  $t$ . Typically  $T_0$  is set to the beginning of systole and  $T$  to the end of systole to calculate the systolic displacement.

Displacement may be estimated from PW TVI recordings [13], but the calculation is more commonly based on color TVI data [7,14,15]. The method has been validated in vitro using a balloon phantom [11].

The displacement can be presented as a time-trace from an ROI, as a CAMM, or as a 2-D color-coded image. The latter is also known as a “Tissue Tracking” image, and an example is shown in Figure 1.6. A stepwise constant color coding, as opposed to a continuous color coding, is used for the Tissue Tracking image. With this method of color coding, it is possible to determine the strain, in addition to the displacement itself. Regions with narrow color bands have high strain, and regions with wide color bands have low strain. This concept will be described in more detail in the next section.

Figure 1.7 shows a velocity time-trace and the corresponding displacement time-trace from the basal part of the interventricular septum in a normal heart.

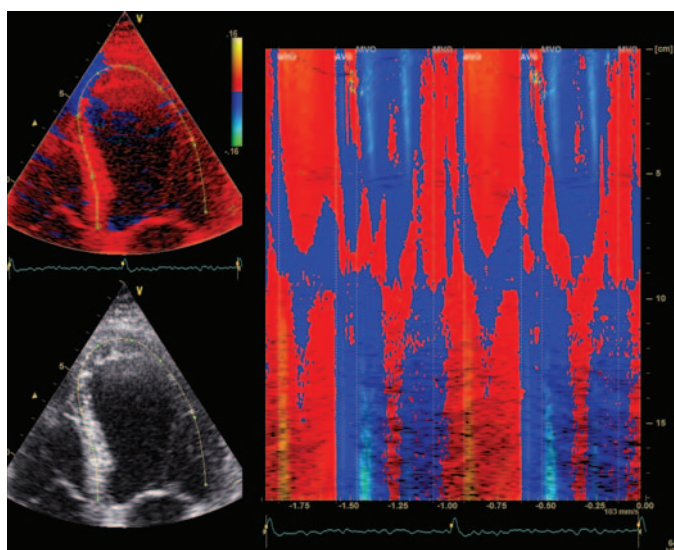


**Figure 1.5** Example of a TVI CAMM over two cardiac cycles. The CAMM shows a map of the velocities at the locations indicated by the CAMM curve in the left panels. In this example, the upper, middle, and lower parts of the CAMM correspond to the septum, the apex, and the lateral wall, respectively. AVO, aortic valve opening; AVC, aortic valve closure; MVO, mitral valve opening; MVC, mitral valve closure.

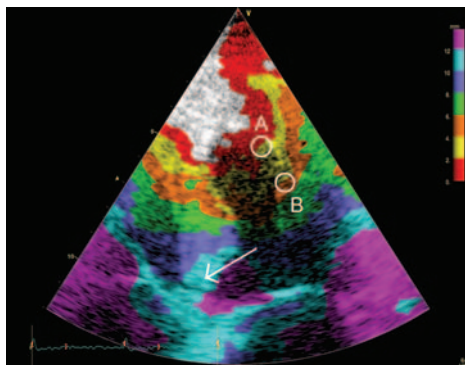


**Figure 1.6** Example of a Tissue Tracking image of the heart of a normal volunteer, showing the end-systolic displacement. The start and end integration times are shown as red markers on the ECG trace. In this example, the basal part of the septum (arrow) is colored cyan, indicating a displacement of more than 10 mm. Similarly, the tissue in region A has moved 2 mm and the tissue in region B has moved 4 mm.

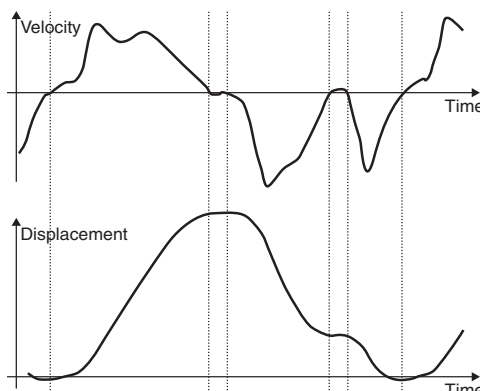


**Figure 1.7** Comparison of velocity (top panel) and displacement (lower panel). The horizontal lines represent zero velocity or displacement, whereas the vertical dotted lines indicate when the velocity trace crosses zero.

As seen in these plots, the velocity is the slope of the displacement trace. When the velocity is positive, the displacement increases, and when the velocity is negative, the displacement decreases. When the velocity crosses zero, the displacement has a positive or negative peak, depending on the direction of the zero crossing.

When reporting displacement values, both the start and end integration times should be specified, for example: “The end-diastolic to end-systolic displacement was 10 mm.” It is also important to specify in what direction the displacement was measured, that is, longitudinal or radial.

## Concepts of strain and strain rate

Strain and strain rate are measures of changes in shape, that is, deformations. The use of these measures to describe mechanics of the heart muscle was introduced by Mirsky and Parmley in 1973 [16]. The strain and strain rate measures can be defined and estimated in various ways, as will be described in the following sections.

### Definition of strain

Strain is a mechanical characteristic that describes the deformation of objects. There are several different ways to measure strain. For 1-D deformations, that is, shortening or lengthening, perhaps the simplest measurement is *conventional* or *engineering strain*  $\varepsilon^*$ . It describes the relative change in length between two states. For an object of initial length  $L_0$  that is being stretched or compressed to a new length  $L$ , the conventional strain is defined as:

$$\varepsilon = \frac{L - L_0}{L_0}$$

The Greek letter epsilon ( $\varepsilon$ ) is commonly used as a symbol for conventional strain. The strain value is dimensionless and can be presented as a fractional number or as a percentage (by multiplying with 100). For instance, a fractional strain of  $-0.2$  corresponds to a percentage strain of  $-20\%$ . The strain is positive if  $L$  is larger than  $L_0$ , meaning that the object has lengthened, and negative if  $L$  is smaller than  $L_0$ , meaning that the object has shortened. If  $L$  equals  $L_0$ , there has been no change in length, and the strain is zero.

Other measures for 1-D strain include *natural strain*<sup>†</sup>, which is defined as:

$$\varepsilon' = \ln\left(\frac{L}{L_0}\right)$$

\*This strain measure has been named Lagrangian strain in the echocardiographic literature, but use of this term is not advised, because Lagrangian only means that the reference state is fixed, which is true for many strain measures. It is also known as longitudinal strain, but use of this term is not advised for cardiac applications, because it can be confused with the longitudinal direction of the ventricle.

<sup>†</sup>Natural strain is also termed logarithmic or true strain in the literature.

The name reflects the use of the natural logarithm function  $\ln$ . Natural strain has the same properties as conventional strain regarding the sign: it is positive for lengthening, negative for shortening, and zero for no change in length. The actual strain, however, is slightly different for each method. Compared to that of conventional strain, the natural strain amplitude is smaller for positive strains and larger for negative strains. For instance, a conventional strain of 20% corresponds to a natural strain of 18.2%, and a conventional strain of  $-20\%$  corresponds to a natural strain of  $-22.3\%$ .

The conventional and natural strains have a fixed nonlinear relationship:

$$\begin{aligned}\varepsilon' &= \ln(\varepsilon + 1) \\ \varepsilon &= \exp(\varepsilon') - 1\end{aligned}$$

Note that, in these formulas, the strains are represented as fractional numbers. For percentage strains, the corresponding formulas are:

$$\begin{aligned}\varepsilon'_\% &= 100 \ln \left( \frac{\varepsilon_\%}{100} + 1 \right) \\ \varepsilon_\% &= 100 \left( \exp \left( \frac{\varepsilon'_\%}{100} \right) - 1 \right)\end{aligned}$$

When reporting strain values, it should be specified whether conventional or natural strain is used. In addition, both the initial and the final reference states should be specified, for example: "The end-diastolic to end-systolic conventional strain was  $-20\%$ ." When measuring 1-D strains in a 2- or 3-D object, it is also important to specify in what direction the 1-D strains were measured.

### Two- or three-dimensional strain

For 2- or 3-D deformations, the concept of strain becomes more complex. In the given coordinate system, one can use the 1-D strain in any spatial direction using the same definitions as presented earlier in this section. This type of strain is termed normal strain, because the deformation is normal to an imaginary plane. In addition, there might be shear strains, measuring changes in angle, as illustrated in Figure 1.8. The maximal and minimal

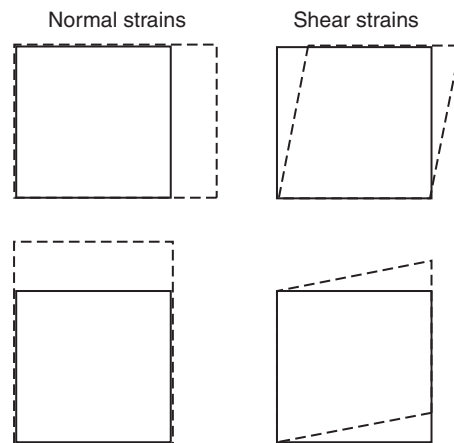


**Figure 1.8** Illustration of normal strains (left) and shear strains (right).

strains might not occur in any of the coordinate directions; therefore, it is common to specify the directions and magnitudes of the maximal and minimal strains. These specifications are termed the principal strains and principal strain directions. Note that, if one aligns the coordinate system to the principal strain directions, there will be no shear strains.

### Definition of strain rate

The strain rate is the temporal derivative of the strain:

$$\dot{\varepsilon} = \frac{d\varepsilon}{dt}$$

This definition means that, whereas strain indicates the amount of deformation, strain rate indicates the rate of the deformation. The relation between strain rate and strain can be compared to the relation between velocity and displacement. Assuming the velocity is constant, displacement equals time multiplied by velocity. Similarly, assuming the strain rate is constant, strain equals time multiplied by strain rate. A positive strain rate means that the length of the object is increasing, whereas a negative strain rate means that the length is decreasing. If the length is constant, the strain rate is zero.

The notation for strain rate is an epsilon with a dot above it ( $\dot{\varepsilon}$ ), indicating the temporal derivative. Because this notation is cumbersome in many

instances, the acronym SR is commonly used to represent the strain rate. The unit of the strain rate is normally 1/sec or sec<sup>-1</sup>, which may be read as “per second.”\* In other applications, the unit Hertz (Hz) is used for sec<sup>-1</sup>, but this method is not recommended for strain rate. Hertz means number of oscillations per second, whereas for strain rate, it is more correct to speak of amount of deformation per second. A strain rate of  $-2 \text{ sec}^{-1}$  applied over 1 sec would result in a relative strain of  $-2$ , and a corresponding percentage strain of  $-200\%$ .

Note that, whereas the strain is a measurement of deformation relative to a reference state, the strain rate is an instantaneous measurement. There is no need to specify a reference state for strain rate, only the time of the measurement, for example: “The mid-systolic strain rate was  $-1.0 \text{ sec}^{-1}$ .”

Because there are several definitions of strain, there are a corresponding number of similar definitions for strain rate. In particular, the derivative of *natural strain* is<sup>†</sup>:

$$\dot{\varepsilon}' = \frac{d\varepsilon'}{dt} = \frac{1}{L} \frac{dL}{dt}$$

### Estimation of strain and strain rate from ultrasound data

One way to measure strain is by M-mode through any of the cardiac walls [17,18]. By measuring the wall thickness before ( $L_0$ ) and after ( $L$ ) contraction, the transmural conventional strain can be calculated as:

$$\varepsilon = \frac{L - L_0}{L_0}$$

Another method is to use the displacement map provided by the Tissue Tracking modality. Consider the two regions marked A and B in Figure 1.6, and

the distance between them  $L$ , which in this example is measured to 15 mm. Because region A is on the red–yellow color transition, it has moved 2 mm toward the transducer since the beginning of systole. Similarly, region B has moved 4 mm. This finding means that the length of the segment between A and B has been reduced by 2 mm. The original distance  $L_0$  was thus  $15 + 2 = 17$  mm. By inserting these values into the equation for strain, one can calculate the strain to  $-12\%$ . Generally, the closer together two color transitions are, the higher is the strain on the segment between them. A similar calculation may be performed based on PW TVI data [13].

Although accurate, these methods are relatively cumbersome to perform, especially for multiple cardiac segments. A faster method is to use TVI and calculate the strain rate and strain from the velocity data, as described in the following section.

### Strain rate and velocity gradient

The spatial velocity gradient was one of the first parameters to be derived from TVI recordings [19–22]. With the assumption that the spatial velocity distribution within the estimation area is linear, the 1-D natural strain rate in an object is equivalent to the spatial velocity gradient [9]:

$$\dot{\varepsilon}' = \frac{dv}{dx}$$

This relation can be illustrated by considering the small object in Figure 1.9, which is being deformed. The instantaneous length is defined by the positions of the endpoints as  $L = x_b - x_a$ . Because the temporal derivative of spatial position

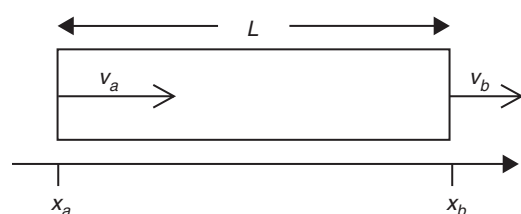


**Figure 1.9** Illustration of a tissue segment of length  $L$  that is being deformed. The velocities of the endpoints  $x_a$  and  $x_b$  are  $v_a$  and  $v_b$ , respectively.

\*In rare instances, the notation %/sec is seen for strain rate, meaning that the strain rate is multiplied by 100. A strain rate of  $-1 \text{ sec}^{-1}$  corresponds to  $-100\%/\text{sec}$ .

<sup>†</sup>The formula is derived using the relation  $d(\ln(u))/dt = (du/dt)/u$ .

is velocity, the natural strain rate of the object can be written as:

$$\dot{\varepsilon}' = \frac{1}{L} \frac{dL}{dt} = \frac{1}{L} \left( \frac{dx_b}{dt} - \frac{dx_a}{dt} \right) = \frac{v_b - v_a}{L} = \frac{dv}{dx}$$

Here,  $v_a$  and  $v_b$  are the instantaneous velocities of the endpoints of the segment.

In practice, it is rarely feasible to accurately track the endpoints of such a segment, and a fixed “strain length”  $\Delta x$  may be used instead. As long as the velocities are linearly increasing or decreasing

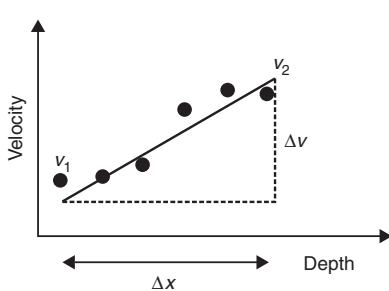


**Figure 1.10** Illustration of the two methods to estimate strain rate from velocity data. The velocities  $v_1$  and  $v_2$  are the actual velocities of the endpoints, whereas  $\Delta v$  is the velocity difference of the endpoints of the regression line. See text for an explanation of the estimation methods.

within the region, this method will give exactly the same answer.

As illustrated in Figure 1.10, the velocity gradient may be estimated using only the two velocity estimates  $v_1$  and  $v_2$  from the endpoints of the estimation area as:

$$\dot{\varepsilon}' = \frac{v_2 - v_1}{\Delta x}$$

or a linear regression of all the velocity samples within the area may be performed\*:

$$\dot{\varepsilon}' = \frac{\Delta v}{\Delta x}$$

This method of measuring strain rate has been validated *in vitro* using tissue-mimicking phantoms [23,24] and *in vivo* versus wall motion scoring with standard echocardiography [25].

Note that the strain rate estimation is performed separately for each frame in a cine-loop and that the ROI may be moved from frame to frame to follow the motion of the myocardium, as explained earlier. Figure 1.11 shows an example of a color-coded strain rate image and an extracted strain rate trace.

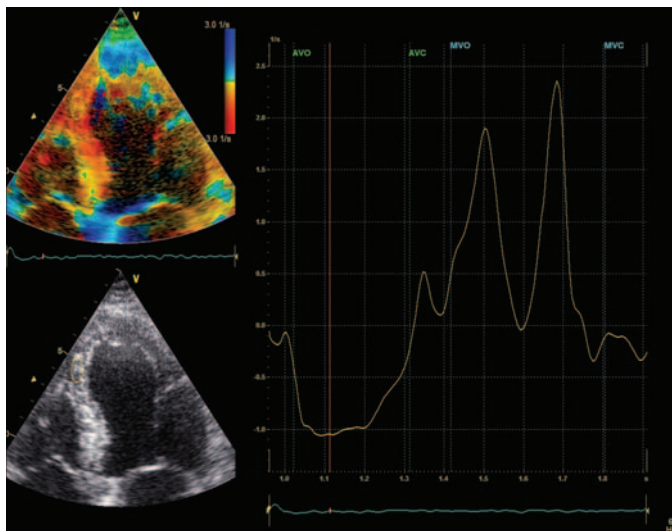


**Figure 1.11** Mid-systolic strain rate images (left) and an extracted strain rate trace (right). The yellow ellipse in each strain rate image indicates the sample region for the trace. In healthy segments, the strain rate is typically negative in systole, indicating shortening, and positive in diastole, indicating lengthening. AVO, aortic valve opening; AVC, aortic valve closure; MVO, mitral valve opening; MVC, mitral valve closure.

\*In ultrasound, velocities have been defined as positive for motion toward the transducer, whereas in the equations here, the velocities are defined as positive for increasing depth. This discrepancy may be accounted for by negating the velocity values before calculating the velocity gradient.

The color coding of strain rate typically ranges from yellow for low negative strain rates to red for high negative strain rates, and from light cyan for low positive strain rates to dark blue for high positive strain rates. A green color is sometimes used for the near zero strain rates.

### Integrating strain rate to get strain

When the strain rate has been calculated for each time point during the deformation, the strain can be found as the temporal integral of the strain rate:

$$\varepsilon' = \int_{T_0}^T \dot{\varepsilon}'(t) dt$$

Here,  $T_0$  and  $T$  are the time points of the start and end of the deformation. Note that it is the natural strain that is found through this integral. To find the more commonly used conventional strain, one might use the conversion formula:

$$\varepsilon = \exp(\varepsilon') - 1$$

Note also that, in commercially available post-processing tools, this function is normally performed automatically, so that it is the conventional strain that is presented to the user. The strain imaging method has been validated *in vivo* versus sonomicrometry [26] and tagged magnetic resonance imaging [27]. The color coding for strain is typically

red for negative strain and blue for positive strain, as illustrated in Figure 1.12.

### Artifacts and methods to improve signal quality

As are all ultrasound modalities, tissue velocity and strain imaging are also affected by noise components such as random thermal noise and reverberations. These noise components may degrade the quality of the velocity and strain rate measurements. In addition, angle mismatches between the ultrasound beams and the examined structure may cause errors. The artifacts, and suggestions of how to reduce them, are reviewed in the following sections.

### Reverberation artifacts

Reverberations are false echoes resulting from multiple reflections within the body. In the gray-scale image they are seen as false echoes or reduced contrast. The reverberations are often caused by tissue layers close to the body surface. These layers are relatively motionless, and the reverberation artifacts are, therefore, often seen as immobile structures mixed with the true signal.

In PW TVI, reverberations can be seen as an increased intensity at zero velocity, as shown in Figure 1.13. In many cases, it is still relatively easy to identify the true velocity signal. PW TVI may,

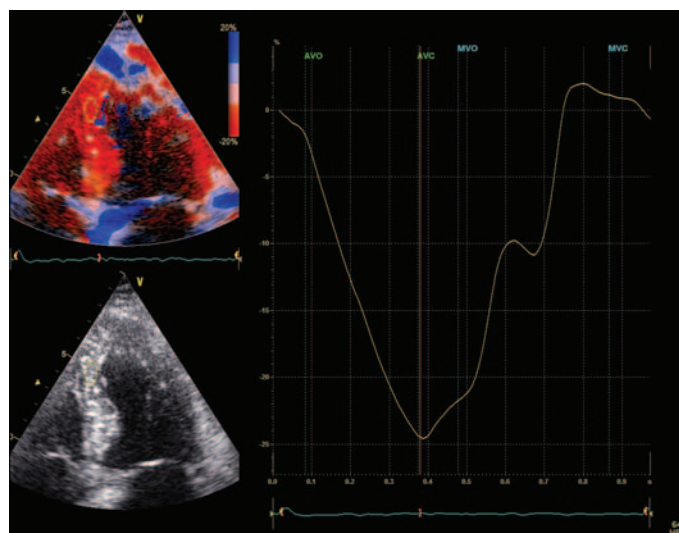


**Figure 1.12** End-systolic strain images (left) and an extracted strain rate trace (right). The yellow ellipse in each strain rate image indicates the sample region for the trace. In healthy segments, the strain is typically negative at end-systole, indicating shortening, and returns to zero at end-diastole. AVO, aortic valve opening; AVC, aortic valve closure; MVO, mitral valve opening; MVC, mitral valve closure.

therefore, be a preferred method for velocity measurements in patients with poor acoustic windows.

For color TVI, strong reverberations may cause a bias in the mean velocity estimate, as shown by the trace in Figure 1.13. Typically the bias is toward zero velocity. The amount of bias depends on the intensity of the reverberation signal relative to the tissue velocity signal. However, the sign of the velocity is seldom affected, so it might be difficult to detect reverberations from the TVI color display, as illustrated in the central part of Figure 1.14.

In strain rate imaging, reverberations may cause large errors, as illustrated in Figure 1.14. A small local bias in the velocity will cause large changes in the spatial velocity gradient and, thus, the strain rate. A typical reverberation artifact in strain rate is a strong blue and red stripe next to each other. Figure 1.15 shows an example of how a strain rate artifact may be detected by using CAMM.

Displacement and strain are calculated from velocity and strain rate; therefore, reverberation errors in velocity and strain rate will also cause errors in displacement and strain. Because strain rate is most affected by reverberation errors, strain will be more affected than displacement.

Unfortunately, there is little the user can do when there is reverberation noise, other than trying to get the best scanning window when performing the imaging. When analyzing the strain rate data, it is important to recognize the reverberation artifacts and to avoid the regions affected. CAMM may, as illustrated in Figure 1.15, be a good tool to get an overview of the amount of reverberation artifacts

in the strain rate and may be used prior to detailed analysis.

### Angle dependence

All basic Doppler methods are angle dependent. It is only the velocity component in the ultrasound beam direction that is picked up. If the true velocity direction is known – or assumed – the true velocity may be calculated by dividing the measured velocity component by  $\cos(\theta)$ , where  $\theta$  is the angle between the ultrasound beam and the true velocity direction [20]. This explanation means that, as the angle increases, the measured velocity component decreases from 100% of the true velocity at zero angle to 0% at a 90°, as illustrated in Figure 1.16.

For strain rate, the angle dependence is more complex. Assuming, for simplicity, that the beam

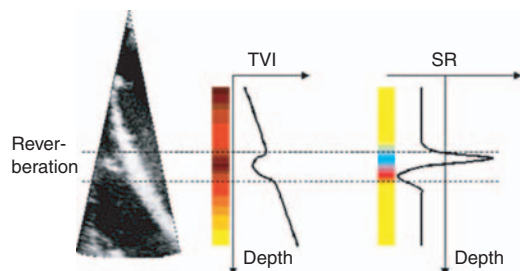


**Figure 1.14** Illustration of effect of a local reverberation in the mid-septum on the tissue velocity and strain rate (SR). The color bars indicate the coloring of the septum in mid-systole, whereas the plots show the actual velocities and strain rates at different depths along the septum. The dashed lines indicate the region affected by the reverberation.

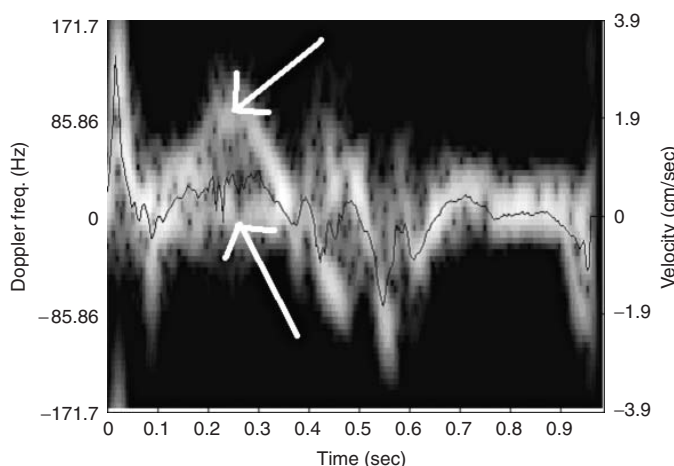


**Figure 1.13** PW TVI from a region with strong reverberations. The upper arrow shows the true signal, and the lower arrow shows the reverberation artifact centered around zero Doppler frequency. The black trace shows the corresponding TVI trace based on color TVI. As one can see, the TVI trace underestimates the correct velocity value.

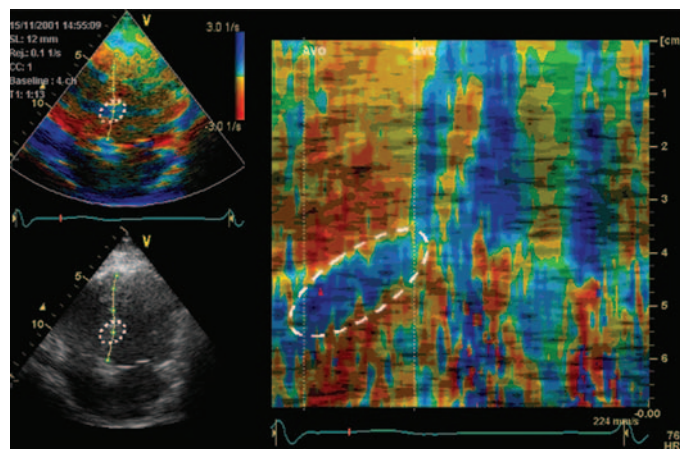


**Figure 1.15** Strain rate image (top left) and a derived CAMM image (right) showing an artifact region covering the basal part of the interventricular septum (white ellipses). Artifacts can often more easily be detected in the CAMM display than in the 2-D strain rate image. AVO, aortic valve opening; AVC, aortic valve closure; MVO, mitral valve opening; MVC, mitral valve closure.

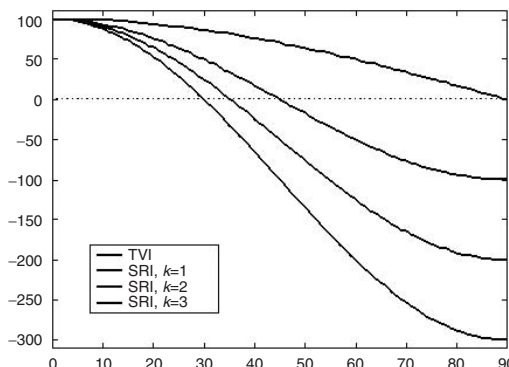


**Figure 1.16** Angle dependence of TVI and strain rate imaging (SRI) for three different assumptions of the radial-longitudinal relationship ( $k$ ). The graphs show how many percent of the true value is picked up when the angle between the ultrasound beam and the desired direction increases. For TVI, it is assumed that the true velocity is in the direction of the ultrasound beam. Notice that, whereas the measured velocity component drops to 0% at 90°, the strain rate becomes zero at 45° or lower.

is perpendicular to the circumferential direction, which usually is the case for apical imaging, a relation can be formulated. Assuming also no shear, the measured strain rate is a component of both the longitudinal ( $l$ ) and the radial ( $r$ ) strain rates [28]:

$$\dot{\varepsilon} = \dot{\varepsilon}_l \cos^2 \theta + \dot{\varepsilon}_r \sin^2 \theta$$

Figure 1.16 shows the angle dependence of the measured strain rate as the percentage of the

longitudinal strain rate for various values of the assumed linear relation:

$$k = -\frac{\dot{\varepsilon}_r}{\dot{\varepsilon}_l}$$

Since the value of  $k$  is generally unknown, it is not possible to angle-correct the measured strain rate. Also, the assumptions of no shear and linear relation between radial and longitudinal strain rates are in general not fulfilled; therefore, the model is somewhat inaccurate. However, the model may give some indications of the angle dependence of the estimate.

Note that strain rate is more angle dependent than tissue velocity. For example, assuming  $k = 3$ , the measured strain rate is reduced to 50% of the true value at 20°, whereas the measured tissue velocity is still 94% of the true value at the same angle. It is, therefore, important to align the ultrasound beams with the muscle when measuring longitudinal strain rates and strains. To be able to accomplish this alignment, it might be necessary to image the different walls and segments of the heart with different probe positions.

Uematsu et al. [20] have suggested using angle-corrected velocities as a basis for the strain rate estimation. The method relies on user input to define the true direction of the motion. With this method, the strain and strain rate in any spatial direction may be calculated, except in the regions where the assumed motion directions are perpendicular to the ultrasound beams. In these regions, it is not possible to angle-correct the velocities.

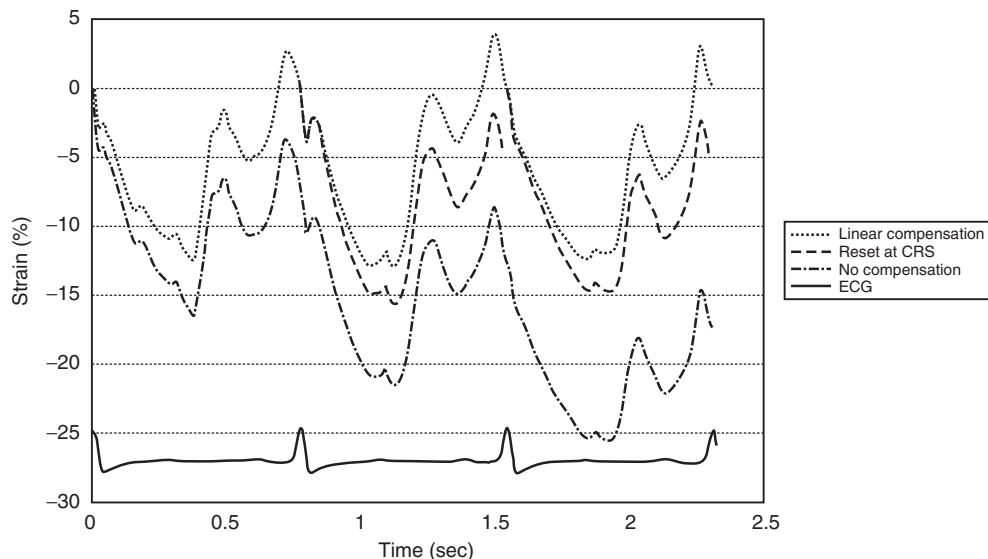


**Figure 1.17** Drift compensation of a strain trace. The dash-dotted trace is the original uncompensated strain trace, while the dashed and dotted traces are drift compensated. The dashed trace is reset at every QRS but does not

necessarily return to zero at the end of each heart beat. The dotted brace is forced to end at zero at each beat through linear compensation. ECG, electrocardiogram trace.

### Drift and drift compensation

Ideally, for displacement and strain traces, the curve should return to the same value, normally zero, at the start of each heartbeat. Artifacts such as those mentioned earlier may result in a drift from beat to beat, meaning that the curve does not return to the same value.

This drift may be compensated in two ways: by forcing the curve to start at the same value in every heartbeat, or through linear compensation of the values in all the time points. Figure 1.17 shows examples of the two methods on a strain trace. Note that the peak strain value is changed when using linear compensation. For the reset-at-zero method, the difference between start and end within a heartbeat is not changed. For example, in the second heartbeat in Figure 1.17, the peak strain in the trace reset at QRS is  $-16\%$ . By subtracting the starting value for the uncompensated trace ( $-6\%$ ) from the peak value ( $-22\%$ ), the exact same peak strain of  $-16\%$  is found.

### Noise reduction by averaging

Spatial and temporal averaging may be helpful to reduce random noise. Note that reverberation

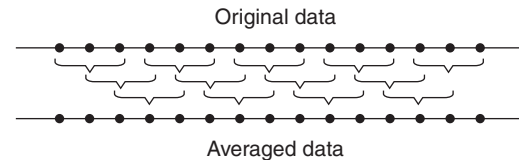


**Figure 1.18** Illustration of the “sliding window” technique that can be used in the averaging process. The averaged data may have the same sample resolution as the original data, but neighboring samples will be correlated.

artifacts and errors caused by angle mismatch are generally not of random nature, so averaging will generally not improve these artifacts.

All averaging techniques may be performed using a “sliding window” technique as illustrated in Figure 1.18. Every sample in the averaged data is based on a set of samples in the original data. The set can be a collection of spatial and/or temporal samples. Spatial averaging is usually performed along the ultrasound beams (axial averaging), perpendicular to them (lateral averaging), or a combination of the two. Temporal averaging may be performed by combining data from a set of frames.

Note that the sample resolution in the averaged data is the same as in the original data, but that

neighboring samples in the averaged data will be correlated. This finding means that averaging should not be performed in the directions where the user wants to measure differences. For example, if the user wants to study differences between subendocardial and subepicardial longitudinal strain rate, no averaging should be performed between the beams in apical views.

A special form of temporal averaging can be performed by averaging only samples from the same time after QRS in several heartbeats. This type of averaging is termed *cine-compound*.

## References

- 1 Yoshida T, Mori M, Nimura Y, et al. Analysis of heart motion with ultrasonic Doppler methods and its clinical applications. *Am Heart J* 1961; **61**: 61–75.
- 2 Kostis JB, Mavrogeorgis E, Slater A, Bellet S. Use of a range-gated, pulsed ultrasonic Doppler technique for continuous measurement of velocity of the posterior heart wall. *Chest* 1972; **62**: 597–604.
- 3 Isaaz K, Thompson A, Ethevenot G, Cloez JL, Bremilla B, Pernot C. Doppler echocardiographic measurement of low velocity motion of the left ventricular posterior wall. *Am J Cardiol* 1989; **64**: 66–75.
- 4 McDicken WM, Sutherland GR, Moran CM, Gordon LN. Colour Doppler velocity imaging of the myocardium. *Ultrasound Med Biol* 1992; **18**: 651–4.
- 5 Sutherland GR, Stewart MJ, Groundstroem KW, et al. Color Doppler myocardial imaging: a new technique for the assessment of myocardial function. *J Am Soc Echocardiogr* 1994; **7**: 441–58.
- 6 Yamazaki N, Mine Y, Sano A, et al. Analysis of ventricular wall motion using color-coded tissue Doppler imaging system. *Jpn J Appl Phys* 1994; **33**: 3141–6.
- 7 Pan C, Hoffmann R, Kuhl H, Severin E, Franke A, Hanrath P. Tissue tracking allows rapid and accurate visual evaluation of left ventricular function. *Eur J Echocardiogr* 2001; **2**: 197–202.
- 8 Heimdal A, Stoylen A, Torp H, Skjaerpe T. Real-time strain rate imaging of the left ventricle by ultrasound. *J Am Soc Echocardiogr* 1998; **11**: 1013–9.
- 9 D'hooge J, Heimdal A, Jamal F, et al. Regional strain and strain rate measurements by cardiac ultrasound: principles, implementation and limitations. *Eur J Echocardiogr* 2000; **1**: 154–70.
- 10 Kasai C, Namekawa K, Koyano A, Omoto R. Real-time two-dimensional blood flow imaging using an autocorrelation technique. *IEEE Trans Sonics Ultrason* 1985; **32**: 458–64.
- 11 Wu Y, Irvine T, Mori Y, Li X, Sahn DJ. In vitro validation of tissue Doppler left ventricular regional wall velocities by using a novel balloon phantom. *J Tongji Med Univ* 2001; **21**: 337–40.
- 12 Donovan CL, Armstrong WF, Bach DS. Quantitative Doppler tissue imaging of the left ventricular myocardium: validation in normal subjects. *Am Heart J* 1995; **130**: 100–4.
- 13 Hartley CJ, Latson LA, Michael LH, Seidel CL, Lewis RM, Entman ML. Doppler measurement of myocardial thickening with a single epicardial transducer. *Am J Physiol* 1983; **245**: H1066–72.
- 14 Cain P, Khoury V, Short L, Marwick TH. Usefulness of quantitative echocardiographic techniques to predict recovery of regional and global left ventricular function after acute myocardial infarction. *Am J Cardiol* 2003; **91**: 391–6.
- 15 Cain P, Baglin T, Khoury V, Case C, Marwick TH. Automated regional myocardial displacement for facilitating the interpretation of dobutamine echocardiography. *Am J Cardiol* 2002; **89**: 1347–53.
- 16 Mirsky I, Parmley WW. Assessment of passive elastic stiffness for isolated heart muscle and the intact heart. *Circ Res* 1973; **33**: 233–43.
- 17 Guth B, Savage R, White F, Hagan A, Samtoy L, Bloor C. Detection of ischemic wall dysfunction: comparison between M-mode echocardiography and sonomicrometry. *Am Heart J* 1984; **107**: 449–57.
- 18 Shapiro E, Marier DL, St John Sutton MG, Gibson DG. Regional nonuniformity of wall dynamics in normal ventricle. *Br Heart J* 1981; **45**: 264–70.
- 19 Fleming D, Xia X, McDicken WN, Sutherland GR, Fenn L. Myocardial velocity gradients detected by Doppler imaging. *Br J Radiol* 1994; **67**: 679–88.
- 20 Uematsu M, Miyatake K, Tanaka N, et al. Myocardial velocity gradient as a new indicator of regional left ventricular contraction: detection by a two-dimensional tissue Doppler imaging technique. *J Am Coll Cardiol* 1995; **26**: 217–23.
- 21 Palka P, Lange A, Fleming AD, et al. Differences in myocardial velocity gradient measured throughout the cardiac cycle in patients with hypertrophic cardiomyopathy, athletes and patients with left ventricular hypertrophy due to hypertension. *J Am Coll Cardiol* 1997; **30**: 760–8.
- 22 Derumeaux G, Ovize M, Loufoua J, Pontier G, Andre-Fouet X, Cribier A. Assessment of nonuniformity of transmural myocardial velocities by color-coded issue Doppler imaging. *Circulation* 2000; **101**: 1390–5.
- 23 Belohlavek M, Bartleson VB, Zobitz ME. Real-time strain rate imaging: validation of peak compression and expansion rates by a tissue-mimicking phantom. *Echocardiography* 2001; **18**: 565–71.

- 24 Hashimoto I, Mori Y, Rusk RA, et al. Strain rate imaging: an in vitro “Validation” study using a physiologic balloon model mimicking the left ventricle. *Echocardiography* 2002; **19**: 669–77.
- 25 Stoylen A, Heimdal A, Bjornstad K, Torp HG, Skjaerpe T. Strain rate imaging by ultrasound in the diagnosis of regional dysfunction of the left ventricle. *Echocardiography* 1999; **16**: 321–9.
- 26 Urheim S, Edvardsen T, Torp H, Angelsen B, Smiseth OA. Myocardial strain by Doppler echocardiography. Validation of a new method to quantify regional myocardial function. *Circulation* 2000; **102**: 1158–64.
- 27 Edvardsen T, Gerber BL, Garot J, Bluemke DA, Lima JA, Smiseth OA. Quantitative assessment of intrinsic regional myocardial deformation by Doppler strain rate echocardiography in humans: validation against three-dimensional tagged magnetic resonance imaging. *Circulation* 2002; **106**: 50–6.
- 28 Heimdal A. *Doppler based ultrasound imaging method for noninvasive assessment of tissue viability* [Doktor ingenør thesis]. Trondheim: Norwegian University of Science and Technology; 1999.

# Principles and different techniques for speckle tracking

Jan D'hooge

## Introduction

Despite the publication of numerous studies showing the additional information that can be provided by Doppler-derived myocardial velocity and deformation data in both the experimental and clinical setting [1], the widespread use of this methodology remains limited. This finding can likely be attributed to the fact that Doppler-derived velocity and deformation data are one-dimensional [2], that is, only the velocity and deformation component along an image line can be assessed, resulting in an angle-dependency of the measurements [3]. Although careful data acquisition can avoid any major difficulty in data analysis and interpretation, it requires a certain level of expertise and the associated training. Moreover, this angle-dependency decreases the reproducibility of the measurement between observers and between studies. On top of that, extracting meaningful deformation data requires manual tracking of the region of interest throughout the cardiac cycle, which is a tedious and time-consuming task.

All of the above-mentioned problems can be overcome if a method were available that not only allows one to measure the velocity along the image line (cf. Doppler-based methods) but also perpendicular to the image line, that is, in two dimensions. Indeed, as explained later in this Chapter, this strategy would allow reconstruction of any in-plane velocity/deformation component, thereby solving the angle-dependency problem. Moreover, it would enable automated in-plane tracking of the region of interest, speeding up the analysis process tremendously.

Two-dimensional (2-D) motion, that is, velocity, estimation using ultrasound has been an active field of research for many years, and multiple approaches have been proposed, such as methods based on speckle tracking [4], multiple-beam Doppler [5], and spatial modulation of the sound field [6]. However, it has not been until relatively recently that ultrasound image quality and computer capacity were adequate to have some of these methods mature into practical research tools or commercial products. This Chapter will introduce the fundamental principles behind multidimensional motion estimation based on speckle tracking and will touch on some of the approaches taken for its practical implementation.

## Principle of speckle tracking

The fundamental principle of 2-D velocity estimation based on speckle tracking is very simple: a particular segment of myocardial tissue shows in the ultrasound image as a pattern of gray values (Figure 2.1). Such a pattern, resulting from the spatial distribution of gray values, is commonly referred to as a *speckle pattern*. This pattern characterizes the underlying myocardial tissue acoustically and is (assumed to be) unique for each myocardial segment. It can, therefore, serve as a fingerprint of the myocardial segment within the ultrasound image.

If the position of the myocardial segment within the ultrasound image changes, we can assume that the position of its acoustic fingerprint will change accordingly. Tracking of the acoustic pattern during the cardiac cycle within the ultrasound image thus allows one to follow the motion of this myocardial

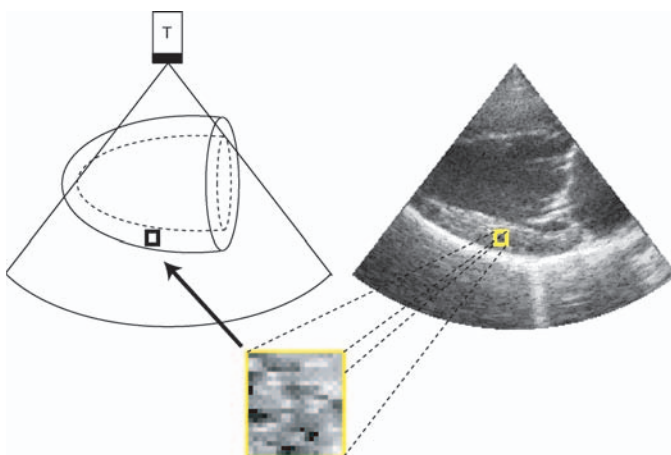


**Figure 2.1** A particular segment of myocardium results in a specific spatial distribution of gray values, that is, speckle pattern, in the ultrasound image. This pattern can be used as an acoustic marker of the tissue. By following the (2-D) motion of the pattern within the image, we can obtain the 2-D motion of the underlying myocardial segment. T, transducer.

segment within the (2-D) image. This finding is the basic principle of speckle tracking.

Fundamental to this methodology is that speckle patterns are preserved between image frames. To understand whether this assumption is reasonable or not, it is essential to know how speckle patterns originate. This process is explained in the following sections.

### Physical origin of speckle

Ultrasonic imaging is based on the pulse-echo experiment: an ultrasound pulse is transmitted, and subsequently the reflected echo signal is detected (Video clip 1 ). Reflections occur at transitions between different types of tissue (e.g., blood–muscle) or at specific sites, much smaller than the wavelength, where the local sound velocity or mass density is different from its surroundings (i.e., collagen fibers within the myocardium). The latter reflections are relatively small in amplitude and are commonly referred to as *scatter* reflections. The sites at which scattering occurs are defined as *scattering sites* or simply *scatterers*.

Each scatterer will reflect the incident wave as it receives it but at lower amplitude (determined by the exact acoustical and geometrical characteristics of the individual scatterer). As myocardial tissue contains many scattering sites, the signal detected by the transducer is the superposition, that is, interference, of the individual reflections occurring at the individual scatterers (Figure 2.2). Because the distance from the transducer to each of these scatterers is slightly different, their ultrasound

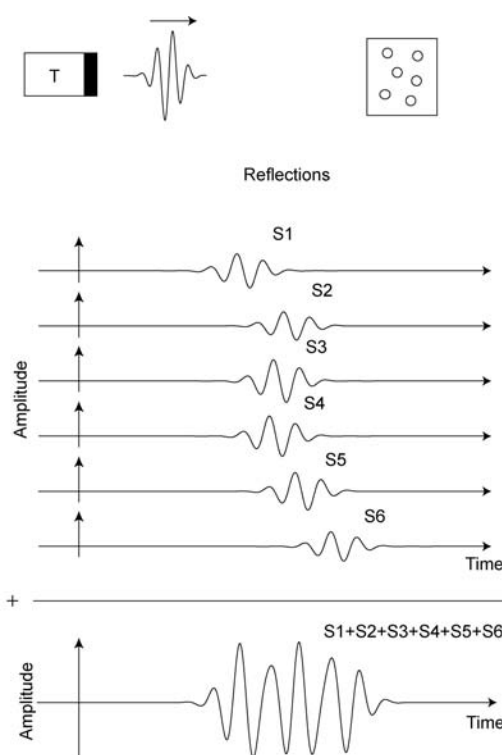


**Figure 2.2** Each scattering site (circle) within a myocardial segment (square) will reflect the wave transmitted by the transducer (T) as it receives it, but at lower amplitude. Due to small differences in travel distance from the transducer to the scattering site, the individual reflections ( $S_1$ – $S_6$ ) arrive at slightly different times. The received RF signal ( $S_1 + \dots + S_6$ ) is the summation (i.e., interference) of each of the individual scatter reflections.

reflections will also arrive at slightly different times (Figure 2.2). This finding will occasionally result in constructive interference (and thus a high-amplitude signal) and occasionally in destructive interference (and thus a low-amplitude signal).

The received signal is called the radiofrequency (RF) signal and is used to construct an ultrasound image. The envelope of the RF signal is detected and color coded in such a way that high-amplitude reflections are represented as bright pixels in the image, whereas low-amplitude reflections are dark (Figure 2.3).

The exact spatial distribution of the gray values within the ultrasound image, that is, the speckle pattern, can thus be attributed to constructive and destructive interference of reflections from the individual scatterers within the myocardium. The exact position of each of the scatterers with respect to the transducer will determine the way in which their reflections interfere, how the resulting RF signal will look, and how the corresponding gray values will be distributed. In other words, the exact scatter positions determine the speckle characteristics.

Speckle is commonly defined as the spatial distribution of gray values in the ultrasound image. However, because speckle originates from a distribution of RF signal amplitudes, it can also be defined as this RF amplitude distribution. In the remainder of this chapter, we will refer to “speckle” as the spatial gray-scale distribution, whereas “RF speckle” is the underlying RF amplitude distribution.

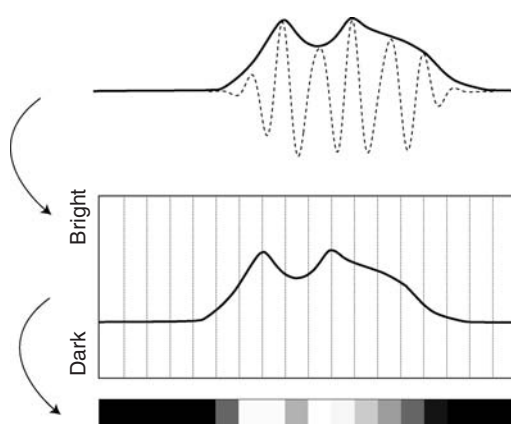


**Figure 2.3** After detection of the envelope (top; bold line) of the RF signal (top; dashed line), high-amplitude reflections are color-coded lighter, whereas low-amplitude reflections are dark (bottom).

### Speckle motion

If tissue showing a particular scatter signal moves away from the transducer, that is, along the image line, all of the individual reflections will arrive late due to the increased traveling time of the ultrasonic waves. However, their relative arrival times are (to a very good approximation) preserved and so is the interference between them. An identical but time-delayed signal is thus detected (Figure 2.4A). In the ultrasound image, we see the same spatial distribution of gray values – speckle pattern – occurring at a position further away from the transducer.

If on the other hand, the tissue moves parallel to the transducer, that is, perpendicular to the image line, the scatterers within this myocardial segment will not continue to reflect ultrasound, as they are no longer within the ultrasound beam (Figure 2.4B). This particular signal (speckle pattern) can no longer be detected along this ultrasound line. However, if we change the position of the ultrasound transducer to acquire the next line of a 2-D image, the relative scatter positions are identical and the same RF signal (and speckle pattern) is measured (Figure 2.4C). In the ultrasound image, we see the same speckle pattern occurring in a neighboring image line. The only requirement for this side-wise detection to work is that the motion of the tissue be much slower than the motion of the ultrasound beam, that is, the acquisition of subsequent image lines. Because sound waves travel at a velocity of approximately 1,530 m/sec and myocardial tissue typically moves at velocities on the order of centimeters per second (approximately 10,000 times slower), this condition is clearly met. We can, thus, conclude that motion of RF signals and the associated speckle patterns do indeed follow the motion of the underlying tissue.

### Conservation of speckle

From the above reasoning, it is clear that speckle patterns are only preserved if the interference between the individual scatter reflections remains identical. This finding only holds true when the amplitude and relative time delays between the individual reflections remain constant between the acquisitions of subsequent image frames. In other words, the relative positions of the scattering sites with respect to the transducer should not change between subsequent image frames.

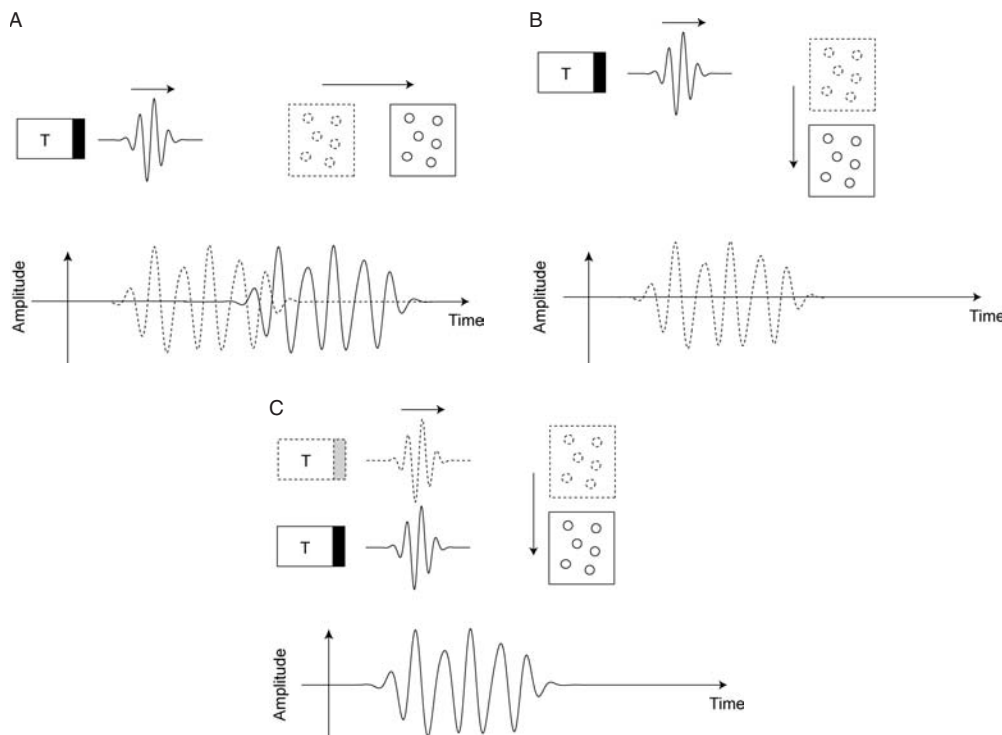


**Figure 2.4** (A) Motion of the scattering region along the direction of wave propagation, that is, along the image line, time shifts all individual scattering reflections by the same amount. The reflected signal (solid line setup) is, thus, identical to the premotion signal (dashed line setup) but shifted in time. T, transducer. (B) Motion perpendicular to the direction of wave propagation results in a loss of reflected signal, as the scattering sites are no longer

within the ultrasound beam. Dashed lines represent the premotion setup and reflections. T, transducer. (C) Motion of the transducer (T), that is, the ultrasound beam, can restore the original situation and re-create the original signal. In B-mode imaging, this suggests that the signal is shifted to a neighboring image line. Dashed lines represent the premotion setup and reflections.

Rotation, deformation (i.e., strain), and out-of-plane motion will change these relative positions/amplitudes and will cause speckle patterns to change between acquisitions. As speckle tracking uses this pattern to identify the position of a particular tissue segment within the ultrasound image, such speckle decorrelation should be limited because it makes tracking impractical. This can easily be done by acquiring image frames quickly after one another to limit the amount of rotation, strain, and out-of-plane motion between subsequent frames. In other words, speckle decorrelation can be limited by acquiring data at a sufficiently high frame rate. Obviously, image artifacts such as reverberations can also reduce the interframe correlation between speckle patterns and should be avoided. In general, high-quality data sets will remain a prerequisite for optimal speckle tracking results.

It is clear that the exact same reasoning holds for the speckle motion in three dimensions. Given that volumetric data can be taken at a sufficient frame rate (to limit decorrelation of speckle between subsequent volumes), speckle tracking should thus be feasible for 3-D motion estimation [7–9]. Approaches to 3-D motion estimation will be discussed later in this book.

## Speckle tracking: practical implementation

### General approaches for tracking speckle patterns

Given a sufficiently high frame rate, it can be assumed that particular speckle patterns are preserved between subsequent image frames [10]. To track these patterns over the entire image sequence,

numerous methods have been described and implemented.

An important category of speckle tracking methods are the ones based on so-called *block-matching* [11]. In this approach, a region in the image is selected (referred to as the *kernel*) and sought for in the next image frame by subsequently trying out different positions and by determining the similarity between the kernel and the pattern observed in that position (Video clip 2 ). The position where the similarity between the kernel (i.e., the original gray-scale pattern) and the observed pattern is maximal is assumed to be the new position of the speckle pattern. Several measures of similarity can be defined [12,13]. In this way, the in-plane velocity vector is obtained. This procedure is repeated for all pixels (or a number of selected pixels/regions) in the image to obtain a velocity vector field. By repeating this measurement between all image pairs within the image sequence, a dynamic velocity vector field is obtained.

An alternative approach to track speckle is the method of *optical flow* [14–17]. In this approach, it is assumed that gray values do not change over time, that is, that the principle of *conservation of gray value* holds. A change of gray value in a particular pixel can then only be attributed to motion of this gray value to another location. This concept is identical to the principle of conservation of mass where local changes in mass density are due to mass flowing in or out of the region but cannot be due to creation or destruction of mass within the volume. The principle of conservation of gray value in combination with an additional boundary condition (e.g., that the motion field is spatially smooth) allow for the estimation of the velocity vector in all pixels within the image. As for the block-matching approach, this procedure is repeated in time to obtain a dynamic velocity vector field.

The optical flow approach works particularly well for small interframe displacement, a condition that might not always be met in cardiac data sets. For this reason, a combined block-matching-optical flow approach, exploiting the strength of both, has been proposed [18].

### **Radiofrequency versus gray-scale tracking**

The block-matching approach described above can be applied to either the RF signal directly

(cf., RF speckle, defined above) [19,20] or to the corresponding speckle pattern in the gray-scale image [21–24]. Because RF speckle is a high-frequency signal (see Figure 2.3), small between-frame motion can be detected, whereas its corresponding gray-scale speckle, derived from the (lower frequency) envelope signal, is less sensitive to small displacements [10]. For this reason, speckle tracking of gray-scale images does not necessarily perform well on high frame-rate data (as between-frame motion is simply too small to be detected accurately, and estimation errors accumulate over the cardiac cycle). An intermediate frame rate allowing sufficient motion between frames while still preserving speckle might, therefore, improve tracking results [25]. Note that this advantage of RF tracking does not hold for detecting motion perpendicular to the beam [26]. On the other hand, RF speckles decorrelate faster and are more sensitive to noise. As a result, RF speckle tracking typically requires data to be acquired at a higher frame rate. This requirement combined with processing signals containing higher frequencies (requiring a larger bandwidth) result in longer computation times, making their (close to) real-time implementation more challenging. Because both RF and gray-scale approaches offer advantages, a hybrid method combining the strengths of both, as recently proposed [27,28], might be very promising.

### **Regularization of the estimated velocity vector field**

Regardless of the method used for speckle tracking, velocity vector estimates are in general noisy and may require correction before further processing. The process of correcting the initial velocity vector estimates by applying additional boundary conditions based on a priori knowledge about the characteristics of the velocity field is called *regularization*. For example, we might know (a priori) that it is very unlikely for neighboring pixels to have a completely different velocity vector. We could then force the measured neighboring velocity vectors to be similar in both amplitude and direction during the regularization process. Similarly, the velocity patterns within the myocardial wall could be forced to follow a particular distribution as predicted by a biomechanical model of myocardial motion.

Many regularization methods can be thought of and have been used.

- *Median filtering*: neighboring velocities (in space and/or time) should be similar; outliers are removed by replacing each initial estimate with the median value of itself and its neighbors [20].
- *Weighted smoothing*: define a quality measure of the velocity estimate and take this into account when smoothing the velocity field by replacing each estimate with the weighted average of itself and its neighbors or with the weighted fitting of a polynomial [29]. As a quality measure, one might use, for example, the maximal similarity obtained in a particular speckle while tracking it to the next frame; if the similarity between the original and tracked pattern is low, there has likely been decorrelation and the velocity estimate is likely less accurate.
- *Myocardial boundaries*: although speckle patterns can change between image frames, endo- and epicardial boundaries should persist and should remain continuous in space and time. This feature makes them particularly interesting for regularization. For example, the endocardial boundary will typically show as a dark-to-bright transition in the image (blood-to-myocardium) and can be seen as a special kind of speckle pattern that is particularly reliable for tracking. During the subsequent weighted smoothing, the *boundary speckles* could be given a more important weight.
- *Elastic model*: As myocardium might be modeled as an elastic material, material particles cannot swap positions, that is, a mid-myocardial particle will be located between a subendocardial particle and a subepicardial particle at all times. They cannot change positions, and if change in position occurs as the result of the estimated motion, the estimates must be wrong and corrected. This finding might be combined with the requirement that tissue is incompressible, which puts an additional constraint on the distribution of the amplitude and direction of the velocity vectors [30].

This list is far from complete and is only intended to give a general impression of how velocity regularization can be achieved. Regularization is an important aspect of any motion-estimation problem and can have a major impact on the performance and accuracy of the proposed methodology. Obviously, if inadequate a priori information is introduced in this regularization procedure, measurements

might become very robust but at the same time very wrong, as we might force the measurements to follow the (inadequate) a priori defined velocity field characteristics. For example, if we force all velocity vectors within the image to be of the same amplitude and direction as we would believe this to accurately describe overall heart motion, a very robust measurement of global heart motion might be obtained, but we would never be able to observe a base-to-apex velocity gradient. Good validation methods under realistic conditions are, thus, required to evaluate the performance of the combined speckle tracking–regularization methodology.

## **Resolution of the dynamic velocity vector field**

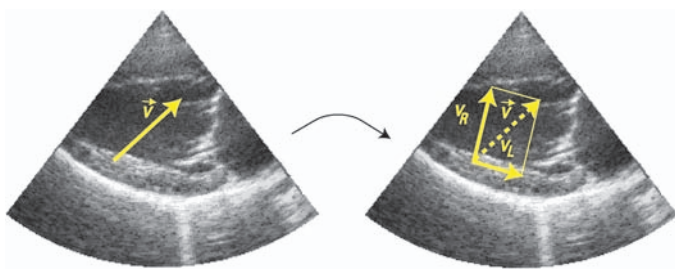
In general, it is not possible to define the exact spatial, temporal, and velocity resolution of speckle-tracked velocity vector fields, as they strongly depend on the exact methodology used for both speckle tracking and the subsequent regularization process. It can be said that, in theory, RF-based methods allow obtaining higher spatial, temporal, and velocity resolution because they use a signal with a higher frequency content. However, as these methods are at the same time more sensitive to decorrelation and noise, they might require more severe regularization, which in turn might limit their resolution. Given that current velocity vector estimation methods are relatively rough, a significant amount of regularization is required, resulting in an effective spatial resolution on the order of  $0.5 \times 0.5 \text{ cm}^2$  to  $1 \times 1 \text{ cm}^2$  at a temporal resolution going from approximately 8–35 msec (for the gray-scale methods) to approximately 2.5–10 msec (for the RF methods).

## **Postprocessing the dynamic velocity vector field**

### **Two-dimensional myocardial velocity imaging**

The result of the speckle tracking procedure in combination with the subsequent regularization process is an estimate of the in-plane velocity vector in all (or a subset of) pixels in each of the frames of the ultrasound data set, that is, a dynamic velocity vector field. This vector field can be visualized directly as vectors superimposed on the gray-scale

**Figure 2.5** The in-plane velocity vector (left) can be decomposed into different components. Typically, the physiologically relevant axes are used (right), for example, the radial ( $v_R$ ) and longitudinal ( $v_L$ ) axes in a parasternal long axis view. The orientation of these physiological axes needs to be defined.



images, in which the length of the vector represents the instantaneous velocity amplitude [31,32].

Alternatively, the velocity vectors can be decomposed into components that are of particular physiologic relevance. For example, in a parasternal long-axis view, the velocity vector can be decomposed into its radial and longitudinal components (Figure 2.5), whereas in a parasternal short-axis image, the radial and circumferential components are obtained. Obviously, the directions of the physiologic axes within the image have to be known. Most often, direction is determined by manually defining one of these axes (e.g., the longitudinal one) through manual or semiautomatic delineation of the endo- or epicardial boundary in one of the image frames. Given that the velocity vector field is known for all pixels within the image, these boundaries can subsequently be moved automatically throughout the cardiac cycle based on the underlying estimated velocity vector. In this way, the physiologic axes are known throughout the complete ultrasound data set with minimal user interaction. Therefore, the true radial, longitudinal, or circumferential velocity profiles throughout the cardiac cycle (using appropriate imaging views) can be reconstructed, independent of the angle between the ultrasound image line and the direction of motion as in the Doppler-based approach. Clearly, an automated boundary detection method could further speed up the extraction of these velocity traces.

## Two-dimensional myocardial strain imaging

When two neighboring points of the same object, that is, the myocardium, move at different velocities, the object is changing shape (Video clip 3 ). Otherwise, the object is merely moving but not deforming. It can be shown that the spatial gradient in myocardial velocities represents the rate of

myocardial deformation, that is, the strain rate [2]. Strain can subsequently be derived by temporal integration of the strain rate curve. Indeed, if the rate of deformation is known at each time instance during the cardiac cycle, the total amount of deformation can easily be calculated. This principle is well known and is the basis for many Doppler-based strain (rate) imaging studies. As Doppler-based methods only measure the velocity component along the image line, the derived strain (rate) data are also limited to reflecting the deformation (rate) along the ultrasound line [2].

Given that speckle tracking allows measuring all in-plane components of the velocity vector in all pixels, the above-mentioned concept can simply be generalized. Indeed, the gradient along the image line (the gradient in the axial [ $A$ ] direction) of the velocity component along the image line ( $v_A$ ) represents the strain rate along the image line ( $\dot{\epsilon}_{AA}$ ). This process is what is done in the Doppler-based methodology. In exactly the same way will the gradient perpendicular to the image line (in the lateral [ $L$ ] direction) of the velocity component perpendicular to the image line ( $v_L$ ) correspond to the rate of deformation perpendicular to this line ( $\dot{\epsilon}_{LL}$ ) (Video clip 4 ). Finally, the rate of shear deformation can be extracted by calculating the gradient along the image line ( $A$  direction) of the velocity component perpendicular to the image line ( $v_L$ ) and vice versa. All components of 2-D deformation rate can be represented in a strain rate tensor, that is, a  $2 \times 2$  matrix:

$$\begin{pmatrix} \dot{\epsilon}_{AA} & \dot{\epsilon}_{AL} \\ \dot{\epsilon}_{LA} & \dot{\epsilon}_{LL} \end{pmatrix} = \begin{pmatrix} \frac{\partial v_A}{\partial A} & \frac{\partial v_A}{\partial L} \\ \frac{\partial v_L}{\partial A} & \frac{\partial v_L}{\partial L} \end{pmatrix}$$

Once this tensor is known, the exact deformation rate in any direction can be calculated similar to

the decomposition of the velocity vector in different components. Typically, the directions of interest would be the physiologically relevant axes such as the longitudinal, radial, and circumferential ones. Again, as for the velocity vector decomposition, the definition of the relevant physiological directions within the image is required.

For numerical simplicity, in practice a slightly different approach is often taken in the sense that different myocardial points are tracked over the cardiac cycle based on the underlying velocity vectors. Then, at any point in time ( $t$ ) within the cardiac cycle, the distance between individual points ( $L[t]$ ) along a particular direction, for example, the longitudinal one, can be compared to the initial distance ( $L_0$ ) along that direction. This strategy defines the strain curve in this direction directly using the definition that strain ( $\epsilon$ ) is equal to the relative change in length:  $(L(t) - L_0)/L_0$ . Once the strain curve is known, the strain rate can be obtained as its first temporal derivative.

## Conclusions

Different methodologies have been proposed for measuring the in-plane motion of the myocardial tissue by ultrasound. Speckle tracking is currently of particular interest as it has evolved into useful research tools and commercial applications. Regularization of the initial (speckle-tracked) velocity vectors is an important aspect of the estimation process and can have a major impact on the estimated velocities and the derived deformation. Good validation of each of these approaches is, thus, required before application in the clinical routine.

## References

- 1 Sutherland GR, Di Salvo G, Claus P, D'hooge J, Bijnens B. Strain and strain rate imaging: a new clinical approach to quantifying regional myocardial function. *J Am Soc Echocardiogr* 2004; **17**: 788–802.
- 2 D'hooge J, Heimdal A, Jamal F, et al. Regional strain and strain rate measurements by cardiac ultrasound: principles, implementation and limitations. *Eur J Echocardiogr* 2000; **1**: 154–70.
- 3 Castro PL, Greenberg NL, Drinko J, Garcia MJ, Thomas JD. Potential pitfalls of strain rate imaging: angle dependency. *Biomed Sci Instrum* 2000; **36**: 197–202.
- 4 Trahey GE, Allison JW, von Ramm OT. Angle independent ultrasonic detection of blood flow. *IEEE Trans Biomed Eng* 1987; **34**: 965–7.
- 5 Hoskins PR. Peak velocity estimation in arterial stenosis models using colour vector Doppler. *Ultrasound Med Biol* 1997; **23**: 889–897.
- 6 Jensen JA. A new estimator for vector velocity estimation. *IEEE Trans Ultrason Ferroelectr Freq Control* 2001; **48**: 886–94.
- 7 Meunier J. Tissue motion assessment from 3D echographic speckle tracking. *Phys Med Biol* 1998; **43**: 1241–54.
- 8 Papademetris X, Sinusa AJ, Dione DP, Duncan JS. Estimation of 3D left ventricular deformation from echocardiography. *Med Image Anal* 2001; **5**: 17–28.
- 9 Chen X, Xie H, Erkamp R, et al. 3-D correlation-based speckle tracking. *Ultrason Imaging* 2005; **27**: 21–36.
- 10 Ramamurthy BS, Trahey GE. Potential and limitations of angle-independent flow detection algorithms using radio frequency and detected echo signals. *Ultrason Imaging* 1991; **13**: 252–68.
- 11 Trahey GE, Hubbard SM, von Ramm OT. Angle independent ultrasonic blood flow detection by frame-to-frame correlation of B-mode images. *Ultrasonics* 1988; **26**: 271–6.
- 12 Viola F, Walker WF. A comparison of the performance of time-delay estimators in medical ultrasound. *IEEE Trans Ultrason Ferroelectr Freq Control* 2003; **50**: 392–401.
- 13 Langeland S, D'hooge J, Torp H, Bijnens B, Suetens P. Comparison of time-domain displacement estimators for two-dimensional RF tracking. *Ultrasound Med Biol* 2003; **29**: 1177–86.
- 14 Horn B, Schunk B. Determining optical flow. *Artif Intell* 1981; **17**: 185–203.
- 15 Mailloux G, Bleau A, Bertrand M, Petitclerc R. Computer analysis of heart motion from 2-dimensional echocardiograms. *IEEE Trans Biomed Eng* 1987; **34**: 356–64.
- 16 Meunier J, Bertrand M, Mailloux G, et al. Local myocardial deformation computed from speckle motion. Proceedings of the IEEE Meeting on Computers in Cardiology; 1988. Chicago (IL).
- 17 Suhling M, Arigovindan M, Jansen C, Hunziker P, Unser M. Myocardial motion analysis from B-mode echocardiograms. *IEEE Trans Image Process* 2005; **14**: 525–36.
- 18 Behar V, Adam D, Lysansky P, Friedman Z. Improving motion estimation by accounting for local image distortion. *Ultrasonics* 2004; **43**: 57–65.
- 19 D'hooge J, Konofagou E, Jamal F, et al. Two-dimensional ultrasonic strain rate measurement of the human heart in-vivo. *IEEE Trans Ultrason Ferroelectr Freq Control* 2002; **49**: 281–6.
- 20 Langeland S, D'hooge J, Wouters PF, et al. Experimental validation of a new ultrasound method for the simultaneous assessment of radial and longitudinal myocardial

- deformation independent of insonation angle. *Circulation* 2005; **112**: 2157–62.
- 21 Behar V, Adam D, Lysyansky P, Friedman Z. The combined effect of nonlinear filtering and window size on the accuracy of tissue displacement estimation using detected echo signals. *Ultrasonics* 2004; **41**: 743–53.
- 22 Ingul CB, Torp H, Aase SA, Berg S, Stoylen A, Slordahl SA. Automated analysis of strain rate and strain: feasibility and clinical implications. *J Am Soc Echocardiogr* 2005; **18**: 411–8.
- 23 Amundsen BH, Helle-Valle T, Edvardsen T, et al. Noninvasive myocardial strain measurement by speckle tracking echocardiography: validation against sonomicrometry and tagged magnetic resonance imaging. *J Am Coll Cardiol* 2006; **47**: 789–93.
- 24 Langeland S, Wouters PF, Claus P, et al. Experimental assessment of a new research tool for the estimation of two-dimensional myocardial strain. *Ultrasound Med Biol* 2006; **32**: 1509–13.
- 25 Ha JS, Walker WF, Hossack JA. Determination of an optimal image frame interval for frame-to-frame ultrasound image motion tracking. *IEEE Trans Ultrason Ferroelectr Freq Control* 2005; **52**: 386–96.
- 26 Bohs LN, Geiman BJ, Anderson ME, Gebhart SC, Trahey GE. Speckle tracking for multi-dimensional flow estimation. *Ultrasonics* 2000; **38**: 369–75.
- 27 Patil AV, Hossack JA. Multi-resolution hybrid strain estimator for elastography. Proceedings of the IEEE Ultrasonics Symposium; 2006. Vancouver, Canada.
- 28 Lopata RGP, Nillesen MM, Gerrits IH, Thijssen JM, Kapusta L de Korte CL. In vivo 3D cardiac and skeletal muscle strain estimation. Proceedings of the IEEE Ultrasonics Symposium; 2006. Vancouver, Canada.
- 29 Rappaport D, Adam D, Lysyansky P, Riesner S. Assessment of myocardial regional strain and strain rate by tissue tracking in B-mode echocardiograms. *Ultrasound Med Biol* 2006; **32**: 1181–92.
- 30 Lubinski MA, Emelianov SY, Raghavan KR, Yagle AE, Skovoroda AR, O'Donnell M. Lateral displacement estimation using tissue incompressibility. *IEEE Trans Ultrason Ferroelectr Freq Control* 1996; **43**: 247–56.
- 31 Suhling M, Jansen C, Arigovindan M, et al. Multiscale motion mapping: a novel computer vision technique for quantitative, objective echocardiographic motion measurement independent of Doppler: first clinical description and validation. *Circulation* 2004; **110**: 3093–9.
- 32 Vannan MA, Pedrizzetti G, Li P, et al. Effect of cardiac resynchronization therapy on longitudinal and circumferential left ventricular mechanics by velocity vector imaging: description and initial clinical application of a novel method using high-frame rate B-mode echocardiographic images. *Echocardiography* 2005; **22**: 826–30.

# Physiologic and magnetic resonance imaging validation of strain techniques

*Thor Edvardsen and Otto A. Smiseth*

## Introduction

Echocardiographic estimation of segmental left ventricular (LV) contractility is routinely accomplished through visual interpretation of endocardial motion and myocardial thickening [1]. This method is subjective, requires an experienced observer, and is at best only semiquantitative. Quantitative analysis based on tracing the endocardial border is hampered by endocardial “dropout” and trabeculations [2]. The development of echocardiographic techniques such as tissue Doppler and speckle tracking echocardiography has enabled more accurate assessment of ventricular function. Tissue Doppler techniques can measure several different myocardial functional parameters: velocity, acceleration, displacement, strain rate, and strain. These modalities have been validated by sonomicrometry in experimental studies and by magnetic resonance imaging (MRI) in clinical studies. Speckle tracking echocardiography has recently been introduced for measurements of myocardial strain and has been validated in experimental and clinical studies. All these new methods can be applied to assess right ventricular (RV) function as well, but validation has been done mostly for LV function. The purpose of this chapter is to describe how these new techniques were validated and to report the most important findings from these validation studies.

## Validation studies of tissue Doppler imaging

The Doppler principle has traditionally been used to measure blood flow velocities, but it may also be

used to measure myocardial velocities and other tissue velocities. Separation between velocities in myocardium and blood is possible due to different signal amplitudes and Doppler frequencies. The principles of pulsed-wave tissue Doppler imaging (TDI) was introduced by Isaaz and colleagues in the 1980s [3], and the color tissue Doppler technique was introduced in the early 1990s by McDicken and associates and Sutherland and coworkers [4,5]. Briefly, by filtering out the low-intensity flow signals, the strong tissue signals derived from myocardial motion are sent directly into the autocorrelator without high-pass filtering [6]. By convention, velocities toward the transducer are positive, and velocities away from the transducer are negative. By marking a region of interest on the two-dimensional (2-D) image, a velocity trace throughout the cardiac cycle can be generated for this region.

The accuracy and validity of TDI to measure myocardial velocities has been confirmed in test phantoms and *in vivo* [5–7]. This confirmation includes studies over a wide range of inotropic states, different loading conditions, and myocardial ischemia and reperfusion [1,2,8–10].

However, the velocity pattern during ischemia is complicated, and the isovolumic phases should be studied in addition to the ejection phase for a reliable diagnosis of regional ischemia [8]. In the normal left ventricle, the isovolumic contraction (IVC) period is dominated by a positive velocity spike of short duration, which represents slight longitudinal shortening before LV ejection. With the onset of ejection, myocardial velocities accelerate rapidly, and peak velocity is reached during early systole.

The most prominent pattern during normal isovolumic relaxation (IVR) is a negative velocity spike of short duration, representing slight elongation of the ventricle before the onset of filling.

The most common findings in moderate ischemia are decreased peak early ejection and mid-ejection velocities due to a decrease in systolic shortening [8]. In severely ischemic and dyskinetic myocardium, however, large IVC and IVR velocities dominate the velocity trace and are the strongest markers of myocardial dysfunction, and ejection velocities have very low amplitudes. Because myocardial ejection velocities remain most often positive or even slightly negative, they do not reflect the marked impairment of myocardial function. Analysis of the

myocardial pressure–segment length loop explains these velocity patterns. In severe ischemia, the ischemic segment behaves like passive tissue, and deformation occurs predominantly during the isovolumic phases, when most of the LV pressure change occurs. There is lengthening during IVC and shortening during IVR, and the segment length trace resembles the LV pressure trace. Due to the curvilinear shape of the LV pressure–segment length loop, there is little deformation during ejection (Figure 3.1) [8].

Although there are important limitations in the ability of peak systolic velocity to serve as a quantitative marker of regional function in ischemic myocardium [11], a more comprehensive analysis

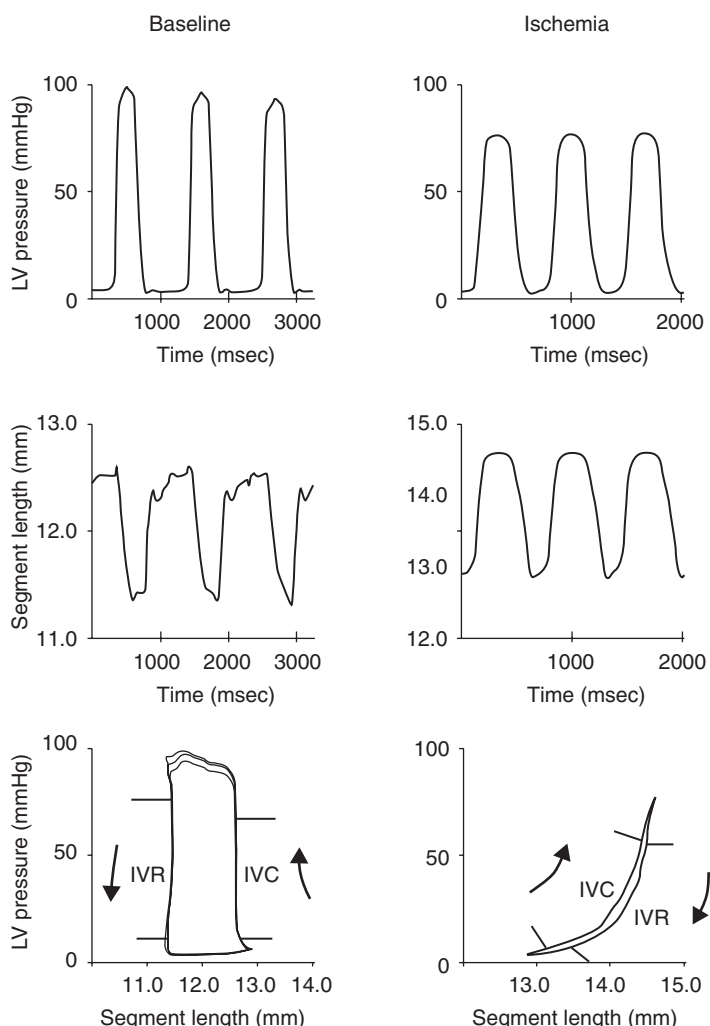


**Figure 3.1** LV pressure and segment lengths and pressure-segment length loops at baseline (left) and during ischemia induced by left anterior descending artery (LAD) occlusion (right). Note that, during ischemia, the pressure–segment length loop rotated in the direction opposite of that during baseline. Note also that, during ischemia, the changes in LV segment length occurred predominantly during IVC and IVR. Modified from Edvardsen et al. [8].

of the myocardial Doppler velocity signal may enhance the ability of TDI to identify ischemic myocardium. This analysis includes measurement of myocardial velocities during IVC and IVR in addition to ejection velocities [8,11].

Reperfused myocardium contains a variable amount of necrosis surrounded by viable and transiently stunned epicardium [12]. This structural and functional heterogeneity complicates interpretation of wall motion abnormalities by conventional echocardiography. There are experimental studies to support the idea that TDI may differentiate nontransmural from transmural myocardial infarction during reperfusion and, therefore, could help to assess myocardial viability [13].

### Validation studies of Doppler strain by sonomicrometry

Quantitation of myocardial function in terms of strain and strain rate has been available for a long time in cardiac physiology using implanted myocardial markers [14]. Strain ( $\epsilon'$ ) is a dimensionless quantity and is produced by application of stress [15]. It represents the fractional or percentage change from the original or unstressed dimension and includes both myocardial shortening (negative strains) and lengthening (positive strains). Calculations of myocardial strain in cardiac mechanics follow the approach proposed by Mirsky and colleagues [16,17] and express strain as percentage or fractional change in dimension. Thus, systolic strain will be a measure of percentage shortening when measurements are done in the long axis, and percentage thickening for radial measurements in the short axis. Recent studies have demonstrated that myocardial strain and strain rate can be calculated from myocardial velocities as a real-time imaging modality [15,18].

A pilot study of myocardial strain rate assessed from myocardial velocities and Doppler shifts was published in 1998 by Heimdal et al. They showed that normal persons had a spatially homogeneous distribution of strain rates, whereas patients with myocardial infarction had areas with reduced strain rates, corresponding to the ischemic regions (Figure 3.2).

### Validation

The first study to validate if Doppler-derived strain could quantify regional myocardial function was

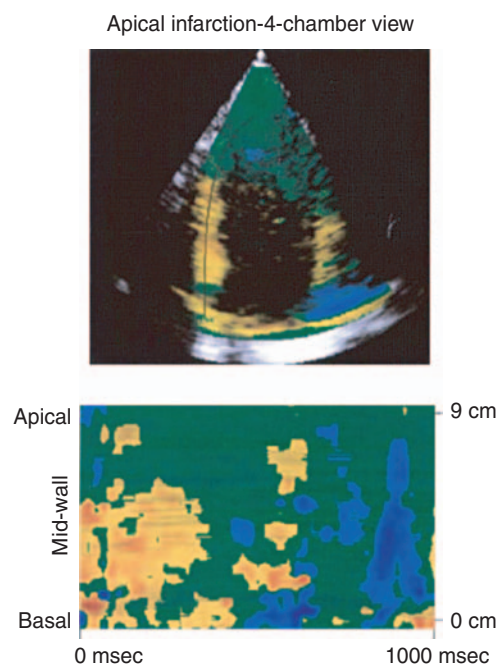


**Figure 3.2** Top: Strain rate imaging (SRI) of heart with apical myocardial infarction. Image taken in mid-systole. The green area indicates where there is no contraction. The black line in the septum indicates where the curved SRI M-mode in the bottom panel is taken. Bottom: SRI M-mode of the septum for one heart cycle. Strain rate is indicated by the following color map: red, below  $-1.0 \text{ sec}^{-1}$ ; yellow,  $-1.0$  to  $-0.3 \text{ sec}^{-1}$ ; green,  $-0.3$  to  $+0.3 \text{ sec}^{-1}$ ; dark blue, above  $+1.0 \text{ sec}^{-1}$ . Negative strain rate means local shortening, positive means local elongation, and near zero strain rate means no deformation. Modified from Heimdal et al. [18].

published by Urheim et al. [15]. The technique was tested against sonomicrometry as reference in an experimental model at baseline conditions, during left anterior descending artery occlusion, and after intravenous volume loading [19]. During coronary occlusion, strain by either method showed early systolic stretching in the LV long axis, followed by postsystolic shortening (Figure 3.3) [20]. Strain by sonomicrometry correlated well with strain by Doppler.

Peak LV systolic elastance (Emax) is an index of LV contractility and can be measured during transient caval occlusion as the slope of the end-systolic pressure-volume relationship [21]. Urheim et al. [15] showed that systolic strain was markedly increased

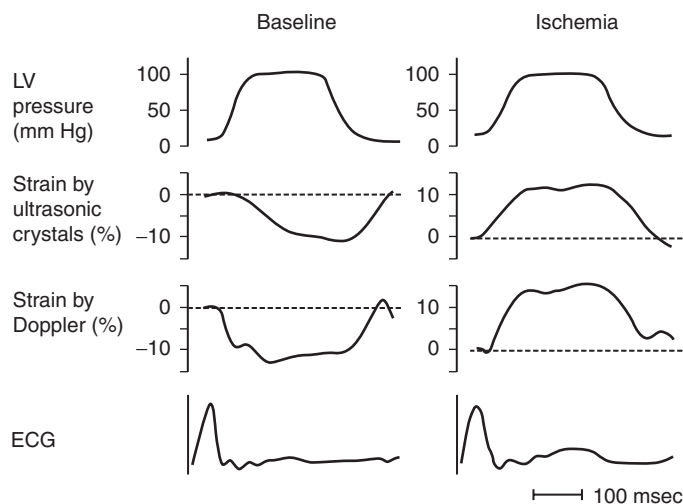


**Figure 3.3** LV pressure, electrocardiogram (ECG), and longitudinal myocardial strain by ultrasonic crystals and by Doppler before and during ischemia. Both methods demonstrate systolic shortening during baseline and systolic lengthening during ischemia. Adapted from Urheim et al. [15].

during volume loading but could not attribute these findings to increased LV contractility, because  $E_{max}$  remained unchanged during the same intervention. This finding suggests that Doppler-derived strain and strain rate are load-sensitive. Later, Greenberg et al. demonstrated that strain rate is a more sensitive marker of inotropy than is strain [22].

### Comparison of strain and velocity

The major strength of strain rate and strain is that they reflect local myocardial function. In contrast, myocardial tissue velocities represent the net effect of the contractile and elastic properties of the area under investigation and motion caused by traction and tethering from other regions [15], as well as being influenced by cardiac translational artifacts. Similarly, strain rate is more uniformly distributed along the different regions of the left ventricle (Figure 3.4), whereas myocardial velocity decreases from base toward apical parts of the left ventricle [15,23,24]. For these reasons, strain techniques are, in principle, the optimal modalities for assessment of regional myocardial function.

However, the tissue Doppler-based approaches to measurement of strain also have major limitations. Doppler-derived strain is highly angle-dependent; when the ultrasound beam is 45 degrees off the LV axis, strain approaches 0% and does not reflect true myocardial function [15]. This angle dependency will particularly limit the ability to assess strain and

strain rates in myocardial areas close to the LV apex and often also from the basal LV parts when they curve toward the mitral annulus.

Calculation of the regional velocity-time integral from the mitral annuli (displacement imaging) has been introduced as an alternative modality to strain for assessment of myocardial function. Displacement imaging was compared to strain rate imaging and tissue velocities and tested in an experimental and human model [11]. This study found that strain is superior to velocity and displacement imaging for grading of myocardial segmental dysfunction. Peak systolic velocity could not differentiate between hypokinetic and dyskinetic myocardium, whereas systolic strain by tissue Doppler echocardiography-derived strain rate and strain measurements (SDE) was an excellent tool for quantification of function in nonischemic as well as ischemic myocardium. Furthermore, strain was superior to velocity and displacement imaging for defining the anatomical extension of dysfunctional myocardium.

### Strain wave morphology

The ability to identify viable myocardium after an ischemic injury is of great importance. Traditionally, conventional stress echocardiography has been used for this purpose, but visual detection of functional recovery might be difficult [25]. Jamal et al. [26] showed in an experimental model that normalization of the strain curve during dobutamine infusion and the increase in both strain rate and strain

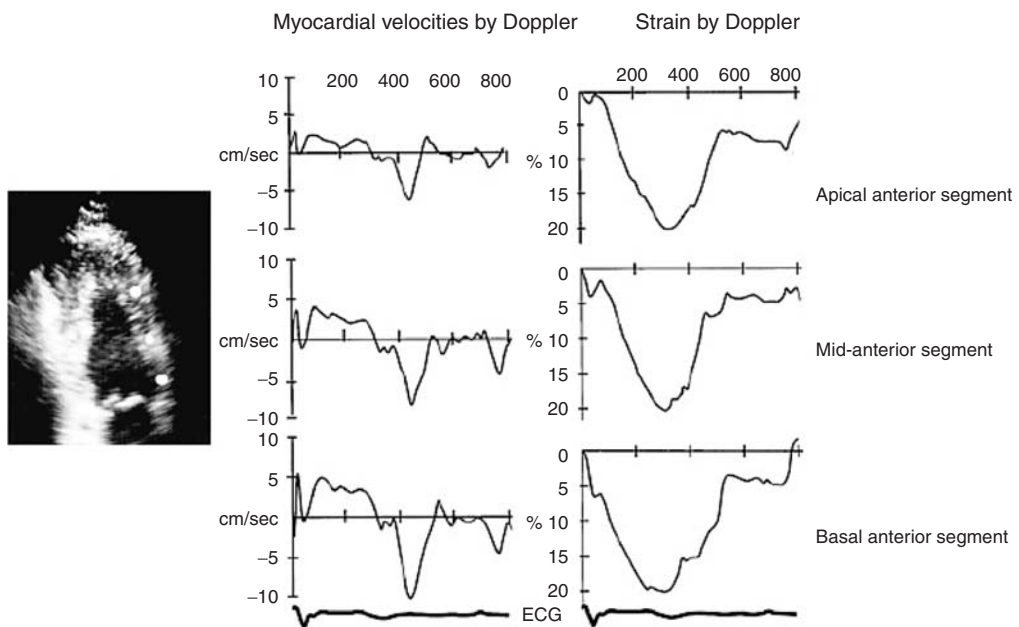


**Figure 3.4** Comparison of myocardial Doppler velocities (left) and strains (right) by TDI. Measurements were performed simultaneously during the same heartbeat and captured from apical, mid, and basal segments

(white dots) in the anterior wall. Myocardial velocities decrease from the base toward the apex, whereas myocardial strains are uniform along the LV long axis. Adapted from Edvardsen et al. [24].

could differentiate between reperfused but stunned and nonviable ischemic myocardium.

In normal myocardium, virtually all contraction occurs during systole with very little postsystolic shortening [27]. In ischemic myocardium, however, there can be substantial postsystolic shortening. Therefore, postsystolic motion has been introduced as a potentially useful marker of ischemic dysfunction. The mechanism of postsystolic shortening can be either delayed active contraction, passive recoil of dyskinetic myocardium, or a combination of both. In moderately ischemic myocardium, postsystolic shortening was found to be due to delayed active contraction [20]. Postsystolic shortening is, however, caused by a passive mechanism when it occurs in necrotic myocardium. The necrotic myocardium simply recoils when the stretching force is removed in late systole or early diastole [20]. Therefore, postsystolic shortening is a relatively nonspecific feature of ischemic myocardium. An experimental study has demonstrated that postsystolic shortening that far exceeds systolic lengthening may be a marker of tissue viability [28], but this finding needs further validation in clinical studies.

### Strain by cardiac magnetic resonance imaging

Noninvasive measurement of strain in humans was first made possible with tagged MRI [29,30]. Tags are temporary features generated by spatial modulation of magnetization (SPAMM) that are superimposed on the myocardium [29,31]. This technique can be applied on the myocardium from both short- and long-axis views and can provide 3-D functional information about myocardial function (Figure 3.5). The myocardium will appear with a spatially encoded pattern that moves with the tissue and can be analyzed to reconstruct myocardial motion. The patterns remain over a period of approximately 500 msec during the cardiac cycle and follow the deformation pattern of the myocardium itself. An improved technique, called complementary SPAMM (CSPAMM), allows the tag pattern to last during the entire cardiac cycle [32,33]. The cardiac motion can be divided into different types of movements: circumferential and longitudinal contraction and rotation. All these complicated patterns can be accurately assessed with tagged MRI.

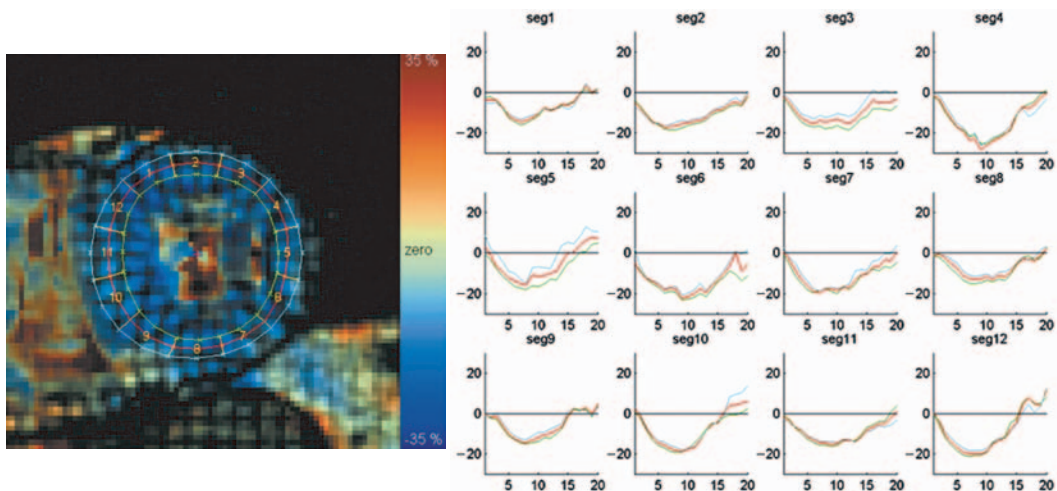


**Figure 3.5** Illustration of MRI tagging from a normal individual. Strain analyzed by harmonic phase software (HARP, Diagnosoft, Inc.) at left. At right, strain curves from 12 segments in a short-axis view during the heart cycle.

The main limitations of strain measurement by MRI have been a low sampling rate and a long examination time. The reconstruction set of the data and the analyzing period has been time-consuming, but can now be done very rapidly using HARP software (Harmonic phase tool, Diagnosoft, Inc.) [34]. This analysis allows quantification of systolic and diastolic myocardial function from large population groups with high accuracy [35–37].

#### Comparison of myocardial strain with different techniques

Tissue Doppler measures velocity within a defined sample volume, but not within a defined piece of myocardium [24]. The sample volume is usually placed in a permanent area in space during the cardiac cycle, and all measurements are done with reference to an external point (the transducer). Due to cardiac motion, the difference between the Doppler measurements and the real myocardial deformation may be significant. This limitation applies to all TDI modalities. It can, in part, be compensated for by using tracking algorithms that move the sample volume continuously or manually in steps during the heart cycle. In contrast, strain by MRI uses the positions of the tags to describe the motion of a fixed point within the myocardium itself. Strain by Doppler measures the velocity at two locations along the Doppler sample beam, whereas MRI measures the motion of two distinct points in the myocardium.

Another important difference is that TDI measurements are dependent on the direction of the Doppler angle in relation to myocardial motion. Strain by Doppler is confined to a 1-D space, whereas strain by MRI can be assessed in two dimensions from one image plane. Furthermore, the MRI technique accounts for through-plane motion effects occurring perpendicularly to the imaging plane, whereas no such correction can be applied for the SDE strain measurements. Strains by MRI can be assessed from the three normal orthogonal directions (radial, circumferential, and longitudinal). Strain by Doppler is not suited to measurement of circumferential strain. As discussed in the next section, speckle tracking echocardiography may compensate for most of these limitations of Doppler-based strain.

#### Validation studies of speckle tracking echocardiography

The complex overall motion of the heart can be divided into three different types of movements: circumferential contraction and rotation (assessed by short-axis view interrogation) and longitudinal contraction (assessed from the long-axis view) [2]. Until recently, only assessment of longitudinal contraction in terms of strain and velocities has been available from Doppler-derived modalities. Radial thickening, which is a result of longitudinal and circumferential shortening, can be assessed from the

anterior and posterior walls [38]. In longitudinal views, Doppler velocities should not be measured near the apex, because the apical curvature suggests large angle problems. This finding is a significant limitation when studying patients with coronary artery disease, as pathology may be limited to the apical segments [15,39].

Speckle tracking echocardiography has been introduced as a method for angle-independent quantification of myocardial strain [40]. The distance between natural acoustic markers (speckles) is measured within a predefined myocardial area as a function of time and parameters of myocardial deformation can be calculated. Strain measurements by the speckle tracking technique are therefore direct measures of myocardial deformation. The most important advantages of using this new technique is independence of insonation angle and of cardiac translation motion [39,41,42].

Speckle tracking has recently been validated in experimental and clinical studies, and the results so far have been promising. Langeland et al. found that two deformation components were able to simultaneously assess both radial and longitudinal strain from the same view in five open-chest sheep and that these measurements were accurate, as compared with sonomicrometry [41]. Furthermore, they found that automatic tracking by the dedicated software was less time consuming than the Doppler-based methods. Amundsen et al. tested another software tool in a combined experimental and clinical model and compared the echocardiographic results to sonomicrometry and MRI tagging, respectively [43]. Speckle tracking echocardiography was tested at baseline, during preload changes, and during regional myocardial ischemia and correlated well with strain measured by sonomicrometry. The results from the clinical part of the study confirmed that speckle tracking echocardiography has the potential to become a clinical bedside tool for quantifying myocardial strain [43].

The wringing motion of the left ventricle consists of systolic twisting and early diastolic untwisting [42]. This complex motion pattern has been studied by MRI tagging but echocardiography has until now been unsuited to its assessment [33]. To explore if speckle tracking echocardiography could assess LV rotation and twist, Notomi et al. studied

13 patients and compared echocardiography to tagged MRI. Another study by Helle-Valle and associates studied LV torsion and twist in an animal model and in humans [39]. The latter study showed that regional LV rotation and twist could be assessed by echocardiography during different stages of inotropy and regional ischemia, and concluded that LV rotation and twist can be measured accurately by speckle tracking echocardiography (Figure 3.6).

The assessment of circumferential strain has for long been the preferred method for quantification of LV function by tagged MRI [24,34]. A study by Becker et al. using contrast-enhanced MRI as reference confirms that circumferential strain by speckle tracking echocardiography may predict the transmurality of myocardial necrosis. These results suggest that speckle tracking echocardiography provides a comprehensive assessment of myocardial function, which includes longitudinal strain from all parts of the LV long axis, circumferential strain, and LV rotation or twist.

As for most echocardiographic methods, the need for good image quality is important. The quality of the recordings must be high to achieve correct tracking of the speckles. This achievement requires proper adjustment of frame rate, probe frequency, and image focus [39]. Reverberations are a major source of error and assessment of strain within a field of reverberations should be avoided. The best compromise between image quality and acceptable lateral resolution is a frame rate between 60 and 100 frames per second [39,43]. This rate suggests that the time resolution for speckle tracking echocardiography might be too low for assessment of strain rate.

## Conclusion

Several validation studies during the past years confirm that tissue Doppler echocardiography can analyze myocardial function with great accuracy. Speckle tracking echocardiography is another promising tool for assessment of myocardial function independent of insonation angle of the ultrasound beam. The clinical place of speckle tracking echocardiography, however, needs to be better defined.

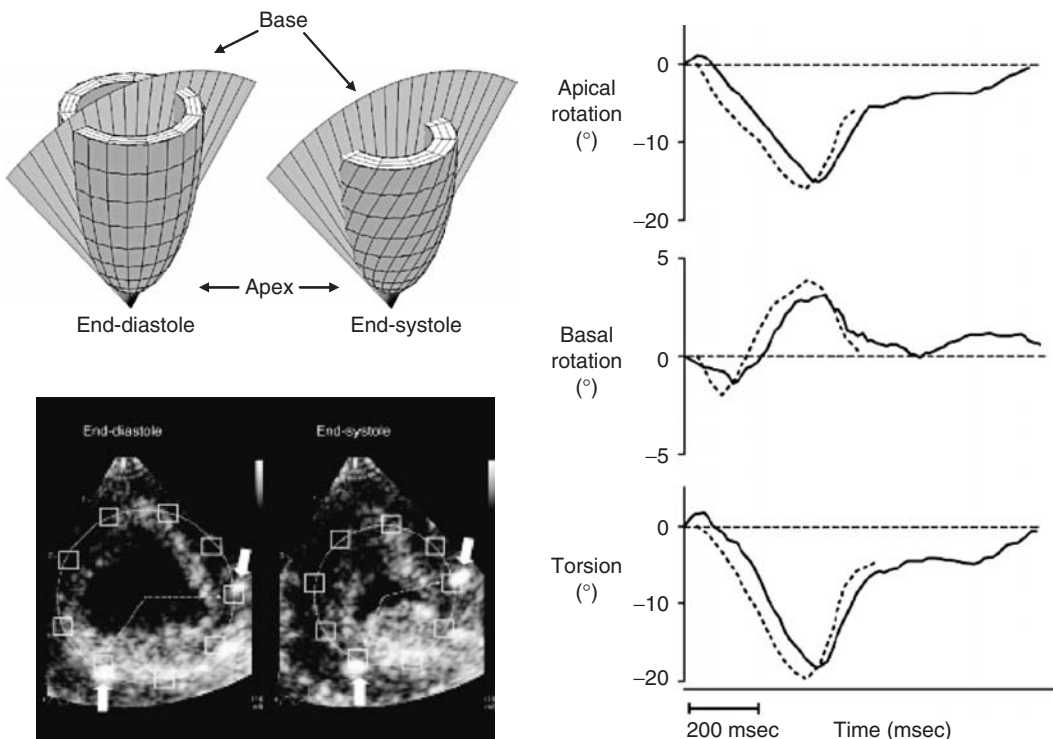


**Figure 3.6** Upper left panel: Schematic illustration of LV twist from end end-diastole to end end-systole. When viewed from the apex, apical rotation is counterclockwise and basal rotation, clockwise. Courtesy of Stein Inge Rabben, PhD. Lower left panel: End-diastolic and end-systolic apical, 2-D, gray-scale echocardiographic images from an animal experiment. The regions of interest (ROIs, white squares) and best-fit (circles) are indicated. The thin, dashed arrows point to ROIs, and the thick solid

arrows point to crystals. The change in position of arrows from end diastole to end systole confirmed the counter-clockwise rotation. Right panel: Representative examples of apical and basal rotation and torsion as measured by MRI tagging and speckle tracking strain. Rotation by MRI was not feasible for a complete heart cycle because of tag fading. Dashed and solid lines indicate rotation measured by MRI and speckle tracking strain, respectively. Modified from Helle-Valle et al. [39].

## References

- 1 Gorcsan J III, Strum DP, Mandaroni WA, Gulati VK, Pinsky MR. Quantitative assessment of alterations in regional left ventricular contractility with color-coded tissue Doppler echocardiography. Comparison with sonomicrometry and pressure-volume relations. *Circulation* 1997; **95**: 2423–33.
- 2 Derumeaux G, Ovize M, Loufoua J, et al. Doppler tissue imaging quantitates regional wall motion during myocardial ischemia and reperfusion. *Circulation* 1998; **97**: 1970–7.
- 3 Isaaz K, Thompson A, Ethevenot G, Cloez JL, Bremilla B, Pernot C. Doppler echocardiographic measurement of low velocity motion of the left ventricular posterior wall. *Am J Cardiol* 1989; **64**: 66–75.
- 4 McDicken WN, Sutherland GR, Moran CM, Gordon LN. Colour Doppler velocity imaging of the myocardium. *Ultrasound Med Biol* 1992; **18**: 651–4.
- 5 Sutherland GR, Stewart MJ, Groundstroem KW, et al. Color Doppler myocardial imaging: a new technique for the assessment of myocardial function. *J Am Soc Echocardiogr* 1994; **7**: 441–58.
- 6 Edvardsen T, Aakhus S, Endresen K, Bjørnerheim R, Smiseth OA, Ihlen H. Acute regional myocardial ischemia identified by 2-dimensional multiregion tissue Doppler imaging technique. *J Am Soc Echocardiogr* 2000; **13**: 986–94.
- 7 Miyatake K, Yamagishi M, Tanaka N, et al. New method for evaluating left ventricular wall motion by color-coded tissue Doppler imaging: in vitro and in vivo studies. *J Am Coll Cardiol* 1995; **25**: 717–24.

- 8 Edvardsen T, Urheim S, Skulstad H, Steine K, Ihlen H, Smiseth OA. Quantification of left ventricular systolic function by tissue Doppler echocardiography: added value of measuring pre- and postejection velocities in ischemic myocardium. *Circulation* 2002; **105**: 2071–7.
- 9 Voigt JU, Arnold MF, Karlsson M, et al. Assessment of regional longitudinal myocardial strain rate derived from Doppler myocardial imaging indexes in normal and infarcted myocardium. *J Am Soc Echocardiogr* 2000; **13**: 588–98.
- 10 Oki T, Fukuda K, Tabata T, et al. Effect of an acute increase in afterload on left ventricular regional wall motion velocity in healthy subjects. *J Am Soc Echocardiogr* 1999; **12**: 476–83.
- 11 Skulstad H, Urheim S, Edvardsen T, et al. Grading of myocardial dysfunction by tissue Doppler echocardiography a comparison between velocity, displacement, and strain imaging in acute ischemia. *J Am Coll Cardiol* 2006; **47**: 1672–82.
- 12 Kloner RA, Ellis SG, Lange R, Braunwald E. Studies of experimental coronary artery reperfusion. Effects on infarct size, myocardial function, biochemistry, ultrastructure and microvascular damage. *Circulation* 1983; **68** (Pt 2): I8–15.
- 13 Derumeaux G, Loufoua J, Pontier G, Cribier A, Ovize M. Tissue Doppler imaging differentiates transmural from nontransmural acute myocardial infarction after reperfusion therapy. *Circulation* 2001; **103**: 589–96.
- 14 Ellis RM, Franklin DL, Rushmer RF. Left ventricular dimensions recorded by sonocardiometry. *Circ Res* 1956; **4**: 684–8.
- 15 Urheim S, Edvardsen T, Torp H, Angelsen B, Smiseth OA. Myocardial strain by Doppler echocardiography. Validation of a new method to quantify regional myocardial function. *Circulation* 2000; **102**: 1158–64.
- 16 Mirsky I, Pasternac A, Ellison RC. General index for the assessment of cardiac function. *Am J Cardiol* 1972; **30**: 483–91.
- 17 Mirsky I, Parmley WW. Assessment of passive elastic stiffness for isolated heart muscle and the intact heart. *Circ Res* 1973; **33**: 233–43.
- 18 Heimdal A, Stoylen A, Torp H, Skjaerpe T. Real-time strain rate imaging of the left ventricle by ultrasound. *J Am Soc Echocardiogr* 1998; **11**: 1013–9.
- 19 Bugge-Asperheim B, Leraand S, Kiil F. Local dimensional changes of the myocardium measured by ultrasonic technique. *Scand J Clin Lab Invest* 1969; **24**: 361–71.
- 20 Skulstad H, Edvardsen T, Urheim S, et al. Postsystolic shortening in ischemic myocardium: active contraction or passive recoil? *Circulation* 2002; **106**: 718–24.
- 21 Suga H, Sagawa K, Shoukas AA. Load independence of the instantaneous pressure–volume ratio of the canine left ventricle and effects of epinephrine and heart rate on the ratio. *Circ Res* 1973; **32**: 314–22.
- 22 Greenberg NL, Firstenberg MS, Castro PL, et al. Doppler-derived myocardial systolic strain rate is a strong index of left ventricular contractility. *Circulation* 2002; **105**: 99–105.
- 23 Edvardsen T, Skulstad H, Aakhus S, Urheim S, Ihlen H. Regional myocardial systolic function during acute myocardial ischemia assessed by strain Doppler echocardiography. *J Am Coll Cardiol* 2001; **37**: 726–30.
- 24 Edvardsen T, Gerber BL, Garot J, Bluemke DA, Lima JA, Smiseth OA. Quantitative assessment of intrinsic regional myocardial deformation by Doppler strain rate echocardiography in humans: validation against three-dimensional tagged magnetic resonance imaging. *Circulation* 2002; **106**: 50–6.
- 25 Kvitting JP, Wigstrom L, Strotmann JM, Sutherland GR. How accurate is visual assessment of synchronicity in myocardial motion? An In vitro study with computer-simulated regional delay in myocardial motion: clinical implications for rest and stress echocardiography studies. *J Am Soc Echocardiogr* 1999; **12**: 698–705.
- 26 Jamal F, Strotmann J, Weidemann F, et al. Noninvasive quantification of the contractile reserve of stunned myocardium by ultrasonic strain rate and strain. *Circulation* 2001; **104**: 1059–65.
- 27 Voigt JU, Lindenmeier G, Exner B, et al. Incidence and characteristics of segmental postsystolic longitudinal shortening in normal, acutely ischemic, and scarred myocardium. *J Am Soc Echocardiogr* 2003; **16**: 415–23.
- 28 Lyseggen E, Skulstad H, Helle-Valle T, et al. Myocardial strain analysis in acute coronary occlusion: a tool to assess myocardial viability and reperfusion. *Circulation* 2005; **112**: 3901–10.
- 29 Axel L, Dougherty L. MR imaging of motion with spatial modulation of magnetization. *Radiology* 1989; **171**: 841–5.
- 30 Zerhouni EA, Parish DM, Rogers WJ, Yang A, Shapiro EP. Human heart: tagging with MR imaging – a method for noninvasive assessment of myocardial motion. *Radiology* 1988; **169**: 59–63.
- 31 Axel L, Dougherty L. Heart wall motion: improved method of spatial modulation of magnetization for MR imaging. *Radiology* 1989; **172**: 349–50.
- 32 Fischer SE, McKinnon GC, Maier SE, Boesiger P. Improved myocardial tagging contrast 1. *Magn Reson Med* 1993; **30**: 191–200.
- 33 Stuber M, Scheidegger MB, Fischer SE, et al. Alterations in the local myocardial motion pattern in patients suffering from pressure overload due to aortic stenosis. *Circulation* 1999; **100**: 361–8.
- 34 Garot J, Bluemke DA, Osman NF, et al. Fast determination of regional myocardial strain fields from tagged

- cardiac images using harmonic phase MRI. *Circulation* 2000; **101**: 981–8.
- 35 Edvardsen T, Detrano R, Rosen BD, et al. Coronary artery atherosclerosis is related to reduced regional left ventricular function in individuals without history of clinical cardiovascular disease: the Multiethnic Study of Atherosclerosis. *Arterioscler Thromb Vasc Biol* 2006; **26**: 206–11.
- 36 Rosen BD, Edvardsen T, Lai S, et al. Left ventricular concentric remodeling is associated with decreased global and regional systolic function: the Multi-Ethnic Study of Atherosclerosis. *Circulation* 2005; **112**: 984–91.
- 37 Edvardsen T, Rosen BD, Pan L, et al. Regional diastolic dysfunction in individuals with left ventricular hypertrophy measured by tagged magnetic resonance imaging—the Multi-Ethnic Study of Atherosclerosis (MESA). *Am Heart J* 2006; **151**: 109–14.
- 38 Jamal F, Kukulski T, D'hooge J, De Scheerder I, Sutherland G. Abnormal post-systolic thickening in acutely ischemic myocardium during coronary angioplasty: a velocity, strain, and strain rate doppler myocardial imaging study. *J Am Soc Echocardiogr* 1999; **12**: 994–6.
- 39 Helle-Valle T, Crosby J, Edvardsen T, et al. New noninvasive method for assessment of left ventricular rotation: speckle tracking echocardiography. *Circulation* 2005; **112**: 3149–56.
- 40 Bohs LN, Trahey GE. A novel method for angle independent ultrasonic imaging of blood flow and tissue motion. *IEEE Trans Biomed Eng* 1991; **38**: 280–6.
- 41 Langeland S, D'hooge J, Wouters PF, et al. Experimental validation of a new ultrasound method for the simultaneous assessment of radial and longitudinal myocardial deformation independent of insonation angle. *Circulation* 2005; **112**: 2157–62.
- 42 Notomi Y, Lysyansky P, Setser RM, et al. Measurement of ventricular torsion by two-dimensional ultrasound speckle tracking imaging. *J Am Coll Cardiol* 2005; **45**: 2034–41.
- 43 Amundsen BH, Helle-Valle T, Edvardsen T, et al. Noninvasive myocardial strain measurement by speckle tracking echocardiography: validation against sonomicrometry and tagged magnetic resonance imaging. *J Am Coll Cardiol* 2006; **47**: 789–93.

# Designation of tissue Doppler normal range\*

Jing Ping Sun, Zoran B. Popović, Neil L. Greenberg, Xiao-Fang Xu, Craig R. Asher, William J. Stewart, James D. Thomas

## Introduction

### Normal physiology of the cardiac function

#### The cardiac cycle

Consider the sequence of events that occurs during a single heartbeat, or cardiac cycle (Figure 4.1). Before mechanical activity begins, an electrical signal is delivered to the myocardium. Electrical signaling is accomplished by specialized conduction system tissue that controls the heart rate (HR) in response to various influences (especially sympathetic and parasympathetic stimulation); it provides a normal sequence of activation of the chambers that maximizes efficient contraction and filling. At the cellular level, the electrical signal initiates biochemical processes underlying contraction. With respect to HR, specialized conduction system cells have the property of spontaneous electrical depolarization; they function as pacemakers that control the rate of the heart. The sinoatrial node, located in the right atrium (RA), is the component of the specialized conduction system that has the fastest spontaneous depolarization rate and, therefore, normally controls HR. It is directly influenced by the autonomic nervous and neuroendocrine systems, which modulate beat-to-beat and long-term variation in HR.

With normal physiology, the mechanical cycle (Figure 4.1) begins at ventricular end-diastole, the

instant just before active tension generation, or systole. Onset of systole is signaled by a sudden, rapid rise in intraventricular pressure. Soon thereafter, ventricular systolic pressure exceeds atrial pressure, at which time the mitral and tricuspid valves close. Ventricular pressures then continue to rise rapidly until the aortic and pulmonic pressures are exceeded, resulting in opening of the aortic valve and pulmonic valves and onset of *ejection* of blood into the systemic and pulmonary circulations. Between mitral/tricuspid valve closure and aortic/pulmonic valve opening, ventricular volume is constant. This phase is termed *isovolumic contraction*. During ejection, ventricular and aortic/pulmonic artery pressures rise and then fall together. The aortic and pulmonic valves close and ejection ends when ventricular pressure falls below aortic and pulmonic artery pressure, signaled by the *dicrotic notch* of the respective arterial pressures. In the left ventricle, a period then ensues during which pressure continues to fall rapidly until it drops below left atrial (LA) pressure, when the mitral valve (MV) opens. Because the aortic and mitral valves are closed and the ventricular volumes are constant, this period is termed *isovolumic relaxation*. Although pulmonic valve closure and tricuspid valve opening are shown as separated in time in Figure 4.1, the point at which right ventricular (RV) pressure falls below pulmonic artery pressure

\* Reprinted with additions from JOURNAL OF THE AMERICAN SOCIETY OF ECHOCARDIOGRAPHY, 2004;17:132–138: Noninvasive Quantification of Regional Myocardial Function Using Doppler-derived Velocity, Displacement, Strain Rate, and Strain in Healthy Volunteers: Effects of Aging, Jing Ping Sun, Zoran B. Popović, Neil L. Greenberg, Xiao-Fang Xu, Craig R. Asher, William J. Stewart, James D. Thomas. With Permission from American Society of Echocardiography.

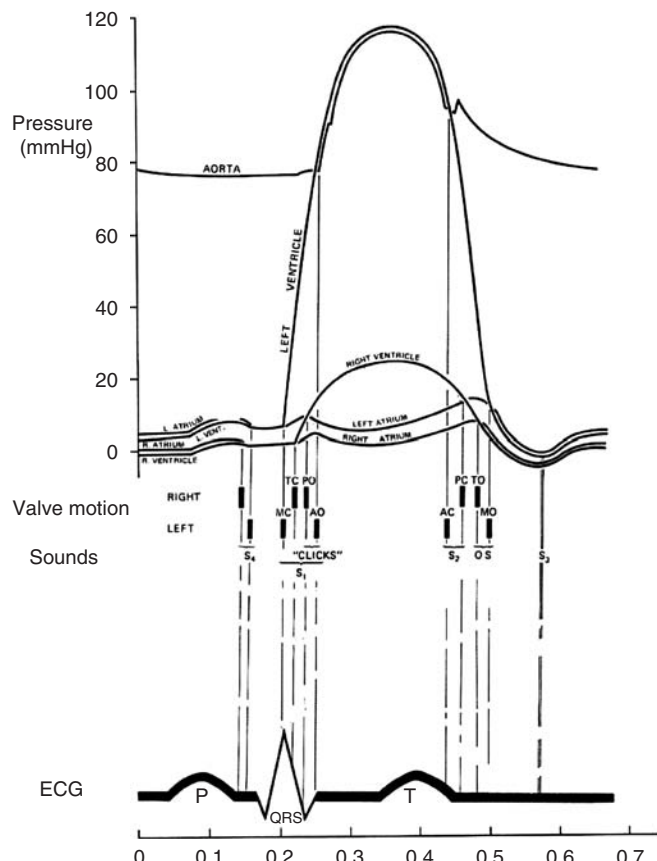


**Figure 4.1** Electrical and mechanical events during the cardiac cycle. Shown here are pressure curves of great vessels and cardiac chambers, valvular events, timing of heart sounds, and an electrocardiogram (ECG). MC and TC, mitral and tricuspid valve closure; PO and AO, pulmonic and aortic valve opening; AC and PC, aortic and pulmonic valve closure; TO and MO, tricuspid and mitral valve opening.

is so low that the RV isovolumic relaxation period is almost nonexistent [1].

The importance of pulsed Doppler echocardiography in estimating cardiac function is extremely high. Its value is in the evaluation of global, not regional, heart function.

A pulsed Doppler tissue image is a tool for evaluation of cardiac function (Figure 4.2).

Schulman et al. [2] studied 128 healthy subjects 25–88 years of age. They concluded that, in healthy subjects, early diastolic temporal discordance, which reflects ventricular restoring forces (suction), is age-independent. A similar temporal discordance can be demonstrated between late diastolic filling and LA contraction; this finding suggests that suction effects initiated in early diastole still contribute to late left ventricular (LV) filling concomitantly with LA contraction. With advancing age, however, isovolumic relaxation time prolongs and the timing of peak LA contraction and that of late diastolic flow

(A-wave) progressively converge (atrial mechanical alignment), providing a novel method to identify healthy persons with increased dependency on LA contraction for late diastolic filling.

The ratio of the transmitral early peak velocity ( $E'$ ) evaluated by conventional Doppler imaging over early mitral annulus velocity ( $E'$ ) evaluated by tissue Doppler imaging has been proposed as a non-invasive marker for LV filling pressure. Sutter et al. [3] evaluated 174 normal patients and 86 patients with hypertension and LV hypertrophy to assess the effects of age, gender, and LV hypertrophy on  $E'$  and  $E/E'$ . Age appeared to be the strongest determinant of  $E'$  and  $E/E'$ , suggesting that, in normal patients and in those with LV hypertrophy, age-dependent cutoff values should be considered.

The quantification of regional myocardial function remains a challenge in clinical cardiology. Traditional methods for evaluation of regional myocardial function using echocardiography are subjective

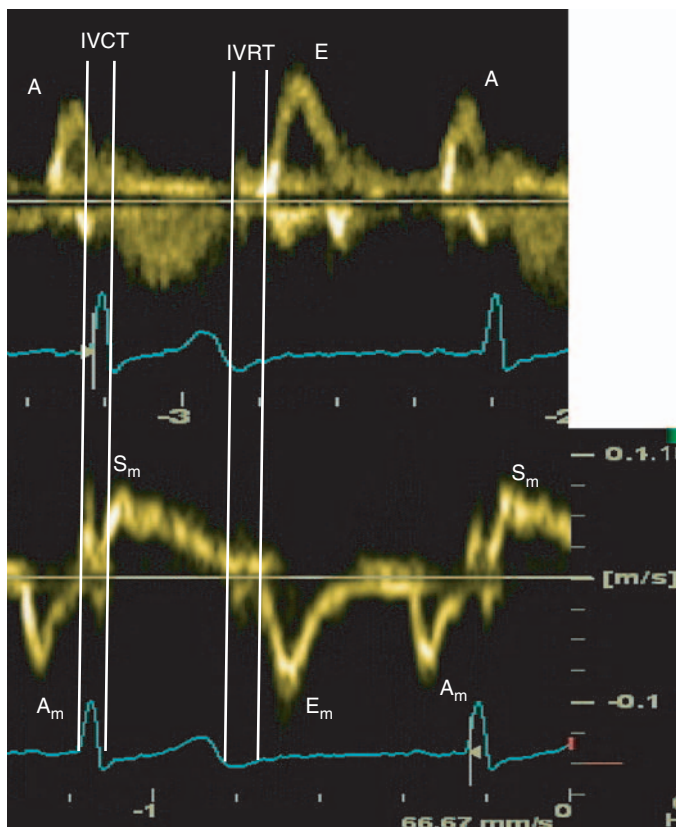


**Figure 4.2** Relationship between Doppler transmural flow (upper panel) and Doppler tissue imaging (DTI) of mitral septal annulus (lower panel) in a normal 40-year-old healthy woman. Vertical lines refer to electrocardiography used as reference for measurements of time. Mitral inflow is biphasic, early diastolic (E) and atrial contraction (A). DTI wall motion profile is triphasic peak systolic (Sm), early diastolic (Em), and atrial contraction (Am). E and Em began simultaneously as did A and Am. IVRT, isovolumic relaxation time.

and only partially quantitative [4–6]. Magnetic resonance imaging permits three-dimensional (3-D) data acquisition that allows quantification of local myocardial function, in particular the six components of local strain [7,8]. However, magnetic resonance imaging has inadequate temporal resolution to provide information on brief mechanical events in the cardiac cycle and is available in only a few centers greatly limiting its clinical use. New ultrasound technology allows for high-frequency imaging, which is able to detect very brief events during the cardiac cycle. Doppler tissue echocardiography (DTE) can now resolve myocardial velocities throughout a 2-D sector at frame rates >150 frames/sec [9,10] with potential application in assessing regional ischemia [11]. There are additional parameters that can be derived from DTE velocity data to further the evaluation of myocardial function. For example, integrating the velocities throughout systole yields tissue displacement, the total amount of tissue movement during systole. By displaying this movement in color, it is possible to display, in one map, overall systo-

lic function. Alternatively, one may calculate the spatial derivative of velocity within the 2-D map to derive strain rate, a fundamental measure of tissue contraction and relaxation that avoids many of the translation and tethering dependencies of tissue velocity alone [12–15]. Segmental deformation by DTE has been validated against sonomicrometry during experimental ischemia [16], and several clinical reports have demonstrated quantitative assessment of regional myocardial function during acute intervention [13,14]. Strain rate is calculated as  $(V_1 - V_2)/L$ , where  $V_1$  and  $V_2$  are the velocity of point 1 and 2, and  $L$  is the distance between points 1 and 2 [12,17]. To avoid the noise inherent in any differentiation method, strain rate data may be integrated throughout systole to obtain strain, a dimensionless measure of the total deformation that the myocardium undergoes during contraction. Strain is calculated as  $(L - L_0)/L_0$ , where  $L_0$  is original length and  $L$  is the length at end of systole. When acquired from the apex, normal myocardium has a negative strain during systole and a positive strain during diastole (Figure 4.3).

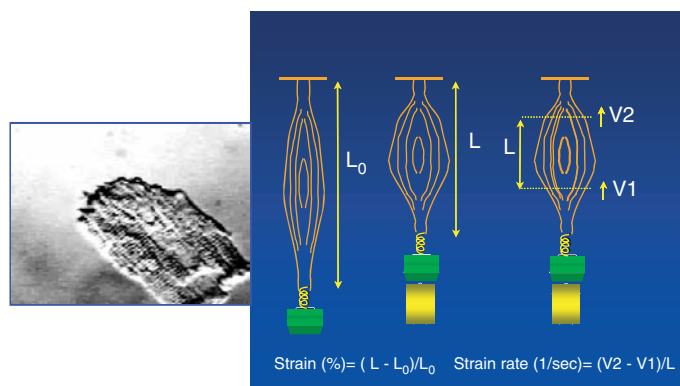


**Figure 4.3** The mechanism of myocardial strain and strain rate.

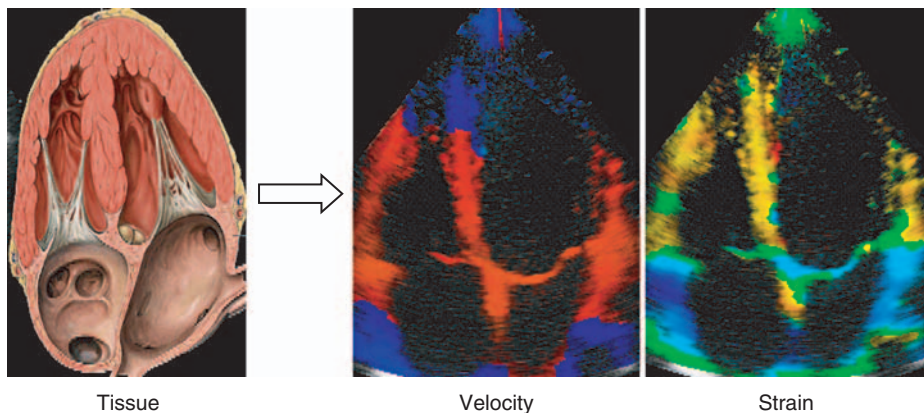


**Figure 4.4** Color coding of tissue velocity and strain.

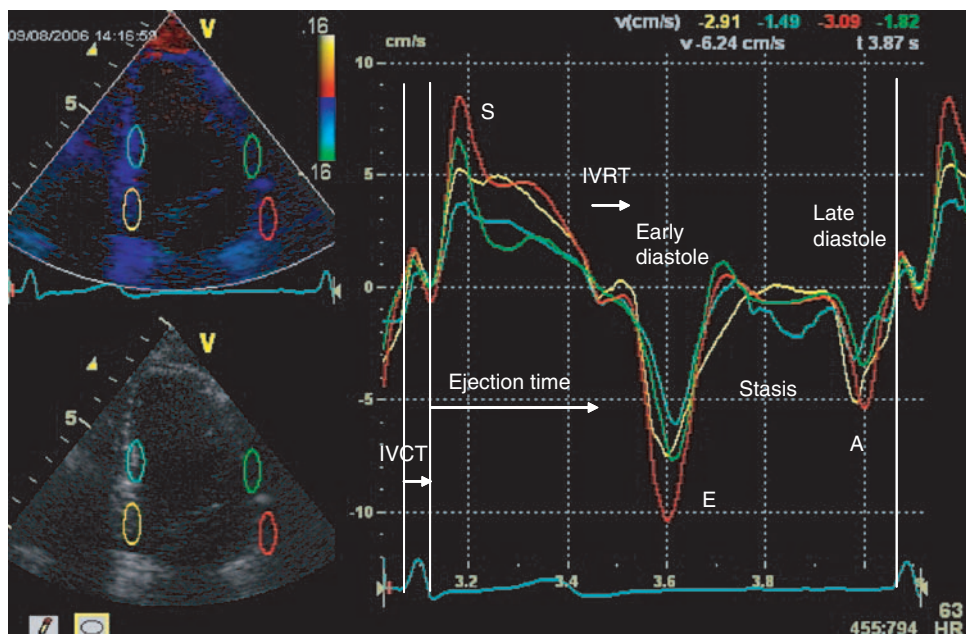


**Figure 4.5** Myocardial velocity (cm/sec). IVRT, isovolumic relaxation time; IVCT, isovolumic contraction time.

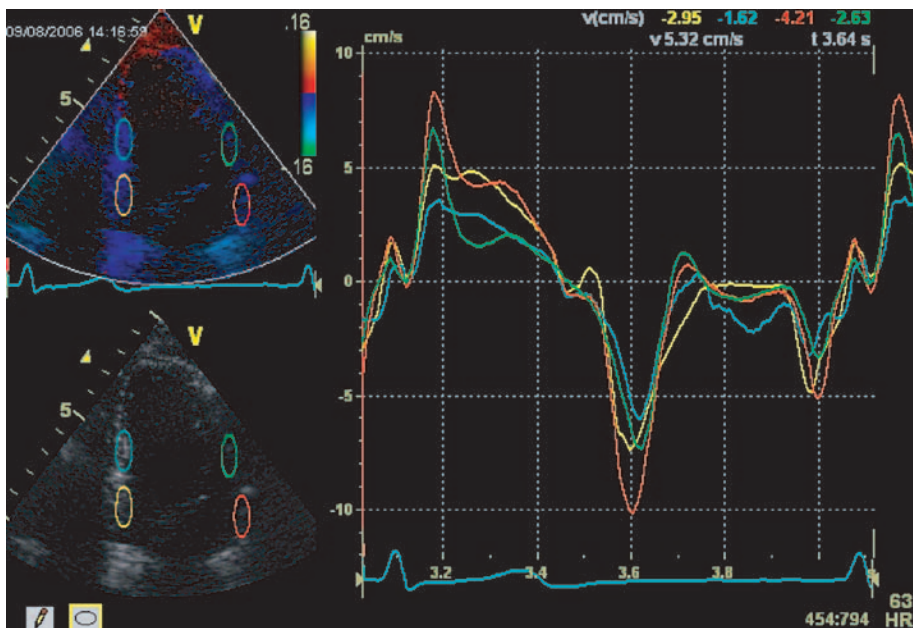


Figure 4.6 Myocardial longitudinal segmental velocity from four-chamber view (cm/sec). See also Video clip 5

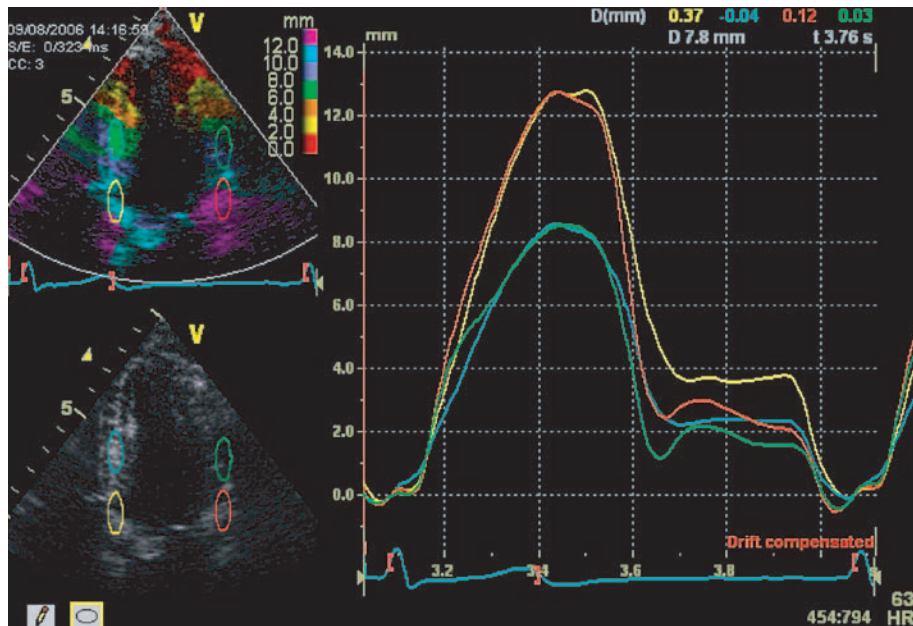


Figure 4.7 Myocardial longitudinal segmental tissue displacement (mm) in a normal subject. See also Video clip 6

The tissue Doppler image also provides a way to measure the segmental myocardial velocity and displacement, which are valuable parameters in clinical practice. The following figures demonstrate the normal patterns of DTE for the parameters velocity (Figures 4.5 and 4.6), displacement

(Figure 4.7), strain rate (Figure 4.8), and strain (Figure 4.9). Different color curves represent different segments.

Although promising, experience with these new Doppler tissue entities is limited. Therefore, the aims of the author were to determine (1) normal values

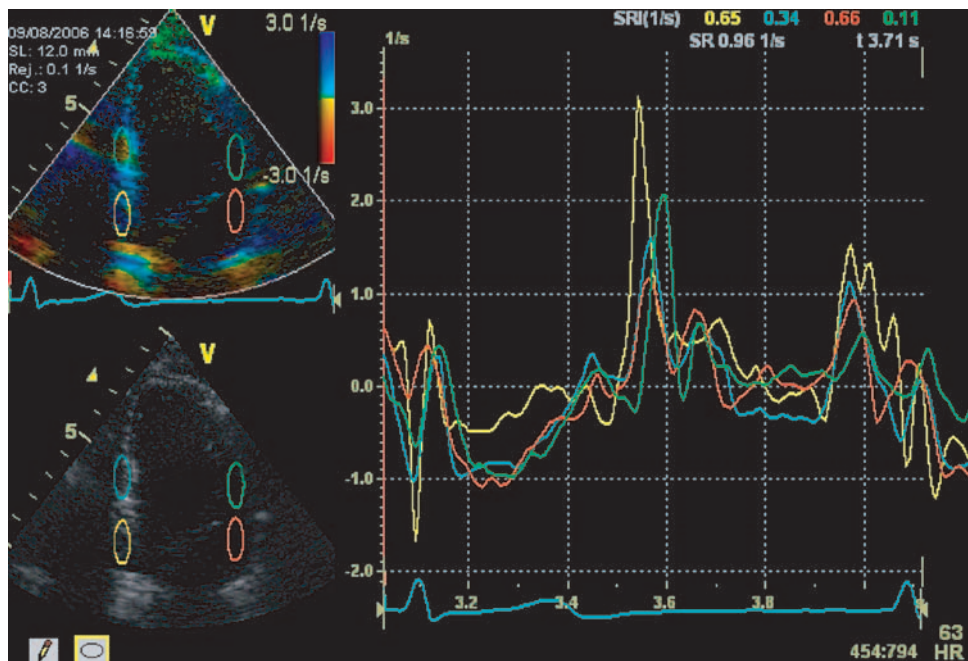


Figure 4.8 Myocardial longitudinal segmental strain rate (1/sec). See also Video clip 7

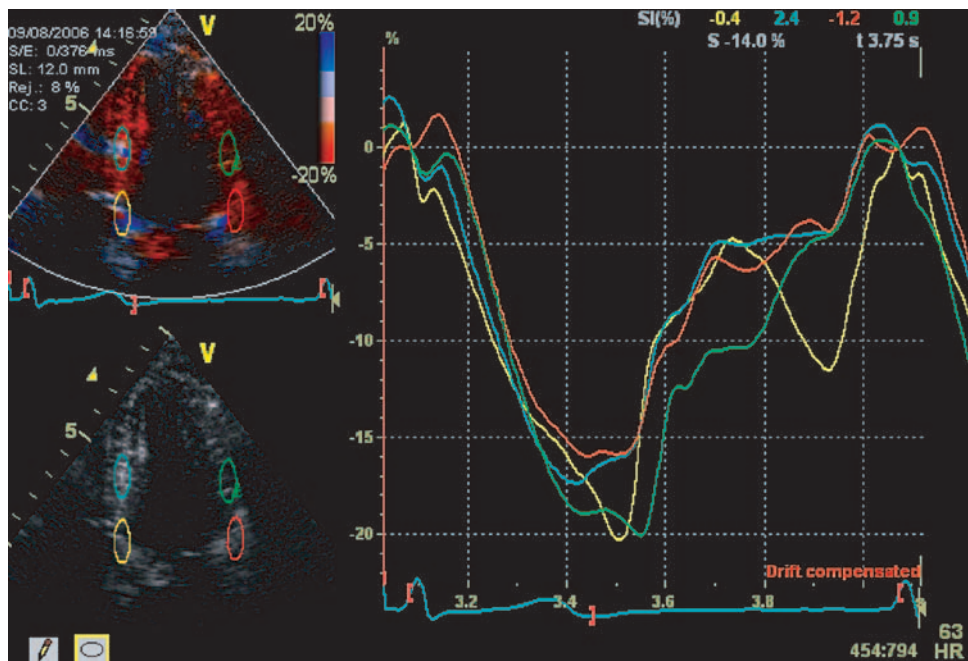


Figure 4.9 Myocardial longitudinal segmental strain (%) in a normal subject. See also Video clip 8

for tissue velocity, displacement, strain rate, and strain for the myocardial wall segments in the left ventricle; (2) whether these values change with age; and (3) the reproducibility of these parameters. Such normative values should allow these techniques to be applied in clinical practice with greater confidence than currently enjoyed.

## Methods

### Population

The institutional review board on human research approved this study, and all participants gave informed consent. Healthy volunteers free of any known cardiovascular disease and between the ages of 18 and 76 years were recruited. All volunteers underwent a thorough history and physical examination and had a normal ECG. None of them reported taking any kind of cardioactive medications (except aspirin).

### Echocardiographic study

A complete echocardiographic study was performed on all participants using an ultrasound machine (Vivid Five, General Electric, Milwaukee) equipped with a 2.5 MHz probe with digital storage capacity. Participants were placed in the left lateral decubitus position, and standard echocardiographic views were obtained in 2-D and DTE modes, including parasternal long, parasternal short, apical four-chamber, and apical two-chamber. Three complete cardiac cycles of both 2-D and DTE data from each echocardiographic view were collected and stored in a cine-loop format. Real-time color DTE was acquired as data superimposed on an underlying 2-D gray-scale image at a frame rate of 150/sec, a depth of 16 cm, and a sector angle of 60 degrees. Special attention was paid to the color Doppler velocity range settings to avoid any aliasing within the image. If detected, increasing the pulse repetition frequency (typically between 1 and 2 kHz) eliminated aliasing.

Regional myocardial wall velocity, displacement (also termed "tracking" by the manufacturer), strain rate, and strain analysis was performed offline using customized computer software (Echopac, version 6.3, General Electric) running on a Power Mac G3 (Apple Computer, Inc., Cupertino, CA). In the apical four- and two-chamber views, each LV wall analyzed was divided into three segments: basal,

mid, and apical. To improve signal-to-noise ratio, median data from a sample region ( $5 \times 5$  pixels) positioned in the center of each segment was used. To ensure that measurements reflected motion of a myocardial tissue segment throughout the cardiac cycle, the position of the sample region was manually adjusted frame by frame to maintain its position within the myocardium. Strain rate and strain were computed using the strain length option set to 15 mm. To reduce noise, the data were taken from three consecutive heart cycles and averaged.

### Reproducibility

To obtain interobserver variability, two echocardiographers with experience in interpreting DTE evaluated raw data from 18 random cases in a blinded manner. Readers were asked to focus on two segments (basal and apical) within two walls (septal and lateral) and measure velocity, displacement, strain rate, and strain independently from each other. Intraobserver variability was similarly tested on 12 randomly selected cases by one experienced echocardiographer 1 week apart. Both interobserver and intraobserver variabilities were expressed as the mean and SD of the signed (not absolute) difference between the measurements.

### Statistical analysis

Data are presented as mean  $\pm$  SD. We assumed that DTE parameters of individual segments were influenced by both the wall level (apical = 0, mid = 1, or basal = 2), and by the wall curvature (geometry), with septal and inferior walls being less curved as a result of the compression by the right ventricle and diaphragm, respectively. Analysis of covariance was performed with LV level, LV wall curvature (lateral and anterior walls = 0, septal and inferior walls = 1), their interaction, and sex as fixed factors; patient identification as a dummy variable to adjust for between-patient differences; and age as a covariate. Reproducibility of DTE parameters was tested by evaluating the Pearson correlation and  $K$  coefficients on interobserver and intraobserver measurement data. A  $P$  value less than 0.05 was considered statistically significant.

## Results

In all, 100 healthy volunteers were recruited. The mean age was  $43 \pm 15$  years (range, 18–76 years),

and 52 were men. There were 22 participants between 18 and 29 years of age, 23 between 30 and 39 years, 26 between 40 and 49 years, 14 between 50 and 59 years, and 15 older than 60 years of age. Their resting heart rates varied between 44 and 86 bpm (mean,  $66 \pm 11$  bpm), and their blood pressure varied from 80 to 120 over 60 to 80 mmHg (mean,  $110 \pm 10/70 \pm 10$  mmHg).

### Echocardiographic studies

We analyzed 1,200 segments in the healthy population. Although great care was taken to ensure the quality of the data collected, 61 segments (5.1%) were excluded from the final analysis. The reasons for exclusion were mostly technical, either the presence of an artifact or a low signal-to-noise ratio. Most of the segments excluded from analysis were either anterior or lateral wall apical segments (58 segments). It is important to note that walls that were parallel to the scan line (septal and inferior walls) provided better image quality than the ventricular walls that could less easily be placed along the scan line (anterior and lateral walls).

### Two-dimensional echocardiography

Standard 2-D and Doppler echocardiography was performed on all of 102 volunteers. Cardiac dimensions, wall thickness, chamber size, and global and regional LV systolic function was normal in all. The average stroke volume was  $66 \pm 19$  ml;

mean LV ejection fraction was  $64 \pm 7\%$ . There was trivial to  $1^+$  regurgitation across the mitral valve in 35, the tricuspid valve in 44, and the pulmonary valve in 30 patients.

### DTE velocities

The systolic (S)-wave velocities of individual regions are presented in Table 4.1. There was a significant impact of wall level ( $P < 0.0001$ ), with no effect of wall curvature, and a moderate correlation with aging ( $r = 0.29$ ;  $P < 0.0001$ ). There was no effect of sex. The overall relationship (with  $r = 0.56$ ) for S-wave values was:

$$\begin{aligned} \text{S-wave} (\pm 1.9 \text{ cm/sec}) \\ = 6.1 + 1.5 \times \text{Level} - 0.06 \times \text{Age} \end{aligned}$$

where *Level* equals 0, 1, and 2 for apical, mid, and basal LV wall segments, respectively, and *Age* is represented in years.

The early (E)-wave velocities of individual regions are presented in Table 4.2. There was a significant impact of wall level ( $P < 0.0001$ ) and wall curvature ( $P < 0.0001$ ), small but significant effects of level by wall interaction ( $P < 0.004$ ), and a moderate correlation with aging ( $r = 0.42$ ;  $P < 0.0001$ ). There was no effect of sex. The overall relationship ( $r = 0.56$ ) for E-wave values was:

$$\begin{aligned} \text{E-wave} (\pm 2.5 \text{ cm/sec}) \\ = 10.5 + 1.0 \times \text{Curvature} + 2.2 \times \text{Level} - 0.39 \\ \times \text{Curvature} \times \text{Level} - 0.12 \times \text{Age} \end{aligned}$$

**Table 4.1** Segmental systolic velocity in age groups.

Age (years)	<i>Basal</i>	<i>Middle</i>	<i>Apex</i>	<i>Basal</i>	<i>Middle</i>	<i>Apex</i>
					<i>Ventricular septal (cm/sec)</i>	<i>Left ventricular lateral wall (cm/sec)</i>
18–29	$6.6 \pm 1.2$	$4.7 \pm 1.1$	$3.1 \pm 1.3$	$7.6 \pm 2.5$	$6.9 \pm 3.3$	$5.4 \pm 3.3$
30–39	$6.2 \pm 0.9$	$4.6 \pm 1.1$	$3.0 \pm 1.5$	$7.3 \pm 2.4$	$5.6 \pm 2.6$	$4.1 \pm 2.5$
40–49	$6.1 \pm 1.0$	$4.5 \pm 0.9$	$3.0 \pm 0.9$	$6.1 \pm 2.1^{\dagger}$	$5.4 \pm 2.3$	$3.8 \pm 2.4$
50–59	$5.4 \pm 1.2$	$4.3 \pm 0.9$	$2.7 \pm 0.9$	$4.3 \pm 0.9^*$	$3.0 \pm 1.1^*$	$2.1 \pm 1.2^*$
60–77	$5.3 \pm 1.0^{\dagger}$	$4.1 \pm 0.7^{\dagger}$	$2.9 \pm 0.9$	$5.1 \pm 2.2^{\dagger}$	$4.1 \pm 1.9^{\dagger}$	$2.6 \pm 1.8^{\dagger}$
Average	$6.0 \pm 1.1$	$4.5 \pm 0.9$	$3.0 \pm 1.1$	$6.3 \pm 2.4$	$5.2 \pm 2.8$	$3.8 \pm 2.7$
				<i>Ventricular inferior wall (cm/sec)</i>	<i>Left ventricular anterior wall (cm/sec)</i>	
18–29	$7.1 \pm 1.3$	$5.6 \pm 1.2$	$4.3 \pm 0.9$	$7.5 \pm 2.5$	$5.2 \pm 2.9$	$3.4 \pm 2.0$
30–39	$6.9 \pm 1.8$	$5.5 \pm 1.6$	$3.8 \pm 1.2$	$7.4 \pm 2.5$	$5.3 \pm 1.9$	$3.4 \pm 1.7$
40–49	$6.6 \pm 1.0$	$5.2 \pm 0.8$	$3.8 \pm 0.9^{\dagger}$	$6.6 \pm 2.1$	$4.6 \pm 2.1$	$3.0 \pm 1.9$
50–59	$5.9 \pm 0.5^{\dagger}$	$4.6 \pm 0.6^{\dagger}$	$3.2 \pm 1.0^{\dagger}$	$5.0 \pm 1.3^{\dagger}$	$3.2 \pm 1.5$	$1.9 \pm 1.2$
60–77	$5.6 \pm 1.0^{\dagger}$	$4.4 \pm 0.9^{\dagger}$	$3.2 \pm 0.9^*$	$4.8 \pm 1.6^{\dagger}$	$3.0 \pm 1.7^{\dagger}$	$2.2 \pm 1.3$
Average	$6.5 \pm 1.3$	$5.1 \pm 1.2$	$3.7 \pm 1.1$	$6.4 \pm 2.3$	$4.4 \pm 2.3$	$2.9 \pm 1.8$

\*vs. 18- to 29-year group,  $P < 0.001$ .

<sup>†</sup>vs. 18- to 29-year group,  $P < 0.05$ .

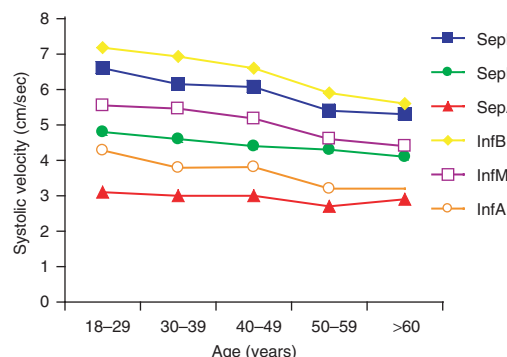


Figure 4.10 The correlation between segmental systolic velocity and age.

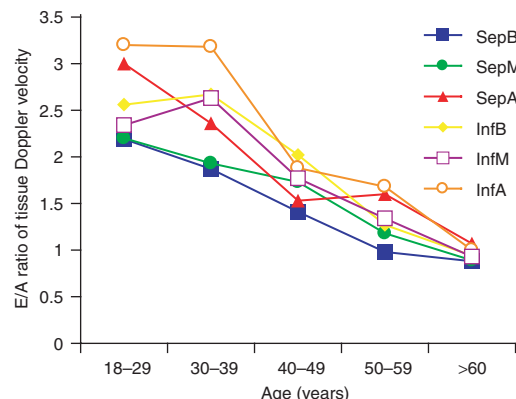


Figure 4.11 The correlation between E/A ratio and age.

Table 4.2 Segmental early diastolic velocity in age groups.

Age (years)	Basal			Middle			Apex		
	Ventricular septal (cm/sec)			Basal			Apex		
18-29	9.3±1.9	7.2±2.0	5.2±2.1	10.3±2.5	9.2±2.9	6.8±3.6			
30-39	8.7±2.0	7.6±1.6	5.0±2.1	9.6±2.5	7.7±2.9	5.0±2.6			
40-49	8.1±1.8	7.2±1.9	4.7±1.9	8.7±2.2	7.2±2.6	4.4±2.5			
50-59	6.8±1.8	6.3±1.5	4.7±2.1	6.6±2.0	4.4±1.6	2.9±1.8			
60-77	5.6±1.3	5.3±1.3	4.0±1.4	6.2±2.4	4.0±2.3	2.4±1.3			
Average	7.9±2.1	6.9±1.9	4.8±1.9	8.5±2.8	6.8±3.2	4.5±2.9			
<i>Ventricular inferior wall (cm/sec)</i>									
18-29	10.1±2.0	8.1±2.0	5.7±2.1	9.6±2.8	7.6±3.4	4.6±2.5			
30-39	10.0±2.0	8.0±1.8	5.7±1.8	8.7±2.1	7.1±2.5	4.7±2.2			
40-49	9.9±2.1	7.9±1.9	6.2±1.9	8.3±2.0	6.3±2.6	4.2±2.9			
50-59	7.1±2.3	6.0±1.3	4.3±1.8	7.2±1.9	4.6±2.3	2.5±1.4			
60-77	6.7±1.6	5.2±1.2	4.2±1.4	5.8±1.7	3.5±1.5	1.4±1.1			
Average	9.0±2.4	7.2±2.0	5.4±2.0	8.1±2.5	6.0±2.9	3.7±2.6			

where Curvature equals 1 for the straighter septal and inferior walls and 0 for the more curved lateral and anterior walls.

The atrial (A) contraction, or late diastolic filling, wave velocities of individual regions are presented in Table 4.3. There was a significant impact of level ( $P < 0.0001$ ) and wall ( $P < 0.0001$ ), small but significant effects of level by wall interaction ( $P = 0.002$ ), and a moderate correlation with aging ( $r = 0.39$ ;  $P < 0.0001$ , increasing with age in contrast to the S- and E-waves that decrease with age). There was no effect of sex. The overall relationship ( $r = 0.64$ ) for A-wave values was:

A-wave ( $\pm 1.7$  cm/sec)

$$= 0.66 + 1.65 \times \text{Curvature} + 1.1 \times \text{Level} \\ + 0.50 \times \text{Curvature} \times \text{Level} + 0.04 \times \text{Age}$$

where Curvature  $\times$  Level represents the interaction between level and wall curvature.

### Myocardial strain rate

The peak systolic strain rates (Ssr) of individual regions are presented in Table 4.4. There was a significant impact of wall ( $P = 0.003$ ), level ( $P = 0.001$ ), and level by wall interaction ( $P < 0.001$ ), with no effect of sex. The overall relationship ( $r = 0.33$ ) for peak systolic strain rate values was:

$$\begin{aligned} \text{Ssr} (\pm 0.63 \text{ 1/sec}) \\ = 1.1 + 0.23 \times \text{Curvature} + 0.25 \times \text{Level} \\ - 0.40 \times \text{Curvature} \times \text{Level} \end{aligned}$$

The E-wave diastolic strain rates (Esr) of individual regions are presented in Table 4.5. Only

**Table 4.3** Segmental late diastolic velocity in age groups.

Age (years)	Basal	Middle	Apex	Basal	Middle	Apex
<i>Ventricular septal (cm/sec)</i>				<i>Left ventricular lateral wall (cm/sec)</i>		
18–29	4.9±1.4	3.9±1.4	2.3±1.2	3.1±1.4	2.1±1.4	1.3±1.0
30–39	5.4±1.4	4.4±1.3	2.7±1.3	3.9±2.0	2.5±1.4	1.3±1.0
40–49	6.2±1.6	4.8±1.8	3.1±1.0	3.7±1.7	2.8±1.8	1.7±1.6
50–59	7.2±1.3	5.6±1.1	3.3±1.7	3.6±0.9	2.6±1.3	1.7±1.7
60–77	7.0±1.9	6.5±1.7	4.3±2.0	5.1±2.3	3.2±1.4	2.6±1.7
Average	6.0±1.7	4.9±1.7	3.1±1.5	3.8±1.8	2.6±1.5	1.7±1.4
<i>Ventricular inferior wall (cm/sec)</i>				<i>Left ventricular anterior wall (cm/sec)</i>		
18–29	4.9±1.5	4.0±1.3	2.6±1.1	3.1±1.4	2.1±1.1	1.0±0.8
30–39	4.8±2.4	3.9±1.6	2.5±1.3	3.2±1.6	2.1±1.2	1.0±0.6
40–49	6.2±2.1	5.2±1.9	3.5±1.3	4.0±1.8	2.8±2.1	1.8±1.8
50–59	6.4±1.7	5.2±1.6	3.3±1.7	4.2±1.4	3.3±2.5	2.0±1.5
60–77	7.3±1.1	5.9±1.1	4.4±1.3	5.2±1.7	3.8±2.1	1.4±1.1
Average	5.8±1.1	4.8±1.7	3.2±1.5	3.9±1.7	2.7±1.9	1.4±1.3

**Table 4.4** Segmental systolic strain rate in age groups.

Age (years)	Basal	Middle	Apex	Basal	Middle	Apex
<i>Ventricular septal (1/sec)</i>				<i>Left ventricular lateral wall (1/sec)</i>		
18–29	1.0±0.4	1.4±0.5	1.4±0.4	1.5±0.5	1.2±0.7	1.4±0.8
30–39	1.2±0.7	1.6±0.9	1.5±0.4	1.5±0.5	0.9±0.5	1.0±0.6
40–49	1.1±0.4	1.2±0.4	1.3±0.4	1.6±0.8	0.8±0.3	1.0±0.6
50–59	0.9±0.5	1.1±0.3	1.3±0.3	1.4±0.8	0.9±0.3	0.9±0.4
60–77	0.7±0.3	1.1±0.2	1.3±0.5	1.4±0.4	0.8±0.4	0.8±0.3
Average	1.0±0.5	1.3±0.5	1.4±0.4	1.5±0.6	0.9±0.5	1.1±0.6
<i>Ventricular inferior wall (1/sec)</i>				<i>Left ventricular anterior wall (1/sec)</i>		
18–29	0.9±0.2	0.8±0.3	1.2±0.7	1.6±1.0	1.4±0.7	1.3±1.0
30–39	1.0±0.4	0.9±0.4	1.3±1.0	1.5±0.8	1.1±0.4	1.5±0.7
40–49	0.9±0.4	0.9±0.3	1.4±0.9	1.7±0.7	1.0±0.4	1.0±0.6
50–59	0.9±0.3	1.0±0.4	1.2±0.5	1.6±0.8	1.1±0.4	0.9±0.6
60–77	0.9±0.4	0.9±0.4	1.2±0.6	1.5±0.4	1.0±0.4	0.7±0.3
Average	0.9±0.4	0.9±0.4	1.2±0.8	1.6±0.8	1.1±0.5	1.1±0.8

level by wall interaction had significant effect on E-wave diastolic strain rate, with no correlation with aging ( $P = \text{not significant}$ ). There was no effect of sex. The overall relationship ( $r = 0.32$ ) for E-wave values was:

$$\text{Esr} (\pm 0.87 \text{ sec}^{-1}) = 1.3 + 0.42 \times \text{Curvature} \\ + 0.15 \times \text{Level} - 0.30 \times \text{Curvature} \times \text{Level}$$

The A-wave diastolic strain rates (Asr) of individual regions are presented in Table 4.6. There was a significant impact of wall ( $P < 0.0001$ ), level ( $P < 0.0001$ ), and level by wall interaction

( $P < 0.0001$ ), and a weak correlation with aging ( $r = 0.30$ ;  $P < 0.0001$ ). There was no effect of sex. The overall relationship ( $r = 0.44$ ) for A-wave values was:

$$\text{Asr} (\pm 0.71 \text{ sec}^{-1}) \\ = 0.07 + 0.88 \times \text{Curvature} + 0.25 \times \text{Level} \\ - 0.39 \times \text{Curvature} \times \text{Level} + 0.02 \times \text{Age}$$

### Myocardial displacement and strain

The peak displacements ( $D$ ) of individual regions are presented in Table 4.3. There was a significant

**Table 4.5** Segmental early diastolic strain rate in age groups.

Age (years)	<i>Basal</i>	<i>Middle</i>	<i>Apex</i>	<i>Basal</i>	<i>Middle</i>	<i>Apex</i>
<i>Ventricular septal (1/sec)</i>						
18–29	1.9±0.6	1.7±0.5	2.3±0.9	2.3±1.1	2.1±1.2	2.2±0.8
30–39	2.1±1.2	1.8±0.8	2.4±0.9	2.2±1.6	2.1±1.8	1.8±1.2
40–49	2.2±1.0	1.6±0.6	2.5±0.9	1.5±0.7	1.8±0.8	1.9±1.1
50–59	1.8±0.8	1.6±0.6	2.1±1.0	2.0±0.9	1.7±0.7	1.3±0.7
60–77	1.6±0.6	1.8±0.9	2.0±0.7	1.7±0.8	1.7±1.2	1.2±0.6
Average	2.0±0.9	1.7±0.7	2.3±0.9	1.9±1.1	1.9±1.2	1.8±1.0
<i>Ventricular inferior wall (1/sec)</i>						
18–29	1.7±0.9	1.8±0.6	2.0±0.8	2.2±0.9	2.0±0.5	1.6±0.8
30–39	1.7±1.0	1.7±0.7	2.0±0.8	2.0±0.9	1.8±0.7	2.3±0.9
40–49	2.0±0.8	1.9±1.2	1.9±0.9	2.1±1.3	1.8±0.6	1.5±0.8
50–59	1.9±0.8	1.4±0.4	1.8±0.8	1.9±0.6	2.0±0.7	1.3±0.6
60–77	1.8±1.0	1.5±0.6	1.5±0.7	1.8±0.9	1.9±0.8	1.2±0.5
Average	1.9±0.9	1.7±0.8	1.8±0.8	2.0±0.9	1.9±0.7	1.6±0.8

**Table 4.6** Segmental late diastolic strain rate in age groups.

Age (years)	<i>Basal</i>	<i>Middle</i>	<i>Apex</i>	<i>Basal</i>	<i>Middle</i>	<i>Apex</i>
<i>Ventricular septal (1/sec)</i>						
18–29	1.2±0.5	1.0±0.4	1.3±0.7	0.9±0.5	0.6±0.4	0.5±0.4
30–39	1.4±0.8	1.2±0.5	1.4±0.7	0.8±0.5	0.7±0.7	0.5±0.5
40–49	1.6±1.1	1.5±0.9	1.8±0.5	0.9±0.3	0.8±0.4	0.7±0.6
50–59	2.0±1.0	2.0±0.7	1.7±1.0	1.0±0.6	0.7±0.6	0.7±0.6
60–77	1.7±0.6	2.1±0.8	2.4±0.5	1.2±0.7	1.2±0.9	1.1±1.0
Average	1.5±0.9	1.5±0.8	1.7±0.8	0.9±0.6	0.8±0.6	0.7±0.7
<i>Ventricular inferior wall (1/sec)</i>						
18–29	1.0±0.4	1.0±0.7	1.1±0.8	1.1±0.6	0.9±0.5	0.4±0.5
30–39	1.0±0.6	0.8±0.5	1.2±0.8	1.5±1.1	0.7±0.3	0.6±0.4
40–49	1.4±1.1	0.9±0.5	1.5±0.7	1.3±0.8	1.0±0.5	0.6±0.4
50–59	1.4±0.8	1.3±0.6	1.3±0.5	2.5±1.2	1.2±0.7	0.7±0.9
60–77	1.3±0.6	1.5±0.4	1.7±0.6	1.7±0.9	1.1±0.6	0.9±0.7
Average	1.2±0.8	1.0±0.6	1.4±0.7	1.5±1.0	1.0±0.5	0.6±0.6

impact of wall ( $P < 0.0001$ ) and level by wall interaction ( $P = 0.007$ ), and a weak but significant correlation with aging ( $r = 0.12$ ;  $P < 0.0001$ ). There was no effect of sex. The overall relationship ( $r = 0.81$ ) for displacement values was:

$$D (\pm 0.2 \text{ cm}) = 0.57 + 0.29 \times \text{Level} + 0.04 \\ \times \text{Curvature} \times \text{Level} - 0.005 \times \text{Age}$$

The correlation between segmental displacements and peak systolic velocities was  $r = 0.69$  ( $P < 0.0001$ ).

The peak systolic strains ( $\epsilon$ ) of individual regions are presented in Figure 4.12. There was a significant

impact of side ( $P < 0.001$ ) and level by wall interaction ( $P < 0.0001$ ), with no correlation with aging ( $P = \text{not significant}$ ). There was no effect of sex. The overall relationship ( $r = 0.47$ ) for peak systolic strain was:

$$\epsilon (\pm 6.1\%) = 14.4 + 8.7 \times \text{Curvature} + 3.0 \times \text{Level} \\ - 6.4 \times \text{Curvature} \times \text{Level}$$

The correlation between segmental displacements and peak systolic velocities was  $r = 0.57$  ( $P < 0.0001$ ).

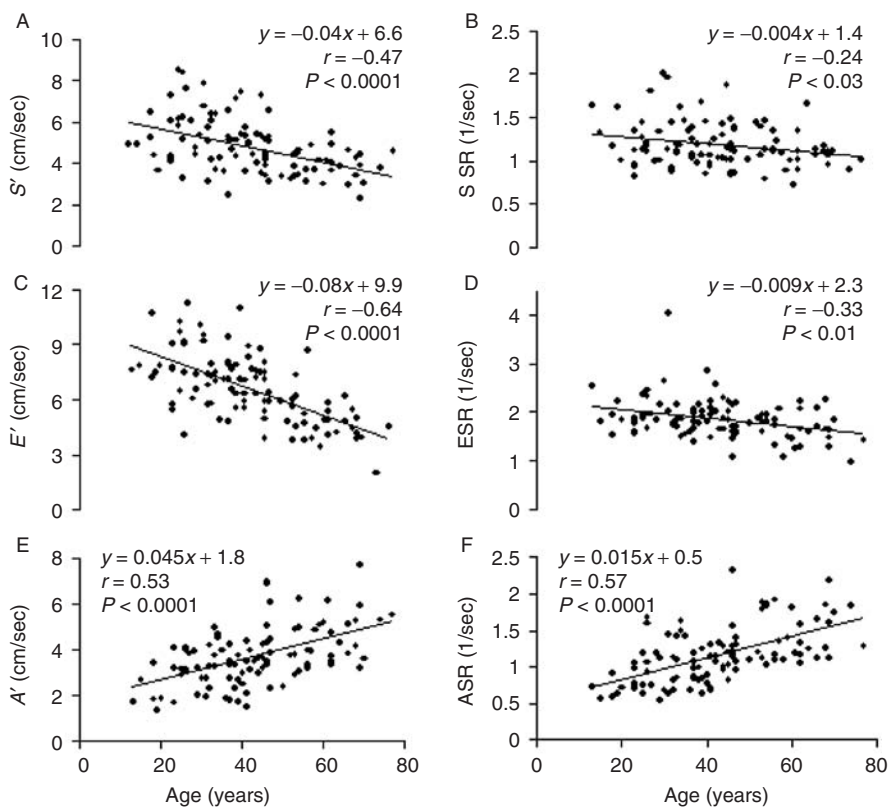


**Figure 4.12** Age-dependence of mean Doppler tissue velocity and strain rate (SR) parameters. To obtain mean Doppler tissue velocity and SR parameters, individual segmental data were averaged for each individual. Age-dependence was less prominent for peak systolic

tissue velocity ( $S'$ ) and SR (A and B) than for early ( $E'$ ) and late ( $A'$ ) diastolic tissue velocities and SR (C to F). Furthermore, regression coefficients were lower for SR when compared with velocity data.

**Table 4.7** Segmental myocardial displacement in age groups.

Age (years)	Septum (mm)			Lateral wall (mm)			Inferior wall (mm)			Anterior wall (mm)		
	Basal	Middle	Apex	Basal	Middle	Apex	Basal	Middle	Apex	Basal	Middle	Apex
18–29	12±2	9±2	5±2	11±3	8±3	5±3	14±2	11±2	8±1	12±3	7±3	4±2
30–39	12±2	9±2	5±2	10±2	6±2	4±2	13±2	10±2	7±2	11±2	7±2	4±2
40–49	12±2	9±2	5±2	9±2	6±2	4±2	14±2	11±2	7±2	10±2	7±2	3±1
50–59	12±2	9±2	6±2	8±2	5±1	3±1	13±3	10±2	6±2	10±3	6±3	3±1
60–77	11±2	9±1	6±2	9±2	5±2	3±1	13±2	10±2	6±2	9±2	6±2	3±2
Average	12±2	9±2	6±2	9±2	6±2	4±2	13±2	10±2	7±2	11±3	7±2	4±2

The effect of aging on displacement and strain measures is shown in Figure 4.13. As can be seen, all parameters except peak systolic strain showed some correlation with age, although it was barely significant for displacement.

### Reproducibility

Data from 72 segments (18 randomly selected volunteers, 4 segments per volunteer) were used to establish interobserver and intraobserver variability. The  $k$  for intraobserver variability in measuring

**Table 4.8** Segmental myocardial systolic strain in age groups.

Age (years)	Septum (%)			Lateral wall (%)			Inferior wall (%)			Anterior wall (%)		
	Basal	Middle	Apex	Basal	Middle	Apex	Basal	Middle	Apex	Basal	Middle	Apex
18–29	18±3	20±6	22±5	17±7	14±5	15±10	14±5	17±4	24±10	23±9	21±8	15±5
30–39	18±5	18±5	25±5	19±7	15±4	15±7	14±7	17±6	21±9	22±7	19±6	17±7
40–49	18±6	19±4	25±5	18±8	14±5	13±6	16±6	19±6	23±8	21±8	20±6	15±6
50–59	17±7	19±6	23±4	20±7	14±6	11±2	15±4	19±6	19±6	25±9	20±5	12±5
60–77	16±6	18±6	23±5	19±6	14±6	12±3	15±6	19±6	20±6	21±6	18±4	12±4
Average	17±5	19±5	24±5	18±7	14±5	13±6	15±6	18±6	22±8	22±8	19±6	15±6

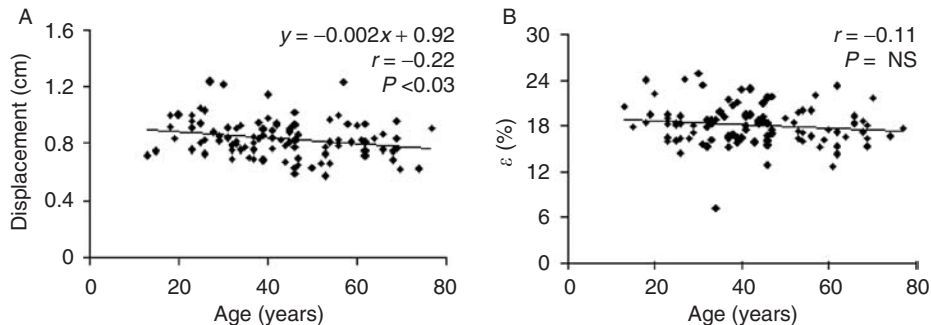


**Figure 4.13** Age-dependence of average tissue displacement (A) and systolic strain ( $\epsilon$ ) (B). To obtain mean Doppler tissue displacement and strain, individual segmental data were averaged for each individual.

The age-dependence of both parameters was less prominent than that for tissue velocity and strain rate parameters. NS, not significant.

systolic velocity is 0.82 ( $P < 0.001$ ), for tissue displacement is 0.73 ( $P < 0.001$ ), for strain rate is 0.58 ( $P < 0.001$ ), and for systolic tissue strain is 0.59 ( $P < 0.001$ ). The Pearson correlation for systolic velocity was  $r = 0.89$  ( $P < 0.001$ ), for tissue displacement was  $r = 0.83$  ( $P < 0.001$ ), for strain rate was  $r = 0.72$  ( $P < 0.001$ ), and for systolic tissue strain was  $r = 0.78$  ( $P < 0.001$ ). The average difference between the measurements for systolic velocity was  $0.01 \pm 0.06$  cm/sec, for tissue displacement was  $0.002 \pm 0.04$  cm, for strain rate was  $0.11 \pm 0.16$  1/sec, and for strain was  $1 \pm 5\%$ . The interobserver variability was equally good, with the  $k$  for velocity was 0.76 ( $P < 0.001$ ), for tissue displacement was 0.7 ( $P < 0.001$ ), for strain rate was 0.53 ( $P < 0.001$ ), and for strain was 0.54 ( $P < 0.001$ ). The Pearson correlation for velocity was  $r = 0.86$  ( $P < 0.001$ ), for tissue displacement was  $r = 0.83$  ( $P < 0.001$ ), for strain rate was  $r = 0.66$  ( $P < 0.001$ ), and for systolic strain was  $r = 0.71$  ( $P < 0.001$ ). The average difference between the two readers for velocity was  $0.02 \pm 0.2$  cm/sec, for tissue displacement was  $0.01 \pm 0.04$  cm, for strain rate was  $0.08 \pm 0.2$  1/sec, and

for systolic strain was  $1 \pm 6\%$ . Velocity and tissue displacement measurements were easier to reproduce compared with strain rate and strain.

## Discussion

In the author's study, we were able to report normal age-adjusted values for systolic tissue velocity, displacement, strain rate, and strain as measured by DTE. Differences in acquired data between the segments of individual walls are demonstrated, as are gradual changes in these values with age. Reproducibility of these measurements and the agreement of the measurements between two readers were acceptable, indicating that these techniques can be implemented into clinical practice.

## Myocardial velocity and Doppler tissue displacement

The velocity of the myocardial wall can be derived from both pulsed and color DTE [18,19]. As we have demonstrated in this study, color DTE imaging is easily obtained and analyzed for any ventricular

segment and can be acquired much more rapidly than applying pulsed Doppler sampling to all regions of interest. However, well-defined values for the healthy population have not previously been available for clinical comparisons.

We have demonstrated the feasibility of obtaining myocardial tissue displacement measurements during systole by using integrated tissue velocities. This technique allows a more complete estimation of the total ventricular systolic function both in global and regional terms. Also, similar to tissue velocities, tissue displacement showed an expected strong base-to-apex gradient in its normal values.

### **Myocardial strain rate and strain**

Myocardial strain reflects tissue deformation referenced to the vector of interrogation, and myocardial strain rate is its derivative with respect to time. In theory, myocardial strain may be measured in all dimensional vectors [20], but in this current echocardiographic approach, only the longitudinal component of myocardial strain is quantified. Strain measurements offer advantages over regional myocardial velocities, which are affected by tethering from other myocardial segments and by translational motion of the entire heart. The impact of such tethering was observed by Yamada et al. [21], who demonstrated a reduced tissue velocity response to dobutamine in nonischemic segments if they were adjacent to ischemic or scarred segments. In contrast, tissue strain is less dependent on these factors. Urheim et al. [13] found that myocardial velocities in the nonischemic basal portion of the LV decreased during apical ischemia, whereas regional strain measured by sonomicrometry and by DTE were unchanged.

### **Regional heterogeneity and effects of aging on left ventricular function**

Magnetic resonance imaging studies have shown that longitudinal strain increases from 15% in the base to 19% in the apex, with no difference between individual LV walls [20]. Similar differences, with some individual wall dependency, were also noted for radial and circumferential strain. Interestingly, a recent echocardiographic study has not corroborated these findings [22]. A probable cause for this discrepancy is the high sensitivity of strain measurement to misalignment of the insonation angle when referenced to the true wall orientation [23]. It is well

known that LV walls show differences in regional curvature [24] and corresponding stress distribution [25]. Indeed, we have found an expected base-to-apex strain and strain rate increase in “flatter” walls, and the opposite change in more “curved” walls.

Interestingly, although it is known that whereas overall LV contractility does not change or may even increase with aging, there is a paucity of data on the effect of age on LV long-axis performance. We observed a highly significant effect of aging on all myocardial velocity indices. Of note, the opposite behavior of E- and A-wave velocities may reflect the development of age-related diastolic dysfunction [26].

However, there was less age-related reduction in total tissue displacement than velocity. This finding likely relates to slower calcium cycling with age, leading to longer systolic contraction periods, allowing total tissue displacement to be preserved despite lower peak velocities [27]. In contrast, the evaluation of strain and strain rate data showed that only the A-wave strain rate showed positive correlation with age. Possibly, this finding may be a result of a higher noise level of strain and strain rate measurement that may mask the effect of aging.

The potential usefulness of Doppler tissue imaging to assess atrial mechanical function in cardiac disease has been demonstrated. Zhang et al. [28] performed a study in which echocardiography with color-coded Doppler tissue imaging was performed in 131 healthy control subjects. They found that assessment of atrial mechanical function by Doppler tissue imaging is feasible in healthy individuals. Atrial velocities are highest in the right atrium, followed by the left atrium, and the lowest at the interatrial septum. Older age and faster heart rate seems to augment peak atrial contraction velocity in the atrial walls. The detailed information will be described in Chapter 21.

In conclusion, this study demonstrated that DTE is a robust and reproducible technique suitable for clinical application in the quantification of regional myocardial function. In this chapter, we define the normal values for the new indices of systolic global and regional wall function that are derived from the DTE data: tissue velocity, displacement, strain rate, and strain. These normal values should assist in bringing DTE into more widespread clinical use.

Further studies are necessary to define the use of tissue displacement, strain rate, and strain in the clinical diagnosis of cardiac disease in unselected populations.

## References

- 1 Smith EE, Guyton AC, Manning RD, White RJ. Integrated mechanisms of cardiovascular response and control during exercise in the normal human. *Prog Cardiovasc Dis* 1976; **18**: 421.
- 2 Schulman SP, Lakatta EG, Fleg JL, Lakatta L, Becker LC, Gerstenblith G. Age-related decline in left ventricular filling at rest and exercise. *Am J Physiol* 1992; **263**: H1932–8.
- 3 De Sutter J, De Backer J, Van de Veire N, Velghe A, De Buyzere M, Gillebert TC. Effects of age, gender, and left ventricular mass on septal mitral annulus velocity ( $E'$ ) and the ratio of transmural early peak velocity to  $E'$  ( $E/E'$ ). *Am J Cardiol* 2005; **95**: 1020–3.
- 4 Parisi AF, Moynihan PF, Folland ED, Feldman CL. Quantitative detection of regional left ventricular contraction abnormalities by two-dimensional echocardiography, II. Accuracy in coronary artery disease. *Circulation* 1981; **63**: 761–7.
- 5 Weiss JL, Bulkley BH, Hutchins GM, Mason SJ. Two-dimensional echocardiographic recognition of myocardial injury in man: comparison with postmortem studies. *Circulation* 1981; **63**: 401–8.
- 6 Visser CA, Kan G, Lie KI, Becker AE, Durrer D. Apex two-dimensional echocardiography: alternative approach to quantification of acute myocardial infarction. *Br Heart J* 1982; **47**: 461–7.
- 7 Beyar R, Shapiro EP, Graves WL, et al. Quantification and validation of left ventricular wall thickening by a three-dimensional volume element magnetic resonance imaging approach. *Circulation* 1990; **81**: 297–307.
- 8 Rademakers FE, Rogers WJ, Guier WH, et al. Relation of regional cross-fiber shortening to wall thickening in the intact heart: three-dimensional strain analysis by NMR tagging. *Circulation* 1994; **89**: 1174–82.
- 9 Sutherland GR, Stewart MJ, Groundstroem KW, et al. Color Doppler myocardial imaging: a new technique for the assessment of myocardial function. *J Am Soc Echocardiogr* 1994; **7**: 441–58.
- 10 Miyatake K, Yamagishi M, Tanaka N, et al. New method for evaluating left ventricular wall motion by color-coded tissue Doppler imaging: in vitro and in vivo studies. *J Am Coll Cardiol* 1995; **25**: 717–24.
- 11 Bach DS, Armstrong WF, Donovan CL, Muller DW. Quantitative Doppler tissue imaging for assessment of regional myocardial velocities during transient ischemia and reperfusion. *Am Heart J* 1996; **132**: 721–5.
- 12 Heimdal A, Stoylen A, Torp H, Skjaerpe T. Real-time strain rate imaging of the left ventricle by ultrasound. *J Am Soc Echocardiogr* 1998; **11**: 1013–9.
- 13 Urheim S, Edvardsen T, Torp H, Angelsen B, Smiseth OA. Myocardial strain by Doppler echocardiography: validation of a new method to quantify regional myocardial function. *Circulation* 2000; **102**: 1158–64.
- 14 Jamal F, Kukulski T, D'Hooge J, De Scheerder I, Sutherland, G. Abnormal postsystolic thickening in acutely ischemic myocardium during coronary angioplasty: a velocity, strain, and strain rate Doppler myocardial imaging study. *J Am Soc Echocardiogr* 1999; **12**: 994–6.
- 15 Voigt JU, Arnold MF, Karlsson M, et al. Assessment of regional longitudinal myocardial strain rate derived from Doppler myocardial imaging indexes in normal and infarcted myocardium. *J Am Soc Echocardiogr* 2000; **13**: 588–98.
- 16 Gorcsan J III, Strum DP, Mandarino WA, Gulati VK, Pinsky MR. Quantitative assessment of alterations in regional left ventricular contractility with color-coded tissue Doppler echocardiography: comparison with sonomicrometry and pressure-volume relations. *Circulation* 1997; **95**: 2423–33.
- 17 Mirsky I, Parmley WW. Assessment of passive elastic stiffness for isolated heart muscle and the intact heart. *Circ Res* 1973; **33**: 233–43.
- 18 Chapman J. The technical aspects of Doppler ultrasound. In: Chapman J, Southland GR, eds. *The noninvasive evaluation of hemodynamics in congenital heart disease*. Boston: Kluwer Academic Publishers; 1990. pp. 36–51.
- 19 Kukulski T, Voigt JU, Wilkenshoff UM, et al. A comparison of regional myocardial velocity information derived by pulsed and color Doppler techniques: an in vitro and in vivo study. *Echocardiography* 2000; **17**: 639–51.
- 20 Moore CC, Lugo-Olivieri CH, McVeigh ER, Zerhouni EA. Three-dimensional systolic strain patterns in the normal human left ventricle: characterization with tagged MR imaging. *Radiology* 2000; **214**: 453–66.
- 21 Yamada E, Garcia M, Thomas JD, Marwick TH. Myocardial Doppler velocity imaging – a quantitative technique for interpretation of dobutamine echocardiography. *Am J Cardiol* 1998; **82**: 806–9, A9–10.
- 22 Kowalski M, Kukulski T, Jamal F, et al. Can natural strain and strain rate quantify regional myocardial deformation? A study in healthy subjects. *Ultrasound Med Biol* 2001; **27**: 1087–97.
- 23 Castro PL, Greenberg NL, Drinko J, Garcia MJ, Thomas JD. Potential pitfalls of strain rate imaging: angle dependency. *Biomed Sci Instrum* 2000; **36**: 197–202.
- 24 DeAnda A Jr, Moon MR, Nikolic SD, et al. A method to assess endocardial regional longitudinal curvature of the left ventricle. *Am J Physiol* 1995; **268**: H2553–60.

- 25 DeAnda A Jr, Komeda M, Moon MR, et al. Estimation of regional left ventricular wall stresses in intact canine hearts. *Am J Physiol* 1998; **275**: H1879–85.
- 26 Yuda S, Short L, Leano R, Marwick TH. Abnormal left ventricular filling with increasing age reflects abnormal myocardial characteristics independent of ischemia or hypertrophy. *Am J Cardiol* 2003; **91**: 63–7.
- 27 Lakatta EG, Sollott SJ. Perspectives on mammalian cardiovascular aging: humans to molecules. *Comp Biochem Physiol A Mol Integr Physiol* 2002; **132**: 699–721.
- 28 Zhang Q, Kum LCC, Lee PW, et al. Effect of age and heart rate on atrial mechanical function assessed by Doppler tissue imaging in healthy individuals. *Am Soc Echocardiogr* 2006; **19**: 422–8.



# 2

## PART 2

### Application to hemodynamic evaluation



# Assessment of filling pressure at rest

*Jianwen Wang and Sherif F. Nagueh*

## **Heart failure and left ventricular filling pressure**

In the United States, heart failure affects approximately 4.8 million people, with 500,000 new cases diagnosed each year. Diastolic dysfunction plays an important role in the pathophysiology of heart failure, and the prevalence of heart failure with preserved ejection fraction can be close to or over 50% among patients presenting with heart failure [1,2]. Furthermore, the survival rate of patients with heart failure and preserved ejection fraction (EF) is slightly lower than or similar to that of patients with reduced EF [1,2]. Even in patients with depressed EF, left ventricular (LV) filling pressures determine exercise tolerance independent of the severity of systolic dysfunction [3]. Accordingly, estimation of LV filling pressures is important not only for the diagnosis but also for the management of patients with heart failure. Importantly, reduction of LV filling pressures is an important goal for patients with acute decompensated heart failure [4].

LV filling at rest is influenced by myocardial relaxation, atrioventricular compliance, left atrial (LA) systolic function, pericardial constraint, right ventricular (RV) filling, and LA pressure. Cardiovascular diseases that impair myocardial relaxation and/or increase chamber stiffness affect LV filling. In the heart with impaired myocardial relaxation, left atrial contractility increases to maintain normal LV filling and LA pressure. However, with myocardial disease progression, this compensation becomes inadequate and LA pressure is elevated, leading to dyspnea. At first, this condition occurs only with exertion, but later on, it occurs at rest.

Cardiac catheterization is still the gold standard for assessment of LV filling pressures. During left heart catheterization, two close surrogates of LA pressure can be obtained: LV mean diastolic pressure [5], and pre-A pressure. LV mean diastolic pressure is derived using a high fidelity pressure catheter, but pre-A pressure can be reliably obtained using a fluid filled catheter. During right heart catheterization, mean pulmonary capillary wedge pressure (PCWP) is obtained and provides a reliable estimate of LA pressure in the absence of significant mitral stenosis. The wedge position is identified by fluoroscopy, venous pressure waveform, and most reliably with an arterial level of O<sub>2</sub> saturation.

LV end-diastolic pressure (EDP) is higher than all of the above filling pressures and has its own Doppler correlates. In patients with diastolic dysfunction, LV EDP is the earliest pressure to become abnormally elevated, at a time when mean LA pressure can be normal. As diastolic dysfunction progresses and/or with exercise or ischemia, LA pressure increases. However, the use of cardiac catheterization for routine management of heart failure patients is not practical due to its invasive nature and the accompanying risks, including bleeding and infection. Given its versatility, portability, and reasonable accuracy, echocardiography has become the primary tool for the noninvasive estimation of LV filling pressures at rest.

## **Role of standard echocardiography in assessment of left ventricular filling pressure**

Conventional two-dimensional (2-D) echocardiography plays a key role in the evaluation of LV

structural (LA, LV size, wall thickness, valvular pathology, and so on) and functional changes in patients presenting with heart failure. Specifically, 2-D echocardiography is the most widely used tool to measure LV EF and, thus, can distinguish between patients with preserved and reduced EF. Using 2-D echocardiography, it is possible to measure LV volumes and wall thickness/mass. Patients with pathologic LV hypertrophy usually have impaired LV relaxation, and this finding can be used in conjunction with additional Doppler data (see below) to predict LV filling pressures. In particular, increased wall thickness in combination with an E (early diastolic) dominant mitral flow pattern usually suggest elevated LV filling pressures.

In addition, in patients with chronic cardiovascular diseases, LA volume is positively related to the stage of diastolic dysfunction and the chronic elevation of LV filling pressures [6]. Several LA volumes can be measured: maximum volume (before mitral valve opening), minimum volume (after LA contraction), and emptying volume (the difference between them). Using 2-D imaging, LA volumes can be measured using three different algorithms: three-axis method, single-plane area-length, and biplane area-length. The most accurate method is the biplane method, but the LA volume from an apical four-chamber view (Figure 5.1) may be used as it provides a close approximation of the biplane volume [7]. Aside from diastolic dysfunction, LA volume can increase in patients with mitral valve pathology and in those with atrial arrhythmias. Accordingly, it should be used in conjunction with

other Doppler parameters to draw inferences about the presence or absence of diastolic dysfunction and the status of LV filling pressures.

### Mitral inflow

The mitral inflow pattern is the cornerstone to evaluating LV filling and diastolic function [8]. It is recorded in an apical four-chamber view by placing a 1- to 2-mm sample volume at the level of the mitral valve annulus and then tips, using pulsed-wave Doppler. In addition, it is important to record the time interval between aortic valve closure and mitral valve opening or the isovolumic relaxation time (IVRT; Figure 5.2). This recording is achieved by acquiring a Doppler spectral trace from midway between the LV outflow tract and mitral valve tips. The mitral inflow pattern is primarily determined by the transmural pressure gradient (i.e., both LV and LA pressures). With active calcium reuptake by the sarcoplasmic reticulum and the detachment of actin-myosin cross-bridges, myocardial relaxation begins and myocardial tension drops rapidly. In addition, the twisted myocardial fibers recoil and provide an important suction mechanism that helps lower LV pressure, resulting in a positive LA-LV pressure gradient that leads to mitral valve opening and early diastolic flow (E velocity). With ongoing LV filling, LV pressure rises, resulting in a slow down of diastolic inflow and a rapid deceleration of the E velocity. As LV pressure rises further, the LA-LV pressure gradient dissipates, resulting in no flow during mid-diastole or diastasis period. In late diastole, LA contraction leads to a higher

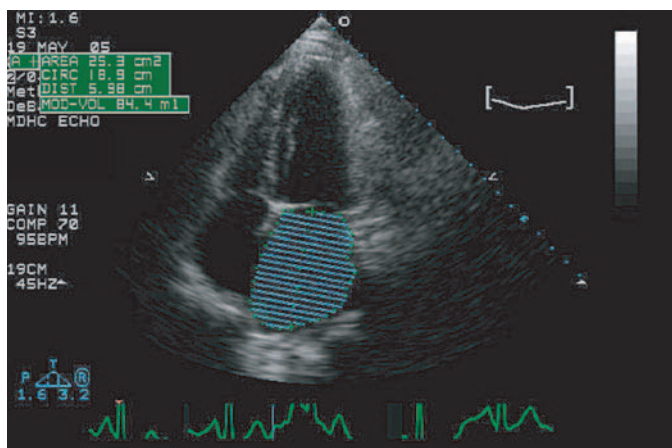


**Figure 5.1** Measurement of maximum left atrial volume by the multiple discs method in the apical four-chamber view.

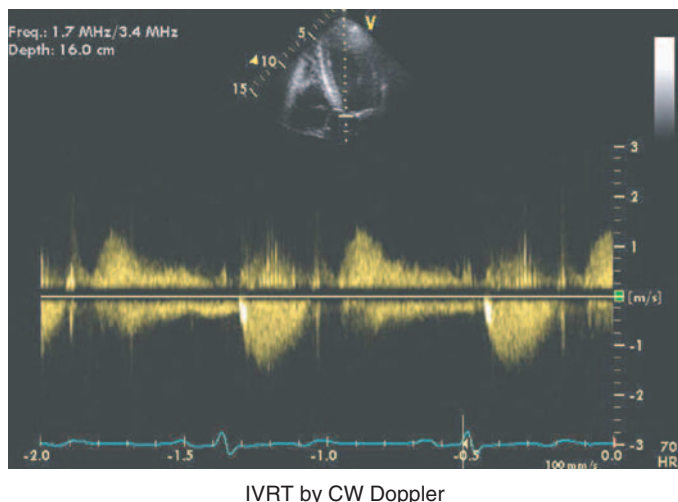


**Figure 5.2** Measurement of isovolumic relaxation time by continuous waves Doppler. The vertical arrows indicate the time interval between aortic valve closure and mitral valve opening.

LA pressure and a positive LA–LV pressure gradient and another phase of antegrade flow: the A velocity. Therefore, in young healthy subjects, the mitral inflow pattern is E-wave dominant with an E/A ratio  $>1.5$  and a short E-wave deceleration time (DT,  $<220$  msec) and IVRT ( $<90$  msec). However, in older subjects with slowing down of LV relaxation rate, the E velocity and the E/A ratio decrease, along with a prolongation of DT and IVRT. Heart rate can also bring about changes in the inflow pattern, such that with tachycardia, the A velocity tends to increase and becomes more dominant [8], resulting in a lower E/A ratio. With a further increase in heart rate, E and A velocities can merge completely, resulting in a single waveform. These rate-dependent changes can pose important limitations to drawing accurate conclusions about LV diastolic function using the mitral inflow profile.

With myocardial disease, sarcoplasmic reticulum  $\text{Ca}^{2+}$  uptake slows down, leading to incomplete LV relaxation, increased early diastolic LV pressures, and reduced transmitral pressure gradient. Accordingly, mitral E velocity and E/A ratio decrease ( $<1$ ), with prolongation of IVRT ( $>90$  msec) and DT ( $>220$  msec). This stage is classified as stage I diastolic dysfunction. To maintain LV filling, LA pressure increases, leading to a positive LA–LV pressure gradient and a higher E velocity than expected for the degree of impaired LV relaxation. In these cases, the mitral inflow pattern is described as pseudonormal, with an E/A ratio  $>1$  along with

an IVRT  $<90$  msec and a DT  $<220$  msec. This stage of diastolic dysfunction is classified as stage II. With further progression of cardiac disease, LV stiffness and diastolic pressures increase, necessitating a further rise in LA pressure to maintain LV filling. The result is an E/A ratio  $>2$  and very short DT ( $<150$  msec) and IVRT ( $<70$  msec) or a *restrictive filling pattern*. This stage of diastolic function is classified as stage III. In advanced cases with markedly elevated LV late diastolic pressures, *diastolic mitral regurgitation* can be observed (Figure 5.3). In stages II and III of LV diastolic dysfunction, the mitral inflow pattern can be reversed to that of stage I by reducing the preload using diuretics (Figure 5.4) or performing a Valsalva maneuver. On the other hand, stage I of diastolic dysfunction can progress to stage II or III by increasing preload. Eventually, a stage is reached when irreversible pathological changes develop, possibly related to loss of viable myocytes and advanced fibrosis [9], where the filling pattern could not be reversed by reducing preload. At this stage, LV diastolic function is stage IV, and portends an ominous outcome [8].

Patients with cardiac disease and LV diastolic dysfunction stages II to IV have increased LV filling pressures, and several equations have been published to predict LV filling pressures based on the mitral inflow profile. These equations are reliable in patients with depressed EF, but are least accurate in patients with normal EF [8,10].

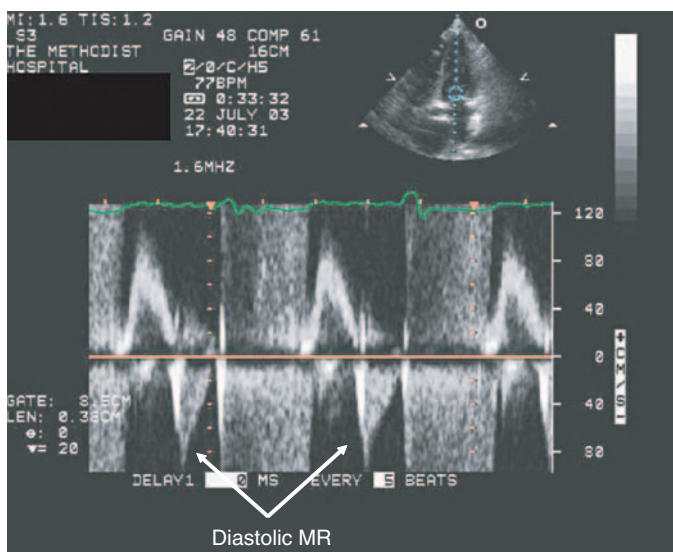


**Figure 5.3** Pulsed-wave Doppler recording of mitral inflow from a patient with markedly elevated left ventricular end-diastolic pressure. The arrows point to diastolic mitral regurgitation signals. MR, mitral regurgitation.

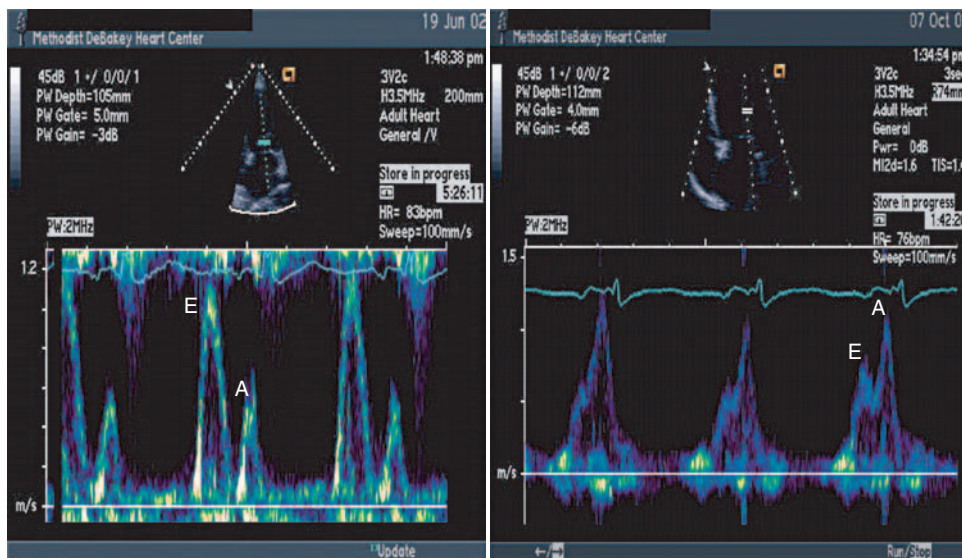


**Figure 5.4** Changes in mitral inflow pattern with medical therapy. Recordings were obtained from a patient with dilated cardiomyopathy. At baseline, there is restrictive LV filling (left). After 3–4 months of oral therapy, the inflow

pattern is one of impaired relaxation, indicating a marked reduction in LV filling pressures. E, early diastolic velocity; A, late diastolic velocity.

### Pulmonary venous flow

Pulmonary venous flow can provide useful insights into LA filling and pressure. The pressure gradient between the pulmonary veins and the LA is the main determinant of pulmonary venous flow. During early systole, LA pressure decreases due to LA relaxation, which results in an S1-wave. Later, another systolic wave is recorded, S2, which is dependent on

RV stroke volume, and the compliance of the pulmonary veins and the LA [11]. Diastolic antegrade flow into the LA occurs due to a decrease in LA pressure with mitral valve opening. Accordingly, with impaired LV relaxation, diastolic forward flow into the LA decreases, with most of the antegrade flow occurring during systole. After LA contraction, LA pressure exceeds pulmonary venous pressure,

leading to flow reversal out of the LA and into the pulmonary veins: Ar velocity. This velocity is dependent on LV late diastolic pressures and LA contractility. In addition, pulmonary venous flow is affected by respiration, heart rate, and age. In normal young subjects, predominant forward flow occurs in diastole (Figure 5.5). With aging, this pattern is reversed and most of the antegrade flow occurs in systole [12]. Therefore, the age of a given patient should be considered when using pulmonary venous flow velocities to draw inferences about LV filling pressures.

In patients with cardiac disease and depressed EF, pulmonary venous flow can be used to predict LA pressure. With normal LA pressure, predominant forward flow occurs in systole, whereas in those with increased filling pressures, predominant flow occurs in diastole [13]. It is possible to express this ratio as time velocity integral of forward systolic flow/total antegrade flow or the systolic filling fraction (SFF). Patients with depressed EF and increased LA pressure, usually have an SFF < 40%. However, the accuracy of SFF is compromised in patients with normal EF [10], hypertrophic cardiomyopathy [14], nonsinus rhythm [15], and normal young individuals. Other investigators have reported on the diagnostic accuracy of the deceleration time of

the antegrade diastolic flow velocity. These reports were initially encouraging [16], but in our experience, this index is most accurate in patients with depressed (Figure 5.6), but not normal EF [17]. On the other hand, with normal LA contractility, Ar velocity and its duration are directly related to LV late diastolic pressures (LA afterload). As these pressures increase, forward flow across the mitral valve with atrial contraction decreases, whereas reverse flow or Ar velocity in the pulmonary veins becomes more prominent. Furthermore, it is possible to measure the time interval between this velocity and that of mitral A velocity (at annulus level) to predict LV EDP [10,17–19]. An Ar velocity >30 cm/sec and an Ar–A duration >35 msec are usually associated with increased LV EDP (Figure 5.7). Unlike all of the above velocity and time measurements, this interval is not altered by age [12], although impaired atrial function may compromise the Ar velocity.

### Color M-mode flow propagation velocity

Systolic and diastolic flow into the left ventricle can be recorded with color M-mode with a high spatial and temporal resolution. In particular, the flow propagation velocity ( $V_p$ ) in early diastole can be

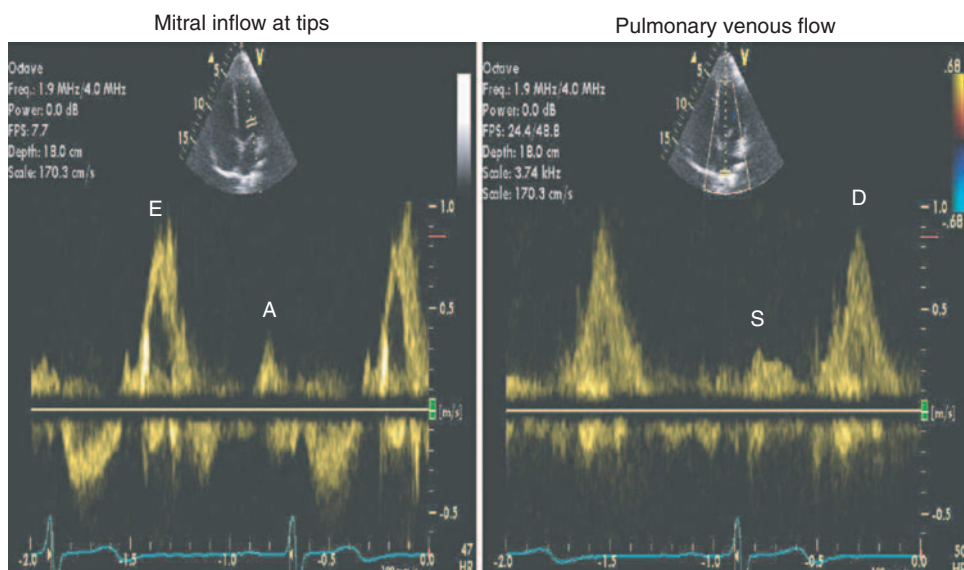


**Figure 5.5** Mitral (left) and pulmonary venous flow (right) recorded from a normal subject. Note the predominant diastolic filling in the mitral inflow profile and the

antegrade diastolic filling in pulmonary venous flow. E, early diastolic velocity; A, late diastolic velocity; S, systolic velocity; D, antegrade diastolic velocity.

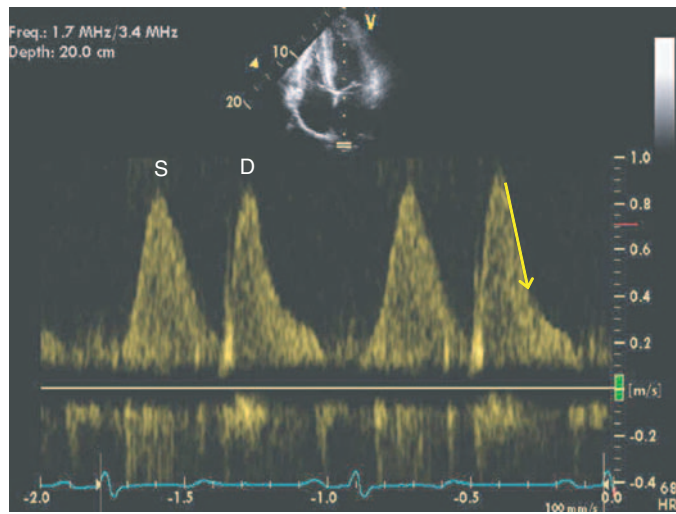


**Figure 5.6** Pulmonary venous recording from a patient with increased left atrial pressure. Notice the steep deceleration time (161 msec) of the diastolic velocity, as indicated by the arrow. S, systolic velocity; D, antegrade diastolic velocity.

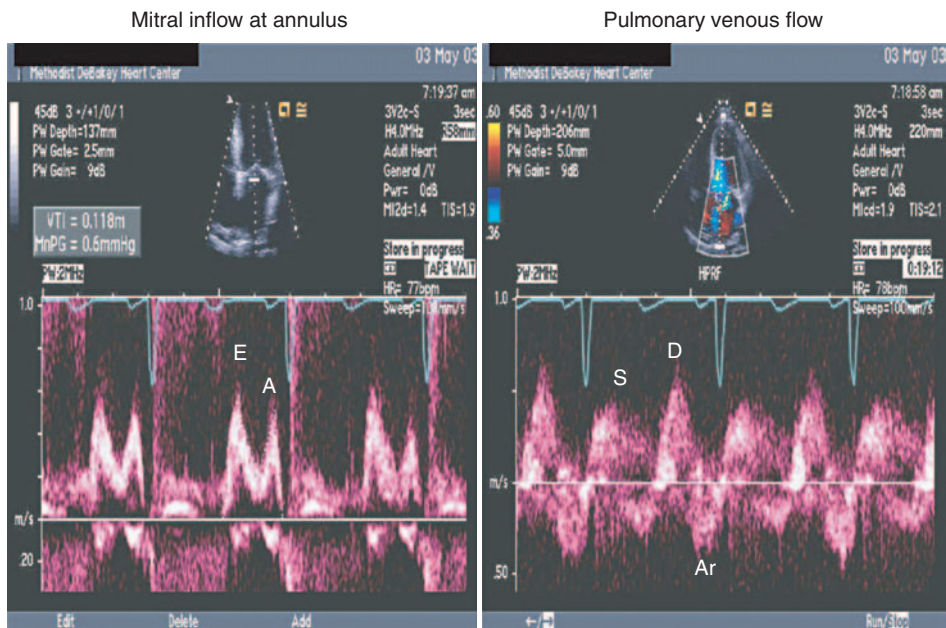


**Figure 5.7** Mitral (left) and pulmonary venous flow (right) from a patient with increased left ventricular end-diastolic pressure. Notice the prominent Ar signal in pulmonary venous flow. Ar-A duration was 60 msec. E, early

diastolic velocity; A, late diastolic velocity; S, systolic velocity; D, antegrade diastolic velocity; Ar, atrial reversal velocity in pulmonary veins.

measured and used as an index of LV relaxation. V<sub>p</sub> can be measured using at least two different approaches. The first is to measure the slope of the transition from no color to color [15,20]. In the second approach, the slope of the first aliasing velocity from the mitral tips to a point 4 cm distally into the

left ventricle is measured [21]. Here, it is important to have an aliasing zone, and it is possible to obtain a clear aliasing zone by using baseline shift. Animal [22,23] and human [20,22–24] studies have shown a significant inverse correlation between V<sub>p</sub> and the time constant of LV relaxation. However, whereas

the published animal studies have shown no significant effect of preload on Vp [22], human reports were not consistent. In fact, there are studies in patients with normal [25] and depressed [26] EF, showing Vp to be positively affected by preload. Other determinants of Vp include LV volumes, particularly end-systolic volume [27], and heart rate.

Vp has been used in conjunction with transmitral E velocity to correct for the influence of LV relaxation on mitral E and, thus, predict LV filling pressures [21]. E/Vp is useful in patients with depressed EF (Figure 5.8), where a ratio of 2.5 appears most accurate in identifying patients with mean wedge pressure >15 mm Hg, with a sensitivity of 78% and a specificity of 77% [17]. However, it can lead to erroneous results in patients with normal EF [17]. This limitation of Vp is likely due to the confounding effect of LV end-systolic volume on its relation with LV relaxation, such that patients with normal (or hyperdynamic) EF, and normal or reduced end-systolic volume, yet impaired LV relaxation, can have a normal or increased Vp velocity [27], which fails to uncover the presence of reduced LV relaxation and, thus, cannot correct for the influence of relaxation on mitral E velocity.

## Role of tissue Doppler imaging in assessment of left ventricular filling pressure

### Mitral annulus early diastolic velocity (Ea)

The motion of the mitral annulus mirrors the composite movement of the left ventricle in the longitudinal direction. The left ventricle moves toward the apex in systole and recoils toward the base during diastole. Using M-mode recordings, Feigenbaum et al. evaluated the amplitude of mitral annular motion as an index of LV systolic function almost four decades ago [28]. Using tissue Doppler, mitral annular velocity signals can be recorded in the vast majority of subjects from an apical transducer position. Tissue Doppler is based on filtering out the low-amplitude, high-frequency signals caused by blood flow, but keeping the lower frequency, high-amplitude signals of myocardial origin. During systole, two signals can be recorded: one during isovolumic contraction ( $S_{IVC}$ ) and the other during ejection (Sa). During diastole, two signals are usually recorded in patients with sinus rhythm: an early diastolic velocity (Ea) and a late

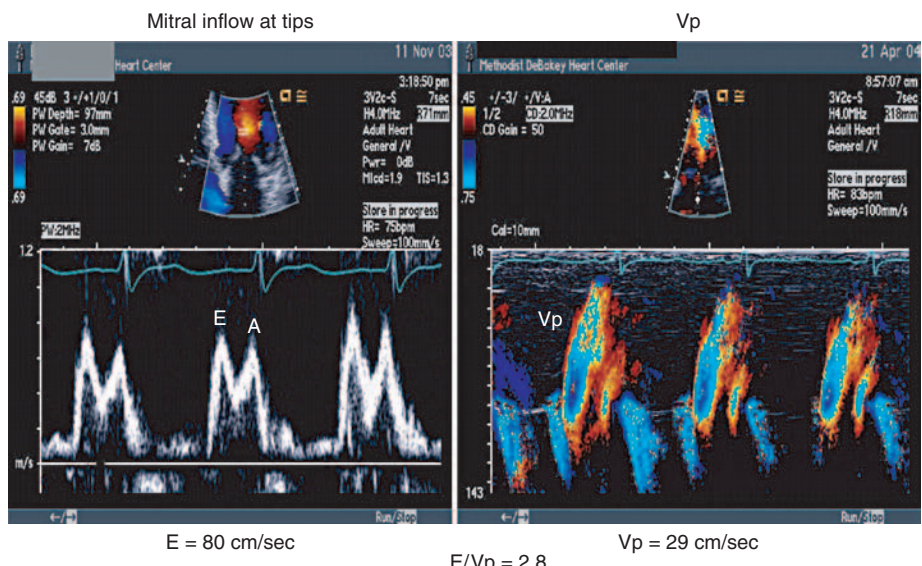


**Figure 5.8** Mitral inflow (left) and Vp velocity by color M-mode (right) from a patient with LV systolic dysfunction and pseudonormal LV filling pattern. Notice that the E/Vp ratio is increased at 2.8, indicative of increased LV filling pressures. E, early diastolic velocity; A, late diastolic velocity; Vp, early diastolic flow propagation velocity by color M-mode.

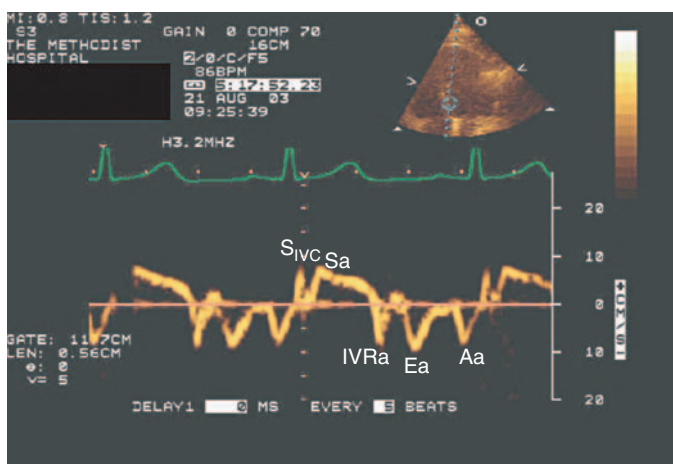


**Figure 5.9** Tissue Doppler signals from the septal side of the mitral annulus.  $S_{IVC}$ , systolic velocity during isovolumic contraction; Sa, systolic velocity during ejection; IVRa, diastolic annular velocity during the isovolumic relaxation period; Ea, early diastolic mitral annulus velocity; Aa, late diastolic mitral annulus velocity.

diastolic velocity (Aa). In addition, a diastolic velocity can be observed during the isovolumic relaxation period (Figure 5.9). Many published studies have examined the utility of Ea as an index of LV relaxation. Whereas Ea is usually recorded by pulsed-wave tissue Doppler for the assessment of LV diastolic function, it can also be recorded by 2-D color tissue Doppler. However, Ea by color Doppler is indicative of the mean and not the peak velocity value [29] and, as such, is lower than Ea by pulsed Doppler. Because the validation studies with Ea used pulsed Doppler, this is the recommended technique to acquire Ea for the subsequent estimation of LV filling pressures.

There are several observations that support the use of Ea for the assessment of LV relaxation. To start with, Ea velocity decreases with age [30] and has a significant correlation with invasive indices of LV relaxation in animal [31,32] and human [33–35] studies. In addition, myocardial Ea velocity is directly related to the beta-adrenergic receptor density [36] and inversely to the extent of interstitial fibrosis [36] and local tumor necrosis factor- $\alpha$  and inducible nitric oxide synthase levels in patients with coronary artery disease [37]. The values of Ea at different mitral annulus sites are different. Ea is higher at the lateral mitral annulus than at the septal annulus. Therefore, the cutoff values of Ea for predicting impaired relaxation are different when using different mitral annulus sites. In patients <60 years old, an Ea <8.5 cm/sec at septal annulus or <10 cm/sec at the lateral annulus is usually associated with impaired LV relaxation.

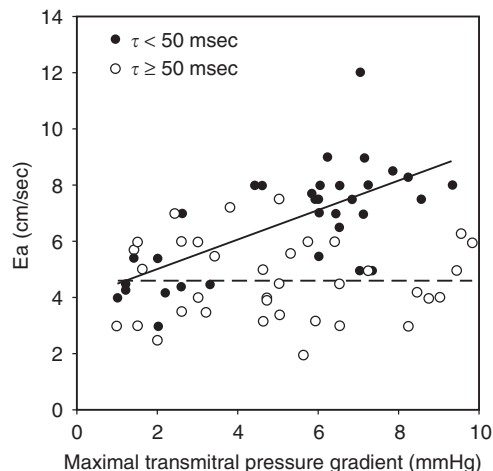


**Figure 5.10** Relation between maximal transmural pressure gradient and Ea velocity in the presence of normal or enhanced LV relaxation (solid circles and continuous line), and impaired left ventricular relaxation (open circles and interrupted line). Reproduced with permission from Nagueh et al. [31].

However, the relation of Ea with preload is not a simple one. In the presence of normal or enhanced LV relaxation, Ea is directly related to filling pressures [31,32]. However, in the presence of impaired LV relaxation, preload appears to have minimal influence on Ea [31,32] (Figure 5.10). The latter finding accounts for the reasonable accuracy of Ea in identifying patients with diastolic dysfunction and pseudonormal LV filling [30], as well as its use with mitral E in the E/Ea ratio (Figure 5.11) to predict LV filling pressures [17,30,35] (Figure 5.12).

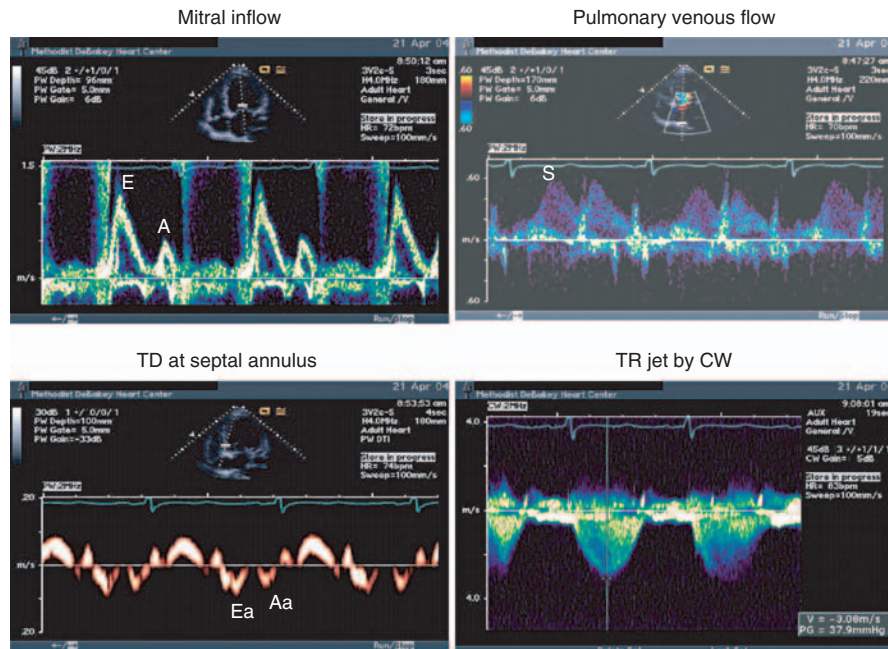


**Figure 5.11** Doppler signals from a patient with increased left ventricular filling pressures. Upper left image shows mitral inflow with an E/A ratio  $>2$ . Upper right image shows pulmonary venous flow. Notice that systolic (S) and diastolic (D) antegrade velocities are almost equal; therefore, the systolic filling fraction is not indicative of increased filling pressures. Lower left image shows tissue Doppler (TD) velocities

at the septal side of the mitral annulus with an Ea velocity of 8 cm/sec, and E/Ea ratio of 15. Lower right image shows the tricuspid regurgitation (TR) jet with a peak velocity of 3.1 cm/sec, corresponding to a pulmonary artery systolic pressure of at least 38 mmHg (not taking into consideration right atrial pressure).

This ratio was examined in several patient groups and by many investigators, including in patients with tachycardia [38,39], hypertrophic cardiomyopathy [14], cardiac transplants [40], and atrial fibrillation [41].

For clinical application, one needs to take into consideration, the presence or absence of cardiac disease, LV EF, presence or absence of regional dysfunction, presence or absence of mitral valve/annular disease, and heart rate/cardiac rhythm. For patients without cardiac disease, Ea is not a reliable index of LV relaxation and the ratio should not be used to predict filling pressures. This finding is due to the direct relation between filling pressures and Ea in subjects with normal LV relaxation [42].

In patients with LV systolic dysfunction, the E/Ea ratio can be used to estimate LV filling pressures. When using septal Ea, an E/Ea ratio of 20 provides the highest accuracy [17] in identifying patients with mean wedge pressure  $>15$  mmHg, with a specificity of 88% but a sensitivity of 59%.

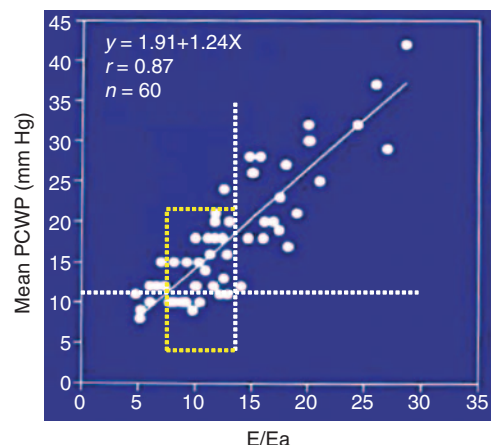


**Figure 5.12** Relation between wedge pressure and E/Ea ratio in 60 patients with cardiac disease. Notice that, for a ratio of 8, most patients had a mean wedge pressure  $\leq 12$  mmHg, whereas for a ratio  $>15$ , most patients had a mean wedge pressure  $>12$  mmHg. However, for an E/Ea ratio of 8–15 (outlined by the box in the graphic display), a wide scatter is present, and patients may have a normal or increased wedge pressure. PCWP, pulmonary capillary wedge pressure.

On the other hand, with lateral Ea, a ratio of 11 appears most accurate [17], with a sensitivity of 85% and a specificity of 82%. When an average (anterior, inferior, septal, and lateral) Ea velocity is available [17], a cutoff value of 15 should be considered (sensitivity of 74% and specificity of 82%). For patients with normal EF, lateral Ea is preferable and a cutoff E/Ea ratio of 10 (sensitivity 79%, specificity 80%) can be used to identify patients with increased filling pressures [17].

The presence of regional dysfunction is a challenge for the accuracy of the E/Ea ratio. This finding is the result of different regional Ea velocity values (Figure 5.13) because of local dysfunction or normal/compensatory hyperdynamic function in sites not involved with ischemia/MI [43]. Accordingly, the use of an average Ea velocity is essential in these cases, and a simplified approach with the average of only septal and lateral Ea velocities can provide a reasonable estimate [17], although this remains a limitation for the accuracy of this method in many cases.

In patients with moderate to severe annular calcification, and those with mitral stenosis, Ea can be reduced despite the presence of normal LV

relaxation [44]. Conversely, in patients with hemodynamically significant mitral regurgitation (MR) and normal EF (and even in some patients with MR and depressed EF), Ea can be increased despite impaired LV relaxation [44,45]. Accordingly, the E/Ea ratio should not be used in these patient groups, and other indices should be used instead (see below).

The presence of sinus tachycardia poses challenges to the estimation of LV filling pressures by Doppler. This finding is due in part to the merging of mitral velocities, and at times, complete merging with a single velocity is observed [38,39]. However, in several patients, annular velocities can be still be identified with separate Ea and Aa peaks, and the E/Ea ratio (Figure 5.14) can provide a reasonable estimate of filling pressures [38,39]. Similar to the performance of most of the Doppler approaches in patients with normal EF, the accuracy of E/Ea is lower in patients with sinus tachycardia and normal EF. This finding is likely related to the inclusion of normal subjects, lower accuracy of mitral E velocity by itself in this group, and potentially the confounding effect of tachycardia on Ea. In an animal model, right atrial pacing was used to increase

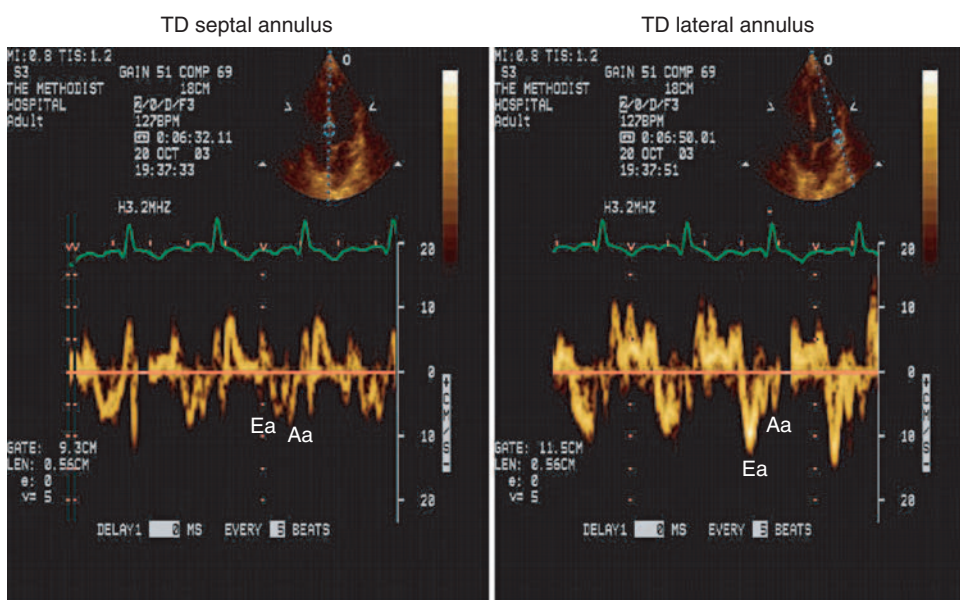


**Figure 5.13** Tissue Doppler (TD) signals from a patient with an anteroseptal myocardial infarction. Notice that, while septal Ea is 6 cm/sec, lateral Ea is increased at 13 cm/sec. In this case, the average of septal and lateral Ea is a better

indicator of left ventricular relaxation. Ea, early diastolic mitral annulus velocity; Aa, late diastolic mitral annulus velocity.

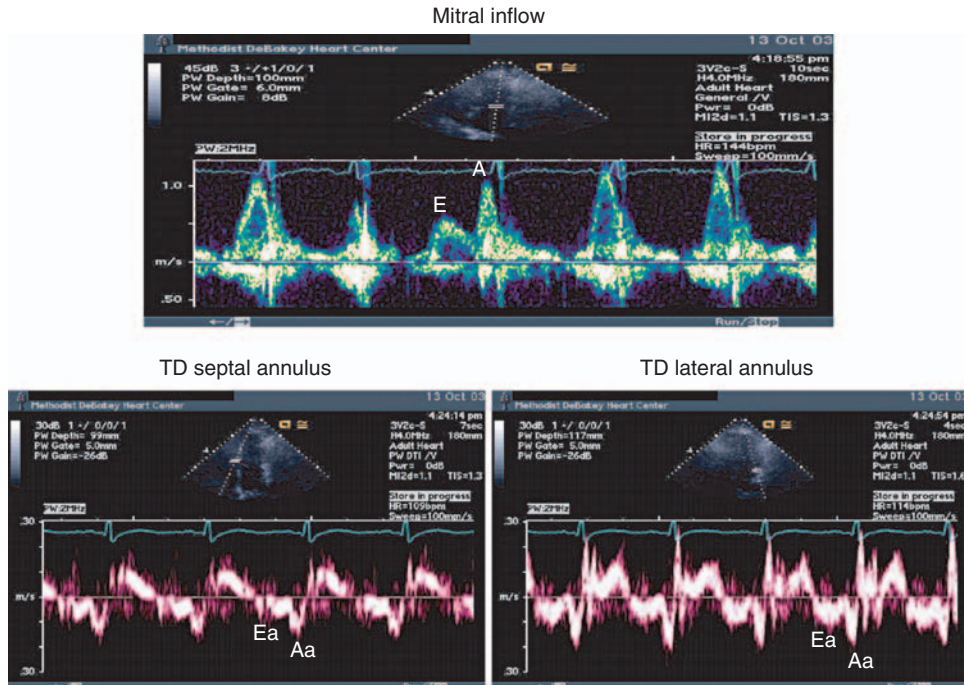


**Figure 5.14** Doppler signals from a patient with sinus tachycardia. Upper image shows the mitral inflow profile. Notice the complete merging of E and A velocities, resulting in a late peaking single velocity for most of the recorded beats. However, the second beat is an atrial premature beat that is followed by a compensatory pause. As a result, the underlying mitral filling pattern of impaired relaxation (stage I diastolic dysfunction) is

readily appreciated in the third cycle. Tissue Doppler (TD) signals from the septal side of the mitral annulus (left) and the lateral side (right) are shown in the lower panel. Ea velocity at either side is ~10 cm/sec, and the E/Ea ratio is 5, which is indicative of normal/reduced left ventricular filling pressures. Ea, early diastolic mitral annulus velocity; Aa, late diastolic mitral annulus velocity.

heart rate, and tachycardia was observed to lower Ea velocity through a decrease in the transmитral pressure gradient despite a normal LV relaxation [43].

### Other tissue Doppler-based measurements

Given the above limitations of E/Ea, other tissue Doppler-based indexes have been investigated for clinical utility. One of these indexes is the time difference between the onset of mitral inflow E velocity and the onset of mitral annulus Ea velocity ( $T_{E-Ea}$ ). In patients with impaired LV relaxation, the onset of Ea is delayed due to prolonged relaxation. However, the increased LA pressure leads to earlier opening of the mitral valve and, thus, an earlier onset of mitral E velocity. Consequently, mitral annulus Ea occurs later than mitral E velocity (Figure 5.15). This time interval, or  $T_{E-Ea}$ , has been shown to have a significant correlation with

the time constant of LV relaxation in animal [32,46] and human [46] studies. Furthermore, given the dependence of IVRT (see above) on LV relaxation and LA pressure, the ratio of IVRT to  $T_{E-Ea}$  can be used to predict LV filling pressures [44,46]. The complete relation between these variables is given by the equation:

$$\text{LA pressure} = \text{LV}_{es} \times e^{-IVRT/T_{E-Ea}}$$

where  $\text{LV}_{es}$  is LV end-systolic pressure, which can be derived noninvasively as  $0.9 \times$  systolic blood pressure. In the absence of mitral valve disease, an  $\text{IVRT}/(T_{E-Ea})$  ratio  $<2$  predicts  $\text{PCWP} > 15 \text{ mm Hg}$  with high accuracy. Furthermore, using this approach, LA pressure can be estimated in patients with mitral regurgitation and stenosis where the E/Ea ratio has major limitations [44]. In patients with mitral regurgitation, an  $\text{IVRT}/(T_{E-Ea})$  ratio  $<5.59$  predicts a mean  $\text{PCWP} > 15 \text{ mmHg}$  with

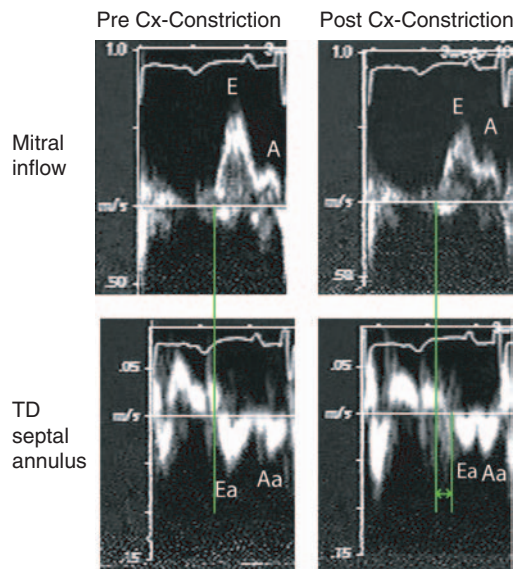


**Figure 5.15** Recording of mitral inflow and tissue Doppler (TD) velocities at septal side of mitral annulus from an experimental study. The left panel shows the signals at baseline, and the right panel shows the signals after left ventricular dysfunction due to constriction of the circumflex coronary artery (Cx). At baseline, mitral E and annular Ea occurred simultaneously. However, after constriction of the circumflex coronary artery, Ea was reduced and delayed. Reproduced with permission from Rivas-Gotz et al. [46].

high accuracy, irrespective of LV EF. Likewise, in patients with mitral stenosis, a ratio  $<4.16$  is highly accurate in identifying increased filling pressures [44]. Aside from  $T_{E-Ea}$ , the absolute value of the time to onset of Ea can be useful by itself for the assessment of LV relaxation [43,47]. In one study, the time interval between aortic valve closure and peak Ea in the mid-posterior wall had a strong correlation with  $\tau$  in patients with hypertension [47].

It is possible to derive the mitral annulus peak (and mean) acceleration rate during the isovolumic relaxation period and early diastolic filling from the mitral annulus velocity spectrum. In an animal study, the peak acceleration rate during the isovolumic relaxation period at the septal side of the mitral annulus has been shown to correlate well with  $LV - dP/dt$  and  $\tau$ , but not with LA pressure [48], that is, it behaves as an index of LV relaxation that is preload-independent. On the contrary, in the same

study, peak acceleration during early LV filling was closely related to LA pressure, but not  $LV - dP/dt$  or  $\tau$ , that is, an index of LV filling pressures only [48]. However, we noted in an animal model with a wide range of loading conditions that the peak and mean acceleration rates of Ea (early diastolic filling) have a positive correlation with the transmural pressure gradient only in the stages with normal or enhanced LV relaxation, but with no relation when  $\tau$  was  $\geq 50$  msec [49]. Furthermore, in cardiac patients, the peak acceleration rate of Ea was an index of LV relaxation rather than filling pressures and provided no incremental information over the Ea velocity alone [49].

In addition to early diastolic measurements, Aa can also be used to gain insight into LV filling pressures. Aa is primarily determined by LA systolic function and afterload, that is, LV end-diastolic pressure. Aa is reduced in patients with increased LV EDP. This correlation is most useful in patients with depressed EF [50], but is less accurate when LV EF is normal [17]. However, overall, it appears to offer limited incremental information over other Doppler measurements, although in one study [50], an Aa velocity  $<5$  cm/sec was a powerful independent predictor of death or hospitalization for worsening congestive heart failure.

### Doppler estimation of left ventricular filling pressures in atrial fibrillation

In atrial fibrillation, there are several limitations to many of the above indices. These limitations include the absence of A velocity in mitral and pulmonary venous flow signals and Aa in tissue Doppler velocity curves. Likewise, LA volumes and the systolic filling fraction have limited accuracy. In addition, LV filling shows beat to beat variation. Despite these limitations, it is still possible to estimate LV filling pressures. Similar to patients in sinus rhythm with depressed EF, DT of the mitral diastolic velocity can be applied [15,51]. Other useful parameters include the peak acceleration rate of the mitral diastolic velocity and IVRT [15]. Data averaged from 10 consecutive cycles provide the highest accuracy, whereas measurements from a single cycle corresponding to the average heart rate provide a reasonable approximation [15]. In addition, it is useful to look at the variability of the mitral diastolic velocity with the RR cycle length (Figure 5.16),

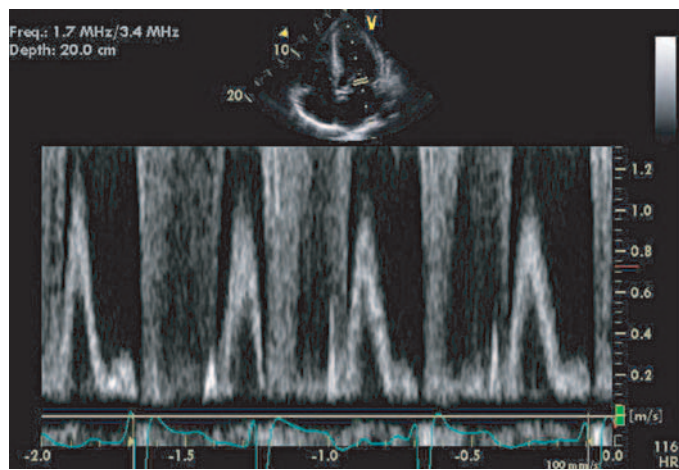


**Figure 5.16** Mitral inflow from a patient with atrial fibrillation and increased LV filling pressures. Notice that there is minimal beat to beat variation in the mitral diastolic peak velocity, despite the varying RR intervals.

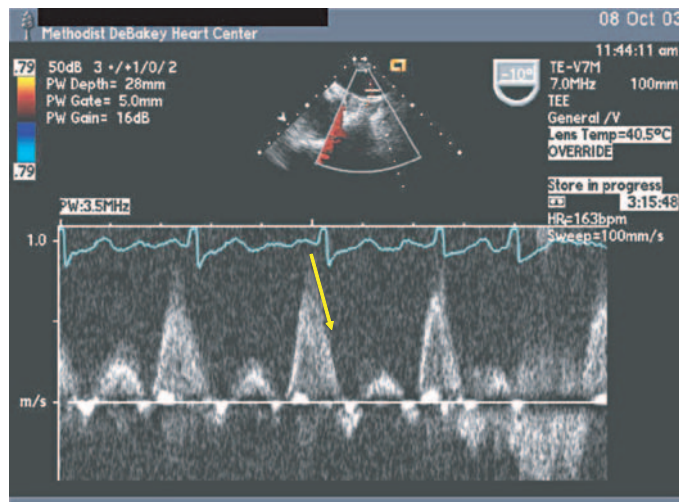


**Figure 5.17** Pulmonary venous flow from a patient with atrial fibrillation and increased LV filling pressures. Notice the steep deceleration (arrow) and short deceleration time (DT) of the diastolic velocity.

at least qualitatively, as patients with increased filling pressures have less beat to beat variation in the mitral velocity [15]. Additional methods of potential utility include DT of pulmonary venous diastolic velocity [52] (Figure 5.17), E/Vp ratio [15], and E/Ea ratio [41], albeit with only modest correlations with filling pressures.

### Prognostic power of E/Ea

E/Ea ratio can predict exercise capacity in different pathophysiologic conditions and across several age groups. In cardiac patients, elevated LV filling pressures rather than slow relaxation per se impair exercise capacity, and among patients with prolonged LV relaxation, only those with  $E/Ea \geq 10$  have objective

evidence of reduced exercise tolerance [53]. In another study that examined the determinants of exercise tolerance in patients with mitral regurgitation, the independent determinants were higher E/Ea ratio, atrial fibrillation, and reduced forward stroke volume [54]. Similar findings were noted in patients with atrial fibrillation [55].

Aside from predicting symptoms and exercise tolerance, Ea velocity [56,57] and E/Ea ratio [58–61] provide independent prognostic information with respect to cardiac morbidity and mortality in patients hospitalized with congestive heart failure [58], acute myocardial infarction [59], atrial fibrillation [60], and end-stage renal failure [61]. In these studies, an Ea velocity  $<3$  cm/sec and

an E/Ea ratio  $>15$  were significant independent predictors of cardiac events, including hospitalization and death. Likewise, the predictive power of this ratio was shown in children with hypertrophic cardiomyopathy, where E/Ea ratio readily predicted adverse clinical outcomes, including death, cardiac arrest, ventricular tachycardia, and significant cardiac symptoms [62].

## Future research

Myocardial velocity measurements are affected by translation and tethering, aside from intrinsic myocardial function at the site of acquisition. Accordingly, segments adjacent to an area of infarction may have abnormally low velocities, despite normal systolic and diastolic function. For the same reason, mitral annulus velocities can be altered (see above) in the presence of regional dysfunction, compromising the accuracy of E/Ea ratio for the prediction of LV filling pressures. In that regard, deformation indexes (strain rate and strain) that are not affected by tethering and translation can be more helpful. Recently, it became feasible to obtain these measurements by ultrasound using either the Doppler principle or tissue speckle tracking. Several animal and human studies have validated the systolic measurements, but there are very limited data on the evaluation of diastolic function by strain rate imaging. In particular, two studies in humans have been published showing the significant correlation between early diastolic strain rate and V<sub>p</sub>,  $\tau$ , and LV end-diastolic pressure in patients with hypertrophic cardiomyopathy [63,64]. In an attempt to obtain a global measurement from each of the segmental strain rate values, investigators used the average from 12 or 16 myocardial segments [64]. However, this approach is cumbersome. Alternatively, global strain and strain rate curves can be obtained using tissue speckle tracking, by considering the total myocardium as the region of interest [65]. We recently investigated the utility of global diastolic strain rate for the assessment of LV relaxation and noticed that the strain rate signal during the isovolumic relaxation period was significantly correlated with invasive indices of LV relaxation, but not LV end-diastolic pressure. However, global strain rate during early diastolic filling showed a significant positive correlation

with LV filling pressures [66]. The clinical application of these indices appears promising, providing incremental value in humans.

## References

- Owan TE, Hodge DO, Herges RM, Jacobsen SJ, Roger VL, Redfield MM. Trends in prevalence and outcome of heart failure with preserved ejection fraction. *N Engl J Med* 2006; **355**: 251–9.
- Bhatia RS, Tu JV, Lee DS, et al. Outcome of heart failure with preserved ejection fraction in a population-based study. *N Engl J Med* 2006; **355**: 260–9.
- Szlachcic J, Massie BM, Kramer BL, Topic N, Tubau J. Correlates and prognostic implication of exercise capacity in chronic congestive heart failure. *Am J Cardiol* 1985; **55**: 1037–42.
- Mehra MR. Optimizing outcomes in the patient with acute decompensated heart failure. *Am Heart J* 2006; **151**: 571–9.
- Yamamoto K, Nishimura RA, Redfield MM. Assessment of mean left atrial pressure from the left ventricular pressure tracing in patients with cardiomyopathies. *Am J Cardiol* 1996; **78**: 107–10.
- Tsang TS, Barnes ME, Gersh BJ, Bailey KR, Seward JB. Left atrial volume as a morphophysiologic expression of left ventricular diastolic dysfunction and relation to cardiovascular risk burden. *Am J Cardiol* 2002; **90**: 1284–9.
- Lester SJ, Ryan EW, Schiller NB, Foster E. Best method in clinical practice and in research studies to determine left atrial size. *Am J Cardiol* 1999; **84**: 829–32.
- Nishimura RA, Tajik AJ. Evaluation of diastolic filling of left ventricle in health and disease: Doppler echocardiography is the clinician's Rosetta Stone. *J Am Coll Cardiol* 1997; **30**: 8–18.
- Yong Y, Nagueh SF, Shimoni S, et al. Deceleration time in ischemic cardiomyopathy: relation to echocardiographic and scintigraphic indices of myocardial viability and functional recovery after revascularization. *Circulation* 2001; **103**: 1232–7.
- Yamamoto K, Nishimura RA, Chaliki HP, Appleton CP, Holmes DR Jr, Redfield MM. Determination of left ventricular filling pressure by Doppler echocardiography in patients with coronary artery disease: critical role of left ventricular systolic function. *J Am Coll Cardiol* 1997; **30**: 1527–33.
- Appleton CP. Hemodynamic determinants of Doppler pulmonary venous flow velocity components: new insights from studies in lightly sedated normal dogs. *J Am Coll Cardiol* 1997; **30**: 1562–74.
- Klein AL, Abdalla I, Murray RD, et al. Age independence of the difference in duration of pulmonary venous atrial

- reversal flow and transmural A-wave flow in normal subjects. *J Am Soc Echocardiogr* 1998; **11**: 458–65.
- 13 Kuecherer HF, Muhiudeen IA, Kusumoto FM, et al. Estimation of mean left atrial pressure from transesophageal pulsed Doppler echocardiography of pulmonary venous flow. *Circulation* 1990; **82**: 1127–39.
  - 14 Nagueh SF, Lakkis NM, Middleton KJ, Spencer WH III, Zoghbi WA, Quinones MA. Doppler estimation of left ventricular filling pressures in patients with hypertrophic cardiomyopathy. *Circulation* 1999; **99**: 254–61.
  - 15 Nagueh SF, Kopelen HA, Quinones MA. Doppler estimation of left ventricular filling pressure in patients with atrial fibrillation. *Circulation* 1996; **94**: 2138–45.
  - 16 Kinnaird TD, Thompson CR, Munt BI. The deceleration time of pulmonary venous diastolic flow is more accurate than the pulmonary artery occlusion pressure in predicting left atrial pressure. *J Am Coll Cardiol* 2001; **37**: 2025–30.
  - 17 Rivas-Gotz C, Manolios M, Thohan V, Nagueh SF. Impact of left ventricular ejection fraction on estimation of left ventricular filling pressures using tissue Doppler and flow propagation velocity. *Am J Cardiol* 2003; **91**: 780–4.
  - 18 Rossvoll O, Hatle LK. Pulmonary venous flow velocities recorded by transthoracic Doppler ultrasound: relation to left ventricular diastolic pressures. *J Am Coll Cardiol* 1993; **21**: 1687–96.
  - 19 Appleton CP, Galloway JM, Gonzalez MS, Gaballa M, Basnight MA. Estimation of left ventricular filling pressures using two-dimensional and Doppler echocardiography in adult patients with cardiac disease. Additional value of analyzing left atrial size, left atrial ejection fraction and the difference in duration of pulmonary venous and mitral flow velocity at atrial contraction. *J Am Coll Cardiol* 1993; **22**: 1972–82.
  - 20 Brun P, Tribouilloy C, Duval AM, et al. Left ventricular flow propagation during early filling is related to wall relaxation: a color M-mode Doppler analysis. *J Am Coll Cardiol* 1992; **20**: 420–32.
  - 21 Garcia MJ, Ares MA, Asher C, Rodriguez L, Vandervoort P, Thomas JD. An index of early left ventricular filling that combined with pulsed Doppler peak E velocity may estimate capillary wedge pressure. *J Am Coll Cardiol* 1997; **29**: 448–54.
  - 22 Garcia MJ, Smedira NG, Greenberg NL, et al. Color m-mode Doppler flow propagation velocity is a preload insensitive index of left ventricular relaxation: animal and human validation. *J Am Coll Cardiol* 2000; **35**: 201–8.
  - 23 Stugaard M, Smiseth OA, Risoe C, Ihlen H. Intraventricular early diastolic filling during acute myocardial ischemia, assessment by multigated color m-mode Doppler echocardiography. *Circulation* 1993; **88**: 2705–13.
  - 24 Takatsuji H, Mikami T, Urasawa K, et al. A new approach for evaluation of left ventricular diastolic function: spatial and temporal analysis of left ventricular filling flow propagation by color M-mode Doppler echocardiography. *J Am Coll Cardiol* 1996; **27**: 365–71.
  - 25 Graham RJ, Gelman JS, Donelan L, Mottram PM, Peverill RE. Effect of preload reduction by haemodialysis on new indices of diastolic function. *Clin Sci (Lond)* 2003; **105**: 499–506.
  - 26 Troughton RW, Prior DL, Frampton CM, et al. Usefulness of tissue Doppler and color M-mode indexes of left ventricular diastolic function in predicting outcomes in systolic left ventricular heart failure (from the ADEPT Study). *Am J Cardiol* 2005; **96**: 257–62.
  - 27 Ohte N, Narita H, Akita S, Kurokawa K, Hayano J, Kimura G. Striking effect of left ventricular systolic performance on propagation velocity of left ventricular early diastolic filling flow. *J Am Soc Echocardiogr* 2001; **14**: 1070–4.
  - 28 Feigenbaum H, Zaky A, Nasser WK. Use of ultrasound to measure left ventricular stroke volume. *Circulation* 1967; **35**: 1092–9.
  - 29 McCulloch M, Zoghbi WA, Davis R, Thomas C, Dokainish H. Color tissue Doppler myocardial velocities consistently underestimate spectral tissue Doppler velocities: impact on calculation peak transmural pulsed Doppler velocity/early diastolic tissue Doppler velocity (E/Ea). *J Am Soc Echocardiogr* 2006; **19**: 744–8.
  - 30 Nagueh SF, Middleton KJ, Kopelen HA, Zoghbi WA, Quinones MA. Doppler tissue imaging: a noninvasive technique for evaluation of left ventricular relaxation and estimation of filling pressures. *J Am Coll Cardiol* 1997; **30**: 1527–33.
  - 31 Nagueh SF, Sun H, Kopelen HA, Middleton KJ, Khoury DS. Hemodynamic determinants of the mitral annulus diastolic velocities by tissue Doppler. *J Am Coll Cardiol* 2001; **37**: 278–85.
  - 32 Hasegawa H, Little WC, Ohno M, et al. Diastolic mitral annular velocity during the development of heart failure. *J Am Coll Cardiol* 2003; **41**: 1590–7.
  - 33 Sohn DW, Chai IH, Lee DJ, et al. Assessment of mitral annulus velocity by Doppler tissue imaging in the evaluation of left ventricular diastolic function. *J Am Coll Cardiol* 1997; **30**: 474–80.
  - 34 Oki T, Tabata T, Yamada H, et al. Clinical application of pulsed Doppler tissue imaging for assessing abnormal left ventricular relaxation. *Am J Cardiol* 1997; **79**: 921–8.
  - 35 Ommen SR, Nishimura RA, Appleton CP, et al. Clinical utility of Doppler echocardiography and tissue Doppler imaging in the estimation of left ventricular filling pressures: a comparative simultaneous Doppler-catheterization study. *Circulation* 2000; **102**: 1788–94.

- 36 Shan K, Bick RJ, Poindexter BJ, et al. Relation of tissue Doppler derived myocardial velocities to myocardial structure and beta-adrenergic receptor density in humans. *J Am Coll Cardiol* 2000; **36**: 891–6.
- 37 Kalra DK, Ramchandani M, Zhu X, et al. Relation of tissue Doppler-derived myocardial velocities to serum levels and myocardial gene expression of tumor necrosis factor-alpha and inducible nitric oxide synthase in patients with ischemic cardiomyopathy having coronary artery bypass grafting. *Am J Cardiol* 2002; **90**: 708–12.
- 38 Nagueh SF, Mikati I, Kopelen HA, Middleton KJ, Quinones MA, Zoghbi WA. Doppler estimation of left ventricular filling pressure in sinus tachycardia. A new application of tissue Doppler imaging. *Circulation* 1998; **98**: 1644–50.
- 39 Sohn DW, Kim YJ, Kim HC, Chun HG, Park YB, Choi YS. Evaluation of left ventricular diastolic function when mitral E and A waves are completely fused: role of assessing mitral annulus velocity. *J Am Soc Echocardiogr* 1999; **12**: 203–8.
- 40 Sundereswaran L, Nagueh SF, Vardan S, et al. Estimation of left and right ventricular filling pressures after heart transplantation by tissue Doppler imaging. *Am J Cardiol* 1998; **82**: 352–7.
- 41 Sohn DW, Song JM, Zo JH, et al. Mitral annulus velocity in the evaluation of left ventricular diastolic function in atrial fibrillation. *J Am Soc Echocardiogr* 1999; **12**: 927–31.
- 42 Firstenberg MS, Levine BD, Garcia MJ, et al. Relationship of echocardiographic indices to pulmonary capillary wedge pressures in healthy volunteers. *J Am Coll Cardiol* 2000; **36**: 1664–9.
- 43 Nagueh SF, Rao L, Soto J, Middleton KJ, Khoury DS. Haemodynamic insights into the effects of ischaemia and cycle length on tissue Doppler-derived mitral annulus diastolic velocities. *Clin Sci (Lond)* 2004; **106**: 147–54.
- 44 Diwan A, McCulloch M, Lawrie G, Reardon MJ, Nagueh SF. Doppler estimation of left ventricular filling pressures in patients with mitral valve disease. *Circulation* 2005; **111**: 3281–9.
- 45 Bruch C, Stypmann J, Gradaus R, Breithardt G, Wichter T. Usefulness of tissue Doppler imaging for estimation of filling pressures in patients with primary or secondary pure mitral regurgitation. *Am J Cardiol* 2004; **83**: 324–8.
- 46 Rivas-Gotz C, Khoury DS, Manolios M, Rao L, Kopelen HA, Nagueh SF. Time interval between onset of mitral inflow and onset of early diastolic velocity by tissue Doppler: a novel index of left ventricular relaxation: experimental studies and clinical application. *J Am Coll Cardiol* 2003; **42**: 1463–70.
- 47 Oki T, Tabata T, Yamada H, et al. Left ventricular diastolic properties of hypertensive patients measured by pulsed tissue Doppler imaging. *J Am Soc Echocardiogr* 1998; **11**: 1106–12.
- 48 Hashimoto I, Bhat AH, Li X, et al. Tissue Doppler-derived myocardial acceleration for evaluation of left ventricular diastolic function. *J Am Coll Cardiol* 2004; **44**: 1459–66.
- 49 Ruan Q, Rao L, Middleton KJ, Khoury DS, Nagueh SF. Assessment of left ventricular diastolic function by early diastolic mitral annulus peak acceleration rate: experimental studies and clinical application. *J Appl Physiol* 2006; **100**: 679–84.
- 50 Yamamoto T, Oki T, Yamada H, et al. Prognostic value of the atrial systolic mitral annular motion velocity in patients with left ventricular systolic dysfunction. *J Am Soc Echocardiogr* 2003; **16**: 333–9.
- 51 Temporelli PL, Scapellato F, Corra U, Eleuteri E, Imparato A, Giannuzzi P. Estimation of pulmonary wedge pressure by transmural Doppler in patients with chronic heart failure and atrial fibrillation. *Am J Cardiol* 1999; **83**: 724–7.
- 52 Chirillo F, Brunazzi MC, Barbiero M, et al. Estimating mean pulmonary wedge pressure in patients with chronic atrial fibrillation from transthoracic Doppler indexes of mitral and pulmonary venous flow velocity. *J Am Coll Cardiol* 1997; **30**: 19–26.
- 53 Skaluba SJ, Litwin SE. Mechanisms of exercise intolerance: insights from tissue Doppler imaging. *Circulation* 2004; **109**: 972–7.
- 54 Messika-Zeitoun D, Johnson BD, Nkomo V, et al. Cardiopulmonary exercise testing determination of functional capacity in mitral regurgitation: physiologic and outcome implications. *J Am Coll Cardiol* 2006; **47**: 2521–7.
- 55 Lee SH, Jung JH, Choi SH, et al. Exercise intolerance in patients with atrial fibrillation: clinical and echocardiographic determinants of exercise capacity. *J Am Soc Echocardiogr* 2005; **18**: 1349–54.
- 56 Wang M, Yip GW, Wang AY, et al. Peak early diastolic mitral annulus velocity by tissue Doppler imaging adds independent and incremental prognostic value. *J Am Coll Cardiol* 2003; **41**: 820–6.
- 57 Wang M, Yip G, Yu CM, et al. Independent and incremental prognostic value of early mitral annulus velocity in patients with impaired left ventricular systolic function. *J Am Coll Cardiol* 2005; **45**: 272–7.
- 58 Dokainish H, Zoghbi WA, Lakkis NM, et al. Incremental predictive power of B-type natriuretic peptide and tissue Doppler echocardiography in the prognosis of patients with congestive heart failure. *J Am Coll Cardiol* 2005; **45**: 1223–6.
- 59 Hillis GS, Moller JE, Pellikka PA, et al. Noninvasive estimation of left ventricular filling pressure by E/e' is a powerful predictor of survival after acute myocardial infarction. *J Am Coll Cardiol* 2004; **43**: 360–7.

- 60 Okura H, Takada Y, Kubo T, et al. Tissue Doppler-derived index of left ventricular filling pressure, E/E', predicts survival of patients with non-valvular atrial fibrillation. *Heart* 2006; **92**: 1248–52.
- 61 Sharma R, Pellerin D, Gaze DC, et al. Mitral peak Doppler E-wave to peak mitral annulus velocity ratio is an accurate estimate of left ventricular filling pressure and predicts mortality in end-stage renal disease. *J Am Soc Echocardiogr* 2006; **19**: 266–73.
- 62 McMahon CJ, Nagueh SF, Pignatelli RH, et al. Characterization of left ventricular diastolic function by tissue Doppler imaging and clinical status in children with hypertrophic cardiomyopathy. *Circulation* 2004; **109**: 1756–62.
- 63 Kato T, Noda A, Izawa H, et al. Myocardial velocity gradient as a noninvasively determined index of left ventricular diastolic dysfunction in patients with hypertrophic cardiomyopathy. *J Am Coll Cardiol* 2003; **42**: 278–85.
- 64 Goto K, Mikami T, Onozuka H, et al. Role of left ventricular regional diastolic abnormalities for global diastolic dysfunction in patients with hypertrophic cardiomyopathy. *J Am Soc Echocardiogr* 2006; **19**: 857–64.
- 65 Reisner SA, Lysansky P, Agmon Y, Mutlak D, Lessick J, Friedman Z. Global longitudinal strain: a novel index of left ventricular systolic function. *J Am Soc Echocardiogr* 2004; **17**: 630–3.
- 66 Wang J, Khoury D, Thohan V, Torre-Amione G, Gagueh SF. Global diastolic strain rate for the assessment of left ventricular relaxation and filling pressures. *Circulation* 2007; **115**: 1376–83.

# Assessment of left ventricular filling pressure with stress

*Jong-Won Ha*

## **Introduction**

Abnormalities of diastolic function have a major role in producing signs and symptoms in patients presenting with heart failure [1–4]. The final result of abnormalities of diastolic dysfunction is an elevation of left ventricular (LV) filling pressure, which is reflected back to the pulmonary circulation, causing pulmonary congestion [5]. When diastolic function is normal, increased cardiac output is maintained by increased diastolic filling without significant rise in filling pressures [6]. However, in the presence of diastolic dysfunction, filling pressure rises more rapidly to cause dyspnea on mild to moderate exertion [7]. Because patients with significant heart disease may have entirely normal hemodynamics by echocardiography or catheterization in the resting state, and as most cardiac symptoms are precipitated by exertion or some other stresses, it may be important to reassess hemodynamic performance during some forms of stress such as exercise. Such an evaluation enables the physician to assess the cardiovascular reserve and the relationship, if any, between specific symptoms and hemodynamic impairment. Although invasive hemodynamic monitoring during exercise would be accurate, a noninvasive demonstration of this phenomenon will be more practical and clinically applicable. In this review, we will focus on noninvasive assessment of LV filling pressure during stress in the evaluation of patients with diastolic dysfunction and exertional dyspnea.

## **Physiologic changes of diastolic function during exercise**

The interpretation of changes in the LV diastolic function that occur during exercise depend greatly

on an appreciation of the adaptations in diastolic function during exercise. During exercise, the increased cardiac output is achieved by having LV stroke volume either maintained or increased concomitantly with increase in heart rate. Because tachycardia decreases the duration of diastole, there is less time for diastolic filling of the left ventricle. Thus, the mean mitral flow rate must increase during exercise to maintain or augment the stroke volume. This increase can be achieved by faster relaxation and an augmented suction effect induced by a higher sympathetic tone during exercise [6,8]. With increased adrenergic stimulation, cyclic adenosine monophosphate-mediated phosphorylation of phospholamban increases the rate of SERCA<sub>2</sub> reuptake of calcium ions by the sarcoplasmic reticulum, which ultimately increases the rate of ventricular relaxation. In addition, enhanced contractility leads to a smaller LV end-systolic volume and correspondingly greater diastolic suction. In conscious dogs, Cheng et al. [6] have shown that, during exercise, sympathetic stimulation and tachycardia produce a downward shift of the early diastolic portion of the LV pressure–volume loop [6]. The enhanced decrease in early diastolic LV pressure produces more rapid flow and maintains LV filling, despite the shortened diastolic filling period during exercise.

Many elderly subjects and patients with hypertension or LV hypertrophy have Doppler echocardiographic evidence of impaired diastolic function, but do not have any symptoms of heart failure at rest. However, in patients with a similar grade of diastolic dysfunction at rest, there can be a spectrum of alterations in diastolic function during exercise (Figures 6.1–6.3). Previous work has shown that marked abnormalities in LV diastolic function may

occur with exercise in patients with clinical evidence of heart failure but normal resting systolic function. Kitzman et al. [7] studied seven patients with New York Heart Association class III or IV heart

failure with one or more documented episodes of pulmonary edema and no significant coronary artery disease. Patients were studied by symptom-limited upright exercise with simultaneous

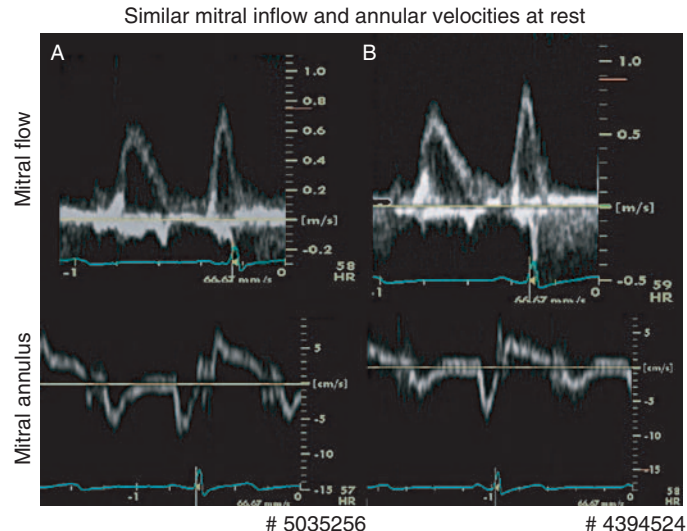


**Figure 6.1** Similar mitral inflow and annular velocity pattern in two different patients.

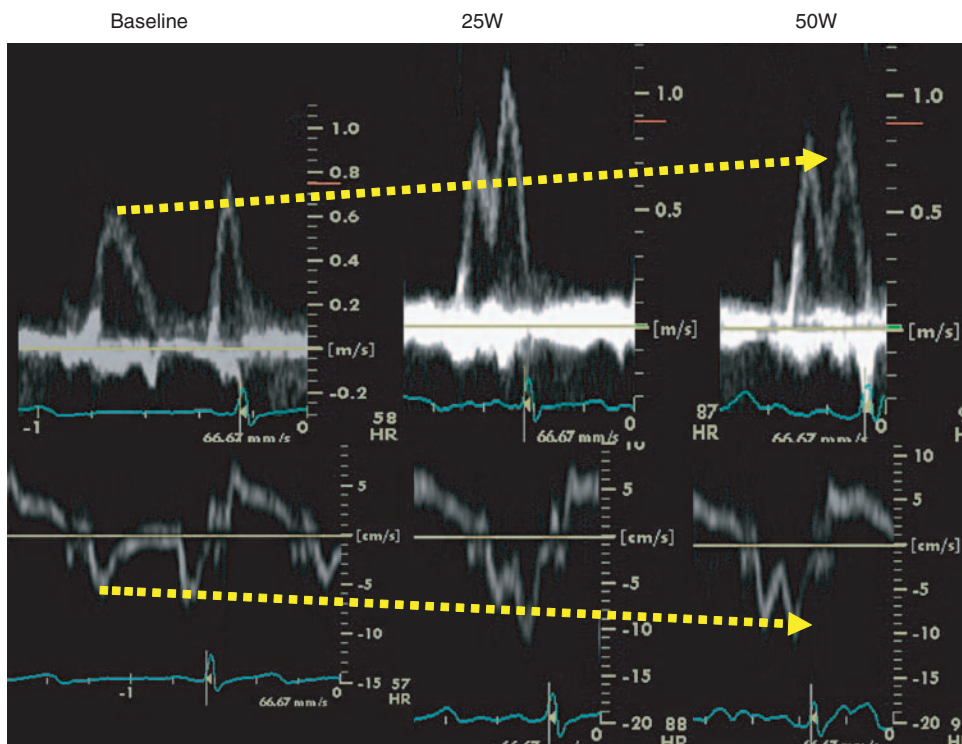


**Figure 6.2** Change of mitral inflow and annular velocity during exercise in patient A. Mitral inflow  $E$  and annular  $E'$  velocities increased during exercise.  $E$ , peak velocity of early filling;  $E'$ , mitral annulus early diastolic velocity.

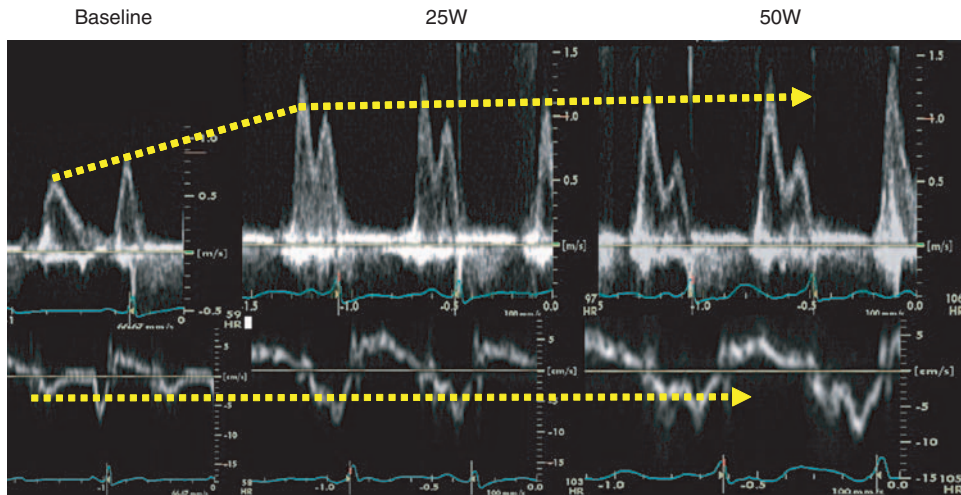


**Figure 6.3** Change of mitral inflow and annular velocity during exercise in patient B. Mitral inflow  $E$  velocity increased during exercise, but  $E'$  velocity did not

increase with exercise, resulting in increase  $E/E'$  during exercise.  $E$ , peak velocity of early filling;  $E'$ , mitral annulus early diastolic velocity.

hemodynamic and radionuclide measurements, and data were compared to those of age- and sex-matched healthy subjects. LV ejection fraction was normal at rest and exercise for both patients and control subjects, but there was a striking rise in pulmonary capillary wedge pressure in the patients with heart failure, compared to controls.

The cause of exercise intolerance in some patients with LV failure is diminished cardiac output, so that inadequate oxygen is delivered to working skeletal muscle to meet the demands of aerobic metabolism. However, in other patients, exercise intolerance is due to the rise in pulmonary capillary wedge pressure, resulting in marked dyspnea. Diastolic functional reserve can be defined as the capacity of the ventricle to accommodate diastolic filling necessary for increased demand, imposed by exercise, without resulting in marked increase in filling pressures. Therefore, in patients suspected of diastolic dysfunction with exertional dyspnea and normal ventricular systolic and diastolic functions, exercise could unmask diastolic abnormalities that were not evident under rest conditions. Some patients have relatively normal or mildly impaired diastolic function at rest but develop a significant deterioration of diastolic function during exercise. Other patients with severe exercise limitation may be found to have relatively preserved diastolic function even during exercise, pointing to other

#### Mode of stress

##### Physical stress

- Treadmill (post-exercise)
- Bicycle (peak exercise)

##### Pharmacologic

- Dobutamine

##### Pacing

- Atrial
- Ventricular

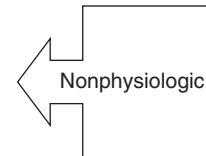


**Figure 6.4** Different modes of stress that can be used for demonstrating elevated filling pressure with stress.

etiologies such as pulmonary disease or deconditioning as the cause of the patient's symptoms. To distinguish these underlying mechanisms, it is important to assess diastolic function during stress or exercise with provocative testing.

#### Mode of stress

In assessing LV filling pressure during stress, the technique used to provoke symptoms should be taken into account (Figure 6.4). The cardiovascular system can be stressed using either active (dynamic exercise) or passive (pacing, pharmacologic) techniques. These stress techniques can also be classified as physiologic (dynamic exercise) or nonphysiologic (pacing, pharmacologic).

## Nonphysiologic stress

### Pacing

Atrial pacing is a feasible and easy way of stressing the heart, especially in patients in whom physical exercise is not possible. However, it must be noted that the hemodynamic changes associated with atrial pacing are different from those associated with physical exercise. During atrial pacing, the heart is stressed without primary autonomic or humoral input [9]. The main hemodynamic changes with atrial pacing are a decrease in LV stroke volume, due to a decrease in LV filling time that is not accompanied by an adequate compensatory increase in systemic venous return [10]. O'Brien et al. [11] demonstrated that patients with coronary artery disease showed an abnormal increase in LV filling pressures when angina was induced by exercise but not when it was provoked by atrial pacing. In atrial pacing, myocardial ischemia and the consequent prolongation of relaxation are apparently observed without significant elevation of LV filling pressures. Thus, during pacing, LV diastolic pressures fell and remained below the control level even during angina. Therefore, to demonstrate an increase in LV filling pressure with stress, pacing is not a suitable technique.

### Dobutamine

Dobutamine has been frequently used to pharmacologically stress the cardiovascular system. Although it is a feasible and easy way of stressing the heart, especially in patients in whom physical exercise is not possible, hemodynamic changes associated with dobutamine are different from those associated with physical exercise. Dobutamine-induced myocardial ischemia results in a decrease in stroke volume with no change in pulmonary capillary wedge pressure. Therefore, LV filling pressure could not be expected to increase during dobutamine administration [12]. It has also been shown that myocardial velocity responses to exercise and dobutamine appear to be different [13]. Similar to atrial pacing, dobutamine may not be a suitable technique to demonstrate an increase in LV filling pressure with stress. However, dobutamine administration may be helpful to evaluate myocardial longitudinal functional reserve in subjects with an inability to exercise. Gorcsan et al. [14] evaluated the myocardial response to low-dose

dobutamine using tissue Doppler echocardiography in 12 normal subjects. They found a 14% increase in  $E'$  velocity after a dobutamine infusion of  $5 \mu\text{g kg}^{-1} \text{min}^{-1}$ , compared with baseline. Because  $E'$  velocity was inversely correlated with the time constant of isovolumic relaxation ( $\tau$ ) [15–17] and administration of dobutamine enhanced LV relaxation and early diastolic recoil, observation of  $E'$  velocity changes during dobutamine administration may be a potential way to assess myocardial longitudinal diastolic functional reserve.

### Exercise

Physical exercise is the most physiological means of gathering data regarding stress-induced elevation of LV filling pressure. Although treadmill exercise has been shown to elicit greater circulatory reserve than bicycle exercise with higher maximal oxygen consumption, echocardiography during supine bicycle exercise allows continuous imaging of the heart during exercise, which made the assessment of LV filling pattern during exercise possible. In addition, an increase in end-systolic and end-diastolic ventricular volumes occurs in the supine position at rest and during exercise [18–21]. These features may make exercise Doppler echocardiography during supine bicycle exercise the optimal approach to demonstrate the increase in LV filling pressures with exercise. In middle-aged healthy subjects, the assessment of mitral inflow and annular velocities during exercise have shown that  $E/E'$  ratio, an accurate estimator of LV filling pressures, did not change significantly after exercise because of proportional increases in both the mitral inflow and annular velocities [22]. This observation represents the normal diastolic response for exercising patients.

On the basis of these observations, efforts have been made to develop a novel noninvasive diagnostic test to detect an exercise-induced increase in diastolic filling pressures using supine bicycle Doppler echocardiography. The preliminary results showed that diastolic stress echocardiography using supine bicycle exercise was technically feasible for demonstrating the change in  $E/E'$  (i.e., filling pressure) with exercise and that the hemodynamic consequences of exercise-induced increase in diastolic filling pressure could be demonstrated noninvasively with this novel technique [23]. In a series of patients referred to the stress echocardiography

laboratory for evaluation of exertional dyspnea, 56% had no evidence of increased filling pressure at rest, and of these, 36% had an increase in filling pressure with exercise on the basis of the E/E' ratio [23]. Although further hemodynamic confirmation will be needed for this approach, supine bicycle Doppler echocardiography is a feasible and appropriate way to demonstrate elevated filling pressure with exercise.

### Hemodynamic validation

Although the increase in E/E' ratio during exercise may be attributed to an increase in filling pressure due to exercise-induced diastolic dysfunction, simultaneous measurements of LV filling pressure and Doppler echocardiography with exercise is warranted to confirm the noninvasive findings. Recent studies using simultaneous measurements of LV filling pressure and Doppler echocardiography with exercise have shown reasonably good correlation between invasively measured LV filling pressures and Doppler-derived E/E' ratio, even with exercise [24,25]. Burgess and colleagues have elegantly demonstrated that the correlation was almost identical during supine cycle ergometry, indicating that E/E' can be used reliably as a convenient noninvasive means of estimating LV diastolic pressures during exercise as well as at rest [25]. The correlation during exercise was best at low filling pressures, and, although there was more scatter at higher levels of LV diastolic pressures, patients could still be grouped into those with and without an elevation of LV diastolic pressures with good sensitivity and specificity (Figure 6.5). Therefore, E/E' ratio can be used to reliably identify patients with elevated LV diastolic pressures [25].

### Observation of left ventricular filling pattern during recovery

One of the practical drawbacks of Doppler echocardiography assessing LV filling during exercise is technical difficulty in obtaining adequate signals for meaningful analysis during rapid heart rates achieved during exercise. Although patients with marked diastolic dysfunction revealed diagnostic changes even at mild or moderate exertion with moderately increased heart rate, a subset of patients

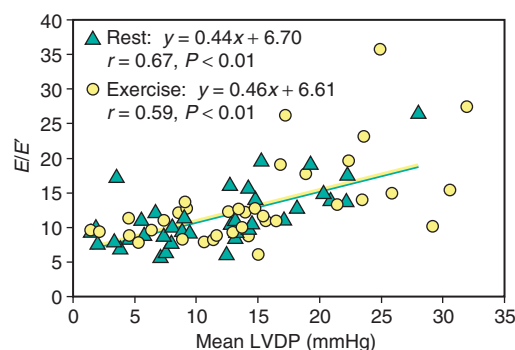


**Figure 6.5** Correlation between mean LV diastolic pressures and ratio of early diastolic transmural velocity to early diastolic tissue velocity ( $E/E'$ ). LVDP, left ventricular diastolic pressure.

develop premature tachycardia even at mild exertion, which makes a meaningful analysis difficult. In a previous report, the test was unsuccessful in 10% of enrolled patients because of tachycardia with low levels of exercise and exercise-induced atrial tachyarrhythmia [23]. Ischemia-induced abnormalities in diastolic function may resolve more slowly during resolution of the ischemia, and diastolic dysfunction induced by myocardial ischemia may persist well beyond recovery of normal systolic function after brief coronary occlusion during coronary angioplasty. Additionally, pulmonary capillary wedge pressure returned to baseline 1 hr after symptom-limited bicycle exercise in patients with LV dysfunction [26]. These results may suggest that exercise-induced diastolic dysfunction causes prolonged diastolic dysfunction that may persist for several days. Figure 6.6 shows mitral flow and annular velocity at rest, during supine bicycle exercise, and recovery in a 56-year-old woman with hypertension and exertional dyspnea. Because of tachycardia even with mild exercise, E/E' could not be measured at 50W of exercise. However, E/E' at recovery was significantly elevated even after cessation of exercise, and it is higher than at rest and during exercise.

It can be speculated that LV filling pressures, assessed noninvasively using E/E' ratio, will return to baseline immediately after cessation of exercise in healthy subjects. In a preliminary study, 73 healthy subjects (age,  $38 \pm 14$  years; 62 male) underwent supine bicycle exercise and mitral inflow parameters and diastolic velocities of the mitral annulus

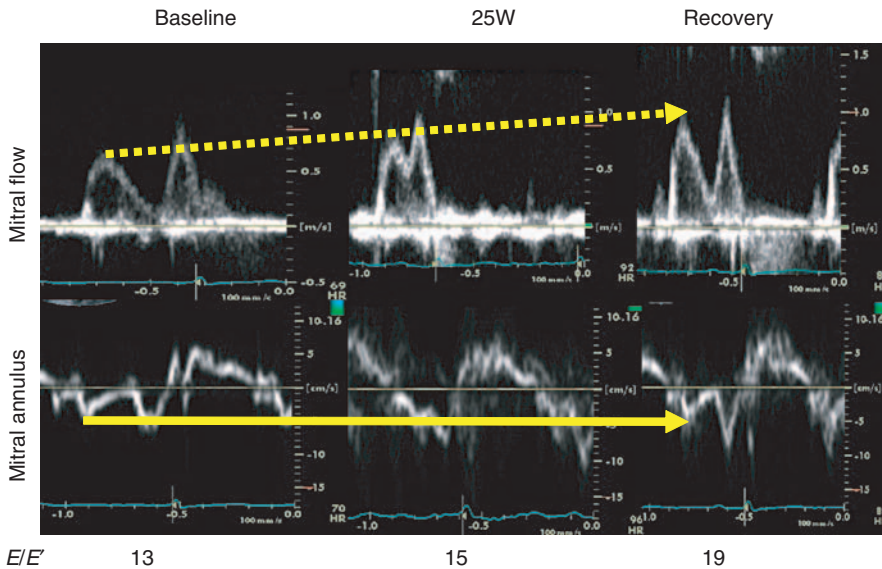


**Figure 6.6** Mitral flow and annular velocity at rest, during supine bicycle exercise, and recovery in a 56-year-old woman with hypertension and exertional dyspnea. Because of tachycardia even with mild exercise,  $E/E'$  could

not be measured at 50W of exercise. Note that  $E/E'$  was significantly elevated even after cessation of exercise, and it is higher than at rest and during exercise.

were recorded at baseline and during recovery 2, 5, 10 min after cessation of exercise. Mean  $E/E'$  ratio at rest was  $7.6 \pm 1.8$ , and it was  $<15$  in all patients. Mean exercise duration was  $837 \pm 184$  sec (range, 390–1,260 sec).  $E/E'$  ratios during recovery 2, 5, 10 min after cessation of exercise were  $8.8 \pm 1.9$ ,  $8.2 \pm 2.0$ , and  $7.8 \pm 1.8$ , and none of the patients had  $E/E' > 15$  during recovery phase. Therefore, in healthy subjects,  $E/E'$  was less than 15 at rest as well as during recovery, for up to 10 min after cessation of exercise [27]. Because  $E/E'$  was not elevated in healthy subjects, elevated  $E/E'$  during recovery may be helpful to detect exercise-induced diastolic dysfunction in subjects with tachycardia even at low levels of exercise.

## Conclusion

Patients with significant heart disease may have entirely normal diastolic hemodynamics assessed in the resting state. Because most cardiac symptoms are precipitated by exertion, therefore, it may be important to assess hemodynamic performance during some forms of stress – especially, exercise – which could unmask diastolic abnormalities that were not evident under rest conditions.

Recent developments in echo-Doppler techniques made noninvasive assessment of LV filling pressure with exercise feasible. The introduction of this “diastolic stress test” would be helpful for better assessment and management of patients with diastolic dysfunction and exertional dyspnea.

## References

- 1 Gaasch WH, Levine HJ, Quinones MA, Alexander JK. Left ventricular compliance: mechanisms and clinical implications. *Am J Cardiol* 1976; **38**: 645–53.
- 2 Grossman W, McLaurin L. Diastolic properties of the left ventricle. *Ann Intern Med* 1976; **84**: 316–26.
- 3 Grossman W, Barry WH. Diastolic pressure–volume relations in the diseased heart. *Fed Proc* 1980; **39**: 148–55.
- 4 Vasan RS, Larson MG, Benjamin EJ, Evans JC, Reiss C, Levy D. Congestive heart failure in subjects with normal versus reduced left ventricular ejection fraction: prevalence and mortality in a population-based cohort. *J Am Coll Cardiol* 1999; **33**: 1948–55.
- 5 Nishimura RA, Appleton CP, Redfield MM, Ilstrup DM, Holmes DR, Tajik AJ. Noninvasive Doppler echocardiographic evaluation of left ventricular filling pressures in patients with cardiomyopathies: a simultaneous Doppler echocardiographic and cardiac catheterization study. *J Am Coll Cardiol* 1996; **28**: 1226–33.

- 6 Cheng CP, Igarashi Y, Little WC. Mechanism of augmented rate of left ventricular filling during exercise. *Circ Res* 1992; **70**: 9–19.
- 7 Kitzman DW, Higginbotham MB, Cobb FR, Sheikh KH, Sullivan MJ. Exercise intolerance in patients with heart failure and preserved left ventricular systolic function: failure of the Frank–Starling mechanism. *J Am Coll Cardiol* 1991; **17**: 1065–72.
- 8 Mizushige K, Matsuo H, Nozaki S, Kwan OL, DeMaria AN. Differential responses in left ventricular filling dynamics with isometric handgrip versus isotonic treadmill exertion. *Am Heart J* 1996; **131**: 131–7.
- 9 David D, Lang RM, Borow KM. Clinical utility of exercise, pacing, and pharmacologic stress testing for the noninvasive determination of myocardial contractility and reserve. *Am Heart J* 1988; **116**: 235–47.
- 10 Sarnoff SJ, Braunwald E, Welch GHJ, Case RB, Stainsby WN, Macruz R. Hemodynamic determinants of oxygen consumption of the heart with special reference to the tension-time index. *Am J Physiol* 1958; **192**: 148–56.
- 11 O'Brien KP, Higgs LM, Glancy DL, Epstein SE. Hemodynamic accompaniments of angina: a comparison during angina induced by exercise and by atrial pacing. *Circulation* 1969; **39**: 735–43.
- 12 Pierard LA, Berthe C, Albert A, Carlier J, Kulbertus HE. Hemodynamic alterations during ischaemia induced by dobutamine stress testing. *Eur Heart J* 1989; **10**: 783–90.
- 13 Pasquet A, Yamada E, Armstrong G, Beachler L, Marwick TH. Influence of dobutamine or exercise stress on the results of pulsed-wave Doppler assessment of myocardial velocity. *Am Heart J* 1999; **138**: 753–8.
- 14 Gorcsan J III, Deswal A, Mankad S, et al. Quantification of the myocardial response to low-dose dobutamine using tissue Doppler echocardiographic measures of velocity and velocity gradient. *Am J Cardiol* 1998; **81**: 615–23.
- 15 Sohn DW, Chai IH, Lee DJ, et al. Assessment of mitral annulus velocity by Doppler tissue imaging in the evaluation of left ventricular diastolic function. *J Am Coll Cardiol* 1997; **30**: 474–80.
- 16 Ommen SR, Nishimura RA, Appleton CP, et al. Clinical utility of Doppler echocardiography and tissue Doppler imaging in the estimation of left ventricular filling pressures: a comparative simultaneous Doppler-catheterization study. *Circulation* 2000; **102**: 1788–94.
- 17 Nagueh SF, Sun H, Kopelen HA, Middleton KJ, Khoury DS. Hemodynamic determinants of the mitral annulus diastolic velocities by tissue Doppler. *J Am Coll Cardiol* 2001; **37**: 278–85.
- 18 Poliner LR, Dehmer GJ, Lewis SE, Parkey RW, Blomqvist CG, Willerson JT. Left ventricular performance in normal subjects: a comparison of the responses to exercise in the upright and supine positions. *Circulation* 1980; **62**: 528–34.
- 19 Freeman MR, Berman DS, Staniloff H, et al. Comparison of upright and supine bicycle exercise in the detection and evaluation of extent of coronary artery disease by equilibrium radionuclide ventriculography. *Am Heart J* 1981; **102**: 182–9.
- 20 Thadani U, West RO, Mathew TM, Parker JO. Hemodynamics at rest and during supine and sitting bicycle exercise in patients with coronary artery disease. *Am J Cardiol* 1977; **39**: 776–83.
- 21 Bygdemar S, Wahren J. Influence of body position on the anginal threshold during leg exercise. *Eur J Clin Invest* 1974; **4**: 201–6.
- 22 Ha JW, Lulic F, Bailey KR, et al. Effects of treadmill exercise on mitral inflow and annular velocities in healthy adults. *Am J Cardiol* 2003; **91**: 114–5.
- 23 Ha JW, Oh JK, Pellikka PA, et al. Diastolic stress echocardiography: a novel noninvasive diagnostic test for diastolic dysfunction using supine bicycle exercise Doppler echocardiography. *J Am Soc Echocardiogr* 2005; **18**: 63–8.
- 24 Talreja DR, Nishimura RA, Oh JK. Non-invasive parameters of diastolic function reflect invasively measured filling pressures during exercise. *Circulation* 2004; **110 Suppl**: III474.
- 25 Burgess MI, Jenkins C, Sharman JE, Marwick TH. Diastolic stress echocardiography: hemodynamic validation and clinical significance of estimation of ventricular filling pressure with exercise. *J Am Coll Cardiol* 2006; **47**: 1891–1900.
- 26 Sato H, Inoue M, Matsuyama T, et al. Hemodynamic effects of the beta 1-adrenoceptor partial agonist xamoterol in relation to plasma norepinephrine levels during exercise in patients with left ventricular dysfunction. *Circulation* 1987; **75**: 213–20.
- 27 Ha JW, Choi EY, Seo HS, et al. Time course of recovery of left ventricular filling pressure after exercise in healthy subjects [abstract]. *Eur J Echocardiogr* 2006.

# 3

## PART 3

# Application in heart failure



# Assessment of systolic heart failure

*John E. Sanderson*

## Introduction

Several different techniques, invasive and non-invasive, have been used to assess systolic function of the ventricles, but none are entirely satisfactory. One of the simplest and most widely used indices is the left ventricular ejection fraction (LVEF), which is the stroke volume expressed as a percentage of the end-diastolic volume. On the basis of the measurement of the LVEF, heart failure is often divided into two major types: systolic heart failure and diastolic heart failure. Those with a low LVEF (usually taken as <45%) are assumed to have a primary systolic abnormality and those with a normal LVEF to have a primary diastolic problem. There are several problems with this scheme both conceptually and in clinical practice [1], which are compounded by the difficulties of measuring accurately the ejection fraction itself. Accurate measurement of LV volumes can be done by two-dimensional (2-D) echocardiography if significant foreshortening of the left ventricle is avoided and if values are averaged from both four-chamber and two-chamber views and preferably from two or three beats. However, in routine clinical practice, and even in many studies of heart failure, EF is unfortunately not measured but only estimated visually (by "eyeball"). Because this method is inaccurate, it is not recommended [2]. Similarly, the estimation of LVEF from radial end-diastolic and end-systolic diameters obtained by M-mode echocardiography from a parasternal window, applying the Teichholz formula, is also not supported, because it involves too many inappropriate and inaccurate assumptions about LV cavity size and shape [2]. In addition, although EF is of some prognostic value in certain situations,

it is affected by preload, afterload, heart rate, dysynchrony, as well as myocardial contractility [3]. There is, therefore, a need for new techniques for assessing global and regional function that can be easily applied in the clinic. Tissue Doppler imaging (TDI, or myocardial velocity imaging) does provide a realistic and practical alternative to the EF for assessing ventricular function, and it also provides robust prognostic information.

## Regional systolic and long-axis function

It is now well appreciated that, in systole, the normal left ventricle shortens longitudinally as well as contracts radially [4,5]. The arrangement of myocardial fibers is not uniform across the wall of the left ventricle; subendocardial and subepicardial muscle bundles are aligned longitudinally, with a slight spiral arrangement, and mid-wall fibers are aligned circumferentially. The latter group is responsible mainly for short-axis or radial contraction of the left ventricle (analogous to the motion of bellows), while the former cause long-axis contraction similar to the motion of a piston [6]. The ventricular long axes of both ventricles connect the apex to the base of the heart. The apex is fixed with respect to the chest wall [7]. The base is considered to be at the atrioventricular (AV) rings. Thus, changes in the long axis can be determined by measuring the movement of the AV rings: their position by M-mode echocardiography and their velocity by Doppler (see Part 1). Rushmer et al. showed that the long axis normally shortens by 10–12% with ejection at the same time as the minor axis falls by 25% [8].

Shortening of the long axis begins during the period of isovolumic contraction, causing cavity shape to become more spherical. As pointed out by Henein and Gibson [6], that this difference can occur demonstrates that motion along the long axis is due to anatomically discrete fibers separate from those supporting the minor axis, rather than the possibility that function in the two directions might merely represent circumferential and longitudinal components of a homogenous set of fibers arranged obliquely. During ejection, the two axes are effectively in phase with one another, although peak long-axis shortening occurs at aortic valve closure, while minor axis falls by a further 1–2 mm, reaching its minimum at the time of mitral valve cusp separation.

Thus, radial, circumferential, and longitudinal shortening and lengthening, all of which contribute importantly to LV global function and create the twisting and untwisting motion of the left ventricle, predominantly involve different muscle bundles or myocardial layers. Probably because of their subendocardial situation, the longitudinal fibers are particularly susceptible to disturbance by various diseases and pathologies. Early work showed that even simple M-mode assessment of the mitral annulus excursion provided a useful and sensitive measure of ventricular function and demonstrated

how it was rapidly affected by ischemia [9]. Evolving from these M-mode-based studies, the newer imaging techniques based on tissue Doppler and now speckle or pixel tracking have produced useful new indices for assessing ventricular function and systolic heart failure.

### Tissue Doppler imaging in experimental heart failure models

In a canine pacing model of congestive heart failure, Tabata et al. [10] studied the relationship of mitral annular velocity changes with EF. Over 20 weeks, LV volume increased as LVEF, stroke volume, and mitral annulus peak systolic velocity significantly decreased. LVEF and mitral annulus systolic velocity closely correlated ( $r = 0.706$ ;  $P < 0.0001$ ). There was a similar fall in the peak early diastolic mitral annular velocity. In a similar pacing model, Hasegawa et al. [11] investigated the mechanism of the reduced early mitral annulus velocity ( $Em$ ) in heart failure. With progressive heart failure,  $Em$  declined and correlated with the time constant of LV relaxation ( $\tau$ ). The peak early mitral inflow velocity ( $E$ ) did not.  $Em$  was also progressively delayed by  $37 \pm 12$  msec so that it occurred after left atrial (LA) to LV pressure crossover (Figure 7.1). They concluded that, under normal circumstances,

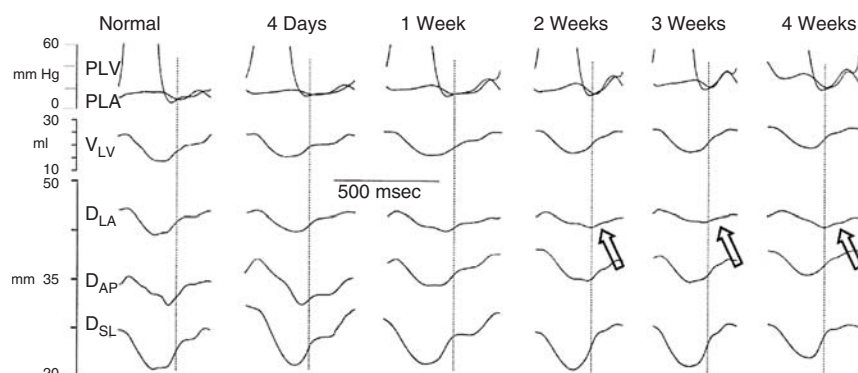


**Figure 7.1** Analog recordings in a conscious animal before (normal) and after producing progressive heart failure (HF) with 4 weeks of rapid pacing. Shown are LA and LV pressures (PLA/PLV), LV volume ( $V_{LV}$ ), and three LV internal dimensions: anteroposterior ( $D_{AP}$ ), septolateral ( $D_{SL}$ ), and long axis ( $D_{LA}$ ). Under normal conditions, the increase in LV volume during early diastolic filling occurs as all three dimensions expand symmetrically. Most of the increase in

LV volume and expansion occurs before the crossover of PLV and PLA (vertical dotted lines). In contrast, after HF, the expansion of the long axis is delayed (arrows), occurring after PLA is greater than or equal to PLV, and most of the early diastolic increase in LV volume and expansion of the short-axis dimensions ( $D_{SL}$  and  $D_{AP}$ ) is complete.

Adapted from Hasegawa et al. [11].

the LV expands symmetrically during rapid, early filling and peak longitudinal expansion (Em) nearly coinciding with the peak mitral inflow velocity (E) in response to a pressure gradient that extends from the LA to LV apex. In heart failure, the synchrony of LV diastolic expansion is altered by the delayed relaxation that is present. Early filling is maintained by an elevated LA pressure, despite slowed relaxation; however, in this situation, longitudinal expansion does not occur during rapid, early filling and it is delayed, occurring after the crossover of LA and LV pressures. Thus, Em appears to provide a consistent measure of diastolic dysfunction that is independent of LA pressure. Therefore, both the peak systolic and early diastolic mitral annular velocities are useful indices of global systolic and diastolic function.

### M-mode measurements

In patients with heart failure, LV long-axis function is always reduced when LV volume is increased, that is, when remodeling has taken place. As in the experimental models, mitral ring amplitude during systole correlates well with LVEF, which incidentally is also true for the tricuspid ring and the right ventricle [12,13]. In addition, Willenheimer et al. found a good relationship between AV plane displacement (or mitral annulus excursion) and 1-year mortality [14]. Those with a displacement value of <6.4 mm had a 37% mortality, whereas those with an excursion >10 mm all survived. However, M-mode measurement of the mitral or tricuspid annulus amplitude is technically more laborious than measuring the peak systolic and diastolic velocities by TDI.

### Peak systolic velocities by tissue Doppler imaging in systolic heart failure

Measurement of mitral ring velocities or basal myocardial velocities has proved to be a relatively simple approach to assessing LV systolic and diastolic function in patients. These simple velocity measurements also have high levels of concordance between observers. Both peak systolic (Sm) and early diastolic (Em) annular or basal velocities are nearly always reduced in patients presenting with the clinical syndrome of systolic heart failure.

In an early study, Yip et al. [15] found that both Sm and Em were markedly reduced compared to normal subjects or even those with intermediate diastolic heart failure. In another study, it was found that Sm averaged from six sites around the mitral annulus also correlates well with LVEF, and a cutoff of >7.5 cm/sec had a sensitivity of 79% and a specificity of 88% in predicting normal global LV function [16]. The Sm is also a sensitive marker of mildly impaired LV systolic function, even in those with a normal LVEF or apparently preserved LV systolic function such as in “diastolic heart failure” [15,17], or diabetics without overt heart disease [18]. Reduced TDI velocities are also present in subjects with hypertrophic cardiomyopathy mutations at a time of subclinical disease when cardiac hypertrophy is not present. TDI can, therefore, be used for early identification of hypertrophic cardiomyopathy [19].

Given the above observations, it is not surprising that peak annular or basal systolic velocities are strong predictors of outcome in several conditions. Wang et al. [20] in a large cohort of 518 subjects (353 with cardiac disease and the rest normal) followed up for 2 years measured the averaged mitral annular velocities from four sites (septal, lateral, anterior, and inferior) from color-coded tissue Doppler images. They found cardiac mortality was significantly higher when both Sm and Em were <3 cm/sec (hazard ratio, 7.5 and 5.3, respectively), although in the multivariate analysis, Em had a stronger impact on mortality than Sm. In another study of a cohort of 182 patients with impaired LV systolic function (defined as a LVEF < 50%), the same group found again that an Em < 3 cm/sec was associated with a significantly higher mortality and this measurement added incremental prognostic value to the standard indices of systolic and diastolic function, including a short deceleration time of the mitral inflow E-wave and the ratio E/Em (Figures 7.2 and 7.3) [21]. In contrast, Nikitin et al. [22] in a study of 185 patients with heart failure and LVEF < 45%, despite optimal pharmacological treatment during a median follow-up of 32 months, found that, on multivariate analysis, only Sm derived from color-coded TDI averaged from six sites and diastolic arterial pressure emerged as independent predictors of outcome (hazard

ratio = 0.648; 95% confidence interval, 0.460–0.912;  $P = 0.013$ ; and hazard ratio = 0.966; 95% confidence interval, 0.938–0.994;  $P = 0.016$ ). They concluded that, in systolic heart failure, the strongest independent echocardiographic predictor of outcome was systolic mitral annular velocity ( $Sm$ ).

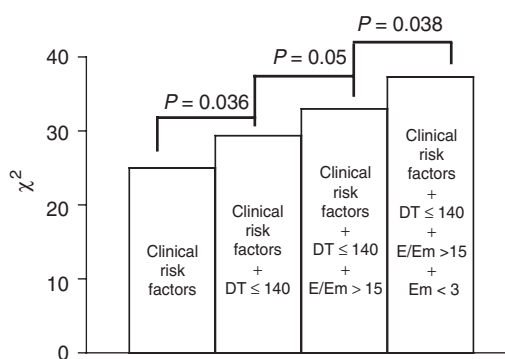


**Figure 7.2** Incremental value of  $Em < 3$  and  $E/Em > 15$  in predicting long-term (median, 48 months) cardiac mortality. The addition of deceleration time (DT),  $E/Em$ , and  $Em$  resulted in significant incremental improvements in the predictive value of a model, including clinical risk factors (age, ischemic heart disease, valvular heart disease, and heart failure):  $\chi^2 = 25.0$  with 5 degrees of freedom for clinical risk factors;  $\chi^2 = 29.4$  with 1 degree of freedom for clinical risk factors plus  $DT \leq 140$  msec;  $\chi^2 = 33.0$  with 1 degree of freedom for clinical risk factors plus  $DT \leq 140$  msec plus  $E/Em > 15$ ; and  $\chi^2 = 37.3$  with 1 degree of freedom for clinical risk factors plus  $DT \leq 140$  msec plus  $E/Em > 15$  plus  $Em < 3$ . Adapted from Wang et al. [21].

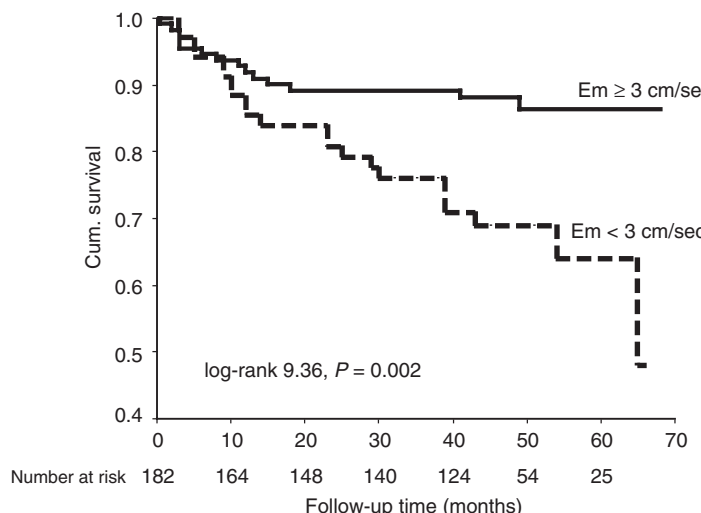


**Figure 7.3** Kaplan–Meier plot demonstrating cardiac mortality in patients classified according to  $Em < 3$  or  $Em \geq 3$  cm/sec. Adapted from Wang et al. [21].

## Assessment of left ventricular filling pressure: E/Em

The ratio  $E/Em$ , peak early mitral inflow velocity/peak annular or basal myocardial velocity, has been shown to correlate well with LV end-diastolic pressure, and an  $E/Em > 15$  can reliably predict an elevated LV diastolic pressure [23]. In addition,  $E/Em$  can be used to estimate LV diastolic pressure on exercise, which could be useful for confirming the diagnosis of heart failure in patients presenting with exertional dyspnea [24]. Burgess et al. [24] found the correlation between mean LV diastolic pressure and  $E/Em$  was fair at rest ( $r = 0.67$ ;  $P < 0.01$ ) but was less strong during exercise ( $r = 0.59$ ;  $P < 0.01$ ), mainly due to increased scatter at the higher mean LV diastolic pressures. However, patients could still be separated into those with or without an elevated LV diastolic pressure with good specificity and sensitivity, and this method could be a useful test to help with diagnosis. In our study [20], we found that, in heart failure patients with reduced LVEF,  $E/Em$  was predictive of cardiac death and an  $E/Em > 15$  had a hazard ratio of 8.43 (95% confidence interval, 1.15–61.9) in a univariate analysis. However, in a multivariable Cox regression analysis,  $Em$  alone was the strongest predictor of cardiac death.

Troughton et al. [25] prospectively studied 225 patients with symptomatic systolic heart failure (LVEF < 35%), with TDI measuring early septal mitral annular velocities. During a median of 429 (238–677) days of follow-up, 18 patients died

and 8 underwent transplantation. In a multiple regression analysis, the ratio of mitral inflow peak E/Em was associated with an increased risk of death or transplant ( $P < 0.05$ ). Those patients with E/Em  $> 17$  had an approximate mortality of 40% at 36 months compared to 5% in those with E/Em  $< 17$  ( $P < 0.001$ ). Similar rates were found with E/Vp, although this finding was less strong. The authors concluded that E/Em from TDI and E/Vp from color M-mode provide powerful prognostic information that is incremental to established indices, including LVEF and mitral early deceleration time.

### Tissue Doppler imaging in heart failure with mitral regurgitation

Alam et al. [26] have confirmed that mitral annular systolic velocities correlate quite well with LVEF, even if mitral regurgitation is present. In addition, Agricola et al. showed that TDI of the lateral mitral annulus in a group of asymptomatic patients with severe mitral regurgitation but normal LVEF could predict those who would develop postoperative LVEF reduction [27]. That is, TDI can detect sub-clinical LV dysfunction that only becomes apparent after the mitral regurgitation is corrected.

### Tricuspid annular velocities and right ventricular function

TDI of the tricuspid annular velocities has also been used to assess right ventricular (RV) function. There is a reasonable correlation between tricuspid annular velocity and RV ejection fraction: an annular velocity  $< 11.5$  cm/sec predicts an RV ejection fraction  $< 45\%$  with a sensitivity of 90% and a specificity of 85% [28]. The same group applied this technique to assessing prognosis in 139 patients with symptomatic heart failure with a mean LVEF of 24% (range, 10–39%). Using a Cox regression model, three effective predictors for both survival and event-free survival emerged: etiology of the heart failure, LV end-diastolic dimension, and peak systolic tricuspid annular velocity [29]. Those patients with a peak systolic velocity of  $< 10.8$  cm/sec had a worse survival rate.

### Tissue Doppler imaging for the diagnosis of systolic heart failure

As suggested above, TDI-derived longitudinal velocities are useful for confirming the diagnosis.

In a more complete study of 50 consecutive patients referred to a heart failure clinic with unexplained breathlessness, the echocardiographic measurement that correlated best with brain natriuretic peptide (BNP) was the longitudinal peak systolic velocity (Figure 7.4), correlating better than LVEF, radial velocities, and mitral inflow patterns [30]. The sensitivity and specificity of a longitudinal systolic velocity of  $< 5.5$  cm/sec (mean of four basal segments) to diagnose heart failure (defined as an elevated BNP) were 94% and 85%, respectively; the negative predictive value was 97% (Table 7.1). In addition, as noted above, the ratio E/Em is a useful index of an elevated LV filling pressure and can also be used for the confirmation of the diagnosis of heart failure. This index is especially useful for

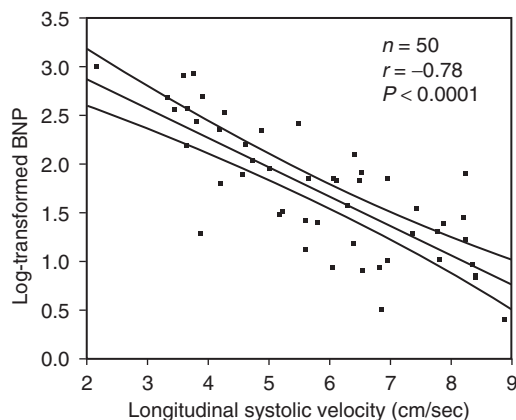


**Figure 7.4** Relationship between BNP levels and peak systolic myocardial velocity (Sm). Adapted from Vinereanu et al. [30].

**Table 7.1** Diagnostic performance of echocardiographic tests to detect patients with a BNP concentration  $> 88$  pg/ml.

Parameter	SENS	SPEC	PPV	NPV
Longitudinal mean systolic velocity $\leq 5.5$ cm/sec	94	85	76	97
Radial systolic velocity $\leq 5.3$ cm/sec	88	61	54	91
Ejection fraction $\leq 50\%$	59	85	67	80

SENS, sensitivity; SPEC, specificity; PPV, positive predictive value; NPV, negative predictive value. All values given are percentages.

those patients with symptoms of heart failure and a normal LVEF or diastolic heart failure.

### **Strain and strain rate in systolic heart failure**

Although strain rate by myocardial Doppler is well validated, its clinical use in overt systolic heart failure has been limited. Peak systolic strain rate correlated well with maximal elastance derived from pressure–volume loops, which is thought to be an index of contractility [31]. Signal noise and hemodynamic changes make it difficult to derive a normal range that is robust [32]. However, despite this difficulty, strain has proved to be a useful way of detecting subclinical abnormalities of systolic function in those with a normal ejection fraction, such as in hypertrophic cardiomyopathy, diabetic heart disease, and Friedrich's ataxia [32]. Zhang et al demonstrated that Strain rate can be used to detect transmurality of a myocardial infarction which is relevant in ischemic cardiomyopathy for determining viability since transmural infarcts are not viable [33]. But for the patient with severe systolic dysfunction the value of strain or strain rate derived from Doppler or speckle tracking is not yet completely known. Some initial data with 2D-strain derived from speckle or pixel tracking indicates that this may be more robust and reliable [34]. This technique can be used to analyse the different components of longitudinal, radial and circumferential function to global function. Becker et al [35] have carried out a similar study to that of Zhang et al but using 2D strain derived from speckle tracking instead of Doppler strain and again showed that discrimination of transmural from non-transmural infarction is possible. Both TDI and 2D strain (speckle tracking) can also be used to assess ventricular torsion or the twisting and untwisting motion of the ventricle. Using TDI Notomi et al elegantly demonstrated the value in studying twist or torsion especially when this is combined with assessment of early diastolic base-to-apex pressure gradients by colour M-mode Doppler which reflects ventricular suction [36]. They confirmed the close relationship between early diastolic untwisting and apex-to-base gradients thus linking systole with diastole. Untwisting and suction are particularly important on exercise as they enable the ventricle to fill rapidly at low pressure

and this was blunted in hypertrophic cardiomyopathy. Reduced and delayed diastolic untwisting will impair diastolic filling and might account for the symptom of breathlessness on exertion despite a ‘normal’ ejection fraction. Notomi et al also found a close relationship between twist/torsion and the annular peak velocities. It may be, therefore, that the annular velocities which are due to the longitudinal motion of the mitral ring up and down are indirectly reflecting ventricular twist and untwist. In addition this work confirms the close link between systolic function and early diastolic filling as was shown earlier by Yip et al [37] Initial studies suggest that untwist is impaired with ageing [38], but little information is available on this important mechanism in systolic heart failure to date. In an earlier study using MRI reduced twist was shown in heart failure by Fuchs et al [39] and with medical therapy there was improvement in regional ejection fraction although rotation only improved at the base. There appeared to be an uncoupling between regional shortening and rotation in chronic heart failure. This is likely to be a fruitful area for further research as it will reveal the linkage between systolic and diastolic function in more detail.

### **Summary**

Tissue Doppler-derived indices of myocardial function have proved to be sensitive and robust measurements and are useful for the diagnosis of heart failure and for predicting outcome. At present, those indices that are based on longitudinal function of the ventricle – annular or basal velocities – are the most simple to use, but new developments such as 2-D strain from speckle tracking are likely to be clinically useful by giving cardiologists better insight into the mechanical performance of the ventricles. There is a great need for measures that can be used to assess more comprehensively regional function that reflects the changes in fiber architecture and structure that accompany the process of heart failure and remodeling. LVEF and most of the other global indices presently used have major limitations and indeed can sometimes mislead.

### **References**

- 1 Sanderson JE. Heart failure with a normal ejection fraction. *Heart* 2007; **93**: 155–8.

- 2 Lang RM, Bierig M, Devereux RB, et al. Recommendations for chamber quantification. *Eur J Echocardiogr* 2006; **7**: 79–108.
- 3 Mahler F, Ross J Jr, O'Rourke RA, Covell JW. Effects of changes in preload, afterload and inotropic state of ejection and isovolumic phase measures of contractility in the conscious dog. *Am J Cardiol* 1975; **35**: 626–34.
- 4 Jones CJ, Raposo L, Gibson DG. Functional importance of the long axis dynamics of the human left ventricle. *Br Heart J* 1990; **63**: 215–20.
- 5 Buchalter MB, Weiss JL, Rogers WJ, Zerhouni EA, Weisfeldt ML, Beyar R. Noninvasive quantification of left ventricular rotational deformation in normal humans using magnetic resonance imaging myocardial tagging. *Circulation* 1990; **81**: 1236–44.
- 6 Henein MY, Gibson DG. Normal long axis function. *Heart* 1999; **81**: 111–13.
- 7 Hamilton WF, Rompf JH. Movements of the base of the heart and the relative constancy of the cardiac volume. *Am J Physiol* 1932; **102**: 559–65.
- 8 Rushmer RF, Crystal DK, Wagner C. The functional anatomy of ventricular contraction. *Circ Res* 1952; **1**: 162–70.
- 9 Henein MY, Gibson DG. Long axis function in disease. *Heart* 1999; **81**: 229–31.
- 10 Tabata T, Cardon LA, Armstrong GP, et al. An evaluation of the use of new Doppler methods for detecting longitudinal function abnormalities in a pacing-induced heart failure model. *J Am Soc Echocardiogr* 2003; **16**: 424–31.
- 11 Hasegawa H, Little WC, Ohno M, et al. Diastolic mitral annular velocity during the development of heart failure. *J Am Coll Cardiol* 2003; **41**: 1590–7.
- 12 Feigenbaum H, Zaky A, Nasser WK. Use of ultrasound to measure left ventricular stroke volume. *Circulation* 1967; **38**: 1092–9.
- 13 Pai RG, Bodenheimer MM, Pai SM, Koss JH, Adamick RD. Usefulness of systolic excursion of the mitral annulus as an index of left ventricular systolic function. *Am J Cardiol* 1990; **67**: 222–4.
- 14 Willenheimer R, Cline C, Erhardt L, Israelsson B. Left ventricular atrioventricular plane displacement: an echocardiographic technique for rapid assessment of prognosis in heart failure. *Heart* 1997; **78**: 230–6.
- 15 Yip G, Wang M, Zhang Y, Fung JW, Ho PY, Sanderson JE. Left ventricular long axis function in diastolic heart failure is reduced in both diastole and systole: time for a redefinition? *Heart* 2002; **87**: 121–5.
- 16 Alam M, Wardell J, Andersson E, Samad BA, Nordlander R. Effects of first myocardial infarction on left ventricular systolic and diastolic function with the use of mitral annular velocity determined by pulsed wave Doppler tissue imaging. *J Am Soc Echocardiogr* 2000; **13**: 343–52.
- 17 Yu CM, Lin H, Yang H, Kong SL, Zhang Q, Lee SW. Progression of systolic abnormalities in patients with “isolated” diastolic heart failure and diastolic dysfunction. *Circulation* 2002; **105**: 1195–201.
- 18 Vinereanu D, Nicolaides E, Tweddel AC, et al. Subclinical left ventricular dysfunction in asymptomatic patients with Type II diabetes mellitus, related to serum lipids and glycated haemoglobin. *Clin Sci (Lond)* 2003; **105**: 591–9.
- 19 Nagueh SF, Bachinski LL, Meyer D, et al. Tissue Doppler imaging consistently detect myocardial abnormalities in patients with hypertrophic cardiomyopathy and provides a novel means for an early diagnosis before and independently of hypertrophy. *Circulation* 2001; **104**: 128–30.
- 20 Wang M, Yip GW, Wang AY, et al. Peak early diastolic mitral annulus velocity by tissue Doppler imaging adds independent and incremental prognostic value. *J Am Coll Cardiol* 2003; **41**: 820–6.
- 21 Wang M, Yip G, Yu CM, et al. Independent and incremental prognostic value of early mitral annulus velocity in patients with impaired left ventricular systolic function. *J Am Coll Cardiol* 2005; **45**: 272–7.
- 22 Nikitin NP, Loh PH, Silva R, et al. Prognostic value of systolic mitral annular velocity measured with Doppler tissue imaging in patients with chronic heart failure caused by left ventricular systolic dysfunction. *Heart* 2006; **92**: 775–9.
- 23 Nagueh SF, Middleton KJ, Kopelen HA, Zoghbi WA, Quinones MA. Doppler tissue imaging: a noninvasive technique for evaluation of left ventricular relaxation and estimation of filling pressures. *J Am Coll Cardiol* 1997; **30**: 1527–33.
- 24 Burgess MI, Jenkins C, Sharman JE, Marwick TH. Diastolic stress echocardiography: hemodynamic validation and clinical significance of estimation of ventricular filling pressure with exercise. *J Am Coll Cardiol* 2006; **47**: 1891–900.
- 25 Troughton RW, Prior DL, Pereira JJ, et al. New echocardiographic indices of diastolic function have significant prognostic value in systolic heart failure: preliminary results from the ADEPT study. *Circulation* 2003; **108** (Suppl IV): 593.
- 26 Alam M, Wardell J, Andersson E, Nordlander R, Samad B. Mitral annular velocities in congestive heart failure with or without mitral regurgitation. *J Am Soc Echocardiogr* 2003; **16**: 240–5.
- 27 Agricola E, Galderisi M, Oppizzi M, et al. Pulsed tissue Doppler imaging detects early myocardial dysfunction in asymptomatic patients with severe mitral regurgitation. *Heart* 2004; **90**: 406–10.
- 28 Meluzin J, Spinarova L, Bakala J, et al. Pulsed Doppler tissue imaging of the velocity of tricuspid annular systolic motion: a new, rapid, and non-invasive method

- of evaluating right ventricular systolic function. *Eur Heart J* 2001; **22**: 340–8.
- 29 Meluzin J, Spinarova L, Dusek L, Toman J, Hude P, Krejci J. Prognostic Importance of the right ventricular function assessed by Doppler tissue imaging. *Eur J Echocardiogr* 2003; **4**: 262–71.
- 30 Vinereanu D, Lim PO, Frenneaux MP, Fraser AG. Reduced myocardial velocities of left ventricular long-axis contraction identify both systolic and diastolic heart failure – a comparison with brain natriuretic peptide. *Eur J Heart Fail* 2005; **7**: 512–9.
- 31 Greenberg NL, Firstenberg MS, Castro PL, et al. Doppler-derived myocardial systolic strain rate is a strong index of left ventricular contractility. *Circulation* 2002; **105**: 99–105.
- 32 Marwick T. Measurement of strain and strain rate by echocardiography: ready for prime time? *J Am Coll Cardiol* 2006; **47**: 1313–27.
- 33 Zhang Y, Chan AKY, Yu CM, Yip GWK, Fung JWH, Lam WMM, So NM, Wang M, Wu EB, Wong JT, Sanderson JE. Strain Rate Imaging Differentiates Transmural From Non-transmural Myocardial Infarction: A Validation Study Using Delayed-enhancement Magnetic Resonance Imaging. *J Am Coll Cardiol* 2005; **46**: 864–71.
- 34 Leitman M, Lysyansky P, Sidenko S, et al. Two-dimensional strain—a novel software for real-time quantitative echocardiographic assessment of myocardial function. *J Am Soc Echocardiogr* 2004; **17**: 1021–9.
- 35 Becker M, Hoffman R, Kuhl HP, et al. Analysis of myocardial deformation based on ultrasonic pixel tracking to determine transmurality in chronic myocardial infarction. *Eur Heart J* 2006; **27**: 2560–2566.
- 36 Notomi Y, Martin-Miklovic MG, Oryszak SJ, et al. Enhanced ventricular untwisting during exercise: a mechanistic manifestation of elastic recoil described by Doppler tissue imaging. *Circulation* 2006; **113**: 2524–33.
- 37 Yip GW, Zhang Y, Tan PY, Wang M, Ho PY, Brodin L-A, Sanderson JE. Left ventricular long axis function changes in early diastole and systole: impact of systolic function on diastole. *Clin Sci* 2002; **102**: 515–522.
- 38 Takeuchi M, Nakai H, Kokumai M, Nishikage T, Otani S, Lang RM. Age-related changes in left ventricular twist assessed by two-dimensional speckle-tracking imaging. *J Am Soc Echocardiogr* 2006; **19**: 1077–84.
- 39 Fuchs E, Muller MF, Oswald H, Thony H, Mohacsi P, Hess OM. Cardiac rotation and relaxation in patients with chronic heart failure. *Eur J Heart Fail* 2004; **6**: 715–722.

# Assessment of diastolic heart failure

*Gabriel W. Yip and Cheuk-Man Yu*

## Introduction

Heart failure is a major health problem requiring significant health care resources, especially in the elderly population. It is the fourth leading cause of death from vascular diseases in China, accounting for 13 and 16 per 100,000 person-years among men and women, respectively [1]. In the United States, almost 5 million Americans live with symptoms of heart failure, and a further 550,000 are diagnosed annually. There are 1.1 million hospital admissions of patients with the primary diagnosis of heart failure and approximately 3 million admissions a year with primary and secondary diagnoses of heart failure [2,3]. Community-based epidemiology prevalence studies show that more than half of patients with symptoms of heart failure have preserved left ventricular ejection fraction (LVEF) [4–7]. They also possess a high frequency of risk factors and comorbidities. This condition is more common in elderly women, especially those with a history of hypertension, LV hypertrophy, and in some cases, with diabetes mellitus, coronary artery disease, and atrial fibrillation [8–10]. Over the past 15 years, remarkable progress has been made in management of systolic heart failure (SHF) through advances in diagnostic devices and medical therapy. There is as yet no proven therapy for heart failure with preserved EF, except a modest reduction in hospitalization by Candesartan therapy, without a robust cardiovascular survival benefit [11]. Worse still, the mortality of preserved EF was similar to that with reduced EF, 22–29%, of those with preserved EF within one year of hospital discharge, and 65% died within five years [4,12,13]. Furthermore, it has been shown that even the

presence of a mild form of diastolic dysfunction in asymptomatic subjects is associated with a fivefold increase in mortality compared to the asymptomatic subjects with normal diastolic function [14]. Thus, the concept of diastolic dysfunction has evolved markedly because of increasing clinical recognition and the ability to diagnose heart failure with preserved EF. Indeed, should this increasing trend be confirmed and continue to grow, heart failure with preserved LVEF may become the most common form of heart failure. There is an urgent need for coordinated efforts to address this growing epidemic.

## Is assessment of diastolic function necessary?

Considerable debate exists as to whether these patients should be labeled as having diastolic heart failure (DHF), heart failure with preserved systolic LV function (HF-PSF), or heart failure with normal ejection fraction (HFNEF). In the absence of a discriminatory role for LV diastolic dysfunction, the latter term is preferred in the recently revised American College of Cardiology–American Heart Association guidelines for the diagnosis and management of heart failure [15]. The diagnosis of heart failure is essentially clinical, though it can be mimicked nonmyocardial as well as myocardial abnormalities [16–17] (Table 8.1). Furthermore, there is evidence of subtle regional abnormalities of myocardial long-axis function in some of these patients, suggestive of mild systolic dysfunction and early phase ventricular muscular pump failure in the presence of a still normal hemodynamic pump function [18–25]. DHF appears to be part of a continuous spectrum from “normal” aging to SHF,

**Table 8.1** Differential diagnosis in a patient with heart failure and normal left ventricular ejection fraction.

- Incorrect diagnosis of HF
- Inaccurate measurement of LVEF
- Primary valvular disease with severe stenosis or regurgitation
- Restrictive (infiltrative) cardiomyopathies  
Amyloidosis, sarcoidosis, hemochromatosis
- Pericardial constriction  
Cardiac tamponade, constrictive pericarditis
- Episodic or reversible LV systolic dysfunction
- Severe hypertension, myocardial ischemia
- HF associated with high metabolic demand (high-output states)  
Anemia, thyrotoxicosis, arteriovenous fistulae
- Right heart failure  
Pulmonary hypertension associated with pulmonary vascular disorders  
Right ventricular infarct  
Arrhythmogenic right ventricular dysplasia  
Atrial septal defect  
Intracardiac mass  
Atrial myxoma, Apical eosinophilic thrombus
- Pulmonary vein stenosis
- Congenital heart diseases
- Diastolic dysfunction of uncertain origin
- Obesity

HF, heart failure; LV, left ventricular; and LVEF, left ventricular ejection fraction.

Modified from Hunt SA, Abraham WT, Chin MH, et al. ACC/AHA 2005 Guideline Update for the Diagnosis and Management of Chronic Heart Failure in the Adult – Summary Article: A Report of the American College of Cardiology/American Heart Association Task Force on Practice Guidelines (Writing Committee to Update the 2001 Guidelines for the Evaluation and Management of Heart Failure). *J Am Coll Cardiol* 2005; 46: 1116–43.

reflecting heart failure as one disease entity with various phenotypes having a mixture of varying degrees of systolic and diastolic abnormalities [24]. DHF denotes a patient population that presents with symptoms and signs of heart failure, relatively normal EF, increased filling pressure, and evidence of diastolic dysfunction, but without other nonmyocardial abnormalities responsible for heart failure. In addition, a significant difference in structural and functional abnormalities of cardiomyocytes induced by hypertension exists between the two

phenotypes [25]. Invasive and noninvasive measurements of the LV global diastolic properties of DHF patients are abnormal [26–28], albeit gathered from a highly selective, small cohort of relatively young, predominantly male patients, under the assumption that ventricular characteristics and pathophysiological mechanisms are the same in all other patients with HFNEF [29]. Thus, the contention that the dominant functional abnormality of DHF resides in diastole and that the heart failure syndrome is related to but unlikely caused by the subtle abnormalities in regional systolic function is far from conclusive at this time.

## Echocardiography as a tool for assessment of heart failure

Echocardiography is an excellent noninvasive tool for the assessment of ventricular size and both systolic and diastolic function, and it is routinely used in patients with heart failure. The evaluation of diastolic function is not easily obtained by other techniques, and this feature is where echocardiography has its advantages. Furthermore, echocardiography can help to (1) confirm the clinical diagnosis of heart failure with elevated LV filling pressures, perhaps in conjunction with brain natriuretic peptide (BNP) measurements [30,31], and, if uncertain, with exercise testing; (2) determine etiology and mechanism and, therefore, treatable factors, for example, presence of ischemia, LV hypertrophy, dyssynchrony, and remodeling; and (3) prognosticate the medium-term of survival of these patients [32]. Clinical use of BNP levels in association with echocardiographic parameters can improve diagnostic accuracy and prognosis [33,34]. However, heart failure does remain a strictly clinical diagnosis. This review will discuss the role of echocardiography in diagnosis and management of DHF patients in whom newer echocardiographic techniques suggest that they have abnormal systolic function.

Comprehensive echocardiography in contemporary practice consists of M-mode, two-dimensional (2-D), Doppler flow, color flow imaging, and tissue Doppler imaging (TDI), all of which should be performed and interpreted collectively in relation to clinical findings. Cardiac function is truly normal

when myocardial contractility, diastolic function, and filling pressures are normal not only at rest but also during exertion. It is not uncommon that heart failure patients may remain largely asymptomatic (stage B) for a period of time until development of symptoms and signs of heart failure. There is no clear consensus worldwide regarding diagnostic echocardiographic criteria for DHF. Disagreement exists over what should be considered a normal EF, how soon the EF must be assessed after heart failure has been diagnosed, and whether measurement of hemodynamics or other tests for the presence of diastolic dysfunction must be performed. Recently, two different standardized diagnostic criteria for diastolic HF were suggested. The European criteria require clinical heart failure with a normal EF (defined as >45%) and some objective quantification (transmitral or pulmonary venous Doppler echocardiography or invasive hemodynamics) of diastolic dysfunction [35]. The criteria suggested by Vasan and Levy require a normal EF (>50%) and invasive hemodynamic data to confirm *definite* diastolic HF. Classification as *probable* or *possible* diastolic HF is based on time from patient's symptom onset to EF determination (<3 days for probable and >3 days for possible) and on supportive clinical features [36]. Invasive measurement of global diastolic parameters based on end-diastolic pressure–volume relationships is impractical in routine clinical practice, and invasive and noninvasive parameters do not necessarily stratify patients for their severity of diastolic dysfunction (e.g., pseudonormal vs. restrictive filling pattern) and prognosis. Furthermore, the criteria still need further prospective validation and testing of their ability to identify patients with a worse prognosis who might respond to a standardized treatment approach. They are further limited by failure to include newer echocardiographic techniques, for example, TDI, strain echocardiography, and speckle tracking echocardiography (STE) for LV torsional assessment. As a result, the previous European guidelines [37].

In practice, a normal EF on 2-D echocardiography in patients with clinical evidence of heart failure immediately suggests the potential diagnosis of DHF. Doppler, color flow imaging, and myocardial tissue imaging can confirm or exclude the

### How to assess diastolic function step by step approach

- 1** Are there 2-D findings for diastolic dysfunction?
- 2** Does mitral inflow velocity pattern indicate diastolic dysfunction?
- 3** Is myocardial relaxation abnormal?
- 4** If abnormal, is filling pressure elevated at rest and/or with exertion?
- 5** Is constrictive pericarditis a possibility?

**Figure 8.1** Stepwise approach in assessment of diastolic function.

diagnosis of DHF by assessing valvular abnormality and intrinsic diastolic function and estimating diastolic filling pressure [38,39] (Figure 8.1). Early identification of diastolic dysfunction in asymptomatic (stage B) patients by echocardiography may provide an opportunity to manage the underlying etiology appropriately to prevent its progression to overt DHF (stage C of development of heart failure). The response and rationale of slowing the heart rate and vasodilator or diuretic treatment may also be guided and monitored by the judicious use of echocardiography, although there is no hard endpoint drug trial selecting patients based on LV filling abnormalities. Ultimately, an ideal drug will improve myocardial relaxation, fibrosis or stiffness, and LV filling pressures at rest and during exertion without untoward effects.

### Traditional Doppler echocardiographic indices of diastolic function

The most commonly used Doppler indices are Doppler transmitral velocities, the early E-wave and late A-wave and their ratio, the deceleration time (DT) of the E-wave, and the isovolumic relaxation time (IVRT; Table 8.2). These variables are used for the evaluation of impaired relaxation and the semiquantitation of filling pressures [39]. Although transmitral filling patterns are fundamental to the assessment of LV diastolic function, they have several limitations. Normal values need to be adjusted for age [35,41,42] (Table 8.3). The early mitral deceleration time correlates well with filling pressures in patients with sinus rhythm and a reduced LVEF of <40% [43,44], but not in

**Table 8.2** What to measure in diastolic function assessment.

- 2-D echo features (e.g., LVEF, wall thickness, septal motion, LA volume)
- Mitral inflow velocities (E-wave, A-wave, E/A ratio)
- Mitral E-wave deceleration time
- Isovolumic relaxation time
- Pulmonary vein systolic and diastolic velocities (PVs2, PVd, S/D ratio)
- Pulmonary vein atrial systolic reversal (PVar) +.3
- Difference between PVar and mitral A-wave duration
- Mitral annular velocities as measured by tissue Doppler imaging: E' (early), A' (late), and ratio of mitral E to Doppler tissue E'
- Color M-mode flow propagation

**Table 8.3** Age adjusted normal cut offs for selected diastolic parameters (Refs. 35, 40–41).

	<40 years	40–60 years	>60 years
E deceleration time (msec)	<220	140–250	140–275
Septal E' velocity (cm/sec)	>9	>7	>6
Lateral E' velocity (cm/sec)	>11	>10	>7

Adapted from Mottram PM, Marwick TH. *Heart* 2005; 91: 681–95.

patients with DHF where the LV systolic function is relatively preserved. They may change rapidly with preload alteration and atrial fibrillation [45]. Pseudonormalization of the inflow pattern is a further major limitation. To overcome this problem, either a preload reduction technique, for example, Valsalva maneuver [46–48] or sublingual glyceryl trinitrate [49], or less load-dependent indices of LV filling can be used, usually in combination with transmural parameters. This strategy may include assessment of the pulmonary venous flow pattern [44,48,50–52]. The reduction of preload (left atrial [LA] pressure) in patients with pseudonormal flow (raised filling pressures coupled with abnormal relaxation) should reveal the underlying abnormal relaxation pattern.

### Preload alteration

The Valsalva maneuver is largely a qualitative technique without an accurate quantitative cutoff value. Patients who perform this maneuver and can reduce the transmural E/A ratio by an absolute value of  $\geq 0.5$ , the E velocity  $\geq 50\%$ , or to complete reversal of the E/A ratio have raised filling pressures independent of systolic function. Unfortunately, some patients are not able to perform an adequate Valsalva maneuver (e.g., as assessed by ability of forcefully exhaling into an analog manometer to achieve an intrathoracic pressure of  $\geq 30$  mmHg), and careful attention to signal acquisition, especially keeping the sample volume position at the mitral valve tips during the maneuver, and measurement is crucial. In cases where there is slight fusion of the mitral E- and A-waves, the absolute late diastolic velocity (A) should be determined by subtracting the E velocity at onset of A (especially if  $\geq 0.4$  m/sec) from the measured peak A velocity. Even with these measures, adequate signals were obtained in only 61% of patients [50]. The use of sublingual nitrate to alter preload, although more predictable, is not feasible in many practice settings.

### Pulmonary venous Doppler velocities

Pulmonary venous flow is obtained during transthoracic imaging by placing a 3- to 4-mm sample volume at 1 to 2 mm into a pulmonary vein, commonly the right paraseptal (superior) vein in apical four-chamber view [53]. The Doppler signal consists of forward waves in early ventricular systole (PVs1; seen in approximately 30% of transthoracic studies) [53], late ventricular systole and isovolumic relaxation (PVs2; largest of the two systolic waves), early ventricular diastolic wave (PVd), and flow reversal during atrial systole (PVar). The PVs1 is caused by atrial relaxation and also systolic descent of the mitral annulus that is responsible for the normal X descent on the atrial pressure pulse [54–56]. The PVs2, however, is attributed to transpulmonary propagation of the RV systolic pressure pulse [56] and also reflected pressure waves from pressure changes in the left atrium [57] (Figure 8.2). Normally, most flow into the left atrium occurs in systole. However, when the LA pressure increases, antegrade systolic flow decreases and flow occurs predominantly in diastole. A systolic filling fraction

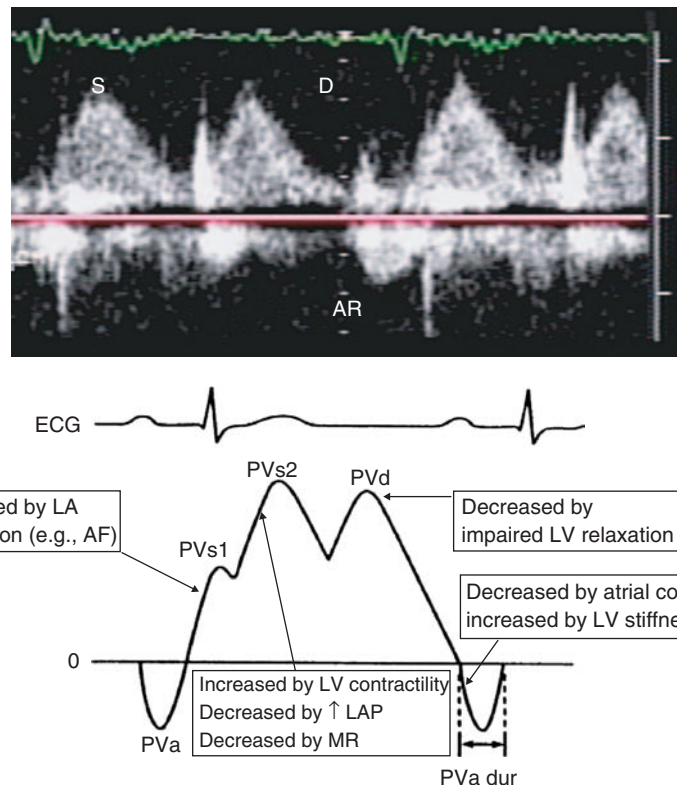


**Figure 8.2** Normal pulmonary venous Doppler flow pattern. S, Systolic flow; PVs1, early pulmonary venous systolic forward flow; PVs2, late pulmonary venous systolic forward flow; PVd or D, pulmonary venous diastolic forward flow. AR or PVa, pulmonary venous flow reversal

due to atrial contraction; PVa dur, duration of pulmonary venous flow reversal due to atrial contraction. Modified from Oh et al. *The Echo Manual*, 2nd edn. Lippincott Williams & Wilkins; 1999, p. 50.

<40% correlates well with a mean LA pressure >15 mm Hg when the LVEF < 50%, but this correlation is poor in patients with DHF [44]. PVar flow into the pulmonary vein with atrial contraction occurs because of a positive pressure gradient between the left atrium and the pulmonary vein and is influenced by pre-A LV diastolic pressure (atrial preload), LV stiffness and LV end-diastolic pressure (LVEDP, atrial afterload), as well as atrial systolic function. When LVEDP increases, antegrade flow across the mitral valve decreases and PVar flow into the vein becomes more prominent (both in duration and velocity). A PVar velocity >35 cm/sec and an Ar-A duration ≥30 msec correctly predict an LVEDP > 15 mm Hg, irrespective of LV systolic function [44,52]. The major limitations are that these signals are difficult to obtain and interpret and are greatly affected by heart

rhythm (e.g., atrial fibrillation) and the presence of mitral stenosis (MS) or regurgitation (MR), independent of LA pressure (blunt/absent/reversal of systolic flow in MR or prolonged diastolic flow and its deceleration time in MS). The technical feasibility of obtaining adequate signals has been reported to be in <80% of unselected patients [50].

### Left atrial size

LA volume is a sensitive indicator of chronicity as well as severity of diastolic dysfunction and is a predictor of common cardiovascular outcomes such as atrial fibrillation, stroke, congestive heart failure, and cardiovascular death [58]. The American Society of Echocardiography has recommended quantification of LA size by biplane 2-D echocardiography using either the method of discs (by Simpson's rule) or the area-length method [59].

The LA volume indexed to body surface area is optimally interpreted as a continuous variable, using a reference point of  $22 \pm 5 \text{ ml/m}^2$  as normal [60]. However, its specificity is compromised in atrial fibrillation and mitral valve disease that commonly increase LA size. Thus, other techniques have been developed. The most extensively validated ones are the determination of blood flow propagation within the left ventricle with the use of color M-mode and tissue Doppler assessment of mitral annulus motion during diastole.

## New echocardiographic indices for assessing diastolic heart failure

### Color M-mode flow propagation velocity

Early diastolic flow propagation velocity by color M-mode in an apical four-chamber view displays velocity information along a scan line that extends from the mitral valve to the LV apex with superior temporal resolution (2.5–10 msec), spatial resolution (~1 mm), and velocity resolution directly proportional to the Nyquist limit. The slope of this early surge of blood into the left ventricle has been termed *flow propagation velocity* ( $V_p$ ), which is slowed in impaired LV relaxation. One of the most commonly used clinical methods of measuring  $V_p$  is by the slope of the first aliasing velocity (normal  $V_p \geq 45 \text{ cm/sec}$ ), along the bright yellow or blue isovelocity line during early filling, from the mitral valve plane to 4 cm distally into the LV cavity at a horizontal sweep speed of 100 mm/sec [45].  $V_p$  correlates with invasive indices of LV relaxation, including the time constant tau ( $\tau$ ), and is relatively preload-independent under physiological conditions [60,61]. It is also affected by LV geometry, base-to-apex intraventricular pressure gradients, and synchronicity of myocardial relaxation [63,64]. The ratio of mitral inflow E velocity to  $V_p$  allows estimation of filling pressure during sinus rhythm or atrial fibrillation. A  $E/V_p$  ratio  $>1.5$  is suggestive of increased ( $>15 \text{ mm Hg}$ ) pulmonary capillary wedge pressure (PCWP), especially in the setting of LV dilatation and reduced EF [65,66]. The  $V_p$  measurements become problematic when the slope of the first aliasing velocity becomes curvilinear toward the LV apex or too steep and becomes normalized by enhanced intraventricular gradients, despite

delayed relaxation in a small hypertrophied left ventricle [67], and minute deviation of the slope results in a large variation of  $V_p$  values.

### Tissue Doppler echocardiography

Because of its high reproducibility, feasibility, and relatively preload-independence, tissue Doppler recording of the early diastolic mitral annular velocity ( $E'$ ) in conjunction with the mitral inflow velocity (E) has become the first line of diastolic evaluation. Myocardial relaxation is impaired in almost all patients with diastolic dysfunction, which is best assessed by the  $E'$  velocity of the mitral annulus using TDI. While early diastolic transmural velocity (E) increases progressively as LV filling pressure increases, the mitral annular  $E'$  velocity remains decreased at all stages of diastolic dysfunction [68]. Therefore, LV filling pressure correlates well with the ratio between mitral E and mitral annular  $E'$  velocity ( $E/E'$ ) [50,69], and it has been validated in the presence of preserved or poor LV systolic function [50], sinus tachycardia [70], atrial fibrillation [71], heart transplant [72], and hypertrophic cardiomyopathy [73]. The lateral mitral annular velocity has been used frequently in this validation, with  $E/E' > 10$  reliably predicting PCWP  $>12 \text{ mmHg}$  [68], but the septal  $E'$  has also been used with similar results. A ratio of E/septal  $E' > 15$  was highly specific for mean LV diastolic pressure (mean LVDP)  $>15 \text{ mmHg}$  and, similarly, a ratio  $< 8$  was highly sensitive for a normal mean LVDP [50]. However, with regional dysfunction, an average of both velocities should be obtained and used in drawing conclusions about diastolic function and filling pressures. In addition, a septal  $E'$  velocity  $> 8 \text{ cm/sec}$  by TDI can distinguish patients with constrictive pericarditis (CP) from those with a restrictive cardiomyopathy where the velocity is reduced [67]. In CP, septal  $E'$  is normal or even increased because the circumferential and lateral motion of the mitral annulus is limited by pericardial adhesion that augments the longitudinal motion of the medial annulus. Thus, an inverse relationship between septal  $E/E'$  and PCWP is seen in CP, in contrast to a direct correlation in myocardial diseases [74]. These findings can be incorporated into clinical practice to provide a noninvasive assessment of diastolic filling of the heart (Figure 8.3). The Doppler patterns from normal, abnormal relaxation to pseudonormal LV filling are illustrated

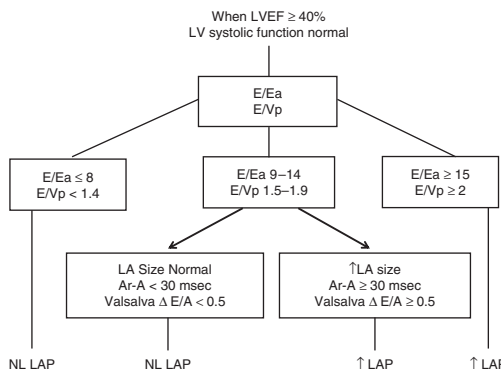


**Figure 8.3** Suggested screening assessment for diastolic function and filling pressures. The 2-D and Doppler echocardiographic variables can be used to readily classify diastolic function. \*In general, high filling pressures should be confirmed with multiple parameters (i.e., E/E', E/Vp, A-dur difference, response to Valsalva maneuver, tricuspid regurgitant velocity, and so on).

in videoloops 9–11 . Doppler variables should always be interpreted in the context of ventricular size and function, as well as left atrial size.

### Dynamic diastology

A subset of patients with chronic stable DHF may have symptoms of increased filling pressure only with exertion. As long as diastolic filling period (DFP) is well preserved at rest, filling pressure remains relatively normal, but when the DFP is shortened by tachycardia or atrial fibrillation, these patients do not have diastolic reserve to compensate and usually experience exertional dyspnea and exercise intolerance, resulting from increased LV filling pressure rather than the slow myocardial relaxation exhibited at rest [75]. The confirmation of a cardiac versus noncardiac etiology for exertional dyspnea has potential therapeutic and prognostic implications. Because the E/E' ratio can assess LV filling pressure at rest, the same parameter can be measured with exercise. A cutoff value of 13 for exercise E/E' identifies patients with an LV diastolic pressure of >15 mmHg during exercise, independent of the presence of myocardial ischemia. Moreover, a postexercise E/E' cutoff value of >10 predicts those with a reduced exercise capacity (<8 metabolic equivalents) with a sensitivity of 71% and a specificity of 69% [76]. The conversion of an *impaired relaxation* pattern at rest to a *pseudonormal* pattern immediately after

exercise is indicative of elevation of LA pressure with exercise, and suggests that the slow LV relaxation is functionally important in a particular patient [77]. Similarly, augmentation of BNP with exercise might also have diagnostic potential in this situation. Whereas resting tissue Doppler measures have recently been shown to provide prognostic information in patients with a range of cardiac diseases [78,79], the prognostic implications of elevated exercise E/E' remain to be defined.

### Temporal relationship between mitral inflow and annulus velocities

Conventional Doppler measurements have limitations in predicting LA pressure (LAP) in patients with mitral valve disease, given the confounding effect of valve area, LV relaxation, and stiffness. In addition, annulus E' velocity is reduced in patients with MS, whereby the stroke volume is reduced despite a normal LVEF, but is increased in those with MR in parallel to the increased stroke volume and regurgitant volume. Previous studies highlighted an important limitation in using E/E' for the prediction of LAP in patients with significant mitral valve disease, especially myxomatous disease [80]. However, the time interval between the onset of early diastolic mitral inflow velocity (E) and annular early diastolic velocity (E') by TDI,  $T_{E-E'}$ , which is well related to the time constant of LV relaxation ( $\tau$ ) in canine and clinical studies [81,82], is not subject to these variables. The mitral annulus velocity normally precedes the transmural flow by approximately  $22 \pm 19$  msec [83], but this temporal relationship becomes reversed with progressive diastolic dysfunction as blood is pushed into the left ventricle under high filling pressure rather than initiated and augmented by LV relaxation. Because IVRT is directly proportional to  $\tau$  but inversely to LAP ( $IVRT \propto \tau/LAP$ ), the PCWP, an indirect measure of the LAP, is related to the ratio of  $IVRT/T_{E-E'}$ . There are different cutoff values of  $IVRT/T_{E-E'}$  for different patient populations to predict  $PCWP > 15$  mmHg: a value of 2 for patients with sinus rhythm without mitral valve disease, 3 for patients with MR, 4.16 for MS patients, and 5.59 for atrial fibrillation patients [84]. The difference in  $T_{E-E'}$  is small and requires mean annulus E' values from four locations in apical four- and two-chamber views with two different cardiac cycles. Sohn et al. [85] questioned the clinical validity of

the formula IVRT/  $T_{E-E'}$  when the onsets of E and E' were simultaneous, and IVRT/ $T_{E-E'}$  became zero in the majority of their cases, although  $T_{E-E'}$  was measured from one location with different cycle lengths. To reduce measurement errors and measurement time, the onset of both mitral E and E' from a single cardiac cycle may be simultaneously recorded using the regular pulsed-wave Doppler echocardiography with a sample volume placed between the septal (or lateral) mitral annulus and the mitral leaflet [86]. Further clinical investigation and experience will determine the reliability and role of IVRT/  $T_{E-E'}$  in assessing filling pressure.

### **Left ventricular dyssynchrony in diastolic heart failure**

The success of cardiac resynchronization therapy has underscored the importance of dyssynchrony in the pathophysiology of SHF, independent of the QRS duration [86]. However, limited data exist for DHF patients in that approximately 33–39% showed evidence of systolic dyssynchrony and 56–58% of diastolic dyssynchrony [88,89]. Interestingly, 25% of the DHF patients demonstrated isolated systolic dyssynchrony, and the correlation between systolic and diastolic dyssynchrony was poor [89], in contrast to the close curvilinear relationship between the mean annulus systolic and early diastolic velocities seen in a range of cardiac diseases and normal subjects [90]. Systolic dyssynchrony in DHF is associated with reduced peak basal myocardial velocities, lower stroke work, and an even lower normal EF than in those without systolic dyssynchrony [88]. This finding suggests that systolic dyssynchrony contributes to a wider spectrum of systolic dysfunction in DHF, casting further doubts on the orthodox view that DHF is purely a clinical entity of diastolic dysfunction. Future studies on dynamic exercise changes of LV dyssynchrony in patients with DHF may be relevant to this ongoing debate [91].

### **Strain echocardiography**

Assessment of myocardial velocity, strain, and strain rate by TDI has proved to be more accurate than visual evaluation of global and regional function [92,93]. TDI-derived parameters have consistently demonstrated the presence of subclinical

systolic long-axis dysfunction in many of the precursor conditions to DHF, such as diabetes [94], hypertension [95], and LV hypertrophy [96], due to susceptibility of the underlying subendocardial longitudinal fibers to effects of fibrosis, ischemia, and hypertrophy. Myocardial strain or strain rate derived from the time integral of spatial velocity gradients between two adjacent color tissue Doppler velocities (velocity regression approach) is superior to myocardial velocities and wall motion score in detection of regional ischemia [93,97]. However, there are no published data that have compared these techniques in DHF patients.

Strain measurements derived from STE are direct measures of myocardial deformation (natural or Lagrangian strain) and recently have been introduced as a method to compensate for the inherent angle-dependence of TDI-derived measures [98], to reduce analysis time, and to further improve signal-to-noise ratio and data quality [99]. This novel technique tracks frame-to-frame movement (from 40 to 90 frames/sec) of natural acoustic markers (speckles) on standard gray-scale images of the myocardium. The technical aspects are covered in Chapter 2. The relatively low frame rate and smoothing may result in less-detailed strain or strain rate curves and may not permit accurate timing measurements. Nonetheless, amplitude parameters correlate well with strain measurements obtained by velocity regression [98] and magnetic resonance tissue tagging [100].

In addition to estimating radial and longitudinal strain simultaneously, STE offers torsional, or twisting, motion assessment [101,102] derived from circumferential strain at different short-axis levels of the heart that is promoted by the virtue of a single myofiber band forming a double helix in the left ventricle, which changes gradually from a right-handed helix in the subendocardium to a left-handed helix in the subepicardium [103]. Accordingly, LV torsion is defined as apical rotation relative to the base. When viewed from the apex, the systolic rotation of the base is clockwise and that of the apex counterclockwise. The LV untwisting begins just slightly before the end of systole as defined by aortic valve closure, followed in time by the peak intraventricular gradient and then long-axis lengthening and short-axis expansion that may precede or coincide with peak early diastolic

filling. However, like many diastolic parameters, there are age-related changes in LV torsion, with increased peak systolic twisting but reduced and delayed untwisting velocities [104]. During exercise, using TDI-based techniques, both twisting and untwisting velocities are increased primarily due to increased apical rotations and are significantly greater than the corresponding changes in LV length and radius. This lusitropic enhancement during exercise is blunted in patients with hypertrophic cardiomyopathy, not only in peak torsional values but also in timing of untwisting being delayed within the cardiac cycle [105]. Thus, there is compelling evidence that a transition from LV twisting to LV untwisting, which are normally closely coupled, is the mechanical event that initiates LV relaxation and that a prominent mechanism for exercise intolerance in hypertrophic cardiomyopathy is an inability to enhance diastolic untwisting, resulting in less diastolic suction, impaired LV filling, and increased LAP. Future directions will be to study these measures in other conditions associated with DHF, such as hypertensive heart disease and infiltrative disorders of the myocardium and whether these conditions can be followed clinically as a response to pharmacological therapy, as our future therapy expands to include agents that are targeted primarily at diastolic function.

## Conclusions

Over the past 20 years, echocardiography has advanced significantly and now provides more practical and clinically relevant information about DHF than other imaging modalities. Tissue Doppler and strain echocardiography have emerged to add incremental value over traditional volumetric analysis and EF and should help advance our understanding of important clinical issues and further clarify mechanisms of DHF. In summary, comprehensive evaluation of diastolic function by echocardiography can (1) provide diagnostic information for DHF, (2) estimate LV filling pressure reliably, (3) distinguish constrictive pericarditis from myocardial DHF, (4) distinguish patients with cardiac from noncardiac exertional dyspnea, (5) provide mechanistic insights of pathophysiology of DHF as a disease of ventricular pump function, and

(6) monitor therapeutic response using various novel echocardiographic parameters.

## References

- He J, Gu D, Wu X, et al. Major causes of death among men and women in China. *N Engl J Med* 2005; **353**: 1124–34.
- Thom T, Haase N, Rosamond W, et al. Heart disease and stroke statistics 2006 – update: a report from the American Heart Association Statistics Committee and Stroke Statistics Subcommittee. *Circulation* 2006; **113**: e85–151.
- DeFrances CJ, Podgornik MN. 2004 National hospital discharge survey. *Adv Data* 2006; **371**: 1–19.
- Bursi F, Weston SA, Redfield MM, et al. Systolic and diastolic heart failure in the community. *JAMA* 2006; **296**: 2209–16.
- Gheorghiade M, Abraham WT, Albert NM, et al. Systolic blood pressure at admission, clinical characteristics, and outcomes in patients hospitalized with acute heart failure. *JAMA* 2006; **296**: 2217–26.
- Hogg K, Swedberg K, McMurray J. Heart failure with preserved left ventricular systolic function: epidemiology, clinical characteristics, and prognosis. *J Am Coll Cardiol* 2004; **43**: 317–27.
- Yip GW, Ho PP, Woo KS, Sanderson JE. Comparison of frequencies of left ventricular systolic and diastolic heart failure in Chinese living in Hong Kong. *Am J Cardiol* 1999; **84**: 563–7.
- Davie AP, Francis CM, Caruana L, Sutherland GR, McMurray JJ. The prevalence of left ventricular diastolic filling abnormalities in patients with suspected heart failure. *Eur Heart J* 1997; **18**: 981–4.
- Kitzman DW, Little WC, Brubaker PH, et al. Pathophysiological characterization of isolated diastolic heart failure in comparison to systolic heart failure. *JAMA* 2002; **288**: 2144–50.
- Yancy CW, Lopatin M, Stevenson LW, De Marco T, Fonarow GC; ADHERE Scientific Advisory Committee and Investigators. Clinical presentation, management, and in-hospital outcomes of patients admitted with acute decompensated heart failure with preserved systolic function: a report from the Acute Decompensated Heart Failure National Registry (ADHERE) Database. *J Am Coll Cardiol* 2006; **47**: 76–84.
- Yusuf S, Pfeffer MA, Swedberg K, et al. Effects of Candesartan in patients with chronic heart failure and preserved left ventricular ejection fraction: the CHARM-Preserved trial. *Lancet* 2003; **362**: 777–81.
- Owan TE, Hodge DO, Herges RM, Jacobsen SJ, Roger VL, Redfield MM. Trends in prevalence and outcome of heart failure with preserved ejection fraction. *N Engl J Med* 2006; **355**: 251–9.

- 13 Bhatia RS, Tu JV, Lee DS, et al. Outcome of heart failure with preserved ejection fraction in a population-based study. *N Engl J Med* 2006; **355**: 260–9.
- 14 Redfield MM, Jacobsen SJ, Burnett JC Jr, Mahoney DW, Bailey KR, Rodeheffer RJ. Burden of systolic and diastolic ventricular dysfunction in the community: appreciating the scope of the heart failure epidemic. *JAMA* 2003; **289**: 194–202.
- 15 Hunt SA. ACC/AHA 2005 guideline update for the diagnosis and management of chronic heart failure in the adult – summary article: a report of the American College of Cardiology/American Heart Association Task Force on Practice Guidelines (writing committee to update the 2001 guidelines for the evaluation and management of heart failure). *J Am Coll Cardiol* 2005; **46**: e1–82.
- 16 Litwin SE, Grossman W. Diastolic dysfunction as a cause of heart failure. *J Am Coll Cardiol* 1993; **22**: 49A–55A.
- 17 Vasan RS, Benjamin EJ, Levy D. Congestive heart failure with normal left ventricular systolic function: clinical approaches to the diagnosis and treatment of diastolic heart failure. *Arch Intern Med* 1996; **156**: 146–57.
- 18 Yip G, Wang M, Zhang Y, Fung JW, Ho PY, Sanderson JE. Left ventricular long axis function in diastolic heart failure is reduced in both diastole and systole: time for a redefinition? *Heart* 2002; **87**: 121–5.
- 19 Petrie MC, Caruana L, Berry C, McMurray JJ. “Diastolic heart failure” or heart failure caused by subtle left ventricular systolic dysfunction? *Heart* 2002; **87**: 29–31.
- 20 Nikitin NP, Witte KK, Clark AL, Cleland JG. Color tissue Doppler-derived long-axis left ventricular function in heart failure with preserved global systolic function. *Am J Cardiol* 2002; **90**: 1174–7.
- 21 Yu CM, Lin H, Yang H, Kong SL, Zhang Q, Lee SW. Progression of systolic abnormalities in patients with “isolated” diastolic heart failure and diastolic dysfunction. *Circulation* 2002; **105**: 1195–1201.
- 22 Bruch C, Gradaus R, Gunia S, Breithardt G, Wichter T. Doppler tissue analysis of mitral annular velocities: evidence for systolic abnormalities in patients with diastolic heart failure. *J Am Soc Echocardiogr* 2003; **16**: 1031–6.
- 23 Vinereanu D, Nicolaides E, Tweddel AC, Fraser AG. “Pure” diastolic dysfunction is associated with long-axis systolic dysfunction: implications for the diagnosis and classification of heart failure. *Eur J Heart Fail* 2005; **7**: 820–8.
- 24 De Keulenaer G, Brutsaert DL. Systolic and diastolic heart failure: different phenotypes of the same disease? *Eur J Heart Fail* 2006 [Epub ahead of print].
- 25 van Heerebeek L, Borbely A, Niessen HW, et al. Myocardial structure and function differ in systolic and diastolic heart failure. *Circulation* 2006; **113**: 1966–73.
- 26 Zile MR, Gaasch WH, Carroll JD, et al. Heart failure with a normal ejection fraction: is measurement of diastolic function necessary to make the diagnosis of diastolic heart failure? *Circulation* 2001; **104**: 779–82.
- 27 Zile MR, Baicu CF, Gaasch WH. Diastolic heart failure: abnormalities in active relaxation and passive stiffness of the left ventricle. *N Engl J Med* 2004; **350**: 1953–9.
- 28 Baicu CF, Zile MR, Aurigemma GP, Gaasch WH. Left ventricular systolic performance, function, and contractility in patients with diastolic heart failure. *Circulation* 2005; **111**: 2306–12.
- 29 Maurer MS, King DL, El-Khoury Rumbarger L, Packer M, Burkhoff D. Left heart failure with a normal ejection fraction: identification of different pathophysiological mechanisms. *J Card Fail* 2005; **11**: 177–87.
- 30 Davis M, Espiner E, Richards G, et al. Plasma brain natriuretic peptide in assessment of acute dyspnoea. *Lancet* 1994; **343**: 440–4.
- 31 Maisel AS, McCord J, Nowak RM, et al. Bedside B-type natriuretic peptide in the emergency diagnosis of heart failure with reduced or preserved ejection fraction: results from the Breathing Not Properly Multinational Study. *J Am Coll Cardiol* 2003; **41**: 2010–7.
- 32 Sanderson JE. Heart failure with a normal ejection fraction. *Heart* 2005; **93**: 155–8.
- 33 Dokainish H, Zoghbi WA, Lakkis NM, et al. Optimal non-invasive assessment of LV filling pressures: a comparison of tissue Doppler echocardiography and BNP in patients with pulmonary artery catheters. *Circulation* 2004; **109**: 2432–9.
- 34 Dokainish H, Zoghbi WA, Lakkis NM, et al. Incremental predictive power of B-type natriuretic peptide and tissue Doppler echocardiography in the prognosis of patients with congestive heart failure. *J Am Coll Cardiol* 2005; **45**: 1223–6.
- 35 Paulus WJ, for the European Study Group on Diastolic Heart Failure. How to diagnose diastolic heart failure. *Eur Heart J* 1998; **19**: 990–1003.
- 36 Vasan RS, Levy D. Defining diastolic heart failure: a call for standardized diagnostic criteria. *Circulation* 2000; **101**: 2118–21.
- 37 Paulus WJ, Tschope C, Sanderson JE, et al. How to diagnose diastolic heart failure: a consensus statement on the diagnosis of heart failure with normal left ventricular ejection fraction by the Heart Failure and Echocardiography Associations of the European Society of Cardiology. *Eur Heart J*. 2007; Apr 11 (Epub ahead of print)
- 38 Oh JK. Echocardiography as a noninvasive Swan-Ganz catheter. *Circulation* 2005; **111**: 3192–4.
- 39 Oh JK, Hatle L, Tajik AJ, Little WC. Diastolic heart failure can be diagnosed by comprehensive two-dimensional

- and Doppler echocardiography. *J Am Coll Cardiol* 2006; **47**: 500–6.
- 40 Appleton CP, Hatle LK, Popp RL. Relation of trans-mitral flow velocity patterns to left ventricular diastolic function: new insights from a combined hemodynamic and Doppler echocardiographic study. *J Am Coll Cardiol* 1988; **12**: 426–40.
  - 41 Rakowski H, Appleton C, Chan KL, et al. Canadian consensus recommendations for the measurement and reporting of diastolic dysfunction by echocardiography: from the Investigators of Consensus on Diastolic Dysfunction by Echocardiography. *J Am Soc Echocardiogr* 1996; **9**: 736–60.
  - 42 De Boeck BW, Cramer MJ, Oh JK, van der Aa RP, Jaarsma W. Spectral pulsed tissue Doppler imaging in diastole: a tool to increase our insight in and assessment of diastolic relaxation of the left ventricle. *Am Heart J* 2003; **146**: 411–9.
  - 43 Nishimura RA, Appleton CP, Redfield MM, Ilstrup DM, Holmes DR Jr, Tajik AJ. Noninvasive Doppler echocardiographic evaluation of left ventricular filling pressures in patients with cardiomyopathies: a simultaneous Doppler echocardiographic and cardiac catheterization study. *J Am Coll Cardiol* 1996; **28**: 1226–33.
  - 44 Yamamoto K, Nishimura RA, Chaliki HP, Appleton CP, Holmes DR Jr, Redfield MM. Determination of left ventricular filling pressure by Doppler echocardiography in patients with coronary artery disease: critical role of left ventricular systolic function. *J Am Coll Cardiol* 1997; **30**: 1819–26.
  - 45 Garcia MJ, Thomas JD, Klein AL. New Doppler echocardiographic applications for the study of diastolic function. *J Am Coll Cardiol* 1998; **32**: 865–75.
  - 46 Schwammthal E, Popescu B, Popescu A, et al. Noninvasive assessment of left ventricular end-diastolic pressure by the response of the transmitral A-wave velocity to a standardized Valsalva maneuver. *Am J Cardiol* 2000; **86**: 169–74.
  - 47 Dumesnil JG, Gaudreault G, Honos GN, Kingma JG Jr. Use of Valsalva maneuver to unmask left ventricular diastolic function abnormalities by Doppler echocardiography in patients with coronary artery disease or systemic hypertension. *Am J Cardiol* 1991; **68**: 515–9.
  - 48 Brunner-La Rocca H, Rickli H, Attenhofer-Jost C, Jenni R. Left ventricular end-diastolic pressure can be estimated by either changes in transmitral inflow pattern during Valsalva maneuver or analysis of pulmonary venous flow. *J Am Soc Echocardiogr* 2000; **13**: 599–607.
  - 49 Hurrell DG, Nishimura RA, Ilstrup DM, Appleton CP. Utility of preload alteration in assessment of left ventricular filling pressure by Doppler echocardiography: a simultaneous catheterization and Doppler echocardiographic study. *J Am Coll Cardiol* 1997; **30**: 459–67.
  - 50 Ommen SR, Nishimura RA, Appleton CP, et al. Clinical utility of Doppler echocardiography and tissue Doppler imaging in the estimation of left ventricular filling pressures: a comparative simultaneous Doppler catheterization study. *Circulation* 2000; **102**: 1788–94.
  - 51 Keren G, Sherez J, Megidish R, Levitt B, Laniado S. Pulmonary venous flow pattern – its relationship to cardiac dynamics. A pulsed Doppler echocardiographic study. *Circulation* 1985; **71**: 1105–12.
  - 52 Rossqvist O, Hatle LK. Pulmonary venous flow velocities recorded by transthoracic Doppler ultrasound: relation to left ventricular diastolic pressures. *J Am Coll Cardiol* 1993; **21**: 1687–96.
  - 53 Jensen JL, Williams FE, Beilby BJ, et al. Feasibility of obtaining pulmonary venous flow velocity in cardiac patients using transthoracic pulsed wave Doppler technique. *J Am Soc Echocardiogr* 1997; **10**: 60–6.
  - 54 Keren G, Sonnenblick EH, LeJemtel TH. Mitral annulus motion. Relation to pulmonary venous and transmural flows in normal subjects and in patients with dilated cardiomyopathy. *Circulation* 1988; **78**: 621–9.
  - 55 Appleton CP. The hemodynamic determinants of Doppler pulmonary venous flow velocity components: new insights from studies in lightly sedated normal dogs. *J Am Coll Cardiol* 1997; **30**: 1562–74.
  - 56 Smiseth OA, Thompson CR, Lohavanichbutr K, et al. The pulmonary venous systolic flow pulse—its origin and relationship to left atrial pressure. *J Am Coll Cardiol* 1999; **34**: 802–9.
  - 57 Hellevik LR, Segers P, Stergiopoulos N, et al. Mechanism of pulmonary venous pressure and flow waves. *Heart Vessels* 1999; **14**: 67–71.
  - 58 Abhayaratna WP, Seward JB, Appleton CP, et al. Left atrial size: physiologic determinants and clinical applications. *J Am Coll Cardiol* 2006; **47**: 2357–63.
  - 59 Lang RM, Bierig M, Devereux RB, et al. Recommendations for chamber quantification a report from the American Society of Echocardiography's Guidelines and Standards Committee and the Chamber Quantification Writing Group, developed in conjunction with the European Association of Echocardiography, a branch of the European Society of Cardiology. *J Am Soc Echocardiogr* 2005; **18**: 1440–63.
  - 60 Tsang TSM, Barnes ME, Gersh BJ, Bailey KR, Seward JB. Left atrial volume as a morphophysiologic expression of left ventricular diastolic dysfunction and relation to cardiovascular risk burden. *Am J Cardiol* 2002; **90**: 1287–9.
  - 61 Stugaard M, Smiseth OA, Risoe C, Ihlen H. Intraventricular early diastolic filling during acute myocardial ischemia, assessment by multigated color M-mode Doppler echocardiography. *Circulation* 1993; **88**: 2705–13.
  - 62 Garcia MJ, Smedira NG, Greenberg NL, et al. Color M-mode Doppler flow propagation velocity is a preload

- insensitive index of left ventricular relaxation: animal and human validation. *J Am Coll Cardiol* 2000; **35**: 201–8.
- 63 Stugaard M, Risoe C, Ihlen H, Smiseth OA. Intracavitary filling pattern in the failing left ventricle assessed by color M-mode Doppler echocardiography. *J Am Coll Cardiol* 1994; **24**: 663–70.
- 64 Steine K, Stugaard M, Smiseth OA. Mechanisms of retarded apical filling in acute ischemic left ventricular failure. *Circulation* 1999; **99**: 2048–54.
- 65 Garcia MJ, Ares MA, Asher C, Rodriguez L, Vandervoort P, Thomas JD. An index of early left ventricular filling that combined with pulsed Doppler peak E velocity may estimate capillary wedge pressure. *J Am Coll Cardiol* 1997; **29**: 448–54.
- 66 Nagueh SF, Kopelen HA, Quinones MA. Assessment of left ventricular filling pressures by Doppler in the presence of atrial fibrillation. *Circulation* 1996; **94**: 2138–45.
- 67 Rajagopalan N, Garcia MJ, Rodriguez L, et al. Comparison of new Doppler echocardiographic methods to differentiate constrictive pericardial heart disease and restrictive cardiomyopathy. *Am J Cardiol* 2001; **87**: 86–94.
- 68 Sohn D, Chai I, Lee D, et al. Assessment of mitral annulus velocity by Doppler tissue imaging in the evaluation of left ventricular diastolic function. *J Am Coll Cardiol* 1997; **30**: 474–80.
- 69 Nagueh SF, Middleton KJ, Kopelen HA, Zoghbi WA, Quinones MA. Doppler tissue imaging: a noninvasive technique for evaluation of left ventricular relaxation and estimation of filling pressures. *J Am Coll Cardiol* 1997; **30**: 1527–33.
- 70 Nagueh S, Mikari I, Kopelen H, Middleton K, Quinones M, Zoghbi W. Doppler estimation of left ventricular filling pressure in sinus tachycardia. A new application of tissue Doppler imaging. *Circulation* 1998; **98**: 1644–50.
- 71 Sohn D, Song J, Zo J, et al. Mitral annulus velocity in the evaluation of left ventricular diastolic function in atrial fibrillation. *J Am Soc Echocardiogr* 1999; **12**: 927–31.
- 72 Sundereswaran L, Nagueh SF, Vardan S, et al. Estimation of left and right ventricular filling pressures after heart transplantation by tissue Doppler imaging. *Am J Cardiol* 1998; **82**: 352–7.
- 73 Nagueh SF, Lakkis NM, Middleton KJ, Spencer WH III, Zoghbi WA, Quinones MA. Doppler estimation of left ventricular filling pressures in patients with hypertrophic cardiomyopathy. *Circulation* 1999; **99**: 254–61.
- 74 Ha J, Oh J, Ling L, et al. Annulus paradoxus: transmural flow velocity to mitral annular velocity ratio is inversely proportional to pulmonary capillary wedge pressure in patients with constrictive pericarditis. *Circulation* 2001; **104**: 976–8.
- 75 Skaluba S, Litwin S. Mechanisms of exercise intolerance. Insights from tissue Doppler imaging. *Circulation* 2004; **109**: 972–7.
- 76 Burgess MI, Jenkins C, Sharman JE, Marwick TH. Diastolic stress echocardiography: hemodynamic validation and clinical significance of estimation of ventricular filling pressure with exercise. *J Am Coll Cardiol* 2006; **47**: 1891–900.
- 77 Mottram PM, Haluska BA, Marwick TH. Response of B-type natriuretic peptide to exercise in hypertensive patients with suspected diastolic heart failure: correlation with cardiac function, hemodynamics, and workload. *Am Heart J* 2004; **148**: 365–70.
- 78 Wang M, Yip GW, Wang AY, et al. Peak early diastolic mitral annulus velocity by tissue Doppler imaging adds independent and incremental prognostic value. *J Am Coll Cardiol* 2003; **41**: 820–6.
- 79 Wang M, Yip GW, Yu CM, et al. Independent and incremental prognostic value of early diastolic annular velocity in patients with impaired left ventricular systolic function. *J Am Coll Cardiol* 2005; **45**: 272–7.
- 80 Bruch C, Stypmann J, Gradaus R, Breithardt G, Wichter T. Usefulness of tissue Doppler imaging for estimation of filling pressures in patients with primary or secondary pure mitral regurgitation. *Am J Cardiol* 2004; **93**: 324–8.
- 81 Hasegawa H, Little WC, Ohno M, et al. Diastolic mitral annular velocity during the development of heart failure. *J Am Coll Cardiol* 2003; **41**: 1590–7.
- 82 Rivas-Gotz C, Khoury DS, Manolios M, Rao L, Kopelen HA, Nagueh SF. Time interval between onset of mitral inflow and onset of early diastolic velocity by tissue Doppler: a novel index of left ventricular relaxation: experimental studies and clinical application. *J Am Coll Cardiol* 2003; **42**: 1463–70.
- 83 Garcia MJ, Rodriguez L, Ares M, Griffin BP, Thomas JD, Klein AL. Differentiation of constrictive pericarditis from restrictive cardiomyopathy: assessment of left ventricular diastolic velocities in longitudinal axis by Doppler tissue imaging. *J Am Coll Cardiol* 1996; **27**: 108–14.
- 84 Diwan A, McCulloch M, Lawrie GM, Reardon MJ, Nagueh SF. Doppler estimation of left ventricular filling pressures in patients with mitral valve disease. *Circulation* 2005; **111**: 3281–9.
- 85 Sohn D, Kim Y, Park Y, Choi Y. Clinical validity of measuring time difference between onset of mitral inflow and onset of early diastolic mitral annulus velocity in the evaluation of left ventricular diastolic function. *J Am Coll Cardiol* 2004; **43**: 2097–101.
- 86 Oh JK, Tajik K. The return of cardiac time intervals: the phoenix is rising. *J Am Coll Cardiol* 2003; **42**: 1471–4.
- 87 Yu CM, Fung WH, Zhang Q, Sanderson JE. Understanding non-responders of cardiac resynchronization

- therapy-current and future perspectives. *J Cardiovasc Electrophysiol* 2005; **16**: 1117–24.
- 88 Wang J, Kurrelmeyer KM, Torre-Amione G, Nagueh SF. Systolic and diastolic dyssynchrony in patients with diastolic heart failure and the effects of medical treatment. *J Am Coll Cardiol* 2007; **49**: 88–96.
  - 89 Yu CM, Zhang Q, Yip GW, et al. Diastolic and systolic asynchrony in patients with diastolic heart failure: a common but ignored condition. *J Am Coll Cardiol* 2007; **49**: 97–105.
  - 90 Yip GW, Zhang Y, Tan PY, et al. Left ventricular long-axis changes in early diastole and systole: impact of systolic function on diastole. *Clin Sci (Lond)* 2002; **102**: 515–22.
  - 91 Lafitte S, Bordacher P, Lafitte M, et al. Dynamic ventricular dyssynchrony: an exercise-echocardiographic study. *J Am Coll Cardiol* 2006; **47**: 2253–9.
  - 92 Urheim S, Edvardsen T, Torp H, Angelsen B, Smiseth OA. Myocardial strain by Doppler echocardiography. Validation of a new method to quantify regional myocardial function. *Circulation* 2000; **102**: 1158–64.
  - 93 Edvardsen T, Skulstad H, Aakhus S, Urheim S, Ihlen H. Regional myocardial systolic function during acute myocardial ischemia assessed by strain Doppler echocardiography. *J Am Coll Cardiol* 2001; **37**: 726–30.
  - 94 Fang ZY, Najos-Valencia O, Leano R, Marwick TH. Patients with early diabetic heart disease demonstrate a normal myocardial response to dobutamine. *J Am Coll Cardiol* 2003; **42**: 446–53.
  - 95 Wang M, Yip GWK, Wang A, et al. Tissue Doppler imaging provides incremental prognostic value in patients with hypertension and left ventricular hypertrophy. *J Hypertens* 2005; **23**: 183–91.
  - 96 Kato TS, Noda A, Izawa H, et al. Discrimination of nonobstructive hypertrophic cardiomyopathy from hypertensive left ventricular hypertrophy on the basis of strain rate imaging by tissue Doppler ultrasonography. *Circulation* 2004; **110**: 3808–14.
  - 97 Voigt JU, Exner B, Schmiedehausen K, et al. Strain rate imaging during dobutamine stress echocardiography provides objective evidence of inducible ischemia. *Circulation* 2003; **107**: 2120–6.
  - 98 Leitman M, Lysansky P, Sidenko S, et al. Two dimensional strain – a novel software for real-time quantitative echocardiographic assessment of myocardial function. *J Am Soc Echocardiogr* 2004; **17**: 1021–9.
  - 99 Langeland S, D'hooge J, Wouters PF, et al. Experimental validation of a new ultrasound method for the simultaneous assessment of radial and longitudinal myocardial deformation independent of insonation angle. *Circulation* 2005; **112**: 2157–62.
  - 100 Amundsen BH, Helle-Valle T, Edvardsen T, et al. Non-invasive myocardial strain measurement by speckle tracking echocardiography: validation against sonomicrometry and tagged magnetic resonance imaging. *J Am Coll Cardiol* 2006; **47**: 789–93.
  - 101 Helle-Valle T, Crosby J, Edvardsen T, et al. New non-invasive method for assessment of left ventricular rotation: speckle tracking echocardiography. *Circulation* 2005; **112**: 3149–56.
  - 102 Notomi Y, Lysansky P, Setser RM, et al. Measurement of ventricular torsion by two-dimensional ultrasound speckle tracking imaging. *J Am Coll Cardiol* 2005; **45**: 2034–41.
  - 103 Torrent-Guasp F, Ballester M, Buckberg GD, et al. Spatial orientation of the ventricular muscle band: physiologic contribution and surgical implications. *J Thorac Cardiovasc Surg* 2001; **122**: 389–92.
  - 104 Takeuchi M, Nakai H, Kokumai M, Nishikage T, Otani S, Lang RM. Age-related changes in left ventricular twist assessed by two-dimensional speckle-tracking imaging. *J Am Soc Echocardiogr* 2006; **19**: 1077–84.
  - 105 Notomi Y, Martin-Miklovic MG, Oryszak SJ, et al. Enhanced ventricular untwisting during exercise: a mechanistic manifestation of elastic recoil described by Doppler tissue imaging. *Circulation* 2006; **113**: 2524–33.

# Assessment of dyssynchrony and its application

Cheuk-Man Yu, Qing Zhang and Jeffrey Wing-Hong Fung

## Introduction

Assessment of cardiac dyssynchrony (also called asynchrony) is increasingly recognized as an important aspect of cardiac assessment by echocardiography. Dyssynchrony refers to the uncoordinated movement of the heart, commonly the ventricle(s). Dyssynchrony may occur during ventricular contraction (systolic dyssynchrony) or during relaxation (diastolic dyssynchrony). However, systolic dyssynchrony has been more extensively investigated than diastolic dyssynchrony, and its clinical implications have also been characterized in some disease models. Systolic dyssynchrony can be defined as uncoordinated timing of contraction in different regions (or segments) of the myocardium, that is, the profile of myocardial segmental contraction does not occur simultaneously. Systolic dyssynchrony can be further divided into *intraventricular* (within the left ventricle) and *interventricular* (between the left and right ventricle) dyssynchrony. In a normal heart, the left ventricle contracts and relaxes in a synchronous manner. Systolic dyssynchrony in patients with heart failure has been investigated extensively in recent years, after development of the pacing therapy known as cardiac resynchronization therapy (CRT). However, systolic dyssynchrony has also been described in other cardiac disease conditions. Several imaging methods have been suggested to evaluate cardiac dyssynchrony: noninvasive imaging techniques, such as radionuclide ventriculography and cardiac magnetic resonance imaging, and invasive techniques, such as measuring the changes of regional

volumetric curves and electroanatomic mapping. However, echocardiography, in particular myocardial imaging, is the most commonly used tool for such a purpose because of its noninvasive nature, no use of radiation, wide availability, and conceptual design to evaluate regional function. This chapter will summarize the methods of assessing cardiac dyssynchrony by myocardial imaging, their implication in cardiac diseases, as well as their application in patient management.

## Methods of assessment of cardiac dyssynchrony by myocardial imaging

Several myocardial imaging techniques allow the assessment of systolic and diastolic dyssynchrony. Table 9.1 summarizes the techniques, roles, advantages, and disadvantages of these echocardiographic tools for assessment of systolic dyssynchrony.

### Tissue Doppler imaging

Tissue Doppler imaging (TDI) is a special form of Doppler echocardiography to detect the velocity of the contracting or relaxing myocardium, which is direction-specific. The myocardial velocity curve can either be constructed online by spectral pulsed TDI, or reconstituted offline from the two-dimensional (2-D) color TDI image. To assess cardiac function and dyssynchrony, TDI can be performed in the apical four-chamber, two-chamber, and three-chamber (or apical long-axis) views to examine the long-axis motion of the heart or, alternatively, the parasternal short-axis views to examine

**Table 9.1** Summary of various echocardiographic tools for the assessment of systolic dyssynchrony.

<i>Echo technology</i>	<i>Methods of assessing dyssynchrony</i>	<i>Views</i>	<i>Methods to assess systolic dyssynchrony</i>	<i>Strength</i>	<i>Limitations</i>
Pulse TDI [4]	Time to onset or peak systolic velocity in ejection phase ( $T_s$ )	Apical view(s)	<ul style="list-style-type: none"> <li>Difference between two or multiple segments</li> </ul>	<ul style="list-style-type: none"> <li>Predict +ve CRT response</li> <li><math>T_s</math> is robust and reproducible</li> </ul>	<ul style="list-style-type: none"> <li>Not true offline analysis</li> <li>Time consuming during online patient scanning for multiple segments</li> <li>Angle dependent</li> </ul>
Color TDI [6,12,46]	Time to onset or peak systolic velocity in ejection phase ( $T_s$ )	Apical view(s)	<ul style="list-style-type: none"> <li>Standard deviation of <math>T_s</math> (6, 8 or 12 segments)</li> <li>Maximal difference in <math>T_s</math> (6, 8 or 12 segments)</li> <li>Difference between 2 segments/walls, e.g., Septo-lateral delay</li> </ul>	<ul style="list-style-type: none"> <li>Predict +ve CRT response</li> <li>Allows offline analysis</li> <li>Highly comprehensive by analysis of multiple segments</li> <li><math>T_s</math> is robust and reproducible</li> <li>Can transform into other postprocessing imaging</li> </ul>	<ul style="list-style-type: none"> <li>Learning curve</li> <li>Angle dependent</li> </ul>
Tissue Tracking [54]	Tissue tracking illustrates systolic displacement as color codes	Apical view(s)	<ul style="list-style-type: none"> <li>No standardized methodology available</li> </ul>	<ul style="list-style-type: none"> <li>Correlates with gain in systolic function after CRT</li> </ul>	<ul style="list-style-type: none"> <li>Semiquantitative</li> <li>May not differentiate isovolumic from ejection phase contraction in the color coding</li> <li>Amount of motion as indirect marker of dyssynchrony</li> <li>Angle dependent</li> </ul>
Displacement imaging [14,15,53]	Time to maximal systolic displacement ( $T_d$ )	Apical view(s)	<ul style="list-style-type: none"> <li>The "SD" or "maximal difference" methods can be applied for <math>T_d</math></li> </ul>		<ul style="list-style-type: none"> <li>Weak predictive value for CRT response</li> <li>Angle-dependent</li> </ul>
DLC or postsystolic shortening [54]	+ve & dominant velocity after AV closure by TDI, and -ve strain rate	Apical view(s)	<ul style="list-style-type: none"> <li>Number of LV segments with DLC</li> </ul>	<ul style="list-style-type: none"> <li>Correlates with gain in systolic function after CRT</li> </ul>	<ul style="list-style-type: none"> <li>Semiquantitative</li> <li>Lack of standardized definition</li> <li>Angle-dependent</li> </ul>
Strain [14,52,53,56]	Time to peak -ve strain ( $T_\varepsilon$ )	Apical view(s)	<ul style="list-style-type: none"> <li>The "SD" or "maximal difference" methods can be applied for <math>T_\varepsilon</math></li> </ul>	<ul style="list-style-type: none"> <li>Change in regional strain may reflect change in dyssynchrony</li> </ul>	<ul style="list-style-type: none"> <li>Role of time to peak -ve strain unsure</li> <li>Relatively large variability</li> <li>Learning curve</li> <li>Technically demanding</li> <li>Angle-dependent</li> </ul>

*Continued*

**Table 9.1** Continued

<i>Echo technology</i>	<i>Methods of assessing dyssynchrony</i>	<i>Views</i>	<i>Methods to assess systolic dyssynchrony</i>	<i>Strength</i>	<i>Limitations</i>
Strain rate imaging [14,56]	Time to peak –ve strain rate (Ts <sub>r</sub> )	Apical view(s)	<ul style="list-style-type: none"><li>• SD of Ts<sub>r</sub> &amp;</li><li>• Maximal difference in Ts<sub>r</sub> (of two or multiple LV segments)</li></ul>	<ul style="list-style-type: none"><li>• Differentiate translational motion “theoretically”</li></ul>	<ul style="list-style-type: none"><li>• Role of time to peak –ve strain rate not confirmed</li><li>• Large observer variability</li><li>• Learning curve</li><li>• Strong technical demand</li><li>• Angle-dependent</li></ul>
Tissue synchronization imaging (TSI) [16,17]	Time to peak +ve myocardial velocity sampled automatically	Apical view(s)	<ul style="list-style-type: none"><li>• Same as TDI methods for offline velocity assessment</li></ul>	<ul style="list-style-type: none"><li>• Quick visual appreciation of regional wall dyssynchrony</li><li>• Faster than TDI method “theoretically”</li><li>• Both quantitative &amp; qualitative</li></ul>	<ul style="list-style-type: none"><li>• Setting of beginning &amp; end of TSI is critical</li><li>• Intrinsic problems of automated sampling of Ts</li><li>• Learning curve</li><li>• Technically demanding</li><li>• Angle-dependent</li></ul>
2-D Speckle tracking	Time to peak radial strain (Tε)	Short-axis view	Difference among two or more segments	<ul style="list-style-type: none"><li>• Angle-independent</li><li>• Predict +ve CRT response</li></ul>	<ul style="list-style-type: none"><li>• Need excellent 2-D image</li><li>• Need to sample a large area of interest based on arbitrary settings (e.g., equal myocardial thickness in all segments)</li></ul>

DLC, Delay longitudinal contraction.

circumferential fiber function. The examination of long-axis motion is recommended because of the anatomical architecture of the ventricle. It has been shown that the majority of the myocardial fibers, in particular those of the endocardial and epicardial layers, are aligned in an oblique manner contributing to long-axis function [1]. Furthermore, the elegant work from Torrent-Guasp and colleagues illustrated in human dissection that the ventricles are wrapped by a continuous piece of myocardium in an oblique manner forming a helical structure [2,3]. As a result, the main axis of contraction of the heart is in the longitudinal direction. However, in the event of heart failure with left ventricular (LV) dilatation, the helical heart will criss-cross in a more horizontal manner. This finding implicates the potential importance of examining circumferential fiber function.

### **Spectral pulsed tissue Doppler imaging**

Spectral pulsed TDI has a good temporal resolution with highly robust signals [4]. As myocardial velocity curves have to be created online, only assessment of one segment is possible at any time. Therefore, simultaneous comparison of multiple sites is precluded. Furthermore, repeated sampling from offline analysis is not possible.

### **Offline two-dimensional color tissue Doppler imaging**

The 2-D color TDI cine-loops of multiple beats can be stored digitally for offline analysis. This offline analysis allows the comparison of multiple segments from each view simultaneously and is a much quicker way of assessing myocardial function and synchronicity. This method can also reduce the time for online image acquisition. The offline analysis can be performed in a blinded manner to provide an objective way of assessment in which repeated measurements by different persons are possible. For both spectral pulsed Doppler and 2-D color TDI methods, the QRS complex is often referenced when systolic mechanical dyssynchrony is assessed [5–7].

### **Color M-mode tissue Doppler imaging**

From the 2-D color TDI images, color M-mode TDI images can be constructed. Although this method has been used to identify regional

dyssynchrony [8,9], it is mainly a qualitative technique to identify regional dyssynchrony and is largely superseded by the quantitative methods from analysis of myocardial velocity curves.

### **Indices of systolic dyssynchrony by tissue Doppler imaging**

Several TDI-based indices of systolic dyssynchrony have been proposed in the literature, mostly for the assessment of intraventricular dyssynchrony within the left ventricle. However, evaluation of interventricular dyssynchrony is also possible by TDI. Technically, the following principles of quantitative assessment of systolic dyssynchrony can be considered (Figure 9.1):

- The time from the beginning of QRS complex to onset of systolic velocity.
- The time from the beginning of QRS complex to peak systolic velocity in ejection phase ( $T_s$ ).
- The time from the beginning of QRS complex to peak postsystolic shortening velocity.

Although “systolic” velocity usually refers to the ejection phase (period between aortic valve opening and closure) in most studies, some researchers examine postsystolic shortening (positive myocardial velocity occurring after aortic valve closure and greater than the ejection peak, which happened at the global timing of the isovolumic relaxation phase or early diastole). On the basis of the above principles, one can establish indices of systolic dysynchrony from simple (e.g., septal–lateral delay, septal–posterior delay), intermediate (six basal LV segments, septal vs. free-wall segments in basal and mid-levels), or more comprehensive (e.g., six basal, six mid-LV segments) models of mechanical dysynchrony [10–13]. When multiple segments are examined, indices of systolic dyssynchrony can be computed by either the standard deviation or maximal difference in the time measurement [11–13]. Appendix 9.1 describes the method of assessing systolic dyssynchrony based on the standard deviation method of  $T_s$  from a six basal, six mid-LV segmental model (Dyssynchrony Index or  $T_s$ -SD).

### **Indices of diastolic dyssynchrony by tissue Doppler imaging**

Methods for assessing diastolic dyssynchrony are described much less often than those for systolic dyssynchrony. The commonly accepted approach

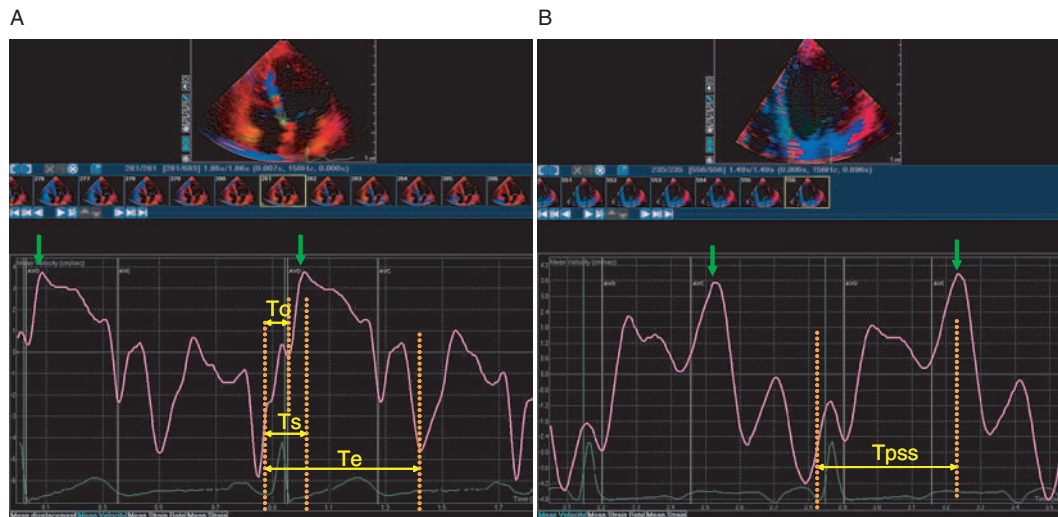


**Figure 9.1** An illustration of TDI to assess intraventricular mechanical dyssynchrony. During offline analysis of 2-D color TDI images, the sampling window is placed within the myocardium to create the myocardial velocity curve. The ejection period can be confirmed by the use of aortic valve opening (AVO) and closure (AVC) markers based on Doppler echocardiography of the LV outflow tract or

aortic valve. (A) To assess systolic dyssynchrony, the time to onset ( $To$ ) or peak systolic velocity ( $Ts$ ) can be measured on multiple segments to calculate various indices of dyssynchrony. (B) Other researchers also use the time to peak postsystolic shortening velocity ( $Tpss$ ). To assess diastolic dyssynchrony, the time to peak early diastolic velocity ( $Te$ ) is measured.

is to measure the time to peak early diastolic velocity of multiple LV segments from the myocardial velocity curve of TDI (Figure 9.1). Similar to systolic dyssynchrony, indices of diastolic dyssynchrony can be computed by either the standard deviation ( $Te-SD$ ) or maximal difference in the time measurement [7].

### Displacement Imaging and tissue tracking

Displacement imaging is derived from the temporal integration of myocardial velocity curves (i.e., velocity–time integral) from TDI data. This illustrates the cumulated amount of myocardial excursion during different phases of the cardiac cycle and presents it on a “curve” format (Figure 9.2) [14,15]. When the amount of myocardial displacement is presented semiquantitatively by transforming into color codes (each represent an incremental displacement of 2 cm) and overlay onto the 2-D images, it is called *tissue tracking*. To assess systolic dyssynchrony quantitatively, the time to maximal systolic displacement can be measured from displacement imaging at either apical or parasternal views [14,15].

### Strain imaging

Strain mapping is another postprocessing mapping of TDI data that calculates the amount of myocardial

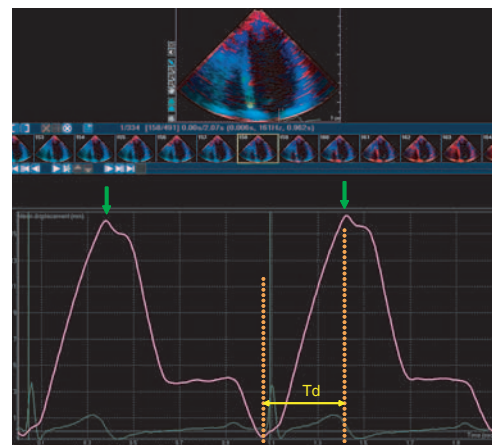


**Figure 9.2** An illustration of displacement imaging, which is derived from velocity time integration of TDI. On the apical view, the systolic motion will be depicted as positive displacement, which will return back to the zero point during diastole. To assess systolic dyssynchrony, the time to peak positive displacement (arrow) can be measured in multiple segments ( $Td$ ).

deformation in a cumulative manner throughout the cardiac cycle. In a normal heart, systolic strain reaches its maximal value during end-systole. In patients with LV dyssynchrony, variation of

the timing to peak strain may occur. Strain can be assessed in both parasternal short-axis (septal-posterior strain delay only) and apical views (strain delay in multiple segments) (Figure 9.3) [14].

### Strain rate imaging

Strain rate imaging reflects the rate of change of strain in the cardiac cycle, that is, the first derivative or slope of the strain curve. Therefore, strain rate imaging is a measure of the rate of deformation of the myocardium (Figure 9.4). Theoretically, strain and strain rate imaging are superior to tissue velocities and displacement mapping, because translational motion from passive motion can be eliminated, such as respiration and tethering of adjacent segments. However, current technical limitations (artifacts and random noise) outweigh the theoretical advantages of strain rate imaging. The time to peak negative strain rate has been used to measure systolic dyssynchrony, although it was found to be significantly inferior to tissue velocities in a comparative study [12].

### Tissue synchronization imaging

Tissue synchronization imaging (TSI) portrays regional dyssynchrony on 2-D images by transforming the timing of regional peak positive velocity of

TDI data into color codes, which allows immediate visual identification of regional delay in systole by comparing the color mapping of orthogonal walls (Figure 9.5; Video clips 12 and 13  [16–18]). In addition, quantitative measurement of regional delay is possible. Because this imaging modality is derived from TDI data, indices of systolic dyssynchrony similar to that of TDI can be generated. At the present moment, it is recommended that quantitative analysis be performed by measurement at the myocardial velocity curve (which is the same as those from TDI) rather than directly from the color-coded TSI images to avoid technical errors during sampling.

### Speckle tracking

As explained in other chapters, speckle tracking allows the examination of regional function through measurement of the excursion of gray-scale speckles on conventional 2-D images. This deformation is transformed into a regional strain curve over the cardiac cycle (Figure 9.6). Speckle tracking has the main advantage of being angle-independent, which renders the assessment of regional function possible in both parasternal short-axis and apical views. To assess systolic dyssynchrony, the time to peak strain can be measured

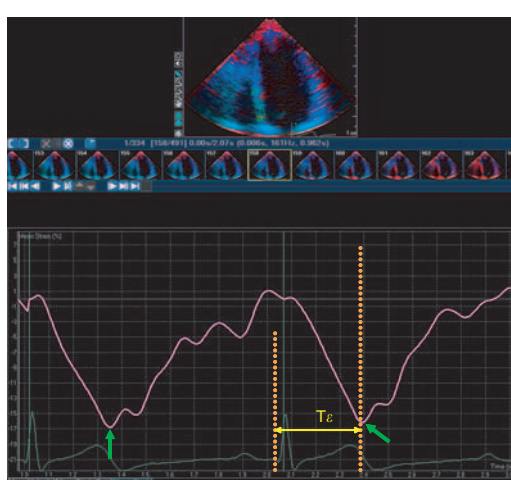


**Figure 9.3** An illustration of tissue Doppler-derived strain imaging. In the apical view, systolic strain is a negative value, which reverses back to the zero point during diastole. To assess systolic dyssynchrony, the time to peak negative strain (arrows) can be measured in multiple segments ( $T\epsilon$ ).

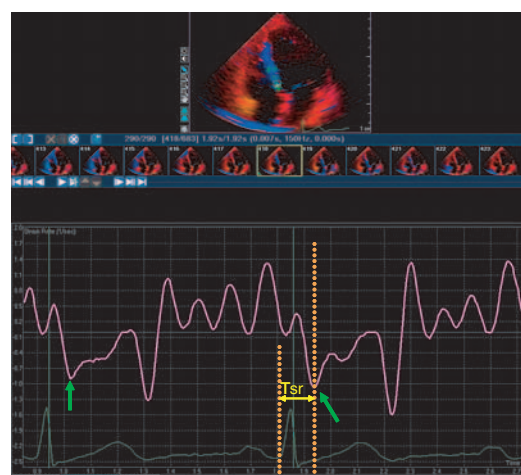


**Figure 9.4** An illustration of tissue Doppler-derived strain rate imaging. In the apical view, systolic strain rate is a negative value. During diastole, two positive peaks arise as a result of early and late diastolic relaxation. To assess systolic dyssynchrony, the time to peak negative strain rate (arrows) can be measured in multiple segments ( $Ts$ ).

A

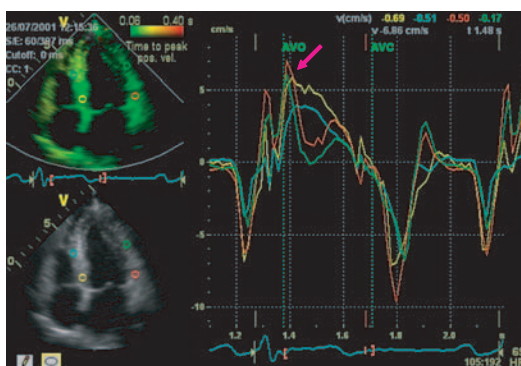
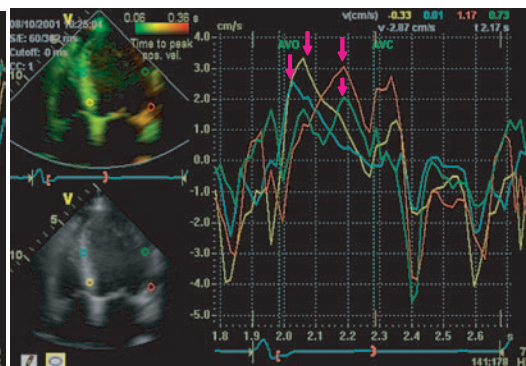


**Figure 9.5** An illustration of TSI. The TSI method was set up to measure the time to peak myocardial systolic velocity (arrows) between the aortic valve opening and closure, that is, at ejection phase. The Ts values are displayed in various colors, depending on the severity of delay, in the

B



sequence of green, yellow, orange, and red. The myocardial curves from TDI signals are shown simultaneously to verify the findings of TSI. (A) A normal subject. (B) A patient with congestive heart failure and systolic dyssynchrony. See also Video clips 12 and 13 (▶).

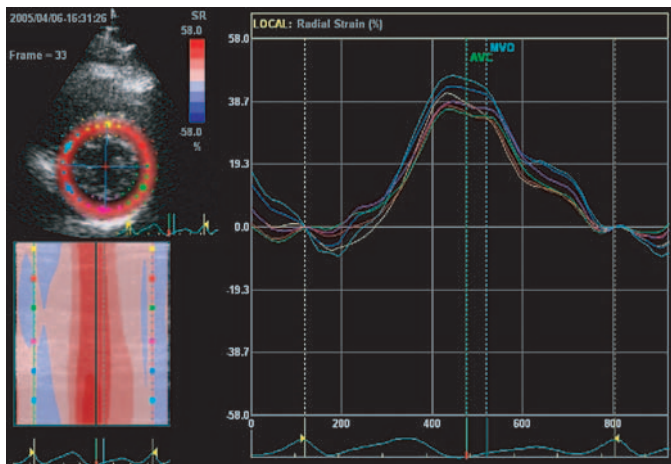


**Figure 9.6** An illustration of 2-D speckle tracking. The radial strain curves were constructed offline. This image shows the radial strain at the level of the papillary muscle. The radial strain is positive during systole, and the time to peak radial strain can be measured as a marker of dyssynchrony. In this normal subject, the time to peak strain is the same in all the segments.

at two or multiple segments to reveal regional delay [19].

### Cardiac dyssynchrony in myocardial diseases

#### Cardiac dyssynchrony in heart failure with systolic dysfunction

In a subset of patients with heart failure and systolic dysfunction who have wide QRS complexes on electrocardiogram, systolic dyssynchrony commonly occurs as a result of electromechanical delay in the ventricle(s). Morphologically, the prolonged QRS can be manifested in the form of bundle branch

block (left [LBBB] or right [RBBB]) or intraventricular conduction delay. QRS prolongation ( $>120$  msec) has been described to occur in one quarter to half of the disease population [20]. However, TDI studies confirmed the hypothesis that systolic dyssynchrony does not occur in all patients with wide QRS complex, only in approximately 70% [7,21,22]. Furthermore, these studies also revealed that systolic dyssynchrony occurred in between 27% and 43% of heart failure patients with normal QRS duration ( $<120$  msec), depending on methodology.

In systolic heart failure, systolic dyssynchrony plays an important role in disease progression.

Interventricular dyssynchrony, especially in the presence of paradoxical septal motion in systole, may adversely affect right ventricular (RV) function, which further impedes venous return to the left ventricle. Intraventricular dyssynchrony will result in a fragmented profile of ineffective contraction, with prolongation of isovolumic contraction and relaxation time. The regional shifting rather than ejection of blood from the left ventricle results in worsening of regional wall stress and aggravation of mitral regurgitation. These factors, together with activation of neurohormonal and proinflammatory cytokine pathways, will accelerate cardiac dilation, resulting in progressive LV dilatation and cardiac remodeling (Figure 9.7).

### **Diastolic heart failure (heart failure with preserved systolic function)**

At least one third of the patients admitted for acute heart failure have preserved systolic function, or diastolic heart failure. These patients are probably in the spectrum of a less severe form of disease, as prognosis in general is better than that for systolic heart failure. In diastolic heart failure, preservation of systolic function is usually defined by an ejection

fraction (see Chapter 8) >45% and evidence of LV diastolic dysfunction. Whether cardiac dyssynchrony may occur in these patients has not been explored until very recently; two studies simultaneously reported that systolic and diastolic dyssynchrony is prevalent [23,24]. The study by Yu et al. examined 373 heart failure patients, which included 281 with systolic heart failure and 92 with diastolic heart failure, and compared them with 100 normal controls [23]. Systolic and diastolic dyssynchrony were assessed by Ts-SD and Te-SD of the 12 LV segments by TDI. Normal synchrony, isolated systolic dyssynchrony, isolated diastolic dyssynchrony, and combined systolic and diastolic dyssynchrony were observed in 39%, 25%, 22%, and 14% of diastolic heart failure patients, respectively; and these rates were 26%, 31%, 17%, and 26%, respectively, in systolic heart failure patients ( $\chi^2 = 10.01$ ;  $P = 0.019$ ) [23]. Also, the study observed that the correlation between systolic and diastolic dyssynchrony as well as between myocardial velocities and corresponding mechanical dyssynchrony appeared weak. Another study by Wang et al. examined 60 patients with diastolic heart failure, 60 with systolic heart failure, and 35 normal controls.

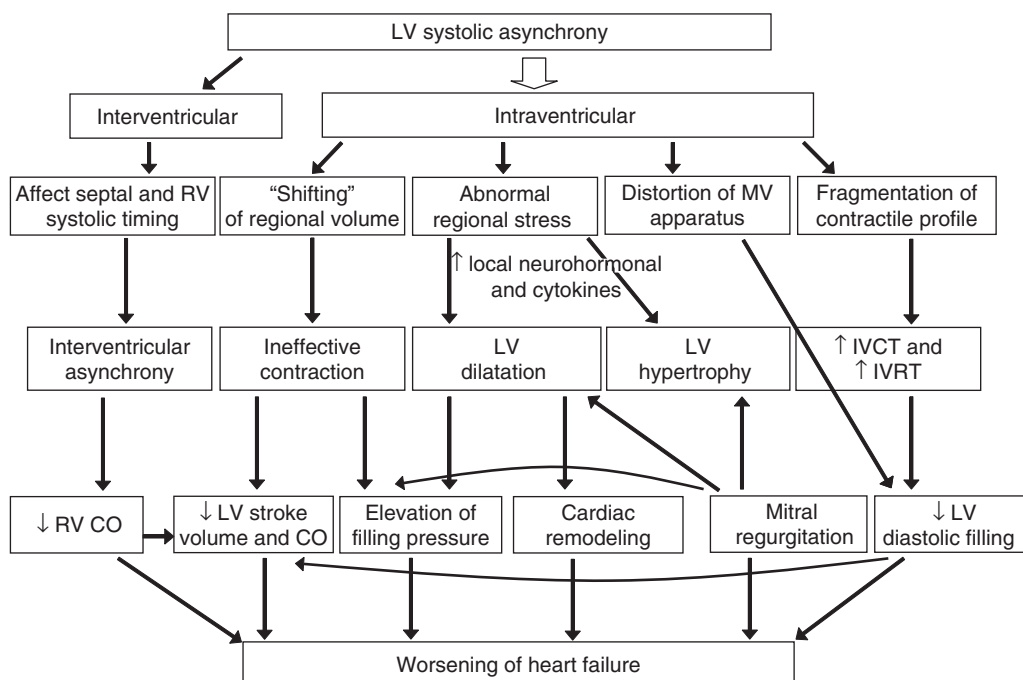


**Figure 9.7** The pathophysiologic mechanism of systolic dyssynchrony on LV remodeling and worsening of heart failure.

Systolic and diastolic dyssynchrony was defined by the maximal difference in time to onset or peak systolic velocity of four LV walls by apical four- and two-chamber views [24]. The prevalence of normal synchrony, isolated diastolic dyssynchrony, and combined systolic and diastolic dyssynchrony were observed in 42%, 25%, and 33%, respectively, in diastolic heart failure patients, and 42%, 20%, and 40%, respectively in systolic heart failure patients. Interestingly, the authors also reported a reduction of diastolic intraventricular time delay after medical therapy in the diastolic heart failure group ( $39 \pm 23$  vs.  $28 \pm 20$  msec;  $P=0.02$ ) [24]. Therefore, it is clear that systolic and diastolic dyssynchrony commonly occur in diastolic heart failure. However, their clinical implication warrants further exploration.

### Right ventricular pacing-induced systolic dyssynchrony

Patients with LBBB pattern, even without LV systolic dysfunction, exhibit systolic intraventricular dyssynchrony apart from interventricular dyssynchrony [25]. This finding has been further substantiated by TDI studies [26,27]. More commonly, LBBB pattern can be iatrogenically induced in patients receiving RV pacing for complete heart block and sick sinus syndrome. It is increasingly recognized that RV pacing is potentially deleterious, as the risk of heart failure is increased when cumulated ventricular pacing exceeds 40% [28]. In this regard, TDI provides helpful insight into cardiac dyssynchrony, which is likely to be a key contributing factor for the development of heart failure. A study by Kang et al. examined the severity of cardiac dyssynchrony in 29 patients with RV pacing, 13 patients with LBBB and ejection fraction >50%, 22 patients with LBBB and ejection fraction <35%, and 27 normal controls [29]. Systolic and diastolic dyssynchrony was defined by the coefficient of variation (mathematically similar to the standard deviation method) of Ts of four basal and four mid-LV walls by apical four- and two-chamber views [29]. The systolic Dyssynchrony Index was increased in all the disease groups, but was significantly higher in the pacing-induced LBBB and LBBB with low ejection fraction groups (Figure 9.8). For diastolic dyssynchrony, the order of decreasing severity is LBBB with low ejection fraction, LBBB with normal ejection fraction, and pacing-induced LBBB.

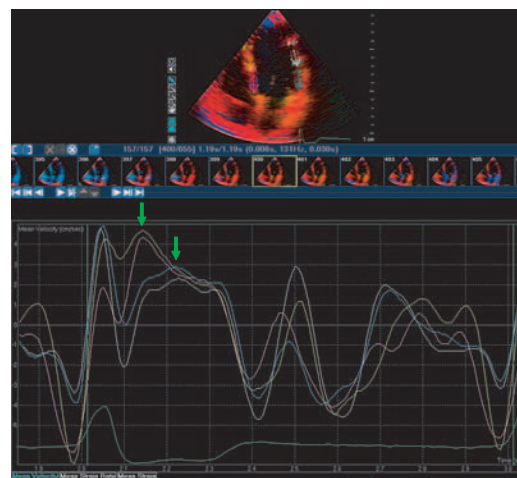


**Figure 9.8** An example of cardiac dyssynchrony induced by RV apical pacing. This patient has evidence of septal–lateral delay (80 msec) as illustrated by the time difference to peak systolic velocity (arrows) between the two walls.

In addition, diastolic dyssynchrony also appeared to correlate with ejection fraction in pooled analysis.

### Left ventricular hypertrophy

Hypertension is the most common cardiovascular disease. LV hypertrophy is a common sequela, which is associated with increased cardiovascular morbidity and mortality. Data are limited on the prevalence and severity of cardiac dyssynchrony in LV hypertrophy, although it was probably the first disease to be investigated for the presence of dyssynchrony by TDI. Pai and Gill examined 18 patients with LV hypertrophy and 20 healthy controls by spectral pulsed TDI, and the time to onset of systolic wave was measured at basal, mid-, and apical levels in the apical four- and two-chamber views [30]. Systolic dyssynchrony was evident by the prolonged coefficient of variation of the time domain in patients with LV hypertrophy ( $14 \pm 9$  vs.  $6 \pm 4$  msec;  $P < 0.01$ ), although the difference in diastolic dyssynchrony was borderline ( $20 \pm 10$  vs.  $15 \pm 7$  msec;  $P = 0.06$ ) [30].

### Prognostic implication of cardiac dyssynchrony in heart failure

The prognostic importance of systolic dyssynchrony in heart failure was first reported by Bader et al. [31]

who examined 104 patients with ejection fraction  $\leq 45\%$  (mean of 31%) [31]. These patients had a wide range of QRS duration. Intraventricular delay was examined by spectral pulsed TDI in the apical four- and two-chamber views in which the time to the onset of ejection phase velocity was measured from the basal LV segments and the maximal time difference was calculated. Interventricular dyssynchrony was measured by Doppler echocardiography by the difference between the aortic and pulmonary pre-ejection period. During 1-year follow-up, although there was no mortality, 86 patients (83%) were admitted for worsening heart failure. Intraventricular but not interventricular dyssynchrony was found to be the most important independent predictor of a heart failure event ( $\beta = 1.47$ ;  $P < 0.001$ ) by Cox multivariate analysis [31].

The prognostic value of systolic dyssynchrony independent of QRS duration was further illustrated by another study in which 106 heart failure patients with ejection fraction  $<35\%$  (mean of 28%) and QRS  $\leq 120$  msec were followed up for a mean of  $17 \pm 11$  months [32]. Intraventricular dyssynchrony was measured by offline 2-D color TDI analysis from apical four- and two-chamber views, in which Ts-SD and maximal difference in Ts (Ts-diff) was calculated from the eight basal and mid-LV segments. Clinical events of heart failure or cardiac transplantation occurred in 35 (33%) patients and mortality in 18 (17%) patients (Figure 9.9).

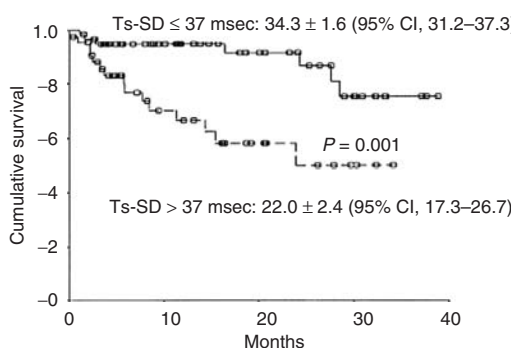


**Figure 9.9** Survival of patients with narrow QRS heart failure stratified by assessment of systolic dyssynchrony from TDI of eight LV segments. Those patients with a Ts-SD  $\leq 37$  msec are associated with a lower mortality than those with significant dyssynchrony. Reprinted with permission from Cho et al. [32].

From the receiver operating characteristic (ROC) curves, a Ts-SD value of  $>37$  msec has a sensitivity of 68% and specificity of 71% to predict event-free survival, and these figures were 70% and 68%, respectively, for a Ts-diff value of  $>91$  msec [32]. The hazard ratio for the cutoff values for Ts-SD and Ts-diff were 3.89 and 4.26, respectively. Importantly, QRS duration was not an independent prognosticator in these patients who did not exhibit wide QRS complex. Therefore, assessment of systolic dyssynchrony in heart failure patients provides important prognostic information independent of QRS duration.

### Role of cardiac dyssynchrony assessment in cardiac resynchronization therapy

CRT is now an established therapy for patients with advanced New York Heart Association (NYHA) class III or IV heart failure, low ejection fraction of  $<35\%$ , and prolonged QRS duration of  $>120$  msec [33]. The latter criterion signifies the presence of electromechanical delay. The clinical benefits of CRT were confirmed by multicenter trials and included the improvement of heart failure symptoms, exercise capacity (e.g., 6-Minute Hall Walk distance), quality of life, and long-term cardiovascular morbidity and mortality [34–37]. Apart from clinical benefits, CRT also improved the structural and functional aspects of the left ventricle, resulting in reverse remodeling, regression of LV hypertrophy, and improvement of systolic function [5,38,39]. Also, early LV reverse remodeling after CRT for 3 to 6 months is a predictor of favorable long-term clinical outcome [40]. Despite the compelling evidence of CRT benefits, lack of clinical or LV reverse remodeling response has been observed in approximately one third of patients [35,41]. One of the main reasons for the lack of response is that some patients with wide QRS complex did not exhibit systolic dyssynchrony [42]. Conversely, studies based on TDI revealed that systolic dyssynchrony is actually present in a significant proportion of heart failure patients with narrow QRS complex [7,43]. Therefore, the role of assessment of systolic dyssynchrony by myocardial imaging in the CRT era includes:

- Understanding the mechanisms of benefit of CRT from the mechanical perspective.

- Predicting responders of CRT by baseline indices of systolic dyssynchrony.
- Potentially to select heart failure patients for CRT, in particular in those with narrow QRS complex and coexisting systolic dyssynchrony.

### **Understanding the mechanisms of benefit of cardiac resynchronization therapy from mechanical perspectives**

The mechanisms of benefit of CRT can be examined from a mechanical perspective. The six basal, six mid-segmental model of the left ventricle adopted by Yu et al. [5] measured the Ts by color-coded TDI from the three orthogonal apical views. In heart failure patients with prolonged QRS duration, widespread LV delay was observed among various LV segments, with a large variation in regional Ts. CRT achieved systolic synchronicity by homogeneously delaying those early contracting segments to a time similar to the delayed segments (Figure 9.10). Therefore, not only was septal-to-lateral delay abolished, other patterns of delay were also corrected [5]. Furthermore, improvement of regional displacement, strain, and strain rate has been reported [14]. When interventricular dyssynchrony was examined, the septal-RV free-wall delay

was also improved after CRT [5]. The improvement of intraventricular dyssynchrony is probably the main mechanism for mediating the echocardiographic benefits of CRT, which include LV reverse remodeling [5,44,45], improvement of systolic function [44–46], reduction of mitral regurgitation [5,45], and gain in LV diastolic filling time [5]. Interestingly, all the echocardiographic benefits are pacing-dependent, as withholding pacing resulted in progressive worsening of these indices [5].

Improvement of mitral regurgitation is another cardinal echocardiographic feature in CRT. With reduction of regurgitant volume into the left atrium, atrial filling pressure is reduced and LV volume overload is decreased. This change enhances the process of LV reverse remodeling. Mechanisms for the reduction of mitral regurgitation are likely related to the improvement of systolic dyssynchrony, which also affects the movement of papillary muscles that distorted the normal timing of movement of the mitral apparatus. This finding was demonstrated by the study of Kanzaki et al. [47] in which interpapillary muscle delay was present by measuring the time to peak strain in the short-axis view. Such delay was greatly reduced after CRT, which correlated with a reduction in mitral regurgitant fraction ( $r = 0.77$ ;  $P < 0.001$ ).

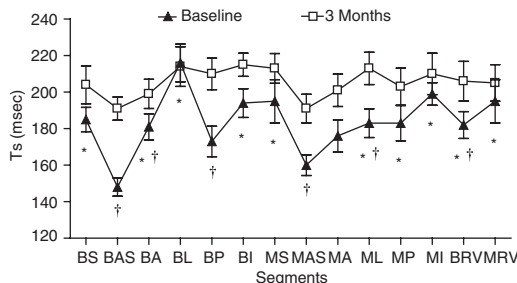


**Figure 9.10** Changes in the time to peak myocardial systolic velocity in the ejection phase (Ts) before (filled triangles) and after (white squares) CRT. At baseline, there was marked regional variation in Ts among the LV segments. The Ts was earliest in the basal anteroseptal segment and latest in the basal lateral segment. After CRT, the Ts were homogeneously delayed to a timing close to that of the basal lateral segment so that regional variation in Ts was abolished. \* $P < 0.05$  versus basal anteroseptal segment at baseline.  $\dagger P < 0.05$  when comparing the same segment before and after pacing therapy. B, basal; M, mid; A, anterior; AS, anteroseptal; I, inferior; L, lateral; P, posterior; S, septal; RV, right ventricle. Reprinted with permission from Cardiac Resynchronization Therapy by Yu et al., Blackwell.

### **Predicting responders of cardiac resynchronization therapy from indices of systolic dyssynchrony**

To predict and differentiate responders from non-responders of CRT, echocardiographic assessment of systolic dyssynchrony has a unique role. Several echocardiographic techniques and their derived indices of dyssynchrony have been proposed. However, to apply an echocardiographic index of systolic dyssynchrony in clinical practice, it is mandated that a cutoff value is identified objectively to determine whether systolic dyssynchrony is clinically relevant. Furthermore, a good index should be able to predict a favorable response with a high sensitivity to be incorporated as a screening test; and a high specificity as a rule-in test to ascertain the presence of systolic dyssynchrony. Table 9.2 summarizes the key studies that examined systolic dyssynchrony by myocardial imaging technologies and have suggested cutoff values of predicting a favorable response to CRT [4,6,12,16,17,19,46,48–50].

**Table 9.2** Published criteria of systolic dyssynchrony by TDI that predict a favorable echocardiographic response to CRT.

Author	Sample size	Criteria	Follow up period	Definition of responders	Cutoff value	Sensitivity (%)	Specificity (%)
Bax [46]	25	Septal-lateral delay in Ts (ejection phase)	Acute (within 24 hours)	Absolute $\uparrow$ ejection fraction $\geq 5\%$	$>60$ msec	76	87.5
Bax [51]	85	Septal-lateral delay in Ts (ejection phase)	12 months	Clinical: $\downarrow$ NYHA $\geq 1$ & $\uparrow$ 6MHW $\geq 25\%$	$\geq 65$ msec	80	80
Yu [12]	54	Ts-SD of six basal, six mid-LV segments (ejection phase)	6 months (echo) 3 months	$\downarrow$ LVVs $>15\%$ $\downarrow$ LVVs $>15\%$	$>31.4$ msec	92 96	92 78
Yu [49]	QRS 27 QRS $>150$ msec: 31	Ts-SD of six basal, six mid-LV segments (ejection phase)	3 months	$\downarrow$ LVVs $>15\%$	$>32.6$ msec (Derived from normal population)	83 100	86 78
Penicka [4]	49	Ts (onset) of BS, BL, BP, & BRV by summation of inter- and intraventricular delay	6 months	Relative $\uparrow$ ejection fraction $\geq 25\%$	$>102$ msec	96	71
Notabartolo [48]	49	Maximal difference in Ts in six basal segments (both ejection phase and postsystolic shortening)	3 months	$\downarrow$ LVVs $> 15\%$	$>110$ msec	97	55
Gorcsan [16]	29	Septo-posterior delay (both ejection phase and postsystolic shortening)	Acute	$\uparrow$ Stroke volume $\geq 15\%$	$>65$ msec	87	100
Yu [17]	56	Lateral wall delay Ts-SD of 6-basal, 6 mid-LV segments (ejection phase)	3 months	$\downarrow$ LVVs $>15\%$	Qualitative $>34.4$ msec	47 87	89 81
Dohi [50]	38	Septal-posterior strain	Acute	$\uparrow$ Stroke volume $\geq 15\%$	$\geq 130$ msec	95	88
Suffoletto [19]	50	Septal-posterior radial strain (2-D speckle tracking)	$8 \pm 5$ months	$\geq 15\% \uparrow$ in ejection fraction	$\geq 130$ msec	89%	83

BS, basal septal; BL, basal lateral; BP, basal posterior; BRV, basal right ventricular; LVVs, left ventricular end-systolic volume; TDI, tissue Doppler imaging; TSI, tissue synchronization imaging, Ts, time to peak myocardial systolic velocity; Ts(onset), time to onset of myocardial systolic velocity; Ts-SD, standard deviation of time to peak myocardial systolic velocity.

### Tissue Doppler imaging

Bax et al. [46] evaluated 25 patients with color-coded TDI by a two basal segmental model in an acute study. Responders were defined as those with an increase in LV ejection fraction by  $\geq 5\%$ . After CRT, LV ejection fraction increased from  $22 \pm 5\%$  to  $31 \pm 10\%$  and the septal-lateral delay decreased from  $71 \pm 38$  msec to  $36 \pm 34$  msec. A septal-lateral delay at baseline  $\geq 60$  msec has a sensitivity of 76% and specificity of 87.5% of predicting an increase in ejection fraction (Figure 9.11) [46]. Subsequently, the same group examined 85 patients for a follow-up period of 1 year [51]. When chronic responders were defined by an improvement in NYHA functional class by  $\geq 1$  score and a gain by  $\geq 25\%$  in 6-Minute Hall Walk distance, the response rate was 73%. This study also revealed that a septal-lateral delay  $\geq 65$  msec predicted clinical response with a sensitivity and specificity of 80%. Importantly, patients who were above this cutoff value had a lower mortality than those who were below [51].

Notabartolo et al. [48] examined the myocardial velocity curves from offline 2-D color TDI analysis by choosing the highest peak velocity in either ejection phase or postsystolic shortening among the six basal LV segments from the three apical views [48]. The maximal difference in time to peak velocity among these six segments, or peak velocity difference, was measured. In 49 patients who received CRT, a peak velocity difference  $> 110$  msec at baseline predicted LV reverse remodeling (defined as a reduction of LV end-systolic volume  $> 15\%$ ) at 3-month follow-up with a sensitivity of 97%, although the specificity was only 55% [48]. On the other hand, examination of ejection phase velocity seems to provide a better trade-off between sensitivity and specificity. When the Dyssynchrony Index (or Asynchrony Index, Ts-SD) of the six basal, six mid-segmental model was used with a cutoff value of 32.6 msec, it was possible to segregate responders from nonresponders defined by LV reverse remodeling (Figures 9.11) [6]. Because the degree of QRS prolongation might have impact on the response rate to CRT, a further study was conducted to examine whether such difference existed between patients with QRS = 120–150 msec and those with QRS  $> 150$  msec [49]. This study illustrated that the response rate of LV reverse remodeling was lower in the less-wide QRS group

(46%) than those with QRS  $> 150$  msec (68%). Intriguingly, only responders had significant systolic dyssynchrony and Ts-SD was improved after CRT. On the other hand, nonresponders only had mild systolic dyssynchrony, which was worsened by CRT [49]. Therefore, implantation of CRT to patients without dyssynchrony may have deleterious effects on cardiac function. Furthermore, the predictive value of LV reverse remodeling response is lower in patients with QRS = 120–150 msec than in those with QRS  $> 150$  msec (sensitivity of 83% vs. 100%) [49].

Another way of assessing systolic dyssynchrony is to measure the time to onset of mechanical contraction in the ejection phase. The work by Penicka et al. [4] used pulsed Doppler TDI at three basal LV segments (basal septal, lateral, and posterior wall) as well as basal RV segment by apical four-chamber and apical long-axis views. Intraventricular dyssynchrony was defined as the maximal electromechanical delay among the three basal LV segments, whereas interventricular dyssynchrony was defined as the maximal delay between the RV segment and the three LV sites. The result was that adding intra- and interventricular dyssynchrony predicted a relative increase in ejection fraction by 25%. A cutoff value  $\geq 102$  msec had an accuracy of 88% [4].

Few studies have compared multiple echocardiographic indices of systolic dyssynchrony at the same time. When this strategy was attempted in two studies [12,17], they confirmed that Ts-SD had the best predictive value for LV reverse remodeling when compared with indices that were derived from a smaller number of segments, for example, from two to eight LV segments. In one study, 18 echocardiographic parameters derived from TDI or strain rate imaging were compared for their predictive value for LV reverse remodeling after CRT for 3 months. Ts-SD has the greatest value of correlation coefficient ( $r = -0.74$ ;  $P < 0.001$ ) and area of ROC curve (area = 0.94;  $P < 0.001$ ) (Figures 9.12 and 9.13) [12]. Also, improvement of interventricular dyssynchrony appeared to be a secondary event, which failed to predict LV reverse remodeling [12]. From the ROC curve, a cutoff value of 31.4 msec was derived, which is very close to the cutoff value  $+2$  SD of the normal population, 32.6 msec [6]. This cutoff value gives a sensitivity of 96% and specificity of 78% [12].

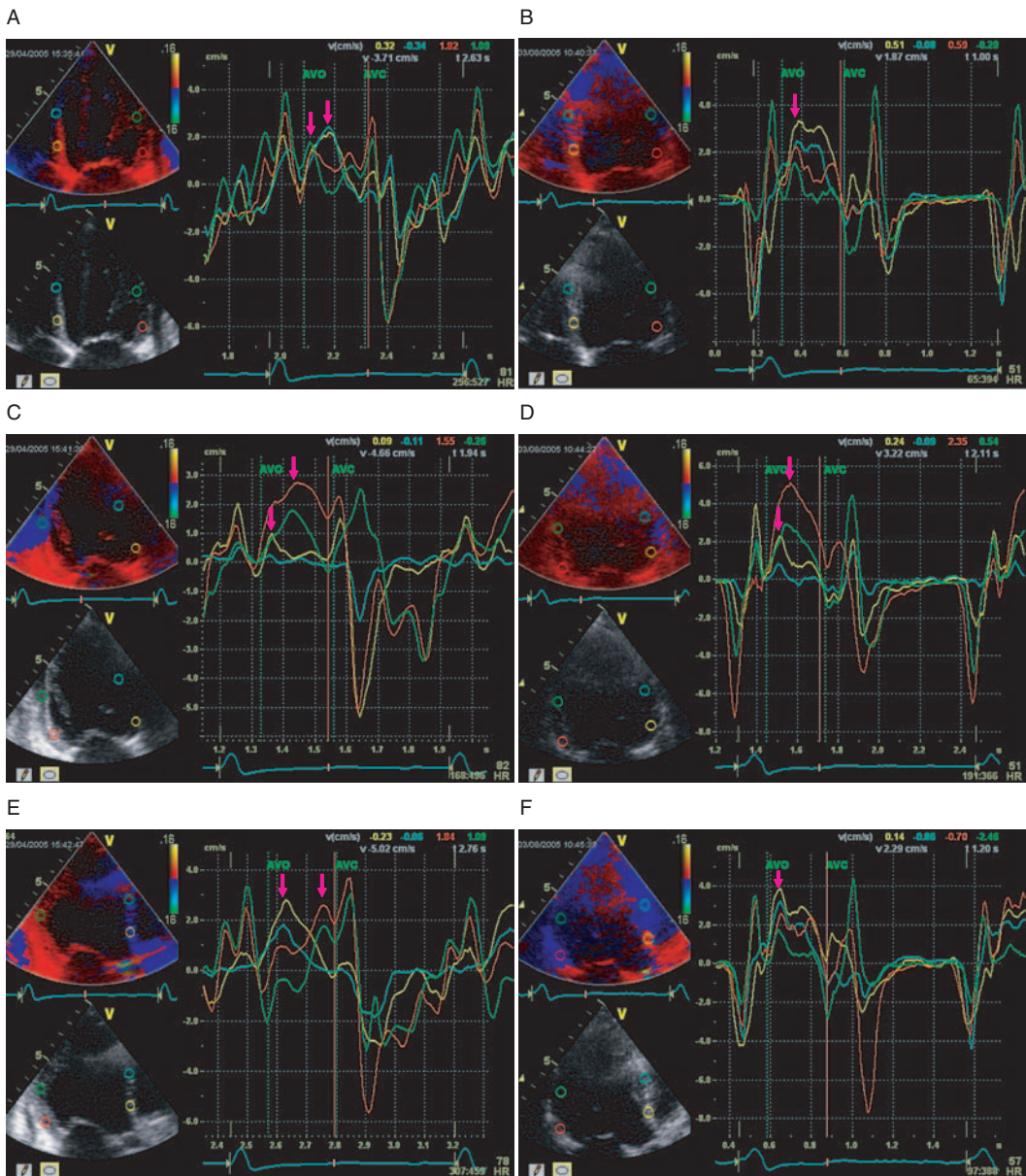


**Figure 9.11** Color TDI with myocardial velocity curves reconstructed at apical four-chamber (A, B), apical two-chamber (C, D), and long-axis (E, F) views before (A, C, E) and after (B, D, F) CRT. The use of three apical views can establish the six basal, six mid-segmental model to examine for systolic dyssynchrony. Aortic valve opening (AVO) and closure (AVC) markers are tagged relative to the electrocardiogram (ECG) signal to provide a temporal guidance on ejection period. Delay in the time to peak

systolic velocity is evident in the septal, inferior, and posterior walls at baseline (arrows). After CRT, there is realignment of the contractile profile, in particular in the ejection phase where the peak contractions occur at approximately the same time (arrows). The Dyssynchrony Index (or Ts-SD) of the six basal, six mid-segmental model decreased from 55 msec before CRT to 17 msec after the therapy. Septal-lateral delay was also improved.

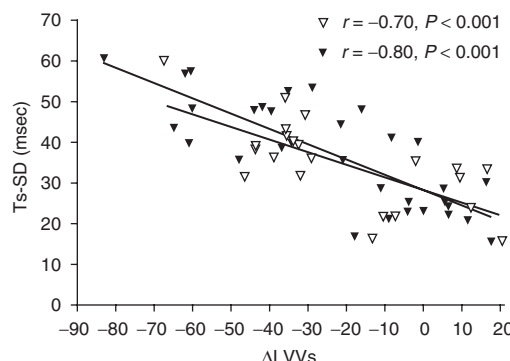


**Figure 9.12** A scatter plot of the change in LV end-systolic volume ( $\Delta$ LVVs) and severity of systolic dyssynchrony as measured by the standard deviation of the time to peak myocardial systolic velocity of the 12 LV segments (Ts-SD). Reprinted with permission from Yu et al. [12].

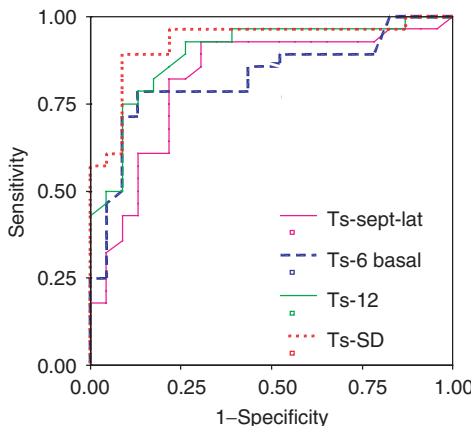


**Figure 9.13** The ROC curves for identification of LV reverse remodeling in all the patients who received CRT for the following parameters: Standard deviation of the time to peak myocardial systolic velocity of the 12 LV segments (Ts-SD), maximal difference in time to peak myocardial systolic velocity among the 12 (Ts-12), or six basal (Ts-6 basal) LV segments as well as difference between the time to peak myocardial systolic velocity between basal septal and lateral segment (Ts-sept-lat). Reprinted with permission from Cardiac Resynchronization Therapy by Yu et al., Blackwell.

### Tissue synchronization imaging

Another evolving technique of measuring systolic dyssynchrony is TSI. As explained, this transforms positive Ts into color mapping that allows a quick qualitative estimation of regional delay, in addition to quantitative assessment of myocardial velocity curves. Gorcsan et al. examined regional wall delay quantitatively by TSI in 29 patients who received

CRT [16]. This acute study defined responders as an increase in stroke volume of  $\geq 15\%$  within 48 hr after CRT. The TSI timing window of assessing dyssynchrony was adjusted to begin with the pre-ejection period and end in early diastolic period, which included the possible occurrence of post-systolic shortening. A delay between the antero septal and posterior wall of  $> 65$  msec predicted the gain in stroke volume with a sensitivity of 87% and specificity of 100% [16]. Another larger study by Yu et al. used TSI to examine only the ejection phase by tagging the beginning and the end of TSI to aortic valve opening and closure, respectively (Figure 9.14; Video clips 14–19 [17]). In 56 patients, qualitative analysis illustrated that the most severe delay occurred at the lateral wall, a specific finding that predicted a favorable LV reverse remodeling response, although the sensitivity was low. However, quantitative analysis from the six basal, six mid-segmental model yielded a sensitivity and specificity of 87% and 81%, respectively [17]. In fact, the predictive values of TSI appeared to be lower than that of TDI when the same indices were compared by their correlation coefficients and ROC curve areas [17]. Therefore, TSI may be a useful adjunctive tool for providing a quick qualitative screening for the presence of severe lateral wall delay. However, when such delay is not present or other regions of delay are suspected, a detailed quantitative assessment of Ts-SD by myocardial velocity curve is advisable.

### Strain imaging

Strain imaging detects the amount of myocardial deformation, and the time to peak strain has been used to assess dyssynchrony. From the parasternal short-axis view, Dohi et al. [50] suggested that a septal–posterior delay in tissue Doppler strain  $\geq 130$  msec predicted an acute improvement of stroke volume of  $\geq 15\%$  after CRT in a study of 38 patients, with a sensitivity of 95% and a specificity of 88%. On the other hand, controversy exists for the role of long-axis strain assessment. The study by Mele et al. [52] examined 37 patients, and responders were defined as those with a relative increase in ejection fraction of  $\geq 20\%$  and/or reduction of LV end-systolic volume  $\geq 15\%$  at 6 months. Criteria for systolic dyssynchrony included septal–posterior motion delay by M-mode

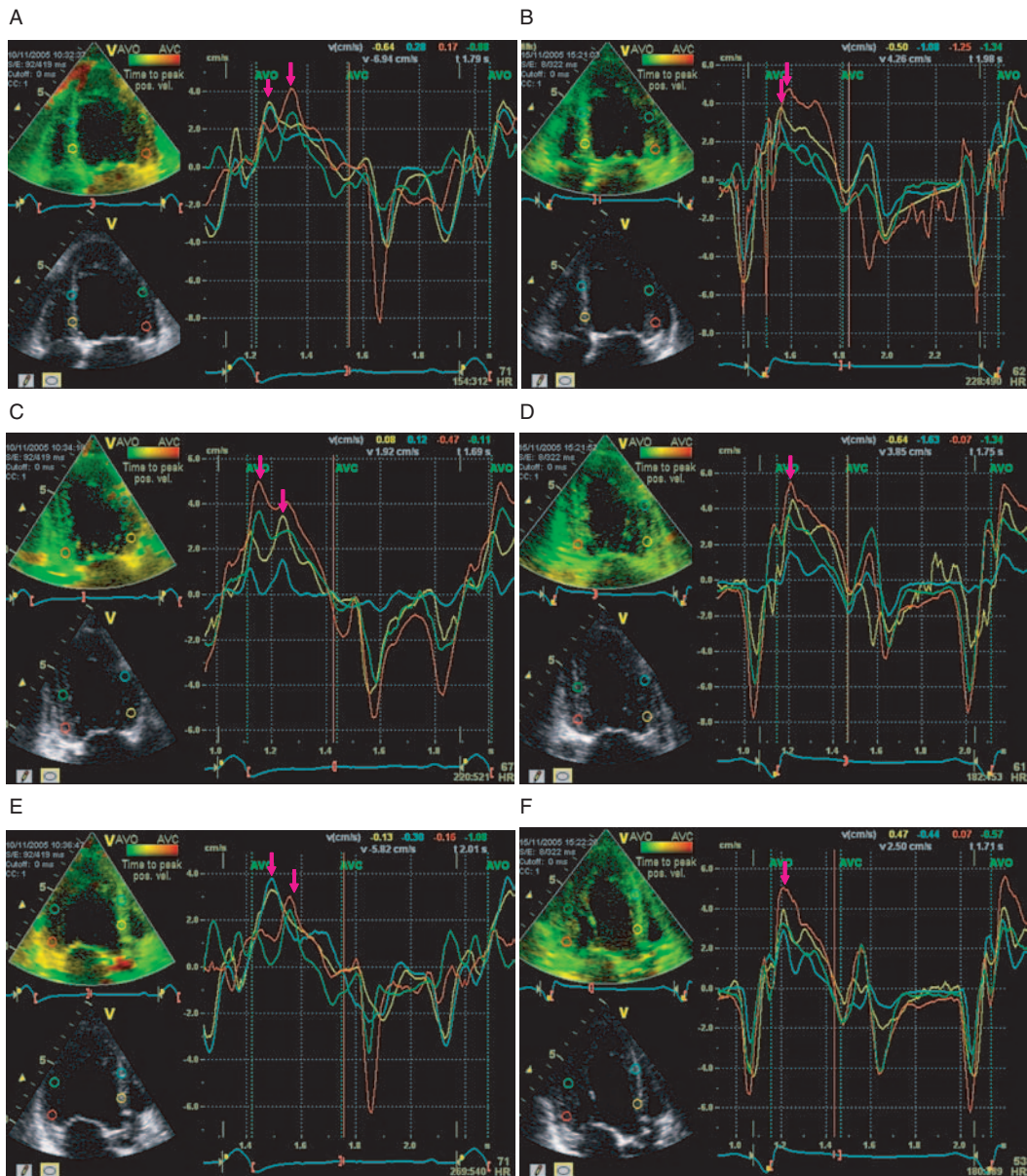


**Figure 9.14** An example of TSI in apical four-chamber (A, B) and apical two-chamber (C, D) views before (A, C) and after (B, D) CRT. The TSI method was set up to measure the time to peak myocardial systolic velocity (Ts) at ejection phase between the opening (AVO) and closure (AVC) of aortic valve. The Ts values were then coded into various colors, depending on the severity of delay, in the sequence of green, yellow, orange and red. Before

CRT, this patient had moderate delay over the lateral wall (orange color) in the four-chamber view; moderate delay of basal to mid-anterior wall (orange color) in the two-chamber view; and moderate delay of posterior wall in the apical long-axis view. Such regional delay was abolished after CRT. The myocardial curves from TDI signals are shown simultaneously to verify and confirm the severity of systolic delay. See also Video clips 14–19

(SPWMD), septal–posterior thickening delay by M-mode plus strain imaging (SPWTD), as well as the standard deviation of the time to peak strain of 12 LV segments at three apical views (Tps-SD) [52]. The study found that SPWMD was unable to predict echocardiographic response. On the other hand, the two parameters from strain imaging predicted a favorable response, although Tps-SD had a tighter correlation coefficient than SPWTD for both changes in ejection fraction ( $r = 0.86$ ;  $P < 0.001$ ) and LV end-systolic volume ( $r = -0.73$ ;  $P < 0.001$ ) [52]. A median cutoff value of Tps-SD  $\geq 60$  msec has been suggested, although its sensitivity and specificity has not been determined. Another recent study by Yu et al. [53] compared tissue velocity, tissue strain, and displacement mapping to predict LV reverse remodeling and gain in ejection fraction in 55 patients who received CRT for 3 months. Both the correlation coefficient and ROC curve area were compared for different models of systolic dyssynchrony, including Ts-SD for 12 and 6 basal LV segments, septal–lateral delay, as well as septal–posterior wall delay. Ts-SD from 12 segments has the best performance in predicting LV reverse remodeling ( $r = -0.76$ ;  $P < 0.001$ ) and gain in ejection fraction ( $r = 0.65$ ;  $P < 0.001$ ) compared with all the other parameters derived from tissue velocity. Interestingly, a similar parameter derived from displacement mapping has a much weaker predictive power for both reverse remodeling ( $r = -0.36$ ;  $P < 0.05$ ) and ejection fraction ( $r = 0.28$ ;  $P < 0.05$ ), whereas none of the strain parameters predicted a favorable response (Figure 9.15) [53]. Therefore, further studies are needed to ascertain the role of strain imaging to identify dyssynchrony and to predict CRT response.

### **Displacement imaging**

It has been suggested that the improvement of displacement in tissue tracking can serve as a surrogate marker of reduced systolic dyssynchrony [54,55]. However, the superiority of displacement mapping to tissue velocity in assessing patients with CRT has not been confirmed in the aforementioned study (Figure 9.16) [53]. It was shown that, for similar models of systolic dyssynchrony (from 2 to 12 LV segments), myocardial velocity had consistently higher predictive values and ROC curve areas for reduction of LV end-systolic volume and gain in ejection fraction than did displacement parameters [53].

### **Strain rate imaging**

Although thought to have theoretical advantage of differentiating active from translational motion, parameters derived from strain rate imaging failed to predict CRT response in a study that examined a large number of parameters derived from 2 to 12 LV segments [12]. Currently, no further study has ascertained the role of strain rate in predicting CRT response, and controversy also exists with respect to the changes of septal and lateral strain rate distribution after CRT [14,56]. Technical improvements in strain rate imaging, including a high signal to noise ratio and good reproducibility, is important before it is sufficiently robust for use in union practice.

### **Speckle tracking**

Speckle tracking measures regional strain from gray-scale images. The study by Suffoletto et al. examined systolic dyssynchrony by evaluating the time to peak radial strain on the parasternal short-axis view at the papillary muscle level [19]. In 50 patients who received CRT for a mean period of  $8 \pm 5$  months, a septal–posterior delay of  $\geq 130$  msec predicted a  $\geq 15\%$  increase in ejection fraction with a sensitivity of 89% and specificity of 83% (Figure 9.17) [19]. The value of short-axis circumferential and radial strain can also be measured as an indicator of LV circumferential fiber function. In another study of 37 patients, Zhang et al. [57] observed that only responders defined by LV reverse remodeling had significant improvement of circumferential and radial strain after CRT for 3 months. Furthermore, improvement of circumferential strain correlated with increased ejection fraction ( $r = 0.51$ ;  $P = 0.001$ ) and decreased LV mid-cavity diameter ( $r = -0.56$ ;  $P < 0.001$ ) [57]. Interestingly, LV torsion was unchanged in responders, but was further reduced in nonresponders defined by LV reverse remodeling. These studies highlight the potential role of using speckle tracking to assess changes in cardiac synchrony and LV function in the CRT era.

### **Systolic dyssynchrony in heart failure patients with normal QRS duration and implication for cardiac resynchronization therapy**

Current guidelines for CRT recommend the prerequisite occurrence of prolonged QRS duration [33]. This patient group constitutes only approximately

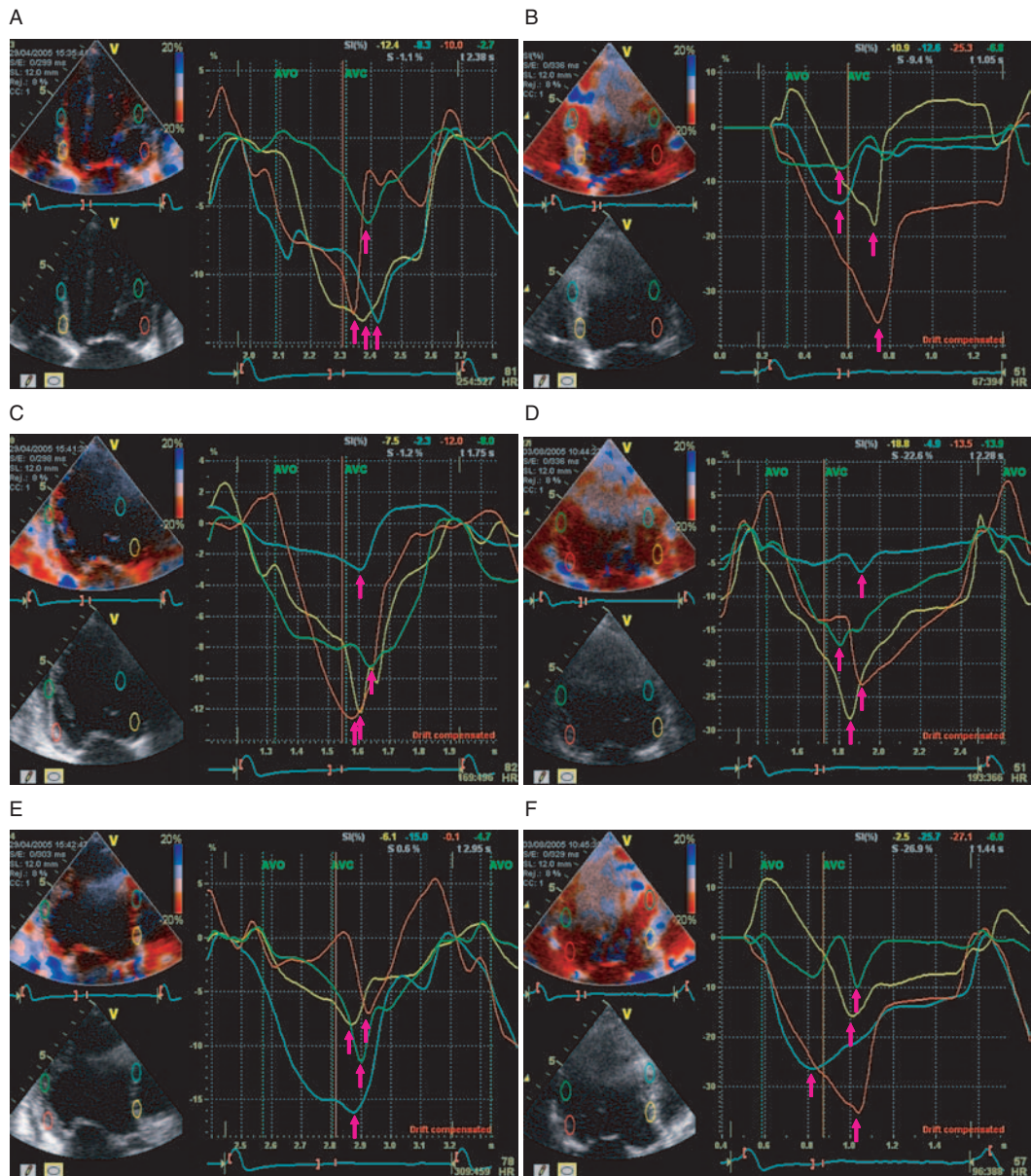


**Figure 9.15** Strain imaging in apical four-chamber (A, B), apical two-chamber (C, D), and apical long-axis (E, F) views before (A, C, E) and after (B, D, F) CRT. Normal systolic strain in apical views is negative with the cumulated values

occurring during end-systole. In this patient, systolic dyssynchrony is illustrated by the dispersion of the time to peak negative strain (arrows). In this case, dispersion of peak systolic strain remain present after CRT.

one quarter of the heart failure population according to large heart failure registries [20,58]. With the use of the TDI technique, it is clear that cardiac dyssynchrony can occur in the failing heart with normal QRS duration. The first report by Yu et al. examined the prevalence of systolic and

diastolic dyssynchrony in 67 heart failure patients with QRS duration >120 msec (in the form of LBBB or intraventricular conduction delay) and in 45 heart failure patients with QRS duration ≤120 msec [7]. By the use of TDI with a cutoff value of  $Ts-SD > 32.6$  msec (derived from 88 normal

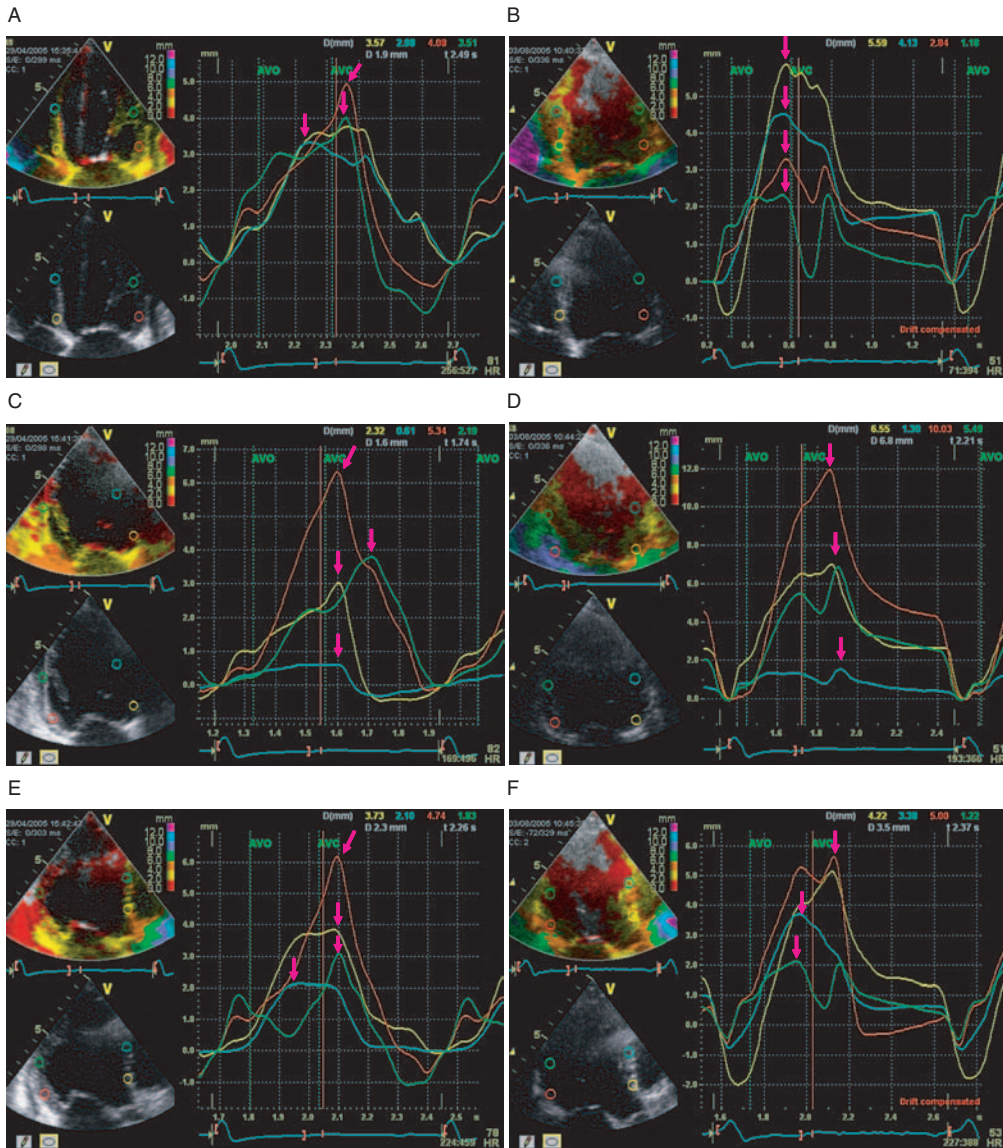


**Figure 9.16** Displacement imaging in apical four-chamber (A, B), apical two-chamber (C, D), and apical long-axis (E, F) views before (A, C, E) and after (B, D, F) CRT. Normal systolic displacement in these views occurs with the largest amplitude at the basal LV segments, which move toward the apex. Therefore, the apex is relatively stationary with respect to long-axis motion. The displacement mapping is cumulative; therefore, it increases in amplitude during

systole and reaches the maximal amplitude at end-systole. In this patient, systolic dyssynchrony is illustrated by the unusually early maximal displacement at some segments, and delayed displacement in others, which extend beyond the aortic valve closure in the others (arrows). After CRT, some degree of improvement is reflected by the realignment of maximal systolic displacement among the segments.

controls), systolic dyssynchrony was present in 43% of heart failure patients with narrow QRS complex and in 64% with wide QRS complex [7]. When the criterion of maximal difference in Ts from the

six basal, six mid-segmental model of >100 msec was used, the prevalence of systolic dyssynchrony was 51% and 73%, respectively (Figure 9.18) [7]. Several subsequent reports also confirmed the

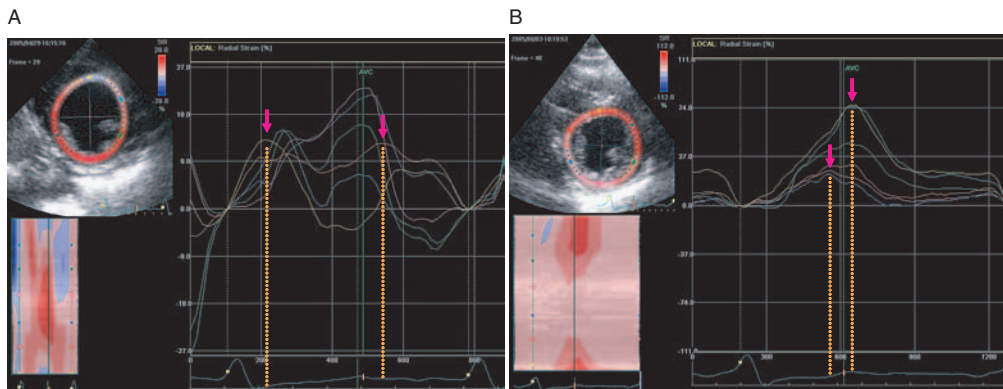


**Figure 9.17** Speckle tracking in parasternal short-axis view (papillary muscle level) to assess systolic dyssynchrony. A heart failure patient with wide QRS complex was studied by radial strain curve in six mid LV segments. The

dotted lines indicate the maximal delay for time to peak positive radial strain before CRT (A) and its improvement at 3 months after CRT (B).

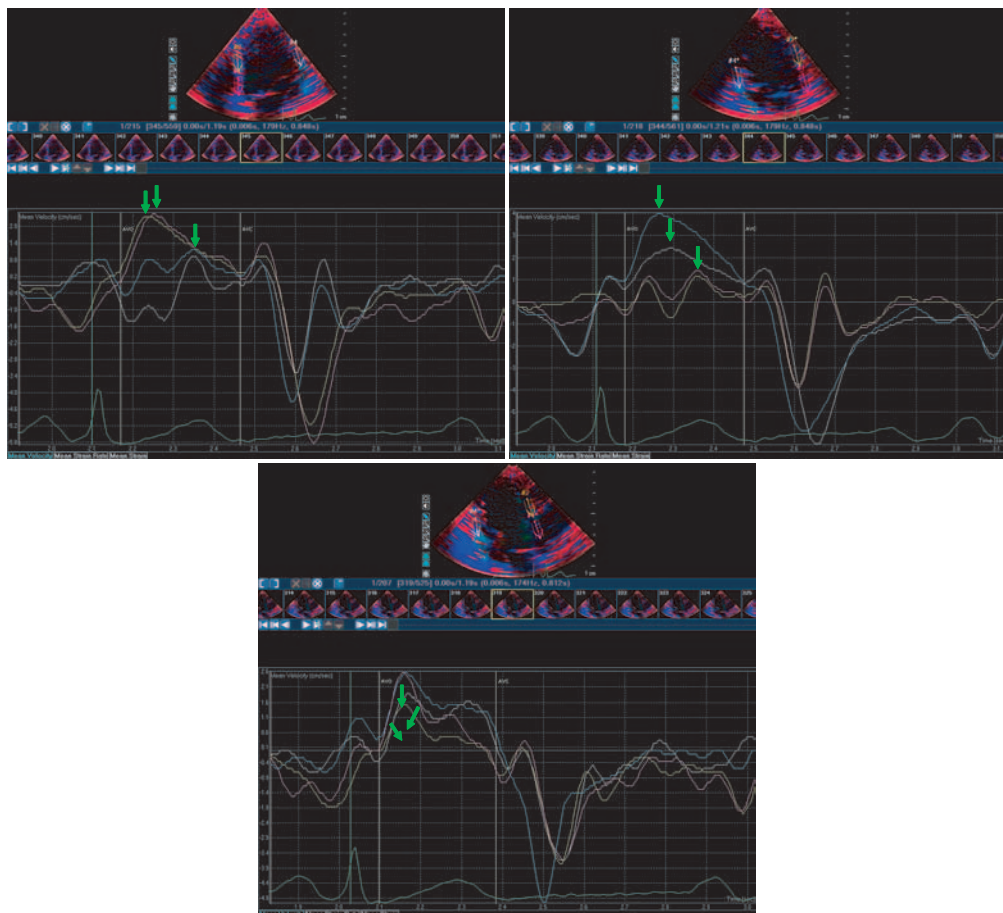


**Figure 9.18** Cardiac systolic dyssynchrony as evidenced by tissue Doppler imaging in a patient with heart failure and normal QRS duration. From the myocardial velocity curves

in the three apical views, there was a delay in Ts at the lateral and anterior segments (arrows) with Ts-SD of 50 msec.

**Table 9.3** Evidence of systolic dyssynchrony by tissue Doppler imaging in heart failure patients with normal QRS duration.

Author	Number	Parameter	Cutoff	Prevalence of intraventricular dyssynchrony (%)		
				QRS <120 msec	QRS >150 msec	
Yu [7]	112	Ts-diff of 12 LV segments	100 msec	51	73	
Yu [7]	112	Ts-SD of 12 LV segments	32.6 msec	43	64	
Sade [15]	36	Anteroseptal-posterior delay in Td (short-axis)	Not specified	36	Not specified	
Bleeker [59]	64	Septal-lateral delay in Ts	60 msec	33	Not included	
Yu [23]	281	Ts-SD of 12 LV segments	33 msec	49	71	
				QRS < 120 msec	QRS = 120–150 msec	QRS > 150 msec
Bleeker [22]	90	Septal-lateral delay in Ts	60 msec	27	60	70
Bader [31]	104	Maximal difference in Ts (onset) of four basal segments	40 msec	56	84	89
Ghio [21]	158	Maximal difference Ts (onset) of four basal or four mid-LV segments	50 msec	30	57	71

Td, time to peak displacement; Ts, time to peak myocardial systolic velocity; Ts (onset), time to onset of myocardial systolic velocity; Ts-SD, standard deviation of time to peak myocardial systolic velocity.

presence of mechanical dyssynchrony in heart failure patients with narrow QRS complex by TDI (Table 9.3) [15,21–23,31,59]. The study by Ghio et al. [21] examined 61 heart failure patients with normal QRS duration, 21 patients with LBBB and QRS between 120 and 150 msec, and 76 patients with QRS duration  $\geq$  150 msec by 2-D color TDI. Intraventricular dyssynchrony was assessed by apical four- and two-chamber views in basal and mid-segments for a maximal difference of time to onset of systolic wave, with a cutoff value of  $>50$  msec. The prevalence of systolic intraventricular dyssynchrony in these three groups was 30%, 57%, and 71%, respectively [21]. Bleeker et al. [22] used a septal-lateral delay  $>60$  msec at basal LV segments and reported that 27% of heart failure patients with QRS duration  $\leq$  120 msec had systolic dyssynchrony; and these rates were 60% and 70%, respectively, in those with QRS between 120 and 150 msec and those with QRS  $>150$  msec. In the subset of patients whose heart failure was caused by idiopathic dilated cardiomyopathy, tissue displacement imaging documented systolic dyssynchrony in 36% (5 of 14) of patients who exhibited anteroseptal–posterior wall delay [15].

The identification of systolic dyssynchrony by TDI in the population with narrow QRS complex may allow to potentially benefit more heart failure patients from CRT. There are three single-center studies that examined the benefit of CRT in such patients [60,61]. The study by Achilli et al. [60] examined 14 heart failure patients with normal QRS duration ( $\leq$ 120 msec). M-mode echocardiography was performed to evaluate systolic dyssynchrony by demonstrating delayed LV wall contraction when compared with global LV diastolic filling by Doppler signals. Interestingly, patients with normal QRS duration have evidence of improvement in NYHA class, 6-Minute Hall Walk distance, reduction in LV diameter and mitral regurgitation, as well as increase in ejection fraction and LV filling time [60]. Another study by Turner et al. [61] compared the change in cardiac function in nine heart failure patients with normal QRS duration before and after CRT. Dyssynchrony was measured by Ts of the six basal LV segments from three apical views. Biventricular pacing resulted in a 2.3% ( $P < 0.05$ ) increase in LV ejection fraction. Furthermore, color TDI showed homogenous delay in Ts in the six basal segments, leading

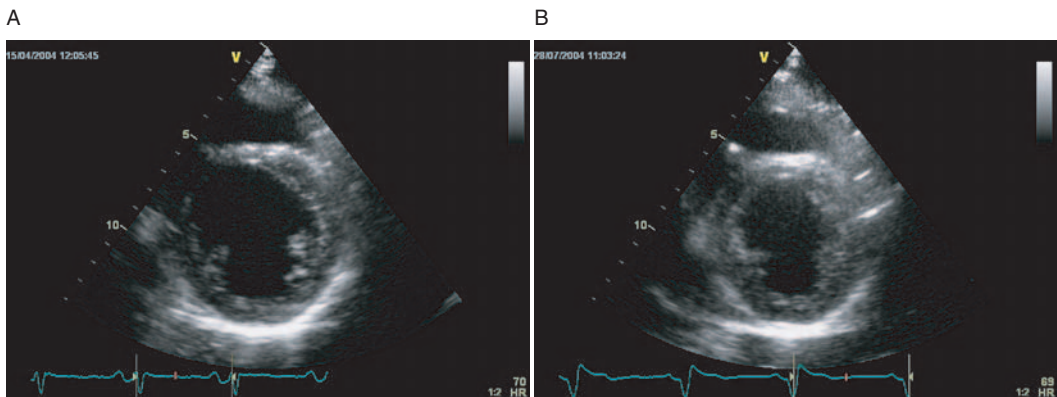


**Figure 9.19** 2-D echocardiography showing LV reverse remodeling in a heart failure patient with normal QRS complex duration and systolic dyssynchrony by TDI who received CRT. On the parasternal short-axis views, there is

an evidence of reduction of LV volume and improvement of myocardial contractility after CRT for 3 months (A, B). The geometry of the heart is also improved favorably. See also Video clips 20 and 21 (6).

to the abolishment of regional delay, a manner similar to that observed in patients with wide QRS complex [5,61]. In fact, acute hemodynamic improvement of cardiac output and pulmonary capillary wedge pressure was also observed in these patients who received CRT [62]. The study by Yu et al. examined 51 heart failure patients with normal QRS duration of <120 msec with coexisting systolic dyssynchrony by Ts-SD [63]. There was significant improvement of NYHA class, maximal exercise capacity, and 6-Minute Hall Walk distance after CRT for 3 months. Echocardiography demonstrated LV reverse remodeling with reduction of LV volume, gain in ejection fraction, and increase in sphericity index (Figure 9.19; Video clips 20 and 21 (6)). There was also reduction of mitral regurgitation and gain in LV filling time [63]. Interestingly, the level of baseline systolic dyssynchrony seems to determine the degree of LV reverse remodeling for a similar extent for both wide and narrow QRS groups (Figure 9.20) [63]. Furthermore, the on-and-off effect of pacing was demonstrated by echocardiography in these patients. By TSI, improvement of systolic dyssynchrony was evident with reduction of Ts-SD [18].

### Dynamic cardiac dyssynchrony

Usually cardiac dyssynchrony is assessed at rest when echocardiography or other imaging modalities are performed. However, it is increasingly

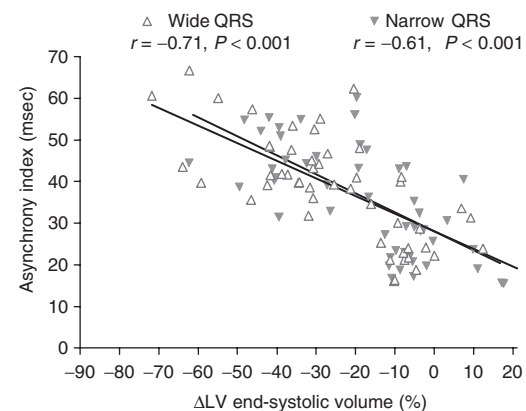


**Figure 9.20** A scatter plot of the change in LV end-systolic volume and severity of systolic asynchrony as measured by Asynchrony Index for heart failure patients with narrow (filled triangles) and wide (white triangles) QRS complexes. The regression lines for both groups nearly superimpose on each other with nearly identical slopes.

conceivable that the status of dyssynchrony may vary from rest to exercise, a condition referred to as dynamic dyssynchrony. A recent study examined the possible occurrence of dynamic dyssynchrony in 65 heart failure patients and 50 matched healthy controls who underwent a symptom-limited bicycle exercise test [64]. Systolic dyssynchrony was assessed by several indices, which included maximal difference in the time to onset or peak

systolic velocity of the six basal segments, Ts-SD, septal-lateral delay in Ts, as well as percentage of LV segments with delayed longitudinal contraction. Interventricular dyssynchrony between pulmonary and aortic outflow was also assessed by Doppler echocardiography. It was observed that, in heart failure patients, LV dyssynchrony increased by at least 20% in 34%, remained stable in 37%, and decreased by at least 20% in 29% of patients. Moreover, 26% of heart failure patients had either exercise-induced or normalization of ventricular dyssynchrony [64]. This finding was in contrast to control subjects with normal LV function in whom exercise did not modify the extent of LV dyssynchrony. The implications of dynamic dyssynchrony necessitate further studies, in particular its change in subjects who might consider CRT.

## Summary

The assessment of cardiac dyssynchrony is gaining importance in clinical practice. Among all the available techniques, myocardial imaging has been most validated and proven useful in clinical practice. Both TDI and its postprocessing imaging as well as speckle tracking technologies have been characterized by various studies, and these powerful tools permit the evaluation of both systolic and diastolic dyssynchrony. Furthermore, cutoff values have been defined in several indices derived from myocardial imaging. Currently, the best described role of dyssynchrony assessment lies in heart failure patients with systolic dysfunction, in particular when CRT is contemplated in those with prolonged QRS complex so as to predict responders to therapy. Furthermore, adjunctive assessment of resting dyssynchrony may help to explore new indications for CRT. Apart from application of dyssynchrony assessment in CRT, it is increasingly recognized that other disease conditions might also result in systolic and diastolic dyssynchrony, such as diastolic heart failure, LV hypertrophy, and idiopathic or RV pacing-induced LBBB in the setting of normal systolic function. Currently, the implications of cardiac dyssynchrony in these diseases are under clinical investigation. Lastly, exercise-induced dynamic dyssynchrony has been recently described

in patients with systolic heart failure. How this condition might affect patient management warrants further clinical investigation.

## Appendix 9.1

### Assessment of Systolic Dyssynchrony Index (or Asynchrony Index, Ts-SD) by tissue Doppler imaging

From the apical four-chamber, two-chamber, and three-chamber (or apical long-axis) views, a six basal, six mid-segmental model is obtained of the left ventricle, namely the septal, lateral, anterior, inferior, anteroseptal, and posterior segments at both basal and mid-levels [6,12]. In systole, myocardial velocities measured are those at the isovolumic contraction phase and ejection phase, both of them are positive in value, that is, apically directed. During diastole, the velocities measured are those at the isovolumic relaxation phase (negative or biphasic profiles) and early diastolic and late diastolic relaxation waves, which are negative in value. To calculate the Ts-SD, the peak myocardial systolic velocity is determined. To measure the time to peak systolic velocity in the ejection phase (Ts) of individual segments, the following are the rules-of-thumb:

- First, use of the aortic valve opening and closure markers that superimpose on TDI tracings to guide for the identification of *ejection* phase is strongly recommended (e.g., from Doppler echocardiography at the LV outflow tract or aortic valve level in the apical five-chamber view).
- Measure the time from the onset of QRS complex to the *highest* systolic peak during the *ejection* phase (between aortic valve opening and closure in general).
  - If there are multiple peaks in ejection phase, take the highest peak (not the first if it is not the highest).
  - If there are two or more peaks in the ejection phase with the same amplitude in velocity, then choose the earliest peak among those with same high velocity.
  - If the segment has only a negative peak in the ejection phase, or the 2-D TDI image quality is too poor to generate a reliable myocardial velocity curve, or the velocity is so noisy with very low and inconsistent velocities, neglect those particular segments and proceed with the rest of the measurable segments.

In general, up to a maximum of three segments can be excluded from analysis, although they should not be the segments from the same wall.

- Do *not* measure Ts on the isovolumic contraction phase, isovolumic relaxation phase, or during postsystolic shortening. If the descending slope of the isovolumic contraction velocity intercept at aortic value opening has a higher velocity than the ejection phase, do not use such values. Similarly, if the ascending slope of postsystolic shortening is higher than ejection phase velocity at intercept of aortic valve closure, do not use this value.

The Ts-SD will then be calculated as the standard deviation of Ts among six basal, six mid-LV segments using any standardized statistical software (e.g., SPSS or Microsoft Excel) – the larger the value of Ts-SD, the more severe the systolic dyssynchrony.

## References

- 1 Henein MY, Gibson DG. Normal long axis function. *Heart* 1999; **81**: 111–3.
- 2 Greenbaum RA, Ho SY, Gibson DG, Becker AE, Anderson RH. Left ventricular fibre architecture in man. *Br Heart J* 1981; **45**: 248–63.
- 3 Torrent-Guasp F, Kocica MJ, Corno A, et al. Systolic ventricular filling. *Eur J Cardiothorac Surg* 2004; **25**: 376–86.
- 4 Penicka M, Bartunek J, de Bruyne B, et al. Improvement of left ventricular function after cardiac resynchronization therapy is predicted by tissue Doppler imaging echocardiography. *Circulation* 2004; **109**: 978–83.
- 5 Yu CM, Chau E, Sanderson JE, et al. Tissue Doppler echocardiographic evidence of reverse remodeling and improved synchronicity by simultaneously delaying regional contraction after biventricular pacing therapy in heart failure. *Circulation* 2002; **105**: 438–45.
- 6 Yu CM, Fung WH, Lin H, Zhang Q, Sanderson JE, Lau CP. Predictors of left ventricular reverse remodeling after cardiac resynchronization therapy for heart failure secondary to idiopathic dilated or ischemic cardiomyopathy. *Am J Cardiol* 2003; **91**: 684–8.
- 7 Yu CM, Lin H, Zhang Q, Sanderson JE. High prevalence of left ventricular systolic and diastolic asynchrony in patients with congestive heart failure and normal QRS duration. *Heart* 2003; **89**: 54–60.
- 8 Ansalone G, Giannantoni P, Ricci R, et al. Doppler myocardial imaging in patients with heart failure receiving biventricular pacing treatment. *Am Heart J* 2001; **142**: 881–96.
- 9 Ansalone G, Giannantoni P, Ricci R, Trambaiolo P, Fedele F, Santini M. Doppler myocardial imaging to evaluate the effectiveness of pacing sites in patients receiving biventricular pacing. *J Am Coll Cardiol* 2002; **39**: 489–99.
- 10 Yu CM, Yang H, Lau CP, et al. Regional left ventricle mechanical asynchrony in patients with heart disease and normal QRS duration: implication for biventricular pacing therapy. *Pacing Clin Electrophysiol* 2003; **26**: 562–70.
- 11 Bax JJ, Ansalone G, Breithardt OA, et al. Echocardiographic evaluation of cardiac resynchronization therapy: ready for routine clinical use? A critical appraisal. *J Am Coll Cardiol* 2004; **44**: 1–9.
- 12 Yu CM, Fung JW, Zhang Q, et al. Tissue Doppler imaging is superior to strain rate imaging and postsystolic shortening on the prediction of reverse remodeling in both ischemic and nonischemic heart failure after cardiac resynchronization therapy. *Circulation* 2004; **110**: 66–73.
- 13 Yu CM, Abraham WT, Bax J, et al. Predictors of response to cardiac resynchronization therapy (PROSPECT) – study design. *Am Heart J* 2005; **149**: 600–5.
- 14 Sun JP, Chinchoy E, Donal E, et al. Evaluation of ventricular synchrony using novel Doppler echocardiographic indices in patients with heart failure receiving cardiac resynchronization therapy. *J Am Soc Echocardiogr* 2004; **17**: 845–50.
- 15 Sade LE, Kanzaki H, Severyn D, Dohi K, Gorcsan J III. Quantification of radial mechanical dyssynchrony in patients with left bundle branch block and idiopathic dilated cardiomyopathy without conduction delay by tissue displacement imaging. *Am J Cardiol* 2004; **94**: 514–8.
- 16 Gorcsan J III, Kanzaki H, Bazaz R, Dohi K, Schwartzman D. Usefulness of echocardiographic tissue synchronization imaging to predict acute response to cardiac resynchronization therapy. *Am J Cardiol* 2004; **93**: 1178–81.
- 17 Yu CM, Zhang Q, Fung JW, et al. A novel tool to assess systolic asynchrony and identify responders of cardiac resynchronization therapy by tissue synchronization imaging. *J Am Coll Cardiol* 2005; **45**: 677–84.
- 18 Yu CM, Zhang Q, Fung JW. Visualization of regional left ventricular mechanical delay by tissue synchronization imaging in heart failure patients with wide and narrow QRS complexes undergoing cardiac resynchronization therapy. *Circulation* 2005; **112**: e93–5.
- 19 Suffoletto MS, Dohi K, Cannesson M, Saba S, Gorcsan J III. Novel speckle-tracking radial strain from routine black-and-white echocardiographic images to quantify dyssynchrony and predict response to cardiac resynchronization therapy. *Circulation* 2006; **113**: 960–8.

- 20 Baldasseroni S, Opasich C, Gorini M, et al. Left bundle-branch block is associated with increased 1-year sudden and total mortality rate in 5517 outpatients with congestive heart failure: a report from the Italian network on congestive heart failure. *Am Heart J* 2002; **143**: 398–405.
- 21 Ghio S, Constantin C, Klersy C, et al. Interventricular and intraventricular dyssynchrony are common in heart failure patients, regardless of QRS duration. *Eur Heart J* 2004; **25**: 571–8.
- 22 Bleeker GB, Schalij MJ, Molhoek SG, et al. Relationship between QRS duration and left ventricular dyssynchrony in patients with end-stage heart failure. *J Cardiovasc Electrophysiol* 2004; **15**: 544–9.
- 23 Yu CM, Zhang Q, Yip GW, et al. Diastolic and systolic asynchrony in patients with diastolic heart failure. *J Am Coll Cardiol* 2007; **49**: 97–105.
- 24 Wang JW, Kurrelmeyer KM, Torre-Amione G, Nagueh SF. Systolic and diastolic dyssynchrony in patients with diastolic heart failure and the effect of medical therapy. *J Am Coll Cardiol* 2007; **49**: 88–96.
- 25 Grines CL, Bashore TM, Boudoulas H, Olson S, Shafer P, Wooley CF. Functional abnormalities in isolated left bundle branch block. The effect of interventricular asynchrony. *Circulation* 1989; **79**: 845–53.
- 26 Niu HX, Hua W, Zhang S, et al. Assessment of cardiac function and synchronicity in subjects with isolated bundle branch block using Doppler imaging. *Chin Med J (Engl)* 2006; **119**: 795–800.
- 27 Ghio S, Constantin C, Klersy C, et al. Interventricular and intraventricular dyssynchrony are common in heart failure patients, regardless of QRS duration. *Eur Heart J* 2004; **25**: 571–8.
- 28 Sweeney MO, Hellkamp AS, Ellenbogen KA, et al. Adverse effect of ventricular pacing on heart failure and atrial fibrillation among patients with normal baseline QRS duration in a clinical trial of pacemaker therapy for sinus node dysfunction. *Circulation* 2003; **107**: 2932–7.
- 29 Kang SJ, Song JK, Yang HS, et al. Systolic and diastolic regional myocardial motion of pacing-induced versus idiopathic left bundle branch block with and without left ventricular dysfunction. *Am J Cardiol* 2004; **93**: 1243–6.
- 30 Pai RG, Gill KS. Amplitudes, durations, and timings of apically directed left ventricular myocardial velocities: II. Systolic and diastolic asynchrony in patients with left ventricular hypertrophy. *J Am Soc Echocardiogr* 1998; **11**: 112–8.
- 31 Bader H, Garrigue S, Lafitte S, et al. Intra-left ventricular electromechanical asynchrony. A new independent predictor of severe cardiac events in heart failure patients. *J Am Coll Cardiol* 2004; **43**: 248–56.
- 32 Cho GY, Song JK, Park WJ, et al. Mechanical dyssynchrony assessed by tissue Doppler imaging is a powerful predictor of mortality in congestive heart failure with normal QRS duration. *J Am Coll Cardiol* 2005; **46**: 2237–43.
- 33 Hunt SA, Abraham WT, Chin MH, et al. ACC/AHA 2005 Guideline update for the diagnosis and management of chronic heart failure in the adult: a report of the American College of Cardiology/American Heart Association Task Force on Practice Guidelines (Writing Committee to Update the 2001 Guidelines for the Evaluation and Management of Heart Failure): developed in collaboration with the American College of Chest Physicians and the International Society for Heart and Lung Transplantation: endorsed by the Heart Rhythm Society. *Circulation* 2005; **112**: e154–235.
- 34 Bargiggia GS, Bertucci C, Recusani F, et al. A new method for estimating left ventricular dP/dt by continuous wave Doppler-echocardiography. Validation studies at cardiac catheterization. *Circulation* 1989; **80**: 1287–92.
- 35 Abraham WT, Fisher WG, Smith AL, et al. Cardiac resynchronization in chronic heart failure. *N Engl J Med* 2002; **346**: 1845–53.
- 36 Bristow MR, Saxon LA, Boehmer J, et al. Cardiac resynchronization therapy with or without an implantable defibrillator in advanced chronic heart failure. *N Engl J Med* 2004; **350**: 2140–50.
- 37 Cleland JG, Daubert JC, Erdmann E, et al. The effect of cardiac resynchronization on morbidity and mortality in heart failure. *N Engl J Med* 2005; **352**: 1539–49.
- 38 St John Sutton MG, Plappert T, Abraham WT, et al. Effect of cardiac resynchronization therapy on left ventricular size and function in chronic heart failure. *Circulation* 2003; **107**: 1985–90.
- 39 Zhang Q, Fung JW, Auricchio A, et al. Differential change in left ventricular mass and regional wall thickness after cardiac resynchronization therapy for heart failure. *Eur Heart J* 2006; **27**: 1423–30.
- 40 Yu CM, Bleeker GB, Fung JW, et al. Left ventricular reverse remodeling but not clinical improvement predicts long-term survival after cardiac resynchronization therapy. *Circulation* 2005; **112**: 1580–6.
- 41 Vasan RS, Benjamin EJ, Larson MG, et al. Plasma natriuretic peptides for community screening for left ventricular hypertrophy and systolic dysfunction: the Framingham heart study. *JAMA* 2002; **288**: 1252–9.
- 42 Yu CM, Fung JWH, Zhang Q, Sanderson JE. Understanding nonresponders of cardiac resynchronization therapy—current and future perspectives. *J Cardiovasc Electrophysiol* 2005; **16**: 1117–24.
- 43 Bleeker GB, Schalij MJ, Molhoek SG, et al. Relationship between QRS duration and left ventricular dyssynchrony in patients with end-stage heart failure. *J Cardiovasc Electrophysiol* 2004; **15**: 544–9.
- 44 Gras D, Leclercq C, Tang AS, Bucknall C, Luttkhuis HO, Kirstein-Pedersen A. Cardiac resynchronization therapy

- in advanced heart failure—the multicenter InSync clinical study. *Eur J Heart Fail* 2002; **4**: 311–20.
- 45 Cazeau S, Leclercq C, Lavergne T, et al. Effects of multisite biventricular pacing in patients with heart failure and intraventricular conduction delay. *N Engl J Med* 2001; **344**: 873–80.
  - 46 Bax JJ, Marwick TH, Molhoek SG, et al. Left ventricular dyssynchrony predicts benefit of cardiac resynchronization therapy in patients with end-stage heart failure before pacemaker implantation. *Am J Cardiol* 2003; **92**: 1238–40.
  - 47 Kanzaki H, Bazaz R, Schwartzman D, et al. A mechanism for immediate reduction in mitral regurgitation after cardiac resynchronization therapy: insights from mechanical activation strain mapping. *J Am Coll Cardiol* 2004; **44**: 1619–25.
  - 48 Notabartolo D, Merlino JD, Smith AL, et al. Usefulness of the peak velocity difference by tissue Doppler imaging technique as an effective predictor of response to cardiac resynchronization therapy. *Am J Cardiol* 2004; **94**: 817–20.
  - 49 Yu CM, Fung JW, Chan CK, et al. Comparison of efficacy of reverse remodeling and clinical improvement for relatively narrow and wide QRS complexes after cardiac resynchronization therapy for heart failure. *J Cardiovasc Electrophysiol* 2004; **15**: 1058–65.
  - 50 Dohi K, Suffoletto MS, Schwartzman D, Ganz L, Pinsky MR, Gorcsan J III. Utility of echocardiographic radial strain imaging to quantify left ventricular dyssynchrony and predict acute response to cardiac resynchronization therapy. *Am J Cardiol* 2005; **96**: 112–6.
  - 51 Bax JJ, Bleeker GB, Marwick TH, et al. Left ventricular dyssynchrony predicts response and prognosis after cardiac resynchronization therapy. *J Am Coll Cardiol* 2004; **44**: 1834–40.
  - 52 Mele D, Pasanisi G, Capasso F, et al. Left intraventricular myocardial deformation dyssynchrony identifies responders to cardiac resynchronization therapy in patients with heart failure. *Eur Heart J* 2006; **27**: 1070–8.
  - 53 Yu CM, Zhang Q, Chan YS, et al. Tissue Doppler velocity is superior to displacement and strain mapping in predicting left ventricular reverse remodeling response after cardiac resynchronization therapy. *Heart* 2006; **19**: 422–8.
  - 54 Sogaard P, Egeblad H, Kim WY, et al. Tissue Doppler imaging predicts improved systolic performance and reversed left ventricular remodeling during long-term cardiac resynchronization therapy. *J Am Coll Cardiol* 2002; **40**: 723–30.
  - 55 Sogaard P, Egeblad H, Pedersen AK, et al. Sequential versus simultaneous biventricular resynchronization for severe heart failure: evaluation by tissue Doppler imaging. *Circulation* 2002; **106**: 2078–84.
  - 56 Breithardt OA, Stellbrink C, Herbots L, et al. Cardiac resynchronization therapy can reverse abnormal myocardial strain distribution in patients with heart failure and left bundle branch block. *J Am Coll Cardiol* 2003; **42**: 486–94.
  - 57 Zhang Q, Fung JW, Yip GW, et al. Preserved circumferential function by 2D speckle tracking determines the favorable improvement of left ventricular geometry and function after cardiac resynchronization therapy. *Circulation* 2006; **114** Suppl II: II-719–20.
  - 58 Farwell D, Patel NR, Hall A, Ralph S, Sulke AN. How many people with heart failure are appropriate for biventricular resynchronization? *Eur Heart J* 2000; **21**: 1246–50.
  - 59 Bleeker GB, Schalij MJ, Molhoek SG, et al. Frequency of left ventricular dyssynchrony in patients with heart failure and a narrow QRS complex. *Am J Cardiol* 2005; **95**: 140–2.
  - 60 Achilli A, Sassara M, Ficili S, et al. Long-term effectiveness of cardiac resynchronization therapy in patients with refractory heart failure and “narrow” QRS. *J Am Coll Cardiol* 2003; **42**: 2117–24.
  - 61 Turner MS, Bleasdale RA, Vinereanu D, et al. Electrical and mechanical components of dyssynchrony in heart failure patients with normal QRS duration and left bundle-branch block: impact of left and biventricular pacing. *Circulation* 2004; **109**: 2544–9.
  - 62 Turner MS, Bleasdale RA, Mumford CE, Frenneaux MP, Morris-Thurgood JA. Left ventricular pacing improves haemodynamic variables in patients with heart failure with a normal QRS duration. *Heart* 2004; **90**: 502–5.
  - 63 Yu CM, Chan YS, Zhang Q, et al. Benefits of cardiac resynchronization therapy for heart failure patients with narrow QRS complexes and coexisting systolic asynchrony by echocardiography. *J Am Coll Cardiol* 2007; **48**: 2251–7.
  - 64 Lafitte S, Bordachar P, Lafitte M, et al. Dynamic ventricular dyssynchrony: an exercise-echocardiography study. *J Am Coll Cardiol* 2006; **47**: 2253–9.



# 4

## PART 4

# Ischemic heart disease



# Experimental studies on myocardial ischemia and viability using tissue Doppler and deformation

*Geneviève Derumeaux*

## Introduction

Complete knowledge of myocardial structure, metabolism, perfusion, and function is crucial to understanding the response of the heart to injury such as ischemia. The effects of ischemia and reperfusion on heart based on studies in experimental models of coronary artery occlusion have been extensively described [1–5]. Brief periods of ischemia of less than 20 min followed by reperfusion are not associated with development of necrosis (reversible injury). If duration of coronary occlusion is extended beyond 20 min, a wavefront of necrosis extends from subendocardium to subepicardium over time. Reperfusion before 3 hr of ischemia salvages ischemic but viable tissue. Reperfusion beyond 3–6 hr does not reduce myocardial infarct size. Late reperfusion may still have a beneficial effect on

reducing or preventing myocardial infarct expansion and left ventricular (LV) remodeling (Figure 10.1).

Therefore, during an episode of transient ischemia, regional LV wall motion abnormalities develop, because myocytes cease contracting within seconds of the onset of acute ischemia. After relief of ischemia, the postischemic but viable myocardium requires hours to days before function is fully restored. This slow return of cardiac function after resolution of ischemia has been called *stunning* and the length of time for function to return is dependent on several parameters, including the duration and the severity of the original ischemic insult and the adequacy of the return of the arterial flow. Stunned myocardium is defined as “prolonged, postischemic dysfunction of viable tissue salvaged by reperfusion.” Hence, an important aspect of stunned myocardium is that there is a flow–function mismatch.

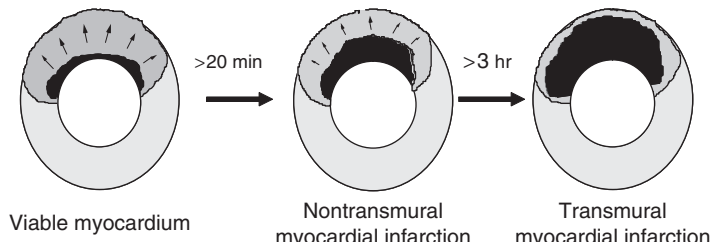


**Figure 10.1** Effect of the duration of coronary occlusion on the transmural extent of myocardial infarction. If the coronary artery occlusion is maintained beyond 20 min, a wavefront of necrosis extends from subendocardium to

subepicardium over time. Reperfusion before 3 hr of ischemia salvages ischemic but viable tissue. Reperfusion beyond 3–6 hr does not reduce myocardial infarct size.

At a time when coronary blood flow has been restored to normal or near normal and ischemia is resolved, the myocardium still does not contract [1,3].

The analysis of fiber thickening across the different layers of myocardial walls is important to take into account to differentiate the various patterns of contractile abnormalities that may occur during acute ischemia, hibernation, or stunning. Conventional assessment of contractile function is based on the measurement of the transmural thickening and does not provide information regarding the transmural distribution of contractile performance. Thus, there is a need for a quantitative approach to study the regional changes in deformation and their timing induced by ischemia. Tissue Doppler imaging (TDI) and strain rate imaging have been introduced as more objective and quantitative methods for assessing myocardial function and have been shown to overcome the limitations of current ultrasound methods in assessing the complex changes in regional myocardial function that occur in differing ischemic substrates. TDI analyzes endocardial and epicardial velocities in real time and measures the myocardial velocity gradient, which is an index of myocardial deformation [6–8]. Strain ( $\epsilon$ )/strain rate (SR) imaging has been shown to be a sensitive technique for quantifying regional myocardial deformation compared with other cardiac imaging modalities [9,10]. In addition, strain rate is less load-dependent than strain and provides, therefore, a better measure of contractility [11].

### **Experimental validation of tissue Doppler imaging and strain rate parameters**

Tissue Doppler imaging and strain rate imaging offer the equivalent of the high-resolution deformation information that is obtainable only by sonomicrometry in the experimental environment. Implanting intramyocardial microcrystals has shown that systolic deformation in the subendocardial layer is higher than deformation in the subepicardial layer [12–14]. Experimental studies have demonstrated that a reduction in coronary flow causes reductions in systolic shortening in the subendocardial layer that far exceed those in the subepicardial layer [13].

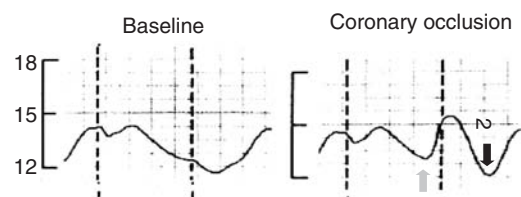


**Figure 10.2** Example of sonomicrometry traces after induction of ischemia by acute coronary artery occlusion. Acute ischemia induces an early systolic thinning, a decrease in maximal systolic thickening, and a delay in the onset of systolic thickening (red arrow), as well as a postsystolic thickening (blue arrow). Adapted from Theroux et al. [15].

The sequence of changes in regional myocardial function consistently induced by acute ischemia has been well defined by both experimental sonomicrometric [14–17] and cardiac ultrasound studies [18–20]. Acute ischemia induces an early systolic thinning, a decrease in maximal systolic thickening, and a delay in the onset of systolic thickening (Figure 10.2). Concomitant with the decrease in maximal systolic thickening, an abnormal ischemia-related thickening of the myocardium occurs after aortic valve closure. This abnormal phenomenon has been termed *postsystolic thickening* or *shortening*. Several experimental studies have demonstrated that the decrease in the rate and degree of systolic thickening was related to the myocardial blood flow.

To investigate whether pulsed TDI could accurately identify and quantify the alterations of myocardial wall motion induced by ischemia, Derumeaux et al. [18] induced various degrees of regional wall motion abnormalities by graded reduction of left anterior descending coronary artery blood flow in open chest pigs and compared the changes in velocities to those in segment lengths as measured by sonomicrometry and in regional myocardial blood flow as assessed by radioactive microspheres. Ischemia resulted in a significant rapid reduction of systolic velocities, a marked increase in isometric relaxation velocity (indicative of postsystolic motion), and an early decrease in the ratio of early to late diastolic velocities (Figure 10.3). Both changes were detected by pulsed TDI within 5 sec of coronary artery occlusion. Although the decrease in systolic velocity significantly correlated

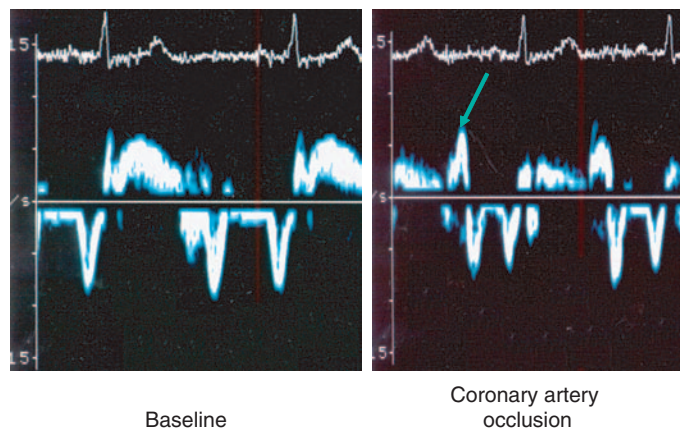


**Figure 10.3** Example of a pulsed-wave tissue Doppler trace during coronary artery occlusion. Ischemia results in a significant rapid reduction of systolic velocities and a marked increase in isometric relaxation velocity, indicative of postsystolic motion (arrow).

with both systolic shortening and regional myocardial blood flow during reduction of coronary artery blood flow, systolic velocities slightly overestimated the degree of regional wall motion abnormalities and failed to distinguish ischemia from reperfusion-induced contractile dysfunction. Indeed, when postischemic contractile dysfunction (myocardial stunning) developed despite restoration of a normal myocardial blood flow, pulsed TDI clearly identified wall motion abnormalities similar to those observed during ischemia. With respect to this finding, estimation of myocardial perfusion through measurement of myocardial wall velocities must be done cautiously and is valid only in situations of ischemia and not reperfusion.

In this regard, experimental studies that examined the complex interaction of changes in myocardial function and flow in postischemic myocardial segments with differing flow reserves have demonstrated the superiority of deformation indices such as myocardial velocity gradient, strain rate, and strain over motion indices (myocardial velocity and displacement).

In a closed chest experimental model, Jamal et al. [19,20] analyzed the spectrum of regional myocardial function changes during and after a transient ischemia of the LV posterior wall induced by an acute total 20 sec occlusion or by 30 min of a severe hypoperfusion followed by 60 min of reperfusion of the left circumflex coronary artery territory. These authors measured the changes in radial strain and strain rate profile of the ischemic posterior wall during ischemia, stunning, and

subsequent dobutamine infusion ( $5\text{--}20 \mu\text{g kg}^{-1} \text{min}^{-1}$ ). During total ischemia and left circumflex coronary artery hypoperfusion, strain and strain rate profiles were consistently modified, showing a delayed onset and a decreased magnitude in regional systolic thickening as well as an increased postsystolic thickening of the posterior wall. Interestingly, end-systolic strain could differentiate total ischemia from severe hypoperfusion (10 ml/min), decreasing from  $32\% \pm 8\%$  to  $16\% \pm 5\%$  (vs.  $60\% \pm 10\%$  at baseline). Occlusion release after 30 sec allowed deformation indices to normalize. However, after 30 min of total left circumflex coronary artery reperfusion following 30 min of a severe hypoperfusion, systolic thickening partially recovered but remained abnormal because of stunning. During dobutamine infusion, systolic thickening of the posterior wall increased incrementally, whereas postsystolic thickening decreased progressively and was not detectable at  $20 \mu\text{g kg}^{-1} \text{min}^{-1}$ . After the dobutamine administration was discontinued, deformation returned to the predobutamine stunning profile. Therefore, these authors demonstrated that, as regional flow was progressively decreased, systolic thickening was progressively reduced, whereas postsystolic thickening concomitantly increased, thus confirming that changes in regional systolic strain and strain rate paralleled stepwise reductions in coronary flow (Figure 10.4).

Derumeaux et al. [8] demonstrated that M-mode TDI allowed interrogation of intramural velocities to quantify LV radial contraction by measuring the transmural myocardial velocity gradient between

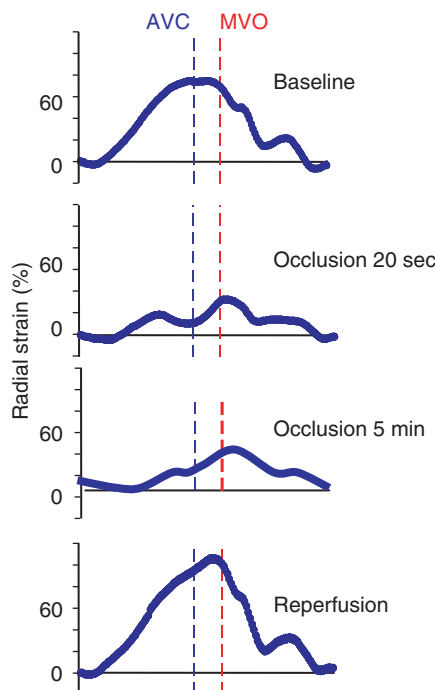


**Figure 10.4** Example of radial strain traces during coronary artery occlusion. As regional flow progressively decreases, systolic thickening is progressively reduced, whereas postsystolic thickening concomitantly increases. AVC, aortic valve closure; MVO, mitral valve opening.

Adapted from Jamal et al. [18,19].

endocardial and epicardial layers as an index of radial deformation. This latter parameter was able to differentiate between ischemia- and reperfusion-induced contractile dysfunction. During left anterior descending coronary artery occlusion, TDI data were closely related to sonomicrometric measurements, and both endocardial and epicardial velocities were markedly and uniformly decreased during ischemia, resulting in the disappearance of the myocardial velocity gradient. This absence of myocardial velocity gradient across the anterior wall during severe flow reduction is congruent with previous investigations that reported the abolition of the transmural thickening gradient during dramatic flow deprivation [21,22]. After reperfusion, wall motion in the distribution of the left anterior descending coronary artery remained severely depressed, indicative of stunning, but M-mode TDI was able to detect a slight but significant increase in the myocardial velocity gradient. This increase

was related to a greater improvement in endocardial than in epicardial velocities early after reflow, likely a consequence of the hyperemic response to the preceding ischemic insult. These data are in close agreement with those from a study by Bolli et al. that reported a comparable time course of nonuniform transmural functional recovery after reflow in dogs submitted to 15 min of left anterior descending coronary artery occlusion followed by 7 days of reperfusion. In that study, dogs exhibited a transmural systolic thickening gradient at baseline that disappeared during ischemia. On reperfusion, the inner/outer gradient first resumed, was maximal during the first hour after reflow, and decreased thereafter [22].

To summarize, although TDI measurement of regional function by peak systolic ejection velocity is easy to perform, reproducible, validated [23], and typically reduced during ischemia, many experimental studies have demonstrated its limited ability to differentiate between different grades of ischemic dysfunction and to distinguish ischemic from postischemic dysfunction. This important limitation of TDI is related to the fact that velocities in one myocardial segment are determined by function in other segments as well, which is due to tethering between segments and cardiac translational motion. Therefore, using motion to represent function has two important drawbacks: (1) peak velocity measurement is dependent on the angle at which the region of interest is imaged; and (2) overall heart motion, cardiac rotation, and contraction in adjacent segments can influence regional velocity estimates.

To overcome the latter problems, strain and strain rate imaging (each reflecting differing aspects of myocardial deformation and both relatively independent of overall heart motion), have been developed and are used to represent regional contractile function. Previous reports indicate that strain imaging in principle provides better quantification of regional function than velocity imaging [24–26].

Recently, Skulstad et al. [27] investigated if grading of ischemic dysfunction by strain imaging was superior to velocity imaging for quantification of regional myocardial dysfunction in a dog model of acute ischemia, using segmental shortening by implanted ultrasonic crystals (from sonomicrometry) and segmental work (from pressure–segment

length loops) as reference methods for regional function. In this animal study, systolic strain correlated well with segmental shortening and work, and differentiated well between nonischemic ( $-13.5 \pm 3.2\%$ ), moderately ischemic ( $-6.5 \pm 2.8\%$ ), and severely ischemic ( $7.1 \pm 13.2\%$ ) myocardium. The ratio postsystolic strain/total strain also differentiated well between levels of ischemia. Peak systolic velocity had weaker correlations with segmental shortening and regional work, and there was marked overlap between values at baseline and at different levels of ischemia. This elegant study was the first one to directly compare the different TDI modalities (strain, tissue velocity, and displacement imaging). The authors demonstrated that strain was superior to velocity and displacement for grading of myocardial segmental dysfunction during experimental ischemia, and they extended their observations in patients with anterior wall infarctions. Peak systolic velocity could not differentiate between hypokinetic and dyskinetic myocardium, whereas systolic strain was an excellent tool for quantification of function in nonischemic as well as ischemic myocardium and for defining the anatomical extent of dysfunctional myocardium.

Therefore, strain and strain rate imaging holds great promise for improving objective quantification and characterization of regional function in the setting of ischemic cardiomyopathies. However, currently, few centers have adopted strain imaging in their routine clinical practice, because some obstacles currently limit the adoption of strain and strain rate imaging, including the following:

- Current assessment of regional function by strain imaging is one-dimensional and does not take into account the complexity of the spatial configuration of myocardial fibers responsible for a strain occurring in three dimensions and involving longitudinal shortening, radial thickening, and rotation.
- Tissue Doppler strain is angle-dependent. Because tissue Doppler strain is derived from relative changes in velocity along a single ultrasound scan line, it can only accurately assess shortening or thickening when this principal vector is aligned with the ultrasound beam.
- High-quality imaging is necessary. Although the tissue Doppler velocity signals are robust, any

potential errors mentioned above become apparent when strain or strain rate imaging is used with below-average image quality.

- Reproducibility needs to be improved before current clinical application.

With the development of the speckle tracking technique, one may expect to resolve some of these limitations and to improve strain imaging data quality and analysis. In conclusion, strain and strain rate imaging appears to be the optimal technique to examine the complex interaction of changes in deformation and flow in ischemic myocardial segments with differing flow reserves.

## Experimental acute ischemia

In addition to their ability to quantify myocardial function, tissue Doppler and strain imaging have a good temporal resolution that enables one to analyze the consequences of acute ischemia during the entire cardiac cycle, including isovolumic periods. Measurement of function during ejection is the most widely used parameter for quantifying regional function during ischemia. However, several studies suggest that analysis of function during the isovolumic LV phases provides additional important diagnostic information.

### Pre-ejection or isovolumic contraction period

Vogel et al. [28] proposed that myocardial isovolumic contraction (IVC) acceleration (IVA) would be a load-independent measure of contractility, as opposed to peak systolic ejection velocity that is preload- and afterload-dependent. These authors demonstrated that IVA reflected myocardial contractility and appeared to be load-independent in a nonischemic animal model, and measurements were taken near the mitral ring, which means they measured global LV function. In a recent experimental study, Lyseggen et al. [29] analyzed IVA as a measure of regional function during myocardial ischemia. This study confirmed that IVA was related to global LV contractility, but IVA did not reflect function in the ischemic myocardium. Thus, IVA appears to have limited potential to serve as a measure of regional function during ischemia.

Experimental studies suggest that longitudinal IVC velocities may determine the degree of

myocardial dysfunction during ischemia [30]. In ventricles with preserved systolic function, there is a dominantly positive longitudinal velocity during IVC, with only a minor negative velocity component. With progressive ischemia, the positive velocity component diminishes, and the negative component increases. During severe ischemia, the positive component is lost and replaced by a large negative IVC velocity. The negative IVC velocity is a reflection of the early systolic lengthening, which is a hallmark of severe ischemia. In addition to these experimental findings, Penicka et al. have shown that a positive IVC velocity after revascularization predicted recovery of function in the reperfused area in patients with myocardial infarction [31]. This study suggests that measurement of IVC velocities may provide important diagnostic information with regard to myocardial viability after coronary reperfusion.

### Postejection or isovolumic relaxation period

Experimental ultrasound studies have demonstrated that, with increasing severity of acute ischemia, the myocardium shortens and thickens after aortic valve closure [32–34]. Postsystolic or postejection shortening (LV long axis) and

postsystolic thickening (short axis) are characteristic features of ischemic myocardium with a concomitant reduction in maximal systolic contraction.

Postsystolic shortening can be imaged by velocity imaging and is, in the long axis, represented by a positive velocity component during isovolumic relaxation (IVR). Postsystolic shortening can be measured directly with strain Doppler echocardiography and is measured as myocardial shortening that occurs after cessation of aortic forward flow (Figure 10.5).

In nonischemic myocardium, virtually all contraction occurs during systole with very little postsystolic shortening. Voigt et al. [35] demonstrated that minor degrees of postsystolic shortening occur in normal myocardium and that it is not pathologic unless it exceeds a substantial fraction (>20%) of total myocardial shortening. The mechanism of postsystolic shortening in normal myocardium is not defined, but may be related to the LV shape changes and untwisting motion that occur during IVR.

In ischemic myocardium, postsystolic shortening has been introduced as a potentially useful marker of ischemic dysfunction. Postsystolic velocity, displacement, and strain differentiate well between nonischemic and ischemic myocardium, with

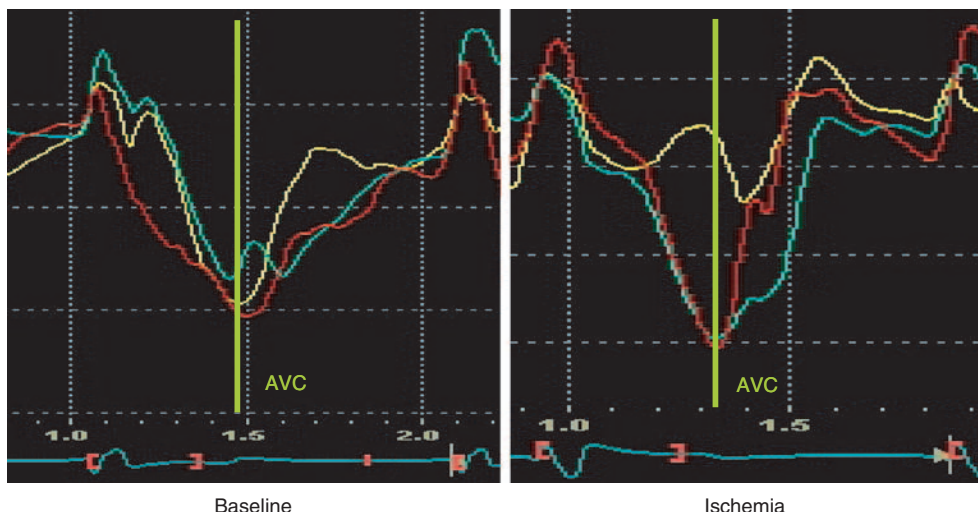


**Figure 10.5** Example of strain curves before and after induction of a myocardial infarction by ablation of the basal septal coronary artery. The basal portion of the interventricular septal wall (yellow curve) is necrotic, whereas the mid- (blue curve) and apical (red curve)

segments are nonischemic. In the basal portion, the strain curve displays a reduced systolic strain and a postsystolic shortening, measured as myocardial shortening that occurs after cessation of aortic forward flow. AVC, aortic valve closure.

strain being the superior marker [26]. Postsystolic strain, however, does not help in grading of ischemic dysfunction, as there is substantial overlap between postsystolic strain values in segments with moderate and severe dysfunction.

To better characterize ischemia-related myocardial dysfunction and to normalize the postsystolic shortening values, a postsystolic strain index has been evaluated. A postsystolic strain index expressed as the ratio between postsystolic shortening and systolic shortening has been proposed by Kukulski et al. [36]. They showed that this index was a highly sensitive and specific marker of myocardial dysfunction during acute myocardial ischemia.

More recently, Skulstad et al. [26] evaluated the ratio between systolic strain and combined systolic and postsystolic strain. This ratio differentiated better between different levels of ischemia than just measuring systolic or postsystolic strain. In contrast, calculating a similar ratio for displacement and velocity did not improve grading of ischemic dysfunction. These experimental results have direct clinical implications. In the setting of stress echocardiography, when postsystolic shortening is absent during baseline, but appears during dobutamine, it is a marker of myocardial ischemia. Voigt et al. demonstrated that the ratio of postsystolic thickening to maximal segmental deformation was the best quantitative parameter to identify stress-induced ischemia [37]. In ischemic myocardium, debate exists whether such an ischemia-induced postsystolic shortening represents an active or passive event. From a clinical perspective, the differentiation between active and passive postsystolic shortening is critical, because active contraction suggests viable myocardium. Postsystolic shortening is nonspecific with regard to tissue viability, because it may occur in entirely passive or necrotic myocardium as well as in actively contracting ischemic myocardium. In passive and dyskinetic myocardium, necrotic segments are stretched in systole by nonischemic segments and recoil during IVR when nonischemic myocardium relaxes and the stretching force drops abruptly.

However, when postsystolic shortening occurs in the absence of systolic lengthening, passive recoil can be excluded; therefore, the postsystolic shortening may represent delayed active contraction. Skulstad et al. [38] suggested that active contraction

also contributes to postsystolic shortening when the postsystolic shortening far exceeds the systolic lengthening in magnitude in a dyskinetic segment [38]. Thus, these authors proposed that the ratio between systolic lengthening and combined late systolic and postsystolic shortening may serve as a marker of active as opposed to passive postsystolic shortening. The rationale for this association is that active wall tension will limit systolic lengthening and enhance active postsystolic shortening [38].

## Myocardial infarction

The noninvasive differentiation of transmural from nontransmural infarcted myocardium is important in clinical practice with regard to assessment of viability. A few experimental studies have demonstrated that, in both acute and chronic myocardial infarction experimental models, the noninvasive measurement of deformation properties can accurately characterize the transmural extent of scar from subendocardial to subepicardial layers. The transmural extension of scar distribution in the infarct zone was proportionally related to the reduction in systolic function measured either by the radial transmural velocity gradient [39] or by strain rate imaging [40] (Figure 10.6).

In addition, the measurement of both systolic and postsystolic deformation both at rest and during a graded dobutamine infusion helps to distinguish between transmural and nontransmural infarcts [40]. A nontransmural infarct will have markedly reduced systolic deformation at rest with some postsystolic shortening. During a low-dose dobutamine challenge, it will exhibit an increase in postsystolic shortening associated with a reduction or no change in systolic strain and strain rate. Conversely, a transmural infarction is characterized by either no measurable systolic deformation or the presence of abnormal thinning/lengthening at rest, with no inducible increase in thickening/shortening during a dobutamine challenge (Figure 10.7).

Therefore, assessment of postsystolic shortening and dobutamine-induced enhancement of postsystolic shortening along with a reduction of systolic thickening differentiates nontransmural from transmural chronic infarctions and might help in patient triage in acute myocardial infarction, in particular when thrombolysis has been the

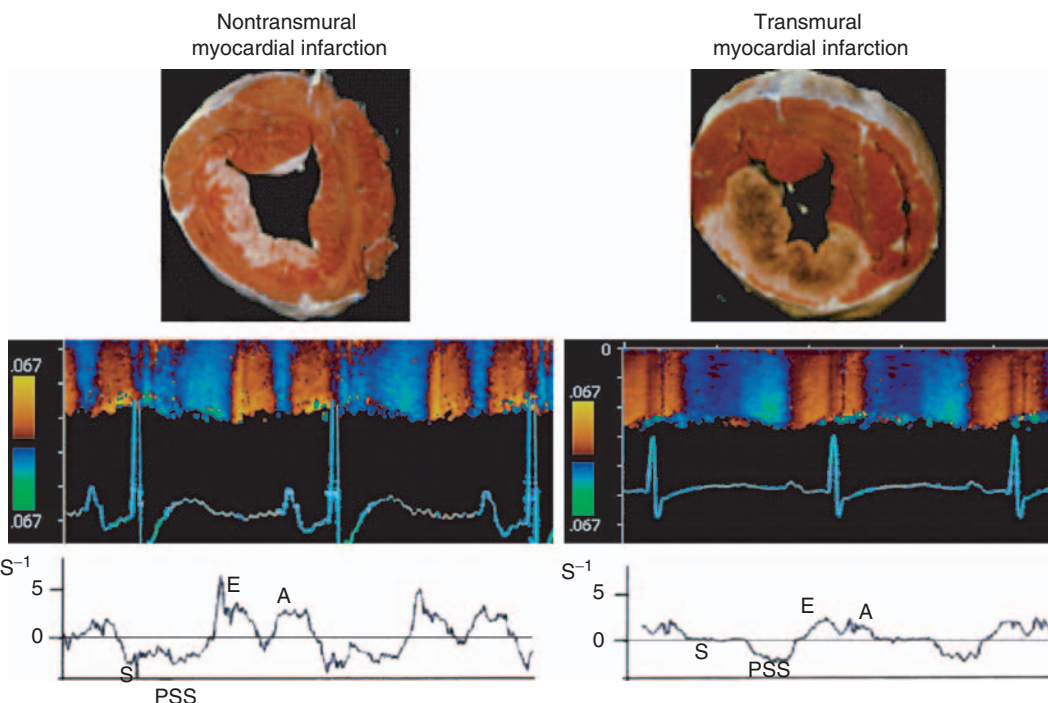


**Figure 10.6** Differentiation between nontransmural and transmural myocardial infarction by the radial transmural velocity gradient (MVG,  $s^{-1}$ ) during systole (S). Abbreviations: early filling (E), atrial contraction (A), post systolic shortening (PSS).

	Baseline			DSE		
	max. SR <sub>sys</sub>	$\varepsilon_{sys}$	PSS	max. SR <sub>sys</sub>	$\varepsilon_{sys}$	PSS
Normal	5 sec <sup>-1</sup>	60%	2%	↗	↗	→
Nontransmural MI	↓	↓	↑	↗	→	↗
Transmural MI	↓	↓	↑	→	→	→

↑ > Normal value      ↗ Increase      ↗ Biphasic response  
 ↓ < Normal value      ↘ Decrease      → No change

**Figure 10.7** A transmural myocardial infarction (MI) is characterized by no measurable systolic deformation at rest, with no inducible increase in thickening/shortening during a dobutamine challenge. DSE, dobutamine stress echocardiography; SR, strain rate;  $\varepsilon$ , strain; PSS, postsystolic shortening. Adapted from Weidemann et al. [40].

primary treatment and additional percutaneous angioplasty is considered.

Recently, Lyseggen et al. [41] found that the ratio of systolic lengthening to combined late and postsystolic shortening identified viable myocardium, and decreases in myocardial compliance (systolic lengthening/systolic pressure rise) defined necrotic myocardium in an open-chest animal

model of coronary occlusion of variable duration to induce differing degrees of transmural necrosis. Partially active myocardium was differentiated from passive increases in myocardial length with pressure-dimensional loops. When the ratio between early systolic lengthening and total shortening (L-S ratio) approached 1, the segment was entirely passive and generated essentially no active force. When the L-S ratio was  $<0.5$  and shortening dominated over lengthening, there was a component of active contraction, consistent with preserved tissue viability. Second, in entirely passive segments (L-S ratio approaching 1), low systolic myocardial compliance, calculated as systolic lengthening divided by systolic LV pressure, proved to be a marker of necrosis. This relation was in part accounted for by marked tissue edema that caused stiffening of necrotic myocardium. Reperfusion of necrotic myocardium caused no change in the L-S ratio but resulted in a rapid, further reduction in compliance. Reperfusion of viable myocardium, however, caused an immediate reduction in the L-S ratio. These observations suggest that the myocardial

L–S ratio and systolic compliance by strain Doppler echocardiography may differentiate between necrotic and viable myocardium and identify reperfusion in acute coronary occlusion.

## Conclusion

In the setting of ischemia, experimental studies have demonstrated that strain imaging has proved to be an accurate method for quantitative evaluation of regional myocardial function and may yield important physiological data. To date, strain rate has not replaced conventional gray-scale imaging in the assessment of regional LV function and the implementation of these new indices into routine clinical practice will need additional clinical and large-scale studies.

## References

- 1 Kloner RA, Jennings RB. Consequences of brief ischemia: stunning, preconditioning, and their clinical implications: part I. *Circulation* 2001; **104**: 2981–9.
- 2 Reimer KA, Jennings RB. The “wavefront phenomenon” of myocardial ischemic cell death, II. Transmural progression of necrosis within the framework of ischemic bed size (myocardium at risk) and collateral flow. *Lab Invest* 1979; **40**: 633–44.
- 3 Heyndrickx GR, Millard RW, McRitchie RJ, Maroko PR, Vatner SF. Regional myocardial functional and electrophysiological alterations after brief coronary artery occlusion in conscious dogs. *J Clin Invest* 1975; **56**: 978–85.
- 4 Kloner RA, Ganote CE, Whalen DA Jr, Jennings RB. Effect of a transient period of ischemia on myocardial cells, II: fine structure during the first few minutes of reflow. *Am J Pathol* 1974; **74**: 399–422.
- 5 Jennings RB, Murry CE, Steenbergen C Jr, Reimer KA. Development of cell injury in sustained acute ischemia. *Circulation* 1990; **82 Suppl**: II2–12.
- 6 Sutherland GR, Steward MJ, Grounstrom KW, et al. Color Doppler myocardial imaging: a new technique for the assessment of myocardial function. *J Am Soc Echocardiogr* 1994; **7**: 441–58.
- 7 Uematsu M, Miyatake K, Tanaka N, et al. Myocardial velocity gradient as a new indicator of regional left ventricular contraction: detection by a two-dimensional tissue Doppler imaging technique. *J Am Coll Cardiol* 1995; **26**: 217–23.
- 8 Derumeaux G, Ovize M, Loufoua J, Pontier G, Andre-Fouet X, Cribier A. Assessment of nonuniformity of transmural myocardial velocities by color-coded tissue Doppler imaging: characterization of normal, ischemic, and stunned myocardium. *Circulation* 2000; **101**: 1390–5.
- 9 Heimdal A, Støylen A, Torp H, Skjærpe T. Real-time strain rate imaging of the left ventricle by ultrasound. *J Am Soc Echocardiogr* 1998; **11**: 1013–9.
- 10 Urheim S, Edvardsen T, Torp H, Angelsen B, Smiseth OA. Myocardial strain by Doppler echocardiography. Validation of a new method to quantify regional myocardial function. *Circulation* 2000; **102**: 1158–64.
- 11 Greenberg NL, Firstenberg MS, Castro PL, et al. Doppler-derived myocardial systolic strain rate is a strong index of left ventricular contractility. *Circulation* 2002; **105**: 99–105.
- 12 Sabbah HN, Marzilli M, Stein PD. The relative role of subendocardium and subepicardium in left ventricular mechanics. *Am J Physiol* 1981; **240**: H920–6.
- 13 Gallagher KP, Osakada G, Matsuzaki M, Miller M, Kemper WS, Ross J. Nonuniformity of inner and outer systolic wall thickening in conscious dogs. *Am J Physiol* 1985; **249**: H241–8.
- 14 Gallagher KP, Stirling MC, Choy M, et al. Dissociation between epicardial and transmural function during acute myocardial ischemia. *Circulation* 1985; **71**: 1279–91.
- 15 Theroux P, Franklin D, Ross J Jr, Kemper WS. Regional myocardial function during acute coronary artery occlusion and its modification by pharmacologic agents in the dog. *Circ Res* 1974; **35**: 896–908.
- 16 Heyndrickx GR, Baig H, Nellens P, Leusen I, Fishbein MC, Vatner SF. Depression of regional blood flow and wall thickening after brief coronary occlusions. *Am J Physiol* 1978; **234**: H653–9.
- 17 Gallagher KP, Kumada T, Koziol JA, Mc Kown MD, Kemper WS, Ross J Jr. Significance of regional wall thickening abnormalities relative to transmural myocardial perfusion in anesthetized dogs. *Circulation* 1980; **62**: 1266–74.
- 18 Derumeaux G, Ovize M, Loufoua J, André-Fouet X, Minaire Y, Cribier A, Letac B. Doppler tissue imaging quantitates regional wall motion during myocardial ischemia and reperfusion. *Circulation* 1998; **97**: 1970–7.
- 19 Jamal F, Szilard M, Kukulsi T, et al. Changes in systolic and postsystolic wall thickening during acute coronary occlusion and reperfusion in closed-chest pigs: implications for the assessment of regional myocardial function. *J Am Soc Echocardiogr* 2001; **14**: 691–7.
- 20 Jamal F, Strotmann J, Weidemann F, et al. Noninvasive quantitation of the contractile reserve of stunned myocardium by ultrasonic strain rate and strain. *Circulation* 2001; **104**: 1059–65.

- 21 Gallagher KP, Stirling MC, Choy M, et al. Dissociation between epicardial and transmural function during acute myocardial ischemia. *Circulation* 1985; **71**: 1279–91.
- 22 Bolli R, Patel BS, Hartley CJ, Thornby JI, Jeroudi MO, Roberts R. Nonuniform transmural recovery of contractile function in stunned myocardium. *Am J Physiol* 1989; **257**: H375–85.
- 23 Gorcsan J, Strum DP, Mandarino WA, Gulati VK, Pinsky MR. Quantitative assessment of alterations in regional left ventricular contractility with color-coded tissue Doppler echocardiography: comparison with sonomicrometry and pressure-volume relations. *Circulation* 1997; **95**: 2423–33.
- 24 Edvardsen T, Skulstad H, Aakhus S, Urheim S, Ihlen H. Regional myocardial systolic function during acute myocardial ischemia assessed by strain Doppler echocardiography. *J Am Coll Cardiol* 2001; **37**: 726–30.
- 25 Edvardsen T, Urheim S, Skulstad H, Steine K, Ihlen H, Smiseth OA. Quantification of left ventricular systolic function by tissue Doppler echocardiography. Added value of measuring pre- and postejection velocities in ischemic myocardium. *Circulation* 2002; **105**: 2071–7.
- 26 Skulstad H, Andersen K, Edvardsen T, et al. Detection of ischemia and new insight into left ventricular physiology by strain Doppler and tissue velocity imaging assessment during coronary bypass operation of the beating heart. *J Am Soc Echocardiogr* 2004; **17**: 1225–33.
- 27 Skulstad H, Urheim S, Edvardsen T, et al. Grading of myocardial dysfunction by tissue Doppler echocardiography: a comparison between velocity, displacement, and strain imaging in acute ischemia. *J Am Coll Cardiol* 2006; **47**: 1672–82.
- 28 Vogel M, Cheung MM, Li J, Kristiansen SB, Schmidt MR, White PA, et al. Noninvasive assessment of left ventricular force–frequency relationships using tissue Doppler-derived isovolumic acceleration: validation in an animal model. *Circulation* 2003; **107**: 1647–52.
- 29 Lyseggen E, Rabben SI, Skulstad H, Urheim S, Risoe C, Smiseth OA. Myocardial acceleration during isovolumic contraction – is it really a sensitive index of myocardial function? *Eur Heart J* 2002; **23 Suppl 1**: 273.
- 30 Edvardsen T, Urheim S, Skulstad H, Steine K, Ihlen H, Smiseth OA. Quantification of left ventricular systolic function by tissue Doppler Echocardiography. Added value of measuring pre- and postejection velocities in ischemic myocardium. *Circulation* 2002; **105**: 2071–7.
- 31 Penicka M, Bartunek J, Wijns W, et al. Tissue Doppler imaging predicts recovery of left ventricular function after recanalization of an occluded coronary artery. *J Am Coll Cardiol* 2004; **43**: 85–91.
- 32 Barletta G, Del Bene R, Lo Sapi O, Gallini C, Fantini F. Post-ejection thickening as a marker of viable myocardium. An echocardiographic study in patients with chronic coronary artery disease. *Basic Res Cardiol* 1998; **93**: 313–24.
- 33 Leone BJ, Norris RM, Safwat A, Foex Pand, Ryder WA. Effects of progressive myocardial ischaemia on systolic function, diastolic dysfunction, and load dependent relaxation. *Cardiovasc Res* 1992; **26**: 422–9.
- 34 Rose J, Schulz R, Martin C, Heusch G. Post-ejection wall thickening as a marker of successful short term hibernation. *Cardiovasc Res* 1993; **27**: 1306–11.
- 35 Voigt JU, Lindenmeier G, Exner B, et al. Incidence and characteristics of segmental postsystolic longitudinal shortening in normal, acutely ischemic, and scarred myocardium. *J Am Soc Echocardiogr* 2003; **16**: 415–23.
- 36 Kukulski T, Jamal F, Herbots L, et al. Identification of acutely ischemic myocardium using ultrasonic strain measurements: a clinical study in patients undergoing coronary angioplasty. *J Am Coll Cardiol* 2003; **41**: 810–9.
- 37 Voigt JU, Exner B, Schmiedehausen K, et al. Strain-rate imaging during dobutamine stress echocardiography provides objective evidence of inducible ischemia. *Circulation* 2003; **107**: 2120–6.
- 38 Skulstad H, Edvardsen T, Urheim S, et al. Postsystolic shortening in ischemic myocardium. Active contraction or passive recoil? *Circulation* 2002; **106**: 718–24.
- 39 Derumeaux G, Loufoua J, Pontier G, Cribier A, Ovize M. Tissue Doppler imaging differentiates transmural from nontransmural acute myocardial infarction after reperfusion therapy. *Circulation* 2001; **103**: 589–96.
- 40 Weidemann F, Dommke C, Bijnens B, et al. Defining the transmurality of a chronic myocardial infarction by ultrasonic strain-rate imaging: implications for identifying intramural viability: an experimental study. *Circulation* 2003; **107**: 883–8.
- 41 Lyseggen E, Skulstad H, Helle-Valle T, et al. Myocardial strain analysis in acute coronary occlusion: a tool to assess myocardial viability and reperfusion. *Circulation* 2005; **112**: 3901–10.

# Assessment of viability

Rainer Hoffmann

## Clinical importance of myocardial viability assessment

Whereas normal myocardium is of course viable, the term *myocardial viability* is used to denote the presence of dysfunctional myocardium that is not entirely necrotic or fibrotic. The identification of dysfunctional but viable myocardium in patients with impaired left ventricular (LV) function has important therapeutic and prognostic implications [1–3]. In the case of chronic LV dysfunction, the impairment may be reversible with coronary revascularization. However, revascularization procedures are beneficial only in cases of sufficient viable myocardium, and transmurally infarcted myocardium does not benefit. Among patients with ischemic cardiomyopathy and viable myocardium, myocardial revascularization is associated with improved systolic function, symptoms, and survival. Several techniques analyzing the morphologic, functional, cellular, or metabolic integrity of the myocardium have been used to define myocardial viability in patients with chronic myocardial infarction [4–6]. More recently, delayed enhancement cardiovascular magnetic resonance imaging has become the standard to evaluate the transmural extent of infarction as well as the remaining myocardial viability in patients with ischemic impairment of LV function [6–8].

## Pathophysiology of acute and chronic left ventricular dysfunction

Reversible myocardial dysfunction has been described in different clinical settings. It may occur after a short period of reversible ischemia (resulting in a state that is called myocardial *stunning*) or it may be due to chronic myocardial malperfusion, a condition that is called myocardial *hibernation*.

Although these entities are separate pathophysiologically, they are often mixed clinically.

Myocardial stunning is the result of a severe ischemic insult, most frequently in acute myocardial infarction. The prototypical situation is the presence of a small area of necrosis with coexistence of stunned myocardium, resulting in a relatively significant acute impairment of myocardial function but the potential for subsequent significant recovery. One of the characteristics of stunned myocardium is that functional recovery is the rule and occurs without any invasive intervention. Myocardial stunning is often recognized a posteriori, by the confirmation of spontaneous improvement of regional function.

Myocardial hibernation typically has a less acute presentation and occurs in the context of chronic ischemic ventricular dysfunction. In contrast to acutely stunned myocardium, revascularization procedures are necessary to improve function in chronically ischemic myocardium. Although initially believed to reflect chronic myocardial malperfusion, hibernating segments often do not have abnormal resting flow, and downregulation of contractility and ultrastructural changes seem to be consequences of recurrent stunning. Hibernating and stunned myocardium can retain contractile reserve, which is recruitable by dobutamine infusion.

## Echocardiographic techniques to define myocardial viability

The combination of two-dimensional (2-D) echocardiography with dobutamine stimulation to evaluate functional reserve was introduced by Pierard et al. [5] in 1990 for analysis of myocardial viability in patients with impaired LV function after acute

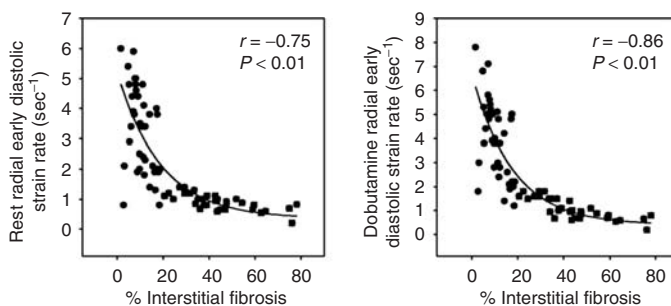


**Figure 11.1** Relation between percent interstitial fibrosis and radial early diastolic strain rate at rest (left panel) and with low-dose dobutamine (right panel). Segments with <20% transmural infarction are shown by circles, whereas those with >20% transmural infarction are shown by squares. From Park et al. [17].

myocardial infarction. Several studies have subsequently confirmed the test to allow accurate assessment of acute as well as chronic ischemic LV dysfunction [9,10]. However, the technique involves subjective analysis of regional function and is, therefore, subject to reader expertise and significant interobserver variability [11,12]. An objective, quantitative approach based on an echocardiographic imaging modality would be desirable.

The advent of tissue Doppler imaging has provided a feasible tool to quantify regional myocardial function [13,14]. Both pulsed Doppler as well as color Doppler imaging techniques have been applied to assess myocardial viability in patients with impaired LV function at rest. The known disadvantages of myocardial velocity analysis by tissue Doppler imaging techniques such as the basoapical velocity gradient and the tethering of myocardial segments from adjacent segments are a significant limitation for the definition of myocardial viability in a specific segment. In particular, point velocities of a specific LV region have not allowed differentiation between active contraction and passive drawing motion related to translation and rotation of the entire heart or contraction of adjacent segments. Myocardial deformation analysis derived from myocardial velocities determined by tissue Doppler imaging circumvents these difficulties. Deformation imaging has, therefore, been applied to analysis of myocardial viability.

In the context of viability analysis, both myocardial velocity and deformation parameters have been analyzed at rest and during dobutamine stimulation to define the functional reserve. Functional reserve during dobutamine stimulation is a marker of structural integrity, in particular of the contractile elements, and thus of myocardial viability. On the basis of experimental studies, which have shown a correlation between

systolic myocardial deformation at rest and the transmurality of myocardial infarction, recent clinical studies have also tried to define myocardial viability from analysis of rest myocardial deformation only [15,16]. Whereas analysis of myocardial viability has long concentrated on the systolic component of myocardial function, recent echocardiographic studies have also included analysis of diastolic function [17,18] (Figure 11.1). Another stimulus for the quantitative echocardiographic analysis of myocardial viability has been the introduction of deformation imaging based on speckle tracking of acoustic pixels in 2-D echocardiographic images [19–21].

The echocardiographic techniques to define myocardial viability in LV dysfunction have been used both in the context of stunning after acute myocardial infarction as well as in the presence of chronic ischemic dysfunction. The previously mentioned echocardiographic techniques have been evaluated (1) in experimental animal models with histologic definition of tissue viability, (2) in clinical studies using either positron emission tomography or magnetic resonance imaging as gold standard for myocardial viability assessment, or (3) in clinical studies using functional recovery after revascularization as an endpoint. However, it is common to all techniques that their use has been limited so far to rather small studies, and application to large patient numbers is still lacking. Thus, the techniques have not yet reached widespread clinical application.

## Myocardial viability assessment from velocity and deformation responses to stress

### Velocity responses

Several studies have analyzed tissue Doppler velocities at rest and during dobutamine stimulation

for assessment of functional reserve as a marker of myocardial viability [18,22–25]. For M-mode tissue Doppler imaging in combination with dobutamine stimulation, the analysis of the velocity gradient between endocardium and epicardium has been reported to have a high sensitivity for the prediction of reversible dysfunction in the postmyocardial infarction setting [23] (Figure 11.2). Pulsed Doppler tissue velocity analysis has been performed on apical views with analysis of tissue velocities confined to the basal segments [24]. This approach determines myocardial viability for the entire ventricular wall from apex to base. Thus, it does not provide precise information on the exact distribution of viability within the wall. An increase of peak systolic velocity at low-dose dobutamine stress indicates viable myocardium as confirmed also in subsequent studies. Whereas earlier studies have concentrated on systolic velocities and the functional reserve with dobutamine stimulation, a recent study analyzed early diastolic myocardial tissue velocities at rest.

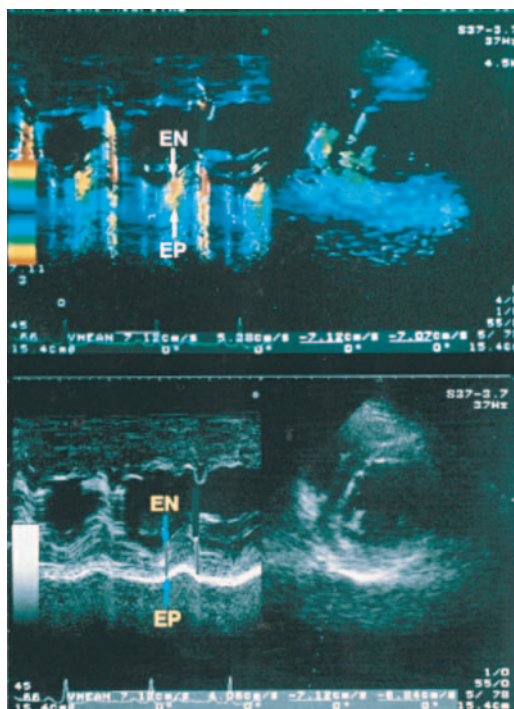


**Figure 11.2** Tissue Doppler imaging in a segment with myocardial viability. Color tissue Doppler imaging M-mode at rest and with dobutamine stimulation showing an increase in tissue velocity. From Nishino et al. [23].

The study demonstrated that diastolic tissue velocities determined at rest are different between viable and nonviable myocardium, providing an additional parameter to distinguish between different viability states [18].

### Deformation responses

A real-time display of strain and strain rate has been introduced for analysis of myocardial deformation based on color tissue Doppler imaging [26]. Experimental studies demonstrated strain and strain rate to be good noninvasive indices of LV contractility, allowing more accurate analysis of LV contractility than myocardial velocities due to elimination of translational artefacts [27,28]. Thus, strain and strain rate analysis are likely to be ideal for the more subtle analysis of myocardial function and myocardial functional reserve required for viability analysis. A subsequent experimental study showed strain rate analysis to allow quantification of the contractile reserve during dobutamine stimulation in stunned myocardium [29]. In a clinical study of 37 patients with ischemic LV dysfunction, the increase in the peak systolic strain rate during low-dose dobutamine stimulation was shown to allow accurate discrimination between different myocardial viability states defined by <sup>18</sup>F-fluorodeoxyglucose positron emission tomography [30] (Figure 11.3). Strain rate imaging proved to be superior to tissue Doppler

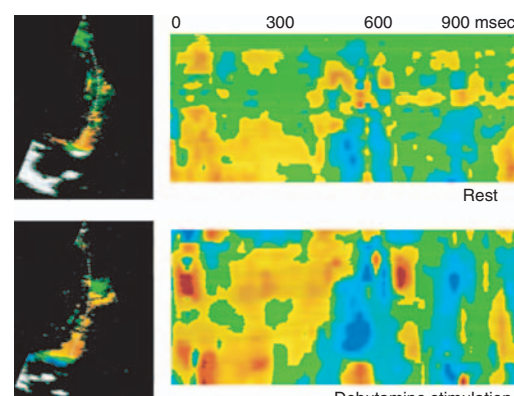


**Figure 11.3** Strain rate imaging of the anterior wall at rest (upper panel) and during dobutamine stimulation (lower panel). The color changes from green to yellow for the mid-anterior segment, indicating an increase of contractility. This segment was shown to be viable by positron emission tomography. From Hoffmann et al. [30].

velocity imaging in the assessment of myocardial viability (area under the receiver operating characteristics curve, 0.89 vs. 0.63). Avoidance of tethering effects affecting local measurements and the absence of a basoapical gradient were thought to be the reasons for greater accuracy of strain rate imaging compared to tissue Doppler velocity imaging.

A subsequent study on 55 stable patients with LV dysfunction due to previous myocardial infarction used recovery of segmental function to define myocardial viability [31] (Figure 11.4). When combined with wall motion scoring, strain rate imaging offered incremental value over wall motion scoring alone for prediction of functional recovery after revascularization. Compared with segments showing functional recovery, segments that failed to recover had lower low-dose dobutamine strain rates, strain rate increments, end-systolic strain, and end-systolic strain increments. An addition of strain rate parameters to wall motion scoring augmented the sensitivity for prediction of functional recovery above wall motion scoring alone (82% vs. 73%;  $P = 0.015$ ; area under the curve, 0.88 vs. 0.73;  $P < 0.001$ ), although specificities were comparable.

The response of diastolic function to dobutamine stimulation has also been used to assess myocardial viability using myocardial deformation imaging. Viable myocardial segments demonstrated an increase in early diastolic E-wave and late diastolic A-wave strain rate, whereas nonviable segments

were less responsive to dobutamine stimulation [32]. The use of diastolic deformation parameters in addition to systolic parameters was evaluated in an animal model [17]. A correlation between the extent of interstitial fibrosis and radial systolic strain rate could be demonstrated at baseline ( $r = -0.5$ ;  $P < 0.05$ ) and with dobutamine stimulation ( $r = -0.63$ ;  $P < 0.01$ ). However, a stronger relation was observed between the extent of interstitial fibrosis and the early diastolic strain rate at rest ( $r = -0.75$ ;  $P < 0.01$ ) and with dobutamine ( $r = -0.86$ ;  $P < 0.01$ ). Thus, among several indexes, diastolic strain rate analysis during dobutamine infusion readily identified segments with >20% transmural infarction and related best to the extent of interstitial fibrosis. Another animal model with postischemic reperfusion and severely reduced systolic deformation proved that diastolic passive deformation parameters (strain and strain rate) allow the distinction between stiff, noncompliant, transmurally infarcted myocardial walls and more compliant walls containing viable but stunned myocardium [33].

In experimental models, myocardial deformation imaging based on tissue Doppler imaging has been shown using sonomicrometry to allow a very accurate analysis of myocardial stretching and compression [27]. However, in clinical practice, myocardial deformation imaging has gained only limited acceptance for viability assessment due to

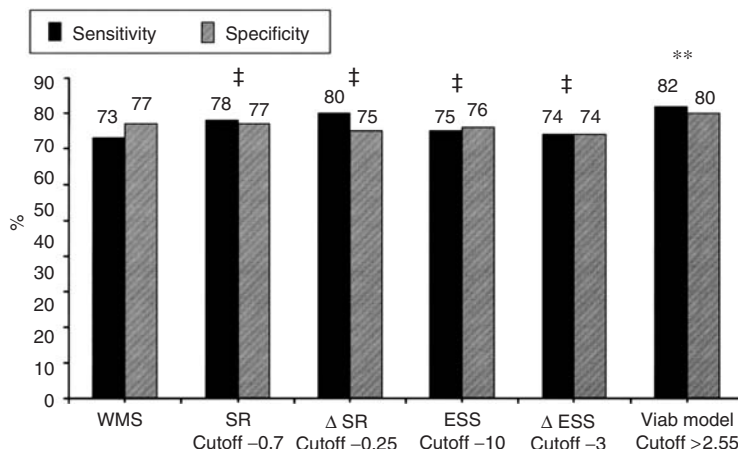


**Figure 11.4** Sensitivity and specificity of wall motion score (WMS) and quantitative methods for predicting regional recovery. The viability (viab) model is derived from the wall motion score and the increment in SR as well as the

strain rate at low-dose dobutamine. Accuracy of SRI parameters vs. WMS:  $^{\ddagger}P > 0.05$ ,  $^{**}P = 0.015$ .) SR, End-systolic strain (ESS), Strain Rate (SRI). From Hanekom et al. [31].

important limitations. These limitations are significant noise artefacts affecting in particular the strain rate analysis and a significant angle dependency, as strain and strain rate values become zero at an angle of 45° between the direction of the Doppler beam and the direction of myocardial deformation [27].

## Deformation imaging at rest only to assess myocardial viability

### Doppler-based deformation

Experimental studies have proven that myocardial deformation imaging performed at rest only may be sufficient to determine myocardial viability [34–36]. In these studies, viable as compared to nonviable myocardium was defined on the basis of rather minor differences in resting function, which can be determined only by very accurate parameters of myocardial function, allowing differentiation of different degrees of functional impairment. Thus, these techniques do not rely on the assessment of functional reserve. M-mode tissue Doppler imaging allowed analysis of myocardial velocity gradients between endocardium and epicardium as a marker of myocardial deformation using epicardial short-axis views [34] (Figure 11.5). The transmurality of acute myocardial infarcts was found to relate to the myocardial velocity gradient determined at rest. Similarly, myocardial strain from endocardium to epicardium defined by Doppler-based strain

imaging correlates closely to transmural scar extension [35] (Figure 11.6). In another animal model using Doppler strain analysis and sonomicrometry, the ratio between systolic lengthening and combined late and postsystolic shortening (L–S ratio) was found to identify viable myocardium, and decreases in myocardial compliance – calculated as systolic lengthening divided by systolic pressure rise – were shown to identify necrotic myocardium [36].

Doppler-based deformation parameters determined only at rest have also been used in clinical studies to define myocardial viability. Tissue Doppler echocardiography-derived strain rate measurements at rest allowed determination of the transmural extent of myocardial infarction defined by contrast-enhanced magnetic resonance imaging in a study on 47 consecutive patients with previous first acute myocardial infarction and 60 age-matched healthy volunteers [15] (Figure 11.7). Peak myocardial velocities and peak myocardial deformation strain rates were measured. Magnetic resonance imaging was used to distinguish between transmural infarction, nontransmural infarction, and subendocardial infarction. Peak systolic strain rate of transmural infarction segments was significantly lower compared to normal myocardium or nontransmural infarction segments ( $P < 0.0005$ ). Transmural infarction could be detected with high sensitivity (90.9%) and high specificity (96.4%) using a cutoff value of  $SRs > -0.59 \text{ sec}^{-1}$ . Thus, differentiation between transmural and nontransmural myocardial

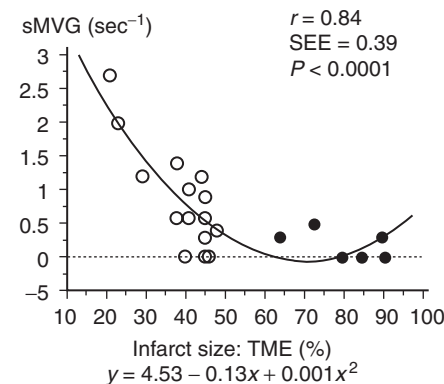
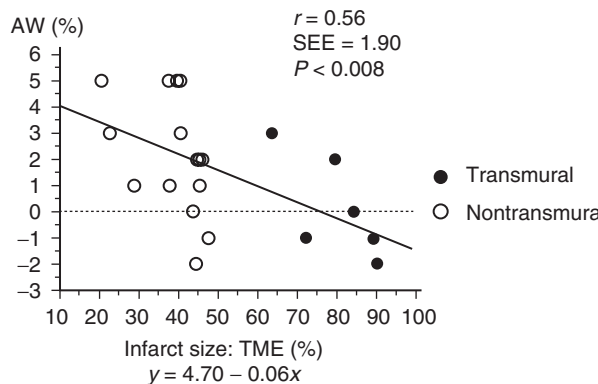


**Figure 11.5** Relationship between transmural extent (TME) of necrosis and anterior wall thickening (left panel) and systolic myocardial velocity gradient (sMVG; right panel). At 60 min after reflow, sMVG was better correlated with

transmural extent of necrosis than anterior wall thickening (AW%). SEE, standard error of estimate. From Derumeaux et al. [34].

infarction and normal myocardium can be obtained with high accuracy, based only on analysis of myocardial deformation at rest using strain rate imaging.

### Speckle tracking-based deformation

Tracking of acoustic markers from frame-to-frame within 2-D echocardiographic images has recently

been described to allow quantification of myocardial deformation [19–21,37]. As discussed in Chapter 2, the main benefit is that this method is angle-independent [19]. Thus, a more accurate assessment of regional myocardial deformation and, thereby, a more reliable analysis of the transmural extent of necrosis may be possible.

Speckle tracking to determine myocardial deformation at rest was used to evaluate the extent of transmural infarction in a study on 47 patients with impaired LV function due to chronic ischemic heart disease [16] (Figure 11.8,11.9). All patients underwent contrast-enhanced magnetic resonance imaging (ceMRI) for the detection of late enhancement. Transmural myocardial infarction based on the ceMRI finding was defined as relative late hyperenhancement of  $\geq 50\%$  and nontransmural myocardial infarction as relative late hyperenhancement  $< 50\%$ . Radial strain analysis allowed distinction of non-transmural infarction from transmural infarction with a sensitivity of 70% and a specificity of 71% (cutoff value for radial strain, 16.5%). The remaining myocardial wall thickness without hyperenhancement had a significant impact on

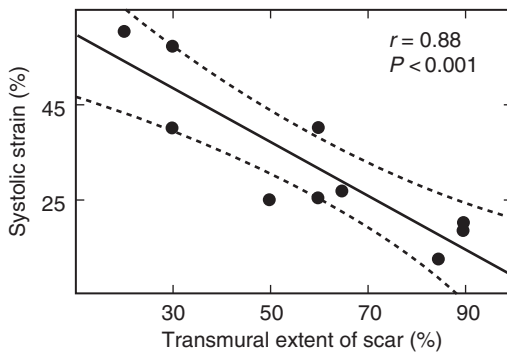


**Figure 11.6** Correlation between transmural extent of scar and systolic strain at rest in the region of interest in experimental nontransmural infarction. From Weidemann et al. [35].

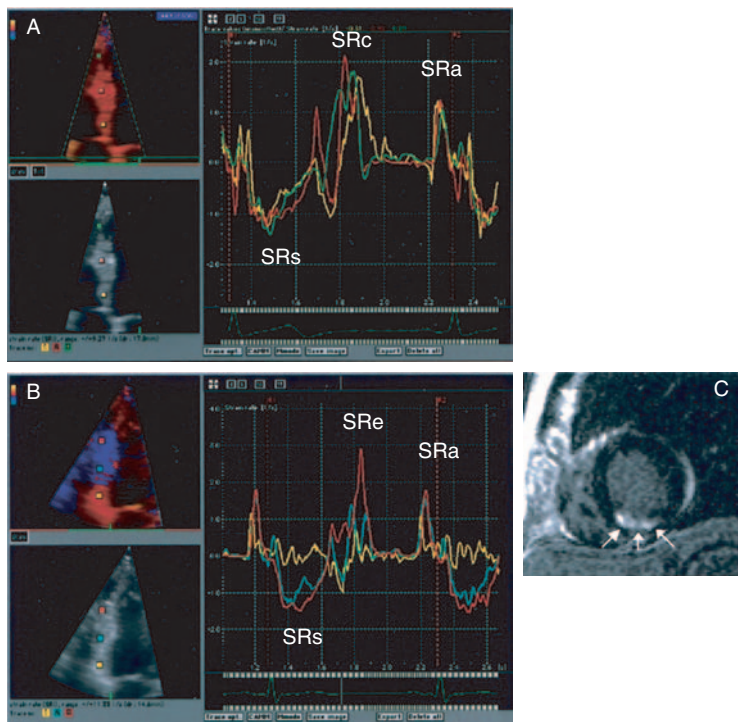


**Figure 11.7** Strain rate profile of a normal subject and a patient with a transmural infarct as defined by magnetic resonance imaging. Peak systolic strain rate (SRs), early diastolic strain rate (SRe), and atrial strain rate (SRa) are uniform in basal, mid-, and apical segments in the normal septum (A). In the patient with a transmural basal inferior infarct, basal SRs is markedly reduced, oscillating around the zero line compared to the mid- and apical segments (B). From Zhang et al. [15].

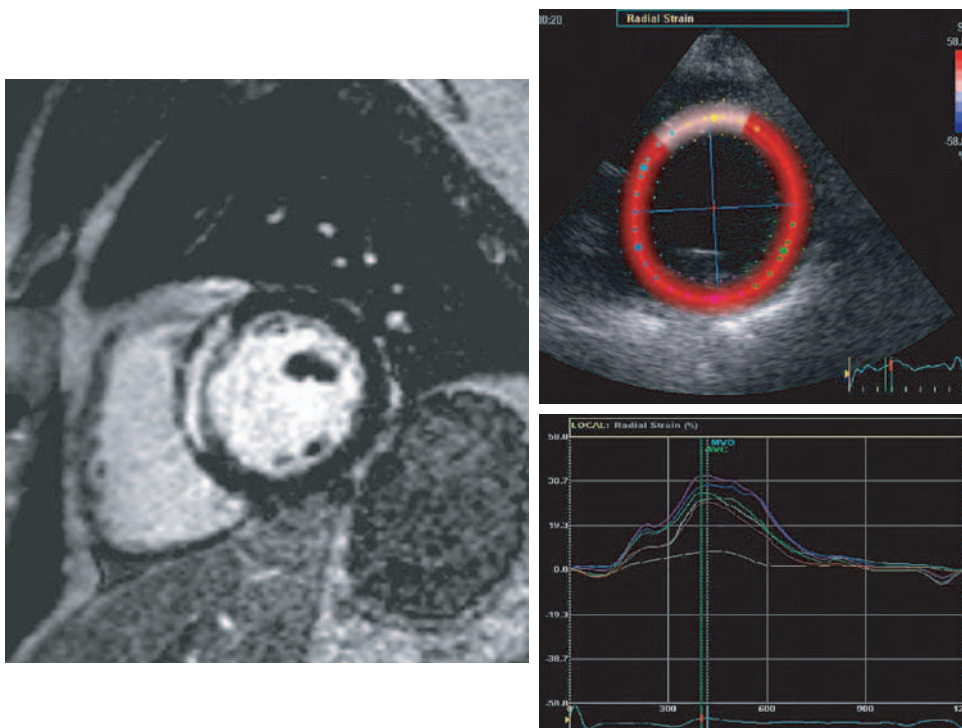


**Figure 11.8** Magnetic resonance imaging (left panel) and systolic radial strain imaging determined from speckle tracking in parasternal short-axis 2-D echocardiographic images (right panels) in a patient with a transmural myocardial infarction of the septum. Magnetic resonance imaging shows almost complete hyperenhancement of the septal wall. The septal segment (segment with yellow dot, upper right panel) shows only purple colorization

in a parametric display of peak systolic strain, indicating impaired peak systolic strain. Tracings of radial strain from a complete cardiac cycle for each of the six segments from the parasternal short-axis view (right lower panel) demonstrate impaired peak systolic strain in the septal segment (yellow tracing). AVC, aortic valve closure; MVO, mitral valve opening. From Becker et al. [16].

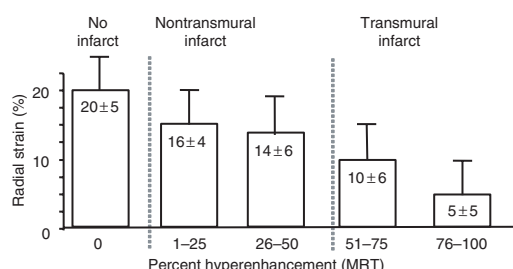


**Figure 11.9** Radial strain values for different degrees of myocardial hyperenhancement. There is decreasing peak systolic radial strain with increasing degree of myocardial hyperenhancement. Segments with transmural infarction defined by hyperenhancement more than 50% have significantly lower peak systolic radial strain than segments with nontransmural infarction defined by myocardial hyperenhancement. From Becker et al. [16].

circumferential (repeated measures analysis of variance [rmANCOVA]  $P < 0.001$ ) and radial (rmANCOVA  $P < 0.001$ ) strain. The thicker the remaining myocardial wall thickness without hyperenhancement, the higher the myocardial deformation parameters ( $r = 0.514$ ;  $P < 0.001$ ).

## Conclusion

Together, tissue Doppler velocity measurements and innovative myocardial deformation imaging techniques allow the identification of myocardial viability in acute and chronic LV dysfunction, as has been demonstrated in experimental and human studies. Both systolic and diastolic function parameters enable assessment of myocardial viability. Other than the measurement of tissue Doppler velocities, the analysis of myocardial deformation

parameters is free of passive tethering effects from adjacent myocardial segments and is, therefore, associated with a higher accuracy in the definition of myocardial viability. Innovative 2-D echocardiography-based deformation imaging techniques appear to allow precise analysis of segmental function from tracking of acoustic tissue pixels without the inherent limitations of tissue Doppler imaging modalities. Whereas analysis of the functional reserve of myocardium with impaired resting function has been shown to have a high accuracy to predict functional recovery after revascularization procedures, recent progress in deformation imaging technology has enabled determination of myocardial viability from local myocardial function at rest. However, the use of both tissue Doppler and speckle tracking techniques has been limited so far to research settings within rather small studies.

Myocardial deformation imaging techniques may be of significant interest for defining myocardial viability in settings where magnetic resonance imaging is not available. However, the clinical utility of these techniques still has to be proven in larger clinical trials.

## References

- 1 Wijns W, Vatner SF, Camici PG. Mechanisms of disease: hibernating myocardium. *N Engl J Med* 1998; **339**: 173–81.
- 2 Tillisch J, Brunken R, Marshall R, Schwaiger M, Mandelkern M, Phelps M, Schelbert H. Reversibility of cardiac wall-motion abnormalities by positron tomography. *N Engl J Med* 1986; **314**: 884–8.
- 3 Picano E, Sicari R, Landi P, et al. Prognostic value of myocardial viability in medically treated patients with global left ventricular dysfunction early after an acute uncomplicated myocardial infarction. *Circulation* 1998; **98**: 1078–84.
- 4 Dilsizian V, Rocco TP, Freedman NMT, Leon MB, Bonow RO. Enhanced detection of ischemic but viable myocardium by the reinjection of thallium after stress-redistribution imaging. *N Engl J Med* 1990; **323**: 141–6.
- 5 Pierard LA, De Landsheere CM, Berthe C, Rigo P, Kulbertus HE. Identification of viable myocardium by echocardiography during dobutamine infusion in patients with myocardial infarction after thrombolytic therapy: comparison with positron emission tomography. *J Am Coll Cardiol* 1990; **15**: 1021–31.
- 6 Fieno DS, Kim RJ, Chen EL, Lomasney JW, Klocke FJ, Judd RM. Contrast-enhanced magnetic resonance imaging of myocardium at risk: distinction between reversible and irreversible injury throughout infarct healing. *J Am Coll Cardiol* 2000; **36**: 1985–91.
- 7 Kim RJ, Wu E, Rafael A, et al. The use of contrast-enhanced magnetic resonance imaging to identify reversible myocardial dysfunction. *N Engl J Med* 2000; **343**: 1445–53.
- 8 Wagner A, Mahrholdt H, Holly TA, et al. Contrast-enhanced MRI and routine single photon emission computed tomography (SPECT) perfusion imaging for detection of subendocardial myocardial infarcts: an imaging study. *Lancet* 2003; **361**: 374–9.
- 9 Smart SC, Sawada S, Ryan T, et al. Low-dose dobutamine echocardiography detects reversible dysfunction after thrombolytic therapy of acute myocardial infarction. *Circulation* 1993; **88**: 405–15.
- 10 Watada H, Ito H, Oh H, et al. Dobutamine stress echocardiography predicts reversible dysfunction and quantitates the extent of irreversibly damaged myocardium after reperfusion of anterior myocardial infarction. *J Am Coll Cardiol* 1994; **24**: 624–30.
- 11 Picano E, Lattanzi F, Orlandini A, Marini C, L'Abbate A. Stress echocardiography and the human factor: the importance of being expert. *J Am Coll Cardiol* 1990; **17**: 666–7.
- 12 Hoffmann R, Lethen H, Marwick T, et al. Analysis of interinstitutional observer agreement in interpretation of dobutamine stress echocardiograms. *J Am Coll Cardiol* 1996; **27**: 330–6.
- 13 Hatle L, Sutherland GR. Regional myocardial function – a new approach. *Eur Heart J* 2000; **21**: 1337–57.
- 14 Gorcsan J III, Stum DP, Mandarino WA, Gulati VK, Pinsky MR. Quantitative assessment of alteration in regional left ventricular contractility with color coded tissue Doppler echocardiography. *Circulation* 1997; **95**: 2423–33.
- 15 Zhang Y, Chan AK, Yu CM, et al. Strain rate imaging differentiates transmural from non-transmural myocardial infarction. *J Am Coll Cardiol* 2005; **46**: 864–71.
- 16 Becker M, Hoffmann R, Kühl HP, et al. Analysis of myocardial deformation based on ultrasonic pixel tracking to determine transmurality in chronic myocardial infarction. *Eur Heart J* 2006; **27**: 2560–6.
- 17 Park TH, Nagueh SF, Khoury DS, et al. Impact of myocardial structure and function postinfarction on diastolic strain measurements: implications for assessment of myocardial viability. *Am J Physiol Heart Circ Physiol* 2006; **290**: H724–31.
- 18 Bountioukos M, Schinkel AF, Bax JJ, et al. Pulsed-wave tissue Doppler quantification of systolic and diastolic

- function of viable and nonviable myocardium in patients with ischemic cardiomyopathy. *Am Heart J* 2004; **148**: 1079–84.
- 19 Langeland S, D'hooge J, Wouters PF, et al. Experimental validation of a new ultrasound method for the simultaneous assessment of radial and longitudinal myocardial deformation independent of insonation angle. *Circulation* 2005; **112**: 2157–62.
- 20 Leitman M, Lysyansky P, Sidenko S, et al. Two-dimensional strain – a novel software for real-time quantitative echocardiographic assessment of myocardial function. *J Am Soc Echocardiogr* 2004; **17**: 1021–9.
- 21 Modesto KM, Cauduro S, Dispensieri A, et al. Two-dimensional acoustic pattern derived strain parameters closely correlate with one-dimensional tissue Doppler derived strain measurements. *Eur J Echocardiogr* 2006; **7**: 315–21.
- 22 Yuan D, Kuhl H, Nowak B, et al. Pulsed tissue Doppler imaging to assess myocardial viability by quantification of regional myocardial functional reserve. *Echocardiography* 2001; **18**: 657–64.
- 23 Nishino M, Tanouchi J, Tanaka K, et al. Dobutamine stress echocardiography at 7.5 mg/kg/min using color tissue Doppler imaging M-mode safely predicts reversible dysfunction early after reperfusion in patients with acute myocardial infarction. *Am J Cardiol* 1999; **83**: 340–4.
- 24 Rambaldi R, Poldermans D, Bax JJ, et al. Doppler tissue velocity sampling improves diagnostic accuracy during dobutamine stress echocardiography for the assessment of viable myocardium in patients with severe left ventricular dysfunction. *Eur Heart J* 2000; **21**: 1091–8.
- 25 Yang HS, Kang SJ, Song JK, et al. Diagnosis of viable myocardium using velocity data of Doppler myocardial imaging: comparison with positron emission tomography. *J Am Soc Echocardiogr* 2004; **17**: 933–40.
- 26 Heimdal A, Stoylen A, Torp H, Skjaerpe T. Real-time strain rate imaging of the left ventricle by ultrasound. *J Am Soc Echocardiogr* 1998; **11**: 1013–9.
- 27 Urheim S, Edvardsen T, Torp H, Angelsen B, Smiseth OA. Myocardial strain by Doppler echocardiography: validation of a new method to quantify regional myocardial function. *Circulation* 2000; **102**: 1158–64.
- 28 Greenberg NL, Firstenberg MS, Castro PL, et al. Doppler-derived myocardial systolic strain rate is a strong index of left ventricular contractility. *Circulation* 2002; **105**: 99–105.
- 29 Jamal F, Strotmann J, Weidemann F, et al. Noninvasive quantification of contractile reserve of stunned myocardium by ultrasonic strain rate and strain. *Circulation* 2001; **104**: 1059–65.
- 30 Hoffmann R, Altiock E, Nowak B, et al. Strain rate measurement by Doppler echocardiography allows improved assessment of myocardial viability in patients with depressed left ventricular function. *J Am Coll Cardiol* 2002; **39**: 443–9.
- 31 Hanekom L, Jenkins C, Jeffries L, et al. Incremental value of strain rate analysis as an adjunct to wall-motion scoring for assessment of myocardial viability by dobutamine echocardiography. *Circulation* 2005; **112**: 3892–900.
- 32 Hoffmann R, Altiock E, Nowak B, et al. Strain rate analysis allows detection of differences in diastolic function between viable and non-viable myocardial segments. *J Am Soc Echocardiogr* 2005; **18**: 330–5.
- 33 Pislaru C, Bruce CJ, Anagnostopoulos PC, et al. Ultrasound strain imaging of altered myocardial stiffness: stunned versus infarcted reperfused myocardium. *Circulation* 2004; **109**: 2905–10.
- 34 Derumeaux G, Loufoua J, Pontier G, Cribier A, Ovize M. Tissue Doppler imaging differentiates transmural from nontransmural acute myocardial infarction after reperfusion therapy. *Circulation* 2001; **103**: 589–96.
- 35 Weidemann F, Dommke C, Bijnens B, et al. Defining the transmurality of a chronic myocardial infarction by ultrasonic strain-rate imaging. *Circulation* 2003; **107**: 883–8.
- 36 Lyseggen E, Skulstad H, Helle-Valle T, et al. Myocardial strain analysis in acute coronary occlusion. *Circulation* 2005; **112**: 3901–10.
- 37 Becker M, Bilke E, Kühl H, et al. Analysis of myocardial deformation based on pixel tracking in 2D echocardiographic images allows quantitative assessment of regional left ventricular function. *Heart* 2006; **92**: 1102–8.

# Use of tissue velocity imaging during stress echocardiography

Thomas H. Marwick

## Introduction

The previous chapters have documented the feasibility and reliability of tissue Doppler techniques for quantifying myocardial function. Although this mode may be used for both global and regional left ventricular assessment, it is the regional assessment that is the most challenging interpretation in routine echocardiography. Regional assessment using wall motion scoring requires skills in recognition of the correct endocardial border; integration of wall thickening as well as wall motion; the ability to distinguish translational motion from motion due to myocardial thickening; comparison with other segments, including those not visualized in the current view; and an ability and preparedness to freeze the image and examine the time course of myocardial motion rather than relying on real-time imaging. Not surprisingly, this series of skills requires significant training and experience, and even experts may have discordant interpretations, particularly when the degree of wall motion abnormality is minor [1,2]. In this context, an easy, quantitative technique such as tissue Doppler imaging may be of value. Additionally, tissue Doppler imaging also gives the opportunity for measuring longitudinal function, which is an important constituent of cardiac motion hitherto largely ignored at echocardiography [3].

## Stress echocardiography and its limitations

The fundamental concept of stress echocardiography is to examine ventricular (usually left ventricular, LV) function before and after some form

of hemodynamic stress [4]. This information is usually used for the evaluation of myocardial ischemia, where the increased oxygen requirements of the myocardium during stress cannot be satisfied by increasing blood flow through a stenosed coronary artery, with resulting wall motion abnormalities. Moreover, the test may be used to identify areas of myocardial viability, where abnormal wall motion at rest may augment in response to either sympathetic stimulation or coronary vasodilation. A third indication for stress echocardiography is to identify subclinical LV dysfunction, as may occur in the early stages of ventricular damage caused by volume loading, or in situations of diffuse myocardial damage as may occur in cardiomyopathy.

## Problems with defining accuracy

Each of these indications for stress echocardiography has different reference standards for the evaluation of the reliability of the technique. In the most common situation – the diagnostic evaluation of chest pain in suspected coronary artery disease – the standard comparator is the coronary angiogram. Although this approach is supported by a long history, it also poses several problems. First, the angiogram, as an anatomic test, offers poor correlation with functional evidence of ischemia in stenoses of intermediate severity (i.e., 50–70% diameter). Second, the angiogram provides visualization of the lumen of the coronary artery rather than the vessel wall, which may be significantly diseased and unable to mount a normal hyperemic response in the absence of significant stenoses. Third, the definition of a normal reference segment at angiography can be challenging, producing problems in the definition of significant stenoses when the

reference segment is itself diseased. Although quantitative coronary angiography has solved some of these problems, particularly relating to the definition of stenosis significance, the optimal invasive comparator would involve measuring coronary flow at rest and stress, or the pressure drop across stenoses, but neither of these comparators has been commonly used. The noninvasive modalities, such as single-photon emission tomography or positron emission tomography have been used in some studies as a reference standard, but this may be inappropriate as these themselves are of imperfect accuracy. Finally, the most meaningful comparator of disease severity is the assessment of prognosis, and the stress echocardiography literature is replete with several outcome studies. However, this does not necessarily parallel the diagnostic accuracy of the test.

Despite these limitations in defining the accuracy of stress echocardiography, the literature over the past 20 years has been highly consistent in identifying a sensitivity and specificity of 80–85% for the detection of significant coronary disease, and a very low event rate (<1% per year or less) for the prognostic significance of a negative scan [4]. Stress echocardiography is listed in the guidelines as a routine test for the evaluation of suspected coronary disease and the prognostic evaluation of patients with cardiac disease [5,6].

### **Limitations of stress echocardiography**

Despite its place as a routine clinical technique, stress echocardiography has several important and well-described limitations that are responsible for many false-positive and false-negative findings (Table 12.1) [7]. Clearly, its reliability is dependent

on the performance of adequate stress, and patients who are unable to exercise maximally, or are tested on drugs that limit the heart rate response may not generate a meaningful test result. A related, but less publicized issue is the impact of transmural wall stress [8]. Even patients attaining an adequate rate pressure product may have false-negative scan results if the LV cavity is small and the blood pressure is low, inferring a low level of wall stress and, therefore, lesser likelihood of ischemia or LV compromise in myopathic conditions.

The routine forms of stress echocardiography are dependent on visual evaluation of the left ventricular response to stress. If the echocardiography image quality is suboptimal, this visual assessment may be difficult or impossible. When left ventricular contraction is dyssynchronous (e.g., patients with left bundle branch block), even good visualization at the endocardial border may be inadequate to permit accurate interpretation, which depends on the ability to assess wall thickening. Following coronary bypass surgery, patients may offer similar challenges with respect to evaluation of the interventricular septum.

There are several limitations to using a technique that is dependent on the development of sufficient ischemia to provoke wall motion abnormalities. For example, in patients with mild single vessel coronary disease, particularly those with borderline exercise capacity, ischemia may either not be provoked or be so limited in extent as to go unrecognized. In patients with multivessel coronary disease, one of several stenoses usually limits exercise capacity, and the recognition of ischemia within the territory of other stenoses may be missed because

**Table 12.1** Causes of false-positive and false-negative stress echocardiograms.

Cause	False-positives	False-negatives
Patient	Cardiomyopathies	Mild CAD Left circumflex disease
Test	HT response to stress	Inadequate stress Antiangular therapy Poor image quality Delayed images poststress
Interpretation	Overinterpretation, bias Localized basal inferior wall abnormalities Abnormal septal motion (LBBB, post-CABG)	Small LV cavity (wall stress)

the workload is insufficient to produce abnormal wall motion. Finally, in patients with previous infarction, the recognition of minor decrements of wall motion, from hypokinesia to akinesia, or the recognition of peri-infarct ischemia, may be difficult because of the subtle change with ischemia.

However, the greatest and probably most correctable limitation of stress echocardiography remains the subjective evaluation of wall motion. Competent interpreters of standard transthoracic echocardiography are not necessarily competent stress echocardiographers. Even for such experienced individuals, a training period of approximately 100 studies is required to attain the accuracy of expert stress echocardiographers [9]. Moreover, the pattern recognition required for accurate interpretation attenuates with disuse, and it is highly likely that an ongoing significant volume of studies is required to maintain skills. Even with these considerations, there remains discordance between expert observers, particularly in individuals with mild disease and suboptimal image quality [1,2]. Standard reading criteria and the improvement of image display using harmonic imaging and side by side display techniques reduce this discordance but remains a significant issue. However, several experimental and clinical studies have indicated that tissue Doppler measurement of myocardial motion closely reflects myocardial excursion. Tissue Doppler might be reasonably expected to address the shortcomings of stress echo.

## Tissue velocity imaging and stress echocardiography

### Technical considerations

Whereas high temporal resolution is important for tissue Doppler imaging generally, it is particularly important for the use of tissue Doppler during stress echo, where peak heart rates may be  $>150$  beats/min. However, there is a balance between temporal and spatial resolution, and the pursuit of very high frame rates may compromise the number of beams across the image. This reduces spatial resolution, to the extent that velocities derived from the blood pool may contaminate the tissue Doppler velocities. In the experimental setting, narrow sector imaging increases the spatial resolution of the acquired data, but this is usually not feasible

in clinical stress echocardiography, which requires comparison between the cardiac walls and, therefore, requires a wide angle acquisition [10]. The same problem with feasibility besets the use of pulsed-wave tissue Doppler during stress [11].

The signal-to-noise ratio of tissue velocity imaging is higher than that of two-dimensional (2-D) echo, but it would be incorrect to consider this technique to be image quality-independent. Indeed, the accuracy of tissue velocity imaging appears to be as dependent on signal quality as standard wall motion scoring.

When tissue Doppler is used as an adjunct to stress echo, there is a trade-off between the imaging resources devoted to gray-scale acquisition and those providing the color tissue Doppler overlay. Acquisition of gray-scale images at a lower frame rate (e.g., 30 frames/sec) provides imaging of satisfactory quality in most cases. However, optimal 2-D image acquisition will require separate 2-D and tissue velocity imaging images, and this is particularly needed if measurement of 2-D strain is considered.

### Imaging considerations

Tissue velocity may be gathered in either the longitudinal, radial, or circumferential directions. The radial approach permits the comparison of the epicardial to endocardial velocity, which is a good marker of ischemia, as this begins in the subendocardium. However, this attraction is outweighed by the angle dependency of Doppler, which precludes the evaluation of velocities in the septal and lateral segments, as well as the difficulty in separating these regional velocities across the thin LV wall. Generally, this radial approach has been used more in experimental studies, where the risk area in an instrumented animal, commonly the left anterior descending, can be compared with a control area in the posterior wall. The failure to interrogate the entire heart, together with some issues of translational and through-plane movement, have limited the applicability of short-axis tissue Doppler imaging in clinical practice.

Most of the tissue Doppler literature pertains to apical imaging, which provides an assessment of long-axis function in the ventricle. Although this approach is ineffective for identification of apical function, as the apex is relatively fixed and velocities

are extremely low, it can be used for interrogation of the remainder of the left ventricle, keeping in mind that there is a velocity gradient from base to apex. An attraction of this strategy is that longitudinal function is provided by subendocardial fibers, which are highly susceptible to ischemia, and long-axis function also appears to be compromised early in myopathic processes, so that the use of stress echocardiography for the evaluation of these diseases may be facilitated by the examination of long-axis function [12].

### Determinants of the tissue velocity response to stress

Myocardial motion may be influenced by both patient and hemodynamic factors. Diastolic function alters with age, as is readily apparent from assessment of transmitral flow, but although there is some influence of age on myocardial systolic function, the influence appears to be relatively less so (Figure 12.1) [13]. These age changes are most prominent in the old and the very young, rather than the 40- to 70-year-old age group, who are the main users of stress testing.

The metabolic milieu may have an influence on myocardial performance. Diabetes and insulin resistance states have been shown to influence not only diastolic but also systolic function [14,15].

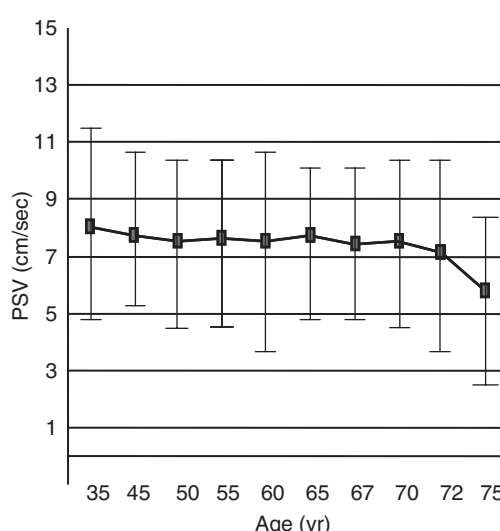


Figure 12.1 Variation of peak systolic velocity (PSV) at peak dobutamine stress according to age.

Hyperlipidemia also appears to influence tissue velocity, possibly through its effect on coronary flow [16]. The role of gender in myocardial performance is debated – tissue velocity appears to be less in women than in men [17] – but this finding is not necessarily matched by differences of myocardial deformation. This may simply reflect the small size of the female heart, although some hormonal influence on myocardial function may be present.

The hemodynamic status of the patient is clearly an influence on tissue velocity. LV volume has a relatively minor impact on velocity in normal individuals, but this influence is highly likely to be an issue in large ventricles (Figure 12.2). LV hypertrophy is also associated with reduced tissue velocity, possibly related to abnormal subendocardial function. Tissue velocity is clearly load-dependent and will be reduced by high afterload, as well as correlating with heart rate, although neither had a major impact on the velocity response to normal studies (Figure 12.2). All of these hemodynamic influences need to be taken into account in evaluating the stress response. Fortunately, dobutamine offers a relatively stereotyped stress response in most individuals, with attainment of a heart rate of approximately 140 beats/min, usually without marked levels of hypertension. In contrast, their hemodynamic response to exercise is vastly heterogenous and poses much more of a challenge in defining the normal range.

The normal response of tissue velocity with stress is a linear increase of both peak velocity and the time velocity integral. Timing parameters fall at low dose, but then tend to plateau between moderate and high dose (Figure 12.3).

### What to measure at tissue Doppler imaging?

Tissue Doppler offers the opportunity to measure both magnitude and timing parameters. The simplest magnitude parameter is to measure peak velocity, which can be assessed during systole, early diastole, or in the isovolumic period. Velocities are reduced in ischemic segments (Figure 12.4). Although diastolic measurements are indeed sensitive to ischemia following stress [18], these are highly sensitive to load and heart rate. Abnormal diastolic responses to stress may not be limited to ischemia but also occur with LV hypertrophy.

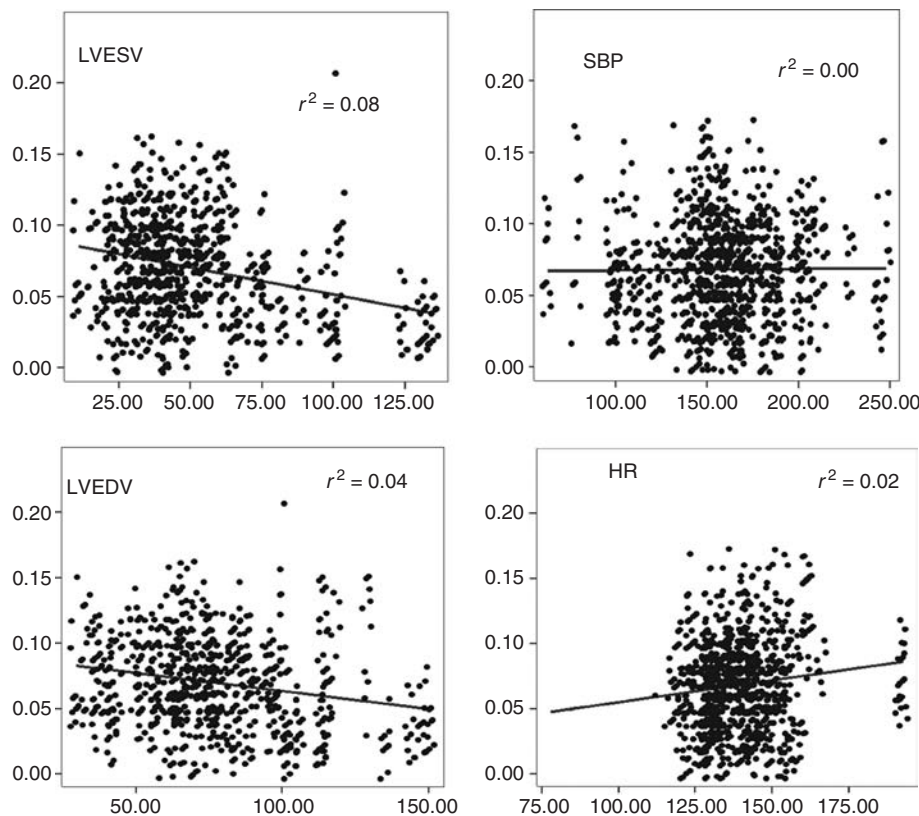


**Figure 12.2** Variation of peak systolic velocity at peak dobutamine stress according to hemodynamics and ventricular volumes. LVESV, LV end-systolic volume; SBP, systolic blood pressure; LVEDV, LV end-diastolic volume, HR, heart rate.

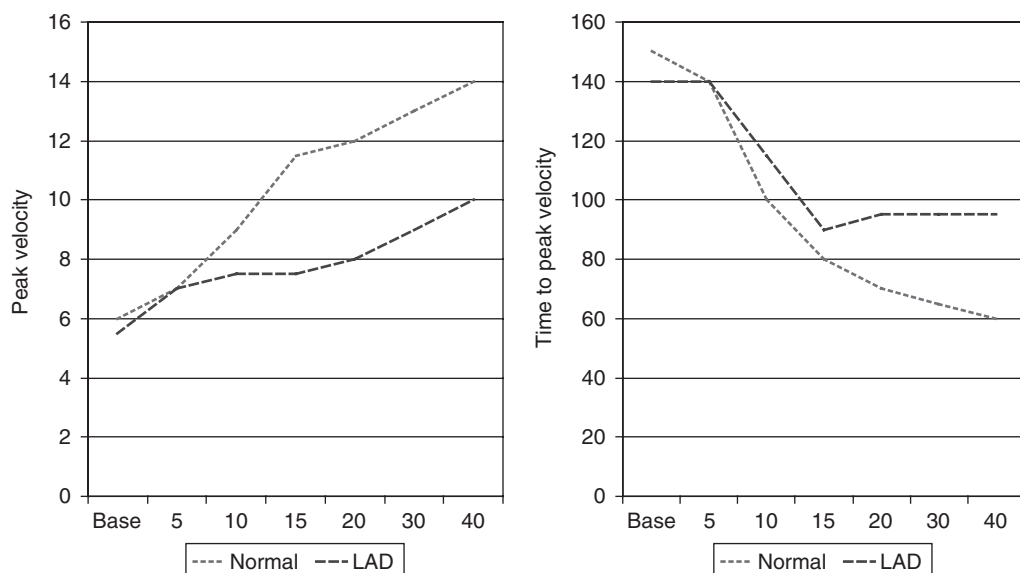


**Figure 12.3** Normal responses of peak velocity (left panel) and time to peak velocity (right panel) to incremental doses of dobutamine. LAD, left anterior descending coronary artery.

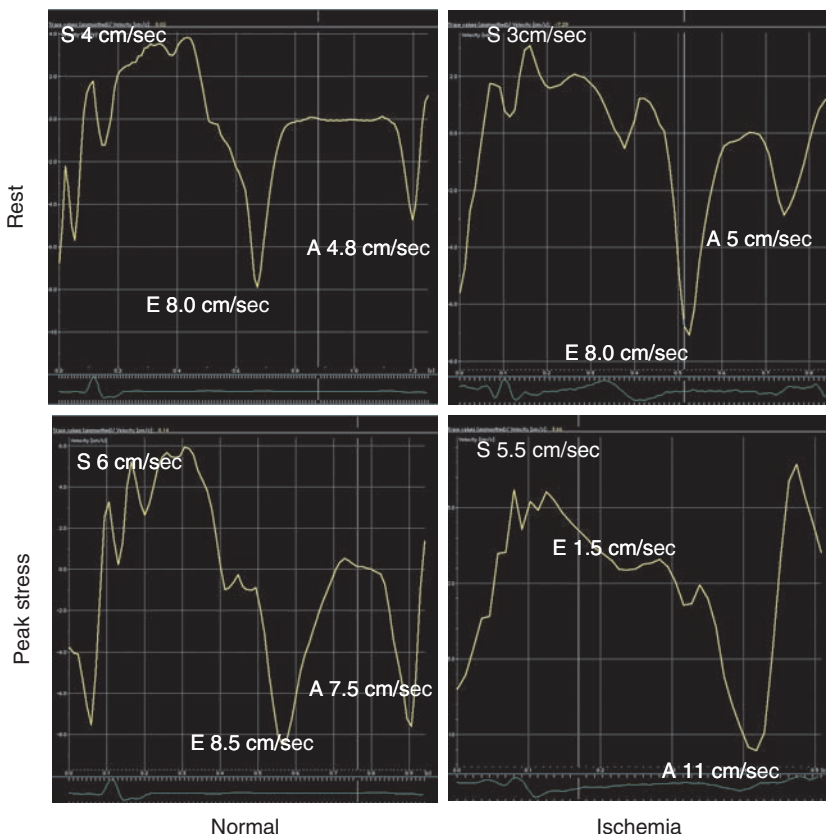


**Figure 12.4** Tissue Doppler velocity profiles in normal (left panel) and ischemic (right panel) basal septal segments. Note that ischemia provokes a marked reduction

of tissue E velocity responses but only a blunted increment of systolic velocity (although still less than normal range).

Systolic responses are simple to evaluate and may be reliably measured in all basal segments. Unfortunately, as there is a velocity gradient from base to apex, a single cutoff velocity cannot be isolated in the entire heart. Systolic velocity can certainly be measured at rest and during stress, potentially allowing the velocity increment to be used as a judge of ischemia. The problem with this strategy is that resting function is more heterogeneous than stress function, causing difficulties in discriminating an optimal cutoff. Isovolumic velocities have been reported by some investigators to be very reliable indices of myocardial function [19,20]. They are load independent as the valves are closed in the isovolumic periods, but their accurate assessment is probably favored by the use of pulsed wave rather than color tissue Doppler, because high temporal resolution is required.

Timing parameters could potentially be attractive for stress echocardiography. Delayed contraction

is a very sensitive indicator of ischemia and is often not recognized if the interpreter fails to freeze and step through the image looking at function from frame to frame. Certainly, real-time evaluation of function is not a good means to assess timing because of the temporal resolution of the human eye [21]. However, although tissue Doppler has a very high temporal resolution, the measurement of timing is highly variable [22], and this technique is insufficiently robust for clinical use.

### Clinical application of tissue velocity imaging with stress echo

#### Feasibility and variability

With the exception of the apex (which is fixed, so tissue velocities are low), interpretable tissue velocities are obtainable in >90% of myocardial segments. The most difficult segments to measure are the anterior and lateral walls, particularly in individuals with suboptimal image quality.

Inter- and intraobserver variability for peak velocity and the time velocity integral varies between 10 and 15%. In the MYDISE study [22], coefficients of variation of peak systolic velocity in basal segments were 9–14% at rest and 11–18% maximal stress in the apical windows, with higher variation in the parasternal windows. Timing parameters are somewhat more variable, with coefficient of variation in the 15–20% range, and diastolic velocities are the most variable, with coefficient of variation of 20%. These variations are an important issue when applying tissue velocity data to individuals rather than groups. Within individuals, individual velocity changes of the order of 30% are required for sequential measurements to be meaningful.

### Tissue velocity responses to ischemia

The initial reports of stress echocardiography in combination with tissue velocity imaging were published over a decade ago. Gorcsan et al. [23] based their work on velocity estimation from the color tissue Doppler and demonstrated that ischemic myocardium demonstrated lower velocities in response to stress. Myocardial velocity was quantified by Yamada et al. [11], using pulsed-wave tissue Doppler to measure peak velocity responses to stress, and demonstrating lower velocities and velocity increments in areas identified by expert wall motion analysis as being ischemic. Wilkenshoff et al. [24] quantified the stress response in normal subjects using color tissue Doppler; Pasquet et al. [25]

reported normal segments to increase velocity by 50%, ischemic segments to demonstrate a blunted velocity response, and scar segments to demonstrate low velocities at baseline. Similar findings were reported from a comparison with perfusion imaging [26], which gave an independent assessment of ischemia, scar, and normal tissue.

### Detection of coronary artery disease

Two major studies compared tissue Doppler with coronary angiography, based upon different strategies. The Brisbane group defined normal ranges for tissue velocity at peak stress (Figure 12.5), based on 300 patients in three groups; patients with normal coronary angiography ( $n = 114$ ), normal segments in normal studies ( $n = 128$ ), and in patients at low probability of coronary disease ( $n = 57$ ) [27]. These velocity cutoffs were then applied to a separate group undergoing dobutamine stress echocardiography and angiography. The results demonstrated that the use of tissue velocity cutoffs could provide an accurate diagnosis of coronary disease in all three coronary perfusion territories but that the accuracy of this approach was not superior to expert wall motion analysis (Figure 12.6). Nonetheless, the investigators did identify a benefit of using this approach with novice readers of stress echo, whose accuracy was improved by use of this approach [28]. Using a parametric display based on these velocity cutoffs, a multicenter study demonstrated higher concordance between

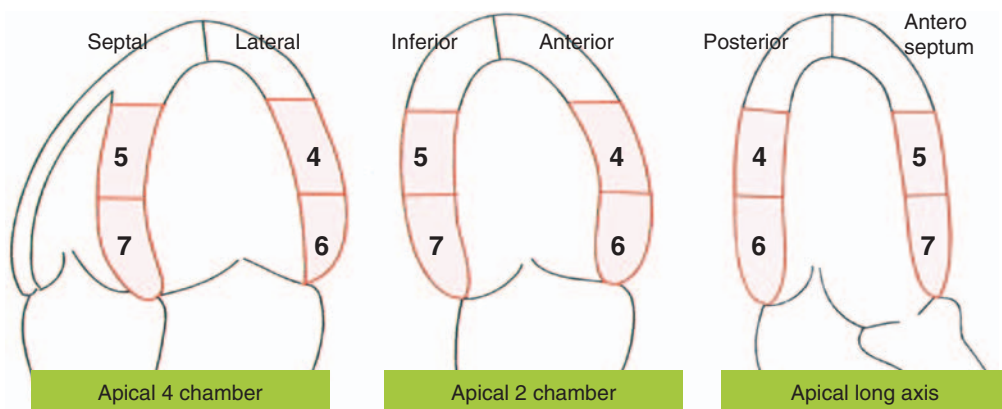


**Figure 12.5** Normal ranges derived from analysis of groups of patients with low probability of coronary disease, no coronary disease at angiography, and no abnormality on wall motion analysis. Adapted from Cain et al. [27].

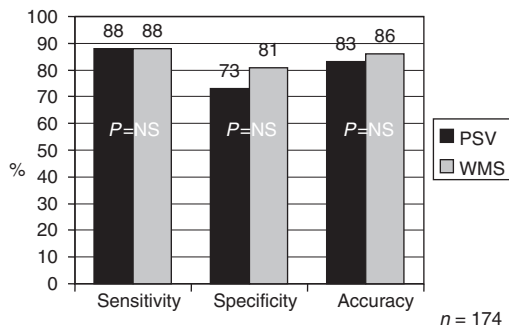


**Figure 12.6** Sensitivity and specificity of peak systolic tissue Doppler velocity (PSV) and expert wall motion scoring (WMS). Tissue Doppler is similar but not superior.

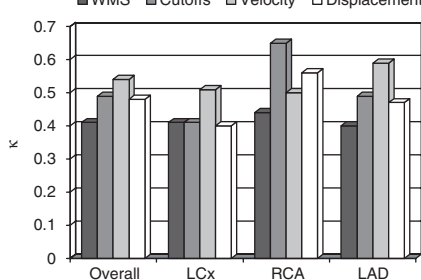
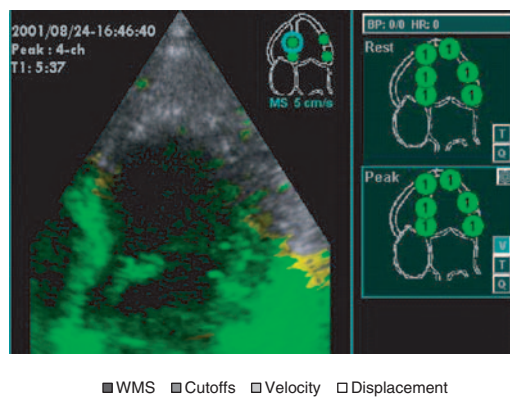


**Figure 12.7** Application of a parametric display based on automated peak velocity analysis (upper frame) to reduce variability between interpreters at three sites. LCx, left circumflex coronary artery; RCA, right coronary artery; LAD, left anterior descending coronary artery.

observers using tissue velocity imaging than was possible with wall motion scoring (Figure 12.7). Subsequent studies with similar design were performed using the time velocity integral of the tissue Doppler profile and, again, showed that this tissue tracking strategy was both feasible and accurate for the detection of coronary artery disease,

although again not superior to expert wall motion analysis [29].

Although the European (MYDISE) group also performed a series of studies to try to understand the role of tissue Doppler in stress echocardiography, there were many differences from the studies discussed above (Table 12.2), and a completely different strategy was used to define the normal response [17]. This group defined a normal velocity response based on a normal population, and combined this with age, gender, and the heart rate response in combination with tissue velocity. This study demonstrated a high level of sensitivity and specificity for the detection of coronary artery disease, but the study did not gather concurrent data for wall motion analysis. The suggestion from these findings is that this multivariate approach to defining normality, rather than using a simple cutoff, could provide a higher level of accuracy than was possible from visual assessment.

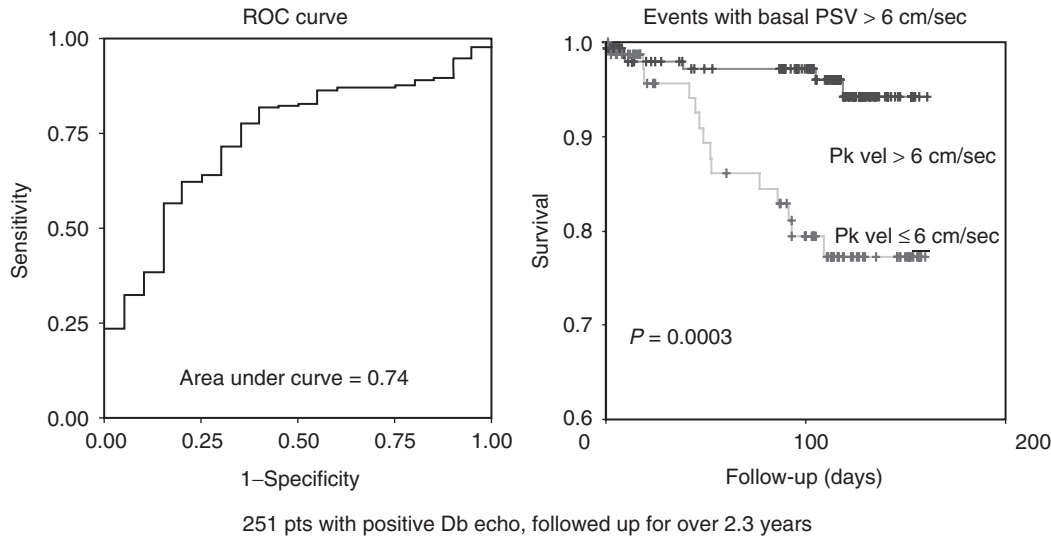
Tissue velocity imaging has several shortcomings in relation to its use during stress echo and has never really become accepted for this use. Strain rate techniques are also technically challenging but have been shown to be superior to wall motion analysis in some studies [30].

### Detection of myocardial viability

The limitations of standard wall motion analysis are no more apparent than in the recognition of viable myocardium. In this most challenging technique, the interpreter needs to distinguish viable from nonviable tissue on the basis of augmentation in response to low-dose dobutamine. Judgments need to be made about subtle differences in hypokinesis, and these changes can occur on a beat-to-beat basis. This is probably the area in which the greatest hope has been focused for the success of stress echocardiography with tissue velocity imaging. Indeed, similar small studies suggested that tissue velocity imaging demonstrated an augmentation of velocity in the setting of viable myocardium, at least as recognized from wall motion assessment [31]. Although regional function at follow-up does correlate with a velocity response at low dose, the accuracy of the test in these studies has been less encouraging than in the original cross-sectional comparisons [32]. One study comparing the technique to positron emission tomography as the gold standard of

**Table 12.2** Comparison between the European ("MYDISE") and Brisbane studies of tissue Doppler stress echocardiography.

	<i>MYDISE</i>	<i>Brisbane</i>	<i>Comparison</i>
Design	Multicentre with core laboratory	Single site	Different
Stress	Dobutamine	Dobutamine	Same
Acquisition	Apical views	Apical views	Same
	Apical segments not used	Apical segments not used	Same
Measurement	Physician-based	Sonographer	Different
	Multiple velocity/time parameters	Peak velocity only	Different
	ROI in basal part of each segment	ROI in central part of each segment	Different
	All stages	Peak stress	Different
Analysis	Multivariate, including age, gender, and hemodynamics	Normal range	Different

**Figure 12.8** Improvement in prognostic assessment of stress echocardiograms using tissue Doppler. In this study, the optimal cutoff (average peak velocity  $<6$  cm/sec) was

designated from receiver operating characteristic curves (ROC, left panel). Application to abnormal tests identified a high risk group (right panel). Adapted from Marwick et al. [35].

viability identified a very limited capacity of the technique to distinguish viable from nonviable tissue [33]. The explanation for this most certainly relates to issues regarding myocardial tethering (discussed below), and strain rate techniques are superior for this purpose [34].

### Prognostic data

While resting tissue velocity and the ratio of transmural flow to tissue velocity ( $E/E'$ ) has been shown to have prognostic value, the prognostic implications of the tissue velocity response to stress

are less well-defined. In a study of patients with positive stress echocardiograms, investigators sought to identify whether tissue velocity adds incremental value to the wall motion assessment alone [35]. This study did demonstrate independent and incremental information from the quantitative approach and was able to define an average peak stress tissue velocity of 6 cm/sec as being a significant determinant of adverse outcome (Figure 12.8). Subsequent clinical follow-up has identified strain rate imaging as a more effective prognostic factor in combination with wall motion analysis [36].

**Table 12.3** Positive and negative aspects of tissue Doppler with stress echocardiography.

Favourable aspects	Unfavourable aspects
Feasible	Works in most patients but not all (e.g., likely to be influenced by LV hypertrophy)
Simple	Velocities vary by location and results susceptible to malpositioning of sample volume
Good evidence base	Image quality remains a problem
Supplement to wall motion scoring rather than replacement	Time-intensive – robust automated peak detection desirable
	Diagnosis of CAD, not ischemia
	Velocities too low to measure in apex
	Unable to distinguish local from translational motion due to tethering of adjacent segments
	Measured velocity influenced by imaging angle

### Limitations of tissue velocity imaging

Despite over a decade of work in a combination of tissue velocity imaging with stress, this technique has not become part of mainstream stress echocardiography practice. The benefits and shortcomings of the technique are listed in Table 12.3. Probably the greatest problem relates to the susceptibility of tissue velocity analysis to tethering. This finding may compromise both sensitivity and specificity. For example, a hypokinetic but viable segment attached to an adjacent area of scar may not be able to declare its viability by an increment of tissue velocity because of tethering of the adjacent scar segment that effectively damps the augmentation of velocity response within the viable tissue. Conversely, a small area of ischemic tissue adjacent to normal tissue may not have a decrement of velocity recognized at peak stress, because the adjacent tissue is moving rapidly and this motion influences the measured velocity in the abnormal zone. These problems relate to the performance of tissue Doppler imaging in the measurement of tissue relative to the transducer rather than relative to adjacent tissue, and could potentially be circumvented by strain rate imaging.

Other problems with tissue velocity imaging relate to its sensitivity to noise, particularly at peak-dose dobutamine, and the difficulty in defining normal response. Although much work has been performed with dobutamine stress, and these results appear to be of some value clinically (see above), their evidence base in combination with vasodilator stressors is limited [37], and particular problems seem pertinent to the application of tissue

velocity imaging with exercise stress – both because velocity falls rapidly after exercise and because peak exercise imaging offers several challenges in terms of image quality.

### Conclusions

There is certainly a need for a quantitative technique in combination with stress echocardiography. In general, tissue velocity has not provided an effective solution to this problem, although a normal tissue velocity response may be reassuring to a less-expert reader and a significant area of ischemia would seem to be unlikely in the setting of a high-velocity response to stress. Nonetheless, as coronary disease is such a regional phenomenon, a more site-specific parameter such as strain rate imaging is likely to be more effective.

### References

- Hoffmann R, Lethen H, Marwick T, et al. Analysis of interinstitutional observer agreement in interpretation of dobutamine stress echocardiograms. *J Am Coll Cardiol* 1996; **27**: 330–6.
- Hoffmann R, Marwick TH, Poldermans D, et al. Refinements in stress echocardiographic techniques improve inter-institutional agreement in interpretation of dobutamine stress echocardiograms. *Eur Heart J* 2002; **23**: 821–9.
- Wandt B. Long-axis contraction of the ventricles: a modern approach, but described already by Leonardo da Vinci. *J Am Soc Echocardiogr* 2000; **13**: 699–706.
- Marwick TH. Stress echocardiography. *Heart* 2003; **89**: 113–8.

- 5 Galati A, Bigi R, Coletta C, et al. Multicenter trial on prognostic value of inducible ischemia, assessed by dobutamine stress echocardiography and exercise electrocardiography test, in patients with uncomplicated myocardial infarction, treated with thrombolytic therapy. *Int J Card Imaging* 1998; **14**: 155–62.
- 6 Ryan TJ, Anderson JL, Antman EM, et al. ACC/AHA Guidelines for the management of patients with acute myocardial infarction. A report of the American College of Cardiology/American Heart Association Task Force on Practice Guidelines (Committee on Management of Acute Myocardial Infarction). *J Am Coll Cardiol* 1996; **28**: 1328–42.
- 7 Gottdiener JS. Overview of stress echocardiography: uses, advantages, and limitations. *Curr Probl Cardiol* 2003; **28**: 485–516.
- 8 Yuda S, Khoury V, Marwick TH. Influence of wall stress and left ventricular geometry on the accuracy of dobutamine stress echocardiography. *J Am Coll Cardiol* 2002; **40**: 1311–9.
- 9 Picano E, Lattanzi F, Orlandini A, Marini C, L'Abbate A. Stress echocardiography and the human factor: the importance of being expert. *J Am Coll Cardiol* 1991; **17**: 666–9.
- 10 Hanekom L, Lundberg V, Leano R, Marwick TH. Optimisation of strain rate imaging for application to stress echocardiography. *Ultrasound Med Biol* 2004; **30**: 1451–60.
- 11 Yamada E, Garcia MJ, Thomas JD, Marwick TH. Myocardial Doppler velocity imaging: a quantitative technique for interpretation of dobutamine echocardiography. *Am J Cardiol* 1998; **82**: 806–9.
- 12 Lee R, Hanekom L, Marwick TH, Leano R, Wahi S. Prediction of subclinical left ventricular dysfunction with strain rate imaging in patients with asymptomatic severe mitral regurgitation. *Am J Cardiol* 2004; **94**: 1333–7.
- 13 Cain P, Napier S, Haluska B, Short L, Marwick TH. Influence of left ventricular size and hemodynamics on the systolic longitudinal myocardial Doppler velocity response to stress. *Am Heart J* 2002; **143**: 169–175.
- 14 Andersen NH, Poulsen SH, Ejskjaer H, Poulsen PL, Mogensen CE. Decreased left ventricular longitudinal contraction in normotensive and normoalbuminuric patients with Type II diabetes mellitus: a Doppler tissue tracking and strain rate echocardiography study. *Clin Sci (Lond)* 2003; **105**: 59–66.
- 15 Fang ZY, Schull-Meade R, Downey M, Prins J, Marwick TH. Determinants of subclinical diabetic heart disease. *Diabetologia* 2005; **48**: 394–402.
- 16 Vinereanu D, Nicolaides E, Tweddel AC, et al. Subclinical left ventricular dysfunction in asymptomatic patients with Type II diabetes mellitus, related to serum lipids and glycated haemoglobin. *Clin Sci (Lond)* 2003; **105**: 591–9.
- 17 Madler CF, Payne N, Wilkenshoff U, et al. Non-invasive diagnosis of coronary artery disease by quantitative stress echocardiography: optimal diagnostic models using off-line tissue Doppler in the MYDISE study. *Eur Heart J* 2003; **24**: 1584–94.
- 18 von Bibra H, Tuchnitz A, Klein A, Schneider-Eicke J, Schomig A, Schwaiger M. Regional diastolic function by pulsed Doppler myocardial mapping for the detection of left ventricular ischemia during pharmacologic stress testing: a comparison with stress echocardiography and perfusion scintigraphy. *J Am Coll Cardiol* 2000; **36**: 444–52.
- 19 Lind B, Nowak J, Cain P, Quintana M, Brodin LA. Left ventricular isovolumic velocity and duration variables calculated from colour-coded myocardial velocity images in normal individuals. *Eur J Echocardiogr* 2004; **5**: 284–93.
- 20 Pauliks LB, Vogel M, Madler CF, et al. Regional response of myocardial acceleration during isovolumic contraction during dobutamine stress echocardiography: a color tissue Doppler study and comparison with angiographic findings. *Echocardiography* 2005; **22**: 797–808.
- 21 Kvitting JP, Wigstrom L, Strotmann JM, Sutherland GR. How accurate is visual assessment of synchronicity in myocardial motion? An in vitro study with computer-simulated regional delay in myocardial motion: clinical implications for rest and stress echocardiography studies. *J Am Soc Echocardiogr* 1999; **12**: 698–705.
- 22 Fraser AG, Payne N, Madler CF, et al. Feasibility and reproducibility of off-line tissue Doppler measurement of regional myocardial function during dobutamine stress echocardiography. *Eur J Echocardiogr*. 2003; **4**: 43–53.
- 23 Gorcsan J, Deswal A, Mankad S, et al. Quantification of the myocardial response to low-dose dobutamine using tissue Doppler echocardiographic measures of velocity and velocity gradient. *Am J Cardiol* 1998; **81**: 615–23.
- 24 Wilkenshoff UM, Sovany A, Wigstrom L, et al. Regional mean systolic myocardial velocity estimation by real-time color Doppler myocardial imaging: a new technique for quantifying regional systolic function. *J Am Soc Echocardiogr* 1998; **11**: 682–92.
- 25 Pasquet A, Armstrong G, Beachler L, Lauer MS, Marwick TH. Analysis of segmental myocardial Doppler velocity as a quantitative adjunct to exercise echocardiography. *J Am Soc Echocardiogr* 1999; **12**: 901–12.
- 26 Pasquet A, D'Hondt AM, Verhelst R, Vanoverschelde JL, Melin J, Marwick TH. Comparison of dipyridamole stress echocardiography and perfusion scintigraphy for cardiac risk stratification in vascular surgery patients. *Am J Cardiol* 1998; **82**: 1468–74.
- 27 Cain P, Baglin T, Case C, Spicer D, Short L, Marwick TH. Application of tissue Doppler to interpretation of

- dobutamine echocardiography: comparison with quantitative coronary angiography. *Am J Cardiol* 2001; **87**: 525–31.
- 28 Fathi RB, Cain P, Nakatani S, Yu H, Marwick TH. Effect of tissue Doppler on the accuracy of novice and expert interpreters of dobutamine echocardiography. *Am J Cardiol* 2001; **88**: 400–5.
- 29 Cain P, Baglin T, Khoury V, Case C, Marwick TH. Automated regional myocardial displacement for facilitating the interpretation of dobutamine echocardiography. *Am J Cardiol* 2001; **89**: 1347–53.
- 30 Voigt JU, Exner B, Schmiedehausen K, et al. Strain-rate imaging during dobutamine stress echocardiography provides objective evidence of inducible ischemia. *Circulation* 2003; **107**: 2120–6.
- 31 Rambaldi R, Poldermans D, Bax JJ, et al. Doppler tissue velocity sampling improves diagnostic accuracy during dobutamine stress echocardiography for the assessment of viable myocardium in patients with severe left ventricular dysfunction. *Eur Heart J* 2000; **21**: 1091–8.
- 32 Cain P, Khoury V, Short L, Marwick TH. Usefulness of quantitative echocardiographic techniques to predict recovery of regional and global left ventricular function after acute myocardial infarction. *Am J Cardiol* 2003; **91**: 391–6.
- 33 Hoffmann R, Altio E, Nowak B, et al. Strain rate measurement by Doppler echocardiography allows improved assessment of myocardial viability inpatients with depressed left ventricular function. *J Am Coll Cardiol* 2002; **39**: 443–9.
- 34 Hanekom L, Jenkins C, Short L, Marwick TH. Accuracy of strain rate techniques for identification of viability at dobutamine stress echo: a follow-up study after revascularization. *Circulation* 2005; **112**: 3892–900.
- 35 Marwick TH, Case C, Leano R, et al. Use of tissue Doppler imaging to facilitate the prediction of events in patients with abnormal left ventricular function by dobutamine echocardiography. *Am J Cardiol* 2004; **93**: 142–6.
- 36 Bjork Ingul C, Rozis E, Slordahl S, Marwick TH. Incremental value of strain rate imaging to wall motion analysis for prediction of outcome in patients undergoing dobutamine stress echocardiography. *Circulation* 2007; **112**: 3892–900.
- 37 Davidavicius G, Kowalski M, Williams RI, et al. Can regional strain and strain rate measurement be performed during both dobutamine and exercise echocardiography, and do regional deformation responses differ with different forms of stress testing? *J Am Soc Echocardiogr* 2003; **16**: 299–308.

# Strain and strain rate imaging in ischemia

*Hsin-Yueh Liang, Jeroen J. Bax and Theodore P. Abraham*

## Introduction

The World Health Organization estimates that the global number of deaths from CAD will rise to 11.1 million by 2020 [1]. The reference standard for the detection of significant coronary atherosclerosis (plaque) is coronary angiography. However, this method is an invasive procedure involving radiation and nephrotoxic contrast dye, thus exposing patients to some risk and is, therefore, not suitable for widespread clinical screening. Noninvasive techniques such as treadmill exercise testing or imaging-based stress testing have gained popularity over the past several years for detection of CAD.

Conventional dobutamine stress echocardiography (DSE) has been well-validated for the diagnosis of angiographically significant CAD [2] and as a strong predictor of subsequent cardiac events in a wide variety of patient populations [3]. The interpretation of DSE is based on the assessment of stress-induced changes in systolic wall thickening or wall motion analysis. Worsening or new wall motion abnormality (WMA) suggests induced ischemia. However, this technique is semiquantitative, subjective, and prone to wide variability. Furthermore, the analysis is restricted to systolic events, because the human eye is unable to reliably resolve rapid diastolic mechanical events [4]. This chapter will focus on the potential role of novel echocardiographic techniques, namely, strain rate imaging for the evaluation of CAD.

## Tissue Doppler and strain echocardiography

Tissue Doppler imaging (TDI) measures myocardial velocity relative to a fixed point (the transducer)

and has been introduced to quantify regional myocardial function. With high temporal resolution (typically >200 frames/sec), TDI depicts change of tissue velocity during consecutive phases of a cardiac cycle objectively. Tissue velocity increases progressively from apical to basal segments, because the obtained velocity represents a cumulative velocity of all segments apical to the analyzed segments.

Strain (S) measures deformation of myocardium, representing the percentage of change in length related to its original dimension (%) as a function of applied force, defined by Mirsky and Parmley [5]. Strain rate (SR) is the temporal derivative of strain and reflects velocity of deformation, with a unit of 1/sec. Shortening or thinning of myocardium is by convention shown with a negative value. Lengthening or thickening is shown with a positive value. Typically, normal left ventricular (LV) myocardium shortens in longitudinal and circumferential directions and thickens along the radial direction during systole, whereas it lengthens in longitudinal and circumferential directions and thins in radial direction during diastole. During isovolumic contraction and isovolumic relaxation, a biphasic appearance of SR is seen (Figure 13.1). In contrast to TDI, strain and SR are homogeneously distributed from the base to the apex. Theoretically, strain is less susceptible than tissue velocity to cardiac translational motion and the tethering effect of adjacent segments [6].

Heimdal et al. introduced that TDI-derived real-time SR is calculated from the regional Doppler velocity gradient between two points along the ultrasonic beam. TDI-derived strain echocardiography (SE) is angle-dependent, because only velocities parallel to the ultrasonic scan line can be estimated

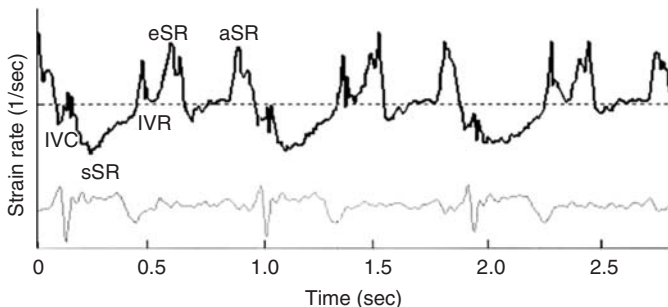


**Figure 13.1** An example of SE in longitudinal direction. sSR, peak systolic SR; eSR, early diastolic SR; aSR, late diastolic SR; IVC and IVR, biphasic appearance of strain curve. Modified and adapted from *J Am Coll Cardiol* 2002; 39: 1531–7.

accurately [6]. Two-dimensional speckle tracking strain echocardiography (2DSE) identifies unique ultrasound patterns in each frame. These individual speckle patterns are tracked frame by frame through the entire cardiac cycle. The in-plane frame-to-frame displacement of each pattern over time is used to calculate velocity, and this velocity is used to derive SR. Because it does not use Doppler techniques, the 2DSE method is not sensitive to the angle of insonation [7,8]. Both TDI-derived SE and 2DSE have been validated against sonomicrometry and tagged magnetic resonance imaging (MRI) in vitro and in vivo, under different conditions [8–12]. Abraham et al. [13] demonstrated that SE closely tracked standard physiological parameters (force–velocity–length relations) of regional contractile function in vitro, under conditions of varying afterload. The maximal value of the first LV pressure–time derivative ( $dP/dt_{\max}$ ) is the gold standard for the assessment of global LV function. In the control group, dobutamine induced an increase in both peak systolic SR (sSR) and  $dP/dt_{\max}$ , with an excellent linear correlation between these parameters ( $r = 0.85$ ) [14]. The area of the regional LV pressure–segment length loop is a measure of regional myocardial work and reflects energy consumption. The positive loop area indicates active work, whereas a negative value indicates passive work. Skulstad et al. [12] has shown that systolic strain (sS) had an excellent correlation with segmental work ( $r = 0.90$ ); therefore, they were able to differentiate active and passive contractile segments. Thus, it should not be surprising that SE is being used to transfer the concepts of ischemia-related change in regional deformation from animal models to the clinical setting.

### Acute ischemia

Work in experimental models indicates that TDI and SE can track regional ischemia by means of recognition of changes in local mechanics. For example, acute coronary artery ligation resulted in reduced TDI systolic velocity and longitudinal sS suggested dyskinesia (stretching). Strain values were unchanged in remote segments while systolic velocity was reduced, indicating that strain is less susceptible to tethering artifacts [9]. During serial imaging, changes in S occurred earlier than change in tissue velocity and wall motion, and the difference between ischemic and nonischemic segments was greater for S ( $P < 0.001$ ) than tissue velocity [15]. When the severity of the coronary occlusion was adjusted to produce various levels of ischemia, S appeared to be more sensitive than tissue velocity in differentiating between moderate and severe grades of ischemia [9].

Moderate ischemia was obtained by gradually reducing coronary flow (by  $47 \pm 6\%$ ) and severe ischemia by complete occlusion. The peak systolic velocity overlapped between moderately and severely ischemic myocardium, sS appeared an excellent tool for quantifying function in moderately as well as severely ischemic myocardium ( $P < 0.01$ ) and defining the anatomical extent of dysfunctional myocardium. Thus SE was superior to tissue velocity for grading of myocardial segmental dysfunction [9].

In a clinical study, 73 patients with stable angina were examined during coronary artery angioplasty. Balloon inflation induced a marked reduction in S in both the radial ( $P < 0.001$ ) and longitudinal ( $P < 0.05$ ) directions. Concomitantly, postsystolic strain increased significantly in both directions ( $P < 0.001$  and  $P < 0.05$  in radial and longitudinal

directions, respectively). Upon reperfusion, S, postsystolic strain, and maximal strain ( $S + \text{post-systolic strain}$ ) returned to near preocclusion values. In comparison with control, baseline, and reperfusion data, the post-systolic strain index (post-systolic strain/max strain) measured during percutaneous coronary angioplasty was more sensitive in identifying acutely ischemic myocardium, with a sensitivity of 92% and 95% and a specificity of 89% and 89% in radial and longitudinal directions, respectively (Figure 13.2) [16]. Similar findings were reported by Edvardsen et al. who demonstrated that S showed expansion (dyskinesis) in the apical septal segment ( $7.5 \pm 6.5\%$  vs.  $-17.7 \pm 7.2\%$ ;  $P < 0.001$ ) (Figure 13.3) and reduced shortening in the mid-septal segment ( $P < 0.05$ ) during left anterior descending coronary artery (LAD) occlusion in 17 patients undergoing angioplasty. Segments not supplied by the LAD showed no changes in S. However, tissue velocity and

wall motion scores changed in segments not supplied by the LAD, again indicating that SE may be superior to tissue velocity and visually recognized wall motion abnormality in detecting systolic regional dysfunction related to acute ischemia [17].

## Chronic ischemia

Voigt et al. [19] demonstrated the feasibility and accuracy of strain rate amplitude and timing parameters in predicting ischemia in 44 patients with known or suspected CAD during clinical DSE. The increase of longitudinal sSR to dobutamine stimulation was blunted in the ischemic segments. In ischemic segments defined by simultaneous perfusion scintigraphy, the increase in longitudinal sSR in ischemic segments was blunted (from  $-1.6 \pm 0.8$  to  $-2.0 \pm 1.1/\text{sec}$ ;  $P < 0.05$ ) compared with nonischemic segments (from  $-1.6 \pm 0.6$  to  $-3.4 \pm 1.4/\text{sec}$ ;  $P < 0.01$ ) in response to dobutamine stimulation. Strain remained unchanged in nonischemic segments (from  $-17 \pm 6\%$  to  $-16 \pm 9\%$ ;  $P < 0.05$ ), whereas strain value decreased in ischemic segments (from  $-16 \pm 7\%$  to  $-10 \pm 8\%$ ;  $P < 0.05$ ). The color-coded strain rate curve in M-mode (Figure 13.4) also showed delayed onset and ending of shortening and deterioration of systolic function in ischemic

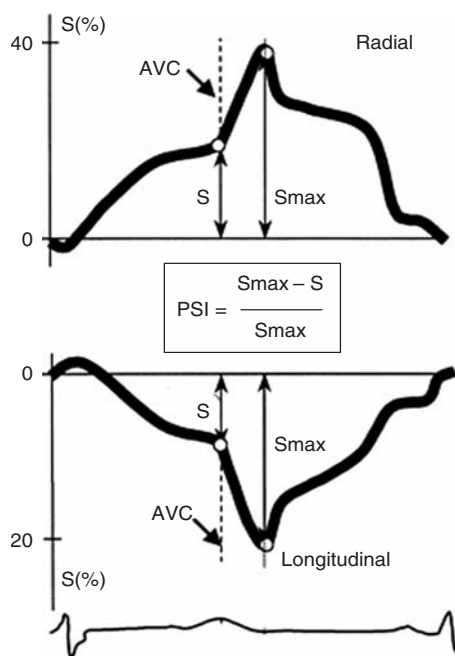


**Figure 13.2** Parameters derived from strain profiles. A schematic representation of radial and longitudinal ischemic strain profiles. Systolic ( $sS$ ) and maximal strains ( $S_{\text{max}}$ ) were measured at end-systole and peak deformation, respectively. Post-systolic strain was calculated as the difference between  $S_{\text{max}}$  and  $sS$  (absolute change). PSI, post-systolic index. Modified and adapted from Kukulski et al. [16].

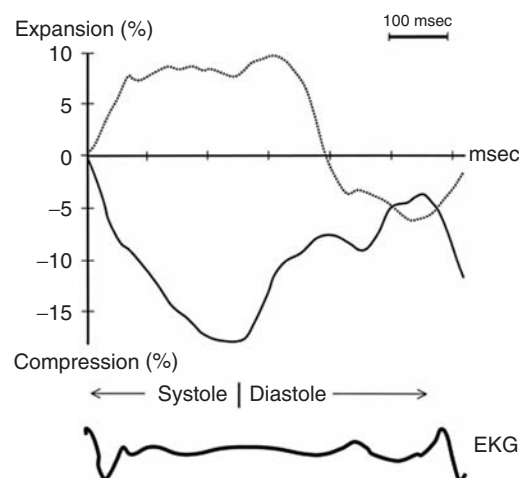


**Figure 13.3** Strain profiles from different segments in the same heartbeat during LAD occlusion. The profile from the basal septum (solid line) showing compression (normal deformation) and from the ischemic apical septum (dashed line) showing expansion (paradoxical motion). Adapted from Edvardsen et al. [17].

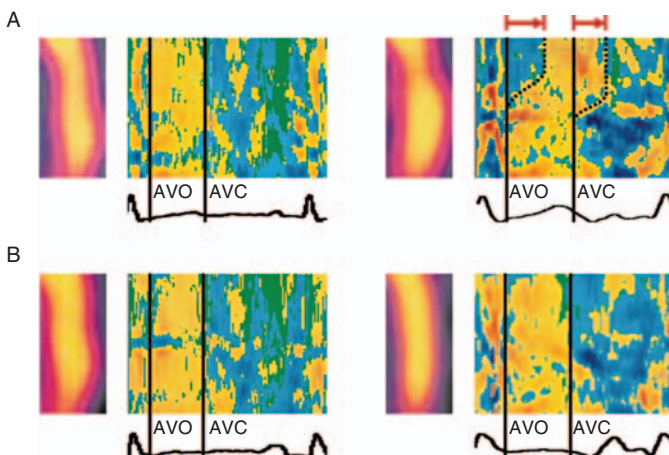


**Figure 13.4** Perfusion scintigrams and color-coded strain rate curved M-modes of a patient's anteroapical wall at baseline (left) and during dobutamine stress (right). (A) Ischemic response. Note normal strain rate patterns at rest and delayed onset of myocardial shortening and marked postsystolic strain in apical region at peak stress (red arrows). (B) The same patient after successful revascularization of the left anterior descending coronary artery. Normal strain rate patterns both at rest and at peak stress. The middle of the lower left curved M-mode shows a typical artifact, identifiable by its band-like shaped color inversion (yellow/blue). Adapted from Voigt et al. [19].

myocardium during inotropic stimulation, and this mode was more accurate than conventional visual DSE (86% vs. 81% and 89% vs. 82% in sensitivity and specificity, respectively). Moreover, a postsystolic strain index  $>35\%$  resulted in an area under the curve of 0.90, with a sensitivity of 82%, and a specificity of 85% for the detection of ischemia stress-induced perfusion defect by thallium scintigraphy [19].

Yip et al. [20] demonstrated that SE tracks dobutamine-induced changes in regional myocardial perfusion during nonocclusive coronary stenosis in an experimental model. In this study, dobutamine stimulation caused a significant increase in regional myocardial blood flow (as measured by microspheres) and sSR, with a decrease in time to onset of relaxation. This response was blunted during nonocclusive coronary stenosis, which consistently reduced dobutamine-induced increase in regional blood flow by approximately 50% of the prestenosis level. These changes in regional mechanics occurred in the absence of changes in global systolic and diastolic function derived from invasive LV measurements. Furthermore, sSR correlated closely with regional myocardial blood flow ( $r=0.70$ ), suggesting that strain parameters were able to predict quantitative changes in regional myocardial blood flow during dobutamine stress [20].

A brief episode of severe ischemia followed by restoration of regional perfusion may produce prolonged myocardial dysfunction with a gradual return of contractile activity, a condition termed

myocardial *stunning* [14,21]. Stunned myocardium has been shown to retain significant contractile reserve, with improvement in ventricular function gradually over the course of days to weeks. Myocardial stunning is also an important feature of unstable angina [22]. The response of dysfunctional myocardium to dobutamine is widely used in clinical stress tests to identify viable but stunned myocardium monitored by conventional two-dimensional echocardiography. Jamal et al. [14] have demonstrated that decreased radial sSR and S failed to fully recover at rest, after 60 min of reperfusion in stunned myocardium created by reduction of coronary blood flow. During an incremental dobutamine infusion, reperfused but stunned myocardium tended to normalize the abnormal resting strain curve. “Normalization” was characterized by a return in end-systolic strain to normal or near-normal values with concomitant reduction in the percentage of postsystolic thickening/shortening, and by the increase in both SR and S (Figure 13.5). In contrast, ongoing ischemia with inadequate flow reserve was characterized by a further reduction in end-systolic strain during dobutamine infusion and an increase in percentage of postsystolic thickening/shortening (Table 13.1) [14].

In an experimental study, Weidemann et al. [23] have shown that the transmurality of a chronic myocardial infarction is related to the change in deformation parameters measured at rest and during dobutamine infusion. In the nontransmural infarcted myocardium, sSR and S were significantly

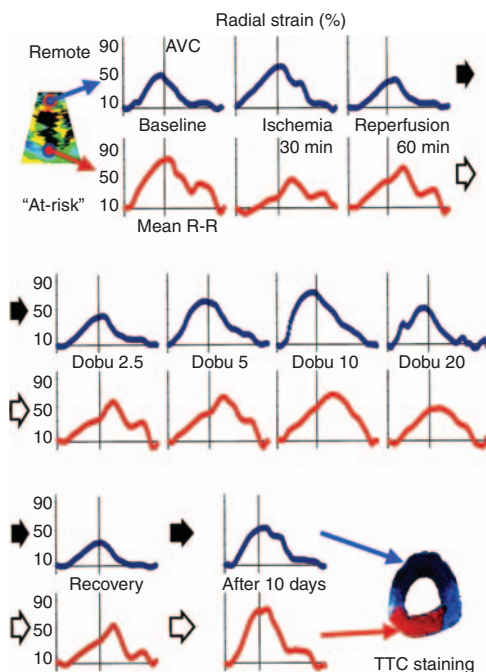


**Figure 13.5** Stunning group: typical example of changes in radial strain profile of at-risk posterior wall (red) and remote septum (blue) during circumflex artery hypoperfusion, reperfusion, and dobutamine (Dobu) challenge. Regional ischemia resulted in a decreased systolic strain and marked asynchronous and delayed contraction of posterior wall. Abnormal strain pattern persisted on reperfusion because of stunning. During dobutamine infusion, deformation profile normalized gradually. After 10 days of reperfusion, segmental function of posterior wall recovered totally. Myocardial staining confirmed matching of interrogated region with area at risk of LCx and absence of myocardial necrosis. AVC indicates aortic valve closure. Adapted from Jamal et al. [14].

lower compared with normally perfused areas at rest. The dobutamine infusion induced a biphasic sSR response with an initial increase at low dose and a decrease at higher infusion rates. S remained at low level without significant changes during the stress test. The ratio of postsystolic strain to S was significantly higher at baseline and increased further in response to the incremental dobutamine challenge. Histopathologic studies demonstrated an excellent correlation between S and the extension of scar tissue into the myocardium ( $r = 0.88$ ;  $P < 0.01$ ).

On the other hand, sSR was significantly reduced with almost no S in the transmural infarct myocar-

**Table 13.1** Summary of radial deformation characteristics at rest and during dobutamine stress for each ischemic substrate.

	Rest			Dobutamine stress		
	sSR	sS	PSI	sSR	sS	PSI
Control	5/s	60%	2%	↗	/↘	⇒
Stunning	↓	↓	↑	↗	↗	↘
Acute ischemia	↓	↓	↑	↘	↘	↗
Nontransmural MI	↓	↓	↑	/↘	⇒	↗
Transmural MI	↓↓	↓↓	↑↑	⇒	⇒	⇒

MI indicates myocardial infarction; ↓, lower vs. control; ↑, higher vs. control; ↗, no change vs. rest; ↘, increase vs. rest values; ↙, decrease vs. rest value; and /↘, initial increase at low-dose dobutamine and a further decrease with higher dobutamine dose. (Adapted from *Circulation* 2003; 107: 883–8).

dium at rest. Both deformation parameters showed no change during the graded dobutamine infusion, whereas postsystolic strain to S ratio was significantly higher than in controls (Figure 13.6) [23].

## Myocardial infarction

In a clinical study, SE demonstrated longitudinal stretching in the infarcted regions (strain,  $+1.5 \pm 4.3\%$ ) compared with longitudinal shortening (strain,  $-15 \pm 3.9\%$ ) in the remote myocardium ( $P < 0.001$ ). Radial mechanics were similarly affected, demonstrating a radial strain of  $-6.9 \pm 4.1\%$  (dyskinesis) versus  $14.3 \pm 5.0\%$  ( $P < 0.001$ ), respectively. Myocardial strain by SE and tagged MRI correlated well ( $r = 0.89$  and  $r = 0.96$  for longitudinal and radial strain, respectively;  $P < 0.001$ ) in healthy individuals and in patients with infarction [11].

The distinction between nontransmural and transmural necrosis after myocardial infarction is clinically important, because an increase in the degree of infarct transmularity is associated with a greater number of infarct-related complications, such as LV dysfunction, arrhythmia, and an increased incidence of sudden death [24].

In an experimental study, segments were divided based on transmularity of the infarct, as identified by triphenyltetrazolium chloride staining. Those with  $<50\%$  myocardial thickness involvement

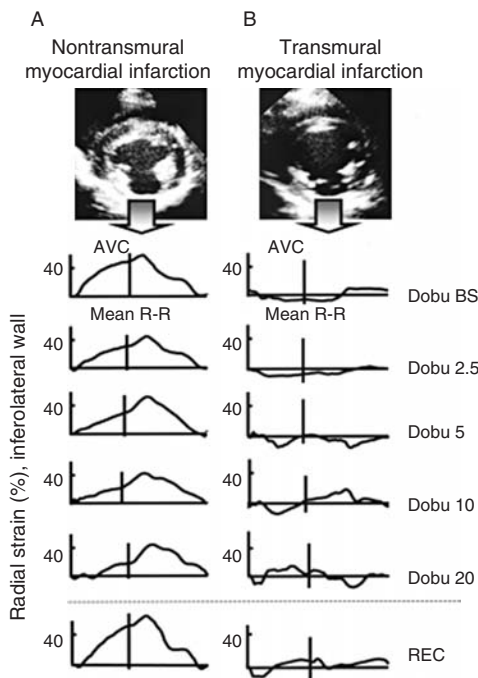


**Figure 13.6** Example of changes in radial strain profiles over one heart cycle in a nontransmural and a transmural infarcted wall. (A) Nontransmural myocardial infarction. At dobutamine baseline, systolic thickening (strain) of nontransmural infarcted myocardium is reduced, and after aortic valve closure, “at-risk” wall continues to thicken during isovolumic relaxation period (postsystolic thickening), resulting in a delayed thickening peak. Incremental dobutamine challenge resulted in a stepwise reduction in systolic thickening, whereas postsystolic thickening increased progressively with increasing dobutamine dose. After dobutamine administration was discontinued, deformation returned to predobutamine baseline profile. (B) Transmural myocardial infarction: At baseline, there is no systolic thickening (strain) of transmural infarcted inferolateral wall. During incremental dobutamine challenge, systolic deformation properties of at-risk wall did not change. AVC indicates aortic valve closure; BS, baseline; Dobu, dobutamine infusion ( $\mu\text{g kg}^{-1} \text{min}^{-1}$ ); REC, recovery. Adapted from Weidemann et al. [23].

(endocardial layers) were identified as having nontransmural infarctions and those with >50% myocardial thickness involvement were identified as having transmural infarction. Coronary occlusion resulted in wall motion abnormality and reduction in systolic velocity and radial sSR.

Sixty minutes after reperfusion, wall motion remained severely and similarly depressed in both groups ( $P = \text{baseline}$  for both). Systolic velocity

and sSR failed to increase significantly in the transmural group. In contrast, both endocardial and epicardial systolic velocity and sSR increased significantly in the nontransmural group. Radial sSR enabled differentiation of transmural from nontransmural infarction as early as 60 min after reperfusion. Overall, sSR analysis provided superior sensitivity for the distinction between transmural and nontransmural infarction as compared to wall motion and systolic velocity data. sSR recovered significantly after reperfusion in the nontransmural subgroup, suggesting that active contraction of a functionally significant amount of viable myocardial tissue resumed as a consequence of reperfusion [25].

In another study of 41 patients with their first myocardial infarction, the extent of late enhancement (expressed as a percentage of the myocardial wall thickness), was assessed with contrast MRI and used to classify the myocardium into no-scar (0%), nontransmural infarction (up to 75%), and transmural infarction (>75%). In the absence of significant differences in the levels of maximal creatine kinase and thrombolysis in myocardial infarction (TIMI) flow before and after intervention, sSR in the no-scar and nontransmural groups increased significantly 3 days after successful percutaneous coronary intervention, whereas sSR remained reduced in the transmural group. In parallel, S increased only in the no-scar and nontransmural infarct groups. Compared with wall motion abnormality, sSR and S were the best parameters for prediction of absence of transmurality after percutaneous coronary intervention with a sensitivity of 95% and a specificity of 91% using a sSR of  $-0.6 \text{ sec}^{-1}$  as the cutoff value.

In the chronic phase of this study (5 months postinfarction), both sSR and S recovered to normal values in the no-scar group, recovered partially in the nontransmural infarct group, and stayed low (similar to baseline) in the transmural infarct group [26].

$^{18}\text{F}$ -Fluorodeoxyglucose ( $^{18}\text{FDG}$ ) positron emission tomography (PET) remains the reference technique for detection of viable myocardium, because of its high sensitivity. In 37 patients with reduced LV function (ejection fraction,  $43.5 \pm 9.9\%$ ) due to a previous myocardial infarction, sSR at rest was  $-0.85 \pm 0.39 \text{ sec}^{-1}$  for myocardium defined as

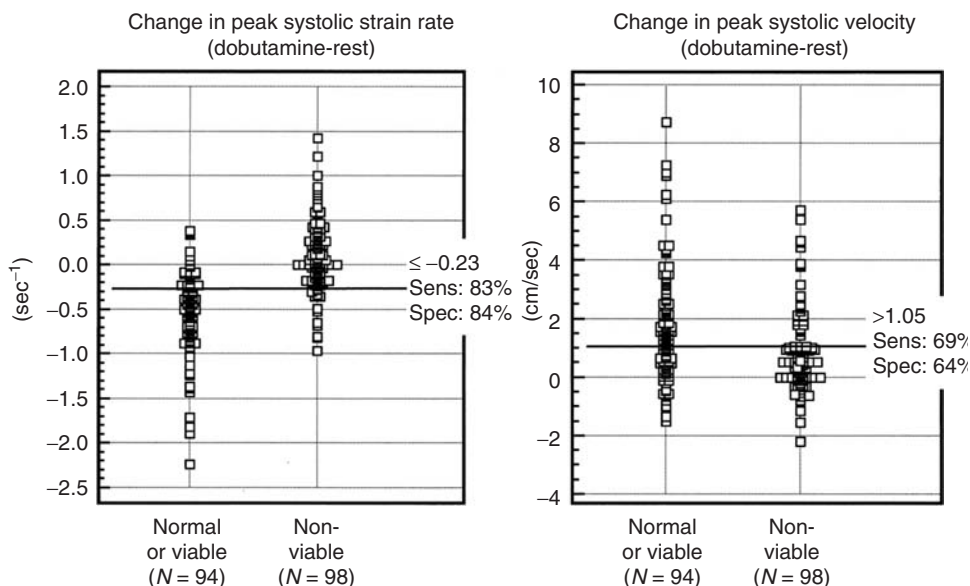


**Figure 13.7** Plot of increase in strain rate during dobutamine stimulation determined by strain rate imaging and increase in tissue velocities during dobutamine stimulation determined by tissue Doppler imaging for myocardial

segments defined as normal or viable and for those defined as nonviable by  $^{18}\text{F}$ -fluorodeoxyglucose positron emission tomography. Adapted from Hoffmann et al. [27].

normal function or viable by  $^{18}\text{FDG}$  PET, and  $-0.64 \pm 0.32 \text{ sec}^{-1}$  for myocardium defined as nonviable by  $^{18}\text{FDG}$  PET ( $P < 0.001$ ). In dysfunctional segments at rest, sSR of viable myocardium did not differ significantly from that of nonviable myocardium ( $-0.61 \pm 0.36 \text{ sec}^{-1}$  vs.  $-0.66 \pm 0.42 \text{ sec}^{-1}$ ;  $P = 0.59$ ). During low-dose dobutamine ( $10 \mu\text{g}/\text{kg}$  per min) stimulation, sSR increased significantly for viable myocardium, whereas it remained unchanged for nonviable myocardium ( $-1.22 \pm 0.43$  vs.  $-0.60 \pm 0.32 \text{ sec}^{-1}$ ;  $P < 0.0001$ ). The increase in sSR was also significantly different between viable and nonviable myocardium ( $-0.61 \pm 0.36$  vs.  $0.07 \pm 0.35 \text{ sec}^{-1}$ ;  $P < 0.0001$ ) (Figure 13.7).

The agreement between  $^{18}\text{FDG}$  PET and conventional visual wall motion analysis, tissue velocity, and SE for the identification of viability were 66%, 66%, and 83% of segments, respectively. An increase in sSR from rest to low-dose dobutamine by more than  $-0.23 \text{ sec}^{-1}$  allowed accurate discrimination of viable from nonviable myocardium, as determined by  $^{18}\text{FDG}$  PET, with a sensitivity of 83% and a specificity of 84%, whereas the sensitivity of conventional DSE and tissue velocity was 75% and 69% and the specificity was 63% and 64%, respectively [27].

## Diastolic mechanics in ischemia

Early diastolic relaxation is an active energy-dependent process. Bonow et al. used radionuclide scintigraphy to demonstrate impaired diastolic relaxation at rest in the absence of systolic dysfunction in patients with CAD, which improved after successful coronary angioplasty [28].

In an animal study, Pislaru et al. have demonstrated that delayed onset of diastole in ischemic regions by SE correlated well with the spatial distribution of myocardium at risk as identified by postmortem tissue staining. The extent of myocardium at risk was better delineated by delayed diastole than by visual wall motion analysis [29]. In another study, the same investigators demonstrated that the ratio of early to late diastolic SR and S could differentiate normal from stunned (viable) and infarcted (nonviable) myocardium. These differences in diastolic mechanics appeared to be related to a difference in myocardial stiffness [30].

Systolic and diastolic strain rates were examined in 27 patients with CAD, wherein ischemic segments were identified by perfusion scintigraphy. All patients underwent percutaneous coronary

intervention and success was defined as a reduction of coronary artery stenosis by at least 40% with TIMI grade 3 flow. Before intervention, there was no difference in sSR between ischemic and nonischemic segments. Furthermore, intervention did not significantly change sSR in ischemic and nonischemic segments. However, eSR was significantly lower in the ischemic than in the nonischemic segments ( $1.82 \pm 0.71$  vs.  $2.03 \pm 0.64 \text{ sec}^{-1}$ ;  $P < 0.01$ ). Moreover, intervention resulted in a significant increase in eSR in the ischemic (from  $1.82 \pm 0.71$  to  $2.29 \pm 0.92 \text{ sec}^{-1}$ ;  $P < 0.001$ ), but not in the nonischemic segments [31].

In another study of 61 patients with chest pain referred for coronary angiography, patients with at least one coronary artery stenosis  $\geq 70\%$  were defined as ischemic and those with stenosis  $< 50\%$  in all three vessels as normal controls. There was no difference in global function between the two groups. The sSR and eSR ( $-0.8 \pm 0.2$ ;  $-0.6 \pm 0.2$ ;  $-0.6 \pm 0.2$ ;  $P < 0.05$  for sSR and  $0.9 \pm 0.3$ ;  $0.8 \pm 0.3$ ;  $0.8 \pm 0.3$ ;  $P = 0.02$  for eSR in the LAD, left circumflex, and right coronary artery territories, respectively) at rest were significantly decreased in ischemic segments compared with normal controls. The combination of sSR and eSR, using  $-0.85 \text{ sec}^{-1}$  and  $0.96 \text{ sec}^{-1}/\text{s}$  as cutoff values, yielded a sensitivity of 92% to detect angiographic coronary artery stenosis  $\geq 70\%$ . Peak eSR was the most specific parameter (93%) (Figure 13.8) [32].

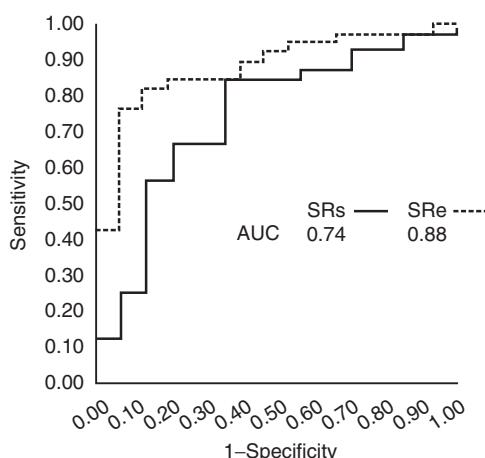


Figure 13.8 Receiver operating characteristic curves for sSR and eSR to detect ischemia. AUC = area under the curve.

In a study of patients ( $n = 37$ ) with prior myocardial infarction and reduced LV function (ejection fraction,  $44 \pm 10\%$ ), wall motion analysis and  $^{18}\text{FDG}$  PET imaging at rest were used to classify segments into normal, dysfunctional with viable myocardium, or dysfunctional with non-viable myocardium. Peak eSR was significantly lower for the combined dysfunctional segments compared with the normal segments. There was no difference in eSR at rest between viable and nonviable. During dobutamine stimulation, eSR increased significantly for normal and viable segments, whereas eSR remained unchanged for nonviable segments. Peak aSR was also significantly lower for the combined dyssynergic dysfunctional segments at rest compared with the normal segments. During dobutamine stimulation, aSR increased in all three subgroups and the increase was larger in viable segments compared with nonviable segments ( $1.00 \pm 0.56$  vs.  $0.71 \pm 0.58 \text{ sec}^{-1}$ ;  $P < 0.001$ ). In the 94 segments dysfunctional segments classified as viable by PET, 63 segments had normal perfusion and metabolism, whereas 31 segments were viable (impaired perfusion with preserved metabolism). There were no differences in eSR and aSR at rest between those viable segments with normal or impaired perfusion [33].

## Future directions

Current TDI-derived SE primarily offers information regarding one-dimensional deformation most commonly interrogated in the longitudinal direction due to the limitations of available windows that allow transducer placement such that the ultrasound beam is parallel to the cardiac walls. However, LV fiber architecture is complex [34], and myocardial deformation is three-dimensional. Recent speckle tracking-based two-dimensional strain technology promises to allow measurement of strain parameters in more than one direction. Furthermore, strain calculations are not based on Doppler and are, therefore, angle-independent [8,35].

Strain imaging continues to rely heavily on offline postprocessing, which is relatively time-consuming and cumbersome. Newer techniques such as speckle tracking strain that allow semi-automated tracking of the region of interest have the potential to reduce analysis time and make measurements more reproducible [36].

Currently, vendors are introducing three-dimensional SE to display simultaneous three-dimensional myocardial deformation. However, a large probe and relatively low frame rate may limit its acceptance in routine practice.

In conclusion, SE allows detailed interrogation of regional systolic and diastolic mechanics not otherwise available by means of conventional echocardiography. This incremental information appears to be of potential use in diagnosis of CAD. Studies in larger, unselected populations will reveal the role of SE in the management of acute and chronic myocardial ischemia.

## References

- 1 Zipes D, Libby P, Bonow RO, Braunwald E. Braunwald's heart disease: a textbook of cardiovascular disease. 7th ed. Philadelphia: Saunders; 2005. p. 1281.
- 2 Pellikka PA. Stress echocardiography in the evaluation of chest pain and accuracy in the diagnosis of coronary artery disease. *Prog Cardiovasc Dis* 1997; **39**: 523–32.
- 3 Chuah SC, Pellikka PA, Roger VL, McCully RB, Seward JB. Role of dobutamine stress echocardiography in predicting outcome in 860 patients with known or suspected coronary artery disease. *Circulation* 1998; **97**: 1474–80.
- 4 Pellikka PA. Stress echocardiography for the diagnosis of coronary artery disease: progress towards quantification. *Curr Opin Cardiol* 2005; **20**: 395–8.
- 5 Mirsky I, Parmley WW. Assessment of passive elastic stiffness for isolated heart muscle and the intact heart. *Circ Res* 1973; **33**: 233–43.
- 6 Heimdal A, Stoylen A, Torp H, Skjaerpe T. Real-time strain rate imaging of the left ventricle by ultrasound. *J Am Soc Echocardiogr* 1998; **11**: 1013–9.
- 7 Leitman M, Lysyansky P, Sidenko S, et al. Two-dimensional strain-a novel software for real-time quantitative echocardiographic assessment of myocardial function. *J Am Soc Echocardiogr* 2004; **17**: 1021–9.
- 8 Langeland S, D'Hooge J, Wouters PF, et al. Experimental validation of a new ultrasound method for the simultaneous assessment of radial and longitudinal myocardial deformation independent of insonation angle. *Circulation* 2005; **112**: 2157–62.
- 9 Urheim S, Edvardsen T, Torp H, Angelsen B, Smiseth OA. Myocardial strain by Doppler echocardiography. Validation of a new method to quantify regional myocardial function. *Circulation* 2000; **102**: 1158–64.
- 10 Korinek J, Wang J, Sengupta PP, et al. Two-dimensional strain – a Doppler-independent ultrasound method for quantitation of regional deformation: validation in vitro and in vivo. *J Am Soc Echocardiogr* 2005; **18**: 1247–53.
- 11 Edvardsen T, Gerber BL, Garot J, Bluemke DA, Lima JA, Smiseth OA. Quantitative assessment of intrinsic regional myocardial deformation by Doppler strain rate echocardiography in humans: validation against three-dimensional tagged magnetic resonance imaging. *Circulation* 2002; **106**: 50–6.
- 12 Skulstad H, Urheim S, Edvardsen T, et al. Grading of myocardial dysfunction by tissue Doppler echocardiography: a comparison between velocity, displacement, and strain imaging in acute ischemia. *J Am Coll Cardiol* 2006; **47**: 1672–82.
- 13 Abraham TP, Laskowski C, Zhan WZ, et al. Myocardial contractility by strain echocardiography: comparison with physiological measurements in an *in vitro* model. *Am J Physiol Heart Circ Physiol* 2003; **285**: H2599–604.
- 14 Jamal F, Strotmann J, Weidemann F, et al. Noninvasive quantification of the contractile reserve of stunned myocardium by ultrasonic strain rate and strain. *Circulation* 2001; **104**: 1059–65.
- 15 Armstrong G, Pasquet A, Fukamachi K, Cardon L, Olstad B, Marwick T. Use of peak systolic strain as an index of regional left ventricular function: comparison with tissue Doppler velocity during dobutamine stress and myocardial ischemia. *J Am Soc Echocardiogr* 2000; **13**: 731–7.
- 16 Kukulski T, Jamal F, Herbots L, et al. Identification of acutely ischemic myocardium using ultrasonic strain measurements. A clinical study in patients undergoing coronary angioplasty. *J Am Coll Cardiol* 2003; **41**: 810–9.
- 17 Edvardsen T, Skulstad H, Aakhus S, Urheim S, Ihlen H. Regional myocardial systolic function during acute myocardial ischemia assessed by strain Doppler echocardiography. *J Am Coll Cardiol* 2001; **37**: 726–30.
- 18 Abraham TP, Nishimura RA, Holmes DR, Jr, Belohlavek M, Seward JB. Strain rate imaging for assessment of regional myocardial function: results from a clinical model of septal ablation. *Circulation* 2002; **105**: 1403–6.
- 19 Voigt JU, Exner B, Schmiedehausen K, et al. Strain-rate imaging during dobutamine stress echocardiography provides objective evidence of inducible ischemia. *Circulation* 2003; **107**: 2120–6.
- 20 Yip G, Khandheria B, Belohlavek M, et al. Strain echocardiography tracks dobutamine-induced decrease in regional myocardial perfusion in nonocclusive coronary stenosis. *J Am Coll Cardiol* 2004; **44**: 1664–71.
- 21 Braunwald E, Kloner RA. The stunned myocardium: prolonged, postischemic ventricular dysfunction. *Circulation* 1982; **66**: 1146–9.

- 22 Zipes D, Libby P, Bonow RO, Braunwald E. *Braunwald's heart disease: a textbook of cardiovascular medicine*. 7th ed. Philadelphia: Saunders; 2005. p. 1124–5.
- 23 Weidemann F, Dommke C, Bijnens B, et al. Defining the transmurality of a chronic myocardial infarction by ultrasonic strain-rate imaging: implications for identifying intramural viability: an experimental study. *Circulation* 2003; **107**: 883–8.
- 24 Zipes D, Libby P, Bonow RO, Braunwald E. *Braunwald's heart disease: a textbook of cardiovascular medicine*. 7th ed. Philadelphia: Saunders; 2005. p. 1198–1216.
- 25 Derumeaux G, Loufoua J, Pontier G, Cribier A, Ovize M. Tissue Doppler imaging differentiates transmural from nontransmural acute myocardial infarction after reperfusion therapy. *Circulation* 2001; **103**: 589–96.
- 26 Weidemann F, Wacker C, Rauch A, et al. Sequential changes of myocardial function during acute myocardial infarction, in the early and chronic phase after coronary intervention described by ultrasonic strain rate imaging. *J Am Soc Echocardiogr* 2006; **19**: 839–47.
- 27 Hoffmann R, Altiok E, Nowak B, et al. Strain rate measurement by Doppler echocardiography allows improved assessment of myocardial viability inpatients with depressed left ventricular function. *J Am Coll Cardiol* 2002; **39**: 443–9.
- 28 Bonow RO, Vitale DF, Bacharach SL, Frederick TM, Kent KM, Green MV. Asynchronous left ventricular regional function and impaired global diastolic filling in patients with coronary artery disease: reversal after coronary angioplasty. *Circulation* 1985; **71**: 297–307.
- 29 Pislaru C, Belohlavek M, Bae RY, Abraham TP, Greenleaf JF, Seward JB. Regional asynchrony during acute myocardial ischemia quantified by ultrasound strain rate imaging. *J Am Coll Cardiol* 2001; **37**: 1141–8.
- 30 Pislaru C, Bruce CJ, Anagnostopoulos PC, et al. Ultrasound strain imaging of altered myocardial stiffness: stunned versus infarcted reperfused myocardium. *Circulation* 2004; **109**: 2905–10.
- 31 Tanaka H, Kawai H, Tatsumi K, et al. Improved regional myocardial diastolic function assessed by strain rate imaging in patients with coronary artery disease undergoing percutaneous coronary intervention. *J Am Soc Echocardiogr* 2006; **19**: 756–62.
- 32 Liang H, Cauduro S, Pellikka P, et al. Usefulness of two-dimensional speckle strain for evaluation of left ventricular diastolic deformation in patients with coronary artery disease. *Am J Cardiol* 2006; **98**: 1581–6.
- 33 Hoffmann R, Altiok E, Nowak B, et al. Strain rate analysis allows detection of differences in diastolic function between viable and nonviable myocardial segments. *J Am Soc Echocardiogr* 2005; **18**: 330–5.
- 34 Greenbaum RA, Ho SY, Gibson DG, Becker AE, Anderson RH. Left ventricular fibre architecture in man. *Br Heart J* 1981; **45**: 248–63.
- 35 Becker M, Hoffmann R, Kuhl HP, et al. Analysis of myocardial deformation based on ultrasonic pixel tracking to determine transmurality in chronic myocardial infarction. *Eur Heart J* 2006; **27**: 2560–6.
- 36 Liang H, Capriotti A, Lardo A, Keel A, Abraham T. Feasibility, validation and diagnostic accuracy of semi-automated regional strain maps: comparison with coronary angiography and magnetic resonance [abstract]. *Circulation Suppl* November 2006.



# 5

## PART 5

# Noncoronary heart disease



# Tissue Doppler echocardiography in the assessment of hypertensive heart disease

*John D. Merlino and Patrick E. BeDell*

## Hypertensive heart disease

Hypertensive heart disease may be defined as the response of the heart to the afterload imposed on the left ventricle by the progressively increasing arterial pressure and total peripheral resistance produced by hypertensive vascular disease [1]. Sequelae of this state include the promotion of left ventricular hypertrophy, ischemic heart disease, cardiac arrhythmias, and congestive heart failure. The heart responds to long-term pressure overload in an attempt to stabilize cardiac output by means of three main pathways: (1) left ventricular hypertrophy through an increase in myocyte thickness and increased deposition of extracellular matrix, (2) adrenergic stimulation of the heart, and (3) moving to a higher position on the Frank–Starling curve by volume expansion [2]. Echocardiographic evaluation demonstrates a range of abnormalities in these patients from left ventricular hypertrophy and increased left ventricular mass, and normal ejection fraction in the compensatory phase to increased left ventricular size and reduced systolic function in failure. The prevalence of left ventricular hypertrophy by echocardiography is estimated at between 20% and 60% for individuals with hypertension. Left ventricular hypertrophy has been shown to be an independent risk factor for predicting myocardial infarction, sudden cardiac death, and heart failure [3].

## Assessment of hypertensive heart disease by two-dimensional and conventional spectral Doppler

Left ventricular hypertrophy secondary to pressure overload and neurohormonal effects [4] is the primary two-dimensional (2-D) echocardiographic finding in patients with long-standing hypertension. M-mode and two-dimensional linear measurements of normal myocardial wall thickness, primarily of the interventricular septum and posterior walls, have been extensively reported and validated and will not be discussed here. The threshold for defining left ventricular hypertrophy by M-mode and two-dimensional echocardiography is accepted as left ventricular wall thickness exceeding 11 mm [5] in the average adult. Additional (2-D) echocardiographic findings of hypertensive heart disease are an increased left ventricular mass, increased wall stress, and increased left atrial size [5]. Increased left atrial size occurs in response to increased left ventricular end-diastolic filling pressures [5]. Although not often used in the clinical setting, left ventricular mass has been shown to have substantial prognostic importance. Its regression is an end goal of antihypertensive therapy [5]. The most common method for determination of left ventricular mass is the area-length method that uses calculations of mean wall thickness and determinations of major and minor

axis of the left ventricle and may be calculated as follows:

$$\text{LV mass} = 1.05 \{ [5/6A_1(a + d + t)] - [5/6A_2(a + d)] \}$$

where  $t$  is the myocardial thickness determined by  $t = \sqrt{(A_2/\pi)}$ ,  $\alpha$  is the semimajor axis measured from the widest minor-axis radius to the apex, and  $d$  is the semiminor axis from the widest short-axis diameter to the mitral valve plane [6]. Left ventricular wall stress is increased in hypertensive persons. Left ventricular hypertrophy is a compensatory mechanism in an attempt to normalize wall stress in response to increased afterload. Left ventricular wall stress may be calculated for meridional, circumferential, or radial stress and may be assessed as global left ventricular stress or regional wall stress [7]. Global meridional or longitudinal end-systolic wall stress may be calculated as follows:

$$\sigma_{m(es)} = 1.33P(A_m/A_c) \times 10^3 \text{ dyn/cm}^2$$

where  $P$  is left ventricular systolic pressure measured by sphygmomanometer,  $A_m$  is the short-axis area traced at the epicardium, and  $A_c$  is the short-axis trace of the blood pool [8]. Wall stress may be calculated continuously throughout the cardiac cycle; however, this method requires invasive measurements of systolic blood pressure.

Conventional spectral Doppler analysis of patients with hypertensive heart disease is primarily used for the assessment of diastolic function of the left ventricle. Diastolic function is evaluated by the interrogation of the transmitral and pulmonary venous inflows using pulsed-wave Doppler. Conventional spectral Doppler analysis of diastolic function by transmitral and pulmonary venous inflows is known to be more load-dependent than tissue Doppler measurements [5].

Interrogation of the transmitral flow in healthy adults without hypertension demonstrates a transmitral flow profile of the E-wave velocity to A-wave velocity ratio of  $>1$  and an E-wave deceleration time of  $>140$  msec [5]. With early diastolic dysfunction due to hypertension and left ventricular hypertrophy, assessment of changes in filling pressures of the transmitral flow by means of pulsed-wave Doppler may demonstrate a reduced velocity of the transmitral E-wave velocity, signaling a decrease in the left ventricle's ability to fill during the rapid

passive early component of diastole, and an increased velocity of the transmitral A-wave component, exceeding that of the E-wave [9]. These findings reflect a shift of diastolic filling volume from the early rapid passive diastolic filling phase to the late active phase of atrial contraction.

Pulsed-wave Doppler analysis of the pulmonary venous inflow in healthy adults produces an inflow pattern in which the S- and D-wave velocities are relatively equal with an A-wave reversal duration less than that of the transmitral A-wave duration [5]. In the presence of early diastolic dysfunction, the S-wave velocity increases as the D-wave velocity decreases in response to increases in early left ventricular end-diastolic filling pressures and decreased left ventricular relaxation [5]. Left ventricular compliance may remain normal during this phase [5].

As disease progresses from mild to moderate diastolic dysfunction, myocardial stiffness increases, left ventricular relaxation further decreases, left ventricular compliance is now abnormal, and as left ventricular end-diastolic pressures continue to rise, a concomitant rise in left atrial pressure occurs. Assessment of the transmitral flow profile demonstrates a *pseudonormal* filling pattern in which the E-wave velocity of the transmitral inflow again exceeds the velocity of the transmitral A-wave velocity and returns to the original ratio of  $>1$  [5]. This pseudonormal pattern is indistinguishable from the *normal* transmitral filling pattern without assessment of the pulmonary venous inflow. Interrogation of the pulmonary venous inflow will demonstrate a pattern of increased diastolic dysfunction with a now reduced S-wave velocity, and a D-wave velocity greater than the S-wave, or a finding of the A-wave duration greater than the transmitral A-wave plus 30 msec [9]. As left ventricular compliance continues to decrease, left atrial pressure continues to rise [9].

As diastolic function continues to deteriorate, interrogation of the transmitral flow demonstrates a *restrictive* flow profile in which  $E/A > 1.5$  with an E-wave deceleration time of  $<140$  msec. Pulmonary venous inflow will demonstrate a further reduction in S-wave velocity or a finding of the A-wave reversal duration greater than the transmitral A-wave plus 30 msec. Left ventricular compliance is now markedly decreased as left atrial pressure

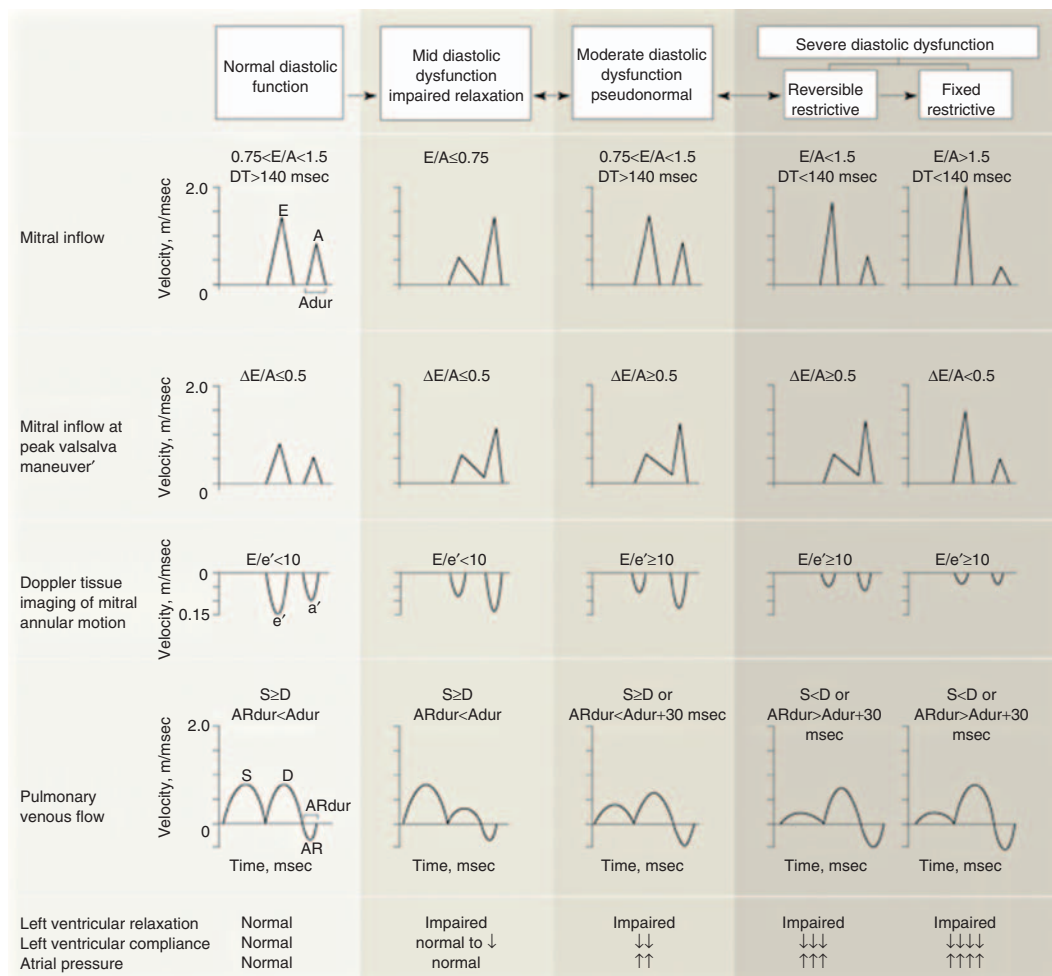


Figure 14.1 "Summary of conventional spectral and tissue Doppler changes with increasing diastolic dysfunction" Printed with permission Redfield MM. et al (2003).

is markedly increased. A summary of the transmural pulsed-wave Doppler changes can be found in Figure 14.1.

### Tissue Doppler echocardiographic findings in hypertensive heart disease

Conventional Doppler findings of transmural inflow in patients with hypertension are highly variable. Hypertensive patients can present with normal transmural inflow filling patterns; however, the more typical presentation is one of diastolic dysfunction. These patterns, however, may be

unreliable given their load-dependent nature [10]. Given this, to more accurately assess left ventricular diastolic and systolic function, it is necessary to find a less load-dependent method of analysis. Tissue Doppler measures are significantly less affected by changes in loading conditions in the heart and, therefore, provide a more reliable measure of the compliance and diastolic function of the left ventricle under various loading conditions [11–14].

Tissue Doppler echocardiography is a relatively new modality in the assessment of heart disease. The nomenclature for describing tissue Doppler waveforms is not well standardized, and significant variations may be noted in the literature. In

this chapter, we use the following terms:  $S_m$ , a positive, peak systolic velocity occurring during ejection;  $E_m$ , a negative velocity corresponding to the conventional Doppler transmitral early, passive E-wave; and  $A_m$ , a negative velocity corresponding to the conventional Doppler transmitral atrial contraction. Tissue Doppler waveforms may be obtained by means of multiple methods: color M-mode, pulsed tissue Doppler, and color-coded tissue Doppler imaging. When discussing pulsed tissue Doppler waveforms, the values expressed are peak values versus color-coded tissue Doppler values that are expressed as mean values obtained from the sample area. Unless otherwise noted, discussions and values presented in this chapter are peak values obtained using pulsed tissue Doppler imaging. A full discussion of the mechanics, advantages, and limitations of tissue Doppler imaging may be found elsewhere in this text.

Current methods of analysis of the left ventricular myocardium by tissue Doppler echocardiography are primarily concentrated on the base to apex longitudinal motion of the left ventricle. Myocardial fibers are oriented circumferentially and longitudinally [15]. Circumferential fibers are located subepicardially, and longitudinal fibers are located in the subendocardium [15]. Contraction of the longitudinal myocardial fibers results in displacement of the mitral annulus toward the apex [16]. As the longitudinal fibers are located in the subendocardium, longitudinal contraction is, therefore, an echocardiographic marker of subendocardial function.

Pathologic left ventricular hypertrophy is associated with subendocardial fibrosis [16]. It has been theorized by Nikolay et al. that a subendocardial defect in norepinephrine uptake may chronically elevate local interstitial catecholamine levels and thereby downregulate  $\beta$ -adrenergic receptors in a spatially heterogeneous distribution between subendocardial and subepicardial layers [17–19]. Because the longitudinal myocardial fibers are located in the subendocardium, they may be more sensitive to changes in the interstitial collagen matrix than the subepicardially located circumferential fibers [16,20–22]. Figure 14.2 demonstrates degrees of myocardial fibrosis from hypertensive patients. Tissue Doppler velocities have been related to the percentage of interstitial fibrosis and

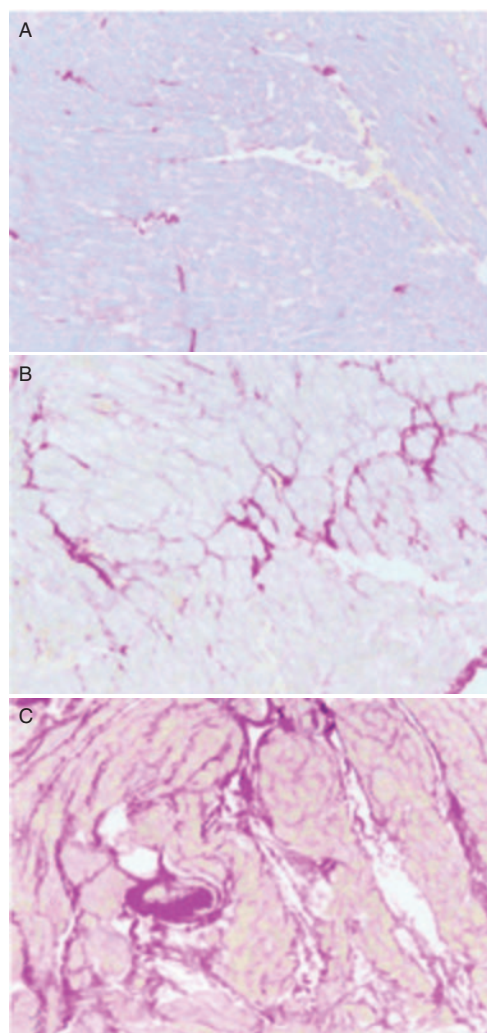


**Figure 14.2** "Endomyocardial tissue from 3 hypertensive patients with minimal interstitial fibrosis (A), mild to moderate interstitial fibrosis (B), and severe fibrosis (C). Sections were stained with picrosirius red, and the interstitial collagen was identified in red" Printed with permission, Diez J. (2000)

the myocardial  $\beta$ -adrenergic receptor density in the myocardium [23].

In a small group of patients with hypertension, coronary artery disease, and globally depressed left ventricular function, Shan et al. [23] measured regional myocardial velocities using tissue Doppler echocardiography. His group then performed biopsies of the corresponding myocardial segments of these hearts. The group found a negative relationship between the degree of interstitial fibrosis

as well as  $\beta$ -adrenoreceptor density and myocardial velocities ( $S_m$  and  $E_m$ ). Their findings provided early evidence that tissue Doppler-assessed myocardial velocities may reflect structural myocardial changes. These data also suggest that the mechanical impact of fibrotic changes in the subendothelial matrix that adversely effect both systolic and diastolic left ventricular performance as assessed by longitudinal tissue Doppler imaging may be detectable before the later involvement of the circumferential fibers, when the impact on systolic and diastolic function is obvious on standard two-dimensional imaging and conventional spectral Doppler.

Fibrotic changes in the myocardium can occur when the rate and extent of collagen degradation and inhibition become unbalanced. Collagen degradation is under the control of the matrix metalloproteinases (MMPs) and their tissue inhibitors (TIMPs). In hypertensive heart disease, if the level of plasma TIMPs are increased and the level of MMPs are decreased, this imbalance will disturb the homeostasis of collagen degradation and promote increased collagen accumulation and fibrosis [24]. Using tissue Doppler echocardiography to assess hypertensive patients with diastolic dysfunction, Nadar et al. [25] found good correlation between the tissue Doppler  $E_m$  and  $E/E_m$  ratio with abnormalities in the MMPs. Their study found a significant inverse correlation between MMP-9 and TIMP-1 with  $E_m$  and a significant positive correlation between the MMPs and  $E/E_m$  ratio. Their work also suggests that changes in the matrix turnover may be responsible for diastolic dysfunction.

Changes in tissue velocity measurements of the myocardium may be found in patients with hypertension before the development of left ventricular hypertrophy or left atrial enlargement [14,26–28]. In general, tissue velocity findings in patients with hypertension include a reduction in the velocity of  $S_m$  and  $E_m$ , an increase in the velocity of the late diastolic  $A_m$  atrial contraction, and a decreased  $E_m/A_m$  ratio. A summary of the changes in tissue Doppler waveforms with hypertension and left ventricular hypertrophy is noted in Figure 14.3 [14,29–31]. Additionally, the ratio of  $E/E_m$ , which has been shown to be directly related to end-diastolic filling pressure and is obtained from the conventional Doppler E-wave and the tissue

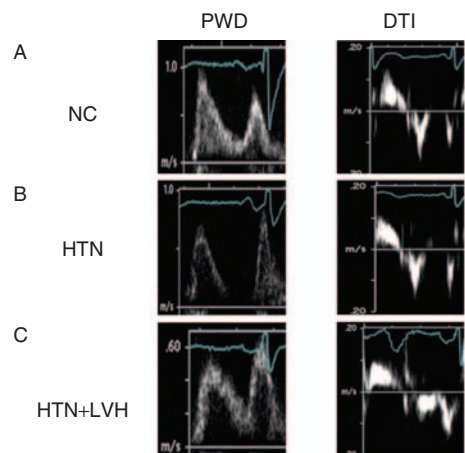


**Figure 14.3** Changes in conventional spectral and tissue Doppler waveforms with hypertension and LVH." adapted with permission, Davila-Roman et al. (2006)

Doppler  $E_m$  from the lateral mitral annulus, is significantly higher in patients with hypertension [31]. Peak systolic and early diastolic measures of strain and strain rate are also impacted in these patients [32].

Rovner et al. [33] performed tissue Doppler measurements in a group of patients with hypertension and patients with hypertension and left ventricular hypertrophy and compared them to normal controls. His group determined that there were statistically significant differences among all three patient groups using the tissue Doppler measurement of  $E/E_m \text{ global}$ , where  $E$  is the transmural peak early diastolic velocity obtained by conventional Doppler, and  $E_m \text{ global}$  is the average of four basal sites (anterior, lateral, septal, and inferior) obtained by tissue Doppler. They also determined that there was a statistically significant difference among all groups if  $E/E_m \text{ septal}$  was substituted for  $E/E_m \text{ global}$ . These findings suggest that the  $E_m \text{ septal}$  obtained by pulsed-wave tissue Doppler is a more sensitive marker for the detection of abnormalities in left ventricular diastolic dysfunction than other individual annulus sites. Furthermore, their study found evidence that suggests elevation of left ventricular filling pressure is an early abnormality in the progression of hypertensive heart disease and that the development of left ventricular hypertrophy is not only associated with abnormal

relaxation, but is accompanied by further increases in left ventricular filling pressures. Bountiokos et al. [31] demonstrated tissue Doppler findings consistent with other investigators. His group found a statistically significant decrease in systolic velocities in patients with normal left ventricular ejection fraction and hypertension versus normal controls. In these hypertensive patients, early diastolic velocities were also reduced. Additionally, his group found  $E/E_m$  to be significantly increased in the hypertensive group. Di Bello et al. [34] assessed previously untreated patients with essential hypertension versus controls. Their study found that conventional Doppler  $E/A$  was able to discriminate between hypertensive patients and normal controls only 25% of the time, but tissue Doppler  $E_m/A_m$  correctly identified normal controls from hypertensive patients 91% of the time. In their study,  $E_m/A_m$  was also found to be useful in the discrimination of normal versus pseudonormal mitral filling waveforms and could be considered an early index of diastolic filling when conventional mitral inflow is normal.

In a study by Yuda et al. [32] in patients with hypertensive left ventricular hypertrophy with normal and abnormal diastolic function, assessed by conventional spectral Doppler, reductions were demonstrated in both peak systolic strain and strain rate in patients with hypertensive left ventricular hypertrophy with and without diastolic dysfunction versus controls. They found a further reduction in peak systolic strain and strain rate between patients with left ventricular hypertrophy and normal diastolic function versus patients with left ventricular hypertrophy and diastolic dysfunction. Their work suggests that the development of left ventricular hypertrophy may precede diastolic dysfunction in some hypertensive persons as assessed by strain imaging. Støylen et al. [35] found similar findings in a group of hypertensive patients with normal left ventricular ejection fraction and diastolic dysfunction. His group found a reduction in systolic and early diastolic tissue velocities and strain rates with no significant increase in late diastolic tissue velocity and strain.

To date, assessment of circumferential motion of the left ventricular myocardium by tissue Doppler echocardiography has been less well-investigated than its longitudinal counterpart. This finding is largely due to technical issues that have been

recently overcome through the advent of color-coded tissue Doppler echocardiography. Evaluation of the myocardium radially is limited to the anteroseptum and posterior wall in the parasternal views due to Doppler angle limitations.

Przewlocka-Kosmala et al. [36] evaluated hypertensive patients with increased left ventricular mass and normal ejection fractions compared to normal controls. Her group measured longitudinal myocardial tissue velocities from six basal sites and circumferential velocities from the mid-anteroseptum and posterior walls. Their study yielded findings similar to other investigators with regard to longitudinal tissue velocities in hypertensive patients: decreased  $S_m$  and  $E_m$  velocities, and a decrease in the  $E_m/A_m$  ratio. Interestingly, these patients had normal two-dimensional echocardiographic measures of circumferential systolic shortening; however, her group found a statistically significant increase in circumferential systolic ( $S_m$ ) velocities from the mid-anteroseptum and a similar, although statistically insignificant, trend in the mid-posterior wall. As with tissue early diastolic longitudinal velocities, early diastolic circumferential velocities and the tissue  $E_m/A_m$  ratio were reduced. This work suggests that the circumferential fibers may act in a compensatory manner to maintain normal ejection fraction in the presence of impaired systolic longitudinal fiber function in hypertensive hearts.

The results of large epidemiological trials suggest that hypertension, or a history of hypertension, accounts for nearly half of all cases of heart failure [37]. Left ventricular hypertrophy and left ventricular diastolic dysfunction are indicators of end-organ damage; either condition may be considered evidence of hypertensive heart disease [38]. Early detection of left ventricular diastolic dysfunction by tissue Doppler echocardiography before the development of left ventricular hypertrophy, detected by conventional two-dimensional echocardiography in hypertensive patients, may represent a clinical finding that may justify earlier treatment aimed at reducing cardiovascular morbidity and mortality [33]. It is significant to note that hypertensive patients with normal conventional Doppler and normal two-dimensional findings may have abnormal tissue Doppler findings. We have previously described hypertensive patients with findings of normal left ventricular ejection fraction with reduced systolic ( $S_m$ ) tissue

Doppler velocities. Given this finding, hypertensive patients with apparently normal systolic function as assessed by conventional methods (left ventricular ejection fraction) may have early systolic dysfunction detectable by tissue Doppler echocardiography. Furthermore, patients previously thought to have congestive heart failure attributed to isolated diastolic dysfunction may, in fact, have concomitant, previously undetectable systolic dysfunction now made detectable by tissue Doppler echocardiography [31]. Table 14.1 demonstrates changes in tissue velocities, strain, and strain rates in hypertensive patients.

### Clinical utility of tissue Doppler echocardiography

Although tissue Doppler imaging has yielded much interesting information about the systolic and diastolic function of the hypertensive heart, tissue Doppler echocardiography has not yet demonstrated much clinical utility in this clinical population. Tissue Doppler has been shown to have clinical utility in the following two areas: (1) estimation of left ventricular filling pressures (see Chapter 5) and (2) differentiation of pathologic left ventricular hypertrophy from physiologic hypertrophy in the athlete's heart. A developing area of clinical utility is the discrimination of the patient with left ventricular hypertrophy as a result of infiltrative

cardiomyopathies from other etiologies of left ventricular hypertrophy.

### Pathologic versus physiologic left ventricular hypertrophy

Athletes who maintain intense, physical training can present with left ventricular hypertrophy and increased left ventricular mass. These findings occur in approximately 2% of elite athletes [39]. Increased left ventricular mass may occur by two means. The chamber size may increase with wall thickness remaining normal or the chamber size may remain normal with an increase in wall thickness [40]. In physiological left ventricular hypertrophy, the increase in ventricular mass is characterized by a normal organization of cardiac structure and no collagen increase [41]. In contrast, in pathologic left ventricular hypertrophy, structural changes and collagen accumulation accompany myocyte hypertrophy and may progressively lead to systolic and diastolic myocardial dysfunction [41–43]. It is important to differentiate patients with increased left ventricular mass due to physical training from those with pathologic hypertension or other conditions from which left ventricular hypertrophy may result so that treatment may be instituted only when appropriate. Figure 14.4 shows the discriminating value of tissue S velocity between physiologic left ventricular hypertrophy and pathologic left ventricular hypertrophy and hypertrophic cardiomyopathy.

**Table 14.1** Changes in tissue Doppler waveforms in hypertension.

	HTN	HTN + LVH
<b>Tissue velocities</b>		
Peak systolic ( $S_m$ )	↓	↓↓
Early diastolic ( $E_m$ )	↓	↓↓
Late diastolic ( $A_m$ )	↑	↑↑
$E_m/A_m$ ratio	↓	↓↓
<b>Strain</b>		
Peak systolic	↓	↓↓
Early diastolic	N/A	N/A
Late diastolic	N/A	N/A
<b>Strain rate</b>		
Peak systolic	↓	↓↓
Early diastolic	↓	↓↓
Late diastolic	↔	↔

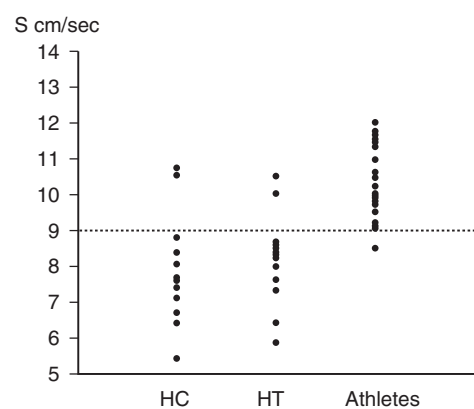


**Figure 14.4** Individual values of 4-site average systolic velocity of mitral annular motion, in patients with HC, systemic hypertension (HT), and in athletes. Dotted line, the best discriminant cut-off value obtained in the analyses of sensitivity and specificity." Printed with permission Fraser A. (2001)

It has been demonstrated that it is possible to distinguish between physiological, adaptive left ventricular hypertrophy caused by exercise, as in athletes, from other pathological processes despite similar left ventricular hypertrophic severity. This finding has been demonstrated in patients [44] and in animal models [45] using the myocardial velocity gradient across the thickness of the left ventricular posterior wall. The myocardial velocity gradient is obtained by sampling the posterior wall myocardium at the level of the subendocardium and subepicardium. The subepicardial layer moves more slowly than the subendothelial layer. Peak systolic and diastolic strain and strain rate may be calculated based on the velocity gradient between these two layers [46]. Derumeaux et al. [45] demonstrated in a group of rats divided into sedentary, exercised, and with aortic banding groups that  $S_m$  values obtained by myocardial velocity gradient were significantly lower in the banded group than in sedentary and exercised animals. This lower  $S_m$  was related to lower endocardial velocities in the banded group, whereas epicardial velocities were similar in the three groups. The group also found  $E_m$  by myocardial velocity gradient was also significantly lower in banded rats than in the other groups. Furthermore, they were able to differentiate the exercise group with physiological hypertrophy from the 2-month banded group representing pathological left ventricular hypertrophy, despite similar left ventricular masses and normal left ventricular fractional shortening and normal left ventricular dP/dtmax.  $S_m$  obtained by myocardial velocity gradient with a cutoff value of  $1 \text{ sec}^{-1}$  clearly separated rats in the banded group, representing pathologic left ventricular hypertrophy, from the exercised animals, representing physiologic hypertrophy, and the sedentary group. Vinereanu et al. using color-coded tissue Doppler [40], demonstrated in a study of athletes, patients with hypertension and left ventricular hypertrophy, and patients with hypertrophic cardiomyopathy that longitudinal systolic  $S_m$  and early diastolic  $E_m$  velocities were decreased in patients with pathologic hypertrophy, but preserved in athletes. Their group found that a mean systolic annular velocity of  $9 \text{ cm/sec}$  (sensitivity 87%, specificity 97%) was the best index to differentiate pathologic from physiologic hypertrophy.

### Infiltrative cardiomyopathies

Although unrelated to hypertensive heart disease, patients with infiltrative cardiomyopathies present with increased left ventricular mass and left ventricular hypertrophy and may be confused with hypertensive heart patients. Tissue Doppler echocardiographic measurements have been shown to be statistically significantly different in patients with amyloid heart [47–50], Fabry cardiomyopathy [51], and Friedreich's ataxia [52] when compared with normal controls. Our current knowledge of tissue Doppler assessment of these conditions is discussed in Chapter 19. The capability of TDI to differentiate patients with left ventricular hypertrophy secondary to infiltrative disease from hypertensive or hypertrophic cardiomyopathy patients has, as of yet, not been investigated, although limited work using speckle tracking echocardiography is under way [53]. These conditions are mentioned here because two-dimensional echocardiography has limited utility in the differentiation of these conditions from patients with hypertensive heart disease. A reliable echocardiographic method to help diagnose these patients would have great clinical utility.

### References

- 1 Frohlich ED, Apstein C, Chobanian AV, et al. The heart in hypertension. *N Engl J Med* 1992; **327**: 998–1008.
- 2 Bristow MR. Mechanisms of development of heart failure in the hypertensive patient. *Cardiology* 1999; **92 Suppl 1**: 3–6.
- 3 Izzo JL Jr, Gradman AH. Mechanisms and management of hypertensive heart disease: from left ventricular hypertrophy to heart failure. *Med Clin North Am* 2004; **88**: 1257–71.
- 4 Muscholl MW, Schunkert H, Muders F, Elsner D, Kuch B, Hense H, Riegger G. Neurohormonal activity and left ventricular geometry in patients with essential arterial hypertension. *Am Heart J* 1998; **135**: 58–66.
- 5 Feigenbaum H, Armstrong W, Ryan T. *Feigenbaum's echocardiography*, 6th ed. Philadelphia: Lippincott Williams & Wilkins; 2005.
- 6 Schiller NB, Shah PM, Crawford M, et al. Recommendations for quantitation of the left ventricle by two-dimensional echocardiography. American Society of Echocardiography Committee on Standards, Subcommittee on Quantitation of Two-Dimensional Echocardiograms. *J Am Soc Echocardiogr* 1989; **2**: 358–67.
- 7 Municino A, de Simone G, Roman M, et al. Assessment of left ventricular function by meridional and circumferential end-systolic stress/minor-axis shortening relations in dilated cardiomyopathy. *Am J Cardiol* 1996; **78**: 544–9.

- 8 Quinones MA, Mokotoff DM, Nouri S, Winters WL, Miller RR. Noninvasive quantification of left ventricular wall stress: validation of method and application to assessment of chronic pressure overload. *Am J Cardiol* 1980; **45**: 782–90.
- 9 Nishimura RA, Tajik AJ. Evaluation of diastolic filling of left ventricle in health and disease: Doppler echocardiography is the clinician's Rosetta Stone. *J Am Coll Cardiol* 1997; **30**: 8–18.
- 10 Falk RH, Comenzo RL, Skinner M. The systemic amyloidosis. *N Engl J Med* 1997; **337**: 898–909.
- 11 Garcia-Fernandez MA, Azevedo J, Moreno M, et al. Regional diastolic function in ischaemic heart disease using pulsed wave Doppler tissue imaging. *Eur Heart J* 1999; **20**: 496–505.
- 12 Lindstrom L, Wranne B. Pulsed tissue Doppler evaluation of mitral annulus motion: a new window to assessment of diastolic function. *Clin Physiol* 1999; **19**: 1–10.
- 13 Sohn DW, Chai IH, Lee DJ, et al. Assessment of mitral annulus velocity by Doppler tissue imaging in the evaluation of left ventricular diastolic function. *J Am Coll Cardiol* 1997; **30**: 474–480.
- 14 Borges MC, Colombo R, Goncalves J, Ferreira J, Franchini K. Longitudinal mitral annulus velocities are reduced in hypertensive subjects with or without left ventricular hypertrophy. *Hypertension* 2006; **47**: 854–60.
- 15 Greenbaum RA, Ho SY, Gibson DG, Becker AE, Anderson RH. Left ventricular fibre architecture in man. *Br Heart J* 1981; **45**: 248–63.
- 16 Jones CJ, Raposo L, Gibson D. Functional importance of the long-axis dynamics of the human left ventricle. *Br Heart J* 1990; **63**: 215–20.
- 17 Beau SL, Saffitz JE. Transmural heterogeneity of nor-epinephrine uptake in failing human hearts. *J Am Coll Cardiol* 1994; **23**: 579–85.
- 18 Beau SL, Tolley TK, Saffitz JE. Heterogeneous transmural distribution of beta-adrenergic receptor subtypes in failing human hearts. *Circulation* 1993; **88**: 2501–9.
- 19 Nikitin NP, Witte K. Applications of tissue Doppler imaging in cardiology. *Cardiology* 2004; **101**: 170–84.
- 20 Pick R, Janicki JS, Weber KT. Myocardial fibrosis in non-human primate with pressure overload hypertrophy. *Am J Pathol* 1989; **135**: 771–81.
- 21 Pearlman ES, Weber KT, Janicki JS, Pietra G, Fishman H. Muscle fiber orientation and connective tissue content in the hypertrophied human heart. *Lab Invest* 1982; **46**: 158–64.
- 22 Huysman JA, Vliegen HW, Van der Laarse A, Eulderink F. Changes in nonmyocyte tissue composition associated with pressure overload of hypertrophic human hearts. *Pathol Res Pract* 1989; **184**: 577–81.
- 23 Shan K, Bick RJ, Poindexter BJ, et al. Relation of tissue Doppler derived myocardial velocities to myocardial structure and beta-adrenergic receptor density in humans. *J Am Coll Cardiol* 2000; **36**: 891–6.
- 24 Ahmed SH, Clark LL, Pennington WR, Webb CS, Bonnema DD, Leonardi AH. Matrix metalloproteinases/tissue inhibitors of metalloproteinases: relationship between changes in proteolytic determinants of matrix composition and structural, functional, and clinical manifestations of hypertensive heart disease. *Circulation* 2006; **113**: 2089–96.
- 25 Nadar S, Tayebjee M, Lip GY. Diastolic dysfunction in hypertensives as assessed by tissue Doppler: relation to matrix metalloproteinases. *Echocardiography* 2004; **21**: 485.
- 26 Huysman JA, Vliegen HW, Van Der Laarse A, Eulderink F. Changes in nonmyocyte tissue composition associated with pressure overload of hypertrophic human hearts. *Pathol Res Pract* 1989; **184**: 577–81.
- 27 Querejeta R, Varo N, Lopez B, et al. Serum carboxy-terminal propeptide of procollagen type I is a marker of myocardial fibrosis in hypertensive heart disease. *Circulation* 2000; **101**: 1729–35.
- 28 Schafer S, Kelm M, Mingers S, Strauer BE. Left ventricular remodeling impairs coronary flow reserve in hypertensive patients. *J Hypertens* 2002; **20**: 1431–7.
- 29 Wang M, Yip GW, Wang AY, et al. Peak early diastolic mitral annulus velocity by tissue Doppler imaging adds independent and incremental prognostic value. *J Am Coll Cardiol* 2003; **41**: 820–6.
- 30 Palka P, Lange A, Fleming AD, et al. Age-related transmural peak mean velocities and peak velocity gradients by Doppler myocardial imaging in normal subjects. *Eur Heart J* 1996; **17**: 940–50.
- 31 Bountiokos M, Schinkel A, Bax J, Lampropoulos S, Poldermans D. The impact of hypertension on systolic and diastolic left ventricular function. A tissue Doppler echocardiographic study. *Am Heart J* 2006; **151**: 1323. e7–12.
- 32 Yuda S, Short L, Leano R, Marwick TH. Myocardial abnormalities in hypertensive patients with normal and abnormal left ventricular filling: a study of ultrasound tissue characterization and strain. *Clin Sci* 2002; **103**: 283–93.
- 33 Rovner A, Fuentes L, Waggoner A, Memon N, Chohan W, Davila-Roman V. Characterization of left ventricular diastolic function in hypertension by use of Doppler Tissue imaging and color M-mode techniques. *J Am Soc Echocardiogr* 2006; **19**: 872–9.
- 34 Di Bello V, Giorgi D, Pedrinelli R, et al. Left ventricular hypertension and its regression in essential arterial hypertension. *Am J Hypertens* 2004; **17**: 882–90.

- 35 Støylen A, Slørdahl S, Skjelvan GK, Heimdal A, Skjaerpe T. Strain rate imaging in normal and reduced diastolic function: comparison with pulsed Doppler tissue imaging of the mitral annulus. *J Am Soc Echocardiogr* 2001; **14**: 264–74.
- 36 Przewlocka-Kosmala M, Kosmala W, Mazurek W. Left ventricular circumferential function in patients with essential hypertension. *J Hum Hypertens* 2006; **20**: 666–71.
- 37 Richards AM, Nicholls MG, Troughton RW. Antecedent hypertension and heart failure after myocardial infarction. *J Am Coll Cardiol* 2002; **39**: 1182–8.
- 38 Schillaci G, Pasqualini L, Verdecchia P, et al. Prognostic significance of left ventricular diastolic dysfunction in essential hypertension. *J Am Coll Cardiol* 2002; **39**: 2005–11.
- 39 Ho CY, Sweitzer NK, McDonough B, et al. Assessment of diastolic function with Doppler tissue imaging to predict genotype in preclinical Hypertrophic cardiomyopathy. *Circulation* 2002; **105**: 2992–7.
- 40 Vinereanu D, Florescu N, Sculthorpe N, Tweddel AC, Stephens MR, Fraser AG. Differentiation between pathologic and physiologic left ventricular hypertrophy by tissue Doppler assessment of long-axis function in patients with hypertrophic cardiomyopathy or systemic hypertension and in athletes. *Am J Cardiol* 2001; **88**: 53–58.
- 41 Medugorac I. Myocardial collagen in different forms of heart hypertrophy in the rat. *Res Exp Med (Berl)* 1980; **177**: 201–11.
- 42 Weber KT, Janicki JS, Pick R, Capasso J, Anversa P. Myocardial fibrosis and pathologic hypertrophy in the rat with renovascular hypertension. *Am J Cardiol* 1990; **65**: 1G–7G.
- 43 Hess OM, Schneider J, Koch R, Bamert C, Grimm J, Krayenbuehl HP. Diastolic function and myocardial structure in patients with myocardial hypertrophy: special reference to normalized viscoelastic data. *Circulation* 1981; **63**: 360–71.
- 44 Palka P, Lange A, Fleming AD, et al. Differences in myocardial velocity gradient measured throughout the cardiac cycle in patients with Hypertrophic cardiomyopathy, athletes and patients with left ventricular hypertrophy due to hypertension. *J Am Coll Cardiol* 1997; **30**: 760–8.
- 45 Derumeaux G, Mulder P, Richard V, et al. Tissue Doppler imaging differentiates physiological from pathological pressure-overload left ventricular hypertrophy in rats. *Circulation* 2002; **105**: 1602–8.
- 46 Garcia MJ, Thomas JD, Klein AL. New Doppler echocardiographic applications for the study of diastolic function. *J Am Coll Cardiol* 1998; **32**: 865–75.
- 47 Koyama J, Ray-Sequin PA, Falk RH. Longitudinal myocardial function by tissue Doppler velocity, strain, and strain rate tissue Doppler echocardiography in patients with AL (primary) cardiac amyloidosis. *Circulation* 2003; **107**: 2446–52.
- 48 Klein AL, Hatle LK, Burstow DJ, et al. Doppler characterization of left ventricular diastolic function in cardiac amyloidosis. *J Am Coll Cardiol* 1989; **13**: 1017–26.
- 49 Klein AL, Hatle LK, Taliercio CP, et al. Serial Doppler echocardiographic follow-up of left ventricular diastolic function in cardiac amyloidosis. *J Am Coll Cardiol* 1990; **16**: 1135–41.
- 50 Koyama J, Davidoff R, Falk R. Longitudinal myocardial velocity gradient derived from pulsed Doppler tissue imaging in AL amyloidosis: a sensitive indicator of systolic and diastolic dysfunction. *J Am Soc Echocardiogr* 2004; **17**: 36–44.
- 51 Pieroni M, Chimenti C, Ricci R, Sale P, Russo M, Frustaci A. Early detection of Fabry cardiomyopathy by tissue Doppler echocardiography. *Circulation* 2003; **107**: 1978–84.
- 52 Dutka DP, Donnelly JE, Palka P, Lange A, Nunez D, Nihoyannopoulos P. Echocardiographic characterization of cardiomyopathy in Friedreich's ataxia with tissue Doppler echocardiographically derived myocardial velocity gradient. *Circulation* 2000; **102**: 1276–82.
- 53 Sun JP, Greenberg NL, Yang XS, et al. Differentiating pathologic left ventricular hypertrophy by speckle tracking echocardiography. Submitted Abstract, ACC; 2007.

# Using myocardial imaging to identify and manage subclinical heart disease in diabetes mellitus and obesity

Niels Holmark Andersen

## Introduction

The diabetic patient is exceptionally susceptible to developing cardiac failure due to the close relation between diabetes and hypertension, left ventricular (LV) hypertrophy, coronary artery disease, and myocardial infarction. Not only is heart failure more common in patients with diabetes, but its outcome is worse [1,2]. Data from the Framingham Study demonstrate significantly elevated heart failure risk ratios of 5.5 and 10.0, respectively, for diabetic men and women 35 to 64 years of age, and the age-adjusted absolute excess risks associated with diabetes are nine more cases of heart failure per 1,000 men or women per year at all ages. Diabetes is also associated with a population-attributable risk for developing congestive heart failure in men (6%) and women (12%) [3,4].

A diabetes-specific myocardial disease, referred to as *diabetic cardiomyopathy*, was first suggested by a Danish endocrinologist, Knud Lundbæk [5]. Rubler et al. later described the presence of congestive heart failure in a small group of patients with diabetes and renal involvement [6] (Figure 15.1; Video clip 22 ). In these patients, the presence of congestive heart failure could not be attributed to coronary artery disease or hypertension and was attributed to cardiomyopathy related to the presence of diabetes.

Cardiac involvement in diabetes is still an enigma. It represents a continuum of preclinical stages, which evolve over time into marked structural and

functional changes in the myocardium. At the end-stage, the diabetic patient suffers from increasing coronary atherosclerosis and will in most cases develop subendocardial or transmural ischemia or infarction, accompanied by dyspnea and angina pectoris (Figure 15.2). In the final stages, such patients often suffer severe pulmonary congestion and angina symptoms due to left atrial and ventricular dilatation and a reduced ejection fraction. The mortality among patients with diabetes and congestive heart failure is substantial [7].

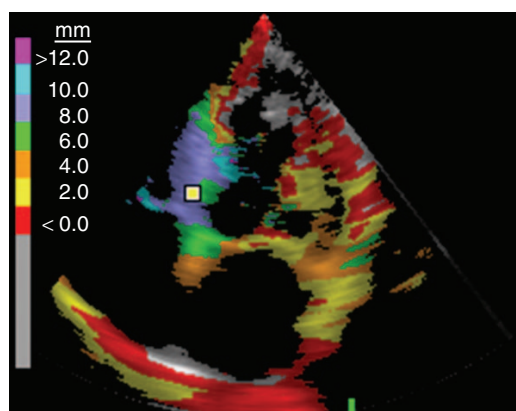


**Figure 15.1** A 63-year-old man with type 2 diabetes mellitus, taking no cardioactive medications, nonhypertensive and with no coronary artery disease. The electrocardiogram (not shown) revealed left bundle-branch block. The tissue tracking image shows significantly reduced long-axis function. See also Video clip 22 .

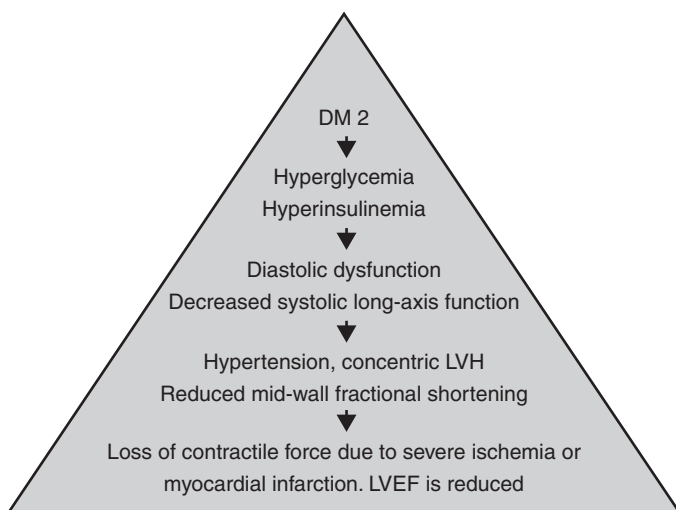


**Figure 15.2** Diagram of the development of heart failure in type 2 diabetes (DM 2). LVH, left ventricular hypertrophy; LVEF, left ventricular ejection fraction. See also Video clip 23

## Myocardial imaging in diabetic patients

Myocardial imaging is the primary approach to the detection of cardiac involvement in diabetes. Since the introduction of tissue Doppler imaging (TDI), substantial knowledge has been gained about the changes in the diabetic heart, knowledge that has brought us a small step closer to understanding the pathophysiological mechanisms behind the diabetic cardiomyopathy.

The presence of LV diastolic dysfunction in patients with normal LV ejection fraction has been proposed as the initial stage in the development of the diabetic cardiomyopathy. This concept is supported by two highly cited Doppler echocardiographic studies that demonstrated the presence of abnormal LV diastolic filling in approximately 50% of normotensive patients with type 2 diabetes and a normal ejection fraction [8,9].

LV hypertrophy (LVH) and diastolic dysfunction are associated with other well known pathophysiological factors, such as microalbuminuria [10,11], hypertension [12] (including the absence of a nocturnal blood pressure dip) [10], endothelial dysfunction [13], and increased carotid intimal thickness [14,15]. The common pathway in these changes is the development of abnormal vascular structure and function.

Systolic dysfunction may occur before or concomitant with diastolic dysfunction. LV systolic function is often described in terms of LV ejection fraction

(LVEF) or fractional shortening (FS), terms that reflect either global or radial shortening of the left ventricle. Although mid-wall FS has been suggested as a measure that could provide additional information about early cardiac involvement in diabetic patients [16], it probably does not provide much information beyond estimation of LV mass [17].

In contrast, the longitudinal systolic contraction of the left ventricle, to which both the outer and inner layers of the myocardium are the primary determinants, seems more susceptible to changes in cardiomyocyte function. These long-axis fibers make a limited contribution to radial shortening (and therefore LVEF); therefore, FS and LVEF do not identify early cardiac involvement. Instead, evaluation of longitudinal function using TDI-derived strain and strain rate appear to be a superior method of quantifying abnormal myocardial contraction or stretching as indicators of subclinical dysfunction [18–20]. When tissue velocity is used as the marker of subclinical disease, the most sensitive marker – in not only diabetic patients but also the elderly and patients with essential hypertension – appears to be the evaluation of systolic rather than systolic function [21–25].

Tissue Doppler echocardiography in asymptomatic type 2 diabetic patients reveals a recognizable pattern of functional changes in the left ventricle in a proportion of patients. This finding has changed the view of subclinical diabetic heart disease (Figure 15.3). The primary indicator in such patients is that their long-axis function is

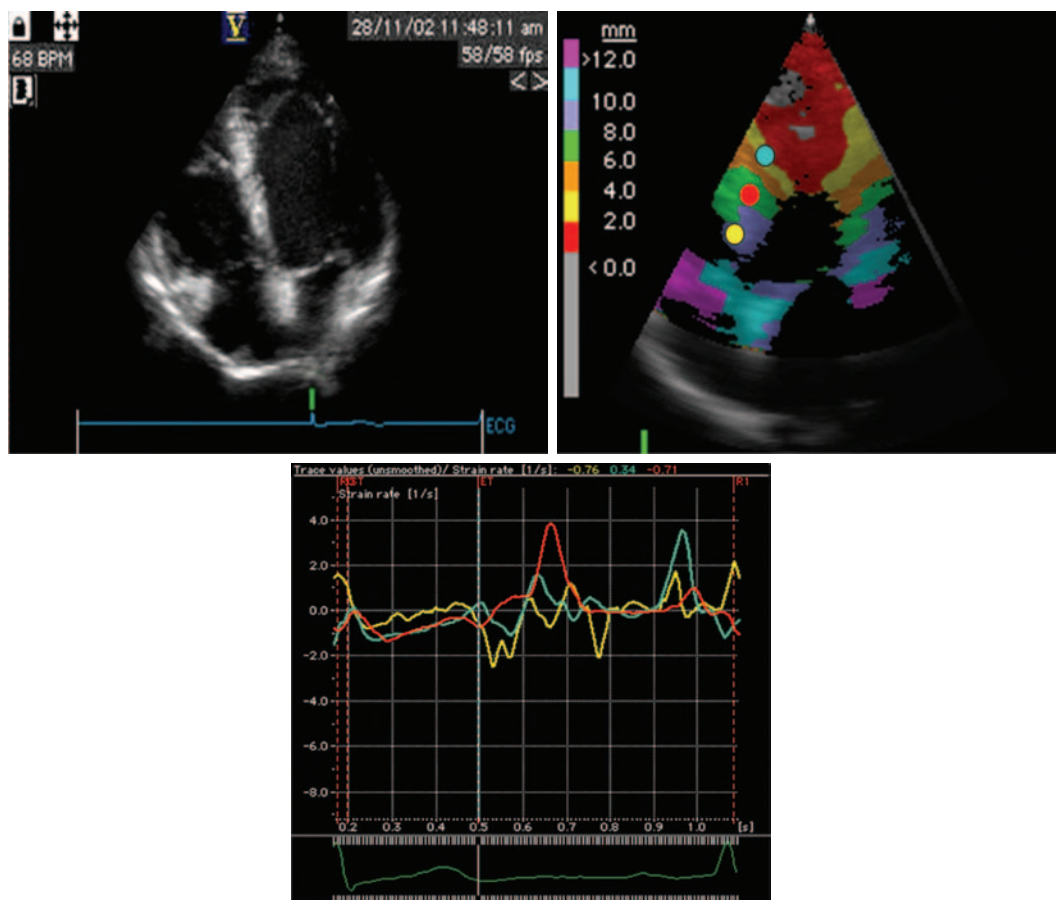


**Figure 15.3** Conventional echocardiography (on the left), tissue Doppler-derived tissue tracking (in the middle), and strain rate imaging of the myocardium (on the right). The patient is a 49-year-old man with type 2 diabetes

and hypertension. Strain rate assessment of the septum reveals decreased long-axis function. The patient is insulin-resistant, and the HbA<sub>1c</sub> is 9%. See also Video clip 24

significantly reduced compared with normal control subjects, even in the earliest stages of the disease, regardless of the presence of LVH [23]. This finding is matched by a compensatory increase in radial function, which exceeds that of normal subjects [26,27] (Video clips 23 and 24 , and explains why this subset of patients has a normal LVEF. This pattern of involvement has been interpreted as evidence of the subendocardium being the primary site of involvement of diabetic myocardial disease. Reduction in function of the longitudinal fibers of the subendocardium leads the radial fibers located in the mid-wall to compensate for the loss of contractile force (Figure 15.4). By inference, reduction of mid-wall function will lead to a more advanced stage of myocardial dysfunction [16].

## Pathophysiological mechanisms

The apparent dysfunction of the subendocardial fibers may be explained by the myocardial milieu of the diabetic patient and the protracted subclinical stage of type 2 diabetes, during which neither physician nor patient is aware of the disease.

## Hypertension

The majority of patients with diabetes, type 1 or type 2, develop hypertension. Patients with type 2 diabetes often suffer from isolated systolic hypertension, partially due to increased stiffening in the large arteries [28]. Over time, elevated blood pressure levels have detrimental effects on LV function, but perhaps more interesting is the question as to

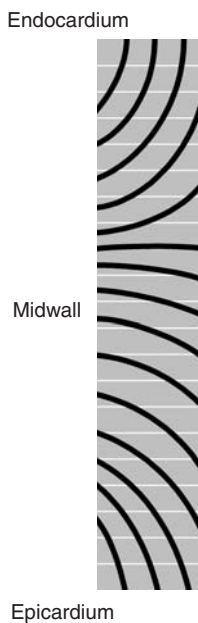


**Figure 15.4** The myocardial muscle fiber orientation.  
Adapted from Streeter et al. [106].

what role the presence of hypertension plays in the early stages of cardiac involvement.

In normal subjects, there is a direct correlation between systolic blood pressure and long-axis function [29]. Nevertheless, a similar correlation between systolic blood pressure and long-axis function has not yet been described in type 2 diabetic patients. Vinereanu and colleagues describe an inverse correlation with diastolic blood pressure, but they also found that the contribution of coexisting arterial hypertension was not significant [27]. Actually, it is even possible to find normotensive diabetic patients with deteriorating long-axis function [23].

Surprisingly, it also appears that lowering blood pressure has no direct relation to long-axis function. A recently published study of 48 type 2 diabetic patients found no connection between a 7 mm Hg systolic blood pressure reduction and changes in systolic strain rate in the long-axis plane. Instead, the study demonstrated a significant correlation between changes in LV mass, which partly reflect changes in blood pressure over time, and long-axis function [30].

However, the role of elevated blood pressure levels cannot be fully discounted, as the MYDID study

demonstrates that the response of patients with type 2 diabetes and hypertension to dobutamine stress at peak systolic velocities ranks under that of normohypertensive patients with diabetes despite similarities in LV mass estimates [31]. The direct relation between long-axis function and arterial hypertension requires further elucidation, but from the available data, it seems that hypertension may play an insignificant role in the mechanism behind the earliest changes in long-axis function and that elevated arterial blood pressure does not truly make its presence felt until a later stage.

### Left ventricular hypertrophy and myocardial fibrosis

The diabetic patient is predisposed to developing LVH. The HyperGen study showed that concentric hypertrophy was the most common type of LVH among type 2 diabetic patients [32]. The pathophysiology behind the different hypertrophy patterns is not fully understood, but it seems that stimulation of myocardial cell growth and activation of the sympathetic nervous system and the renin-angiotensin system (RAS) might preferentially lead to concentric LVH through a direct trophic effect, rather than being due to pressure overload alone [33,34]. In addition, diabetic patients are predisposed to developing a disproportionate amount of myocardial collagen [35], leading to increased stiffness in the left ventricle and possibly also to aggravation of diastolic dysfunction.

The connection between LVH and the loss of long-axis function is well described in both nondiabetic and diabetic patients [10,24,36] (Figure 15.5). Although several different factors contribute to the relation between long-axis function and LV mass, the main factor is the purely mechanical influence exerted by a stiffened and hypertrophic myocardium. Moreover, apoptosis of myocytes, endothelial cells, and fibroblasts is quite pronounced in diabetic individuals [35], especially in patients with hypertension. Such individuals also have more angiotensin II receptors in the apoptotic areas, which indicate the direct influence of the RAS.

A large cross-sectional study by Fang and colleagues showed that one of the major determinants of systolic long-axis dysfunction is a lack of angiotensin converting enzyme (ACE) inhibition, which strongly implicates a direct relation between

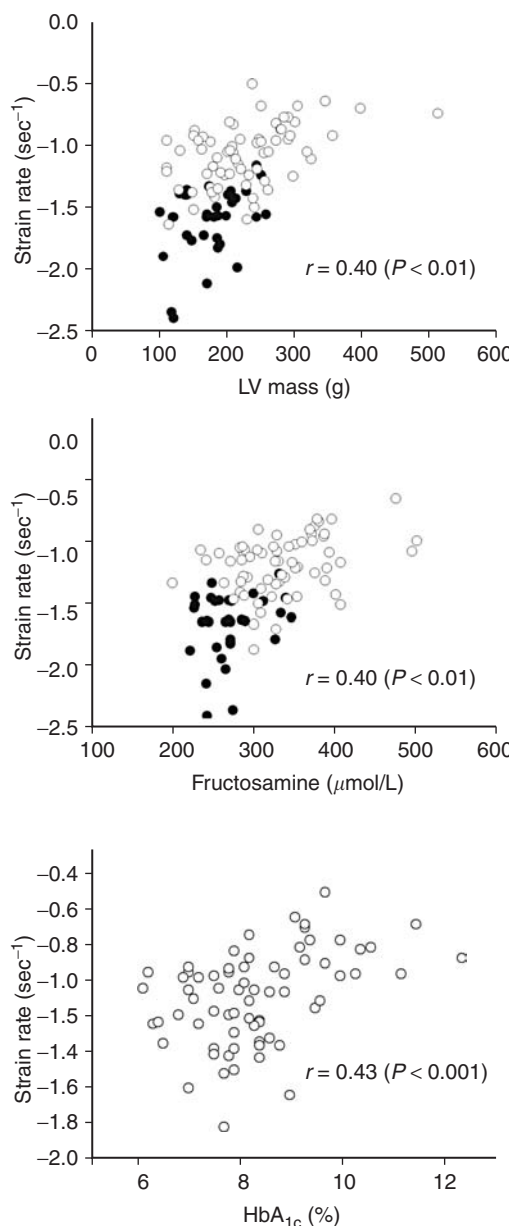


**Figure 15.5** Correlations between strain rate and LV mass, fructosamine, and HbA<sub>1c</sub> in diabetic patients (white circles). Nondiabetic subjects (filled circles) are included to illustrate the relation to normal findings. From Andersen et al. [10].

the deleterious effects of angiotensin II on the myocardium and early signs of cardiac involvement in diabetic patients [37]. At present, there are no randomized studies of ACE inhibition and systolic long-axis function, but a single study found a

correlation between improved long-axis function and reductions in LV mass in patients with the optimized inhibition of RAS blockade [30]. Whether this finding was due to the mechanism of therapy or to the blood pressure lowering itself is not clear.

### Insulin resistance

Insulin resistance is a condition in which normal amounts of insulin are unable to induce a normal insulin response in fatty tissue, skeletal muscle, and liver cells. Insulin resistance elevates free fatty acids in the blood stream, reduces glucose uptake in the skeletal muscle, and reduces liver glucose storage, all effects serving to elevate blood glucose levels. High plasma levels of insulin and blood glucose resulting from insulin resistance are cornerstones in the metabolic syndrome and in type 2 diabetes.

Insulin resistance is linked to obesity, hypertension, LVH, endothelial dysfunction, albuminuria, and coronary heart disease, and seems to have detrimental effects on cardiomyocyte metabolism as well. In short, it may play a significant role in the pathogenesis of decreased cardiac function [38]. Hyperinsulinemia seems to influence cardiomyocyte growth through cellular mechanisms, despite that the cellular mechanisms of insulin are attenuated [39], and hyperinsulinemia can eventually lead to LVH and impaired LV function. Insulin resistance has already been linked to diastolic dysfunction [27] and seems to play a direct role in the early changes in LV systolic function in diabetic patients [40–43]. In a TDI study of LV systolic function in type 2 diabetes, a strong negative correlation was reported between fasting insulin levels, fasting blood glucose levels, and LV systolic strain [37]. These results suggest an additive role of the degree of insulin resistance above and beyond that of hyperglycemia [37]. These findings are supported by another recently published TDI study of obese patients, showing a direct correlation between HOMA-IR values (homeostasis model assessment, surrogate measure of insulin resistance) and systolic strain and strain rate [44]. These findings suggest that correcting insulin resistance would have a favorable effect on systolic long-axis function; in fact, data on this matter are emerging. For instance, a study with 140 type 2 diabetic patients randomized to a lifestyle modification program showed

a significant correlation between improvements in systolic strain and strain rate and improvements in the HOMA index [45]. These findings strongly indicate that myocardial insulin resistance is a potent accessory in the reduction of long-axis function, but that treating insulin resistance leads to improved LV function as a consequence.

The hyperinsulinemia component of insulin resistance can probably account for most of the myocardial changes that occur in obese or type 2 diabetes, but cannot explain the changes seen in lean type 1 diabetic patients. These patients indicate that hyperglycemia may be of considerable importance as well, and this is also true in type 2 diabetes.

### Hyperglycemia

There is a strong correlation between glycemic control and systolic long-axis function in type 2 diabetes. Two separate studies have reported correlations between  $\text{HbA}_{1\text{c}}$  and systolic strain [37] and strain rate [10], with  $r$  values  $> 0.40$  (Figure 15.5), which indicate that the glycemic control of the past 40–60 days has a significant influence on the contractile function of the long-axis plane. The same correlation has been found with s-fructosamine [10], which more or less represents the past 2 weeks of glycemic control.

Changes in  $\text{HbA}_{1\text{c}}$  over time are also significantly related to LV systolic function. For instance, a recently published study of type 2 diabetic patients demonstrates a significant relation between coherent values of  $\text{HbA}_{1\text{c}}$  and LV strain rate over a 12-month follow-up period. Patients with improved glycemic control – defined as a reduction in  $\text{HbA}_{1\text{c}}$  value after 12 months of follow-up (8.3% to 7.4%) – had a significantly improved strain rate compared to that of patients whose  $\text{HbA}_{1\text{c}}$  values had risen compared to baseline (8.2% to 9.1%), even though the two groups had comparable baseline values with regard to systolic blood pressure, LV mass, age, and the duration of diabetes (Figure 15.6) [30].

In type 1 diabetes, the main focus has been on glycemia and diastolic function [46,47]. There is a relation between high glycemic levels and the stiffening of the left ventricle, which seems to diminish when the glycemic levels are reduced [48]. A recently published study, using magnetic resonance imaging, indicated that glycemia and LV systolic function are interrelated in type 1 diabetes

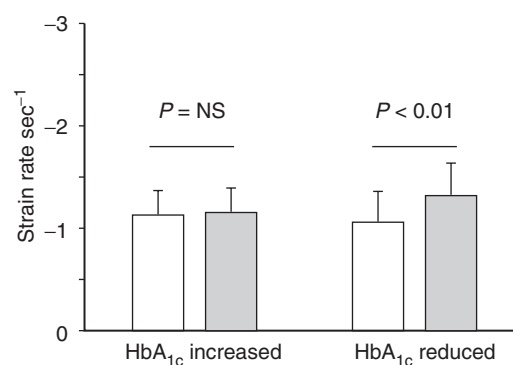


**Figure 15.6** Effects of changes in  $\text{HbA}_{1\text{c}}$  over 12 months in relation to LV systolic strain rate. White bars indicate baseline values, gray bars indicate the 12-month follow-up. The bars display mean values  $\pm$  the standard deviation.  $\text{HbA}_{1\text{c}}$  increased ( $N = 24$ ),  $\text{HbA}_{1\text{c}}$  reduced ( $N = 24$ ). Based on data from Andersen et al. [30].

as well [49]. It is as yet unclear how closely changes in glycemic control are related to LV function in type 1 diabetes, but a recent study demonstrated a significant correlation between alterations in glycemic control and changes in LV function in a subset of type 1 diabetic patients on insulin pump therapy [50].

The mechanism whereby elevated blood glucose levels interfere with the contractile function of the long-axis fibers of the myocardium is unknown, although several theories exist. First, hyperglycemia may directly induce apoptotic cell death and myocyte necrosis [51]. Myocyte apoptosis initiated by hyperglycemia and aggravated by oxidative stress [52] results in myocardial cell loss, which may impair the contractile forces of the myocardium. Chronic hyperglycemia could also affect LV function by means of the reduction of the sarco(endo)plasmatic reticulum  $\text{Ca}^{2+}$ -ATPase [53,54], but this issue is far from settled in humans.

Elevated glucose levels also increase the non-enzymatic glycation of proteins, which induce the irreversible formation and deposit of reactive advanced glycation end-products (AGEs). The formation of AGEs on extracellular matrix components accelerates the process of collagen cross-linking, contributing to myocardial stiffness and hypertrophy [55]. In experimental settings, this phenomenon has been moderated through treatment with a crosslink breaker or an AGE receptor

antibody [56–60]. In human studies, serum levels of AGEs are higher among type 2 diabetic patients with coronary heart disease [61], but little is known about the relation to myocardial function [62,63]. Carboxymethyllysine (CML) is known to bind to a specific AGE receptor (RAGE) and activate NF- $\kappa$ B and proinflammatory cytokine secretion [64], but no significant association has been found between CML and long-axis systolic strain rate in type 2 diabetic patients, with LV function. The lack of any correlation with the noncrosslinking ligand CML brings into question whether CML is related to the involvement of myocardial function in type 2 diabetes. Nevertheless, the correlation between the levels of glycosylated hemoglobin and long-axis function in the study's patients supports the assumption that myocardial crosslinked proteins may, due to glycation, significantly influence myocardial systolic function.

Another issue is glucose transport through the cellular membrane. Increased glucose uptake in hypertrophied hearts is insulin-independent and is associated with, on one hand, the increased expression of the basal glucose transporter GLUT1, and on the other hand, the decreased expression of insulin-regulated glucose transporter GLUT4 [65,66]. These changes in GLUT expression are also partially related to the mitochondrial dysfunction found in the type 2 diabetic patient [67]. Thus, changes in GLUT expression can be partially attributed to hyperglycemia, but they are also a result of insulin resistance [68].

In other words, if glycemic control were optimized, this correction might directly result in improved cardiac function – possibly because it would alter GLUT expression on the surface of the cardiomyocyte, a process that has been shown to have an effect on cardiac function in experimental studies [69,70]. The role of these glucose transporter isoforms and their relation to myocardial function in humans is yet to be clarified.

### **Coronary artery disease or impaired myocardial microperfusion**

Extensive coronary disease is often associated with reduced LV function, and the skeptics might argue that the early stages of diabetic heart disease could be caused by subclinical coronary heart disease. This connection seems unlikely. According to

a large cohort study [71], only 22% of asymptomatic type 2 diabetic patients have silent ischemia, assessed by SPECT. Moreover, the large bulk of data regarding subclinical long-axis function is based upon patients with normal stress echocardiography, which should exclude patients with severe coronary lesions, and one study included the conduct of coronary angiography in selected cases [72]. Finally, the MYDID study was performed on patients with normal coronary angiograms [31].

There is also little reason to justify attribution of these changes to abnormalities of the microcirculation. Although postprandial hyperglycemia has been found to decrease myocardial microperfusion [73], a direct connection to the loss of long-axis function has not been described. Microalbuminuria, a common surrogate for widespread involvement of the microcirculation in diabetes, has not been consistently linked to abnormal long-axis function [10,23]. Finally, a recent study did not find any relationship between abnormal transmural flow and subclinical myocardial long-axis dysfunction in type 2 diabetic patients [74].

### **Biochemical detection**

In a disease as prevalent as diabetes mellitus, the specialized nature of myocardial imaging may limit the availability of echocardiographic assessment to identify myocardial dysfunction. This limitation has increased interest in biochemical detection tools to assess early signs of LV dysfunction, with B-type natriuretic peptide (BNP) seeming to be the most valid method at present. The question is whether BNP can be used as a detection tool in screening for subclinical stages of diabetic heart disease.

Despite its first isolation from the porcine brain [75], BNP is a cardiac hormone that is primarily secreted by the left cardiac ventricle in response to volume expansion and pressure overload [76–78]. BNP levels are elevated in patients with systolic heart failure [79], and in such patients, BNP levels correlate well to their hearts' functional capacities and prognoses [80,81]. In nondiabetic hypertensive individuals with preserved ejection fraction, it seems that increased BNP levels are related to the presence of LVH [82] or diastolic dysfunction [83,84].

In type 2 diabetic patients, BNP levels are elevated when the patient also suffers from congestive heart failure [85], but the same is true for albuminuric patients [86], possibly due to undiagnosed myocardial dysfunction or LVH. However, BNP levels in normoalbuminuric type 2 diabetic patients, have been found to be within normal limits [87,88]. In a study using conventional Doppler, elevated levels of NT-proBNP were only associated with LVH and concomitant left atrial enlargement; moreover, patients with diastolic dysfunction were impossible to identify [88]. Likewise, a study of 101 type 2 diabetic patients with subclinical long-axis dysfunction was not able to link tissue velocities to BNP levels, although BNP was related to LVH [89].

These data suggest that, in the absence of decreased LV ejection fraction, BNP levels in type 2 diabetes may be largely due to the presence of LVH and concomitant left atrial enlargement, and not correlated to the functional status of the diabetic heart. The lack of any relation between BNP and long-axis dysfunction confirms that this very early stage of myocardial dysfunction is insufficient to alter wall stress.

## Intervention

Our recognition and understanding of subclinical myocardial disease in diabetes is currently rudimentary. As yet, it is unknown whether subclinical long-axis dysfunction has any prognostic implications beyond that of standard clinical risk markers such as HbA<sub>1c</sub> [90], blood pressure [91], or microalbuminuria [92]. It seems probable that this will be the case – changes in myocardial function are often witnessed in the absence of other complications of diabetes such as hypertension, microalbuminuria, or retinopathy [23], indicating that long-axis dysfunction might be an independent form of target organ damage in type 2 diabetes.

The appropriate intervention to reverse or at least prevent progression of long-axis dysfunction also remains to be defined. It seems likely that strategies to improve glycemic control and reduce insulin resistance and avoid the progression of LVH through blood pressure lowering therapy will be effective, in support of current guidelines [93]. The role of specific therapies with antifibrotic agents and crosslink breakers remain to be defined.

## Obesity and other variants of diabetic heart disease

Obesity is a multifactorial condition that brings with it increased cardiovascular morbidity and mortality [94]. Several recent studies make connections between changes in the function and structure of the left ventricle and obesity, and some even go so far as to suggest a specific obesity cardiomyopathy [95,96] in which several factors interact.

The obese patient suffers from chronic volume overload, which is probably related to right ventricular (RV) dilation and the reduced RV long-axis function [97]. Despite the prevalence in obstructive sleep apnea in this group, RV dysfunction appears more likely attributable to metabolic disturbance.

Disturbances in LV diastolic function in obese individuals [98] may be partially attributable to abnormalities in ventricular interaction. However, the high prevalence of hypertension in obesity is also likely to be a contributor. The myocardial changes found in hypertensive obese patients seem similar to the changes found in lean hypertensive patients, with one major exception. Increased relative wall thickness and concentric remodeling are often found in the left ventricle [99,100], suggesting that both hypertension and insulin resistance play a role here.

As in type 2 diabetic patients, the substrate metabolism of obese individuals is often deranged, a condition that is actually directly reflected in their myocardial performance. Even in the absence of hypertension, it seems that obesity is associated with significant changes in systolic myocardial deformation properties [44,100,101]. This finding can be found even in children and can involve both the right and left ventricle [102]. Insulin resistance is commonly associated with obesity and seems to be directly linked to LV systolic dysfunction in the nonhypertensive subset of obese individuals [44,95,99,100]. This finding suggests that the myocardium in the obese patient is influenced by the same intrinsic factors as in diabetic patients.

In addition, significant weight loss [103] and physical exercise [104] results in improved LV function for obese patients, a similar reaction to that found in type 2 diabetic patients who improve their

**Table 15.1** Known pathophysiological correlates of long-axis function in type 2 diabetes.

Insulin resistance	Negative correlation to fasting insulin levels (27,37)
Hyperglycemia	Strong negative correlation to HbA <sub>1c</sub> and fructosamine levels (10,30,37)
LV hypertrophy	Negative correlation to LV mass (10,24,36)
Hypertension	No direct relation to blood pressure levels (10,24,27,36,37), possibly an effect through myocardial hypertrophy

glycemic control or reduce their insulin resistance [30,45]. Moreover, this similarity seems to extend to pattern of LV dysfunction, which includes a compensatory increase in radial function [105].

## Conclusions

The availability of TDI has facilitated a closer understanding of the earliest changes in LV function in the diabetic cardiomyopathy. In most cases, the asymptomatic diabetic patient will have significantly reduced systolic long-axis function, often in conjunction with impaired diastolic filling capacities. Such systolic long-axis dysfunction is due to the presence of increased LV mass, insulin resistance, and hyperglycemia, with a limited contribution of hypertension, perhaps mediated by LV mass (summarized in Table 15.1). It is important to note that long-axis dysfunction should not be seen as a chronic, irreversible deterioration of LV function, but as a modifiable change that responds favorably to improvements in glycemic control, LV mass reduction, and improved insulin sensitivity.

## References

- 1 Nichols GA, Gullion CM, Koro CE, Ephross SA, Brown JB. The incidence of congestive heart failure in type 2 diabetes: an update. *Diabetes Care* 2004; **27**: 1879–84.
- 2 Gustafsson I, Brendorp B, Seibaek M, et al. Influence of diabetes and diabetes-gender interaction on the risk of death in patients hospitalized with congestive heart failure. *J Am Coll Cardiol* 2004; **43**: 771–7.
- 3 Levy D, Larson MG, Vasan RS, Kannel WB, Ho KK. The progression from hypertension to congestive heart failure. *JAMA* 1996; **275**: 1557–62.
- 4 Lloyd-Jones DM. The risk of congestive heart failure: sobering lessons from the Framingham Heart Study. *Curr Cardiol Rep* 2001; **3**: 184–90.
- 5 Lundbaek K. Diabetic angiopathy. A specific vascular disease. *Lancet* 1954; **1**: 377–9.
- 6 Rubler S, Drugash J, Yuceoglu YZ, Kumral T, Branwood AW, Grishman A. New type of cardiomyopathy associated with diabetic glomerulosclerosis. *Am J Cardiol* 1972; **30**: 595–602.
- 7 Varela-Roman A, Grigorian SL, Barge CE, Mazon RP, Rigueiro VP, Gonzalez-Juanatey JR. Influence of diabetes on the survival of patients hospitalized with heart failure: a 12-year study. *Eur J Heart Fail* 2005; **7**: 859–64.
- 8 Zabalgoitia M, Ismael MF, Anderson L, Maklady FA. Prevalence of diastolic dysfunction in normotensive, asymptomatic patients with well-controlled type 2 diabetes mellitus. *Am J Cardiol* 2001; **87**: 320–3.
- 9 Poirier P, Bogaty P, Garneau C, Marois L, Dumesnil JG. Diastolic dysfunction in normotensive men with well-controlled type 2 diabetes: importance of maneuvers in echocardiographic screening for preclinical diabetic cardiomyopathy. *Diabetes Care* 2001; **24**: 5–10.
- 10 Andersen NH, Poulsen SH, Poulsen PL, et al. Left ventricular dysfunction in hypertensive patients with Type 2 diabetes mellitus. *Diabet Med* 2005; **22**: 1218–25.
- 11 Salmasi AM, Jepson E, Grenfell A, Kirolos C, Dancy M. The degree of albuminuria is related to left ventricular hypertrophy in hypertensive diabetics and is associated with abnormal left ventricular filling: a pilot study. *Angiology* 2003; **54**: 671–8.
- 12 Bella JN, Palmieri V, Liu JE, et al. Relationship between left ventricular diastolic relaxation and systolic function in hypertension: the Hypertension Genetic Epidemiology Network (HyperGEN) Study. *Hypertension* 2001; **38**: 424–8.
- 13 Charvat J, Michalova K, Chlumsky J, Valenta Z, Kvapil M. The association between left ventricle diastolic dysfunction and endothelial dysfunction and the results of stress myocardial SPECT in asymptomatic patients with type 2 diabetes. *J Int Med Res* 2005; **33**: 473–82.
- 14 Fernandes VR, Polak JF, Edvardsen T, et al. Subclinical atherosclerosis and incipient regional myocardial dysfunction in asymptomatic individuals: the Multi-Ethnic Study of Atherosclerosis (MESA). *J Am Coll Cardiol* 2006; **47**: 2420–8.
- 15 Bertoni AG, Goff DC Jr, D'Agostino RB Jr, et al. Diabetic cardiomyopathy and subclinical cardiovascular disease: the Multi-Ethnic Study of Atherosclerosis (MESA). *Diabetes Care* 2006; **29**: 588–94.

- 16 Hildebrandt P, Wachtell K, Dahlöf B, et al. Impairment of cardiac function in hypertensive patients with Type 2 diabetes: a LIFE study. *Diabet Med* 2005; **22**: 1005–11.
- 17 Verdecchia P, Schillaci G, Borgioni C, et al. Prognostic value of left ventricular mass and geometry in systemic hypertension with left ventricular hypertrophy. *Am J Cardiol* 1996; **78**: 197–202.
- 18 Marwick TH. Measurement of strain and strain rate by echocardiography: ready for prime time? *J Am Coll Cardiol* 2006; **47**: 1313–27.
- 19 Urheim S, Edvardsen T, Torp H, Angelsen B, Smiseth OA. Myocardial strain by Doppler echocardiography. Validation of a new method to quantify regional myocardial function. *Circulation* 2000; **102**: 1158–64.
- 20 Edvardsen T, Urheim S, Skulstad H, Steine K, Ihlen H, Smiseth OA. Quantification of left ventricular systolic function by tissue Doppler echocardiography: added value of measuring pre- and postejection velocities in ischemic myocardium. *Circulation* 2002; **105**: 2071–7.
- 21 Fonseca CG, Dissanayake AM, Doughty RN, et al. Three-dimensional assessment of left ventricular systolic strain in patients with type 2 diabetes mellitus, diastolic dysfunction, and normal ejection fraction. *Am J Cardiol* 2004; **94**: 1391–5.
- 22 Soma J, Dahl K, Wideroe TE. Tissue Doppler imaging of the left ventricle in healthy elderly females does not support the concept of “isolated” diastolic dysfunction. *Blood Press* 2005; **14**: 93–8.
- 23 Andersen NH, Poulsen SH, Eiskjaer H, Poulsen PL, Mogensen CE. Decreased left ventricular longitudinal contraction in normotensive and normoalbuminuric patients with Type II diabetes mellitus: a Doppler tissue tracking and strain rate echocardiography study. *Clin Sci (Lond)* 2003; **105**: 59–66.
- 24 Poulsen SH, Andersen NH, Ivarsen PI, Mogensen CE, Egeblad H. Doppler tissue imaging reveals systolic dysfunction in patients with hypertension and apparent “isolated” diastolic dysfunction. *J Am Soc Echocardiogr* 2003; **16**: 724–31.
- 25 Vinereanu D, Nicolaides E, Tweddel AC, Fraser AG. “Pure” diastolic dysfunction is associated with long-axis systolic dysfunction. Implications for the diagnosis and classification of heart failure. *Eur J Heart Fail* 2005; **7**: 820–8.
- 26 Fang ZY, Leano R, Marwick TH. Relationship between longitudinal and radial contractility in subclinical diabetic heart disease. *Clin Sci (Lond)* 2004; **106**: 53–60.
- 27 Vinereanu D, Nicolaides E, Tweddel AC, et al. Subclinical left ventricular dysfunction in asymptomatic patients with Type II diabetes mellitus, related to serum lipids and glycated haemoglobin. *Clin Sci (Lond)* 2003; **105**: 591–9.
- 28 Smulyan H, Safar ME. The diastolic blood pressure in systolic hypertension. *Ann Intern Med* 2000; **132**: 233–7.
- 29 Andersen NH, Poulsen SH. Evaluation of the longitudinal contraction of the left ventricle in normal subjects by Doppler tissue tracking and strain rate. *J Am Soc Echocardiogr* 2003; **16**: 716–23.
- 30 Andersen NH, Poulsen SH, Poulsen PL, et al. Effects of blood pressure lowering and metabolic control on systolic left ventricular function in Type II diabetes mellitus. *Clin Sci (Lond)* 2006; **111**: 53–9.
- 31 Govind S, Brodin LA, Nowak J, et al. Isolated type 2 diabetes mellitus causes myocardial dysfunction that becomes worse in the presence of cardiovascular diseases: results of the myocardial Doppler in diabetes (MYDID) study 1. *Cardiology* 2005; **103**: 189–95.
- 32 Palmieri V, Bella JN, Arnett DK, et al. Effect of type 2 diabetes mellitus on left ventricular geometry and systolic function in hypertensive subjects: Hypertension Genetic Epidemiology Network (HyperGEN) study. *Circulation* 2001; **103**: 102–7.
- 33 Devereux RB, Roman MJ. Left ventricular hypertrophy in hypertension: stimuli, patterns, and consequences. *Hypertens Res* 1999; **22**: 1–9.
- 34 Verdecchia P, Rebaldi G, Schillaci G, et al. Circulating insulin and insulin growth factor-1 are independent determinants of left ventricular mass and geometry in essential hypertension. *Circulation* 1999; **100**: 1802–7.
- 35 Frustaci A, Kajstura J, Chimenti C, et al. Myocardial cell death in human diabetes. *Circ Res* 2000; **87**: 1123–32.
- 36 Fang ZY, Yuda S, Anderson V, Short L, Case C, Marwick TH. Echocardiographic detection of early diabetic myocardial disease. *J Am Coll Cardiol* 2003; **41**: 611–7.
- 37 Fang ZY, Schull-Meade R, Downey M, Prins J, Marwick TH. Determinants of subclinical diabetic heart disease. *Diabetologia* 2005; **48**: 394–402.
- 38 Sasso FC, Carbonara O, Cozzolino D, et al. Effects of insulin-glucose infusion on left ventricular function at rest and during dynamic exercise in healthy subjects and noninsulin dependent diabetic patients: a radionuclide ventriculographic study. *J Am Coll Cardiol* 2000; **36**: 219–26.
- 39 Poornima IG, Parikh P, Shannon RP. Diabetic cardiomyopathy: the search for a unifying hypothesis. *Circ Res* 2006; **98**: 596–605.
- 40 Fujino T, Ishii Y, Takeuchi T, Hirasawa K, et al. Recovery of BMIPP uptake and regional wall motion in insulin resistant patients following angioplasty for acute myocardial infarction. *Circ J* 2003; **67**: 757–62.
- 41 Peterson LR, Herrero P, Schechtman KB, et al. Effect of obesity and insulin resistance on myocardial substrate metabolism and efficiency in young women. *Circulation* 2004; **109**: 2191–6.

- 42 Monti LD, Landoni C, Setola E, et al. Myocardial insulin resistance associated with chronic hypertriglyceridemia and increased FFA levels in Type 2 diabetic patients. *Am J Physiol Heart Circ Physiol* 2004; **287**: H1225–31.
- 43 Mule G, Nardi E, Cottone S, et al. Influence of metabolic syndrome on hypertension-related target organ damage. *J Intern Med* 2005; **257**: 503–513.
- 44 Di Bello V, Santini F, Di Cori A, et al. Relationship between preclinical abnormalities of global and regional left ventricular function and insulin resistance in severe obesity: a Color Doppler Imaging Study. *Int J Obes (Lond)* 2006; **30**: 948–56.
- 45 Marwick T, Zhang N, Sharman J, Hordern M, Smith L, Prins J. Response of subclinical myocardial dysfunction in diabetes mellitus to lifestyle modification. *Circulation* 2005; **112**: U487.
- 46 Berg TJ, Clausen JT, Torjesen PA, Dahl-Jorgensen K, Bangstad HJ, Hanssen KF. The advanced glycation end product Nepsilon-(carboxymethyl) lysine is increased in serum from children and adolescents with type 1 diabetes. *Diabetes Care* 1998; **21**: 1997–2002.
- 47 Berg TJ, Snorgaard O, Faber J, et al. Serum levels of advanced glycation end products are associated with left ventricular diastolic function in patients with type 1 diabetes. *Diabetes Care* 1999; **22**: 1186–90.
- 48 Grandi AM, Piantanida E, Franzetti I, et al. Effect of glycemic control on left ventricular diastolic function in type 1 diabetes mellitus. *Am J Cardiol* 2006; **97**: 71–6.
- 49 Chung J, Abraszewski P, Yu X, et al. Paradoxical increase in ventricular torsion and systolic torsion rate in type 1 diabetic patients under tight glycemic control. *J Am Coll Cardiol* 2006; **47**: 384–90.
- 50 Andersen NH, Hansen TK, Christiansen JS. Change in glycaemic control are related to the systolic function in type 1 diabetes mellitus. *Scandinavian Cardiovascular Journal*. 2007; **41**: 85–88. DOI: 10.1080/14017430601156384.
- 51 Cai L, Li W, Wang G, Guo L, Jiang Y, Kang YJ. Hyperglycemia-induced apoptosis in mouse myocardium mitochondrial cytochrome C-mediated caspase-3 activation pathway. *Diabetes* 2002; **51**: 1938–48.
- 52 Bojunga J, Nowak D, Mitrou PS, Hoelzer D, Zeuzem S, Chow KU. Antioxidative treatment prevents activation of death-receptor- and mitochondrion-dependent apoptosis in the hearts of diabetic rats. *Diabetologia* 2004; **47**: 2072–80.
- 53 Bidasee KR, Zhang Y, Shao CH, et al. Diabetes increases formation of advanced glycation end products on Sarco (endo) plasmic reticulum Ca<sup>2+</sup>-ATPase. *Diabetes* 2004; **53**: 463–73.
- 54 Abe T, Ohga Y, Tabayashi N, et al. Left ventricular diastolic dysfunction in type 2 diabetes mellitus model rats. *Am J Physiol Heart Circ Physiol* 2002; **282**: H138–48.
- 55 Candido R, Forbes JM, Thomas MC, et al. A breaker of advanced glycation end products attenuates diabetes-induced myocardial structural changes. *Circ Res* 2003; **92**: 785–92.
- 56 Vaitkevicius PV, Lane M, Spurgeon H, et al. A cross-link breaker has sustained effects on arterial and ventricular properties in older rhesus monkeys. *Proc Natl Acad Sci USA* 2001; **98**: 1171–5.
- 57 Asif M, Egan J, Vasan S, et al. An advanced glycation endproduct cross-link breaker can reverse age-related increases in myocardial stiffness. *Proc Natl Acad Sci USA* 2000; **97**: 2809–13.
- 58 Liu J, Masurekar MR, Vatner DE, et al. Glycation end-product cross-link breaker reduces collagen and improves cardiac function in aging diabetic heart. *Am J Physiol Heart Circ Physiol* 2003; **285**: H2587–91.
- 59 Cao Z, Bonnet F, Candido R, et al. Angiotensin type 2 receptor antagonism confers renal protection in a rat model of progressive renal injury. *J Am Soc Nephrol* 2002; **13**: 1773–87.
- 60 Flyvbjerg A, Denner L, Schrijvers BF, et al. Long-term renal effects of a neutralizing RAGE antibody in obese type 2 diabetic mice. *Diabetes* 2004; **53**: 166–172.
- 61 Kilhovd BK, Berg TJ, Birkeland KI, Thorsby P, Hanssen KF. Serum levels of advanced glycation end products are increased in patients with type 2 diabetes and coronary heart disease. *Diabetes Care* 1999; **22**: 1543–8.
- 62 Simm A, Casselmann C, Schubert A, Hofmann S, Reimann A, Silber RE. Age associated changes of AGE-receptor expression: RAGE upregulation is associated with human heart dysfunction. *Exp Gerontol* 2004; **39**: 407–13.
- 63 He CJ, Koschinsky T, Buenting C, Vlassara H. Presence of diabetic complications in type 1 diabetic patients correlates with low expression of mononuclear cell AGE-receptor-1 and elevated serum AGE. *Mol Med* 2001; **7**: 159–68.
- 64 Schalkwijk CG, Baidoshvili A, Stehouwer CD, van Hinsbergh VW, Niessen HW. Increased accumulation of the glycoxidation product Nepsilon-(carboxymethyl) lysine in hearts of diabetic patients: generation and characterisation of a monoclonal anti-CML antibody. *Biochim Biophys Acta* 2004; **1636**: 82–9.
- 65 Paternostro G, Clarke K, Heath J, Seymour AM, Radda GK. Decreased GLUT-4 mRNA content and insulin-sensitive deoxyglucose uptake show insulin resistance in the hypertensive rat heart. *Cardiovasc Res* 1995; **30**: 205–11.
- 66 Nuutila P, Maki M, Laine H, et al. Insulin action on heart and skeletal muscle glucose uptake in essential hypertension. *J Clin Invest* 1995; **96**: 1003–9.
- 67 Lowell BB, Shulman GI. Mitochondrial dysfunction and type 2 diabetes. *Science* 2005; **307**: 384–7.

- 68 Hammarstedt A, Sopasakis VR, Gogg S, Jansson PA, Smith U. Improved insulin sensitivity and adipose tissue dysregulation after short-term treatment with pioglitazone in non-diabetic, insulin-resistant subjects. *Diabetologia* 2005; **48**: 96–104.
- 69 Belke DD, Larsen TS, Gibbs EM, Severson DL. Altered metabolism causes cardiac dysfunction in perfused hearts from diabetic (db/db) mice. *Am J Physiol Endocrinol Metab* 2000; **279**: E1104–13.
- 70 Belke DD, Larsen TS, Gibbs EM, Severson DL. Glucose metabolism in perfused mouse hearts overexpressing human GLUT-4 glucose transporter. *Am J Physiol Endocrinol Metab* 2001; **280**: E420–7.
- 71 Wackers FJ, Young LH, Inzucchi SE, et al. Detection of silent myocardial ischemia in asymptomatic diabetic subjects: the DIAD study. *Diabetes Care* 2004; **27**: 1954–61.
- 72 Kosmala W, Kucharski W, Przewlocka-Kosmala M, Mazurek W. Comparison of left ventricular function by tissue Doppler imaging in patients with diabetes mellitus without systemic hypertension versus diabetes mellitus with systemic hypertension. *Am J Cardiol* 2004; **94**: 395–9.
- 73 Scognamiglio R, Negut C, De Kreutzenberg SV, Tiengo A, Avogaro A. Postprandial myocardial perfusion in healthy subjects and in type 2 diabetic patients. *Circulation* 2005; **112**: 179–84.
- 74 Moir S, Hanekom L, Fang ZY, et al. Relationship between myocardial perfusion and dysfunction in diabetic cardiomyopathy: a study of quantitative contrast echocardiography and strain rate imaging. *Heart* 2006; **92**: 1414–9.
- 75 Sudoh T, Kangawa K, Minamino N, Matsuo H. A new natriuretic peptide in porcine brain. *Nature* 1988; **332**: 78–81.
- 76 Maeda K, Tsutamoto T, Wada A, Hisanaga T, Kinoshita M. Plasma brain natriuretic peptide as a biochemical marker of high left ventricular end-diastolic pressure in patients with symptomatic left ventricular dysfunction. *Am Heart J* 1998; **135**(Pt 1): 825–32.
- 77 Tsutamoto T, Wada A, Maeda K, et al. Plasma brain natriuretic peptide level as a biochemical marker of morbidity and mortality in patients with asymptomatic or minimally symptomatic left ventricular dysfunction. Comparison with plasma angiotensin II and endothelin-1. *Eur Heart J* 1999; **20**: 1799–1807.
- 78 Struthers AD. How to use natriuretic peptide levels for diagnosis and prognosis. *Eur Heart J* 1999; **20**: 1374–5.
- 79 Maisel AS, Krishnaswamy P, Nowak RM, et al. Rapid measurement of B-type natriuretic peptide in the emergency diagnosis of heart failure. *N Engl J Med* 2002; **347**: 161–7.
- 80 McCullough PA, Nowak RM, McCord J, et al. B-type natriuretic peptide and clinical judgment in emergency diagnosis of heart failure: analysis from Breathing Not Properly (BNP) Multinational Study. *Circulation* 2002; **106**: 416–22.
- 81 Omland T, Aakvaag A, Bonarjee VV, et al. Plasma brain natriuretic peptide as an indicator of left ventricular systolic function and long-term survival after acute myocardial infarction. Comparison with plasma atrial natriuretic peptide and N-terminal proatrial natriuretic peptide. *Circulation* 1996; **93**: 1963–9.
- 82 Nishikimi T, Yoshihara F, Morimoto A, et al. Relationship between left ventricular geometry and natriuretic peptide levels in essential hypertension. *Hypertension* 1996; **28**: 22–30.
- 83 Yamaguchi H, Yoshida J, Yamamoto K, et al. Elevation of plasma brain natriuretic peptide is a hallmark of diastolic heart failure independent of ventricular hypertrophy. *J Am Coll Cardiol* 2004; **43**: 55–60.
- 84 Lubien E, DeMaria A, Krishnaswamy P, et al. Utility of B-natriuretic peptide in detecting diastolic dysfunction: comparison with Doppler velocity recordings. *Circulation* 2002; **105**: 595–601.
- 85 Epshteyn V, Morrison K, Krishnaswamy P, et al. Utility of B-type natriuretic peptide (BNP) as a screen for left ventricular dysfunction in patients with diabetes. *Diabetes Care* 2003; **26**: 2081–7.
- 86 Nagai T, Imamura M, Inukai T, Mori M. Brain natriuretic polypeptide in type 2 NIDDM patients with albuminuria. *J Med* 2001; **32**: 169–80.
- 87 Yano Y, Katsuki A, Gabazza EC, et al. Plasma brain natriuretic peptide levels in normotensive noninsulin-dependent diabetic patients with microalbuminuria. *J Clin Endocrinol Metab* 1999; **84**: 2353–6.
- 88 Andersen NH, Poulsen SH, Knudsen ST, Heickendorff L, Mogensen CE. NT-proBNP in normoalbuminuric patients with Type 2 diabetes mellitus. *Diabet Med* 2005; **22**: 188–95.
- 89 Fang ZY, Schull-Meade R, Leano R, Mottram PM, Prins JB, Marwick TH. Screening for heart disease in diabetic subjects. *Am Heart J* 2005; **149**: 349–54.
- 90 Stratton IM, Adler AI, Neil HA, et al. Association of glycaemia with macrovascular and microvascular complications of type 2 diabetes (UKPDS 35): prospective observational study. *BMJ* 2000; **321**: 405–12.
- 91 Adler AI, Stratton IM, Neil HA, et al. Association of systolic blood pressure with macrovascular and microvascular complications of type 2 diabetes (UKPDS 36): prospective observational study. *BMJ* 2000; **321**: 412–9.
- 92 Mogensen CE. Microalbuminuria and hypertension with focus on type 1 and type 2 diabetes. *J Intern Med* 2003; **254**: 45–66.

- 93 Gaede P, Vedel P, Larsen N, Jensen GV, Parving HH, Pedersen O. Multifactorial intervention and cardiovascular disease in patients with type 2 diabetes. *N Engl J Med* 2003; **348**: 383–93.
- 94 Adams KF, Schatzkin A, Harris TB, et al. Overweight, obesity, and mortality in a large prospective cohort of persons 50 to 71 years old. *N Engl J Med* 2006; **355**: 763–78.
- 95 Di Bello V, Santini F, Di Cori A, et al. Obesity cardiomyopathy: is it a reality? An ultrasonic tissue characterization study. *J Am Soc Echocardiogr* 2006; **19**: 1063–71.
- 96 Chinali M, de Simone G, Roman MJ, et al. Impact of obesity on cardiac geometry and function in a population of adolescents: the Strong Heart Study. *J Am Coll Cardiol* 2006; **47**: 2267–73.
- 97 Wong CY, O'Moore-Sullivan T, Leano R, Hukins C, Jenkins C, Marwick TH. Association of subclinical right ventricular dysfunction with obesity. *J Am Coll Cardiol* 2006; **47**: 611–6.
- 98 Sidana J, Aronow WS, Ravipati G, et al. Prevalence of moderate or severe left ventricular diastolic dysfunction in obese persons with obstructive sleep apnea. *Cardiology* 2005; **104**: 107–9.
- 99 Wong CY, O'Moore-Sullivan T, Leano R, Byrne N, Beller E, Marwick TH. Alterations of left ventricular myocardial characteristics associated with obesity. *Circulation* 2004; **110**: 3081–7.
- 100 Peterson LR, Waggoner AD, Schechtman KB, et al. Alterations in left ventricular structure and function in young healthy obese women: assessment by echocardiography and tissue Doppler imaging. *J Am Coll Cardiol* 2004; **43**: 1399–404.
- 101 Levent E, Goksen D, Ozyurek AR, Darcan S, Coker M. Usefulness of the myocardial performance index (MPI) for assessing ventricular function in obese pediatric patients. *Turk J Pediatr* 2005; **47**: 34–8.
- 102 Di Salvo G, Pacileo G, Del Giudice EM, et al. Abnormal myocardial deformation properties in obese, non-hypertensive children: an ambulatory blood pressure monitoring, standard echocardiographic, and strain rate imaging study. *Eur Heart J* 2006; **27**: 2689–95.
- 103 Willens HJ, Chakkro SC, Byers P, et al. Effects of weight loss after gastric bypass on right and left ventricular function assessed by tissue Doppler imaging. *Am J Cardiol* 2005; **95**: 1521–4.
- 104 Gondoni LA, Titon AM, Silvestri G, et al. Short term effects of physical exercise and low calorie diet on left ventricular function in obese subjects: a tissue Doppler study. *Nutr Metab Cardiovasc Dis* 2006.
- 105 Pascual M, Pascual DA, Soria F, et al. Effects of isolated obesity on systolic and diastolic left ventricular function. *Heart* 2003; **89**: 1152–6.
- 106 Streeter DD Jr, Spotnitz HM, Patel DP, Ross J Jr, Sonnenblick EH. Fiber orientation in the canine left ventricle during diastole and systole. *Circ Res* 1969; **24**: 339–47.

# Constrictive pericarditis versus restrictive cardiomyopathy

*Sunil V. Mankad, Seong-Mi Park and Jae K. Oh*

## Introduction

The differentiation of constrictive pericarditis (CP) from restrictive cardiomyopathy (RCM) remains one of the great diagnostic challenges in cardiology [1]. The overlap in clinical presentation and hemodynamic findings seen with CP and RCM often leads to diagnostic uncertainty, and surgical exploration or endomyocardial biopsy is sometimes necessary to establish a definitive diagnosis [2,3]. Despite the emergence of multiple newer imaging techniques such as computed tomography (CT) and magnetic resonance imaging (MRI) that aid in the diagnosis, echocardiography and especially Doppler echocardiography remain pivotal in clinically separating CP from RCM. Although CT and MRI have been demonstrated to be excellent methods of measuring pericardial thickness, the finding of a thickened pericardium does not indicate CP and up to 20% of patients with CP have normal pericardial

thickness by pathologic examination [4]. M-mode (Figure 16.1) and two-dimensional (2-D) echocardiography provide important information about cardiac chamber dimensions, chamber function, pericardial thickening, and pericardial calcification and can characterize the abnormal septal motion seen in CP [5,6]. Routine Doppler echocardiographic techniques are extremely helpful in differentiating CP from RCM. With CP, the following routine Doppler echocardiographic findings are present (Figure 16.2): (1) restrictive mitral inflow velocity ( $E$ ) usually with a  $\geq 25\%$  increase with expiration compared with inspiration and (2) augmented diastolic flow reversals after the onset of expiration ( $\geq 25\%$  of forward diastolic velocity) [7–10]. In a classic study validating these techniques, Doppler echocardiography correctly diagnosed 22 of 25 (88%) patients with CP preoperatively and also predicted functional response to pericardectomy [9]. However, routine Doppler echocardiography

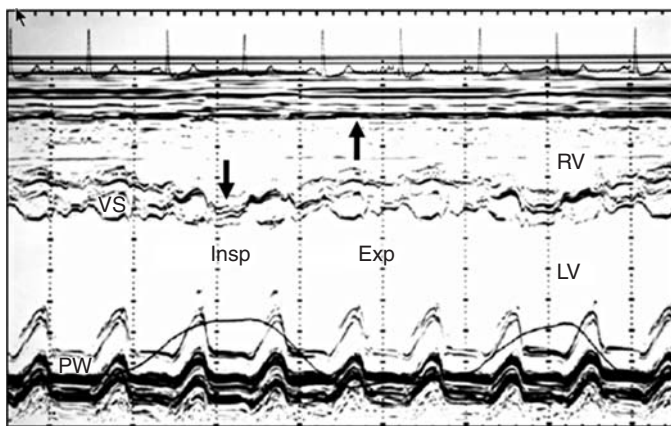


**Figure 16.1** M-mode echocardiogram of the left ventricle with simultaneous respirometer recording. The ventricular septum (VS) shifts toward the left ventricle (LV) with inspiration (downward arrow) and moves toward the right ventricle (RV) with expiration (upward arrow). This ventricular septal motion changes with respiration is related to the increased interventricular dependence in constrictive pericarditis. Reproduced with permission from Oh et al. *The echo manual*. 3rd ed. Philadelphia: Lippincott, Williams, & Wilkins; 2006.

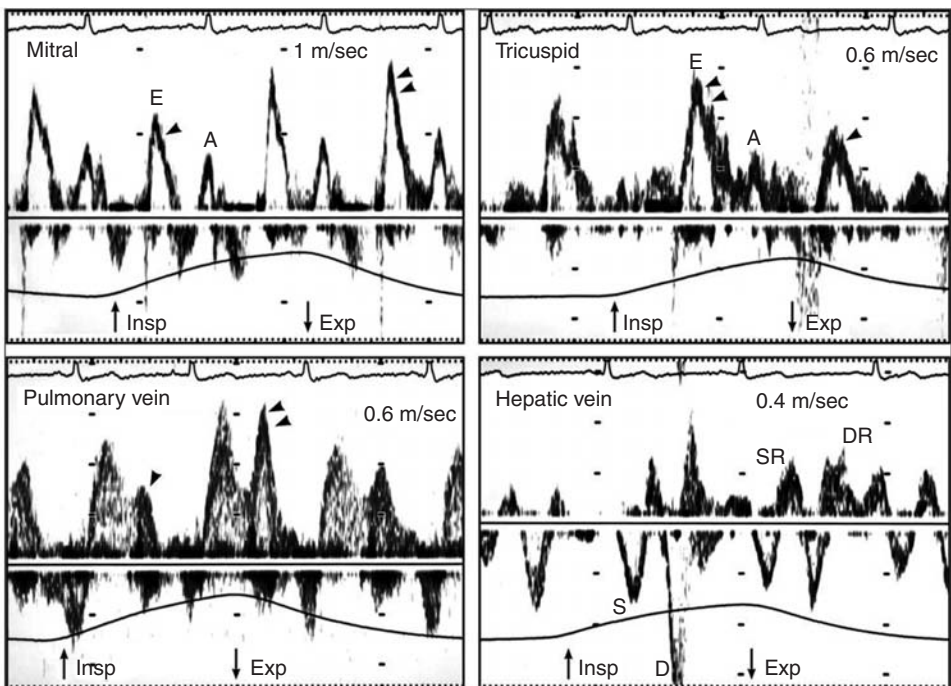


**Figure 16.2** Pulsed-wave Doppler recording of the mitral inflow, tricuspid inflow, pulmonary vein, and hepatic vein velocities of CP with a simultaneous recording

of respiration. Reproduced with permission from Oh et al. *The echo manual*. 3rd ed. Philadelphia: Lippincott, Williams, & Wilkins; 2006.

may be rendered less reliable in certain confounding situations, such as in patients with underlying lung disease or in patients with right ventricular systolic dysfunction. Although the Doppler echo findings of CP in some of these patients may be unmasked with additional echocardiographic maneuvers to reduce preload [11], in some cases, the diagnosis still remains equivocal and indistinguishable from RCM. Therefore, a less load-dependent imaging modality that could distinguish between CP and RCM by directly measuring intrinsic mechanical and elastic properties of the myocardium would likely be of benefit.

### Tissue Doppler echocardiography of the mitral annulus

Tissue Doppler echocardiography (TDE) allows the acquisition of myocardial or mitral annular velocities for online or offline analysis [12,13]. Mitral annular motion was initially reported by Zaky et al. [14] using M-mode echocardiography. The mitral annulus descends toward a stationary

apex during systole and reflects the extent of longitudinal fiber shortening. During diastole, the mitral annulus returns toward the base and is characterized by two distinct waves in patients in sinus rhythm (Figure 16.3). Because the rate of left ventricular relaxation is affected by primary myocardial disease but not by CP, direct determination of myocardial wall expansion or mitral annular velocities may be useful in differentiating RCM from CP. This hypothesis was first tested in a preliminary series of patients by Garcia et al. [15]. They studied 16 consecutive patients referred for right heart failure for evaluation of the presence of CP or RCM. After excluding one patient who was diagnosed with primary pulmonary hypertension, the results of all diagnostic tests were reviewed and patients were classified as either having CP ( $n = 8$ ) or RCM ( $n = 7$ ). Patients then underwent comprehensive routine transmitral Doppler echocardiography and pulsed TDE of the lateral aspect of the mitral annulus during apnea. Systolic and diastolic longitudinal axial velocities of the mitral annulus were recorded (average of three to six beats).

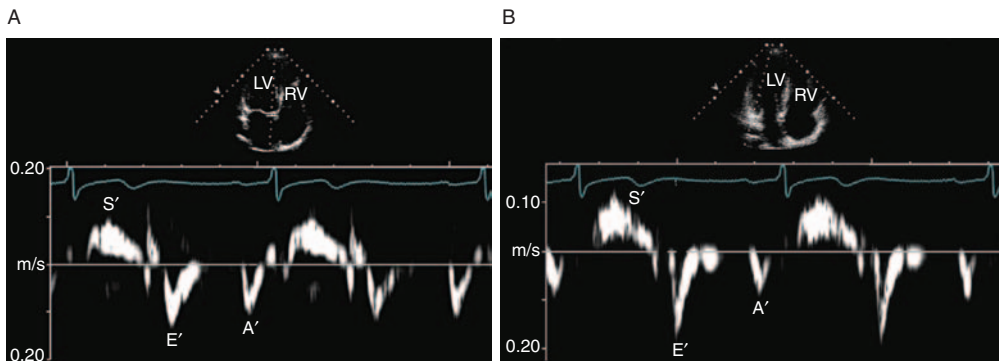


**Figure 16.3** Tissue Doppler velocity recording of the mitral annulus at the septal (A) and lateral (B) location. The recordings show systolic velocity ( $S'$ ), early diastolic velocity ( $E_a$  or  $E'$ ), and late diastolic velocity ( $A_a$  or  $A'$ ).

$E'$  velocity reflects the status of myocardial relaxation and is normally higher at the lateral location ( $>15$  cm/sec) than at the septal or medial location ( $>10$  cm/sec).

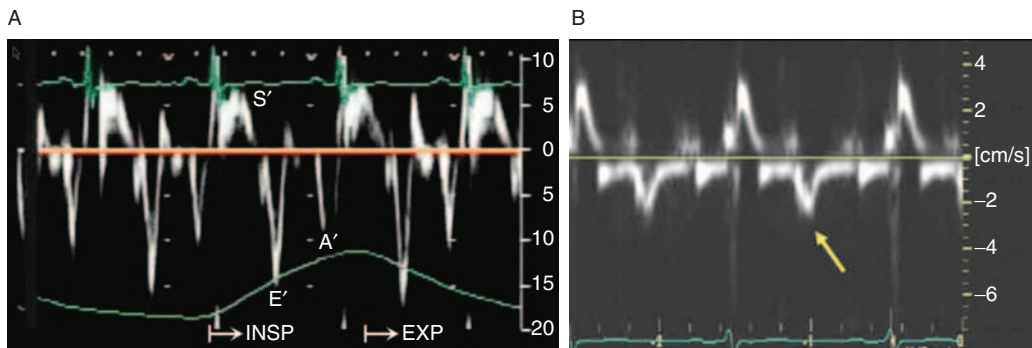


**Figure 16.4** Tissue Doppler velocity recording of the septal mitral annulus in patients with CP (A), and RCM (B).  $E'$  is high in constrictive pericarditis and decreased (arrow) in restrictive cardiomyopathy.

A comparator group of 10 normal healthy volunteers was also studied. Peak systolic mitral annular velocities were higher in the normal ( $10.5 \pm 3.6$  cm/sec) and CP ( $8.4 \pm 1.1$  cm/sec) groups than in the group with RCM ( $6.8 \pm 2.6$  cm/sec;  $P = 0.02$ ). Peak early diastolic velocity ( $E_a$  or  $E'$ ) was similar in the normal ( $14.5 \pm 4.7$  cm/sec) and CP ( $14.8 \pm 4.8$  cm/sec) groups (Figure 16.4A), but was significantly lower in the RCM group ( $5 \pm 1.4$  cm/sec;  $P < 0.001$ ) (Figure 16.4B). Peak E velocity by routine Doppler echocardiography did not correlate with  $E_a$ . The  $E_a/E$  index was significantly different in the normal ( $0.23 \pm 0.09$ ) and CP ( $0.19 \pm 0.07$ ) groups compared with the RCM group ( $0.06 \pm 0.02$ , reaching high statistical significance  $P < 0.001$ ). Thus, this small series indicated that peak velocities of left ventricular expansion in the longitudinal axis were markedly reduced in patients with RCM. A peak  $E_a$  velocity of 8 cm/sec

or an index of 0.11 differentiated the patients with CP from those with RCM with no overlap. Importantly, this study also demonstrated that, in normals and in patients with CP, peak expansion velocity occurred earlier than peak mitral inflow velocity, indicating that TDE-derived longitudinal velocity precedes rather than is driven by the increasing intraventricular volume. This temporal relation was lost in patients with RCM, probably as a result of reduced stored elastic recoil, resulting in more passive filling of the left ventricle.

Ha et al. [16] from our laboratory, evaluated  $E_a$  in a group of 19 surgically confirmed CP patients who had comprehensive preoperative Doppler echocardiography and TDE without typical respiratory variation in mitral inflow velocity. Interestingly, in this consecutive series, 9 of the 19 patients (47%) actually had  $<25\%$  respiratory variation in E velocity (in a larger series by this

same group, the incidence of patients with CP who demonstrated the characteristic respiratory variations in Doppler blood flow velocities was ≈ 88% [8]. They found no significant difference in E velocity, deceleration time, early-to-late ventricular filling ratio, or  $E_a$  between patients with and without respiratory variation of E velocity of 25% or more. Irrespective of the presence or absence of a significant respiratory variation of E velocity,  $E_a$  was relatively normal in all patients with CP (mean =  $12 \pm 4$  cm/sec). It was concluded that, when the respiratory variation in Doppler E velocity is absent or attenuated during the evaluation of patients with suspected CP or RCM, the presence of a preserved  $E_a$  velocity by TDE should support the diagnosis of CP over a primary myocardial disease. Our laboratory has published the largest and most definitive investigation evaluating the ability of mitral annular TDE to differentiate between CP and RCM [17]. We studied 23 patients with surgically confirmed CP, 38 patients with biopsy-proved systemic amyloidosis and typical echocardiographic features of cardiac involvement (i.e., RCM from amyloidosis), and 14 patients with primary RCM (based on echocardiographic features demonstrating biatrial enlargement, nondilated ventricles, and normal ventricular wall thickness) [18]. All patients had a comprehensive evaluation with pulsed-wave Doppler echocardiography of mitral inflow and TDE to measure  $E_a$  at the septal mitral annulus.  $E_a$  was significantly higher in patients with CP than in those with primary RCM or cardiac amyloidosis (CA) ( $12.3 \pm 4.0$  vs.  $5.1 \pm 1.5$  cm/sec;  $P < 0.001$ ) as shown in Figure 16.5. An  $E_a$  cutoff value of 8 cm/sec resulted in 95% sensitivity and 96% specificity for the diagnosis of CP. There was no overlap of  $E_a$  between patients who had CP and those who had RCM from CA. Two patients who had primary RCM had  $E_a \geq 8$  cm/sec. In a subgroup analysis of the patients with RCM,  $E_a$  of patients who had CA was significantly lower than that for patients who had primary RCM ( $4.6 \pm 0.2$  vs.  $6.3 \pm 0.3$  cm/sec;  $P < 0.001$ ). Thus, in the largest series published to date,  $E_a$  by TDE provided accurate discrimination between CP and RCM. The study confirmed that  $E_a$  can be a valuable diagnostic tool in the evaluation of patients with suspected RCM versus CP and should be measured routinely in these patients.

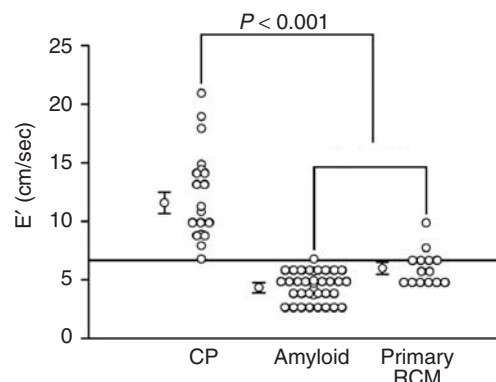


**Figure 16.5** Distribution of septal mitral annulus E' velocity in CP, CA, and primary RCM. Reproduced with permission from Ha et al. [17].

Rajagopalan et al. [19] compared the ability of TDE of the lateral mitral annulus versus respiratory variation of Doppler blood flow velocities in distinguishing between CP ( $n = 19$ ) and RCM ( $n = 11$ ). The systolic longitudinal velocities were not different between the two groups. Patients with CP had a significantly higher  $E_a$  of the lateral mitral annulus than patients with RCM ( $12.7 \pm 4.3$  vs.  $5.3 \pm 2.5$  cm/sec;  $P < 0.001$ ). The acceleration and deceleration rates of  $E_a$  were also significantly higher in the CP group. In addition, a significant difference was found between the  $E_a/E$  index in patients with CP compared to those with RCM ( $0.19 \pm 0.08$  vs.  $0.07 \pm 0.03$ ;  $P < 0.001$ ). A peak  $E_a$  velocity of 8.0 cm/sec differentiated CP from RCM with a sensitivity of 89% and a specificity of 100%. This group found that a 10% respiratory variation of the mitral inflow peak E wave showed 84% sensitivity and 91% specificity and an 18% respiratory variation of pulmonary venous peak diastolic velocity produced 79% sensitivity and 91% specificity in distinguishing between CP and RCM. Although analysis of areas under the receiver operating characteristic curves to determine accuracy as a function of sensitivity and specificity did not reveal any significant differences between TDE and conventional Doppler approaches to differentiate between CP and RCM, TDE did provide additional discriminatory power in patients who had proven CP but who did not meet criteria for respiratory variation of mitral inflow or pulmonary venous flow. The differentiation of CP from RCM should

not be made only by mitral or pulmonary vein flow velocity variation with respiration.

Sengupta et al. [20] evaluated the efficacy of mitral annular velocities by TDE in diagnosing CP in 122 subjects (87 referred for clinically suspected CP and 35 age- and sex-matched controls). Of the 87 patients suspected of having CP, 45 (51.7%) had the diagnosis confirmed at surgery, 11 (12.6%) had RCM, 20 (23.0%) had right heart failure due to cor pulmonale, and the other 11 (12.6%) had chronic pericardial effusions with no hemodynamic evidence of CP on follow-up echocardiography. They measured longitudinal velocities by TDE at both the septal and lateral aspects of the mitral annulus in addition to a comprehensive M-mode, 2-D, and conventional Doppler echocardiographic evaluation. Of the patients with CP, 35 (77.8%) had abnormal features on M-mode and 2-D echocardiography suggestive of CP. Respiratory variation >25% in transmitral E velocity was seen in 30 of 45 patients with CP (66.6%). They noted that  $E_a$  was normal ( $\geq 8$  cm/sec) in 40 of 45 patients with CP (88.9%). Of the 5 patients with CP with decreased  $E_a$  ( $< 8$  cm/sec) in one or both mitral annular regions, 2 had extensive mitral annular

calcification, and the other 3 had significant left ventricular systolic dysfunction (ejection fraction  $< 35\%$ ). Of 11 patients with RCM, 8 (72.7%) had reduced  $E_a$  and 3 showed normal  $E_a$  in one or both aspects of the mitral annulus assessed. They found that a normal  $E_a$  velocity improved recognition of CP, particularly when conventional echo/Doppler findings were equivocal. The overall sensitivity and specificity for diagnosing CP with TDE of the mitral annulus incrementally with M-mode, 2-D, and transmural Doppler flow variation were 88.8% and 94.8%, respectively. The authors concluded that TDE of the mitral annulus was of benefit in distinguishing CP from RCM in most cases, but cautioned against using this method in the presence of extensive mitral annular calcification, left ventricular systolic dysfunction, or segmental discordance between septal and lateral mitral annular longitudinal velocities.

### Annulus paradoxus

One of the most commonly used techniques to estimate left ventricular filling pressures noninvasively is the ratio of  $E/E_a$  obtained by Doppler

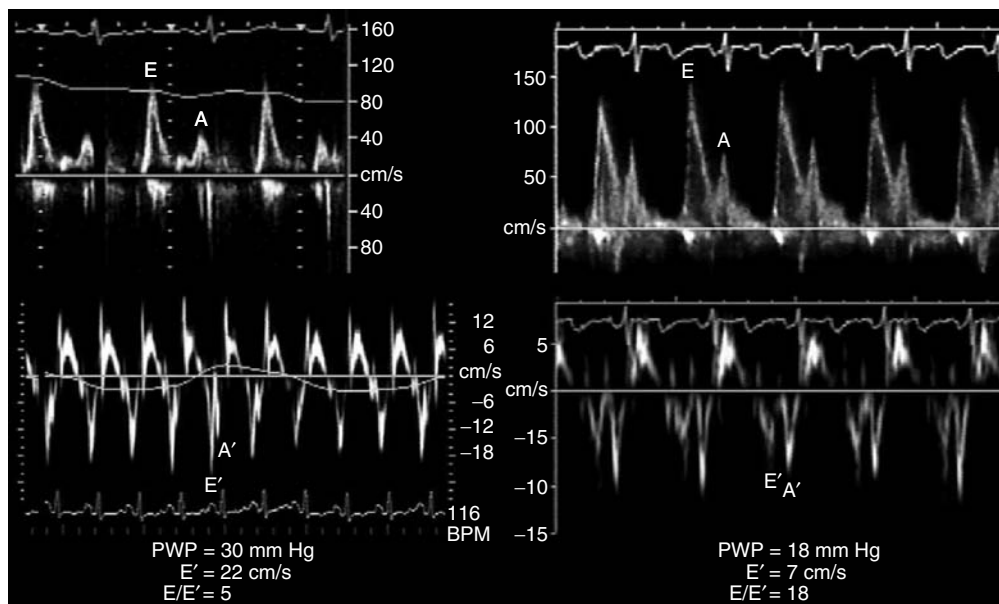


**Figure 16.6** Mitral inflow velocities (upper panel) and mitral annulus velocities (lower panel) from two patients with CP. The patient with worse constriction and higher PCWP (PWP) in left has a higher  $E_a$  or  $E'$  velocity with a

lower  $E/E'$  or  $E/E_a$  ratio than the patient with lesser degree of constriction in right. Reproduced with permission from Ha et al. [22].

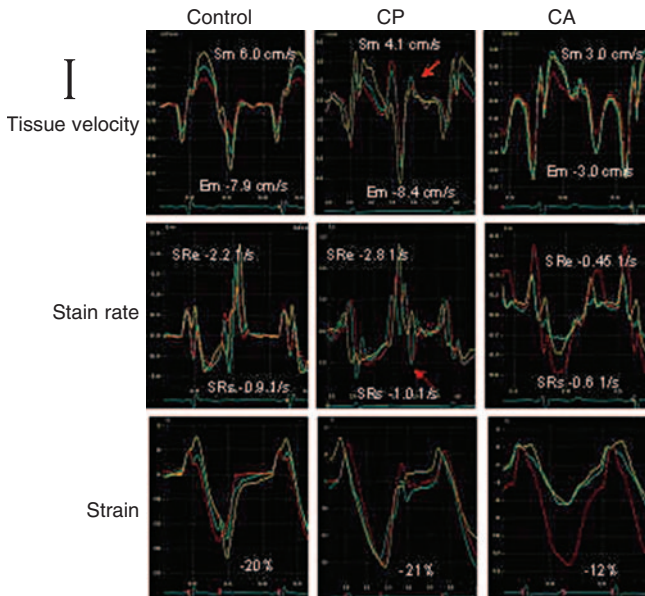


**Figure 16.7** Tissue Doppler longitudinal time-velocity curve of the interventricular septum, demonstrating the characteristic biphasic motion (arrow) seen with CP.

echocardiography and TDE [21]. Ha et al. [23] tested whether this parameter also correctly predicted left ventricular filling pressure in patients with CP. They measured  $E/E_a$  and directly correlated it to invasively determined pulmonary capillary wedge pressure (PCWP) in 10 patients with surgically confirmed CP. They found a significant inverse correlation between  $E/E_a$  and PCWP (Figure 16.6;  $r = -0.74$ ;  $P = 0.014$ ), and despite high left ventricular filling pressures (mean PCWP =  $25 \pm 6$  mm Hg),  $E/E_a$  (mean =  $9 \pm 4$  mm Hg) was  $<15$  in all but one patient. Thus, paradoxical to the positive correlation between  $E/E_a$  and PCWP in patients with myocardial disease, an inverse relationship was found in patients with CP. This phenomenon was termed *annulus paradoxus* [22]. The more severe the constriction with a higher filling pressure, the more accentuated is the longitudinal motion of the mitral annulus (Figure 16.6), a finding supported by the fact that  $E_a$  was decreased after pericardectomy in all three patients who had a repeat measurement of  $E_a$  postoperatively. The normal or even accentuated  $E_a$  in CP likely reflects an exaggerated longitudinal motion of the mitral annulus, because circumferential expansion of the entire heart is limited by the pericardial constriction [22].

### Tissue Doppler echocardiography of interventricular septum

One of the cardinal 2-D and M-mode findings in CP is abnormal motion of the septum [5,6,23–25]. Sengupta et al. evaluated the usefulness of TDE of the interventricular septum and posterior wall in the short axis for diagnosing CP [26]. They performed preoperative TDE in 40 patients with surgically confirmed CP and compared the findings to 35 age- and sex-matched controls and 20 patients with abnormal septal motion from other causes. In 33 of the 40 patients (82.5%) TDE identified abnormal septal motion. A high-velocity polyphasic fluttering of the interventricular septum with peak velocity  $>7$  cm/sec was present in 29 patients (72.5%). This finding included a high-velocity ( $>7$  cm/sec) early diastolic biphasic motion that coincided with the early diastolic notching of the septum on M-mode tracing, followed by multiple recoil/reverberation waves. An example of this abnormal biphasic septal motion seen with tissue Doppler imaging in CP is shown in Figure 16.7. High-velocity early diastolic biphasic motion without recoil was seen in 4 other patients. TDE of the posterior wall revealed that the early diastolic wave was unaltered, whereas the late diastolic wave

was reduced in 24 patients (60%) and absent in 7 patients (17.5%). TDE was superior at identifying abnormalities in septal or posterior wall motion in CP compared to M-mode or 2-D echocardiography (33 vs. 24 patients;  $P = 0.003$ ). TDE also distinguished abnormal septal motion in CP from that in 16 of 20 patients with abnormal septal motion from other etiologies. A high-velocity biphasic early diastolic motion (peak velocity  $\geq 7$  cm/sec) with or without recoil waves had 82.5% sensitivity and 92.7% specificity for diagnosing CP. TDE provides a more precise way to detect the exaggerated interventricular interdependence reflected by the abnormal septal motion characteristic of CP.

### Myocardial velocity gradient

Myocardial velocity gradient (MVG) is an index of myocardial contraction and relaxation that quantifies the spatial distribution of velocities across the myocardium from epicardium to endocardium and is a sensitive parameter of myocardial contractility [27–30]. Therefore, MVG is the same as strain rate in concept and measuring unit described throughout this Book. MVG is relatively independent of translational motion of the heart [31] and also

less load-dependent than conventional Doppler derived estimates of myocardial performance [32]. Palka and colleagues [33] evaluated the use of MVG measured from the left ventricular posterior wall during predetermined phases of the cardiac cycle in differentiating between RCM and CP (10 patients with CP, 15 patients with RCM, and 30 age-matched controls). They found that MVG was significantly lower in RCM patients compared with both CP and normal controls during ventricular ejection ( $2.8 \pm 1.2$  vs.  $4.4 \pm 1.0$  and  $4.7 \pm 0.8$  sec $^{-1}$ , respectively;  $P < 0.01$ ) and during rapid ventricular filling ( $1.9 \pm 0.8$  vs.  $8.7 \pm 1.7$  and  $3.7 \pm 1.4$  sec $^{-1}$ , respectively;  $P < 0.01$ ). Furthermore, during isovolumic relaxation, MVG was positive in RCM patients and negative in both CP patients and normal controls ( $0.7 \pm 4$  vs.  $-1.0 \pm 0.6$  and  $-0.04 \pm 0.3$  sec $^{-1}$ , respectively;  $P < 0.01$ ). During atrial contraction, the posterior wall MVG was significantly lower for both RCM and CP patients compared to normal controls ( $1.6 \pm 1.7$  and  $1.7 \pm 1.8$  vs.  $3.8 \pm 0.9$  sec $^{-1}$ , respectively;  $P < 0.01$  for both groups). However, use of MVG during systole did not allow for a clear-cut distinction between RCM and CP, as some overlap in data points did occur. In addition, the degree of decrease in MVG during ventricular ejection

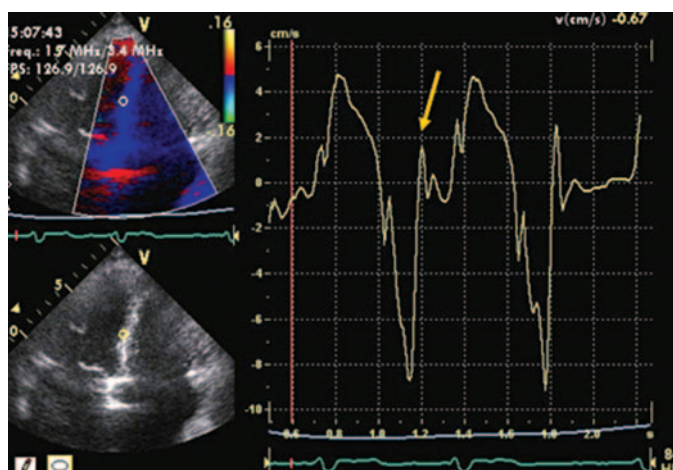


**Figure 16.8** Tissue velocity, strain rate, and strain imaging of ventricular septum. Left column: Normal control. Center column: Patient with CP. Reduced systolic tissue velocity (Sm) but well-preserved systolic strain rate (SRs) and strain were seen. The diastolic waves showed high magnitudes of early diastolic tissue velocity (Em) and early diastolic strain rate (SRe). Note the extra waves immediately after

the Em and SRe waves (red arrows). Right column: Patient with CA. Reduced Sm and Em velocities were seen. SRs, SRe and strain were also severely reduced except apical wall. There was no additional wave during diastole. Yellow wave, basal septum; green wave, mid-septum; red wave, apical septum.

was dependent on the severity of left ventricular hypertrophy. The most robust parameter for separation of RCM from CP was diastolic MVG during rapid ventricular filling. In RCM patients, early diastolic MVG was 78% lower than that measured in CP patients and  $\approx 50\%$  lower than that in normal controls. Finally, the absolute value of MVG during isovolumic relaxation was paradoxically 150% higher in patients with CP compared with normal subjects and most likely explained by the increased dissociation of intrathoracic–intracardiac pressure changes during end-respiration. Importantly, diastolic MVG parameters were independent of the degree of left ventricular hypertrophy. The authors concluded that the clear reduction in both systolic and diastolic parameters of MVG in RCM patients was likely the result of the fibrotic and/or infiltrative process involving the myocardium in this illness [34]. One last important finding in this study was that 24% of the patients studied were in atrial fibrillation and the measurement of MVG was not influenced by whether the patient was in sinus rhythm or atrial fibrillation.

### Strain rate imaging

Limited data exist with regard to the clinical utility of Doppler strain and strain rate imaging in distinguishing CP from RCM. Arnold et al. [35] report two cases of CP in which mitral annular excursion and velocity were reduced. Both patients had prominent calcification at the cardiac base, which may have resulted in reduced annular motion and also likely affected the deformation properties of the basal myocardium. Using strain rate imaging, the authors demonstrated that there was compensation for this finding provided by an inverse movement of the apical halves of the ventricles. The described hypermobility of the usually stationary apex was believed to correspond to the clinical sign of apical retraction seen in CP. Thus, under these circumstances, annular velocities alone did not reflect global longitudinal function of the respective wall. The authors concluded that lateral mitral annular velocities would be more likely affected by this phenomenon than septal mitral annular velocities and suggest preferentially using the septal region for TDE differentiation of CP from RCM. Another possible limitation of mitral annular TDE

may also occur in patients with mixed CP and RCM (e.g., postradiation-induced perimyocardial disease), where  $E_a$  velocity may not be as diagnostic as in isolated CP.

Park et al., in our laboratory, compared strain rate (SR) and strain as well as tissue velocity (TV) of the myocardium (Figure 16.8) in 12 CP patients, 10 patients with CA, and 10 normal controls [36]. The systolic velocity ( $Sm$ ) of both septum and left ventricular lateral wall was reduced similarly in CP and CA (basal septal mean value, 4.35 and 4.43 cm/sec, respectively). The early diastolic velocity ( $Em$ ) was significantly increased in CP patients and decreased in CA patients in all segments (basal septal mean value,  $-8.73$  vs.  $-2.89$  cm/sec;  $P < 0.05$ ). In contrast to the TV measurements, systolic SR ( $SR_s$ ) of CP was well preserved in all segments (basal septal mean value,  $-1.20$  sec $^{-1}$ ). On the other hand, the early diastolic strain rate ( $SRe$ ) was significantly increased and late diastolic strain rate ( $Sra$ ) was markedly reduced in patients with CP, similar to TV recording. In eight patients with CP, TV and SR showed a prominent extra diastolic wave ( $>1.5$  cm/sec and  $<-0.7$  sec $^{-1}$ , respectively) in the opposite direction, immediately after  $Em$  and  $SRe$  at ventricular septum, that was not present in controls and CA. In patients with CA,  $SR_s$  and  $SRe$  were significantly decreased in both septum and left ventricular lateral wall, but not reduced in apical segments. Strain was normal in CP patients, but significantly reduced in CA patients (basal septal mean value,  $-21.4$  vs.  $-8.3$ ;  $P < 0.05$ ). We concluded that SR and strain imaging showed that systolic longitudinal myocardial function was well preserved in patients with CP, although TV showed reduced systolic velocity as low as that of CA. Both TV and SR of CP are characteristic and different from those of CA with a unique diastolic pattern of high  $Em$  and  $SRe$  with mid-diastolic biphasic wave.

### Conclusion

Both RCM and CP are characterized by decreased chamber compliance, but the mechanisms leading to decreased chamber compliance in each of these cardiovascular disorders are fundamentally different. In CP, the diminished left ventricular compliance is secondary to an increase in pericardial

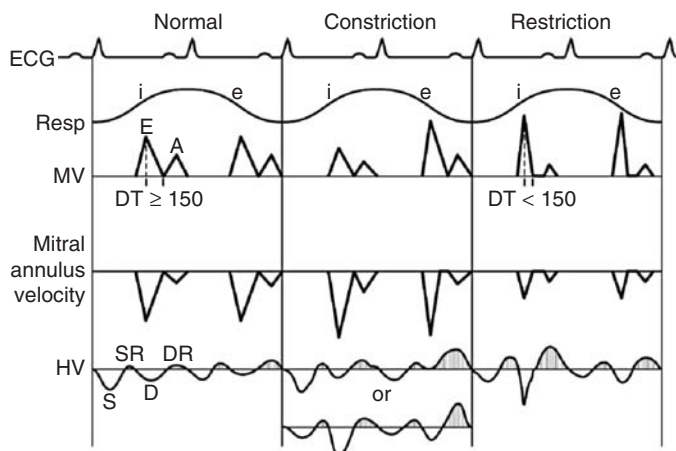


**Figure 16.9** Schematic diagram to demonstrate mitral inflow velocities (MV), mitral annulus tissue velocities, and hepatic vein (HV) Doppler velocities in normal, constriction, and restriction. S, systolic forward flow; D, diastolic forward flow; SR, systolic reversal of flow; DR, diastolic reversal of flow. Reproduced with permission from Oh et al. *The echo manual*. 3rd ed. Philadelphia: Lippincott, Williams, & Wilkins; 2006.

restraint [36,37], and in RCM, the left ventricular wall itself has diminished compliance secondary to an intrinsic myocardial or endocardial pathologic process [38]. The differentiation of CP and RCM can be usually identified by 2-D and conventional Doppler echocardiography, and in some cases, invasive hemodynamic data are also required. Diagnostic certainty and reliability of echocardiography regarding the differentiation of CP versus RCM is enhanced by TDE, which can be used to directly measure the fundamental difference in myocardial relaxation and tissue velocity between these two distinct clinical entities. A summary of mitral inflow, mitral annulus, and hepatic vein velocities of normal, constriction, and restriction is schematically shown in Figure 16.9. Based on these comprehensive echocardiographic parameters, the differentiation between constrictive pericarditis and restrictive cardiomyopathy should be possible in most of the clinical situations.

## References

- Nishimura RA, Connolly DC, Parkin TW, Stanson AW. Constrictive pericarditis: assessment of current diagnostic procedures. *Mayo Clin Proc* 1985; **60**: 397–401.
- Lorell B, Grossman W. Profiles in constrictive pericarditis, restrictive cardiomyopathy and cardiac tamponade. In: Baim DS, Grossman W, eds. *Cardiac catheterization, angiography and intervention*. Baltimore: Williams and Wilkins; 1996. p. 801–57.
- Spodick DH. Constrictive pericarditis. In: Spodick DH, ed. *The pericardium: a comprehensive textbook*. New York: Marcel Dekker, Inc; 1997. p. 214–59.
- Talreja DR, Edwards WD, Danielson GK, et al. Constrictive pericarditis in 26 patients with histologically normal pericardial thickness. *Circulation* 2003; **108**: 1852–7.
- Gibson TC, Grossman W, McLaurin, Moos S, Craige E. An echocardiographic study of the interventricular septum in constrictive pericarditis. *Br Heart J* 1976; **38**: 738–43.
- Tei C, Child JS, Tanaka H, Shah PM. Atrial systolic notch on the interventricular septal echogram: an echocardiographic sign of constrictive pericarditis. *J Am Coll Cardiol* 1983; **1**: 907–12.
- Hatle LK, Appleton CP, Popp RL. Differentiation of constrictive pericarditis and restrictive cardiomyopathy by Doppler echocardiography. *Circulation* 1989; **79**: 357–70.
- Klein AL, Cohen GI, Pietrolungo JF, et al. Differentiation of constrictive pericarditis from restrictive cardiomyopathy by Doppler transesophageal echocardiographic measurements of respiratory variations in pulmonary venous flow. *J Am Coll Cardiol* 1993; **22**: 1935–43.
- Oh JK, Hatle LK, Seward JB, et al. Diagnostic role of Doppler echocardiography in constrictive pericarditis. *J Am Coll Cardiol* 1994; **23**: 154–62.
- Boonyaratavej S, Oh JK, Tajik AJ, Appleton CP, Seward JB. Comparison of mitral inflow and superior vena cava Doppler velocities in chronic obstructive pulmonary disease and constrictive pericarditis. *J Am Coll Cardiol* 1998; **32**: 2043–8.
- Oh JK, Tajik AJ, Appleton CP, Hatle LK, Nishimura RA, Seward JB. Preload reduction to unmask the characteristic Doppler features of constrictive pericarditis: a new observation. *Circulation* 1997; **95**: 796–9.
- Isaaz K, Thompson A, Ethevenot G, Cloez JL, Bremilla B, Pernot C. Doppler echocardiographic

- measurement of low velocity motion of the left ventricular posterior wall. *Am J Cardiol* 1989; **64**: 66–75.
- 13 Isaaz K, Munoz del Romeral L, Lee E, Schiller NB. Quantitation of the motion of the cardiac base in normal subjects by Doppler echocardiography. *J Am Soc Echocardiogr* 1993; **6**: 166–76.
  - 14 Zaky A, Grabhorn L, Feigenbaum H. Movement of the mitral ring: a study in ultrasound cardiography. *Cardiovasc Res* 1967; **1**: 121–31.
  - 15 Garcia MJ, Rodriguez L, Ares M, Griffin BP, Thomas JD, Klein AL. Differentiation of constrictive pericarditis from restrictive cardiomyopathy: assessment of left ventricular diastolic velocities in longitudinal axis by Doppler tissue imaging. *J Am Coll Cardiol* 1996; **27**: 108–14.
  - 16 Ha J-W, Oh JK, Ommen SR, Ling LH, Tajik AJ. Diagnostic value of mitral annular velocity for constrictive pericarditis in the absence of respiratory variation in mitral inflow velocity. *J Am Soc Echocardiogr* 2002; **15**: 1468–71.
  - 17 Ha J-W, Ommen SR, Tajik AJ, et al. Differentiation of constrictive pericarditis from restrictive cardiomyopathy using mitral annular velocity by tissue Doppler echocardiography. *Am J Cardiol* 2004; **94**: 316–9.
  - 18 Ammash NM, Seward JB, Bailey KR, Edwards WD, Tajik AJ. Clinical profile and outcome of idiopathic restrictive cardiomyopathy. *Circulation* 2000; **101**: 2490–6.
  - 19 Rajagopalan N, Garcia M, Rodriguez L, et al. Comparison of new Doppler echocardiographic methods to differentiate constrictive pericardial heart disease and restrictive cardiomyopathy. *Am J Cardiol* 2001; **87**: 86–94.
  - 20 Sengupta PP, Mohan JC, Mehta V, Arora R, Pandian NG, Khandheria BK. Accuracy and pitfalls of early diastolic motion of the mitral annulus for diagnosis in constrictive pericarditis by tissue Doppler imaging. *Am J Cardiol* 2004; **93**: 886–90.
  - 21 Nagueh SF, Middleton KJ, Kopelen HA, Zoghbi WA, Quinones MA. Doppler tissue imaging: a noninvasive technique for evaluation of left ventricular relaxation and estimation of filling pressures. *J Am Coll Cardiol* 1997; **30**: 1527–33.
  - 22 Ha J-W, Oh JK, Ling LH, Nishimura RA, Seward JB, Tajik AJ. Annulus paradoxus – transmural flow velocity to mitral annular velocity ratio is inversely proportional to pulmonary capillary wedge pressure in patients with constrictive pericarditis. *Circulation* 2001; **104**: 976–978.
  - 23 Morgan JM, Raposo L, Clague JC, Chow WH, Oldershaw PJ. Restrictive cardiomyopathy and constrictive pericarditis: non-invasive distinction by digitized M-mode echocardiography. *Br Heart J* 1989; **61**: 29–37.
  - 24 Engel PJ, Fowler NO, Tei CW, et al. M-mode echocardiography in constrictive pericarditis. *J Am Coll Cardiol* 1985; **6**: 471–4.
  - 25 Candell-Riera J, Garcia del Castillo H, Permanyer-Miralda G, Soler-Soler J. Echocardiographic features of the interventricular septum in chronic constrictive pericarditis. *Circulation* 1978; **57**: 1154–8.
  - 26 Sengupta PP, Mohan JC, Mehta V, Arora R, Khandheria BK, Pandian NG. Doppler tissue Imaging improves assessment of abnormal interventricular septal and posterior wall motion in constrictive pericarditis. *J Am Soc Echocardiogr* 2005; **18**: 226–230.
  - 27 Gorcsan J, Strum DP, Mandarino WA, Gulati VK, Pinsky MR. Quantitative assessment of alterations in regional left ventricular contractility with color-coded tissue Doppler echocardiography: comparison with sonomicrometry and pressure-volume relations. *Circulation* 1997; **95**: 2423–33.
  - 28 Gorcsan J, Gulati VK, Mandarino WA, Katz WE. Color-coded measures of myocardial velocity throughout the cardiac cycle by tissue Doppler imaging to quantify regional left ventricular function. *Am Heart J* 1996; **131**: 1203–13.
  - 29 Palka P, Lange A, Fleming AD, et al. Differences in myocardial velocity gradient measured throughout the cardiac cycle in hypertrophic cardiomyopathy, athletes and hypertensive hearts. *J Am Coll Cardiol* 1997; **30**: 760–8.
  - 30 Gorcsan J III, Deswal A, Mankad S, et al. Quantification of the myocardial response to low-dose dobutamine using tissue Doppler echocardiographic measures of velocity and velocity gradient. *Am J Cardiol* 1998; **81**: 615–23.
  - 31 Uematsu M, Nakatani S, Tamagishi M, Matsuda H, Miyatake K. Usefulness of myocardial velocity gradient derived from two-dimensional tissue Doppler imaging as an indicator of regional myocardial contraction independent of translational motion assessed in atrial septal defect. *Am J Cardiol* 1997; **79**: 237–41.
  - 32 Shimizu Y, Uematsu M, Shimizu H, Nakamura K, Yamagishi M, Miyatake K. Peak negative myocardial velocity gradient in early diastole as a noninvasive indicator of left ventricular diastolic function: comparison with transmural flow velocity indices. *J Am Coll Cardiol* 1998; **32**: 1418–25.
  - 33 Palka P, Lange A, Donnelly JE, Nihoyannopoulos P. Differentiation between restrictive cardiomyopathy and constrictive pericarditis by early diastolic Doppler myocardial velocity gradient at the posterior wall. *Circulation* 2000; **102**: 655–62.
  - 34 Benotti JR, Grossman W, Cohn PF. Clinical profile of restrictive cardiomyopathy. *Circulation* 1980; **61**: 1206–12.

- 35 Arnold MF, Voigt J-U, Kukulski T, Wranne B, Sutherland GR, Hatle L. Does atrioventricular ring motion always distinguish constriction from restriction? A Doppler myocardial imaging study. *J Am Soc Echocardiogr* 2001; **14**: 391–5.
- 36 Park SM, Casablang-Verzosa G, Diego B, Espinosa RE, Miller FA, Oh JK. Longitudinal myocardial function of constrictive pericarditis assessed by tissue velocity, strain rate, and strain imaging echocardiography. *J Am Coll Cardiol* (submitted).
- 37 Hirschman JV. Pericardial constriction. *Am Heart J* 1978; **96**: 110–22.
- 38 Katritsis D, Wilmshurst PT, Wendon JA, Davies MJ, Webb-Peploe MM. Primary restrictive cardiomyopathy: clinical and pathological characteristics. *J Am Coll Cardiol* 1991; **18**: 1230–5.

# Use of myocardial imaging to identify and manage subclinical heart disease in thyroid and other endocrine diseases

Vitantonio Di Bello

## Introduction

The cardiovascular system is the target of multiple endocrine signals that may influence its function, to the effects of similar to other types of signals (nutritional signals, nerve inputs, and so on). Endocrine signals are evoked through nuclear receptors (e.g., thyroid hormones) or cell surface receptors that work by initiating second messenger signaling cascades [1]. Cardiovascular tissues are also endocrine organs, and stimuli that affect the cardiovascular system act on hormone receptors; these hormone-signaling systems are interconnected, therefore, the single components are difficult to distinguish [2].

In overt endocrine diseases, the deleterious interactions between the endocrine system and the heart are well known. However, there are conflicting data regarding the significance of early, subclinical phases of endocrine diseases, which likely may be associated with several preclinical myocardial abnormalities [3], including subclinical hypothyroidism and hyperthyroidism, acromegaly, and hyperaldosteronism (Conn's adenoma). Some questions emerge in this debate and need to be addressed: (1) What is the prognostic significance of subclinical cardiac involvement in endocrine disease? (2) Are these myocardial abnormalities reversible upon normalization of endocrine function? (3) Is aggressive treatment necessary for subclinical endocrine diseases?

Knowledge of the basic ultrastructural physiopathological mechanisms of myocardial abnormalities has been recently advanced by the application of the new ultrasound methods focused on the myocardium. These very refined, new ultrasonic techniques capable of studying the physiopathological intramyocardial phenomena include *color Doppler myocardial imaging* (CDMI) and its elaborations (strain and strain rate), which study intramyocardial velocities and allow the analysis of deformation (Figure 17.1) [4,5]; *videodensitometry* (VD) [6,7], which works on gray level scale of digitized video imaging and *integrated backscatter* (IBS) (Figure 17.2) [8,9], which analyzes the variations of myocardial reflectivity in decibels, working on radiofrequency signal. The advantage of these techniques is their relative independence of loading conditions and, in particular – for strain and strain rate – a relative independence from rotational and translational motions of the heart. Furthermore, these techniques permit a very early diagnosis of systolic and diastolic dysfunction, when conventional echo-Doppler parameters of left ventricular (LV) function are still within normal range. In particular, VD and IBS correlate with structural changes, such as myocardial fibrosis, as recently demonstrated by our research group in models of LV hypertrophy secondary to hypertension and aortic stenosis, in acromegaly and in obesity [10–13].

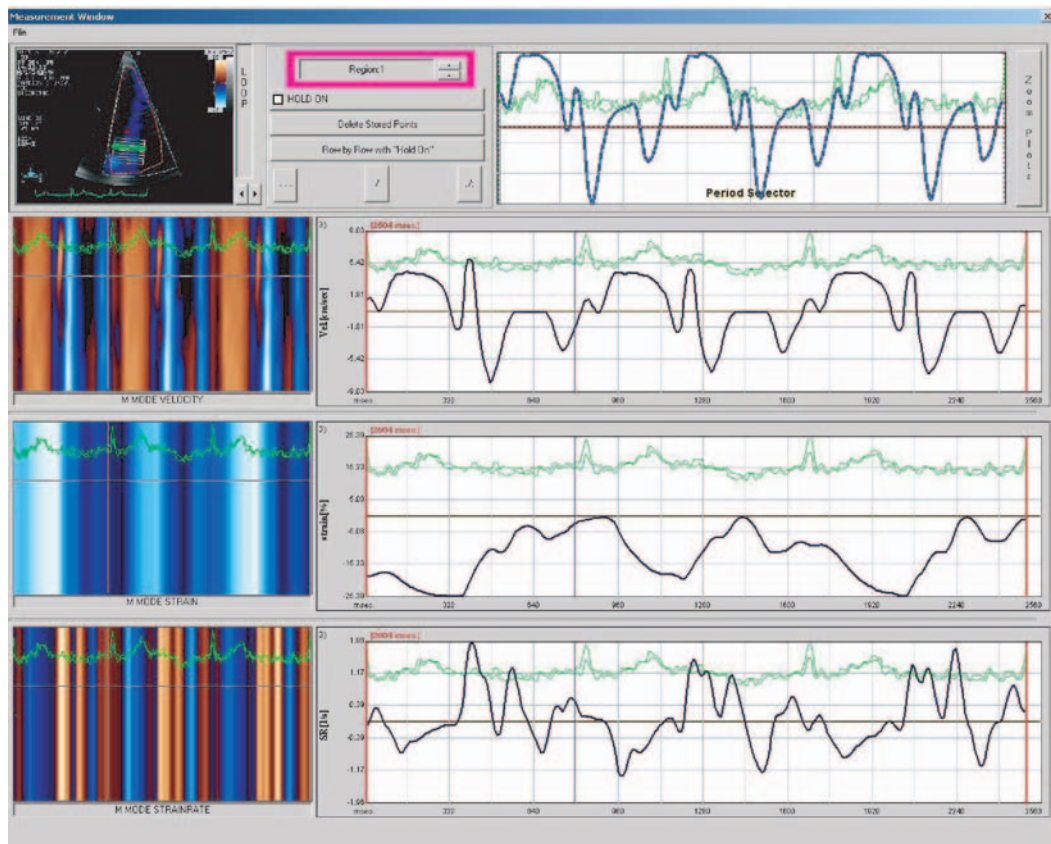


**Figure 17.1** CDMI analysis showing color M-mode and magnitude vs. time curves for velocity, strain, and strain rate.

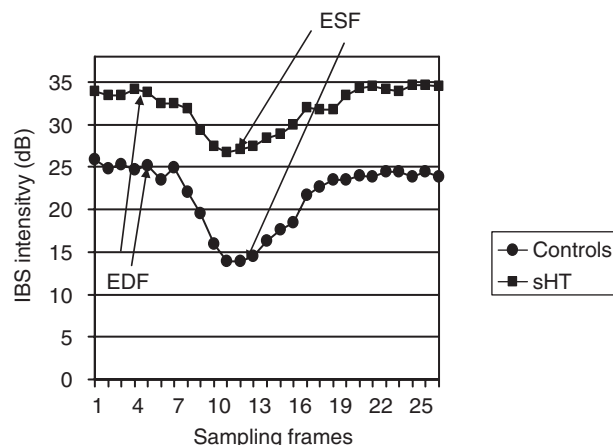
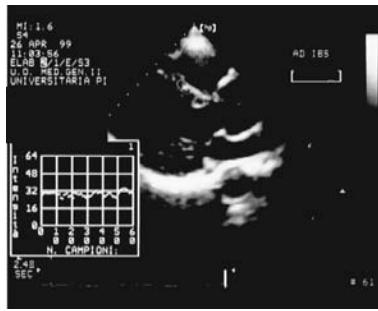


**Figure 17.2** IBS analysis in a patient with sHypoT. IBS intensity in myocardial and reference segments is summarized in the right panel. EDF, end-diastolic frames; ESF, end-systolic frames; sHT, subclinical hypothyroidism.

## Subclinical thyroid dysfunction

The heart is a major target of thyroid hormone and pronounced changes occur in cardiac function in patients with hyper- and hypothyroidism. In this section, we will consider only the subclinical picture of hyper- and hypothyroidism.

### Subclinical hyperthyroidism

Subclinical hyperthyroidism (sHyperT) is characterized by low to undetectable circulating thyrotropin (TSH) levels and normal serum free thyroxin ( $FT_4$ ) and free tri-iodothyronine ( $FT_3$ ) concentrations, in the absence of symptoms and signs of hyperthyroidism [14–16]. Subjects with exogenous or endogenous sHyperT have higher prevalence of palpitations, tremor, heat intolerance, sweating, nervousness, anxiety, reduced feeling of well-being, fear, hostility, and inability to concentrate.

Excess thyroid hormone causes a wide spectrum of cardiovascular changes, secondary to both direct and indirect effects on cardiovascular system and effects mediated by neurohumoral activation. The implications of overt hyperthyroidism in the development of cardiac disease are well known [17]. The more common cardiac abnormalities include increased heart rate, increased LV mass (LVM) with unchanged systolic function, diastolic dysfunction, and the induction of cardiac arrhythmias [18–20].

On the contrary, the involvement of the cardiovascular system in sHyperT is still debated [21,22]. There is growing evidence that endogenous or exogenous TSH suppression is consistent with a condition of tissue hyperthyroidism [23]. Detrimental cardiac effects have been reported in literature but the entity and the actual clinical significance are still debated. sHyperT has been reported to be associated with a significantly lower pre-expulsive period (PEP) and PEP/LVET (LV ejection time) ratio, which suggests the presence of a faster PEP with an LVET comparable to healthy controls [23,24]. In a recent study of 24 untreated patients with sHyperT by Di Bello et al. [25] standard indices of LV systolic function (fractional shortening and ejection fraction) did not differ from that of a healthy control group. These indices are influenced by preload and afterload and being the expression of global ventricular function, they are not sensitive for the detection of early abnormalities of sHyperT.

In this study, the LVM indexed by body surface (LVMbs) values did not differ from controls, in contrast to other studies, and this finding could be explained by the young age of the study population and by the short duration of disease. In the earliest phase of sHyperT an increase of loading conditions, which stimulates the synthesis of contractile proteins inducing LVM increase, does not occur. LV diastolic function evaluated with conventional echocardiography (mitral flow Doppler analysis) showed a slight dysfunction in sHyperT with a slightly, but significantly reduced peak E-wave velocity and a significantly higher peak A-wave velocity, compared to controls. The pulsed-wave tissue Doppler imaging (PW-TDI) analysis at the mitral annular level, an expression of global longitudinal function, showed a significant impairment of the mitral annular velocity in sHyperT patients. In sHyperT patients, the early diastolic phase showed a significantly lower velocity and the late diastolic phase a significantly higher velocity compared to controls. The CDMI analysis confirmed the impairment of regional diastolic function detected by PW-TDI at a global level. Strain rate also confirmed that regional diastolic function was lower in subjects with sHyperT, independently of loading conditions and/or rotational and translational motion artifacts.

The functional intramyocardial phenomena detected at regional level by CDMI showed a significantly higher systolic peak velocity (peak S) and a significantly lower systolic acceleration time in sHyperT. These findings indicate the presence of enhanced systolic regional function (hyperkinesis). Systolic strain was significantly higher in sHyperT compared to controls, indicating a greater systolic deformation of the myocardium in the early phase of sHyperT. Ultrasonic backscatter analysis confirmed the CDMI data by showing a significantly higher Cyclic Variation Index (CVI) at the septum in sHyperT, again indicating increased intrinsic myocardial contractility. Other IBS parameters, in particular those representative of myocardial texture, were comparable in both groups (Figures 17.3 and 17.4).

Cardiac hypercontractility, demonstrated by significant increase of CVI (by IBS) and strain (by CDMI) may be explained by a direct action of thyroid hormones on heart [27,28]. The early

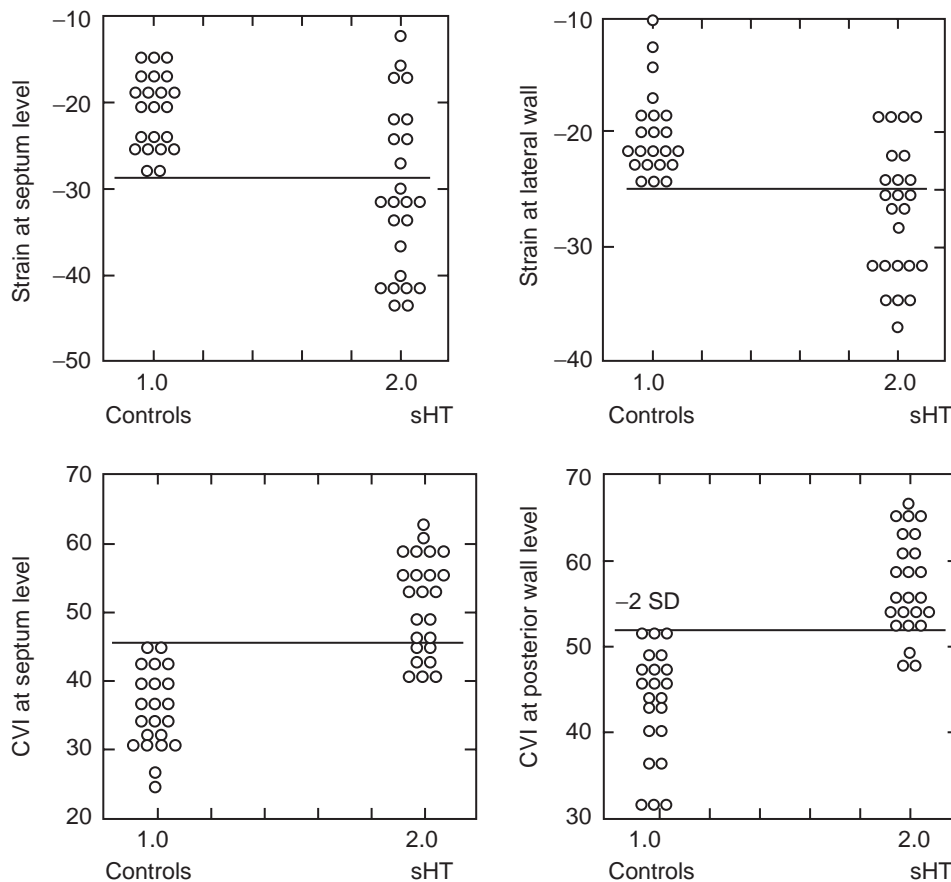


**Figure 17.3** Comparison of individual plots for strain and CVI at the septum and posterior wall level in sHyperT (sHT) and control subjects.

functional myocardial abnormalities in sHyperT were confirmed in our study by the overlap in IBS parameters, which are related to structural changes of myocardial texture, in particular collagen content, which increases as LVM increases. The inverse relationship between LVMbs and lateral wall strain may be explained as a sign of early myocardial hyperdeformability caused by sHyperT, which normalizes when the LVMbs increases (Figure 17.5). The presence of a higher LVM in other series of patients with sHyperT may be explained as a later phenomenon [29]. The persistence of the hypercontractility could induce the development of structural abnormalities that are responsible for the increase of LVM.

The administration of the cardioselective beta-blocker bisoprolol for 6 months significantly improved the mean symptom rating scale score in

patients with exogenous sHyperT [30]. In particular, this therapy reduced the incidence of supraventricular arrhythmias and LVM with subsequent improvement of diastolic function at rest and systolic function during exercise. No data are available, at the moment, regarding the effects of therapy on early systolic and diastolic functional parameters as documented by the new ultrasound techniques.

### Subclinical hypothyroidism

Subclinical hypothyroidism (sHypoT) is an apparently asymptomatic condition characterized by elevated serum TSH concentrations in the presence of normal free thyroid hormone levels [30,31]. It affects 5–15% of the general population, with a particularly high prevalence observed among women over 60 years of age [32,33]. Because patients with sHypoT appear to merely show a biochemical

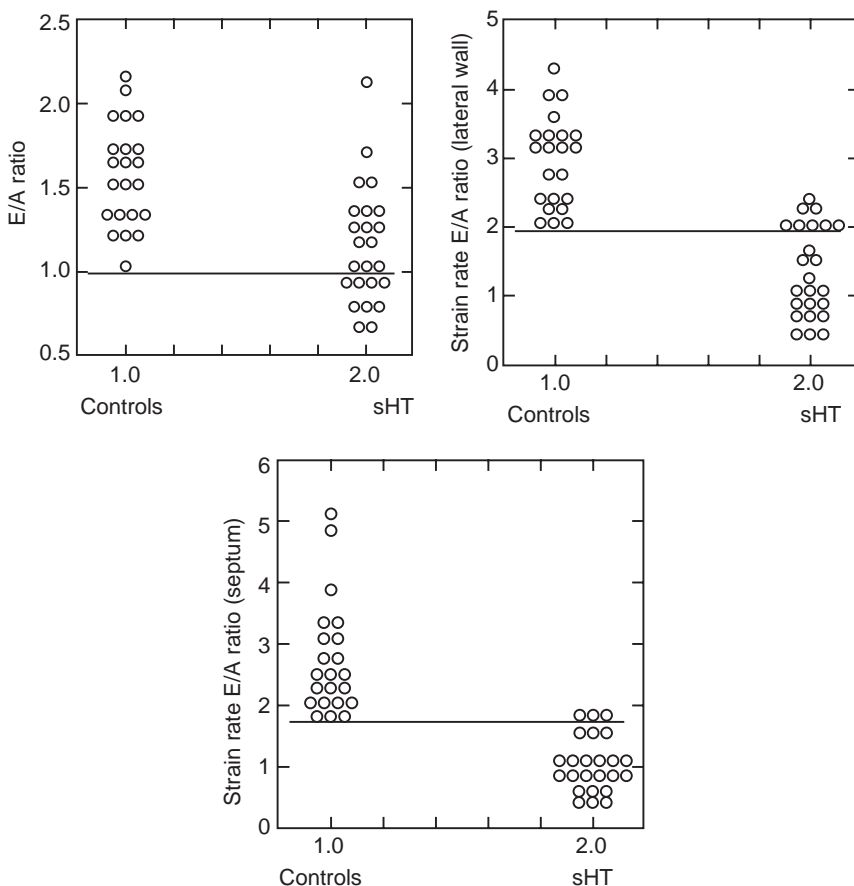


**Figure 17.4** Individual plots for E/A ratio of transmural flow and strain rate E/A ratio both at septum and posterior wall level in patients with sHyperT (sHT) and controls.

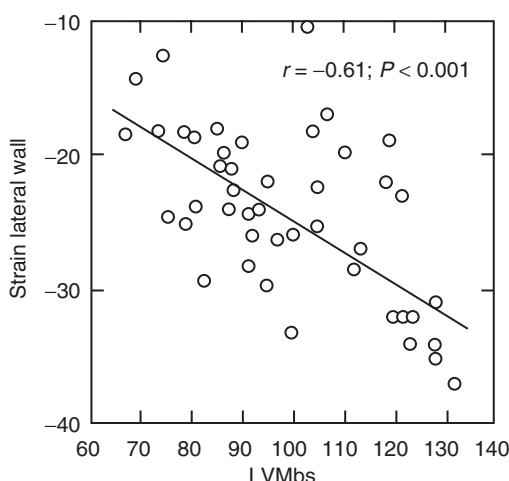


**Figure 17.5** Inverse relationship between LVMbs and lateral wall strain in sHyperT and control subjects.

abnormality, the need for lifelong treatment with thyroxine (L-T4) is still controversial. On the other hand, metabolic, neuromuscular and neurobehavioral abnormalities have been described in subclinical hypothyroidism [34,35]. Furthermore, abnormalities in myocardial contractility associated with changes of lipoprotein profile have been reported. sHypoT seems to be a risk factor for the development of coronary heart disease [36,37]. Indeed, a greater progression of coronary angiographic lesions in sHypoT patients, compared to patients whose TSH levels are within the normal range, has been reported.

Impaired myocardial contractility in overt hypothyroidism has been documented clinically and experimentally [38–40]. However, the presence of similar abnormalities in subclinical hypothyroidism

is still a matter of debate. With conventional Doppler echocardiography, an impairment of LV diastolic function both at rest and during exercise, associated with a clear improvement after L-T4 replacement therapy, has been reported [41–43]. Biondi et al. [44] have documented an impairment of LV diastolic function in sHypoT, reversible after 6 months of L-T4 replacement therapy. On the contrary, other authors have not found abnormalities of systolic time intervals and of ejection fraction, as assessed by simultaneous recording of the aortic and mitral flow velocities or radionuclide ventriculography. These conflicting results might, in part, be related to different patient selection (age, inclusion of patients with unstable sHypoT) and to different diagnostic criteria (wide range of TSH levels, inclusion of patients with low serum FT<sub>4</sub> levels).

The results of studies on the effects of sHypoT on LV structure and function are controversial, particularly with regard to the effects on LV systolic function at rest. These conflicting data could be explained by the selection of patients or to different diagnostic criteria for sHypoT. Di Bello et al. [45] have demonstrated that sHypoT is associated with early abnormalities in both myocardial function and structure and, in a subsequent study, Monzani has reported the effect of L-T4 replacement therapy on myocardial function and structure by means of conventional echocardiography and videodensitometric analysis. These data have been supported by a subsequent blinded, randomized controlled trial of L-T4 replacement therapy in 20 young patients with sHypoT [46]. Patients were strictly selected to exclude those with confounding factors (particularly those affecting the cardiovascular system). Special attention was taken to include only patients with free thyroid hormone levels within the normal range. Baseline and follow-up conventional echocardiography and ultrasonic videodensitometric analysis demonstrated a significant impairment of both LV diastolic and systolic function in subclinical hypothyroidism that were fully reversible with L-T4 replacement therapy. However, abnormalities of LV diastolic function need a longer period of treatment than systolic function parameters to be reversed. A minimal or absent systolic/diastolic excursion of the CVI was found which may be considered as a further early index of altered myocardial function, that is, impaired “intrinsic” myocardial contractile

performance [47]. This interpretation is in agreement with the observed inverse relationship between the PEP/LVET ratio and CVI. In parallel with conventional echocardiographic parameters, a progressive improvement of videodensitometric findings was observed during L-T4 treatment. In fact, a significant increase of CVI was already detectable after 6 months, but its normalization was achieved only after 1 year of replacement therapy. It is noteworthy that CVI and serum TSH level variations were inversely correlated (Figure 17.6). These data confirm the findings of two previous randomized studies using conventional Doppler echocardiography [48,49], one of which evaluated only systolic time intervals, whereas the other was not placebo controlled.

This study demonstrated the complete reversibility of myocardial ultrasonic textural abnormalities observed in sHypoT patients (through the videodensitometric approach) after 1 year of replacement therapy. The behavior of these myocardial textural findings could be considered as the expression of a normalization of the complex myocardial ultrastructure as well as an improvement in intrinsic contractility in treated sHypoT patients.

We recently repeated this work using new ultrasound techniques (IBS and CDMI) in another 24 young patients with newly diagnosed, untreated subclinical hypothyroidism (sHypoT) [50]. In this study, PW-TDI at the mitral annulus, an expression of global longitudinal LV function, identified

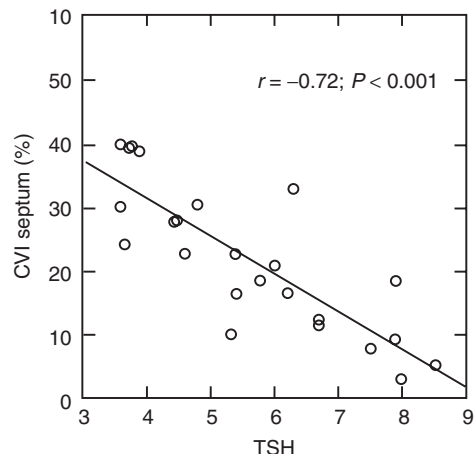
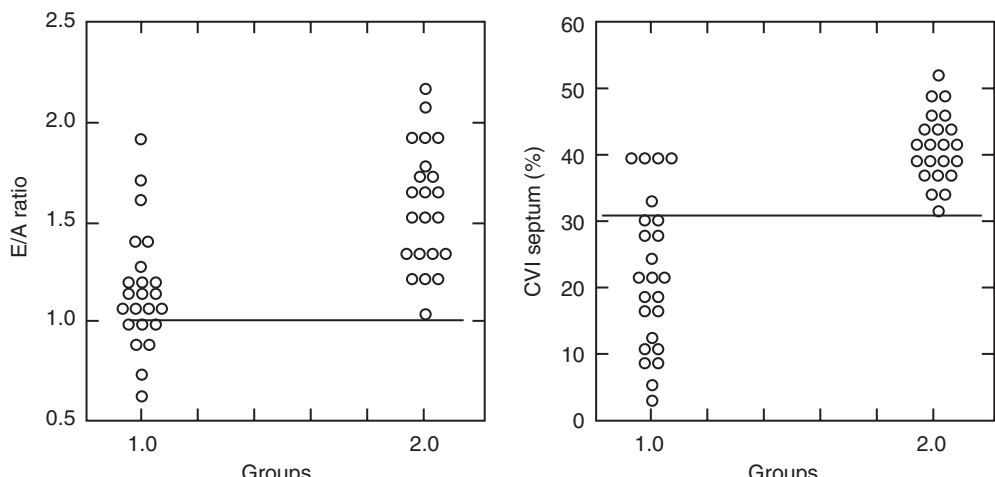


Figure 17.6 Relationship between CVI at the septum level and serum TSH concentration in patients with sHypoT.



**Figure 17.7** The E/A ratio obtained by transmural Doppler (left) and septal CVI obtained by IBS (right) in patients with sHypoT (group 1.0) and in controls (group 2.0).

diastolic LV myocardial abnormalities in sHypoT. Among the new ultrasound parameters, CVI at septum level showed the highest discriminating power (86%) between groups with and without sHypoT, whereas conventional Doppler mitral flow E/A ratio showed a very low discriminating power (33%) (comparison between the two methods;  $P < 0.001$ ) (Figure 17.7). These results were concordant with reports of impaired global longitudinal ventricular diastolic function and alteration of myocardial time intervals with sHypoT [51] and changes in not only diastolic but also systolic function with borderline hypothyroidism [52]. By contrast, conventional echocardiographic indices (e.g., ejection fraction and fractional shortening) were unable to differentiate healthy from sHypoT myocardium.

These data show that myocardial dysfunction in sHypoT is also associated with modifications of both the acoustic properties (IBS) and the velocity of myocardial fiber motion (CDMI) and regional myocardial deformation (systolic strain and strain rate analysis). These results suggest both a reduction in contractility, as well as increased myocardial reflectivity, suggesting an alteration of myocardial texture. Indeed, previous tissue characterization studies using VD documented higher reflectivity in combination with increased collagen fraction (i.e., increased intramyocardial fibrosis) in overt, but not in subclinical, hypothyroid patients [53].

These early abnormalities of myocardial function and texture reinforce the notion that sHypoT is strongly associated with the risk of future cardiovascular events [54].

The mechanisms of these effects of sHypoT are still debated. The role of thyroid autoimmunity in the development of cardiovascular events is also debated. Minimal reductions in hormone activity at the myocardial level may over time lead to biochemical and functional effects qualitatively similar to those of overt hypothyroidism, responsible for the functional myocardial abnormalities. Thyroid hormone deficiency could alter cardiac muscle function by decreasing the activity of several enzymes involved in the regulation of calcium homeostasis [55] and the expression of several contractile proteins [56]. Cardiac muscle functional abnormalities, such as abnormalities in calcium uptake and release that could reduce inotropy, occur in sHypoT, although in a milder manner compared to overt hypothyroidism [57]. Our data suggest that myocardial dysfunction in sHypoT is associated also with modifications of the acoustic properties of the myocardial tissue. An increase in albumin distribution in the extracellular space or an increase in capillary permeability could increase the tissue water content and influence the acoustic properties of the myocardium [58].

In summary, both phases of the cardiac cycle are involved early and simultaneously in sHypoT,

causing a decrease in intramyocardial contractility and an impairment of both active and passive phases of diastole. The application of sensitive, non-invasive techniques, which are relatively independent from loading conditions, permits the detection of subtle functional and textural abnormalities of intramural myocardium, partially undetectable by conventional two-dimensional Doppler echocardiography. Indeed, the high sensitivity of new ultrasonic intramyocardial indices of LV global or regional function in comparison with conventional echo parameters may explain the variations in literature regarding the cardiac consequences of sHypoT.

### Growth hormone excess

Acromegaly is associated with an increased mortality mainly due to cerebral and cardiovascular causes. However, an increasing body of evidence supports the existence of a specific acromegalic cardiomyopathy not related to either hypertension or diabetes. This acromegalic cardiomyopathy is characterized by myocardial hypertrophy and interstitial fibrosis and is due to chronic growth hormone (GH) and insulin-like growth factor-1 (IGF-1) excess. A progressive impairment of acromegalic heart architecture occurs due to increased extracellular collagen deposition and myocyte hypertrophy; in addition, myofibrillar derangement and development of areas of monocyte necrosis and apoptosis in cardiomyocytes and in fibroblasts are considered the ultrastructural hallmarks. In fact, cardiac hypertrophy has been reported in approximately 20% of young acromegalic patients and is a common finding (72%) in older patients with a longer duration of disease [59–63].

Decreased diastolic filling may be found in acromegalic patients using conventional echocardiography. These abnormalities, which reflect the impairment of global cardiac function, may become evident after several years and affect systolic function, mainly during exercise. Systolic derangement is revealed in the late stage of acromegalic cardiomyopathy and is considered secondary to diastolic impairment [64–70].

Mercuro studied 18 patients with active untreated acromegaly and found an impairment of regional systolic function in the presence of a normal

ejection fraction. However, no correlation was shown between these parameters and serum GH or IGF-1 concentrations, nor with the estimated duration of disease [71]. A prospective study [72] reported that patients with active untreated acromegaly had elevated values of the index (which evaluates global cardiac function), in contrast with controls or patients with disease treated medically or surgically. However, because the Tei index is an indicator of global cardiac dysfunction, segmental abnormalities might not have been revealed.

Several studies have shown that some cardiac abnormalities might be reversed by treating acromegaly, mainly in the youngest patients, thus suggesting that prompt therapeutic intervention may avoid or slow progression of cardiac changes. In addition, diastolic function may improve after successful therapy of acromegalic patients.

Bogazzi et al. have recently evaluated early changes of systolic function and the degree of fibrosis using highly sensitive IBS indices [12], and Di Bello et al. [73] have investigated the intramyocardial longitudinal velocities and deformation using both PW-TDI and CDMI indices such as strain rate (SR) and strain ( $\epsilon$ ) in acromegalic patients before and after a 6-month course with somatostatin (SMSA) (Figure 17.8). The study comprised a group of 29 acromegalic patients: 22 with active untreated acromegaly evaluated at baseline and after a 6-month course with Sandostatin LAR 20 mg every 28 days for 6 months and 8 patients treated surgically.

The main findings of these studies are that the acromegalic heart showed (1) increased reflectivity (IBS), probably an expression of abnormal collagen content; (2) significantly lower CVI values compared to controls (IBS) both at the septum and at the posterior wall, an expression of impaired intrinsic contractility; (3) impaired systolic function, shown by the deformation parameters systolic strain and systolic strain rate; and (4) a significant trend toward normalization of the previously described abnormal new ultrasonic indices at the end of a treatment period.

The reduction of systolic deformation is an early myocardial functional abnormality, which develops in parallel with diastolic dysfunction, when common conventional systolic functional indices are normal. The fact that systolic changes are at least as early as diastolic ones is supported by

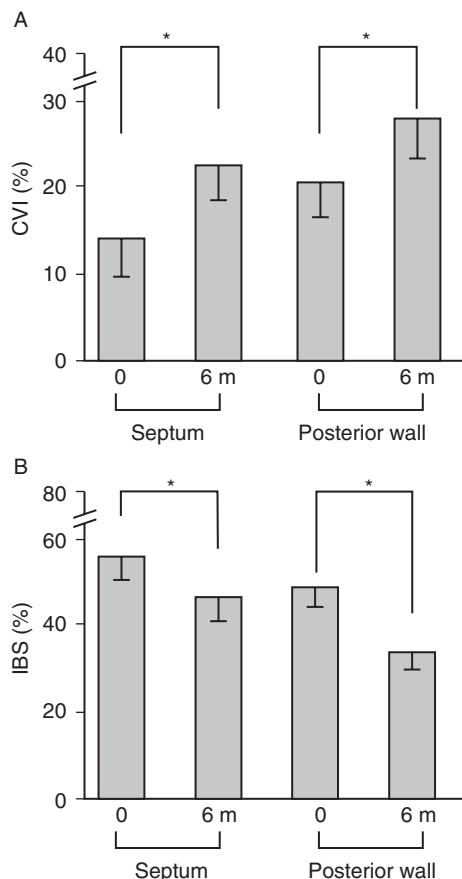


**Figure 17.8** Variation of intrinsic myocardial contractility and collagen content before (0) and after a 6-month course with SMSA analogues (6 m). Myocardial intrinsic contractility, assessed by CVI (A), and collagen content, as evaluated by IBS (B), were measured at either the septum ( $\text{CVI}_{\text{s}}$  and  $\text{IBS}_{\text{s}}$ , respectively) or posterior wall ( $\text{CVI}_{\text{pw}}$  or  $\text{IBS}_{\text{pw}}$ , respectively). \* $P < 0.003$ .

their correlation with serum GH and IGF-1 levels – although this finding does not correlate with the estimated duration of disease. Moreover, strain rate and strain showed a high discriminating power between acromegalic patients and controls (Figure 17.9).

Pharmacological treatment with SMSA produced a significant improvement of indices of myocardial systolic and diastolic function, suggesting that prompt control of disease activity is mandatory in all patients to prevent a further derangement of cardiac function. Prompt control of acromegaly is particularly important because early abnormalities of myocardial contractility and fibrosis content due to GH and IGF-1 excess are susceptible to regression,

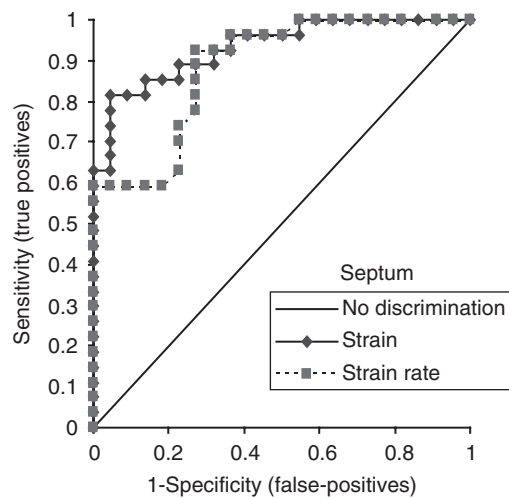


**Figure 17.9** Receiver operator characteristic curves showing the discriminating power of septal strain and strain rate to distinguish acromegalic from control myocardium.

and the likelihood of regression is greater how much earlier the treatment is started.

## Growth hormone deficiency

Hypopituitary patients have a reduced life expectancy, with an approximately twofold higher risk of death from cardiovascular disease (essentially for ischemic heart diseases) compared with healthy controls. The limited reports of conventional echocardiographic findings in this condition show a reduction in LVM, caused by a reduction of LV internal diameter and of thickness both of septum and of posterior wall [74] and a reduction of LV ejection fraction both at basal conditions and at peak exercise. A recent study of 16 hypopituitary, GH-deficient patients, performed using conventional Doppler echocardiography and TDI of the mitral and tricuspid annulus, showed a significant reduction of peak early diastolic (Em) mitral annular velocity [75].

## Hyperaldosteronism

Primary hyperaldosteronism (PA) offers a unique opportunity to investigate the role of excess aldosterone in humans, because angiotensin II is typically suppressed. Doppler flow velocity indices

of early diastolic transmural flow are decreased compared with those of patients with primary (essential) hypertension (EH). These abnormalities are more pronounced in patients with Conn's adenoma, in whom aldosterone excess and renin suppression are also more prominent, and are corrected by adrenalectomy, thus indicating a causative role of excess aldosterone in cardiac fibrosis [76,77]. Rossi et al. [78] compared myocardial texture features known to correlate with extracellular matrix and collagen deposition in 17 patients affected by PA (secondary to an adenoma in the majority of cases) with 10 control subjects with EH (diagnosed after the exclusion of all possible causes of secondary hypertension). PA patients exhibited a higher prevalence of LV hypertrophy and LV remodeling, abnormal filling, and changes in myocardial texture. These findings confirm that excess aldosterone affects cardiac mass independently of arterial blood pressure, that diastole is more dependent on atrial contraction in PA patients, and also that changes in myocardial texture (i.e., fibrosis) are characteristic of PA patients. The EH patients in this trial showed values of  $CVI_s$  and  $CVI_{pw}$  that were almost identical to those found in a larger series of EH patients with normal LV mass and concentric remodeling, making a selection bias unlikely (Figure 17.10). Furthermore, in another series of EH patients with pronounced concentric LV hypertrophy,  $CVI_s$  values were quite similar to those seen in the PA patients, who had a much lower LVM index. Thus, the effects of excess aldosterone appear to be independent of pressure overload in the alteration of myocardial texture.

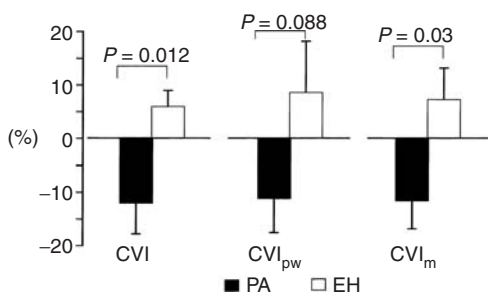


**Figure 17.10** Bar graph showing the mean values of  $CVI_s$ ,  $CVI_{pw}$ , and  $CVI_m$  in patients with PA and EH. The significantly lower values for both indices in PA suggest the presence of cardiac fibrosis.

The abnormalities of the acoustic properties of PA myocardium have several explanations. Increased deposition of extracellular matrix and collagen, as a result of excess aldosterone in PA, may create increased backscatter in systole. In the normal heart, the loss of acoustic myocardial reflectivity during systole is related to the shortening of myocardial fibers during contraction. Augmentation of collagen content, which was found in postmortem specimens of hearts of patients with autopsy-proven adrenal adenoma, could decrease the normal cyclic variation of backscatter by impairing contractility. Secondly, pressure-volume overload, which stretches the myocardium, could change the orientation, structure, or geometry of both the muscle fibers and of the collagen network, thereby influencing the acoustic properties of the myocardium. Whatever the mechanisms, our results indicate that videodensitometric analysis of myocardial texture is a sensitive test, along with LV mass and LV filling changes, for the early identification of cardiac involvement in patients with PA.

Further mechanistic insight has been gained by examining the relationship between individual variables and videodensitometric indices of cardiac fibrosis. There is a direct relationship between  $CVI_s$  and plasma renin activity (PRA), indicating that lower PRA values are associated with higher collagen deposition in the heart. A regression analysis also identified electrocardiogram PQ duration, baseline supine PRA, plasma aldosterone, and age as predictors of CVI. Because the electrocardiogram PQ interval reflects conduction time from the sinoatrial node through the atria, the atrioventricular node, and the Purkinje fibers to the left ventricle, the highly significant ( $P = 0.009$ ) correlation of CVI with PQ duration suggests that fibrosis has important sequelae in the conduction system.

More recently, Kozakova et al. have performed IBS analysis in 42 hypertensive patients (14 with primary aldosteronism, 7 with renovascular hypertension, and 21 with EH) [79]. Myocardial IBS sampled at end-diastole was significantly higher in patients with PA and renovascular hypertension than EH. In the entire population, as well as in the hypertensive subpopulation, myocardial IBS was directly and significantly related to plasma aldosterone and immunoreactive endothelin. These results

suggest that, in human hypertension, circulating aldosterone and immunoreactive endothelin may induce abnormalities in LV myocardial texture, possibly related to increased myocardial collagen content. Moreover, the LV changes of secondary aldosteronism (e.g., in congestive heart failure) should respond to mineralocorticoid receptor blockade with not only improved outcome [80], decreased LVM index, and LV end-diastolic diameter and volume, but also reduction of biochemical markers of myocardial fibrosis and hypertrophy [81].

## Conclusion

New ultrasonic techniques have a high diagnostic sensitivity for the detection of early subclinical abnormalities of myocardial function compared to conventional echocardiography. This very early detection allows the initiation of patients treatment in a more aggressive manner, thereby preventing an evolution toward overt heart failure. On the other hand, more studies are needed to confirm both the diagnostic and prognostic significance of subclinical heart disease associated with endocrine disorders.

## Acknowledgments

I am very grateful to my colleagues at the Echocardiographic Laboratory of the Cardiac Thoracic and Vascular Department of the University of Pisa (Dr. C. Palagi, Dr. M.G. Delle Donne, and Dr. E. Talini) for their precious help and support and to Dr Giovanna Lastrucci for editorial assistance.

## References

- Baxter JD, Young WF, Webb P. Cardiovascular endocrinology: introduction. *Endocr Rev* 2003; **24**: 253–60.
- Ribeiro RC, Kushner PJ, Baxter JD. The nuclear hormone receptor gene superfamily. *Annu Rev Med* 1995; **46**: 443–53.
- Ledenson PW. Thyrotoxicosis and the heart: something old and something new. *J Clin Endocrinol Metab* 1993; **77**: 332–3.
- Edvardsen T, Gerber BL, Garot J, Bluemke DA, Lima JA, Smiseth OA. Quantitative assessment of intrinsic regional myocardial deformation by Doppler strain rate echocardiography in humans. *Circulation* 2002; **106**: 50–6.
- Sutherland GR, Di Salvo G, Claus P, D'hooge J, Bijnens B. Strain and strain rate imaging: a new clinical approach to quantifying regional myocardial function. *J Am Soc Echocardiogr* 2004; **17**: 788–802.
- Skorton DJ, Collins SM. Clinical potential of ultrasound tissue characterization in cardiomyopathies. *J Am Soc Echocardiogr* 1988; **1**: 69–77.
- Di Bello V, Pedrinelli R, Giorgi D, et al. Ultrasonic videodensitometric analysis of two different models of left ventricular hypertrophy: athlete's heart and hypertension. *Hypertension* 1997; **29**: 937–44.
- Lythall DA, Bishop J, Greenbaum RA, et al. Relationship between myocardial collagen and echo amplitude in non fibrotic hearts. *Eur Heart J* 1993; **14**: 344.
- Wickline SA, Thomas LJ III, Miller JG, Sobel BE, Perez JE. A relationship between ultrasonic integrated backscatter and myocardial contractile function. *J Clin Invest* 1985; **76**: 2151–60.
- Di Bello V, Giorgi D, Talini E, et al. Incremental value of ultrasonic tissue characterization (backscatter) in evaluation of left ventricular myocardial structure and mechanics in essential arterial hypertension. *Circulation* 2003; **107**: 74–80.
- Di Bello V, Giorgi D, Viacava P, et al. Severe aortic stenosis and myocardial function: diagnostic and prognostic usefulness of ultrasonic integrated backscatter analysis. *Circulation* 2004; **110**: 849–55.
- Bogazzi F, Di Bello V, Palagi C, et al. Improvement of intrinsic myocardial contractility and cardiac fibrosis degree in acromegalic patients treated with somatostatin analogues: a prospective study. *Clin Endocrinol (Oxf)* 2005; **62**: 590–6.
- Di Bello V, Santini F, Di Cori A, et al. Relationship between preclinical abnormalities of global and regional left ventricular function and insulin resistance in severe obesity: a color Doppler imaging study. *Int J Obes (Lond)* 2006; **30**: 948–56.
- McDermott MT, Woodmansee WW, Haugen BR, Smart A, Ridgway EC. The management of subclinical hyperthyroidism by thyroid specialists. *Thyroid* 2003; **13**: 1133–9.
- Biondi B, Palmieri EA, Lombardi G, Fazio S. Effects of subclinical thyroid dysfunction on heart. *Ann Intern Med* 2002; **137**: 904–14.
- Mercuro G, Panzuto MG, Bina A, et al. Cardiac function, physical exercise capacity, and quality of life during long-term thyrotropin-suppressive therapy with levothyroxine: effect of individual dose tailoring. *J Clin Endocrinol Metab* 2000; **85**: 159–64.
- Kahaly GJ, Dillmann WH. Thyroid hormone action in the heart. *Endocr Rev* 2005; **26**: 704–28.
- Sgarbi JA, Villaca F, Garbelino B, Villar HE, Romaldini JH. The effects of early anti thyroid therapy for endogenous subclinical hyperthyroidism on clinical and heart abnormalities. *J Clin Endocrinol Metab* 2003; **88**: 1672–7.

- 19 Biondi B, Palmieri EA, Lombardi G, Fazio S. Effects of thyroid hormone on cardiac function: the relative importance of heart rate, loading conditions, and myocardial contractility in the regulation of cardiac performance in human hyperthyroidism. *J Clin Endocrinol Metab* 2002; **87**: 968–74.
- 20 Fazio S, Palmieri EA, Lombardi G, Biondi B. Effects of thyroid hormone on the cardiovascular system. *Recent Prog Horm Res* 2004; **59**: 31–50.
- 21 Biondi B, Palmieri EA, Fazio S, et al. Endogenous subclinical hyperthyroidism affects quality of life and cardiac morphology and function in young and middle-aged patients. *J Clin Endocrinol Metab* 2000; **85**: 4701–5.
- 22 Shapiro LE, Sievert R, Ong L, et al. Minimal cardiac effects in asymptomatic athyreotic patients chronically treated with thyrotropin-suppressive doses of L-thyroxine. *J Clin Endocrinol Metab* 1997; **82**: 2592–5.
- 23 Banovac K, Papic M, Bilsker MS, Zakarija M, McKenzie JM. Evidence of hyperthyroidism in apparently euthyroid patients treated with levo-thyroxine. *Arch Intern Med* 1989; **149**: 809–12.
- 24 Surks MI, Ortiz E, Daniels GH, et al. Subclinical thyroid disease. Scientific review and guidelines for diagnosis and management. *JAMA* 2004; **291**: 228–38.
- 25 Di Bello V, Aghini-Lombardi F, Di Cori A, et al. Early abnormalities of left ventricular myocardial characteristics associated with subclinical hyperthyroidism. *J Endocrinol Invest* [submitted].
- 26 Tseng KH, Walfish PG, Persaud JA, Gilbert BW. Concurrent aortic and mitral valve echocardiography permits measurements of systolic time intervals as an index of peripheral tissue thyroid functional status. *J Clin Endocrinol Metab* 1989; **69**: 633–8.
- 27 Dörr M, Wolff B, Robinson DM, et al. The association of thyroid function with cardiac mass and left ventricular hypertrophy. *J Clin Endocrinol Metab* 2005; **90**: 673–7.
- 28 Klein I, Ojamaa K. Thyroid hormone and the cardiovascular system. *N Engl J Med* 2001; **344**: 501–9.
- 29 Ching GW, Franklyn JA, Stallard TJ, Daykin J, Sheppard M, Gammie MD. Cardiac hypertrophy as a result of long-term thyroxine therapy and thyrotoxicosis. *Heart* 1996; **75**: 363–8.
- 30 Biondi B, Fazio S, Carella C, et al. Control of adrenergic overactivity by beta-blockade improves quality of life in patients receiving long term suppressive therapy with levothyroxine. *J Clin Endocrinol Metab* 1994; **78**: 1028–33.
- 31 Surks MI, Ortiz E, Daniels GH, et al. Subclinical thyroid disease. Scientific review and guidelines for diagnosis and management. *JAMA* 2004; **291**: 228–38.
- 32 Tunbridge WM, Evered DC, Hall R, et al. The spectrum of thyroid disease in a community: the Whickham survey. *Clin Endocrinol (Oxf)* 1977; **7**: 481–93.
- 33 Sawin CT, Chopra D, Azizi F, Mannix JE, Bacharach P. The aging thyroid. Increase prevalence of elevated serum thyrotropin levels in the elderly. *JAMA* 1979; **242**: 247–50.
- 34 Canaris GJ, Manowitz NR, Mayor G, Ridgeway EC. The Colorado thyroid disease prevalence study. *Arch Intern Med* 2000; **160**: 526–34.
- 35 Sahin I, Turan N, Kosar F, Tascapan C, Gunen H. Evaluation of autonomic activity in patients with subclinical hypothyroidism. *J Endocrinol Invest* 2005; **28**: 209–13.
- 36 Forfar JC, Walhen CG, Todd TA, et al. Left ventricular performance in subclinical hypothyroidism. *Q J Med* 1985; **224**: 857–65.
- 37 Ridgway EC, Ladenson PW, Cooper DS, Daniels GH, Francis GS, Maloof F. Cardiac function in mild and severe hypothyroidism. *Life Sci* 1982; **30**: 651–8.
- 38 Ridgway EC, Cooper DS, Walker H, Rodbard D, Maloof F. Peripheral responses of thyroid hormone before and after L-thyroxine therapy in patients with subclinical hypothyroidism. *J Clin Endocrinol Metab* 1981; **53**: 1238–42.
- 39 Nyström E, Caidhal K, Fager G, Wikkelso C, Lundberg PA, Lindstedt G. A double-blind cross-over 12 month study of L-thyroxine treatment of women with subclinical hypothyroidism. *Clin Endocrinol (Oxf)* 1988; **29**: 63–76.
- 40 Bough EW, Crowley WF, Ridgway EC, et al. Myocardial function in hypothyroidism: relation to disease severity and response to treatment. *Arch Intern Med* 1987; **138**: 1476–80.
- 41 Cooper DS, Halpern R, Wood LC, Levin AA, Ridgway EC. L-thyroxine therapy in subclinical hypothyroidism. A double blind, placebo-controlled trial. *Ann Intern Med* 1984; **101**: 18–24.
- 42 Forfar JC, Wathen CG, Todd TA, et al. Left ventricular performance in subclinical hypothyroidism. 1985; **224**: 857–65.
- 43 Ridgway EC, Ladenson PW, Cooper DS, Daniels GH, Francis GS, Maloof F. Cardiac function in mild and severe primary hypothyroidism. *Life Sci* 1982; **30**: 651–8.
- 44 Biondi B, Fazio S, Palmieri EA, et al. Left ventricular diastolic dysfunction in patients with subclinical hypothyroidism. *J Clin Endocrinol Metab* 1999; **84**: 2064–7.
- 45 Di Bello V, Monzani F, Giorgi D, et al. Ultrasonic myocardial textural analysis in subclinical hypothyroidism. *J Am Soc Echocardiogr* 2000; **13**: 832–40.
- 46 Monzani F, Di Bello V, Caraccio N, et al. Effect of levothyroxine on cardiac function and structure in subclinical hypothyroidism: a double blind, placebo-controlled study. *J Clin Endocrinol Metab* 2001; **86**: 1110–5.
- 47 Wickline SA, Thomas LJ III, Miller JG, Sobel BE, Perez JE. A relationship between ultrasonic integrated

- backscatter and myocardial contractile function. *J Clin Invest* 1985; **76**: 2151–60.
- 48 Cooper DS, Halpern R, Wood LC, Levin AA, Ridgway EC. L-thyroxine therapy in subclinical hypothyroidism. A double blind, placebo-controlled trial. *Ann Intern Med* 1984; **101**: 18–24.
- 49 Nystrom E, Caidhal K, Fager G, Wikkelso C, Lundberg PA, Lindstedt G. A double-blind cross-over 12 month study of L-thyroxine treatment of women with subclinical hypothyroidism. *Clin Endocrinol (Oxf)* 1988; **29**: 63–76.
- 50 Aghini-Lombardi F, Di Bello V, Talini E, et al. Early textural and functional alterations of left ventricular myocardium in mild hypothyroidism. *Eur J Endocrinol* 2006; **155**: 3–9.
- 51 Vitale G, Galderisi M, Lupoli GA, et al. Left ventricular myocardial impairment in subclinical hypothyroidism assessed by a new ultrasound tool: pulsed tissue Doppler. *J Clin Endocrinol Metab* 2002; **87**: 4350–5.
- 52 Zoncu S, Pigliaru F, Puzzu C, et al. Cardiac function in borderline hypothyroidism: a study by pulsed wave tissue Doppler imaging. *Eur J Endocrinol* 2005; **152**: 527–33.
- 53 Ciulla M, Paliotti R, Tortora R, Valentini P, Cortelazzi B, Beck-Peccoz P. Myocardial ultrasonic reflectivity in patients with thyroid dysfunction: a tissue characterization study. *Cardiovasc Imag* 1997; **9**: 75–7.
- 54 Bartalena L, Pinchera A. Levothyroxine suppressive therapy: harmful and useless or harmless and useful? *J Endocrinol Invest* 1994; **17**: 675–7.
- 55 Rohrer D, Dillmann WH. Thyroid hormone markedly increases the mRNA coding for sarcoplasmatic reticulum  $\text{Ca}^{2+}$ -ATPase in rat heart. *J Biol Chem* 1988; **263**: 6941–4.
- 56 Hoyt RH, Collins SL, Skorton DJ, Eriksen EE, Conyers DC. Assessment of fibrosis in infarcted human hearts by analysis of ultrasonic backscatter. *Circulation* 1985; **71**: 740.
- 57 Lythall DA, Bishop J, Greenbaum RA, et al. Relationship between myocardial collagen and echo amplitude in non fibrotic hearts. *Eur Heart J* 1993; **14**: 344.
- 58 Parving HH, Hansen JM, Neilsen SL, Rossing N, Munck O, Lassen NA. Mechanism of edema formation in myxedema: increased protein extravasation and relatively slow lymphatic drainage. *N Engl J Med* 1979; **301**: 460–6.
- 59 Lie JT, Grossman SJ. Pathology of the heart in acromegaly: anatomic findings in 27 autopsied patients. *Am Heart J* 1980; **100**: 41–5.
- 60 Colao A, Merola B, Ferone D, Lombardi G. Acromegaly. *J Clin Endocrinol Metab* 1997; **82**: 2777–81.
- 61 Hejtmancik MR, Bradfield JY, Herrmann GR. Acromegaly and the heart: a clinical and pathologic study. *Ann Intern Med* 1951; **34**: 1445–56.
- 64 Colao A, Marzullo P, Di Somma C, Lombardi G. Growth hormone and the heart. *Clin Endocrinol (Oxf)* 2001; **54**: 137–54.
- 63 Clayton RN. Cardiovascular function in acromegaly. *Endocr Rev* 2003; **24**: 272–7.
- 64 Colao A, Spinelli L, Cuocolo A, et al. Cardiovascular consequences of early-onset growth hormone excess. *J Clin Endocrinol Metab* 2002; **87**: 3097–104.
- 65 Frustaci A, Chimenti C, Setoguchi M, et al. Cell death in acromegalic cardiomyopathy. *Circulation* 1999; **99**: 1426–34.
- 66 Fazio S, Cittadini A, Biondi B, et al. Cardiovascular effects of short-term growth hormone hypersecretion. *J Clin Endocrinol Metab* 2000; **85**: 179–82.
- 67 Vitale G, Pivonello R, Galderisi M, et al. Cardiovascular complications in acromegaly: methods of assessment. *Pituitary* 2001; **4**: 251–7.
- 68 Lim MJ, Barkan AL, Buda AJ. Rapid reduction of left ventricular hypertrophy in acromegaly after suppression of growth hormone hypersecretion. *Ann Intern Med* 1992; **117**: 719–726.
- 69 Tokgozoglu SL, Erbas T, Aytemir K, Akalin S, Kes S, Oram E. Effects of octreotide on left ventricular mass in acromegaly. *Am J Cardiol* 1994; **74**: 1072–4.
- 70 Lombardi G, Colao A, Ferone D, et al. Cardiovascular aspects in acromegaly: effects of treatment. *Metabolism* 1996; **45**: 57–60.
- 71 Mercuro G, Zoncu S, Colonna P, et al. Cardiac dysfunction in acromegaly: evidence by pulsed wave tissue Doppler imaging. *Eur J Endocrinol* 2000; **143**: 363–9.
- 72 Bruch C, Herrmann B, Schermund A, Bartel T, Mann K, Erbel R. Impact of disease activity on left ventricular performance in patients with acromegaly. *Am Heart J* 2002; **144**: 538–43.
- 73 Di Bello V, Bogazzi F, Di Cori A, et al. Myocardial systolic strain abnormalities in patients with acromegaly: a prospective color Doppler imaging study. *J Endocrinol Invest* 2006; **29**: 544–50.
- 74 Colau A, Vitale G, Pivonello R, Ciccarelli A, Di Somma C, Lombardi G. The heart: an end-organ of GH action. *Eur J Endocrinol* 2004; **151**: S93–101.
- 75 Yurci A, Oflaz H, Meric M, Ozbey N. Mitral and tricuspid annular velocities determined by Doppler tissue imaging in hypopituitary, growth hormone-deficient patients. *Horm Res* 2005; **64**: 107–14.
- 76 Rossi GP, Sacchetto A, Visentin PA, et al. Changes in left ventricular anatomy and function in hypertension and primary aldosteronism. *Hypertension* 1996; **27**: 1039–45.
- 77 Rossi GP, Sacchetto A, Pavan E, et al. Remodeling of the left ventricle in primary aldosteronism due to Conn's adenoma. *Circulation* 1997; **95**: 1471–8.

- 78 Rossi GP, Di Bello V, Ganzaroli C, et al. Excess aldosterone is associated with alterations of myocardial texture in primary aldosteronism. *Hypertension* 2002; **40**: 23–7.
- 79 Kozakova M, Buralli S, Palombo C, et al. Myocardial ultrasonic backscatter in hypertension: relation to aldosterone and endothelin. *Hypertension* 2003; **41**: 230–6.
- 80 Pitt B, Zannad F, Remme WJ, et al. The effect of spironolactone on morbidity and mortality in patients with severe heart failure. *N Engl J Med* 1999; **341**: 709–17.
- 81 Tsutamoto T, Wada A, Maeda K, et al. Effect of spironolactone on plasma brain natriuretic peptide and left ventricular remodeling in patients with congestive heart failure. *J Am Coll Cardiol* 2001; **37**: 1228–33.

# Myocardial imaging in valvular heart disease

*Sudhir Wahi and Thomas H. Marwick*

## Myocardial changes in valvular heart disease

### Myocardial changes and new technologies

Valvular heart disease produces pressure overload (aortic stenosis), volume overload (mitral regurgitation), or both pressure and volume overload (aortic regurgitation) on the left ventricle. Therefore, apart from in patients with mitral stenosis (in whom the left ventricular [LV] myocardium is spared), the adaptive response and function of the myocardium is an important determinant of immediate and longer term prognosis, second only to the severity of the valvular lesion. The status of the myocardium is a key factor in the onset of symptoms and effort tolerance preoperatively and the improvement or progression of LV dysfunction postoperatively, and should, therefore, be a key factor in surgical decision making.

Traditionally, the decision making for intervention in valvular heart disease has been based on a patient's symptoms of effort intolerance and resting indices of LV function [1–4]. Resting LV end-diastolic and end-systolic dimensions and ejection fraction have been the parameters used to follow up patients with valvular heart disease and recommend surgery [4–7]. Two-dimensional (2-D) measurements of LV volumes are useful in population studies, but limitations in accuracy and reproducibility pose problems for decision making. These problems have recently been improved by three dimensional (3-D) measurements (Figures 18.1 and 18.2). Even in groups, however, recent studies have shown these measurements to

be relatively insensitive markers to predict underlying latent LV dysfunction and postoperative outcomes on follow-up [8]. The improvement in surgical techniques and the advent of valve repair has led to a lowering of the threshold to explore surgical options in asymptomatic and minimally symptomatic patients. This paradigm shift comes with its own attendant problems of some premature and unnecessary repairs, in addition to the risk of operative morbidity and mortality and future redo surgery.

Recently, the myocardial response to isotonic exercise using exercise stress echocardiography has been used to predict postoperative outcome after valve repair or replacement. Contractile reserve (CR) or the ability to improve the ejection fraction with exercise has been shown to correlate with postoperative LV dysfunction [8] and outcome after mitral and aortic valve replacement. A loss of CR (i.e., lack of improvement or reduction in post-exercise ejection fraction) suggests subclinical or latent myocardial dysfunction in these patients.

Myocardial tissue Doppler imaging (TDI) [9–11] has helped in the detection of myocardial dysfunction using tissue velocity, strain, and strain rate. The recognition of latent LV dysfunction may also be facilitated by tissue characterization using integrated backscatter (IB). The latter has previously been shown to identify latent LV dysfunction and myocardial fibrosis in patients with LV hypertrophy (LVH) and hypertensive heart disease and in coronary artery disease [12–15]. Although IB can provide information on both tissue reflectivity and function, it is subject to anisotropy.

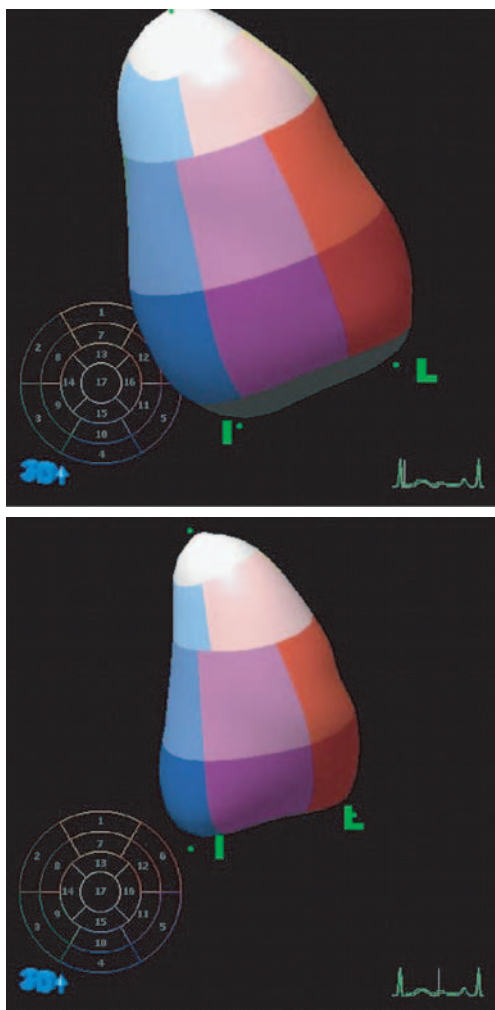


**Figure 18.1** Use of 3-D echocardiography to measure LV volumes in diastole (above) and systole (below).

In contrast, tissue Doppler methods measure contraction in the axis of the ultrasound beam, and 2-D strain can measure deformation in any direction, offering the ability to interrogate the function of longitudinal, radial, or circumferential directions [16]. This ability to measure longitudinal function is important, because long-axis fiber function contributes up to 50% of LV ejection fraction and appears to be affected early in patients with valvular heart disease, particularly in volume overload states [17–21]. Using myocardial tissue imaging, it is now possible to analyze the long-axis function reliably from the apical views [22,23].

### Myocardial changes in chronic pressure overload

The development of native valvular aortic stenosis (AS) results in obstruction to LV emptying and increases the workload of the myocardium, leading in some cases to LVH [24–26]. Concentric LVH is produced by the increase in diameter of the myocardial fibers, and the increase in LV mass directly correlates with the transaortic gradient with significant genetic variation [27]. The cardiac output and LV end-diastolic volume are maintained for a prolonged period, despite a systolic pressure gradient between the left ventricle and peripheral arterial system. During the compensated phase of AS, the increase in wall thickness helps to maintain normal end-systolic wall stress despite the increase in LV pressure.

As the hypertrophy continues, the left ventricle becomes less compliant. Other factors contributing to a reduction in ventricular function are incoordinate contraction, resulting from regional wall motion abnormalities or subendocardial ischemia, and myocardial fibrosis [24]. The cardiac connective tissue or interstitial fibers of the myocardium have an important role in modulating the LVH and remodeling. The increase in transaortic gradient stimulates fibroblast activity and an increase in the ratio of type III to type I collagen [28]. Continued progression of this process ultimately leads to a reduction in stroke volume and cardiac output, and eventual congestive heart failure. With the release of the transaortic obstruction, there is an early reduction of LV mass with a continued remodeling up to 8 years after aortic valve replacement. The delayed remodeling may be related to the regression of the interstitial fibrotic changes [29].

### Myocardial changes in chronic volume overload

Chronic mitral regurgitation (MR) produces a volume overload on the left ventricle, leading to eccentric LVH, with an increase in the length of the myocardial fibers causing chamber dilatation with no significant increase in wall thickness. In the compensated stage, there is a dilatation of the left ventricle with an increase in the LV end-diastolic volume and little or no change in the end-systolic volume. During this phase, the ejection fraction is maintained. The ability of the ventricle to offload the extra regurgitant volume into a low-impedance

left atrium masks the development of the overt contractile dysfunction with maintained ejection performance. LV wall stress is maintained with the increase in LV dimension without an increase in wall thickness [30–32].

### **Myocardial changes in chronic pressure and volume overload**

The left ventricle in chronic aortic regurgitation (AR) is faced with a combination of volume and pressure overload. The volume overload is understandable from the addition of the regurgitant volume to the forward stroke volume. However, AR also produces an increased afterload as the increased stroke volume is ejected into the high impedance aorta. To maintain a normal LV end-systolic wall stress in the face of LV dilatation, there is an increase in LV wall thickness or mass. In a previous study, Dodge et al. [33] have shown that patients with AR have the highest LV mass index when compared with normal subjects, patients with MR, or patients with AS. The combination of volume and pressure overload results in both LV dilatation and hypertrophy [32,34].

Similar to AS and MR patients, the myocardial changes are able to adapt and maintain the ejection fraction and cardiac output for a prolonged period. Even though symptoms of effort intolerance and overt LV dysfunction develop late, these patients often have latent or subclinical contractile dysfunction, which is masked by the loading conditions. Myocardial imaging is a useful means to identify myocardial changes in these patients and to be able to recognize contractile dysfunction despite the alterations of preload and afterload.

### **Changes in diastolic function**

Diastolic dysfunction develops much earlier than overt systolic dysfunction in patients with valvular heart disease. The increased volume and pressure overload produces changes in diastolic compliance and LV diastolic filling pressure. In the initial stage, there is an impairment in early diastolic relaxation of the left ventricle, which can progress to reduced compliance and a restrictive filling pattern. The elevated LV diastolic pressure is also reflected as elevated left atrial (LA) pressure and pulmonary congestion. These changes can account for symptoms of effort intolerance.

The standard Doppler parameters to assess LV filling are highly dependent on preload and intravascular volume. Myocardial imaging using TDI has been found to be a relatively load-independent and reliable measure for the assessment of LV diastolic pressure. Early myocardial tissue velocity ( $E'$  or  $Em$ ) and the ratio of early diastolic filling velocity ( $E$ ) from the transmural pulsed-wave Doppler to early myocardial tissue velocity ( $E'$ ) or  $E/E'$  has been shown to have a better correlation with LV diastolic pressure and pulmonary capillary wedge pressure. In a recent study, Nagueh et al. [35] demonstrated that load increases on average raised the transmural  $E$  velocity by 70%, whereas the same manipulations produced only a 13% change in  $Em$ . Low  $Em$  values are indicative of abnormal LV relaxation even when LV filling pressures are increased.

In the postoperative period, systolic dysfunction improves early, reflecting the resolution of pressure and/or volume overload. In contrast, the improvement of diastolic function and remodeling continues over years and depends on the extent of interstitial fibrosis.

## **Myocardial imaging in mitral valve disease**

### **Mitral regurgitation**

#### **Use in decision making**

Currently, clinical decisions for surgery in patients with MR have been based on resting LV function or ejection fraction and LV dimensions at end-diastole and end-systole. These parameters are insensitive predictors of LV dysfunction in these patients, and awaiting the development of symptoms or overt clinical or echocardiographic LV dysfunction risks the morbidity and mortality associated with congestive heart failure.

The recently updated ACC/AHA guidelines on the management of valvular heart disease have lowered the threshold in recommending earlier surgery in patients with symptoms of effort intolerance, severe MR, and preserved LV function. However, the management of asymptomatic patients with normal LV function remains controversial. Indeed, technological advancements are improving the ability to quantify regurgitation (Figure 18.2), to the

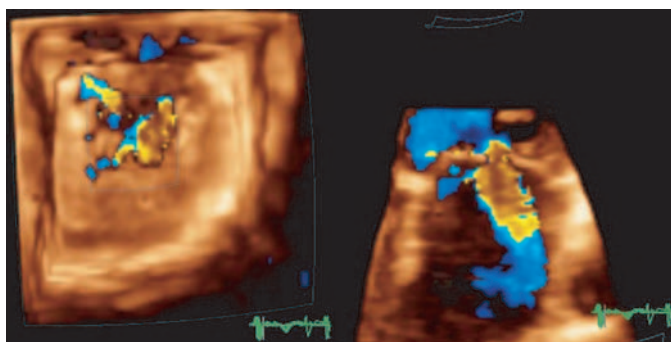


**Figure 18.2** Use of 3-D echocardiography to measure proximal isovelocity surface area and vena contracta.

extent that proof of severe MR has been argued as sufficient indication for surgery, provided that mitral valve (MV) repair is feasible, and a suitably skilled and experienced surgeon is available to perform MV repair [26]. This is clearly difficult to qualify objectively for clinical decision making for these patients. Although early surgery may prevent dysfunction in some patients, widespread early operation may result in more patients undergoing surgery, with implications regarding cost, recurrence (for repairs), and surgical risk or late complications (for replacements).

Moreover, studies support both aggressive (surgery) [36] and conservative (observational) [37] strategies for asymptomatic MR. The former study followed up asymptomatic patients with chronic MR and flail MV leaflets over 10 years, and demonstrated a significantly improved survival and a lower incidence of atrial fibrillation, cardiac death, and incidence of heart failure in the early surgery compared with the medically managed group [36]. In contrast, the study favoring the “watchful waiting” approach showed that waiting until either symptoms occurred or until currently recommended cutoff values for LV size, LV function, or pulmonary hypertension are reached was not associated with adverse outcome [37]. However, this finding contrasts with the first study, showing that *even in patients having early surgery, 27% manifested congestive heart failure in 5–10 years* [36]. The best strategy for avoiding deterioration of LV function might be to identify patients with occult LV dysfunction, and manage them more aggressively.

#### Assessment of contractile reserve

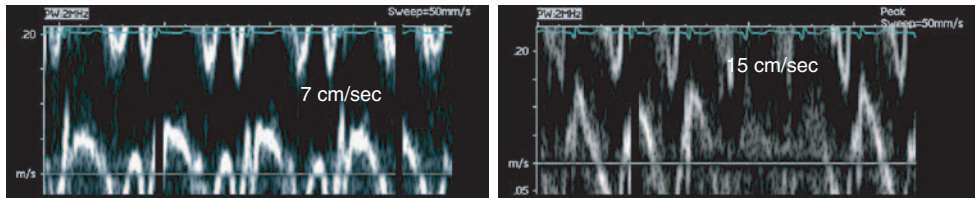
The normal LV response to exercise involves reduction of LV volumes and an increment of ejection

fraction (Video clip 25 ). Failure to augment LV ejection fraction with exercise (loss of CR) may identify subclinical LV dysfunction (Video clip 26 ). In a prospective study in patients with MR undergoing MV surgery [8], change of ejection fraction with exercise and exercise end-systolic volume index had a significantly better correlation ( $r$  value of 0.73 and 0.74, respectively) ( $P < 0.001$ ) than resting ejection fraction in being able to predict postoperative LV ejection fraction on follow-up in asymptomatic patients with severe MR. Although resting dP/dt on Doppler echocardiography was the best resting parameter to predict postoperative LV function, all the exercise parameters – end-systolic volume index, postexercise ejection fraction, and change in ejection fraction (CR) – had significantly higher sensitivities and specificities. Nonetheless, although CR is clinically useful, it has inherent limitations relating to technical difficulty in accurate tracing of the LV volumes, can be time consuming, and may be somewhat subjective.

#### Tissue Doppler imaging

As described in previous chapters, TDI permits the quantification of regional myocardial function, including long-axis function of the left ventricle. Patients with severe MR – even if asymptomatic or minimally symptomatic – tend to have more spherical ventricles due to volume overload. This change in geometry of the left ventricle may reduce its efficiency, in particular, the longitudinal (base–apex) piston function may be compromised even though short-axis function, or radial contractility, usually appears normal. Loss of CR, which is a marker of more severe latent LV dysfunction, correlates with abnormal longitudinal-axis function on exercise (Figure 18.3) [38].

## Patient 1 – Contractile reserve



## Patient 2 – Loss of contractile reserve

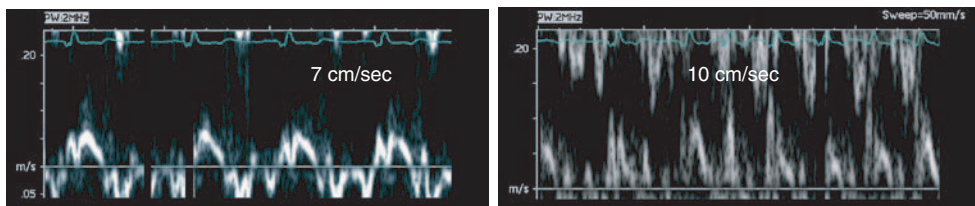


**Figure 18.3** Use of pulsed-wave tissue Doppler before and after exercise to quantify CR in two patients with comparable resting ejection fraction and tissue velocity.

The twofold augmentation in patient 1 confirms CR, whereas a minor increment in patient 2 corresponds to loss of CR.

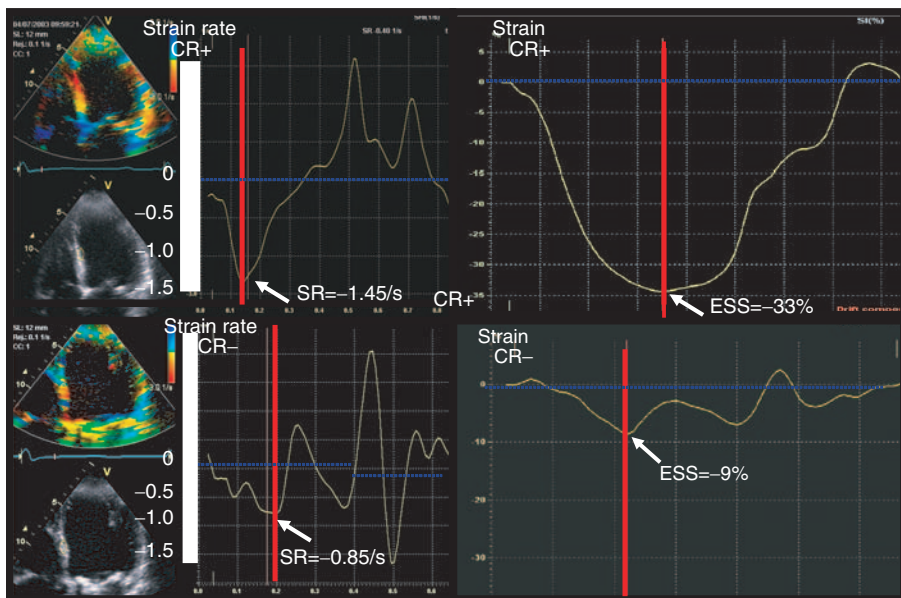


**Figure 18.4** Use of myocardial deformation at rest to predict CR in two patients with comparable resting ejection fraction. The upper panels show normal SR and strain in a

patient with preserved CR. The lower panels show reduced SR and strain in a patient with loss of CR.

### Assessment of myocardial deformation

Measurement of the amount of deformation or extent of shortening with strain rate (SR) imaging may also be used to characterize the myocardium in MR. In a group of patients with asymptomatic MR, with and without CR, SR was the only echocardiographic parameter at rest that is independently

predictive of CR [39]. End-systolic strain and SR were significantly greater in patients with CR when compared to patients without CR (Figure 18.4), but were not significantly different from normal controls. The receiver operating curve confirmed that resting SR had the maximum area under the curve, followed by functional capacity and end-systolic

volume postexercise. Using cutoffs of  $-1.07/\text{sec}$  for SR gives a sensitivity of 91%, specificity of 80%, and an accuracy of 88%. These findings support the presence of subclinical LV dysfunction in asymptomatic patients with severe MR and a normal LV ejection fraction at rest, similar to the detection of subclinical LV dysfunction in a variety of diseases before the development of abnormalities in conventional measures of LV performance. They also provide reassurance that those with normal CR have normal myocardium. This study suggests that evaluation of global long-axis function at rest, using SR imaging, is a feasible method for detecting subclinical LV dysfunction and can accurately predict CR in asymptomatic patients with severe MR. It may be a useful test for the follow-up of these patients and could assist in decisions with regard to the optimal timing of surgery.

To explore the histopathologic correlates of loss of CR and changes in myocardial strain in patients with valvular heart disease, we have evaluated intraoperative LV myocardial biopsy specimens from patients undergoing MV repair or replacement, in the absence of other confounding causes of myocardial fibrosis, including hypertensive heart disease, diabetes mellitus, coronary artery disease, or collagen vascular diseases. Patients with underlying myocardial fibrosis have a lower end-systolic strain at rest (Figure 18.5) and showed a lower cyclic variation of IB, when compared with those without fibrosis [40]. These findings support the concept of the development of myocardial ultrastructural changes before the development of overt LV dysfunction or symptoms, and highlight

the significance of myocardial tissue imaging in these patients with MV disease.

### Mitral stenosis

The left ventricle is not involved in the hemodynamic disturbances of mitral stenosis. The raised LA pressure due to the obstruction of flow across the mitral valve in diastole is reflected in the pulmonary circulation. Over a period of time, this finding can lead to changes in the pulmonary vasculature and development of pulmonary hypertension. Chronic pulmonary hypertension eventually leads to right ventricular (RV) pressure and/or volume overload and dysfunction.

The right ventricle is an important determinant of clinical symptoms, exercise capacity, and prognosis in MS. In this setting, RV performance is affected not only by changes in afterload but also by ventricular interaction and myocardial structure. It has been technically challenging to objectively quantify RV function, due to its complex structure and its pronounced translational movement. Both exercise stress echocardiography and myocardial imaging using TDI and strain may provide assistance in evaluating RV function.

In patients with mild–moderate MS, exercise tolerance has been shown to correlate with RV function and RV systolic pressure at peak exercise, more than resting or peak exercise MV gradients and MV area [41]. Tricuspid annular velocity on TDI is an objective measure of RV systolic performance, and its reduction has been shown to be an independent predictor of prognosis and event-free survival in patients with heart failure as well as after RV infarction [42].

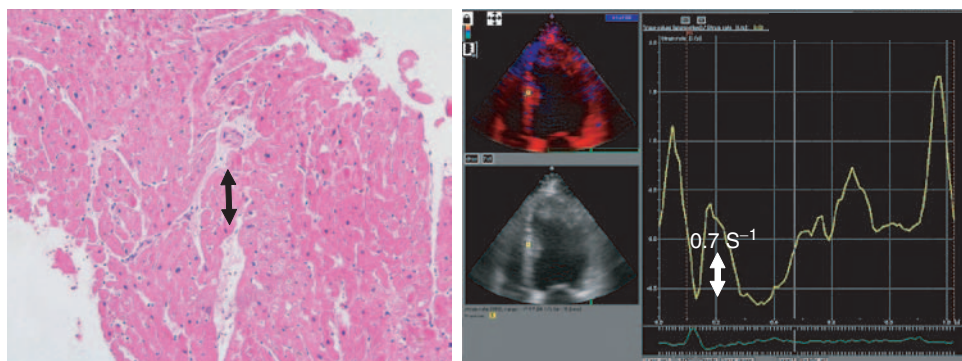


**Figure 18.5** Association of fibrosis (black arrow) with reduction of myocardial deformation at rest (white arrow).

## Myocardial imaging in aortic valve disease

### Aortic regurgitation

#### Use in decision making

Aortic valve replacement for AR is commonly recommended while the patient is still asymptomatic, but selection of the optimum time for surgery may be difficult. Although early surgery has been proposed [43,44], valve replacement carries a 1–3% operative mortality and the ongoing risks of a prosthetic valve warrant consideration, as aortic valve repair is rarely feasible.

Similar to MR, AR also produces a state of volume overload for the left ventricle, which may mask the detection of latent myocardial damage. In these patients, volume and pressure load also produce an increase in LV wall stress and subendocardial ischemia and fibrosis. As in MR, changes in LV geometry may have an adverse impact on the alignment of subendocardial myocardial fibers. As these fibers are aligned longitudinally, the assessment of long-axis function using myocardial tissue Doppler imaging is ideally suited to assess the LV response in AR.

#### Assessment of contractile reserve

In asymptomatic patients with severe AR, CR on exercise echocardiography is a better predictor of subsequent LV decompensation than resting indices of LV function [45]. These results support the findings of Borer et al. [46] who have shown similar results. In their experience, patients who had a worsening in postexercise ejection fraction of >5%, in other words had a negative CR, had a significantly higher incidence of developing heart failure or subclinical LV dysfunction. CR might, therefore, be useful to monitor the early development of myocardial dysfunction in these patients and to optimize the timing of surgery.

#### Myocardial imaging

The development of a resting parameter to assess latent LV dysfunction in AR would be desirable and helpful, especially as many of these patients may be older and unable to exercise adequately on the treadmill or stationary bicycle. In patients with AR, Vinereanu et al. [47] used exercise

echocardiography to subdivide patients based on their CR. They used resting peak systolic velocity of the medial mitral annulus on TDI and the resting systolic excursion of the mitral annulus on M-mode echocardiography to evaluate the LV long-axis function. In their experience, a resting mitral annular excursion of <12 mm and a resting peak systolic velocity of the medial mitral annulus of <9.5 cm/sec were the optimal cutoffs to separate the groups according to their CR. The resting peak systolic velocity of the medial mitral annulus was the better predictor between the two, with a sensitivity of 90% and specificity of 100%.

### Aortic stenosis

Surgical replacement of the aortic valve is the only definitive treatment option for AS, and the timing of surgery is guided by natural history studies, which have shown a prolonged asymptomatic period associated with minimal mortality, followed by a rapid deterioration in mortality after the onset of symptoms of angina, syncope, or heart failure. Thus, symptomatic patients or those with overt LV dysfunction are treated surgically [26]. Whereas this strategy has given very favorable survival findings, and patients' symptoms are improved, many patients remain somewhat limited.

Earlier intervention in AS could certainly be provided, because the widespread availability of noninvasive techniques has enabled many patients to be detected with severe stenosis but no or few symptoms. In these patients, the timing of surgery is controversial. In a study of asymptomatic patients, 2-year event-free survival (death or aortic valve surgery) was 21% for those with a jet velocity >4.0 m/sec compared with 84% in those with a jet velocity <3.0 m/sec [25]. However, the majority of these events were valve replacement surgery – and the indication for surgery was not independent of the echo measurement.

A major argument for earlier valve replacement would be to prevent overt dysfunction. Indeed, the prevalence of diastolic dysfunction remains high in patients with AS – in our experience, this is present in 58% preoperatively, falling to 40% after aortic valve replacement. Findings of moderate to severe diastolic dysfunction are an independent predictor of late mortality (hazard ratio = 1.72)

( $P = 0.0038$ ) and do not diminish with time, suggesting that myocardial changes due to AS may not completely regress after aortic valve replacement [48]. It remains unclear as to whether earlier surgery could spare the ventricle, or what stage could be considered “early”.

However, tissue Doppler imaging may be a useful tool to identify preclinical dysfunction. Patients with moderate–severe AS had significantly lower myocardial velocity in systole ( $S'$ ) and early diastole ( $E'$ ), compared with normal controls, despite preserved fractional shortening and ejection fraction. The ratio of early diastolic filling to the  $E'$  ( $E/E'$ ) correlated with the LV filling pressures – an  $E/E'$  ratio  $\geq 13$  identified elevated LV diastolic filling pressure with a sensitivity of 93% and a specificity of 88% [49]. Another study showed tissue velocity to be reduced in chronically elevated afterload, to a degree similar to patients with dilated cardiomyopathy even in the absence of other identifiable abnormalities of the left ventricle [50]. The mechanism of these myocardial changes may be fibrosis or apoptosis – the latter attributed to impaired myocardial blood flow [51].

The evaluation of myocardial deformation may also have a prominent future role in the assessment of regional LV function in patients with AS. In congenital valvular AS, the  $S'$ ,  $E'$ , and strain rate on TDI were significantly reduced, compared with normal age-matched controls [52]. These reductions in strain and SR imaging correlate with the severity of AS [53]. Conversely, deformation parameters show a subtle improvement in postoperative LV function after aortic valve replacement, preceding changes in LV mass and LV function assessed by conventional echocardiography [54].

## Conclusion

As discussed earlier, in patients with valvular heart disease, the left ventricle is the end-organ that has to adapt to changes in pressure or volume overload or a combination of the two factors. The adequacy of this response over time determines the immediate and long-term prognosis and the development of symptoms in these patients. In addition to assessing the hemodynamic severity of the valvular abnormality, the ability to recognize the myocardial changes early before the onset of overt LV

dysfunction might help in optimizing the timing for surgical intervention in many of these patients.

In our experience, CR at exercise stress echocardiography has been a useful adjunct in assessing the myocardial response in asymptomatic patients with valvular heart disease, particularly patients with MR and AR. CR correlates with the long-term prognosis and the development of LV dysfunction postoperatively in these patients. Nonetheless, assessment of CR may have some technical limitations, so the assessment of myocardial performance from resting echocardiography would be beneficial. The mitral annular velocity on TDI has been shown to correlate with CR in these patients with MR and AR and to provide another useful measure in patients with suboptimal images from technically difficult studies. Deformation indices have further facilitated the assessment of latent myocardial dysfunction from resting parameters. Hopefully in the future, these resting parameters will overcome or at least limit the need for exercise echocardiography.

## References

- Borow KM, Green LH, Mann T, et al. End-systolic volume as a predictor of postoperative left ventricular performance in volume overload from valvular regurgitation. *Am J Med* 1980; **68**: 655–63.
- Goldman MR, Boucher CA, Block PC, et al. Spectrum of congestive heart failure late after aortic valve or mitral replacement: differentiation of valvular versus myocardial cause by radionuclide ventriculogram–ejection fraction. *Am Heart J* 1981; **102**: 751–6.
- Gaasch WH, Carroll JD, Levine HJ, Criscitiello MG. Chronic aortic regurgitation: prognostic value of left ventricular end-systolic dimension and end-diastolic radius/thickness ratio. *J Am Coll Cardiol* 1983; **1**: 775–82.
- Zile MR, Gaasch WH, Carroll JD, Levine HJ. Chronic mitral regurgitation: predictive value of preoperative echocardiographic indexes of left ventricular function and wall stress. *J Am Coll Cardiol* 1984; **3(Pt 1)**: 235–42.
- Bonow RO, Rosing DR, Kent KM, Epstein SE. Timing of operation for chronic aortic regurgitation. *Am J Cardiol* 1982; **50**: 325–36.
- Enriquez-Sarano M, Tajik AJ, Schaff HV, et al. Echocardiographic prediction of left ventricular function after correction of mitral regurgitation: results and clinical implications. *J Am Coll Cardiol* 1994; **24**: 1536–43.
- Stewart WJ. Choosing the “golden moment” for mitral valve repair. *J Am Coll Cardiol* 1994; **24**: 1544–6.

- 8 Leung DY, Griffin BP, Stewart WJ, Cosgrove DM III, Thomas JD, Marwick TH. Left ventricular function after valve repair for chronic mitral regurgitation: predictive value of preoperative assessment of contractile reserve by exercise echocardiography. *J Am Coll Cardiol* 1996; **28**: 1198–205.
- 9 Donovan CL, Armstrong WF, Bach DS. Quantitative Doppler tissue imaging of the left ventricular myocardium: validation in normal subjects. *Am Heart J* 1995; **130**: 100–4.
- 10 Nagueh SF, Middleton KJ, Kopelen HA, Zoghbi WA, Quinones MA. Doppler tissue imaging: a noninvasive technique for evaluation of left ventricular relaxation and estimation of filling pressures. *J Am Coll Cardiol* 1997; **30**: 1527–33.
- 11 Derumeaux G, Ovize M, Loufoua J, et al. Doppler tissue imaging quantitates regional wall motion during myocardial ischemia and reperfusion. *Circulation* 1998; **97**: 1970–7.
- 12 Di Bello V, Talarico L, Picano E, et al. Increased echodensity of myocardial wall in the diabetic heart: an ultrasound tissue characterization study. *J Am Coll Cardiol* 1995; **25**: 1408–15.
- 13 Yuda S, Short L, Leano R, Marwick TH. Myocardial abnormalities in hypertensive patients with normal and abnormal left ventricular filling: a study of ultrasound tissue characterization and strain. *Clin Sci (Lond)* 2002; **103**: 283–93.
- 14 Mottram PM, Haluska B, Leano R, Cowley D, Stowasser M, Marwick TH. Effect of aldosterone antagonism on myocardial dysfunction in hypertensive patients with diastolic heart failure. *Circulation* 2004; **110**: 558–65.
- 15 Mottram PM, Haluska B, Yuda S, Leano R, Marwick TH. Patients with a hypertensive response to exercise have impaired systolic function without diastolic dysfunction or left ventricular hypertrophy. *J Am Coll Cardiol* 2004; **43**: 848–53.
- 16 Greenbaum RA, Ho SY, Gibson DG, Becker AE, Anderson RH. Left ventricular fibre architecture in man. *Br Heart J* 1981; **45**: 248–63.
- 17 Simonson JS, Schiller NB. Descent of the base of the left ventricle: an echocardiographic index of left ventricular function. *J Am Soc Echocardiogr* 1989; **2**: 25–35.
- 18 Jones CJ, Raposo L, Gibson DG. Functional importance of the long axis dynamics of the human left ventricle. *Br Heart J* 1990; **63**: 215–20.
- 19 Isaaz K, Munoz del Romeral L, Lee E, Schiller NB. Quantitation of the motion of the cardiac base in normal subjects by Doppler echocardiography. *J Am Soc Echocardiogr* 1993; **6**: 166–76.
- 20 Gulati VK, Katz WE, Follansbee WP, Gorcsan J III. Mitral annular descent velocity by tissue Doppler echocardiography as an index of global left ventricular function. *Am J Cardiol* 1996; **77**: 979–84.
- 21 Vinereanu D, Ionescu AA, Fraser AG. Assessment of left ventricular long axis contraction can detect early myocardial dysfunction in asymptomatic patients with severe aortic regurgitation. *Heart* 2001; **85**: 30–6.
- 22 Garcia MJ, Rodriguez L, Ares M, et al. Myocardial wall velocity assessment by pulsed Doppler tissue imaging: characteristic findings in normal subjects. *Am Heart J* 1996; **132**: 648–56.
- 23 Gorcsan J III, Gulati VK, Mandarino WA, Katz WE. Color-coded measures of myocardial velocity throughout the cardiac cycle by tissue Doppler imaging to quantify regional left ventricular function. *Am Heart J* 1996; **131**: 1203–13.
- 24 Lund O, Nielsen TT, Pilegaard HK, Magnussen K, Knudsen MA. The influence of coronary artery disease and bypass grafting on early and late survival after valve replacement for aortic stenosis. *J Thorac Cardiovasc Surg* 1990; **100**: 327–37.
- 25 Otto CM, Burwash IG, Legget ME, et al. Prospective study of asymptomatic valvular aortic stenosis. Clinical, echocardiographic, and exercise predictors of outcome. *Circulation* 1997; **95**: 2262–70.
- 26 ACC/AHA guidelines for the management of patients with valvular heart disease. A report of the American College of Cardiology/American Heart Association. Task Force on Practice Guidelines (Committee on Management of Patients with Valvular Heart Disease). *J Am Coll Cardiol* 1998; **32**: 1486–588.
- 27 Rockman HA, Wachhorst SP, Mao L, Ross J Jr. ANG II receptor blockade prevents ventricular hypertrophy and ANF gene expression with pressure overload in mice. *Am J Physiol* 1994; **266(6 Pt 2)**: H2468–75.
- 28 Carver W, Nagpal ML, Nachtigal M, Borg TK, Terracio L. Collagen expression in mechanically stimulated cardiac fibroblasts. *Circ Res* 1991; **69**: 116–22.
- 29 Krayenbuehl HP, Hess OM, Monrad ES, Schneider J, Mall G, Turina M. Left ventricular myocardial structure in aortic valve disease before, intermediate, and late after aortic valve replacement. *Circulation* 1989; **79**: 744–55.
- 30 Braunwald E. Mitral regurgitation: physiologic, clinical and surgical considerations. *N Engl J Med* 1969; **281**: 425–33.
- 31 Urschel CW, Covell JW, Sonnenblick EH, Ross J Jr, Braunwald E. Myocardial mechanics in aortic and mitral valvular regurgitation: the concept of instantaneous impedance as a determinant of the performance of the intact heart. *J Clin Invest* 1968; **47**: 867–83.
- 32 Wisenbaugh T, Spann JF, Carabello BA. Differences in myocardial performance and load between patients with similar amounts of chronic aortic versus chronic mitral regurgitation. *J Am Coll Cardiol* 1984; **3**: 916–23.

- 33 Dodge HT, Kennedy JW, Petersen JL. Quantitative angiographic methods in the evaluation of valvular heart disease. *Prog Cardiovasc Dis* 1973; **16**: 1–23.
- 34 Grossman W, Jones D, McLaurin LP. Wall stress and patterns of hypertrophy in the human left ventricle. *J Clin Invest* 1975; **56**: 56–64.
- 35 Nagueh SF, Lakkis NM, Middleton KJ, Spencer WH III, Zoghbi WA, Quinones MA. Doppler estimation of left ventricular filling pressures in patients with hypertrophic cardiomyopathy. *Circulation* 1999; **99**: 254–61.
- 36 Ling LH, Enriquez-Sarano M, Seward JB, et al. Clinical outcome of mitral regurgitation due to flail leaflet. *N Engl J Med* 1996; **335**: 1417–23.
- 37 Rosenhek R, Rader F, Klaar U, et al. Outcome of watchful waiting in asymptomatic severe mitral regurgitation. *Circulation* 2006; **113**: 2238–44.
- 38 Haluska BA, Short L, Marwick TH. Relationship of ventricular longitudinal function to contractile reserve in patients with mitral regurgitation. *Am Heart J* 2003; **146**: 183–8.
- 39 Lee R, Hanekom L, Marwick TH, Leano R, Wahi S. Prediction of subclinical left ventricular dysfunction with strain rate imaging in patients with asymptomatic severe mitral regurgitation. *Am J Cardiol* 2004; **94**: 1333–7.
- 40 Hanekom L, Lee R, Leano R, Wahi S, Marwick TH. Ultrasound tissue characterization may be used to detect subclinical left ventricular dysfunction and fibrosis in asymptomatic severe mitral regurgitation [abstract]. *Circulation* 2004.
- 41 Meluzin J, Spinarova L, Bakala J, et al. Pulsed Doppler tissue imaging of the velocity of tricuspid annular systolic motion; a new, rapid, and non-invasive method of evaluating right ventricular systolic function. *Eur Heart J* 2001; **22**: 340–8.
- 42 Dokainish H, Abbey H, Gin K, Ramanathan K, Lee PK, Jue J. Usefulness of tissue Doppler imaging in the diagnosis and prognosis of acute right ventricular infarction with inferior wall acute left ventricular infarction. *Am J Cardiol* 2005; **95**: 1039–42.
- 43 Copeland JG, Griep RB, Stinson EB, Shumway NE. Long-term follow-up after isolated aortic valve replacement. *J Thorac Cardiovasc Surg* 1977; **74**: 875–89.
- 44 Forman R, Firth BG, Barnard MS. Prognostic significance of preoperative left ventricular ejection fraction and valve lesion in patients with aortic valve replacement. *Am J Cardiol* 1980; **45**: 1120–5.
- 45 Wahi S, Haluska B, Pasquet A, Case C, Rimmerman CM, Marwick TH. Exercise echocardiography predicts development of left ventricular dysfunction in medically and surgically treated patients with asymptomatic severe aortic regurgitation. *Heart* 2000; **84**: 606–14.
- 46 Borer J, Hochreiter C, Okin PM, Borer JS. Prediction of indications for valve replacement among asymptomatic or minimally symptomatic patients with chronic aortic regurgitation and normal left ventricular performance. *Circulation* 1998; **97**: 523–34.
- 47 Vinereanu D, Ionescu AA, Fraser AG. Assessment of left ventricular long axis contraction can detect early myocardial dysfunction in asymptomatic patients with severe aortic regurgitation. *Heart* 2001; **85**: 30–6.
- 48 Gjertsson P, Caidahl K, Farasati M, Oden A, Bech-Hanssen O. Preoperative moderate to severe diastolic dysfunction: a novel Doppler echocardiographic long-term prognostic factor in patients with severe aortic stenosis. *J Thorac Cardiovasc Surg* 2005; **129**: 890–6.
- 49 Bruch C, Styppmann J, Grude M, Gradaus R, Breithardt G, Wichter T. Tissue Doppler imaging in patients with moderate to severe aortic valve stenosis: clinical usefulness and diagnostic accuracy. *Am Heart J* 2004; **148**: 696–702.
- 50 Eidem BW, McMahon CJ, Ayres NA, et al. Impact of chronic left ventricular preload and afterload on Doppler tissue imaging velocities: a study in congenital heart disease. *J Am Soc Echocardiogr* 2005; **18**: 830–8.
- 51 Galiuto L, Lotriente M, Crea F, et al. Impaired coronary and myocardial flow in severe aortic stenosis is associated with increased apoptosis: a transthoracic Doppler and myocardial contrast echocardiography study. *Heart* 2006; **92**: 208–12.
- 52 Kiraly P, Kapusta L, Thijssen JM, Daniels O. Left ventricular myocardial function in congenital valvar aortic stenosis assessed by ultrasound tissue-velocity and strain-rate techniques. *Ultrasound Med Biol* 2003; **29**: 615–20.
- 53 Kowalski M, Herbots L, Weidemann F, et al. One-dimensional ultrasonic strain and strain rate imaging: a new approach to the quantitation of regional myocardial function in patients with aortic stenosis. *Ultrasound Med Biol* 2003; **29**: 1085–92.
- 54 Iwashashi N, Nakatani S, Kanzaki H, Hasegawa T, Abe H, Kitakaze M. Acute improvement in myocardial function assessed by myocardial strain and strain rate after aortic valve replacement for aortic stenosis. *J Am Soc Echocardiogr* 2006; **19**: 1238–44.

# Use of myocardial imaging to identify and manage systemic diseases

Frank Weidemann and Joerg M. Strotmann

## Introduction

In systemic diseases such as amyloidosis, sarcoidosis, Friedreich's ataxia, Fabry's disease, and muscular dystrophy, the heart is involved in addition to other organs. The prevalence of cardiac involvement in these disorders is highly variable; the clinician needs to know the presence and amount of myocardial involvement (including subclinical involvement), differentiate the condition from comorbid diseases such as hypertensive heart disease, and monitor disease progression. In some of these diseases, a specific therapy is available, and imaging may provide information about the impact of the therapy on the heart [1,2].

Echocardiography is a widely available non-invasive clinical tool for the investigation of cardiac morphology and function. However, in subclinical cardiac dysfunction typical of systemic disease, the routinely used echocardiographic parameters such as left ventricular (LV) ejection fraction or fractional shortening are not sensitive enough to detect this early dysfunction [3–5]. However, other echocardiographic techniques such as tissue Doppler imaging may be able to detect changes in myocardial performance that go beyond the limitations of "simple" measurements of ejection fraction [6]. Strain rate, a regional deformation parameter independent of overall heart motion and tethering effects, can be calculated by postprocessing tissue Doppler data [7]. As described in previous chapters, this parameter has been validated and is mainly related to the intrinsic contractility of

the underlying myocardium and relatively independent of heart rate [8]. When these new techniques were developed, they were mainly used to assess regional myocardial function in coronary heart disease [9]. Later, when it was recognized that these parameters are very sensitive to detect subtle changes in myocardial function, they have also been used to describe cardiac function on the presence of systemic disease [3–5]. The aim of this chapter is to explore the impact of tissue Doppler imaging to identify and to manage cardiac aspects of these diseases.

## Requirements of imaging modalities to assess cardiac function in systemic diseases

When the left ventricle is involved in systemic diseases, it may be a quite homogeneous global pathology, such as in amyloidosis, Friedreich's ataxia, and Fabry's disease, which might be detected with global LV functional parameters, especially in more advanced stages of disease. However, in sarcoidosis, the LV involvement might be more patchy, necessitating regional parameters for the assessment of myocardial function. In addition, some of these patients are followed up for years; therefore, a cardiac function test with a high test-retest reliability is necessary. As most of the patients also have other diseases that involve cardiac function, such as arterial hypertension and coronary artery disease, it is necessary to distinguish this comorbidity from the original systemic disease.

Therefore, noninvasive functional parameters that define cardiac involvement and also the progression of the disease are important. Furthermore, the chosen echocardiographic parameter in these patients has to be reasonably load- and heart rate-independent, especially when follow-up studies are planned.

For the assessment of diastolic function, the ratio of early diastolic mitral inflow ( $E =$  measured by the transmitral blood pool pulsed Doppler) to early diastolic mitral annular motion ( $E'$  = measured by tissue Doppler imaging) seems to be the best parameter to fulfill all these requirements. This parameter is validated [10] and is used more and more in large multicenter trials where the assessment of diastolic dysfunction is crucial. However, although  $E/E'$  ratio is the best single predictor of LV filling pressure, additional echocardiographic parameters such as chamber dimensions and Doppler variables must be considered in the analysis of individual patients [10].

When assessing systolic function by tissue Doppler imaging, regional systolic strain rate might be a good choice of parameter. This factor is related to the intrinsic contractility of the myocardium and is relatively independent of heart rate [8]. However, it is not completely load-independent (especially not afterload-independent), and sometimes the traces are noisy and, thus, difficult to interpret. In general, systemic diseases are associated with hypertrophic myocardium. This connection is advantageous when using tissue Doppler imaging to assess cardiac function in hypertrophic myocardium, if the velocity traces and the strain rate traces are of good quality. Using all these parameters, it is clear that the assessed function is influenced by a combination of the intrinsic function of the underlying myocardium together with potential fibrosis and infiltration of the myocardium.

### **Myocardial imaging in patients with amyloidosis**

Amyloidosis is a systemic disease characterized by the deposition of interstitial amyloid fibrils in various organs, including the heart [11]. The most severe cardiac involvement is seen in primary amyloidosis, where light chain amyloid protein is deposited in the heart [12]. More than 50% of all

amyloidosis-related deaths are attributed to cardiac infiltration [12]. The cardiac involvement is also called *stiff heart syndrome*, with early impairment of diastolic function and relatively preserved systolic function until late in the disease [13]. Using classic echocardiography, typical findings are increased LV wall thickness, sparkling granular myocardial texture, dilated atria, and pericardial effusion [11]. In addition, most patients show diastolic relaxation abnormalities with restrictive filling patterns seen only in the most advanced stages of the disease.

In 2002, Koyama et al. [14] were the first to use pulsed tissue Doppler imaging for the assessment of cardiac involvement. Using this motion-based technique, they showed that diastolic tissue velocities more clearly documented diastolic dysfunction than conventional Doppler-derived indices and were impaired before the presentation of clinical heart failure. In contrast, peak systolic velocities could not differentiate patients with amyloidosis but without congestive heart failure from patients without cardiac amyloidosis [14]. By working with the myocardial velocity gradient (which is analogous to strain rate), Koyoma et al. [15] showed that both diastolic and systolic dysfunction could be detected in patients with congestive heart failure. In addition, they showed that diastolic and systolic abnormalities were seen especially in the lateral wall and not in the interventricular septum [15].

The same group was the first to use strain rate imaging to assess longitudinal function in a large patient cohort with biopsy-proven amyloidosis [16]. They examined one group with no cardiac involvement, a second group with involvement shown by biopsies but no congestive heart failure, and a third group with heart involvement and congestive heart failure. Using strain rate imaging for the assessment of deformation, they showed a significant difference of peak systolic strain rate among all three groups (Figure 19.1). Interestingly, the detection of the subclinical disease was not possible with velocity measurements. Thus, the authors concluded that peak systolic strain rate was useful to detect early involvement in patients with amyloidosis and also for follow-up studies after aggressive chemotherapy or stem cell transplantation [16]. In a recent study by Ogiwara et al. [17] strain rate imaging was

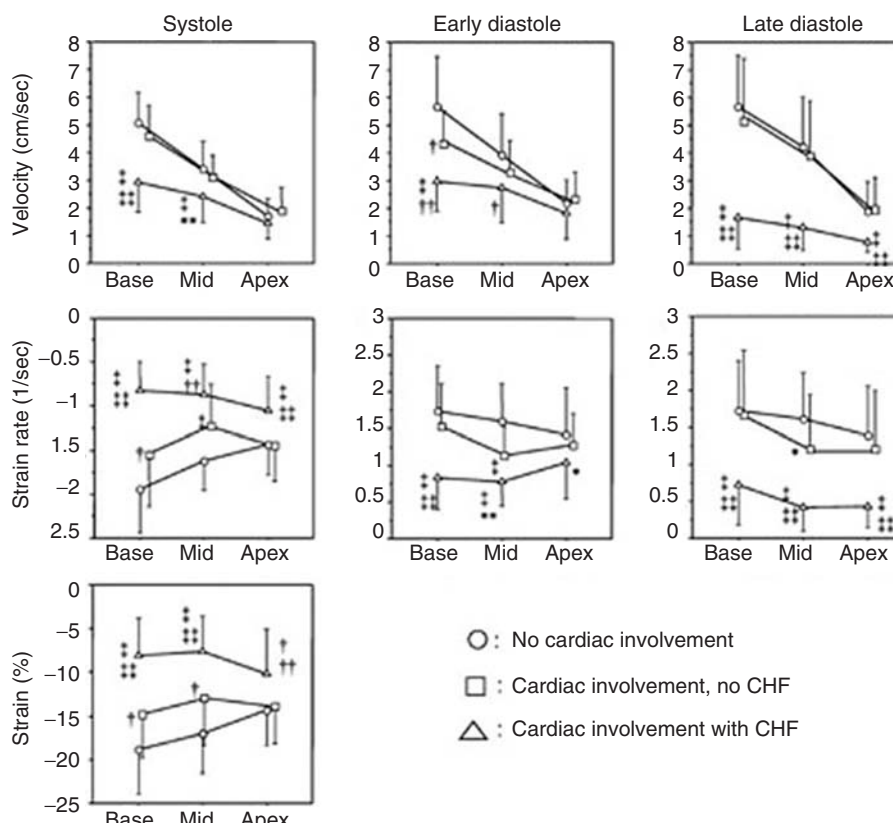


**Figure 19.1** Mean values of tissue velocities, strain rate, and strain calculated from septum, lateral, inferior, and anterior walls of the basal (Base), mid- (Mid), and apical

(Apex) left ventricle in systole and early and late diastole. CHF, congestive heart failure. Adapted from Koyama et al. [16].

used in patients with familial amyloid polyneuropathy and in patients with light-chain amyloidosis; patients with light-chain amyloidosis particularly showed reduced strain rate and strain values. This observation may in part account for the previously recognized differences in heart failure and survival between primary and familial cardiac amyloidosis [18]. By measuring reduced strain values in the right ventricular free wall, it was also suggested that amyloidosis should be regarded as a biventricular disease [19]. However, as no right ventricular biopsies were taken in that study, it is not clear if these deformation abnormalities are driven secondarily to the LV abnormalities or primary by infiltration of the right ventricular free wall. Thus, these new tissue Doppler techniques offer complementary information on the evaluation of cardiac amyloidosis, helpful to the cardiologist with regard

to early diagnosis of amyloid infiltration and patient management.

### Myocardial imaging in patients with sarcoidosis

Sarcoidosis is a multisystem granulomatous disease of unknown etiology often seen in young adults. A wide range of cardiac manifestations of the disease has been described, including conduction abnormalities, mitral regurgitation, congestive heart failure, ventricular aneurysms, pericardial effusion, and sudden death [20]. Typical echocardiographic features in the beginning of the disease include mild thickening of the myocardium [21]. Later, as the disease progresses and scarring occurs, thinning of the myocardium and aneurysms may be observed [22]. The cardiac lesions caused by noncaseating granulomas have a patchy distribution in the left

ventricle, which are often overlooked because of their subclinical disease progression [23]. Thus, global LV parameters such as ejection fraction and fractional shortening are not sensitive enough to detect cardiac involvement.

As cardiac involvement is an independent predictor of mortality and carries a very poor prognosis, noninvasive tools for the assessment of regional myocardial function would be desirable to detect the sarcoid lesion. Initially, cyclic variation of integrated backscatter was used to estimate the acoustic properties of the myocardium and, thereby, to detect cardiac sarcoidosis [23]. Tissue Doppler velocities would probably not be helpful, because they are influenced by global heart motion and tethering effects from the nondiseased myocardium. In contrast, strain rate imaging might be very promising to detect the regional lesions. However, the detection of the cardiac lesions (even with biopsies) is difficult because of the patchy distribution, and it might not be clear if the abnormalities assessed by deformation imaging are due to artifacts or pathology in the tissue investigated. The value of this parameter remains to be investigated. Gadolinium enhancement by magnetic resonance imaging seems to be a sensitive tool for the detection of the sarcoid lesion and might be the test of choice in the future [24].

### **Myocardial imaging in patients with Friedreich's ataxia**

Friedreich's ataxia is an autosomal recessive neurodegenerative disease caused by an intronic GAA triplet repeat expansion. This change leads to a defect in the gene that encodes for a mitochondrial protein named frataxin, resulting in mitochondrial dysfunction [25]. In the heart, this mitochondrial respiratory dysfunction leads to cellular hypertrophy, diffuse fibrosis, and focal myocardial necrosis [26]. Myocardial involvement in Friedreich's ataxia is well documented, with the most common cardiac finding being concentric or asymmetrical LV hypertrophy [3,27]. Clinical signs of cardiac involvement typically occur late in the course of the disease, but heart failure accounts for more than 50% of the deaths from this disease [26]. Few attempts were made to assess regional LV function in Friedreich's ataxia or, indeed, to identify functional abnormalities that indicate early cardiac

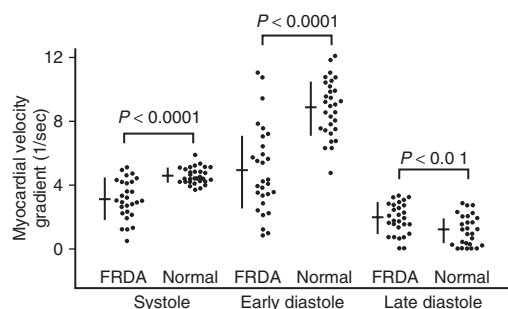


**Figure 19.2** Myocardial velocity gradients in patients with Friedreich's ataxia (FRDA) and control subjects (Normal) in systole and early and late diastole (mean  $\pm$  SD are represented by horizontal and vertical lines, respectively). Adapted from Dutka et al. [3].

involvement in this disease before the development of the new imaging techniques. The measurement of global LV function using ejection fraction does not seem to be sufficiently sensitive enough to detect cardiac involvement [26].

In 2000, Dutka et al. [3] reported on the use of tissue Doppler imaging to extract systolic and diastolic velocity gradients in patients with Friedreich's ataxia who were not experiencing cardiac symptoms and showed reduction of both systolic and diastolic function (Figure 19.2). In addition, they found that age-corrected myocardial velocity gradients in systole and especially in early diastole were inversely related to the size of the GAA triple repeat expansion. Thus, it could be demonstrated that there is a relationship between expansion of the gene defect and tissue Doppler parameters as a marker of cardiac involvement.

The relationship between regional myocardial function assessed by strain rate imaging and the degree of LV hypertrophy in patients with Friedreich's ataxia was investigated in another study (Figure 19.3) [28]. As expected, the magnitude of systolic deformation (end-systolic strain) and the maximal systolic velocity of deformation (peak systolic strain rate) were markedly reduced in the hypertrophic myocardium. Interestingly, impaired systolic and diastolic deformation properties were already present in patients with Friedreich's ataxia who had no evidence of LV hypertrophy and also in nonhypertrophic segments of patients with regional LV hypertrophy [28]. Thus, strain rate imaging could potentially be used to detect functional changes in the myocardium of

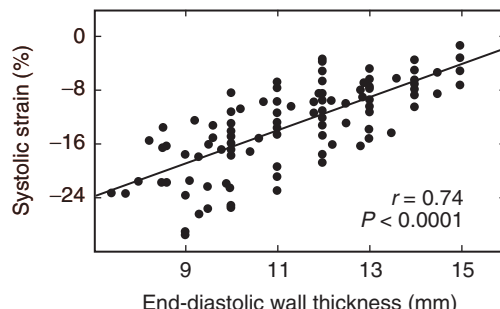


**Figure 19.3** Relationship between cardiac function (systolic strain) and morphology (wall thickness) in Friedreich's ataxia patients. Adapted from Weidemann et al. [28].

Friedreich's ataxia patients before the detection of LV hypertrophy on gray-scale echocardiography. This finding could signify that, in the early stages of the disease when the myocardium does not show macroscopic changes, the mitochondrial respiratory dysfunction was already causing myocardial dysfunction. This finding would suggest that myocardial dysfunction as an early marker of cardiac involvement might occur before the detection of LV hypertrophy on standard imaging. In further agreement with this finding, cardiac bioenergetics (as measured by  $^{31}\text{P}$  magnetic resonance spectroscopy) are abnormal in nonhypertrophic segments of patients with Friedreich's ataxia [25].

In contrast to the changes measured in the left ventricle in Friedreich's ataxia patients, the right ventricle is normally not hypertrophic, and the right ventricular regional longitudinal systolic and diastolic deformation properties are normal [28]. However, as this gene defect for frataxin is present in all myocytes [25], it would seem to be surprising that patients with Friedreich's ataxia have neither a hypertrophic right ventricle nor evidence of regional right ventricle dysfunction. It may be that the combination of the higher pressure development with an associated higher myocardial oxygen consumption [29] in the left ventricle compared to the right ventricle may contribute to the phenotypic expression of the genotypic disorder in the left ventricle of patients. Eventually, in the end-stage of the disease, patients with Friedreich's ataxia present with global dysfunction, a dilated left ventricle, and markedly reduced regional myocardial function measured by tissue Doppler imaging [30].

Since the understanding of the frataxin gene defect, new therapeutic strategies have been developed for patients with Friedreich's ataxia. Idebenone, an antioxidant drug, has been shown to protect mitochondrial respiratory dysfunction [31]. In an initial study of eight patients during 1 year of treatment [1], the reduction of hypertrophy was preceded by an early and linear improvement in cardiac function assessed by strain rate imaging.

### Myocardial imaging in patients with Fabry's disease

Fabry's (or Anderson-Fabry) disease is a rare X-linked lysosomal storage disorder leading to an accumulation of glycosphingolipids (GL3) in all tissues and organs, including the heart. Cardiomyocyte storage results in LV hypertrophy with subsequent diastolic and systolic dysfunction and is of major prognostic importance in Fabry's disease. Vascular storage affects the coronary arteries, with potential consequences for myocardial perfusion. GL3 deposition in the conductive tissue can lead to a variety of atrial and ventricular arrhythmias. The accumulation of GL3 in heart valves promotes valvular thickening and potential malfunction.

According to current observational registry data, approximately 50–60% of patients with Fabry's disease present with cardiac symptoms and one third die from cardiac causes [32]. Pieroni et al. [4] were the first to use pulsed-wave tissue Doppler imaging to assess systolic and diastolic function in patients with Fabry's disease. They showed that, in patients with and without LV hypertrophy, systolic and diastolic velocities were reduced at the septal and lateral mitral ring. Thus, they concluded that the assessment of systolic and diastolic motion by tissue velocities provides the opportunity for pre-clinical diagnosis of Fabry's cardiomyopathy [4].

Strain rate imaging was first used to understand the progression of the cardiomyopathy in a cohort of 51 patients with Fabry's disease [5]. The analysis of peak systolic strain rate showed that functional abnormalities start in the lateral wall. Whereas only longitudinal strain rate is reduced in the early stage, with further progression of disease, radial deformation properties are also impaired. A correlation between radial strain rate and myocardial wall thickness has been demonstrated, with lower strain values for thicker walls (Figure 19.4).

Although this is an X-linked disease, women can be not only carriers but can also progress to Fabry's cardiomyopathy [33]. In general, they develop functional abnormalities 10 years later compared to male patients, and the progression of the disease is variable and slower (Figure 19.5). The detection of abnormalities by tissue Doppler in female carriers should prompt consideration of myocardial biopsy to confirm cardiac involvement. Although right ventricular deformation properties (i.e., strain rate and strain) are not significantly reduced in most patients [5], in more advanced stages of the disease, the right ventricle is affected secondarily due to LV failure [34].

Myocardial biopsy studies have shown that myocardial hypertrophy is accompanied by interstitial fibrosis in Fabry's cardiomyopathy. As in other forms of cardiomyopathy, magnetic resonance

imaging studies can detect advanced stages of myocardial fibrosis by the use of regional late enhancement after gadolinium exposure [35]. Thus, the end-stage of Fabry's cardiomyopathy is characterized by the coexistence of LV hypertrophy, myocardial fibrosis, and severely reduced regional LV function (Figure 19.6) [5]. Fibrosis starts in the mid-myocardial layers of the basal parts of the inferolateral wall, where LV workload is highest [36], and is combined with severely reduced strain rate and strain values at this site. In addition, all fibrotic segments display a characteristic strain rate pattern consisting of a first peak in early systole followed by a rapid fall in strain rate to close to zero and a second peak during isovolumetric relaxation (Figure 19.7). It can be speculated that this typical *double-peak sign* is due to the regionally reduced contractile force combined with the interaction of surrounding segments and cavity pressure.

Specific treatment with enzyme replacement therapy has been available since 2001 in patients with Fabry's disease [37]. In an initial study of 16 patients taking enzyme replacement therapy, both a regression of LV hypertrophy and an increase of strain rate values have been demonstrated after 1 year of therapy. Thus, it was speculated that this new specific therapy results in a combined morphological and functional cardiac improvement [2]. However, function of myocardial segments with fibrosis does not improve during enzyme replacement therapy [38], suggesting that there may be a "point of no return" in Fabry's disease, that is, when LV fibrosis occurs and irreversible damage has been done to the myocardium. For this reason, it is crucial to assess the progression of the heart disease in

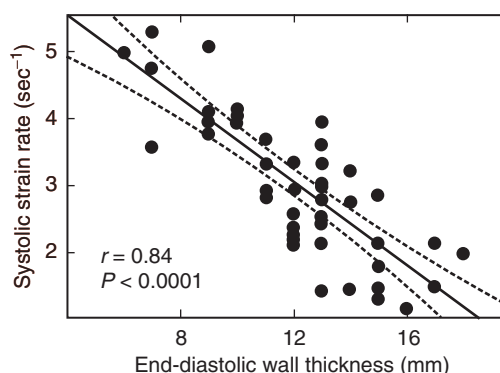


**Figure 19.4** Relationship between cardiac function (systolic strain rate) and morphology (wall thickness) in Fabry's disease patients. Adapted from Weidemann et al. [5].

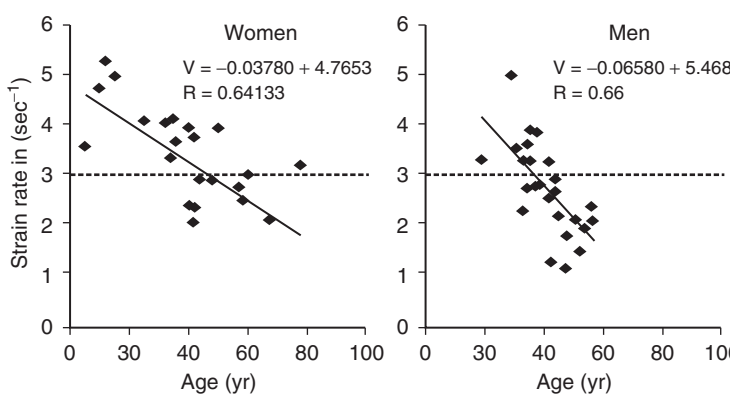


**Figure 19.5** The change in strain rate with ageing in female and male Fabry patients.

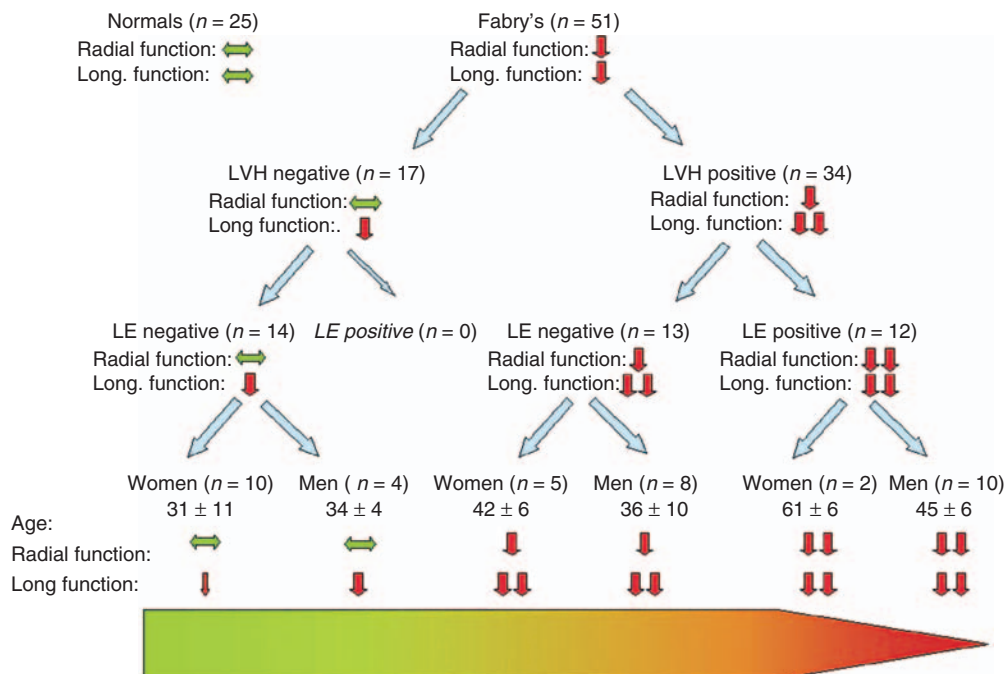


**Figure 19.6** Clinical algorithm to classify patients with Fabry's disease according to sex, LV hypertrophy (LVH), and late enhancement (LE). For each subgroup, radial and longitudinal (long.) function is described semiquantitatively. The arrows signify the comparison of strain

rate values with controls. Note that there is a progressive deterioration of LV function from female patients without hypertrophy and no LE (left side) to male patients with hypertrophy and LE (right side). Adapted from Weidemann et al. [5].

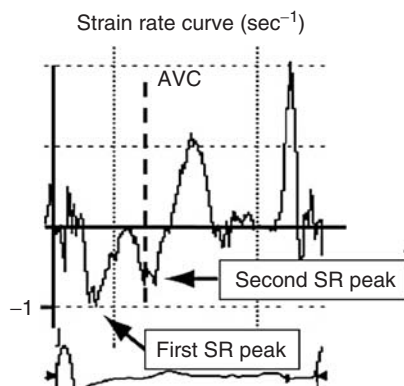


**Figure 19.7** Longitudinal strain rate curve over one heart cycle from a patient with Fabry's disease extracted from a segment with late enhancement. The typical double-peak sign with a first and a second strain rate peak is seen. AVC, aortic valve closure; SR, strain rate.

the individual patient. As most patients are managed by special Fabry centers, it should be easy to standardize the noninvasive staging and follow up the patients by the use of tissue Doppler imaging

over years. This strategy will provide information on the natural history of the disease and also the impact of enzyme replacement therapy on the Fabry's cardiomyopathy.

### Myocardial imaging in patients with muscular dystrophy

Myotonic dystrophy (Steinert's disease) is a systemic disease affecting the skeletal muscle, smooth muscle, and the heart. In a prospective trial with 22 patients, tissue Doppler imaging was able to detect subclinical impairment in patients not suffering from heart failure [39]. Moreover, the degree of tissue velocity reduction correlates with neurologic severity in patients with myotonic dystrophy [39].

Becker's muscular dystrophy is another systemic disease for which progressive muscular weakness and cardiac involvement is caused by dystrophin abnormalities. Pulsed-tissue Doppler velocities have shown both systolic and diastolic velocities to be decreased in affected patients and also in

carriers [40]. It might, therefore, be useful to examine suspected patients with muscular dystrophy not only with conventional echocardiography but also with tissue Doppler imaging to detect subclinical involvement.

## Perspectives for imaging in systemic diseases

Tissue Doppler imaging provides additional information about potential involvement of the heart in patients with systemic disease. Most studies published to date have reported time-averaged values (i.e., averages of several heart beats and temporal smoothing) and compared *different groups* to show significant differences. However, in *individual patients*, the measurement of peak amplitudes (especially strain rate) is technically demanding due to background noise and potential misalignment of the myocardium and the ultrasound beam, and the use of this technology for decision-making and follow-up might best be restricted to specialized centers.

To enter clinical practice in cardiology, innovative noninvasive technologies have to show that they do not only discriminate pathologies at group levels but are also of help in the clinical management of the individual patient. Thus more robust, widely available imaging techniques are needed. This may be provided by two-dimensional strain assessment, which is now possible using speckle tracking based on gray-scale data [41], although the temporal resolution is low; thus, strain rate is difficult to extract. Further studies will need to prove that these new techniques will have an impact on the clinical management of patients with systemic disease.

## Conclusions

For experienced cardiologists, tissue Doppler imaging, along with other conventional echocardiography measurements, is important for the evaluation of patients with systemic disease. However, the limitations of this technique have to be considered, and tissue characterization based just on tissue Doppler imaging might not be possible. The major advantage of this technique is definitely that

subclinical involvement can be detected. In addition, tissue Doppler imaging seems to be a valuable tool to select patients who might benefit from a specific treatment and to monitor myocardial function during treatment.

## References

- 1 Buyse G, Mertens L, Di Salvo G, et al. Idebenone treatment in Friedreich's ataxia: neurological, cardiac, and biochemical monitoring. *Neurology* 2003; **60**: 1679–81.
- 2 Weidemann F, Breunig F, Beer M, et al. Improvement of cardiac function during enzyme replacement therapy in patients with Fabry disease: a prospective strain rate imaging study. *Circulation* 2003; **108**: 1299–301.
- 3 Dutka DP, Donnelly JE, Palka P, Lange A, Nunez DJ, Nihoyannopoulos P. Echocardiographic characterization of cardiomyopathy in Friedreich's ataxia with tissue Doppler echocardiographically derived myocardial velocity gradients. *Circulation* 2000; **102**: 1276–82.
- 4 Pieroni M, Chimenti C, Ricci R, Sale P, Russo MA, Frustaci A. Early detection of Fabry cardiomyopathy by tissue Doppler imaging. *Circulation* 2003; **107**: 1978–84.
- 5 Weidemann F, Breunig F, Beer M, et al. The variation of morphological and functional cardiac manifestation in Fabry disease: potential implications for the time course of the disease. *Eur Heart J* 2005; **26**: 1221–7.
- 6 Sutherland GR, Stewart MJ, Groundstroem KW, et al. Color Doppler myocardial imaging: a new technique for the assessment of myocardial function. *J Am Soc Echocardiogr* 1994; **7**: 441–58.
- 7 Urheim S, Edvardsen T, Torp H, Angelsen B, Smiseth OA. Myocardial strain by Doppler echocardiography. Validation of a new method to quantify regional myocardial function. *Circulation* 2000; **102**: 1158–64.
- 8 Weidemann F, Jamal F, Sutherland GR, et al. Myocardial function defined by strain rate and strain during alterations in inotropic states and heart rate. *Am J Physiol Heart Circ Physiol* 2002; **283**: H792–9.
- 9 Garot J, Derumeaux GA, Monin JL, et al. Quantitative systolic and diastolic transmyocardial velocity gradients assessed by M-mode colour Doppler tissue imaging as reliable indicators of regional left ventricular function after acute myocardial infarction. *Eur Heart J* 1999; **20**: 593–603.
- 10 Ommen SR, Nishimura RA, Appleton CP, et al. Clinical utility of Doppler echocardiography and tissue Doppler imaging in the estimation of left ventricular filling pressures: a comparative simultaneous Doppler-catheterization study. *Circulation* 2000; **102**: 1788–94.

- 11 Sallach JA, Klein AL. Tissue Doppler imaging in the evaluation of patients with cardiac amyloidosis. *Curr Opin Cardiol* 2004; **19**: 464–71.
- 12 Kyle RA, Greipp PR. Amyloidosis (AL). Clinical and laboratory features in 229 cases. *Mayo Clin Proc* 1983; **58**: 665–83.
- 13 Cueto-Garcia L, Reeder GS, Kyle RA, et al. Echocardiographic findings in systemic amyloidosis: spectrum of cardiac involvement and relation to survival. *J Am Coll Cardiol* 1985; **6**: 737–43.
- 14 Koyama J, Ray-Sequin PA, Davidoff R, Falk RH. Usefulness of pulsed tissue Doppler imaging for evaluating systolic and diastolic left ventricular function in patients with AL (primary) amyloidosis. *Am J Cardiol* 2002; **89**: 1067–71.
- 15 Koyama J, Davidoff R, Falk RH. Longitudinal myocardial velocity gradient derived from pulsed Doppler tissue imaging in AL amyloidosis: a sensitive indicator of systolic and diastolic dysfunction. *J Am Soc Echocardiogr* 2004; **17**: 36–44.
- 16 Koyama J, Ray-Sequin PA, Falk RH. Prognostic significance of ultrasound myocardial tissue characterization in patients with cardiac amyloidosis. *Circulation* 2002; **106**: 556–61.
- 17 Ogiwara F, Koyama J, Ikeda S, Kinoshita O, Falk RH. Comparison of the strain Doppler echocardiographic features of familial amyloid polyneuropathy (FAP) and light-chain amyloidosis. *Am J Cardiol* 2005; **95**: 538–40.
- 18 Dubrey SW, Cha K, Skinner M, LaValley M, Falk RH. Familial and primary (AL) cardiac amyloidosis: echocardiographically similar diseases with distinctly different clinical outcomes. *Heart* 1997; **78**: 74–82.
- 19 Lindqvist P, Olofsson BO, Backman C, Suhr O, Waldenstrom A. Pulsed tissue Doppler and strain imaging discloses early signs of infiltrative cardiac disease: a study on patients with familial amyloidotic polyneuropathy. *Eur J Echocardiogr* 2006; **7**: 22–30.
- 20 Bargout R, Kelly RF. Sarcoid heart disease: clinical course and treatment. *Int J Cardiol* 2004; **97**: 173–82.
- 21 Matsumori A, Hara M, Nagai S, et al. Hypertrophic cardiomyopathy as a manifestation of cardiac sarcoidosis. *Jpn Circ J* 2000; **64**: 679–83.
- 22 Sekiguchi M, Yazaki Y, Isobe M, Hiroe M. Cardiac sarcoidosis: diagnostic, prognostic, and therapeutic considerations. *Cardiovasc Drugs Ther* 1996; **10**: 495–510.
- 23 Yasutake H, Seino Y, Kashiwagi M, Honma H, Matsuzaki T, Takano T. Detection of cardiac sarcoidosis using cardiac markers and myocardial integrated backscatter. *Int J Cardiol* 2005; **102**: 259–68.
- 24 Smedema JP, Snoep G, van Kroonenburgh MP, et al. Evaluation of the accuracy of gadolinium-enhanced cardiovascular magnetic resonance in the diagnosis of cardiac sarcoidosis. *J Am Coll Cardiol* 2005; **45**: 1683–90.
- 25 Bradley JL, Blake JC, Chamberlain S, Thomas PK, Cooper JM, Schapira AH. Clinical, biochemical and molecular genetic correlations in Friedreich's ataxia. *Hum Mol Genet* 2000; **9**: 275–82.
- 26 Hewer R. The heart in Friedreich's ataxia. *Br Heart J* 1969; **31**: 5–14.
- 27 Child JS, Perloff JK, Bach PM, Wolfe AD, Perlman S, Kark RA. Cardiac involvement in Friedreich's ataxia: a clinical study of 75 patients. *J Am Coll Cardiol* 1986; **7**: 1370–8.
- 28 Weidemann F, Eyskens B, Mertens L, et al. Quantification of regional right and left ventricular function by ultrasonic strain rate and strain indexes in Friedreich's ataxia. *Am J Cardiol* 2003; **91**: 622–6.
- 29 Kusachi S, Nishiyama O, Yasuhara K, Saito D, Haraoka S, Nagashima H. Right and left ventricular oxygen metabolism in open-chest dogs. *Am J Physiol* 1982; **243**: H761–6.
- 30 Poulsen SH, Sogaard P, Nielsen-Kudsk JE, Egebлад H. Dilated cardiomyopathy in Friedreich's ataxia: 2D echo and tissue-Doppler analysis of left ventricular and atrial function. *Eur J Echocardiogr* 2003; **4**: 331–3.
- 31 Rustin P, von Kleist-Retzow JC, Chantrel-Groussard K, Sidi D, Munnich A, Rotig A. Effect of idebenone on cardiomyopathy in Friedreich's ataxia: a preliminary study. *Lancet* 1999; **354**: 477–9.
- 32 Mehta A, Ricci R, Widmer U, et al. Fabry disease defined: baseline clinical manifestations of 366 patients in the Fabry Outcome Survey. *Eur J Clin Invest* 2004; **34**: 236–42.
- 33 Kampmann C, Baehner F, Whybra C, et al. Cardiac manifestations of Anderson-Fabry disease in heterozygous females. *J Am Coll Cardiol* 2002; **40**: 1668–74.
- 34 Kampmann C, Baehner FA, Whybra C, et al. The right ventricle in Fabry disease. *Acta Paediatr Suppl* 2005; **94**: 15–8; discussion 9–10.
- 35 Moon JC, Sachdev B, Elkington AG, et al. Gadolinium enhanced cardiovascular magnetic resonance in Anderson-Fabry disease. Evidence for a disease specific abnormality of the myocardial interstitium. *Eur Heart J* 2003; **24**: 2151–5.
- 36 Bogaert J, Rademakers FE. Regional nonuniformity of normal adult human left ventricle. *Am J Physiol Heart Circ Physiol* 2001; **280**: H610–20.
- 37 Eng CM, Guffon N, Wilcox WR, et al. Safety and efficacy of recombinant human alpha-galactosidase A-replacement therapy in Fabry's disease. *N Engl J Med* 2001; **345**: 9–16.
- 38 Beer M, Weidemann F, Breunig F, et al. Impact of enzyme replacement therapy on cardiac morphology

- and function and late enhancement in Fabry's cardiomyopathy. *Am J Cardiol* 2006; **97**: 1515–8.
- 39 Fung KC, Corbett A, Krishnadas L. Myocardial tissue velocity reduction is correlated with clinical neurologic severity in myotonic dystrophy. *Am J Cardiol* 2003; **92**: 177–81.
- 40 Agretto A, Politano L, Bossone E, et al. Pulsed Doppler tissue imaging in dystrophinopathic cardiomyopathy. *J Am Soc Echocardiogr* 2002; **15**: 891–9.
- 41 Suffoletto MS, Dohi K, Cannesson M, Saba S, Gorcsan J III. Novel speckle-tracking radial strain from routine black-and-white echocardiographic images to quantify dyssynchrony and predict response to cardiac resynchronization therapy. *Circulation* 2006; **113**: 960–8.

# Tissue Doppler imaging and strain rate imaging to evaluate right ventricular function

*Gabe B. Bleeker, Eduard R. Holman, Theodore P. Abraham and Jeroen J. Bax*

## Introduction

In daily clinical practice, the right ventricle is frequently overlooked during the echocardiographic examination. Adequate function of the right ventricle, however, is of key importance to maintain adequate pulmonary perfusion and to ensure a low systemic venous pressure so as to prevent tissue damage and organ congestion.

Impairment of right ventricular (RV) function may be the result of primary right-sided heart disease, including RV cardiomyopathies, valvular heart disease, or congenital heart disease (particularly in conditions where the right ventricle supports the systemic circulation). In addition, RV dysfunction may be secondary to left-sided cardiomyopathy, valvular heart disease, or pulmonary disease. Finally, left-to-right shunting may lead to RV dysfunction.

It should also be considered that RV dysfunction may affect left ventricular (LV) function, not only by limiting LV preload, but also by adverse systolic and diastolic interaction by means of the intraventricular septum and the pericardium (referred to as ventricular interdependence). The clinical implications of impaired RV function have been studied widely in recent years, and it has become clear that both RV dysfunction and RV dilatation are strong and independent predictors of adverse cardiac events [1–3]. The need for evaluation of the right ventricle and diagnosis of RV dysfunction is evident, and assessment of RV function should

be part of every echocardiographic examination to optimize clinical management and treatment.

At present, conventional two-dimensional (2-D) echocardiography is still considered the cornerstone in the evaluation of RV function. Assessment of RV function by using conventional echocardiography, however, is much more challenging compared to the evaluation of LV function, mostly due to the complex geometry of the right ventricle. When used in a qualitative manner, conventional echocardiography is usually able to provide information about RV function, but if more objective (quantitative) information about RV function is required, conventional echocardiography is frequently insufficient.

In recent years, tissue Doppler imaging (TDI) and strain/strain rate (SR) imaging have been developed and are novel echocardiographic techniques for quantitative analysis of cardiac function. Both techniques have now been widely studied in the quantitative analysis of LV systolic and diastolic function. In particular, TDI has been proven highly accurate and reproducible. More recently, a limited number of studies tested the ability of TDI and strain/SR imaging to quantify RV global and regional function, and the initial results appear promising. The major potential advantages of TDI and strain/SR imaging for assessment of RV function over conventional echocardiography are their independence of geometric assumptions and endocardial border tracing. In addition, both TDI and strain/SR imaging images are feasible in a high number

of patients, even in the presence of low-quality 2-D imaging. This Chapter gives an overview of the current literature on the optimal use of TDI and strain/SR imaging for the quantitative analysis of RV function.

## Tissue Doppler imaging

TDI is an application based on Doppler principles, which can be used to measure myocardial velocities throughout the cardiac cycle. TDI determines the timing, direction, and velocity of wall motion. The myocardial velocity curves can either be constructed online using pulsed-wave (PW) TDI, or reconstructed offline from color-coded TDI images. The advantages of color-coded TDI over PW-TDI are the possibility for offline analysis and the possibility to analyze multiple segments during a single heartbeat, thereby avoiding potential errors from differences in the cardiac cycle.

### Assessment of right ventricular function

One of the most studied parameters for the quantification of RV systolic function is the measurement of the tricuspid annular velocity at the junction of the RV free-wall and the anterior leaflet of the tricuspid valve (Figure 20.1). For example, Meluzin et al. used PW-TDI to assess the tricuspid annular systolic velocity in 44 heart failure patients (mean LV ejection fraction,  $24 \pm 7\%$ ) and in 30 matched

healthy controls. Using a cutoff value of less than 11.5 cm/sec, the authors were able to predict RV dysfunction (defined as RV ejection fraction  $<45\%$ ) with a sensitivity of 90% and a specificity of 85% [4]. This parameter has now also been validated using cardiac magnetic resonance imaging (MRI) [5,6]. In 99 patients, a direct and significant correlation was observed between RV ejection fraction derived from MRI and tricuspid annular systolic velocity ( $r = 0.64$ ;  $P < 0.001$ ). Moreover, identification of patients with a severely reduced RV ejection fraction ( $<30\%$ ) was possible with a 100% sensitivity and 92% specificity using a cutoff value of  $<9$  cm/sec [5,6].

The tricuspid annular systolic velocity measured by TDI can also be used to diagnose RV involvement in patients with acute inferior myocardial infarction. In these patients, the tricuspid annular systolic velocity and the early diastolic velocities are significantly reduced when compared to healthy individuals and patients with inferior infarction without RV involvement. It has been suggested that a peak tricuspid annular systolic velocity  $<12$  cm/sec is predictive for RV involvement in acute inferior infarction (sensitivity 81% and specificity 82%) [7]. Other parameters suggestive for RV involvement included RV diastolic dimension and early diastolic velocity of the tricuspid annulus measured by TDI [7–11]. The value of the tricuspid annular systolic velocity (using either PW-TDI or color-coded TDI) for the assessment of RV function has now been

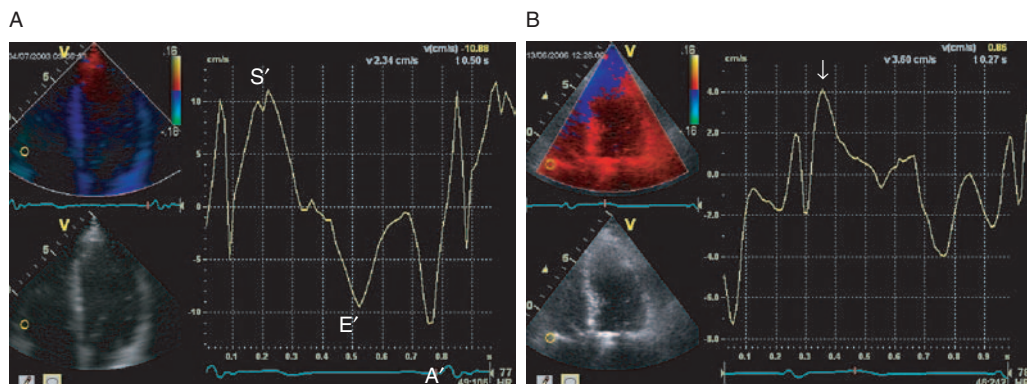


**Figure 20.1** (A) Tracing derived from color-coded tissue Doppler imaging with the sample placed at the junction of the RV free-wall and the anterior leaflet of the tricuspid valve, demonstrating peak systolic velocity (S') as well as

early (E') and late (A') diastolic velocities of the tricuspid annulus in a normal individual. (B) A substantially lower tricuspid annular velocity in a patient with impaired RV function. The arrow indicates peak systolic velocity.

studied in a wide range of pathological conditions, such as coronary artery disease, hypertension, hypothyroidism, pulmonary hypertension, cardiac amyloidosis, hypertrophic cardiomyopathy, pulmonary fibrosis, chronic pulmonary embolism, and congenital heart disease (tetralogy of Fallot). In addition, this parameter proved a strong predictor of patient prognosis in these studies [5,12–19].

Greaves et al. [20] used color-coded TDI to study regional differences in myocardial velocities throughout both the left and the right ventricle in 40 healthy subjects. In both ventricles, longitudinal velocities (apical views) were significantly (79%) higher than in the radial direction (parasternal views). Furthermore, the peak systolic velocities corresponding to RV longitudinal and radial contractions are significantly higher than their respective counterparts in the left ventricle [20].

Another approach for the assessment of RV systolic function using TDI is the measurement of myocardial acceleration during isovolumic contraction (IVA) (Figure 20.2). This index is unaffected by RV shape or loading conditions. In 22 pediatric patients with pulmonary regurgitation after repair of tetralogy of Fallot and 27 age-matched healthy controls, the IVA was strongly related with RV function and significantly lower compared to normal controls [12,13]. A basal septal IVA  $>1.1$  m/sec $^2$  predicted an RV ejection fraction  $>45\%$  (derived from MRI) with a sensitivity of 91% and a specificity of 94% (Figure 20.2) [6].

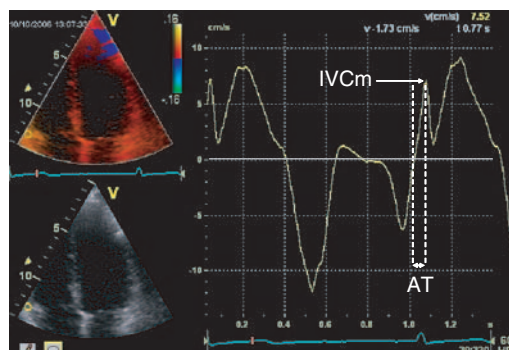


**Figure 20.2** The measurement of myocardial acceleration during IVA. The IVA is measured by dividing the myocardial velocity during isovolumic contraction (IVCm) by the time interval from onset of the myocardial velocity during isovolumic contraction to the time at peak systolic velocity of this wave (AT).

The Tei index of the right ventricle (Figure 20.3) can be used to combine assessment of systolic and diastolic function, proven to be a marker of global RV function, and is normally measured using conventional Doppler echocardiography. Harada et al. [21] used TDI to calculate the RV Tei index and noted a correlation of 0.81 ( $P < 0.001$ ) with RV Tei index derived from conventional pulsed Doppler, thus representing a simple method of assessing RV myocardial performance. Moreover, the TDI-derived Tei index has the advantage of simultaneous recording of systolic and diastolic velocity patterns (Figure 20.3).

In addition to the peak systolic velocity of regional RV contraction, the TDI curve of the tricuspid annulus can also be used to measure the peak early diastolic velocity ( $E'$ ) and peak late diastolic velocity ( $A'$ ), allowing evaluation of RV diastolic function, which may for example be affected in heart failure, hypertrophic cardiomyopathy, and inferior infarction (Figure 20.1) [4,8,14–17,22].

### Estimation of right atrial pressure

A potentially interesting application of TDI is its ability to estimate right atrial (RA) pressure. In the left ventricle, the ratio of the transmural peak early diastolic velocity ( $E$ ) measured by conventional Doppler echocardiography to the peak early diastolic velocity of the mitral annulus measured by TDI ( $E'$ ) (the  $E/E'$  ratio) proved to correlate closely with LV filling pressures (Figure 20.4) [23,24]. Nageh et al. tested a comparable parameter in the right

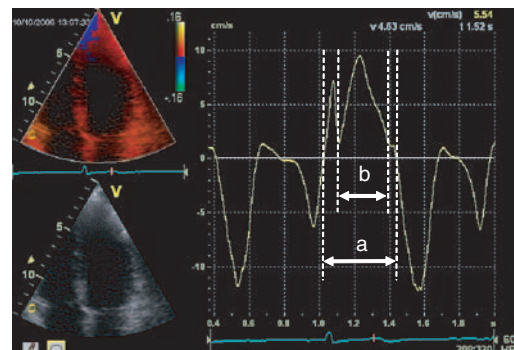


**Figure 20.3** Time intervals of the Tei index of the right ventricle by color-coded TDI. The "a" represents the time interval between the end and onset of tricuspid annular diastolic velocities. The "b" is the duration of the tricuspid annular ejection velocity. The TDI Tei index is calculated as (a-b/b).

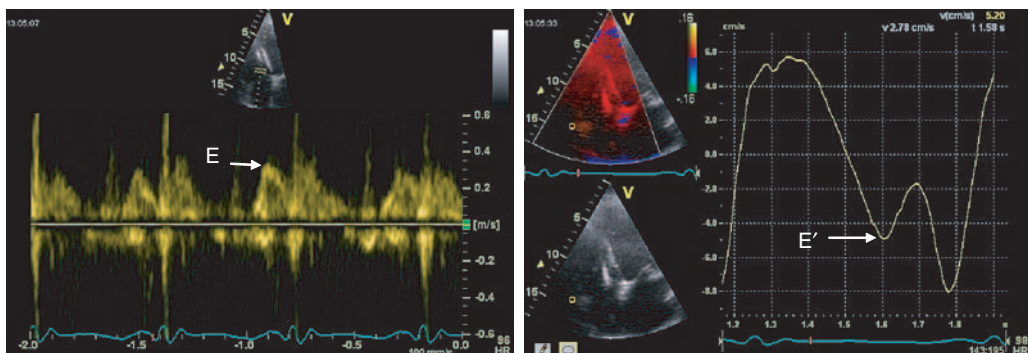


**Figure 20.4** Display of the E/E' ratio of the tricuspid annulus as a marker of RA pressure in a patient with heart failure. The height of the E is measured from the

pulsed-wave Doppler for transtricuspid early diastolic velocity and divided by the height of the E' measured from the tricuspid annulus velocity on color-coded TDI.

ventricle for its ability to estimate RA pressure [25]. Using the ratio between the transtricuspid early diastolic velocity (E) to peak early diastolic velocity of the lateral tricuspid annulus (E'), the E/E' ratio in the RV was calculated in 62 patients and compared to invasive measurements of RA pressure. Mean invasively measured RA pressure was  $13 \pm 6$  mm Hg and had a strong relationship with the tricuspid E/E' ratio ( $r = 0.75$ ;  $P < 0.001$ ), irrespective of RV function. Overall, an E/E' ratio of more than 6 had a sensitivity of 79% and a specificity of 73% to detect a mean RA pressure  $\geq 10$  mm Hg [25]. Of note, the accuracy of this parameter has recently been questioned in patients who are mechanically ventilated [26].

### Strain/strain rate imaging

Strain and SR imaging are postprocessing TDI data that enable quantification of myocardial deformation (strain imaging) or its rate of deformation (SR imaging) between two points in the region of interest within the myocardium. This ability offers strain/SR the potential advantage over TDI (which measures myocardial velocities) of being able to distinguish active from passive myocardial motion. Moreover, the use of strain/SR imaging proved relatively independent of heart rate and loading conditions compared to TDI [27]. Data on the use of strain/SR imaging for the evaluation of RV function are relatively scarce, but preliminary studies reveal promising results for the quantitative assessment of both global and regional RV function.

In addition, the initial results of speckle tracking, which is able to calculate myocardial strain from conventional 2-D echocardiography, will be briefly discussed.

### Global right ventricular function

In recent studies, quantification of RV function proved feasible by measurement of strain (rate) in the longitudinal direction (apical views). In contrast, the analysis of RV radial deformation (parasternal views) is frequently hampered by near-field artifacts and the RV wall is proved too thin for strain analysis. Jamal et al. demonstrated the feasibility of longitudinal strain/SR imaging for the quantification of RV contractile function in an elegant animal experiment [28]. In nine male pigs, the Doppler-derived strain measurements correlated well with sonomicrometry segment length measurements both in the inflow and outflow tract of the right ventricle and under different loading conditions [28].

Urheim et al. compared the accuracy of various conventional and novel echocardiographic parameters in predicting RV stroke volume in patients undergoing right heart catheterization. Invasive RV stroke volume was estimated by the thermodilution technique or Fick formula. Peak RV basal systolic displacement and RV systolic strain best correlated with RV stroke volume. These parameters closely tracked load-related changes in RV stroke volume in patients who underwent vasodilator infusion and reductions in pulmonary vascular resistance. However, indices such as the Tei index and IVA did not correlate closely with RV stroke volume [29].

A recent study by Vitarelli et al. applied strain/SR imaging in a clinical setting in 39 patients with chronic obstructive pulmonary disease (COPD) and 22 healthy control subjects [30]. Strain and SR values were obtained from the RV free-wall and the interventricular septum in the longitudinal views. Strain/SR measurements were feasible in a high number of patients (93%) with a low intra- and inter-observer variability for all measurements (approximately 5%). In the COPD patients with pulmonary hypertension (defined as a pulmonary artery pressure  $> 35$  mm Hg,  $n = 22$ ), strain/SR values were reduced in all segments and significantly lower compared to the control subjects with the highest values in the basal RV free-wall. A significant relationship was observed between peak systolic SR at the basal free-wall site and radionuclide-derived RV ejection fraction ( $r = 0.81$ ;  $P < 0.001$ ). Interestingly, this correlation was somewhat better than the correlation between radionuclide-derived RV ejection fraction and RV ejection fraction calculated from conventional 2-D echocardiography (manual tracing,  $r = 0.63$ ;  $P < 0.005$ ). A cutoff point of systolic strain and peak strain rate at the basal RV free-wall of 25% and  $-4 \text{ sec}^{-1}$  yielded sensitivities of 81% and 85% with specificities of 82% and 88%, respectively, for prediction of preserved global RV systolic function (RV ejection fraction  $\geq 50\%$ ) (Figure 20.5) [30].

Various recent studies confirmed the value of strain/SR imaging for quantification of global RV function in a wide variety of pathological conditions, including pulmonary hypertension, obesity, Friedreich's ataxia, after lung transplantation, and in congenital heart disease (atrial septal defects, tetralogy of Fallot, systemic right ventricle) [27,28,31–39]. For example, Borges et al. calculated strain from the basal segment of the RV free-wall in 37 patients with chronic pulmonary arterial hypertension and RV dysfunction and compared the results to a group of 38 healthy controls (systolic longitudinal deformation  $-8.8 \pm 4.1\%$  vs.  $-24.3 \pm 4.7\%$ , respectively;  $P < 0.001$ ) [32]. After treatment of the patients with pulmonary arterial hypertension with vasodilator therapy, the authors were able to detect improvements in RV function as evidenced by an improvement in systolic longitudinal strain of the basal segment of the RV free-wall ( $-13.3 \pm 6.2\%$ ;  $P < 0.001$ ) [32].

One of the difficulties with assessment of RV function using conventional echocardiographic techniques is its relative dependence on loading conditions. Both volume and pressure overload of the right ventricle are frequently observed in cardiovascular pathological states and are known to affect echocardiographic parameters of RV function. Kjaergaard et al. studied the effects of increasing preload and afterload on the strain/SR-derived

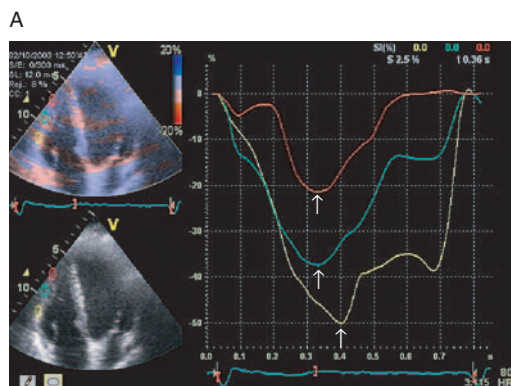
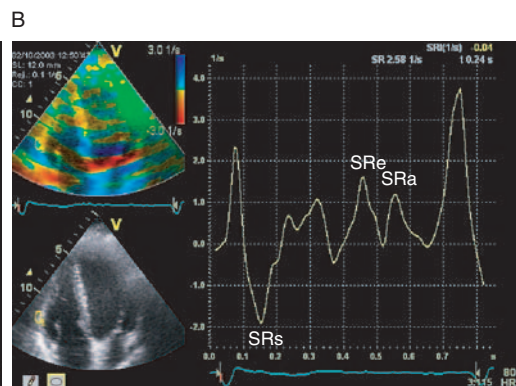


**Figure 20.5** (A) Two-dimensional longitudinal strain imaging (four-chamber view) in a normal individual. The sample volumes are placed in the basal (yellow curve), mid-(blue curve), and apical-segments (red curve) of the RV free-wall (arrows indicate peak strain). Of note, peak strain is highest in the basal part of the RV free-wall.



**(B)** Strain rate imaging (four-chamber view) in a normal individual. The sample volume is placed in the basal part of the RV free-wall. The peak systolic strain rate (SRs) as well as peak early (SRe) and late diastolic (SRa) strain rate can be measured.

indices of RV systolic function (measured as the peak strain/SR of the basal and mid-RV free-wall) [15]. Seventeen healthy subjects were exposed to increased preload by rapid infusion of saline and increased afterload simulated in a controlled hypoxic environment. Again, strain/SR measurements were feasible in more than 90% of patients under all conditions. The strain/SR were not significantly different between baseline conditions (RV basal free-wall peak strain,  $-23 \pm 7\%$ ; peak SR,  $-1.4 \text{ sec}^{-1}$ ) and during increased preload and afterload ( $-26 \pm 8\% / -1.4 \pm 0.5 \text{ sec}^{-1}$  and  $-26 \pm 10\% / -1.7 \pm 0.8 \text{ sec}^{-1}$ , respectively; all  $P = \text{not significant}$ ). These findings demonstrate that strain/SR measurements of RV function are relatively independent of loading conditions [17]. Furthermore, the relative independence from loading conditions of strain/SR-derived indices of RV function was also confirmed in animal experiments [28].

Although evaluation of global RV systolic function is one of the most promising applications of strain/SR imaging, it may also be used for the evaluation of RV diastolic function by measuring the SR during early diastole (E) and late diastole (A). The reproducibility of the diastolic parameters calculated from SR, however, was substantially lower compared to the systolic parameters [15,30].

### **Regional right ventricular function**

Analysis of regional RV function by visual inspection of regional myocardial thickening on conventional 2-D echocardiography remains a major challenge. Strain/SR imaging now allows the offline analysis of deformation in multiple RV segments, which makes this technique particularly well suited for the analysis regional RV function (Figure 20.5). This analysis may provide valuable clinical information in diseases with alterations of the contractile function that are (initially) limited to a specific region of the right ventricle. Several studies demonstrated the feasibility of strain/SR imaging for the analysis of regional RV function. In line with the findings obtained in TDI (myocardial velocities) studies, RV longitudinal strain and SR values are significantly higher in the right ventricle compared to the left ventricle. In addition, the strain/SR values show a heterogeneous distribution throughout the RV (with the basal segments showing the highest values) (Figure 20.5A)), whereas myocardial

deformation is homogenously distributed through the left ventricle, which may be explained by the complex geometry and different muscular arrangements of the right ventricle compared to the left ventricle [40]. Also, the values recorded from the RV inferior wall were significantly lower than those recorded from the RV free-wall [41–43]. A potentially interesting application of strain/SR imaging is the diagnosis of RV involvement in patients suffering from acute inferior myocardial infarction.

The diagnosis of arrhythmogenic right ventricular cardiomyopathy (ARVC) is another potential application for the quantitative analysis of regional RV function by strain/SR imaging. ARVC is a familial disorder that is characterized by the replacement of RV myocardium by fibrous and fatty tissue, resulting in ventricular arrhythmias. The diagnosis of ARVC remains a major challenge, especially in the early asymptomatic stage of the disease. At present, ARVC is usually diagnosed using MRI, but strain/SR imaging could offer a potentially useful noninvasive imaging modality to screen patients for the presence of ARVC, as demonstrated by Herbots et al. who describe a case of a 50-year-old man with ARVC [44]. By using strain/SR imaging, the authors showed an absence of systolic and diastolic deformation throughout the longitudinal RV free-wall, which was confirmed microscopically by the presence of extensive subendocardial fibrosis and replacement of myocytes by fatty tissue throughout the entire RV free-wall [44].

### **Is right ventricular dyssynchrony an issue?**

In addition to the quantification of global and regional RV function, strain/SR also permit assessment of ventricular dyssynchrony. Strain/SR imaging has been extensively studied for the assessment of dyssynchrony within the left ventricle, but the prevalence and hemodynamic effects of RV dyssynchrony on cardiac function have not been evaluated [45]. From a theoretical point of view, RV dyssynchrony may result in an inefficient RV contraction, therefore, reducing the cardiac output. Due to its complex geometry, assessment of RV dyssynchrony is only feasible by measurement of septum-to-RV free-wall delay with the current techniques.

Rajagopalan et al. studied the coexistence of RV dyssynchrony in 34 patients with heart failure [46].

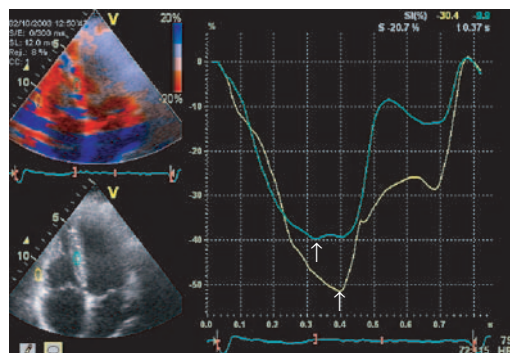


**Figure 20.6** Measurement of RV dyssynchrony in a normal individual. RV dyssynchrony is measured as the difference in time-to-peak strain of the basal part of the RV free-wall (yellow curve) and the basal part of the interventricular septum (blue curve, arrows indicate peak strain).

RV dyssynchrony was defined as the difference in time to peak longitudinal strain between the basal RV free-wall and the basal interventricular septum (Figure 20.6). Mean RV dyssynchrony was  $59 \pm 45$  msec, whereas mean LV dyssynchrony (between septum and LV lateral wall) was  $80 \pm 62$  msec. A strong correlation was observed between RV dyssynchrony and pulmonary artery systolic pressure ( $r = 0.73$ ;  $P < 0.001$ ) and a modest negative correlation between RV dyssynchrony and RV fractional area change ( $r = -0.43$ ;  $P < 0.02$ ) [46]. In addition, RV dyssynchrony proved a strong predictor of disease severity in heart failure patients as it correlates with World Health Organization class and number of hospitalizations [47].

These findings demonstrate that RV dyssynchrony is a frequent observation in patients with heart failure, which correlates with pulmonary hypertension, RV dysfunction, and disease severity. It is currently unclear whether novel heart failure treatment modalities, such as cardiac resynchronization therapy are able to reduce RV dyssynchrony, and it is unknown whether a reduction in RV dyssynchrony will translate into favorable clinical effects.

### Speckle tracking

Data on the use of speckle tracking for quantification of RV function are scarce. The main theoretical advantage of speckle tracking-derived strain (derived from conventional 2-D echocardiography) over TDI-derived strain is its lack of angle

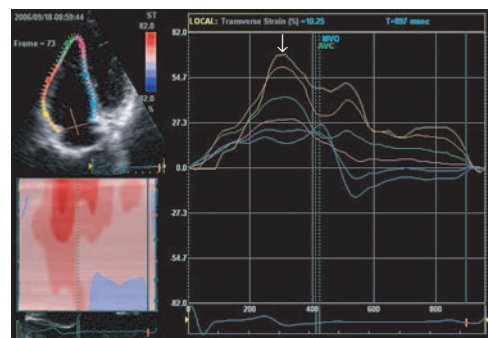


**Figure 20.7** Speckle tracking-derived longitudinal strain in the apical four-chamber view. Longitudinal strain is calculated from multiple circumferential points over the cardiac cycle. The curves are color coded in accordance with the segments on the four-chamber view. Note that the highest peak strain is located in the basal part of the RV free-wall (indicated by the arrow).

dependency, which may result in more reliable strain measurements. Speckle tracking has been used for the assessment of RV function in patients with systemic sclerosis with ( $n = 34$ ) and without ( $n = 5$ ) pulmonary hypertension. Maximum longitudinal strain was derived from the basal-, mid-, and apical-segments of the RV free-wall in the apical four-chamber view (similar to the measurements derived from TDI-derived strain/SR imaging) (Figure 20.7) [48]. A large difference in maximum longitudinal strain of the RV free-wall was observed between patients with and without pulmonary hypertension. The maximum longitudinal strain of the mid-segment of the RV free-wall showed the strongest correlation with pulmonary artery pressure ( $r = 0.65$ ;  $P < 0.001$ ) and pulmonary vascular resistance ( $r = 0.62$ ;  $P < 0.001$ ) [48,49]. De Boeck et al. used speckle tracking-derived strain in a 51-year-old man with drug-refractory Wolff-Parkinson-White syndrome. Using this technique, the authors were able to localize the area of earliest ventricular contraction and the extent of ventricular premature ventricular contraction associated with the accessory bypass (both in the left and the right ventricle) [50].

### Conclusions

To date, the quantitative assessment of RV function has been hampered by the complex anatomy of the right ventricle. The echocardiographic assessment

of the right ventricle has, therefore, mainly been limited to qualitative assessment of RV function, resulting in subjective and operator-dependent measurements. Recently, TDI and strain/SR imaging have been introduced for the quantitative analysis of RV function. At present, the clinical experience with both techniques is limited, but initial studies have demonstrated promising results. The major potential advantage of TDI and strain/SR imaging for assessment of RV function are the independence of geometric assumptions and endocardial border tracing. In addition, both TDI and strain/SR images are feasible in the majority of patients (even in the presence of low-quality 2-D imaging), have a good reproducibility, and are relatively load-independent. Both techniques also permit the quantification of longitudinal systolic and diastolic function for each RV segment separately.

TDI and strain/SR imaging also have limitations. Both techniques are angle-dependent, and interpretations should be performed with caution if tissue movement direction deviates more than 30 degrees from the beam direction. This disadvantage can potentially be overcome by a novel angle-independent echo technique called speckle tracking, which can calculate strain/SR from conventional 2-D images. However, this new technology has a higher dependence on the quality of the 2-D image, and many more studies are necessary to assess the role of speckle tracking in evaluation of RV function.

## References

- 1 Mehta SR, Eikelboom JW, Natarajan MK, et al. Impact of right ventricular involvement on mortality and morbidity in patients with inferior myocardial infarction. *J Am Coll Cardiol* 2001; **37**: 37–43.
- 2 Zehender M, Kasper W, Kauder E, et al. Eligibility for and benefit of thrombolytic therapy in inferior myocardial infarction: focus on the prognostic importance of right ventricular infarction. *J Am Coll Cardiol* 1994; **24**: 362–9.
- 3 de Groote P, Millaire A, Foucher-Hossein C, et al. Right ventricular ejection fraction is an independent predictor of survival in patients with moderate heart failure. *J Am Coll Cardiol* 1998; **32**: 948–54.
- 4 Meluzin J, Spinarova L, Bakala J, et al. Pulsed Doppler tissue imaging of the velocity of tricuspid annular motion. *Eur Heart J* 2001; **22**: 340–8.
- 5 Praz F, Wahl A, Kabok M, et al. Assessment of right ventricular systolic function: comparison between MRI and pulsed wave Tissue Doppler imaging of the tricuspid annulus [abstract]. *Eur Heart J* 2006; **27 Suppl**: 298.
- 6 Sade LE, Gulmez O, Ozyer U, et al. Regional pulsed wave tissue Doppler of the right ventricle for the evaluation of systolic function: validation against cardiac magnetic resonance imaging [abstract]. *Eur Heart J* 2006; **27 Suppl**: 628.
- 7 Zaborska B, Makowska E, Pilichowska E, et al. Pulsed Doppler tissue imaging – a useful tool for diagnosis of acute right ventricular infarction [abstract]. *Eur Heart J* 2006; **27 Suppl**: 627.
- 8 Alam M, Wardell J, Andersson E, Samad BA, Nordlander R. Right ventricular function in patients with first inferior myocardial function: assessment by tricuspid annular motion and tricuspid annular velocity. *Am Heart J* 2000; **139**: 710–15.
- 9 Oguzhan A, Abaci A, Eryol NK, Topsakal R, Seyfeli E. Colour tissue Doppler echocardiographic evaluation of right ventricular function in patients with right ventricular infarction. *Cardiology* 2003; **100**: 41–6.
- 10 Ozdemir K, Altunkeser BB, Icli A, Ozdil H, Gok H. New parameters of right ventricular myocardial infarction and proximal right coronary artery lesion. *Chest* 2003; **124**: 219–26.
- 11 Dokainish H, Abbey H, Gin K, Ramanathan K, Lee PK, Jue J. Usefulness of tissue Doppler imaging in the diagnosis and prognosis of acute right ventricular infarction with inferior wall acute left ventricular infarction. *Am J Cardiol* 2005; **95**: 1039–42.
- 12 Toyono M, Harada K, Tamura M, Yamamoto F, Takada G. Myocardial acceleration during isovolumic contraction as a new index of right ventricular contractile function and its relation to pulmonary regurgitation in patients after repair of tetralogy of Fallot. *J Am Soc Echocardiogr* 2004; **17**: 332–7.
- 13 Turhan S, Tulunay C, Ozduman Cin M, et al. Effects of thyroxine therapy on right ventricular systolic and diastolic function in patients with subclinical hypothyroidism: a study by pulsed wave tissue Doppler imaging. *J Clin Endocrinol Metab* 2006; **91**: 3490–3.
- 14 Kosar F, Sahin I, Aksoy Y, Uzer E, Turan N. Usefulness of pulsed-wave tissue Doppler echocardiography for the assessment of the left and right ventricular function in patients with clinical hypothyroidism. *Echocardiography* 2006; **23**: 471–7.
- 15 Kjaergaard J, Snyder EM, Hassager C, Oh JK, Johnson BD. Impact of preload and afterload on global and regional right ventricular function and pressure: a quantitative echocardiographic study. *J Am Soc Echocardiogr* 2006; **19**: 515–21.
- 16 D'Andrea A, Caso P, Severino S, et al. Different involvement of right ventricular myocardial function in either

- physiologic or pathologic left ventricular hypertrophy: a Doppler tissue study. *J Am Soc Echocardiogr* 2003; **16**: 154–61.
- 17 Burgess MI, Mogulkoc N, Bright-Thomas RJ, Bishop P, Egan JJ, Ray SG. Comparison of echocardiographic markers of right ventricular function determining prognosis in chronic pulmonary disease. *J Am Soc Echocardiogr* 2002; **15**: 633–9.
  - 18 Funabashi N, Sekine T, Fujikawa A, et al. Quantitative evaluation of chronic pulmonary thromboemboli by multislice computed tomography in comparison with pulsed Doppler tissue imaging and brain natriuretic peptide [abstract]. *Eur Heart J* 2006; **27 Suppl**: 630.
  - 19 Pitsiou G, Papadopoulos CE, Dalamanga GE, et al. Right ventricular myocardial function assessment in patients with non-end stage idiopathic pulmonary fibrosis. A tissue Doppler imaging study [abstract]. *Eur Heart J* 2006; **27 Suppl**: 628.
  - 20 Greaves K, Puranik R, O’Leary JJ, Celermajer DS. Myocardial tissue velocities in the normal left and right ventricle: relationships and predictors. *Heart Lung Circ* 2004; **13**: 367–73.
  - 21 Harada K, Tamura M, Toyono M, Yasuoka K. Comparison of the right ventricular Tei index by tissue Doppler imaging to that obtained by pulsed Doppler in children without heart disease. *Am J Cardiol* 2002; **90**: 566–9.
  - 22 Topal E, Ozdemir R, Aksoy Y, et al. Tissue Doppler velocities of the right and left ventricles and their association with C-reactive protein and homocysteine levels in Behcet’s disease. *Am J Cardiol* 2005; **96**: 1739–42.
  - 23 Nagueh SF, Middleton KJ, Kopelen HA, Zoghbi WA, Quinones MA. Doppler tissue imaging: a noninvasive technique for evaluation of left ventricular relaxation and estimation of filling pressures. *J Am Coll Cardiol* 1997; **30**: 1527–33.
  - 24 Ommen SR, Nishimura RA, Appleton CP, et al. Clinical utility of Doppler echocardiography and tissue Doppler imaging in the estimation of left ventricular filling pressures: a comparative simultaneous Doppler-catheterization study. *Circulation* 2000; **102**: 1788–94.
  - 25 Nageh MF, Kopelen HA, Zoghbi WA, Quinones MA, Nagueh SF. Estimation of mean right atrial pressure using tissue Doppler imaging. *Am J Cardiol* 1999; **84**: 1448–51.
  - 26 Michaux I, Filipovic M, Skarvan K, Schneiter S, Seeberger MD. Accuracy of tissue Doppler estimation of the right atrial pressure in anesthetized, paralyzed and mechanically ventilated patients. *Am J Cardiol* 2006; **97**: 1654–6.
  - 27 Eyskens B, Ganame J, Claus P, Boshoff D, Gewillig M, Mertens L. Ultrasonic strain rate and strain imaging of the right ventricle in children before and after percutaneous closure of an atrial septal defect. *J Am Soc Echocardiogr* 2006; **19**: 994–1000.
  - 28 Jamal F, Bergerot C, Argaud L, Loufouat J, Ovize M. Longitudinal strain quantitates regional right ventricular contractile function. *Am J Physiol Heart Circ Physiol* 2003; **285**: H2842–7.
  - 29 Urheim S, Cauduro S, Frantz R, et al. Relation of tissue displacement and strain to invasively determined right ventricular stroke volume. *Am J Cardiol* 2005; **96**: 1173–8.
  - 30 Vitarelli A, Conde Y, Cimino E, et al. Assessment of right ventricular function by strain rate imaging in chronic obstructive pulmonary disease. *Eur Respir J* 2006; **27**: 268–75.
  - 31 Hammoudi N, Tieb K, Ederhy S, et al. Strain and strain rate imaging in the evaluation of right ventricular regional function in systemic sclerosis: a case control matched study [abstract]. *Eur Heart J* 2006; **27 Suppl**: 630.
  - 32 Borges AC, Knebel F, Eddicks S, et al. Right ventricular function assessed by two-dimensional strain and tissue Doppler echocardiography in patients with pulmonary arterial hypertension and the effect of vasodilator therapy. *Am J Cardiol* 2006; **98**: 530–4.
  - 33 Weidemann F, Jamal F, Sutherland GR, et al. Myocardial function defined by strain rate and strain during alterations in inotropic stated and heart rate. *Am J Physiol Heart Circ Physiol* 2002; **283**: H792–9.
  - 34 Weidemann F, Eyskens B, Mertens L, et al. Quantification of right and left ventricular function by ultrasonic strain rate and strain indexes after surgical repair of tetralogy of Fallot. *Am J Cardiol* 2002; **90**: 133–8.
  - 35 Weidemann F, Eyskens B, Mertens L, et al. Quantification of regional right and left ventricular function by ultrasonic strain rate and strain indexes in Friedreich’s ataxia. *Am J Cardiol* 2003; **91**: 622–6.
  - 36 Di Salvo G, Pacileo G, Del Giudice EM, et al. Abnormal myocardial deformation properties in obese non-hypertensive children: an ambulatory blood pressure monitoring, standard echocardiographic and strain rate imaging study. *Eur Heart J* 2006; **27**: 2689–95.
  - 37 Bos JM, Hagler DJ, Silvilairat S, et al. Right ventricular function in asymptomatic individuals with a systemic right ventricle. *J Am Soc Echocardiogr* 2006; **19**: 1033–7.
  - 38 Dambrauskaite V, Herbots L, Claus P, et al. Differential changes in regional right ventricular function before and after a bilateral lung transplantation: an ultrasonic strain and strain rate study. *J Am Soc Echocardiogr* 2003; **16**: 432–6.
  - 39 Eyskens B, Weidemann F, Kowalski M, et al. Regional right and left ventricular function after the Senning operation: an ultrasonic study of strain rate and strain. *Cardiol Young* 2004; **14**: 255–64.
  - 40 Torrent-Guasp F, Ballester M, Buckberg GD, et al. Spatial orientation of the ventricular muscle band: physiologic contribution and surgical implications. *J Thorac Cardiovasc Surg* 2000; **122**: 389–92.

- 41 Weidemann F, Eyskens B, Jamal F, et al. Quantification of regional left and right ventricular radial and longitudinal function in healthy children using ultrasound-based strain rate and strain imaging. *J Am Soc Echocardiogr* 2002; **15**: 20–8.
- 42 Kowalski M, Kukulski T, Jamal F, et al. Can natural strain and strain rate quantify regional myocardial deformation? A study in healthy subjects. *Ultrasound Med Biol* 2001; **27**: 1087–97.
- 43 Goebel B, Arnold R, Koletzki E, et al. Exercise tissue Doppler echocardiography with strain rate imaging in healthy young individuals: feasibility, normal values and reproducibility. *Int J Cardiovasc Imaging* 2006 [epub ahead of print].
- 44 Herbots L, Kowalski M, Vanhaecke J. Characterizing abnormal regional longitudinal function in arrhythmogenic right ventricular dysplasia. The potential clinical role of ultrasonic myocardial deformation imaging. *Eur J Echocardiogr* 2003; **4**: 101–7.
- 45 Bax JJ, Abraham T, Barold SS, et al. Cardiac resynchronization therapy, Issues before implantation. *J Am Coll Cardiol* 2005; **46**: 2153–67.
- 46 Rajagopalan N, Dohi K, Simon MA, et al. Right ventricular dyssynchrony in heart failure: a tissue Doppler imaging study. *J Card Fail* 2006; **12**: 263–7.
- 47 Lopez-Candales A, Dohi K, Rajagopalan N, et al. Right ventricular dyssynchrony in patients with pulmonary hypertension is associated with disease severity and functional class. *Cardiovasc Ultrasound* 2005; **3**: 23.
- 48 Hassan AA, Constandse J, Vonk MC, Sander MH, Van Dijk AP. Right ventricular free wall strain as determined by speckle-tracking decreases in elevated pulmonary arterial pressure and resistance in systemic sclerosis. *Eur Heart J* 2006; **27**: 626.
- 49 Pirat B, McCulloch ML, Zoghbi WA. Evaluation of global and regional right ventricular systolic function in patients with pulmonary hypertension using a novel speckle tracking method. *Am J Cardiol* 2006; **98**: 699–704.
- 50 De Boeck BW, Cramer MJ, Loh P, Doevedans PA. Two-dimensional strain imaging to assess the origin and extent of ventricular preexcitation associated with an accessory bypass. *Circulation* 2006; **113**: e835–9.

# 6

## PART 6

# Coming developments and applications



# Atrial function

*Qing Zhang and Cheuk-Man Yu*

## Introduction

Atrial function is an integral aspect of the proper performance of the circulatory system. In the presence of cardiac diseases, atrial function could be primarily or secondarily affected. Hemodynamic assessment of atrial function using a high-fidelity catheter is limited by its invasive nature and by it possibly not reflecting the true functional status of the atrium, such as the contractility of the chamber [1]. Doppler echocardiography is one of the most common modalities to assess atrial function indirectly by estimating hemodynamic differences between the atrium and the ventricle [2]. In recent years, tissue Doppler imaging (TDI) has been used as a sensitive and reproducible tool for noninvasive evaluation of left and right atrial function [3–10]. This Chapter will discuss the evolution of echocardiographic tools for the assessment of atrial function, in particular the application of TDI in clinical practice.

## Hemodynamic function of the atrium

Hemodynamically, the atrium acts as a facilitator and distributor for optimization of ventricular filling through its three components, that is, reservoir function during ventricular systole, conduit function during early ventricular diastole, as well as active contractile (pump) function during late diastole. The reservoir phase starts with ventricular systole, when venous return is accommodated in the distensible atrial chambers. During the early diastolic phase, blood coming into the atrial chambers from the veins is sucked into the ventricles where the atria act as a conduit to facilitate ventricular filling. In late diastole, muscles of the atria contract

actively to expel the blood into the ventricles, serving as a booster pump.

In normal subjects, the relative contribution of the reservoir, conduit, and pump functions of the atria to the total ventricular filling is approximately 40%, 35%, and 25%, respectively. However, with changes in ventricular filling, the atria are able to adjust the relative proportion of these components to maintain the ventricular stroke volume. For example, impaired ventricular relaxation is associated with decreased conduit function but enhanced reservoir and pump function, due to a lowering of atrioventricular pressure gradient during early diastole. As left ventricular diastolic dysfunction progresses to a pseudonormal or restrictive filling pattern, the contribution of conduit function is significantly increased while reservoir and pump functions are severely impaired [11–13]. Atrial contractile function is determined by its muscle contractility and the intra-atrial pressure at the beginning of atrial systole (atrial preload). According to the Frank–Starling law, an increase in atrial pressure and the associated increase in wall stretch will result in augmentation of the atrial contribution to ventricular filling because of the increase in atrial contractility initially [14]. However, with further deterioration of atrial myocyte function either due to a myopathic process or overdistension of atrial fibers to a critical point, depression of atrial pump performance will occur, despite increased atrial preload [15].

## Methods for evaluation of left atrial function

### Left atrial pressure–volume relationship

The pressure–volume relationship is an accurate modality for the investigation of left atrial (LA)

hemodynamic status [12]. The placement of a high-fidelity, micromanometer-tipped catheter into the LA chamber is necessary to obtain a precise recording of the LA pressure waveform [16]. Simultaneous and continuous measurement of LA volume has been successfully conducted using various noninvasive imaging tools, such as real-time two-dimensional (2-D) or 3-D echocardiography with automated boundary detection, radionuclide angiography, cine computerized tomography, and magnetic resonance imaging [17–19]. The combination of these two waveforms will give rise to an LA pressure–volume graph that is composed of “A” and “V” loops. The active component of the graph, the “A loop,” proceeds in a counterclockwise direction representing LA pump function. The passive component of the graph, the “V loop,” proceeds in a clockwise manner representing LA reservoir function. However, this method is restricted as an investigational tool for mechanistic and conceptual purposes due to its invasive nature. Furthermore, this measure of LA pump function is load-dependent and, therefore, may not serve as the best quantitative index of LA contractility.

### **Echocardiographic assessment of left atrial phasic function**

#### **Left atrial size**

The assessment of LA size can readily be achieved by echocardiography, and it has been shown that LA volume is a more accurate and reproducible estimate than LA dimension [13]. LA enlargement is associated with an increase in risk of atrial fibrillation, heart failure, ischemic stroke, cardiovascular hospitalization, and mortality [20–22]. The three principal LA volumetric measurements, namely the maximal volume just before mitral valve opening (LAVmax), the minimum volume at mitral valve closure (LAVmin), and the volume before the P-wave (LAVmid) can be used to demonstrate the LA phasic function [10,23]. The total emptying volume can be derived from the difference between LAVmax and LAVmin, which is an estimate of reservoir function. The passive emptying volume is calculated as the difference between LAVmax and LAVmid, whereas active emptying volume is obtained by LAVmid minus LAVmin. The active emptying volume is a surrogate index of LA contractile function. LA conduit function is calculated as the difference

between left ventricular (LV) stroke volume and total LA emptying volume, which is the amount of blood flowing from pulmonary veins through the LA chamber into the left ventricle without any share of the left atrium as a pump.

#### **Doppler echocardiographic indices of left atrial function**

It is important to note that Doppler parameters have been shown to be dependent on LA loading conditions, LA contractile state, and LV function [24]; therefore, alteration of LA function by these indices should be interpreted in the context of potential limitations. The pulsed Doppler profile of transmural inflow provides much information on atrial function. The profile consists of an early (E-wave) and late (A-wave) diastolic flow. The transmural E-wave amplitude represents LV filling in early diastole, which is a combined effect of passive and active LV function, although it also reflects LA function as a conduit [25]. The transmural A-wave is often used to evaluate LA contractile performance; therefore, its amplitude and, in particular, the E/A ratio describes atrial contribution to ventricular filling [11].

Spectral pulsed Doppler recording of the pulmonary veins entering the left atrium is also used frequently to assess LA function [11,26]. The first positive deflection (S-wave) during LV systole reflects the reservoir function of the left atrium. The second positive deflection (D-wave) immediately after the opening of mitral valve acts as an index of LA conduit function. The reversal component of the waveform represents LA contraction, which has been shown to correlate closely with mean LA pressure and volume. It is usually combined with transmural A-wave to describe atrial booster pump function.

#### **Left atrial appendage function**

The left atrial appendage (LAA) is a highly contractile pump with a pattern of contraction totally different from that of the LA main body. It is more compliant and, therefore, also plays an important role in LA reservoir function, especially during increases in LA pressure or volume [27]. Meanwhile, LAA is a place where thrombi are often formed and spontaneous echo contrast (SEC) is present. Transesophageal echocardiography provides

essential information regarding LAA structure and function, including planimetric parameters and assessments of blood flow by spectral pulse Doppler at the appendage outlet. LAA size and LAA late emptying and filling velocities can be measured to reflect its systolic and diastolic function [23,27]. In particular, for patients with atrial fibrillation undergoing cardioversion, recovery of LAA mechanical function can be reflected by the progressive increase in emptying and filling velocities.

### Tissue Doppler imaging and atrial function

#### Atrial myocardial performance

With TDI imaging, a sample volume can be placed in an atrial segment of interest to generate a

myocardial velocity curve either online by pulsed TDI or offline by reconstitution of myocardial signals in color TDI. This analysis consists of systolic (Sa-wave), early diastolic (Ea-wave), and late diastolic (atrial contraction, Aa-wave) components. It has been suggested that atrial longitudinal contraction can be directly measured by the Aa-wave, which might be less dependent on loading conditions (Figure 21.1A) [6,10,28,29]. Sa and Ea may also represent passive atrial function [5,30]. Furthermore, TDI-derived measurement of timing variables indirectly reflects atrial electrical activation sequence that follows the known activation process (from right to left atrium) as revealed by invasive electrophysiology [6,8,10,28]. In TDI, a few different imaging modalities can be used, including

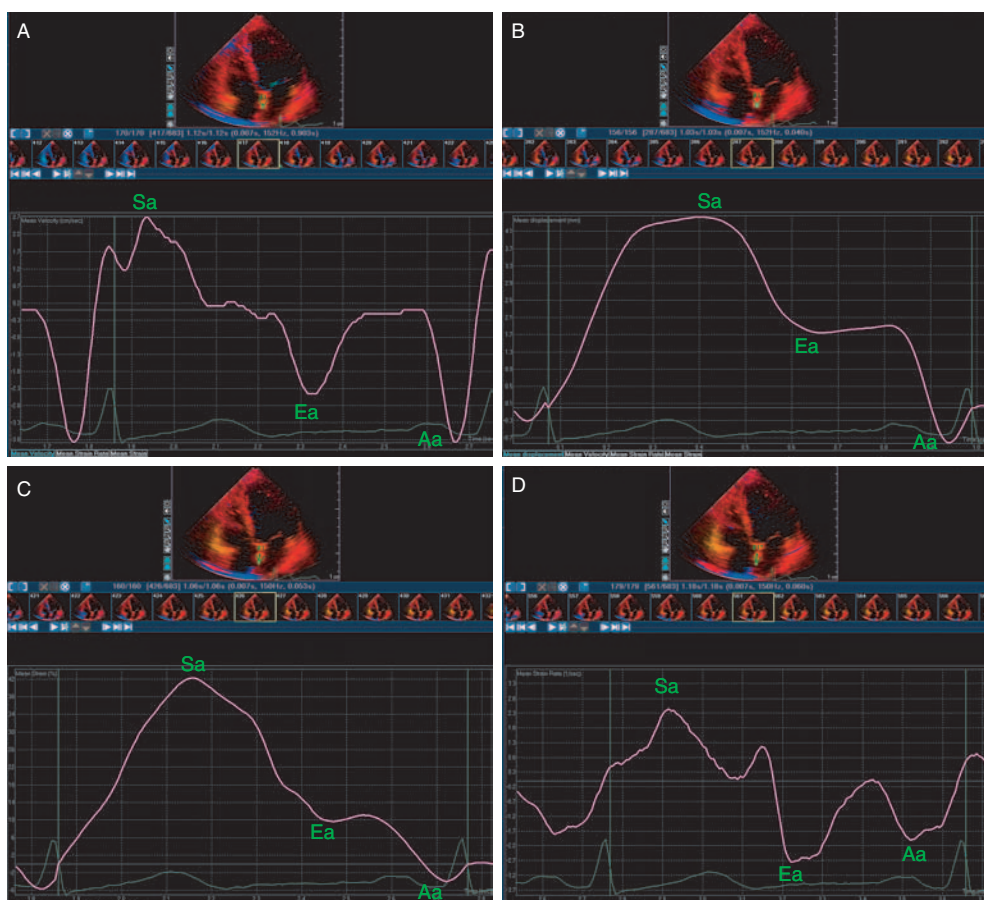


**Figure 21.1** Atrial myocardial performance reflected by TDI. The sample volume was placed at the mid-level of IAS on color TDI image to reconstitute offline the myocardial velocity (A), displacement (B), strain (C), and strain rate

(D) curves. They consist of systolic (Sa-wave), early diastolic (Ea-wave), and late diastolic (atrial contraction, Aa-wave) components.

tissue velocity, displacement, strain, and strain rate (Figure 21.1A, B, C, and D). Usually, a small sample volume (i.e., 2 mm for velocity and not more than 12 mm for length for strain rate) is preferred for the evaluation of regional atrial function in view of the thin-walled structure of the atrium. Moreover, different atrial walls can be readily assessed, in particular by offline analysis of color TDI, such as the LA free-wall, right atrial free-wall, and interatrial septum (IAS). An individual atrial wall can also be approached at different levels, from the atrioventricular rings to the base of the heart [5,6,9,10,28].

### Left atrial appendage myocardial performance

A characteristic triphasic TDI profile (Figure 21.2), independent of the flow, can be obtained readily at the tip and the septal or lateral wall of LAA. The initial upward velocity in sinus rhythm is recorded early in ventricular diastole (before the P-wave). This finding is followed by another upward velocity with higher amplitude (after the P-wave) identical to the late emptying flow, called late systolic wave (LSW). Then, the negative velocity following this event is called the late diastolic wave (LDW) as a result of LAA filling.

## Atrial function in healthy subjects

### Atrial pump function

Studies in healthy subjects have demonstrated the feasibility and reproducibility of TDI parameters, in particular the peak velocity ( $V_a$ ) and peak strain rate ( $SR_a$ ) of active atrial contraction. Both the interobserver and intraobserver variabilities for measuring the  $V_a$  were reported to be within 10% by Yu et al. and other investigators [10,28]. Although  $V_a$  can be measured successfully in nearly all patients,  $SR_a$  was not measured successfully in approximately 5% of patients, due to the relatively higher noise-to-signal ratio [9]. It has been suggested that the right atrial (RA) free-wall has the highest  $V_a$  or  $SR_a$  compared with other atrial sites [6,10]. In a study that included 131 healthy adults 22 to 81 years of age, Zhang et al. found that  $V_a$  was significantly higher in the RA than the LA free-wall ( $9.0 \pm 2.6$  vs.  $7.5 \pm$

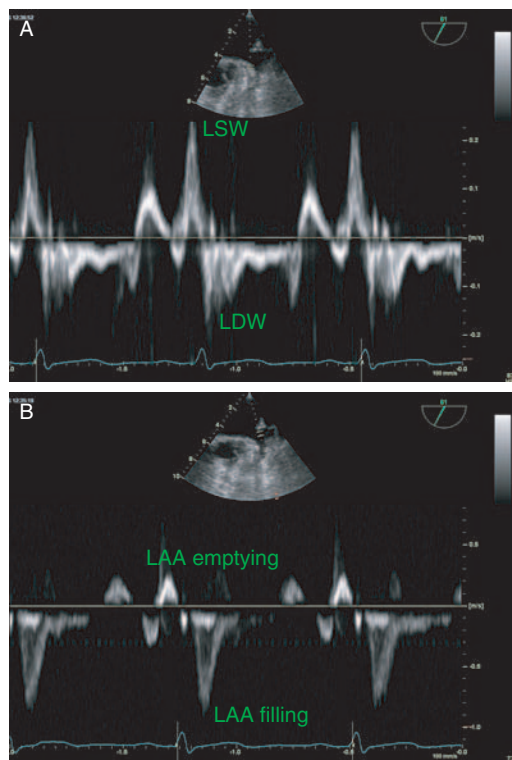


**Figure 21.2** Myocardial performance at LAA. (A) The sample volume was placed at the septal wall of LAA where pulsed TDI was recorded by transesophageal echocardiography. A characteristic triphasic TDI profile includes the initial upward velocity before the P-wave on electrocardiogram, which is followed by another upward velocity with higher amplitude after the P-wave (LSW) and the negative velocity (LDW). (B) The LAA emptying and filling velocities recorded by Doppler echocardiography at the inlet of LAA by transesophageal echocardiography are shown.

$2.4 \text{ cm/sec}$ ;  $P < 0.001$ ), and the IAS had the lowest  $V_a$  ( $5.6 \pm 1.3 \text{ cm/sec}$ ;  $P < 0.001$  vs. other atrial sites) (Figure 21.3) [6]. In fact, the free-walls of both atria have higher mobility and, hence, higher velocities than the bounded IAS. Furthermore, the larger pectinate muscle masses in the right atrium will perhaps generate more pronounced and sustained longitudinal movement, and the lower pressure in the right heart might also accelerate the  $V_a$  of the right atrium. In another study, it was observed that the atrial mechanical function was quite similar in all LA walls. However, longitudinal segmental atrial contraction has shown a decremental gradient for

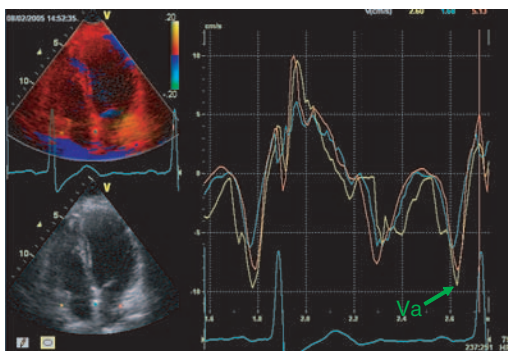


**Figure 21.3** Atrial pump function and electromechanical coupling. In a healthy subject, myocardial velocity curves were reconstituted by placing the sample volumes at the mid-level of RA and LA free-walls and IAS. Typically, the amplitude of peak atrial contraction velocity ( $V_a$ ) is in the order RA > LA > IAS. The time to the onset of atrial contraction is the earliest in RA and the latest in LA.

$V_a$  and SRa from lower (annular) to higher (basal) atrial levels [28].

Aging-associated myocardial hypertrophy and fibrosis leading to decreased compliance of the myocardium have been reported [31]. Consequently, LA pressure rises to maintain adequate LV filling, and the increased atrial wall tension results in chamber dilatation and stretch of the atrial myocardium. The augmentation of LA contractility is explained by the Frank–Starling law [14,32]. This law has been confirmed by TDI studies that measured LA segments directly. The study by Zhang et al. [6] compared normal individuals in “Older Age” ( $\geq 60$  years) and “Younger Age” ( $< 60$  years) groups and found that the  $V_a$  in the right atrium ( $9.6 \pm 2.8$  vs.  $8.0 \pm 2.1$  cm/sec;  $P < 0.01$ ) and left atrium ( $8.1 \pm 2.7$  vs.  $6.7 \pm 1.4$  cm/sec;  $P < 0.001$ ) were significantly higher in the Older Age group. In another study that included 92 healthy subjects, Thomas et al. also observed that the older group ( $\geq 50$  years) had a significantly higher  $V_a$  [14]. The changes in atrial contraction demonstrated by TDI are consistent with previous observations by conventional 2-D and Doppler echocardiography that a shift between LA reservoir, conduit, and pump functions in contribution to LV filling occurs with aging, that is, an increase in atrial active emptying function compensating for a reduction in passive emptying function [33].

## Electromechanical coupling

In atrial TDI studies, the time interval from the beginning of the P-wave on the electrocardiogram to the onset of  $Aa$ -wave on myocardial velocity curve has been adopted as a noninvasive measure of atrial electromechanical delay [6,10]. The electromechanical coupling was the earliest at the right atrium, which was followed by the IAS, and was the latest at the LA lateral wall (Figure 21.3) [6,10]. This sequence is the same as the known electrical activation process revealed by invasive electrophysiologic techniques, which originates from the sinoatrial node of the right atrium, through the IAS, and finally reaches the LA free-wall [34]. The interatrial delays between left and right atrium obtained by different investigators were quite similar as well, ranging from 19 to 24 msec [6,8,10,28], which is consistent with the previous studies that reported 25 msec and 20 msec based on M-mode echocardiography and invasive catheterization, respectively, in normal subjects [35,36].

## Atrial function in cardiac diseases

### Atrial fibrillation and cardioversion

Atrial fibrillation (AF) is the most common cardiac arrhythmia associated with increased morbidity and mortality. A reduction in LA compliance and an increase in the LA pressure have been observed with onset of AF. In the absence of atrial booster pump function, the LA–LV pressure gradient during early LV filling is enhanced by elevation of LA pressure to maintain stroke volume [16]. Restoration and maintenance of sinus rhythm may eliminate the detrimental effects of LA dilatation and AF, as well as prevent the development of atrial cardiomyopathy [37].

Wang et al., in a study of 52 patients with AF of duration less than 1 year and 27 matched normal controls, explored the feasibility of measuring strain rate in atrial walls [5]. It was found that the passive motion velocity and deformation induced by ventricular motion was decreased significantly in AF. When the sample volume was placed at the basal level of LA free-wall, the measured velocity and strain rate at ventricular systole were markedly reduced in AF patients. In another study by Di Salvo et al. where the sample volume was placed at the mid-atrial level, the myocardial

velocity, strain, and strain rate at the period of both ventricular systole and early diastole were decreased significantly [30]. As expected, no atrial deformation could be detected during late diastole. These results may reflect decreased compliance of LA wall in patients with AF which is in agreement with several studies demonstrating that, during AF, the reservoir and conduit function are impaired and the booster pump is absent. The two studies also investigated the predictors of maintenance of sinus rhythm after cardioversion. By multivariate regression analysis adjusted for clinical and other echocardiographic parameters, the reduced atrial deformation of both strain and strain rate during early diastole was found to be an independent predictor of reverting into AF.

Atrial stunning is characterized by reduced atrial mechanical function after restoration of sinus rhythm from AF, which may last several weeks and is associated with increased thromboembolic risk during this vulnerable period [38]. Thomas et al. demonstrated the gradual recovery of atrial pump function after cardioversion using strain rate. In 37 patients after successful cardioversion from chronic AF who were followed up for up to 6 months, the late diastolic strain rate measured at basal atrial walls was significantly lower than normal controls. This finding improved over time, with maximal changes observed in the initial 4 weeks after cardioversion [39].

Most recently, Duytschaever et al. attempted to measure AF cycle length using TDI technique. This is a critical parameter for the perpetuation and termination of AF [40]. The AF cycle length by TDI method was defined as the time interval between two consecutive positive to negative crossings of the baseline of the atrial time velocity curves. There was a good correlation between the cycle length measured from TDI and invasive electrophysiological study. With improvement of the spatial-temporal relationship and imaging technologies, the non-invasive measurement may provide a guide for localizing the target areas for treatment.

### **Ischemic heart disease**

Atrial contractile dysfunction is consistently observed in patients with ischemic heart disease

(IHD) by TDI, irrespective of previous myocardial infarction, coexisting systolic dysfunction, or severity of diastolic dysfunction. Therefore, it appears to be an early echocardiographic feature, even before the occurrence of obvious LV systolic dysfunction. The largest study by Yu et al. comprehensively investigated for the impairment of atrial pump function in 118 patients with known IHD compared with 100 normal subjects [10]. The Va at the mid-level of RA, IAS, and LA wall in the apical four-chamber view was measured to assess atrial contractile function. In patients with IHD, the Va in the left atrium and IAS were drastically reduced. The Va of right atrium was affected by the disease, albeit to a lesser extent. In a subgroup analysis, it was found that atrial function was jeopardized, even in patients without previous myocardial infarction. Moreover, a low LV ejection fraction and the presence of restrictive filling pattern in diastole were important determinants of LA contractile dysfunction. From the regression coefficient, each percent of increase in ejection fraction was associated with an increase in Va in LA by 0.06 cm/sec, while the occurrence of a restrictive filling pattern was associated with a reduction of Va in the left atrium by 3.17 cm/sec [10]. Restrictive filling pattern of diastolic dysfunction has been regarded as the worst form of diastolic dysfunction, which is associated with a poor prognosis [41]. The dramatic reduction of Va in the presence of a restrictive filling pattern, in particular in the LA, implicated the presence of possible LA systolic failure, which has been suggested in these patients. This possibility was also supported by the significantly increased LA size and reduced active emptying fraction observed in the same study [10]. However, atrial electromechanical delay was unaffected in IHD.

### **Mitral valve disease**

#### **Mitral stenosis**

LA pressure and volume increase proportionally to the severity of mitral stenosis. Despite the increase in LA preload, the atrial booster pump contributes less to LV filling even during sinus rhythm because LA contractile force cannot overcome the mechanical obstruction [42]. Moreover, the reduction of

LA compliance and intrinsic myocardial contractility are associated with impaired atrial reservoir and pump function [43]. LAA function is also affected in mitral stenosis, which leads to a reduced contribution of the LAA to overall LA emptying fraction and an increased risk of thrombus formation [44]. TDI was applied in several small-scale studies to assess LAA motion, which confirmed the above findings [45–47]. When the sample volume was placed at the lateral wall or the tip of AA in patients with mitral stenosis and sinus rhythm, the recorded LSW and LDW tissue velocities were markedly reduced when compared with normal controls. In patients with SEC, the systolic velocity was further decreased when compared with those without SEC [46]. Interestingly, at 24 hr after the balloon mitral valvuloplasty, the systolic and diastolic components of the atrial myocardial velocity curve were consistently increased when compared with baseline [48,49]. Furthermore, SEC was decreased or even completely disappeared, and the mean transmural gradient was significantly correlated with LDW tissue velocity before and after the procedure [48]. This finding corroborates the previous finding by invasive LA pressure–volume relationship methods of increases in “A loop” area consistent with enhanced emptying fraction and stroke work [16].

### Mitral regurgitation

Mitral regurgitation causes concomitant atrial and ventricular volume overload. When mitral regurgitation is progressively increased, the augmentation of atrial shortening and expansion occurring at early disease stage is diminished. This finding leads to a reduction in LA emptying fraction [50,51]. The role of TDI to assess atrial pump function in mitral regurgitation has not been adequately explored. Gurlertop et al. studied a group of patients with pure mitral regurgitation and compared them to those with rheumatic mitral stenosis and healthy subjects [45]. It was observed that both LSW and LDW velocities of LAA were reduced in mitral regurgitation, although they were not different from those in mitral stenosis. Because the presence of mitral regurgitation often interferes with the interpretation of LV diastolic function as well as LA mechanical function using conventional 2-D

or Doppler parameters, the use of TDI may provide complementary information for disease assessment in this population.

### Atrial septal defect and transcatheter occlusion

Atrial septal defect (ASD) is a common congenital heart disease, which can be corrected by either surgical and transcatheter closure. The evaluation of atrial mechanical function using TDI has been attempted in this disease entity. Abd El Rahman et al. measured peak strain rate in both the right and left atria during ventricular systolic, early diastolic, and late diastolic phases and reported no difference between patients with ASD and normal controls. However, peak strain rate of late diastolic phase at the mid-LA level was significantly diminished after surgical but not catheter closure of the ASD [52]. Similar findings were also observed by Di Salvo et al. who recruited ASD patients receiving surgical or transcatheter closure for more than 6 months [53]. Compared with normal controls, it was shown that the transcatheter approach conserved both LA and RA regional myocardial properties, whereas peak systolic strain rate in both atria were significantly reduced after surgical correction. However, the baseline atrial performance was not compared in the study. The same author also performed an interesting observation in another study by placing the sampling cursor on the ASD occluder, and demonstrated almost the absence of atrial deformation [54]. Therefore, strain rate was concluded to be a reliable index of atrial lengthening and shortening.

### Conclusion

Assessment of atrial longitudinal contraction by TDI provides reproducible and useful data on atrial mechanical function. These data are often complementary to conventional assessment of atrial size, atrial emptying fraction, and Doppler echocardiography. TDI is particularly helpful to measure atrial contractility directly, which might be less dependent on loading conditions. Furthermore, atrial deformation properties reflecting its stiffness can also be assessed by atrial strain and strain rate. As a result, both active booster pump function as

well as passive reservoir and conduct functions of the atria can be evaluated. However, further studies are needed to explore the clinical utilities of TDI and its postprocessing imaging in a variety of cardiac diseases. With improvement of the imaging and analyzing technologies, this novel tool will help clinicians in decision making and in managing patients with cardiac conditions.

## References

- 1 Stefanidis C, Dernellis J, Toutouzas P. A clinical appraisal of left atrial function. *Eur Heart J* 2001; **22**: 22–36.
- 2 Thomas JD, Weyman AE. Echocardiographic Doppler evaluation of left ventricular diastolic function. Physics and physiology. *Circulation* 1991; **84**: 977–90.
- 3 Hesse B, Schuele SU, Thamilasaran M, Thomas J, Rodriguez L. A rapid method to quantify left atrial contractile function: Doppler tissue imaging of the mitral annulus during atrial systole. *Eur J Echocardiogr* 2004; **5**: 86–92.
- 4 Eryol NK, Topsakal R, Kiranatli B, et al. Color Doppler tissue imaging to evaluate left atrial appendage function in mitral stenosis. *Echocardiography* 2003; **20**: 29–35.
- 5 Wang T, Wang M, Fung JW, et al. Atrial strain rate echocardiography can predict success or failure of cardioversion for atrial fibrillation: a combined transthoracic tissue Doppler and transoesophageal imaging study. *Int J Cardiol* 2007; **114**: 202–9.
- 6 Zhang Q, Kum LC, Lee PW, et al. Effect of age and heart rate on atrial mechanical function assessed by Doppler tissue imaging in healthy individuals. *J Am Soc Echocardiogr* 2006; **19**: 422–8.
- 7 Abbas A, Lester S, Moreno FC, Srivathsan K, Fortuin D, Appleton C. Noninvasive assessment of right atrial pressure using Doppler tissue imaging. *J Am Soc Echocardiogr* 2004; **17**: 1155–60.
- 8 Rein AJ, O'Donnell CP, Colan SD, Marx GR. Tissue velocity Doppler assessment of atrial and ventricular electromechanical coupling and atrioventricular time intervals in normal subjects. *Am J Cardiol* 2003; **92**: 1347–50.
- 9 Inaba Y, Yuda S, Kobayashi N, et al. Strain rate imaging for noninvasive functional quantification of the left atrium: comparative studies in controls and patients with atrial fibrillation. *J Am Soc Echocardiogr* 2005; **18**: 729–36.
- 10 Yu CM, Fung JW, Zhang Q, et al. Tissue Doppler echocardiographic evidence of atrial mechanical dysfunction in coronary artery disease. *Int J Cardiol* 2005; **105**: 178–85.
- 11 Prioli A, Marino P, Lanzoni L, Zardini P. Increasing degrees of left ventricular filling impairment modulate left atrial function in humans. *Am J Cardiol* 1998; **82**: 756–61.
- 12 Rossi A, Zardini P, Marino P. Modulation of left atrial function by ventricular filling impairment. *Heart Fail Rev* 2000; **5**: 325–31.
- 13 Abhayaratna WP, Seward JB, Appleton CP, et al. Left atrial size: physiologic determinants and clinical applications. *J Am Coll Cardiol* 2006; **47**: 2357–63.
- 14 Thomas L, Levett K, Boyd A, Leung DY, Schiller NB, Ross DL. Changes in regional left atrial function with aging: evaluation by Doppler tissue imaging. *Eur J Echocardiogr* 2003; **4**: 92–100.
- 15 Triposkiadis F, Pitsavos C, Boudoulas H, Trikas A, Toutouzas P. Left atrial myopathy in idiopathic dilated cardiomyopathy. *Am Heart J* 1994; **128**: 308–15.
- 16 Stefanidis C, Dernellis J, Stratos C, et al. Assessment of left atrial pressure-area relation in humans by means of retrograde left atrial catheterization and echocardiographic automatic boundary detection: effects of dobutamine. *J Am Coll Cardiol* 1998; **31**: 426–36.
- 17 Waggoner AD, Barzilai B, Miller JG, Perez JE. On-line assessment of left atrial area and function by echocardiographic automatic boundary detection. *Circulation* 1993; **88**: 1142–9.
- 18 Kircher B, Abbott JA, Pau S, et al. Left atrial volume determination by biplane two-dimensional echocardiography: validation by cine computed tomography. *Am Heart J* 1991; **121**: 864–71.
- 19 Rodevan O, Bjørnerheim R, Ljosland M, Maehle J, Smith HJ, Ihlen H. Left atrial volumes assessed by three- and two-dimensional echocardiography compared to MRI estimates. *Int J Card Imaging* 1999; **15**: 397–410.
- 20 Moller JE, Hillis GS, Oh JK, et al. Left atrial volume: a powerful predictor of survival after acute myocardial infarction. *Circulation* 2003; **107**: 2207–12.
- 21 Tsang TS, Abhayaratna WP, Barnes ME, et al. Prediction of cardiovascular outcomes with left atrial size: is volume superior to area or diameter? *J Am Coll Cardiol* 2006; **47**: 1018–23.
- 22 Benjamin EJ, Wolf PA, D'Agostino RB, Silbershatz H, Kannel WB, Levy D. Impact of atrial fibrillation on the risk of death: the Framingham Heart Study [see comments]. *Circulation* 1998; **98**: 946–52.
- 23 Piotrowski G, Goch A, Wlazłowski R, Gawor Z, Goch JH. Non-invasive methods of atrial function evaluation in heart diseases. *Med Sci Monit* 2000; **6**: 827–39.
- 24 Hoit BD, Shao Y, Gabel M, Walsh RA. Influence of loading conditions and contractile state on pulmonary venous flow. Validation of Doppler velocimetry. *Circulation* 1992; **86**: 651–9.

- 25 Rossvoll O, Hatle LK. Pulmonary venous flow velocities recorded by transthoracic Doppler ultrasound: relation to left ventricular diastolic pressures. *J Am Coll Cardiol* 1993; **21**: 1687–96.
- 26 Smiseth OA, Thompson CR, Lohavanichbutr K, Ling H, Abel JG, Miyagishima RT, et al. The pulmonary venous systolic flow pulse – its origin and relationship to left atrial pressure. *J Am Coll Cardiol* 1999; **34**: 802–9.
- 27 Al-Saady NM, Obel OA, Camm AJ. Left atrial appendage: structure, function, and role in thromboembolism. *Heart* 1999; **82**: 547–54.
- 28 Quintana M, Lindell P, Saha SK, et al. Assessment of atrial regional and global electromechanical function by tissue velocity echocardiography: a feasibility study on healthy individuals. *Cardiovasc Ultrasound* 2005; **3**: 4.
- 29 Sirbu C, Herbots L, D'hooge J, et al. Feasibility of strain and strain rate imaging for the assessment of regional left atrial deformation: a study in normal subjects. *Eur J Echocardiogr* 2006; **7**: 199–208.
- 30 Di Salvo G, Caso P, Lo Piccolo R, et al. Atrial myocardial deformation properties predict maintenance of sinus rhythm after external cardioversion of recent-onset lone atrial fibrillation: a color Doppler myocardial imaging and transthoracic and transesophageal echocardiographic study. *Circulation* 2005; **112**: 387–95.
- 31 Bryg RJ, Williams GA, Labovitz AJ. Effect of aging on left ventricular diastolic filling in normal subjects. *Am J Cardiol* 1987; **59**: 971–4X.
- 32 Yamaguchi M, Arakawa M, Tanaka T, Takaya T, Nagano T, Hirakawa S. Study on left atrial contractile performance–participation of Frank – Starling mechanism. *Jpn Circ J* 1987; **51**: 1001–9.
- 33 Schirmer H, Lunde P, Rasmussen K. Mitral flow derived Doppler indices of left ventricular diastolic function in a general population: the Tromso study. *Eur Heart J* 2000; **21**: 1376–86.
- 34 Josephson ME, Scharf DL, Kastor JA, Kitchen JG. Atrial endocardial activation in man. Electrode catheter technique of endocardial mapping. *Am J Cardiol* 1977; **39**: 972–81.
- 35 Braunwald E, Fishman AP, Cournand A. Time relationship of dynamic events in the cardiac chambers, pulmonary artery and aorta in man. *Circ Res* 1956; **4**: 100–7.
- 36 Wang K, Xiao HB, Fujimoto S, Gibson DG. Atrial electromechanical sequence in normal subjects and patients with DDD pacemakers. *Br Heart J* 1995; **74**: 403–7.
- 37 Zipes DP. Atrial fibrillation. A tachycardia-induced atrial cardiomyopathy. *Circulation* 1997; **95**: 562–4.
- 38 Escudero EM, San Mauro M, Laugle C. Bilateral atrial function after chemical cardioversion of atrial fibrillation with amiodarone: an echo-Doppler study. *J Am Soc Echocardiogr* 1998; **11**: 365–71.
- 39 Thomas L, McKay T, Byth K, Marwick TH. Abnormalities of left atrial function after cardioversion: an atrial strain rate study. *Heart* 2006; **93**: 89–95.
- 40 Duytschaever M, Heyse A, de Sutter J, et al. Transthoracic tissue Doppler imaging of the atria: a novel method to determine the atrial fibrillation cycle length. *J Cardiovasc Electrophysiol* 2006; **17**: 1202–9.
- 41 Yu HC, Sanderson JE. Different prognostic significance of right and left ventricular diastolic dysfunction in heart failure. *Clin Cardiol* 1999; **22**: 504–12.
- 42 Stott DK, Marpole DG, Bristow JD, Kloster FE, Griswold HE. The role of left atrial transport in aortic and mitral stenosis. *Circulation* 1970; **41**: 1031–41.
- 43 Sato S, Kawashima Y, Hirose H, Nakano S, Matsuda H, Shimasaki Y. Clinical study of left atrial compliance and left atrial volume in mitral stenosis. *Jpn Circ J* 1991; **55**: 481–6.
- 44 Garcia-Fernandez MA, Torrecilla EG, San Roman D, et al. Left atrial appendage Doppler flow patterns: implications on thrombus formation. *Am Heart J* 1992; **124**: 955–61.
- 45 Gurler top Y, Yilmaz M, Acikel M, et al. Tissue Doppler properties of the left atrial appendage in patients with mitral valve disease. *Echocardiography* 2004; **21**: 319–24.
- 46 Topsakal R, Eryol NK, Ozdogru I, et al. Color Doppler tissue imaging to evaluate left atrial appendage function in patients with mitral stenosis in sinus rhythm. *Echocardiography* 2004; **21**: 235–40.
- 47 Khankirawatana B, Khankirawatana S, Peterson B, Mahrous H, Porter TR. Peak atrial systolic mitral annular velocity by Doppler tissue reliably predicts left atrial systolic function. *J Am Soc Echocardiogr* 2004; **17**: 353–60.
- 48 Karakaya O, Turkmen M, Bitigen A, et al. Effect of percutaneous mitral balloon valvuloplasty on left atrial appendage function: a Doppler tissue study. *J Am Soc Echocardiogr* 2006; **19**: 434–7.
- 49 Bauer F, Verdonck A, Schuster I, et al. Left atrial appendage function analyzed by tissue Doppler imaging in mitral stenosis: effect of afterload reduction after mitral valve commissurotomy. *J Am Soc Echocardiogr* 2005; **18**: 934–9.
- 50 Reed D, Abbott RD, Smucker ML, Kaul S. Prediction of outcome after mitral valve replacement in patients with symptomatic chronic mitral regurgitation. The importance of left atrial size. *Circulation* 1991; **84**: 23–34.
- 51 Kihara Y, Sasayama S, Miyazaki S, et al. Role of the left atrium in adaptation of the heart to chronic mitral regurgitation in conscious dogs. *Circ Res* 1988; **62**: 543–53.

- 52 Abd El Rahman MY, Hui W, Timme J, et al. Analysis of atrial and ventricular performance by tissue Doppler imaging in patients with atrial septal defects before and after surgical and catheter closure. *Echocardiography* 2005; **22**: 579–85.
- 53 Di Salvo G, Drago M, Pacileo G, et al. Atrial function after surgical and percutaneous closure of atrial septal defect: a strain rate imaging study. *J Am Soc Echocardiogr* 2005; **18**: 930–3.
- 54 Di Salvo G, Pacileo G, Caso P, et al. Strain rate imaging is a superior method for the assessment of regional myocardial function compared with Doppler tissue imaging: a study on patients with transcatheter device closure of atrial septal defect. *J Am Soc Echocardiogr* 2005; **18**: 398–400.

# Three-dimensional reconstruction of strain measurement and measurement of strain in three-dimensions

*Asbjorn Stoylen*

## Background

In the assessment of strain rate using tissue Doppler, deformation is measured along the ultrasound beam [1]. From the apical views, this measurement is taken as an approximation to longitudinal strain, but the angle between the beam and the longitudinal direction of the myocardium may significantly influence the measured values. As discussed in Chapter 2, longitudinal strain can be measured along the wall with speckle tracking, truly independent of imaging angle [2,3].

As heart muscle is incompressible, deformation in all three axes (longitudinal, transmural, and circumferential; Figure 22.1) occurs simultaneously [4], and the deformation in all three directions is interrelated [5]. However, as the heart itself is a three-dimensional (3-D) structure, it has to be remembered that 1-D data are being measured along a surface that is curved in three dimensions, analogous to an ellipsoid shell. The reconstruction process expresses 1-D measurements on a 3-D model, and this method should be distinguished from the more complex measurement of 3-D strain, with simultaneous deformation measurements in three dimensions.

Deformation is especially well suited to parametric displays that show contraction by color coding [6], which allows dyssynergy to be readily visualized on a left ventricular map of inhomogeneity of either systolic strain rate or strain. This display

allows pixel strain values to be mapped on the bull's eye, instead of the traditional segmental values. Probably the easiest way to express these data is in a polar map (bull's eye) display, which shows all parts of the ventricle simultaneously. Although the display is analogous to displays of perfusion on myocardial single photon emission computed tomography, the latter involves 3-D reconstruction from tomographic slices, whereas echo acquisition of longitudinal data necessitates reconstructing the 3-D surface from the standard apical planes, as described by Stoylen et al. [7]. The polar map display misrepresents area, with the basal parts being enlarged and the apex diminished, and mathematical correction is required to take the shape of the ventricle into account.

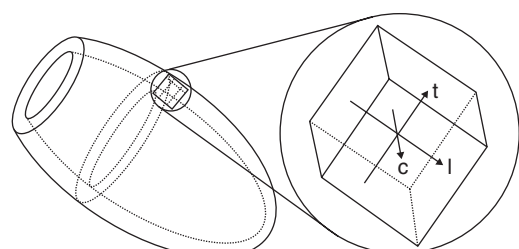


**Figure 22.1** The myocardium, being a thick-walled structure, is a 3-D object. Coordinates relative to the left ventricle are longitudinal (l), circumferential (c), and transmural (t). At any point, the coordinates are at 90° to each other, but all three are parallel to the tangents in the point and, hence, changing direction along the surface.

## Three-dimensional reconstruction of strain measurement

### Reconstruction of a three-dimensional surface

The reconstruction process is based on the following steps:

- Acquisition of 2-D cine-loops from standard apical planes with gray-scale and tissue velocity data.
- Drawing a curved M-mode [8] within the wall from base through apex to base in all three data sets.
- Processing, using
  - Deformation data along the M-mode line
  - Curvature of the M-mode line
  - Interpolation of data around the circumference, assuming a 60° separation of the planes
  - Temporal alignment of the cycles using electrocardiographic data.

The reconstructed data yields a true 3-D distribution of longitudinal (hence, 1-D) strain rate, allowing mapping of the contraction in space (Figure 22.2) in each frame. As the main emphasis has been on the magnitude of regional systolic function, most information can be shown in a single systolic frame in a parametric imaging display. For strain rate, the optimal timing of this

frame will be before mid-systole, close to the time of maximal systolic myocardial velocity. For strain, the optimal frame would be at end-systole, to capture maximal systolic strain. More sophisticated analyses of deformation over time may be performed with early and late parametric displays to visualize the time course of dyssynchrony, and scrolling through each frame allows review of a 4-D data set, in cine-loop format through one heart cycle.

### Possible clinical uses for three-dimensional reconstruction

The first use of 3-D reconstruction might be to facilitate communication. Strain rate imaging is conceptually difficult. A 3-D display can present the data in a visual way that may be easier for non-experts to understand. A 3-D display (as opposed to a polar map) has the advantage of giving a true area representation, but the disadvantage is that, to see the entire ventricular surface, the model has to be rotated on a visual display.

The 3-D data are quantitative. By defining a threshold for normal contraction, the area of reduced contraction can be easily visualized and measured. This area could then be measured as a fraction of total left ventricular area and, thus, be

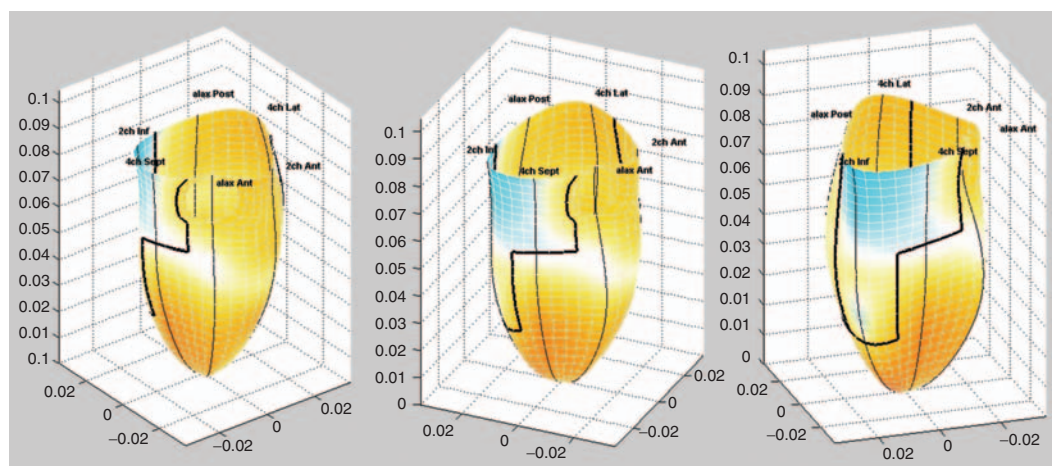


**Figure 22.2** The figure shows a 3-D reconstructed surface from a patient with an inferior infarction, rotated counterclockwise from an anterior view. The image is from a frame before mid-systole, showing longitudinal stretching in the infarct area (blue color), as well as reduced shortening (light yellow color) within the infarct area.

Normal longitudinal systolic shortening is shown in the rest of the ventricle (deep yellow to orange). The area of the infarct relative to the whole ventricle is recognizable. As the underlying information is quantitative, the area can in principle be delineated by a threshold value and the fractional area calculated.

a measure of infarct size [9], which is a prognostically important parameter. A preliminary study has shown the feasibility of this approach. Thus, the model itself may yield new information, subject to further validation studies.

### **Limitations and possible technical solutions**

The present approach is based on freehand scanning of three standard apical planes, which may have several pitfalls.

- Freehand planes mean that there may be a foreshortening in one or more planes, so the true apex will not be at the top of the model.
- The angle between planes is assumed to be 60°, but this may vary in real time.
- The circumferential resolution is only approximately 60°, although this is analogous to the present 16-segment model, and longitudinal resolution is far better.

Although this model gives a fair representation of the volume contained in the ellipsoid, reproducibility could be improved by adding a fourth plane. Modern equipment has the possibility of simultaneous multiplane acquisitions. This method would permit the probe position to be correctly placed at the apex, eliminating foreshortening, and ensure that simultaneous standard imaging planes would be acquired at the desired angle. However, simultaneous multiplane acquisition would result in a reduced frame rate and line density (which would be even lower with full volume 3-D acquisition), and reduction of line density could contribute to numerous artefacts in strain rate imaging [10]. An approach where the position and planes were adjusted first, and then three planes acquired sequentially, would overcome this limitation, although this strategy is not a commercial option so far. Technical improvements, for instance increasing the MLA acquisition (shooting an ultrasound pulse in a wide beam and acquiring simultaneously along more, narrower beams) is possible and may improve both the number of lines and the frame rate of multiplane acquisition in the near future.

Heart rate variability during acquisition would result in problems in aligning the heart cycles in time. Instead of using the electrocardiogram, using a timing reference based on aortic valve closure,

which can be acquired automatically using tissue Doppler data [11], will improve the temporal alignment, especially in systole. This reference can be easily implemented in the software [12].

Peak strain rate is difficult to discern, as strain rate data are noisy. Because parametric imaging focuses more on designation of normal and abnormal deformation than actual peak values, a means of circumventing this would be to use parametric imaging to display only strain rate values above a certain threshold. A similar approach could be used for mapping end- or peak-systolic strain.

Finally, strain rate imaging itself is subject to severe artefacts, especially angle dependence, problems with lateral resolution, dropouts, and reverberations [12]. We have shown that approximately 85% of patients show such artefacts in 3-D reconstruction [9,13] and that 15–20% of segments in segmental analysis should be discarded [12]. This finding means that artefacts must be edited out. Without this editing, the display will have no diagnostic value for inexperienced viewers [13] and automated area measurements would not be feasible. However, at present, only manual editing is possible, based on expert recognition of artefacts versus true pathology, which limits its use.

With parametric imaging, emphasis could switch from high temporal resolution, which allows accurate designation of the true peak value, to high lateral resolution, which will reduce the impact of reverberations and dropouts. In principle, the 3-D reconstruction model is not limited to tissue Doppler measurement, and speckle tracking methods could be displayed in the same way. Similarly, if transmural or circumferential strain could be measured simultaneously over a whole 2-D cine-loop, the 3-D model could map those strain components as well. However, measurement of strain in all three dimensions still has important limitations, which will be discussed in the next section.

### **Measurement of strain in three dimensions**

As discussed above, a 3-D object can be deformed in three dimensions – the main axes related to the heart (left ventricle) are longitudinal, circumferential, and transmural (Figure 22.1).

## Measurements by tissue Doppler

In principle, all three deformations can be measured sequentially by tissue Doppler. *Longitudinal strain rate* has in general been measured in the apical planes [14–16]. Longitudinal strain is fairly uniformly distributed [17] if there is no regional dysfunction, although some inhomogeneity has been described [18]. This finding may be due to the method itself, however, especially angle distortion [10]. This measurement is now clinically useful, although limited by artefacts.

*Transmural strain* has been measured by M-mode, as wall thickening. *Transmural strain rate* can be measured as transmural velocity gradient [19]. Although the algorithm is slightly different in strain rate imaging, it can be shown that the two measurements are comparable [5]. Applying angle correction, transmural deformation could in principle be measured around the circumference of the ventricle [20]. However, accurate angle correction is dependent on applying the true radial vector from the true center of the ventricle and also tracking any translational movement of this center during the heart cycle. Inaccurate angle correction will result in angle distortion as described for longitudinal strain rate. This distortion is a much greater problem than is angle correction for velocity alone [10]. Moreover, segments having thickening perpendicular to the ultrasound beam (e.g., septal and lateral) cannot undergo angle correction. Thus, angle correction applied to transmural strain rate has limited clinical utility, and for practical purposes, transmural measurements are limited to the anteroseptal and inferolateral segments.

*Circumferential strain* is more difficult. First, it varies across the wall with outer circumferential shortening being small, as the outer contour of the left ventricle varies little [21–23], while endocardial circumferential shortening is the highest. Mid-wall circumferential shortening has been proposed as the representative value [24]. Nevertheless, measurement is sensitive to the placement of the sample volume or region of interest, and tracking the inward motion of the endocardium to stay in the mid-wall is a necessity. This again depends on the correct placement and tracking of the center of gravity of the ventricle. Similarly, tissue velocity-based measurements of circumferential strain can only be measured in the segments parallel to the

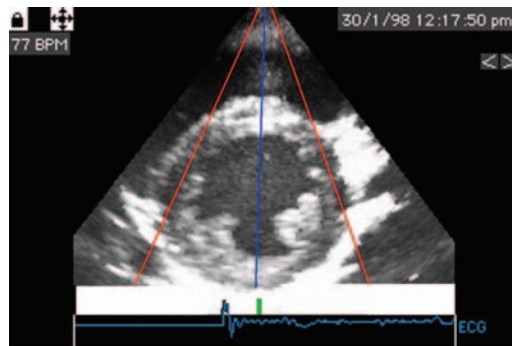


**Figure 22.3** Relation of ultrasound beam direction to the two principal strain directions in the short axis. The figure clearly shows that transmural thickening is only measurable in the anterior and inferior segments where the ultrasound beam is 90° to the wall (blue) and, thus, parallel to the wall thickening direction. Circumferential strain, being parallel to the wall, is only measurable in the segments where the ultrasound beam is tangential to the wall (red), in the anterolateral and anteroseptal parts.

ultrasound beam, typically the anterolateral and anteroseptal. Figure 22.3 shows the areas where tissue velocity-based measurements of transmural and circumferential strain are accessible.

## Measurements in two-dimensions by speckle tracking

Speckle tracking is a new method of measuring deformation, based on the speckle pattern in gray-scale images [25] and is discussed in detail in Chapter 2. This method offers the possibility of angle-independent tracking, thus eliminating the angle distortion inherent in tissue Doppler techniques, and has been validated in experimental studies as well as compared with magnetic resonance images [26,27]. As deformation can also be tracked in two directions at right angles to each other in any 2-D image, this tracking provides longitudinal and transmural strain in apical planes and circumferential and transmural strain in short-axis views. A new application called 2-D strain [3], based on this principle, has been validated against tagged magnetic resonance imaging (MRI) [28]. Although transmural and circumferential strain were measurable in all segments for each cross-sectional view, the correlation and mean difference with tagged MRI were only fair, approximately 50%, and comparable to tissue Doppler in the longitudinal

**Table 22.1** Limitations of 2-D strain.

- Tracking is dependent on image quality.
- Tracking is poor at low and high frame rate;
  - At low frame rate, large changes in the speckle pattern occur from frame to frame, limiting the tracking. This possibly also limits the utility at high heart rates, where there are fewer frames per heart cycle.
  - At high frame rate, line density is reduced, limiting lateral resolution.
- Tracking in the lateral direction is dependent on lateral resolution, that is, line density, which makes the lateral tracking depth sensitive. This limits the assessment of transmural strain in the apical views, and in the short-axis views it affects transmural strain in the lateral and septal segments, as well as circumferential strain in the inferior segments. The effect will be most pronounced in the basal segments, which are deepest both from the apical and parasternal window (Figure 22.4).
- Tracking quality is dependent on the stability of the speckle pattern. As the longitudinal motion of the base is about 15 mm, in the basal and mid-short-axis views there is a considerable out-of-plane motion, so in fact none of the myocardium visible in end-diastole is visible in the same plane in end-systole.
- To give robust results, there is a considerable amount of curve fitting along the wall. This means that the influence of noise is reduced in a different way than with temporal smoothing, but this may also serve to reduce the difference between segments with reduced and normal contraction. This may not reduce the sensitivity of segmental diagnosis, if differences are large enough to give robust cut off values.

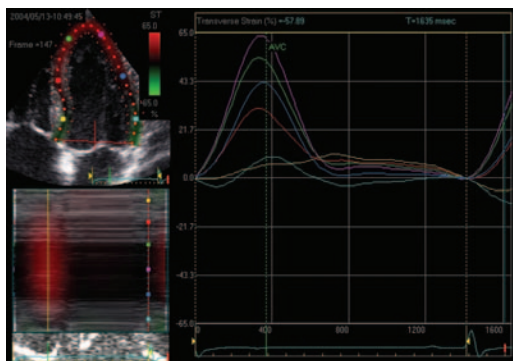


**Figure 22.4** Transverse strain by 2-D speckle tracking. This image from a healthy individual shows 50 to 65% transmural strain in the apical segments (pink and green points and curves), 30 to 45% in the mid-wall segments (red and blue), and <10% in the basal segments (yellow and light blue). The depth dependence of transverse tracking is shown and is a result of decreasing line density with depth in the sector scan.

direction. The limitations of this application are summarized in Table 22.1 (Figure 22.4) [29].

A recent study comparing segmental strain with late enhancement gadolinium MRI [30] has shown a limited sensitivity of transmural and circumferential strain for hypo- and akinesia compared to the presence and transmurality of chronic infarcts. The study also did show a fairly high strain

in transmurally infarcted segments. Both effects might be due to the smoothing and the limited lateral resolution.

### Tracking in true three dimensions

As discussed above, the ideal method would be to derive all strain measurements from one single data set. As full-volume gray-scale acquisition is feasible, speckle tracking in three dimensions could theoretically be applied, giving results similar to MRI tagging, and with a comparable frame rate. However, 3-D gray-scale echocardiography also has limitations, similar to 2-D strain.

- A full volume is constructed from “stitching” of four or more subsectors. This will lead to problems in tracking speckles across “stitches” as they are from different heart cycles, although as most of the deformation occurs in small segments, this may not be of major importance.
- Both frame rate (20–25) and lateral resolution (number of lines in each direction) are too low for effective tracking at present.

However, technical improvement, for instance in increasing the MLA acquisition (shooting an ultrasound pulse in a wide beam and acquiring simultaneously along a greater number of narrower beams), is possible in theory and will improve both the number of lines and the frame rate. Thus, it may become feasible in the near future.

Another approach would be to apply the incompressibility condition in a mathematical model of the left ventricle. As the heart muscle is incompressible (disregarding the small volume changes due to compression of intramyocardial vessels, which may be approximately 5%), the deformations have to balance out so the volume remains constant, so that circumferential and longitudinal shortening balances wall thickening [5] (Figure 22.5). The model is dependent on defining the epicardial border and wall thickness. If the invariance of the outer contour of the left ventricle [21–23] is also applied, only longitudinal shortening and end-diastolic wall thickness would need to be measured, the rest of the deformations could be estimated, and further measurements based on the various techniques could give redundant information to quality-control the robustness of the data. Unlike 3-D speckle tracking, this method is within theoretical possibility with current-generation equipment. A robust method would incorporate automated border detection

and probably tracking, with lateral speckle tracking and longitudinal tissue Doppler or speckle tracking measurements.

Nonetheless, as the three strain directions are interdependent in a very calculable way, it may well be the case that only one strain direction – probably the longitudinal – would be necessary to give all clinically relevant information, although this assumption may not hold if myocardial fiber orientation causes deformation to be nonuniform. However, it remains to be proven in clinical studies that more strain directions give additional information, although they may serve to increase the robustness of the data.

## Conclusions

- Three-dimensional display of strain rate is feasible and may serve as a demonstration tool for visualizing strain and strain rate data. It may also, subject to clinical validation, be a tool for measuring infarct size. In principle, it can be applied to both tissue Doppler and speckle tracking derived data, and in the latter case to both transmural and longitudinal strain.
- Deformation occurs in all three dimensions simultaneously. Strain measurements are possible in all three directions (longitudinal, circumferential, and transmural) sequentially and by speckle tracking in all parts of the left ventricle. However, the method has serious limitations, the importance of these needs to be evaluated in clinical studies.
- Deformation in three dimensions can be measured by incorporating strain measurements with wall thickness in a mathematical model assuming myocardial incompressibility. Deformation by speckle tracking in full-volume 4-D acquisitions is possible, subject to technical improvement in data acquisition.
- The value of measuring strain in three dimensions, either as incremental information or by increased robustness of data, will need to be documented in clinical studies.

## References

- 1 Heimdal A, Stoylen A, Torp H, Skjaerpe T. Real-time strain rate imaging of the left ventricle by ultrasound. *J Am Soc Echocardiogr* 1998; 11: 1013–9.

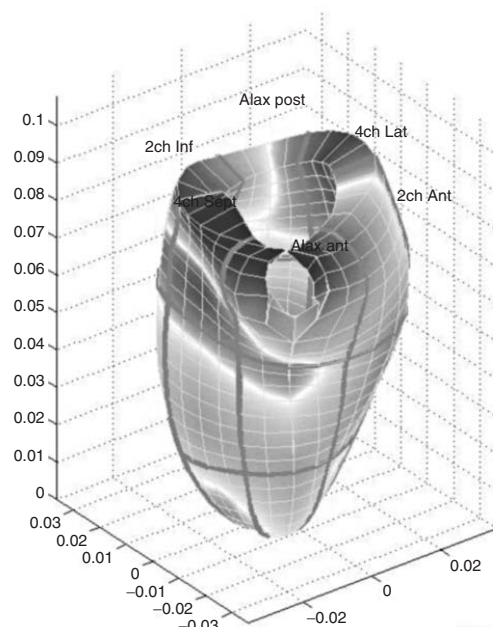


**Figure 22.5** Thick-walled 3-D left ventricular surface model. The model consists of a grid, and each box is considered incompressible. Thus, deformation has to occur in such a way that each box retains its volume. Applying different combinations of measurements as well as conditions on the model will yield all three principal strain directions.

- 2 Amundsen BH, Helle-Valle T, Edvardsen T, et al. Noninvasive myocardial strain measurement by speckle tracking echocardiography: validation against sonomicrometry and tagged magnetic resonance imaging. *J Am Coll Cardiol* 2006; **47**: 789–93.
- 3 Leitman M, Lysyansky P, Sidenko S, et al. Two-dimensional strain-a novel software for real-time quantitative echocardiographic assessment of myocardial function. *J Am Soc Echocardiogr* 2004; **17**: 1021–9.
- 4 D'hooge J, Heimdal A, Jamal F, et al. Regional strain and strain rate measurements by cardiac ultrasound: principles, implementation and limitations. *Eur J Echocardiogr* 2000; **1**: 154–70.
- 5 Stoylen A. *Mathematics of strain and strain rate*. Available from: URL:<http://folk.ntnu.no/stoylen/strainrate/mathematics/index.html>.
- 6 Brodin LA. Tissue Doppler, a fundamental tool for parametric imaging. *Clin Physiol Funct Imaging* 2004; **24**: 147–55.
- 7 Stoylen A, Ingul CB, Torp H. Strain and strain rate parametric imaging. A new method for post processing to 3-/4-dimensional images from three standard apical planes. Preliminary data on feasibility, artefact and regional dyssynergy visualisation. *Cardiovasc Ultrasound* 2003; **1**: 11.
- 8 Brodin LA, van der Linden J, Olstad B. Echocardiographic functional images based on tissue velocity information. *Herz* 1998; **23**: 491–8.
- 9 Malm S, Sagberg E, Frigstad S, Støylen A, Skjærpe T. Effects of contrast on regional left ventricular strain and strain rate measurements. Abstract, Euroecho 9, Florence; December 7–10, 2005. *Eur J Echocardiogr* 2004; **Suppl 1**: 153.
- 10 Stoylen A. *Problem and pitfalls in strain rate imaging*. Available from: URL:<http://folk.ntnu.no/stoylen/strainrate/Howto/Pitfalls.html>.
- 11 Aase SA, Stoylen A, Ingul CB, Frigstad S, Torp H. Automatic timing of aortic valve closure in apical tissue Doppler images. *Ultrasound Med Biol* 2006; **32**: 19–27.
- 12 Ingul CB, Torp H, Aase SA, Berg S, Stoylen A, Slordahl SA. Automated analysis of strain rate and strain: feasibility and clinical implications. *J Am Soc Echocardiogr* 2005; **18**: 411–8.
- 13 Sagberg E, Malm S, Ingul CB, Torp H, Støylen A. Feasibility of 3D reconstructed parametric strain rate data in recognition of myocardial infarction. Abstract, Euroecho 8, Athens; December 1–4, 2004. *Eur J Echocardiogr* 2004; **Suppl**: S143.
- 14 Heimdal A, Stoylen A, Torp H, Skjaerpe T. Real-time strain rate imaging of the left ventricle by ultrasound. *J Am Soc Echocardiogr* 1998; **11**: 1013–9.
- 15 Stoylen A, Heimdal A, Bjørnstad K, Torp HG, Skjaerpe T. Strain rate imaging by ultrasound in the diagnosis of regional dysfunction of the left ventricle. *Echocardiography* 1999; **16**: 321–9.
- 16 Voigt JU, Arnold MF, Karlsson M, et al. Assessment of regional longitudinal myocardial strain rate derived from Doppler myocardial imaging indexes in normal and infarcted myocardium. *J Am Soc Echocardiogr* 2000; **13**: 588–98.
- 17 Stoylen A, Heimdal A, Bjørnstad K, et al. Strain rate imaging by ultrasonography in the diagnosis of coronary artery disease. *J Am Soc Echocardiogr* 2000; **13**: 1053–64.
- 18 Storaas C, Lind B, Brodin LA. Distribution of left ventricular longitudinal peak systolic strain and impact of low frame rate. *Ultrasound Med Biol* 2004; **30**: 1049–55.
- 19 Fleming AD, Xia X, McDicken WN, Sutherland GR, Fenn L. Myocardial velocity gradients detected by Doppler imaging. *Br J Radiol* 1994; **67**: 679–88.
- 20 Uematsu M, Miyatake K, Tanaka N, et al. Myocardial velocity gradient as a new indicator of regional left ventricular contraction: detection by a two-dimensional tissue Doppler imaging technique. *J Am Coll Cardiol* 1995; **26**: 217–23.
- 21 Hamilton WF, Rompf JH. Movements of the base of the ventricle and relative constancy of the cardiac volume. *Am J Physiol* 1932; **102**: 559–65.
- 22 Lundback S. Cardiac pumping and function of the ventricular septum. *Acta Physiol Scand Suppl* 1986; **550**: 1–101.
- 23 Hoffman EA, Ritman EL. Invariant total heart volume in the intact thorax. *Am J Physiol* 1985; **249**: 883–90.
- 24 Almeida P, Cordoba M, Goicoechea J, et al. Relation of midwall circumferential systolic stress to equatorial midwall fibre shortening in chronic aortic regurgitation. Value as a predictor of postoperative outcome. *Br Heart J* 1984; **52**: 284–91.
- 25 Kaluzynski K, Chen X, Emelianov SY, Skovoroda AR, O'Donnell M. Strain rate imaging using two-dimensional speckle tracking. *IEEE Trans Ultrason Ferroelectr Freq Control* 2001; **48**: 1111–23.
- 26 Helle-Valle T, Crosby J, Edvardsen T, et al. New noninvasive method for assessment of left ventricular rotation: speckle tracking echocardiography. *Circulation* 2005; **112**: 3149–56.
- 27 Amundsen BH, Helle-Valle T, Edvardsen T, Torp H, Crosby J, Lyseggen E. Noninvasive myocardial strain measurement by speckle tracking echocardiography: validation against sonomicrometry and tagged magnetic resonance imaging. *J Am Coll Cardiol* 2006; **47**: 789–93.

- 28 Cho GY, Chan J, Leano R, Strudwick M, Marwick TH. Comparison of two-dimensional speckle and tissue velocity based strain and validation with harmonic phase magnetic resonance imaging. *Am J Cardiol* 2006; **97**: 1661–6.
- 29 Stoylen A. *Strain rate imaging. 2D Strain by speckle tracking*. Available from: URL:[http://folk.ntnu.no/stoylen/strainrate/index.html#2D\\_strain](http://folk.ntnu.no/stoylen/strainrate/index.html#2D_strain).
- 30 Becker M, Hoffmann R, Kuhl HP, et al. Analysis of myocardial deformation based on ultrasonic pixel tracking to determine transmurality in chronic myocardial infarction. *Eur Heart J* 2006; **27**: 2560–6.

# Ventricular torsion

Jing Ping Sun

## Introduction

The myofiber geometry of the left ventricle changes gradually from a right-handed helix in the subendocardium to a left-handed helix in the subepicardium. Left ventricular (LV) torsional deformation (or twist) plays an important role with respect to LV ejection and filling [1–4]. During the cardiac cycle, there is a systolic twist and an early diastolic untwist of the LV about its long axis due to oppositely directed apical and basal rotations. As viewed from the LV apex, systolic apical rotation is counterclockwise and basal rotation is clockwise. Current research in clinical cardiac mechanics is moving from short- and long-axis LV function and ejection fraction to three-dimensional (3-D) ventricular deformation studies, including analysis of LV torsion [5]. The magnitude and characteristics of this torsional deformation have been described in different clinical and experimental studies, and it is well established that LV rotation is sensitive to changes in both regional and global LV function [6–16]. Therefore, assessment of LV rotation represents an interesting approach for quantifying LV function. However, sonomicrometry is limited by its invasive nature, and magnetic resonance imaging is limited by its limited availability, which precludes its use in routine clinical practice.

The recent development of 2-D ultrasound speckle tracking imaging has allowed LV twist to be evaluated noninvasively. The accuracy of this novel technology has recently been validated with tagged magnetic resonance imaging [17–20]. This technique simultaneously provides cardiac rotation and radial displacement data, thus providing an opportunity for the construction of twist-displacement loops.

Although heart size increases with somatic maturation [21], the helically oriented myocardial fiber architecture, which creates LV torsion, has been observed in human hearts from neonates to adults, independent of sex and age [22]. LV torsion has recently attracted the attention of LV mechanics researchers and is believed to be a sensitive indicator of systolic and diastolic performance and myocardial molecular properties [23]. Whether torsional biomechanics change during the complex development from infancy to adulthood is not well established, but understanding the biomechanics is important both mechanistically and as it relates to potential diagnostic utility. Tissue Doppler imaging (TDI) can assess myocardial velocity [24] and LV torsion [25] noninvasively, a significant advantage for the examination of children. Investigators from Cleveland Clinic Foundation studied the developmental alterations in LV torsional behavior from infancy to adulthood in normal subjects using TDI. They found that modulation of LV torsion appears to reflect both myocardial mechanical maturation in childhood and further adaptive changes in adulthood, influenced by contractility, loading conditions, and possibly myogenetic changes through life.

## Maturing left ventricular twist during childhood

Distinct patterns of apical basal twisting are seen with maturation: counterclockwise apical rotation was almost constant during childhood, and an age-related increase in LV torsion during childhood results from a striking change in basal rotation, initially counterclockwise in infancy to neutral in early childhood and showing the adult clockwise pattern

in adolescence, a finding that may indicate fundamental myoarchitectural changes in the developing heart or possibly the greater length over which the angulated epicardial fibers can act. Wulfsohn et al. [26] reported that, with growth, myocardial fibers connect points at the base and apex that are farther and farther apart circumferentially. By this growth process, basal rotation becomes more prominent, consequently increasing net LV torsion. Although this small basal rotation has not been emphasized in prior studies, its influence on effective twisting and untwisting in childhood should not be neglected, and it should be taken into account and compared with healthy and pathological states.

### **Enhanced left ventricular torsion in infancy and middle-age adults**

When torque is applied to a cylinder, the angle of twist it produces and the associated shear stress are proportional to the magnitude of the torque and shaft length [27]. LV torsion was higher in infants than in older children, adolescents, and young adults [28]. This result correlates with the finding that contractility is higher in children <2 years of age (due to higher metabolic demand) [29] compared with older children.

Histological data indicate that, in normal subjects, increasing age does not result in cellular hypertrophy [30], although stiffening of the arterial tree may increase afterload and, thereby, alter diastolic function [31]. LV torsion is afterload-dependent [32], and a chronic increase in afterload leads to increasing apical rotation and LV torsion [13]. Higher fiber stress is associated with enhanced torsion, and in general, fiber stress rises with age in adults, predicting that there should be an age-related rise in torsion. Oxenham et al. [33] reported that peak apical rotation and LV torsion were increased in older subjects (69 years), more so than in younger ones (22 years).

### **Effect of aging on left ventricular torsion by two-dimensional speckle tracking imaging**

Nakai et al. [34] studied the effects of aging by using the twist–displacement loop method by two-dimensional (2-D) speckle tracking imaging. First, they found that 2-D speckle tracking imaging

allows the construction of twist–displacement loop noninvasively. Second, there was a tight linear relation between LV twist and radial displacement during systole. Twisting at a given displacement was greater in the older volunteers. Third, during early diastole, there was substantial untwist, despite a small diastolic reversal of systolic displacement, resulting in a different twist–displacement relationship compared with systole. Fourth, during most of the remainder of diastolic filling, less untwisting occurred, despite a substantial diastolic reversal of systolic displacement. Thus, the twist–radial displacement relation is related to the phase of the cardiac cycle.

### **Technical and clinical validations**

It has been demonstrated that regional LV rotation and torsion can be measured accurately by speckle tracking echocardiography when compared against sonomicrometry in anesthetized dogs during baseline dobutamine infusion with apical ischemia and against magnetic resonance imaging tagging in healthy humans. These findings suggest a new echocardiographic approach for the quantification of LV systolic function [35].

Using an animal model, the Author performed an experiment with pigs that were subjected to myocardial infarction by occlusion of the left anterior descending coronary artery (LAD) and followed up for 8 weeks. Regional rotation was quantified noninvasively by ultrasonic speckle tracking imaging before LAD occlusion, immediately at occlusion, and at 4, 6, and 8 weeks after LAD occlusion. The 2-D strain-based LV torsion was assessed at the same time points. Segmental torsion was decreased significantly in the LAD territory areas due to myocardial ischemia and infarction. There were no significant changes of segmental torsion in the adjacent and remote areas over time (Table 23.1).

LV rotations at the mitral (clockwise as negative) and apical (counterclockwise as positive) level are shown in Figure 23.1A and B. Torsion was calculated as the difference between basal and apical rotation (degrees).

Our group also did a study in 44 normal volunteers and 49 patients with cardiomyopathies of different etiologies (amyloid cardiomyopathy,  $n = 4$ ; dilated cardiomyopathy,  $n = 13$ ; coronary artery disease with cardiac infarction,  $n = 8$ ; asymmetrical hypertrophic cardiomyopathy,  $n = 8$ ; and

**Table 23.1** Segmental torsion of each left ventricular wall in a model of LAD ischemia.

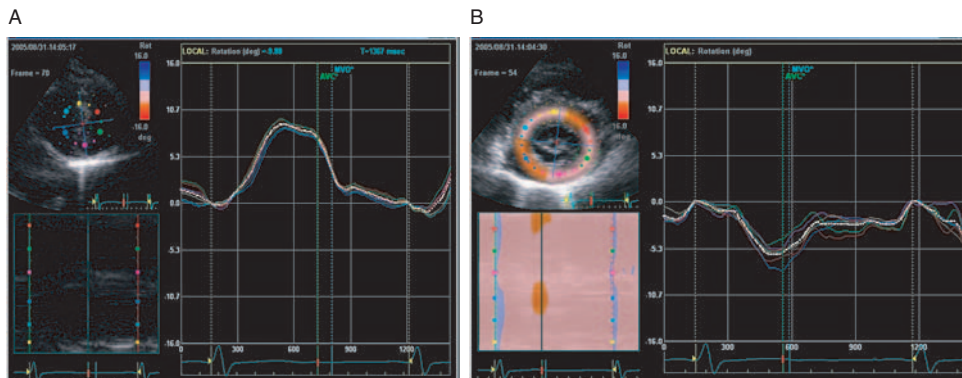
Torsion (degree)	Anterior wall	Inferior wall	Posterior wall	Anterior-septal	Global
Baseline	5.0±2.0	4.4±2.0	5.2±2.5	5.1±1.8	4.7±1.6
AMI	2.5±1.6*	3.2±3.0	3.2±2.6	2.5±1.6*	3.1±1.4
4 weeks	2.6±1.8*	3.2±1.6	3.4±2.5	4.2±2.2	3.6±1.5
6 weeks	2.1±2.1*	3.9±1.9	4.4±2.1	2.8±2.3	3.2±1.6
8 weeks	1.0±1.7**	3.7±3.0	3.2±2.9	2.4±1.5*	2.9±2.3

\*vs. Baseline,  $P < 0.05$ . \*\*vs. Baseline,  $P < 0.01$ .

**Table 23.2** Segmental LV torsion is uniformly decreased in patients with amyloidosis and DCM, but torsion of lateral and anterior wall is preserved in patients with LVH.

LV wall torsion (degree)	Septal	Lateral	Anterior	Inferior	Posterior	Anterior-septal
Normal	9.6±3.9	7.8±3.0	7.7±2.7	9.4±4.0	8.6±3.9	8.6±3.2
Amyloid	1.0±2.3**	1.9±0.2**	3.4±2.3**	1.6±1.6**	0.6±1.6**	2.5±2.5**
DCM	4.5±3.6**	3.5±4.0**	2.6±1.8*	3.9±3.8**	4.6±2.9**	3.7±3.3**
HOCM	2.4±3.6**	6.8±2.2	6.7±3.1	3.5±3.5**	4.9±2.9**	4.2±3.8*
LVH	8.8±2.4	7.7±5.1	7.6±3.5	8.1±4.4	7.4±5.9	7.5±2.4*

\*\*vs. Normal,  $P < 0.005$ . \* $P < 0.05$ .

**Figure 23.1** Representative rotation of apical level (deg) baseline (A) with mitral level (deg) baseline (B). Torsion = apical – mitral rotation (deg).

LV hypertrophy due to hypertension,  $n = 16$ ). The LV segmental torsion was derived from the parasternal short-axis view of mitral and apical level by speckle tracking echocardiography. The results are shown in Table 23.2.

These results indicated that LV segmental torsion was significantly decreased uniformly in the amyloid and dilated cardiomyopathies. These findings are consistent with the diffuse pathological changes

of these two cardiomyopathies. In contrast, the torsions of the anterior and lateral wall were preserved in patients with asymmetrical hypertrophy. The LV hypertrophy due to hypertension is a secondary pathophysiologic change. The LV torsion measurements suggest that LV function is preserved in the early stage of LV hypertrophy.

Our results and previous reports [17,19,25,28, 34,35] suggest that TDI combined with speckle

tracking echocardiography is a new tool for estimating LV segmental and global torsion. In particular, the speckle tracking technique provides us with a very simple and convenient method with which to measure LV torsion using routine available gray-scale imaging.

## References

- 1 McDonald IG. The shape and movements of the human left ventricle during systole: a study by cineangiography and by cineradiography of epicardial markers. *Am J Cardiol* 1970; **26**: 221–30.
- 2 Rademakers FE, Buchalter MB, Rogers WJ, et al. Dissociation between left ventricular untwisting and filling: accentuation by catecholamines. *Circulation* 1992; **85**: 1572–81.
- 3 Gibbons Kroeker CA, Ter Keurs HE, Knudtson ML, Tyberg JV, Beyar R. An optical device to measure the dynamics of apex rotation of the left ventricle. *Am J Physiol Heart Circ Physiol* 1993; **265**: H1444–9.
- 4 Moon MR, Ingels NB Jr, Daughters GT, Stinson EB, Hansen DE, Miller DC. Alterations in left ventricular twist mechanics with inotropic stimulation and volume loading in human subjects. *Circulation* 1994; **89**: 142–50.
- 5 Buckberg GD, Weisfeldt ML, Ballester M, et al. Left ventricular form and function scientific priorities and strategic planning for development of new views of disease. *Circulation* 2004; **110**: e333–6.
- 6 Hansen DE, Daughters GT, Alderman EL, Ingels NB, Stinson EB, Miller DC. Effect of volume loading, pressure loading, and inotropic stimulation on left ventricular torsion in humans. *Circulation* 1991; **83**: 1315–26.
- 7 Yun KL, Niczyporuk MA, Daughters GT, et al. Alterations in left ventricular diastolic twist mechanics during acute human cardiac allograft rejection. *Circulation* 1991; **83**: 962–73.
- 8 Maier SE, Fischer SE, McKinnon GC, Hess OM, Krayenbuehl HP, Boesiger P. Evaluation of left ventricular segmental wall motion in hypertrophic cardiomyopathy with myocardial tagging. *Circulation* 1992; **86**: 1919–28.
- 9 Buchalter MB, Rademakers FE, Weiss JL, Rogers WJ, Weisfeldt ML, Shapiro EP. Rotational deformation of the canine left ventricle measured by magnetic resonance tagging: effects of catecholamines, ischaemia, and pacing. *Cardiovasc Res* 1994; **28**: 629–35.
- 10 DeAnda A Jr, Komeda M, Nikolic SD, Daughters GT Jr, Ingels NB, Miller DC. Left ventricular function, twist, and recoil after mitral valve replacement. *Circulation* 1995; **92**: 458–66.
- 11 Gibbons Kroeker CA, Tyberg JV, Beyar R. Effects of load manipulations, heart rate, and contractility on left ventricular apical rotation: an experimental study in anesthetized dogs. *Circulation* 1995; **92**: 130–41.
- 12 Knudtson ML, Galbraith PD, Hildebrand KL, Tyberg JV, Beyar R. Dynamics of left ventricular apex rotation during angioplasty: a sensitive index of ischemic dysfunction. *Circulation* 1997; **96**: 801–8.
- 13 Stuber M, Scheidegger MB, Fischer SE, et al. Alterations in the local myocardial motion pattern in patients suffering from pressure overload due to aortic stenosis. *Circulation* 1999; **100**: 361–8.
- 14 Nagel E, Stuber M, Lakatos M, Scheidegger MB, Boesiger P, Hess OM. Cardiac rotation and relaxation after anterolateral myocardial infarction. *Coron Artery Dis* 2000; **11**: 261–7.
- 15 Sandstede JJ, Johnson T, Harre K, et al. Cardiac systolic rotation and contraction before and after valve replacement for aortic stenosis: a myocardial tagging study using MR imaging. *AJR Am J Roentgenol* 2002; **178**: 953–8.
- 16 Fuchs E, Muller MF, Oswald H, Thony H, Mohacsi P, Hess OM. Cardiac rotation and relaxation in patients with chronic heart failure. *Eur J Heart Fail* 2004; **6**: 715–22.
- 17 Helle-Valle T, Crosby J, Edvardsen T, et al. New noninvasive method for assessment of left ventricular rotation: speckle tracking echocardiography. *Circulation* 2005; **112**: 3149–56.
- 18 Leitman M, Lysyansky P, Sidenko S, et al. Two-dimensional strain – a novel software for real-time quantitative echocardiographic assessment of myocardial function. *J Am Soc Echocardiogr* 2004; **17**: 1021–9.
- 19 Notomi Y, Lysyansky P, Setser R, et al. Measurement of ventricular torsion by two-dimensional ultrasound speckle tracking imaging. *Am Coll Cardiol* 2005; **45**: 2034–41.
- 20 Reisner SA, Lysyansky P, Agmon Y, Mutlak D, Lessick J, Friedman Z. Global longitudinal strain: a novel index of left ventricular systolic function. *J Am Soc Echocardiogr* 2004; **17**: 630–3.
- 21 Nidorf SM, Picard MH, Triulzi MO, et al. New perspectives in the assessment of cardiac chamber dimensions during development and adulthood. *J Am Coll Cardiol* 1992; **19**: 983–8.
- 22 Fernandez-Teran MA, Hurle JM. Myocardial fiber architecture of the human heart ventricles. *Anat Rec* 1982; **204**: 137–47.
- 23 Bell SP, Nyland L, Tischler MD, McNabb M, Granzier H, LeWinter MM. Alterations in the determinants of diastolic suction during pacing tachycardia. *Circ Res* 2000; **87**: 235–40.
- 24 Miyatake K, Yamagishi M, Tanaka N, et al. New method for evaluating left ventricular wall motion by color-coded

- tissue Doppler imaging: in vitro and in vivo studies. *J Am Coll Cardiol* 1995; **25**: 717–24.
- 25 Notomi Y, Setser RM, Shiota T, et al. Assessment of left ventricular torsional deformation by Doppler tissue imaging: a validation study using tagged magnetic resonance imaging. *Circulation* 2005; **111**: 1141–7.
  - 26 Wulfsohn D, Nyengaard JR, Tang Y. Postnatal growth of cardiomyocytes in the left ventricle of the rat. *Anat Rec* 2004; **277A**: 236–47.
  - 27 Taber LA, Yang M, Podszus WW. Mechanics of ventricular torsion. *J Biomech* 1996; **29**: 745–52.
  - 28 Notomi Y, Srinath G, Shiota T, et al. Maturational and adaptive modulation of left ventricular torsional biomechanics: Doppler tissue imaging observation from infancy to adulthood. *Circulation* 2006; **113**: 2534–41.
  - 29 Stopfkuchen H. Changes of the cardiovascular system during the perinatal period. *Eur J Pediatr* 1987; **146**: 545–9.
  - 30 Olivetti G, Melissari M, Capasso JM, Anversa P. Cardiomyopathy of the aging human heart: myocyte loss and reactive cellular hypertrophy. *Circ Res* 1991; **68**: 1560–8.
  - 31 Oxenham H, Sharpe N. Cardiovascular aging and heart failure. *Eur J Heart Fail* 2003; **5**: 427–34.
  - 32 MacGowan GA, Burkhoff D, Rogers WJ, et al. Effects of afterload on regional left ventricular torsion. *Cardiovasc Res* 1996; **31**: 917–25.
  - 33 Oxenham HC, Young AA, Cowan BR, et al. Age-related changes in myocardial relaxation using three-dimensional tagged magnetic resonance imaging. *J Cardiovasc Magn Reson* 2003; **5**: 421–30.
  - 34 Nakai H, Takeuchi M, Nishikage T, Kokumai M, Otani S, Lang RM. Effect of aging on twist-displacement loop by 2-dimensional speckle tracking imaging. *J Am Soc Echocardiogr* 2006; **19**: 880–5.
  - 35 Helle-Valle T, Crosby J, Edvardsen T, et al. New noninvasive method for assessment of left ventricular rotation: speckle tracking echocardiography. *Circulation* 2005; **112**: 3149–56.

# Automated strain and strain rate

Charlotte Bjork-Ingul and Svein A. Aase

## Benefits of an automated method

Quantitative analysis of echocardiography has been a great technical challenge, and this is especially true for stress echocardiography. Deformation analysis from tissue Doppler imaging (TDI) has been considered to be a truly quantitative approach, but its clinical interpretation can be subjective and, therefore, requires a high level of expertise. Speckle tracking has been recently introduced as an alternative quantitative technique, but application of this method to echocardiography and stress echocardiography is in its infancy.

The clinical adaptation of strain and strain rate has been slow, due to variable data quality and time-consuming analysis. In the first applications using TDI for strain and strain rate analysis, manual positioning of the region of interest in each of the 16 segments was required. To obtain reliable data of the standard analysis myocardial segments have to be tracked through each frame to follow the myocardium throughout the cardiac cycle. Segment size, reverberations, and deviations between the axis of the wall and the directions of the ultrasound beams are all important additional considerations. The timing of cardiac events, such as aortic valve closure (AVC) and opening (AVO), has to be set manually. Both the inter- and intra-observer variability are high, as the method is subjective and dependent on where the operator places the region of interest, and the as well as data-dependent. Traps for less-expert users abound, and apparently adequate curves can be obtained even if the region of interest is misplaced too close to the ventricle.

In contrast, an automated approach could provide objective and rapid analysis as well as high

feasibility and repeatability. In this chapter, we will describe in detail an example of an automated method for analyzing strain and strain rate that has been developed in our laboratory, called *the Trondheim Autostrain method*.

## Segmentation

Automatic segmentation requires automatic localization of anatomical landmarks (the mitral plane and the apex) and automatic localization of the myocardium. Automatic post-processing will give segmental values once the region of interest is defined as regional variation is responsible for much of the variation of deformation measurements, ensuring full repeatability of segmentation would increase *reproducibility* of the automated method, compared to a manual method. Indeed, the variability of automated speckle-based strain has varied from 4–5% within observers to 7–10% between observers [2–4]. In contrast, an automated study based on combined TDI and speckle tracking has shown a higher variability compared to the B-mode-based modalities (Figure 24.1) [5].

Nonetheless, the automated setting of the region of interest with the automated approach may paradoxically reduce the *feasibility* of this method relative to the manual method. This is because the manual method allows the region of interest to be adjusted to avoid unsuitable areas such as reverberations. Automated analysis with a combination of TDI and speckle tracking has been shown to have a feasibility of between 75% and 80% of segments, compared to 92% with manual analysis by TDI [5]. Automated analysis using only speckle tracking resulted in a feasibility of 80% [4].

The issue of feasibility is balanced by analysis time. The total time used for analysis with an

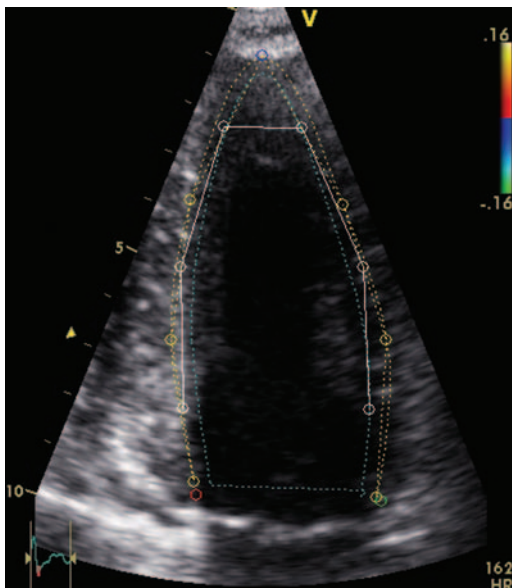


**Figure 24.1** An automated system using TDI for tracking along the ultrasound beam and speckle tracking perpendicular to the ultrasound beam. In this apical four-chamber view from a healthy subject undergoing dobutamine stress echocardiography at peak stress, the left ventricle has been divided automatically into six segments, divided by yellow points. The white points represent the middle of each segment.

automated method was 2 minutes for 16 segments [4] compared to 11 minutes by the manual analysis. Another automated study has shown the duration of analysis to be 3 to 4 minutes per patient for the right ventricle [6].

### Tracking

When tracking is used, a region of interest is set automatically in the myocardium at one frame and then tracked automatically through the cardiac cycle. This method allows the movement of cardiac tissue to be taken into account when extracting curves, although tracking is not mandatory for automated analysis of TDI. The region of interest is defined, automatically eliminating the search for suitable curves, thus resulting in more objective traces.

### Timing

The Trondheim Autostrain method includes algorithms for automatic timing of the cardiac events. This feature allows the analysis process to become more efficient. The use of timing data from the

same cardiac cycle used in analysis also ensures more reliable timing than timing acquired from a different cardiac cycle.

## Acquisition of data using tissue Doppler imaging, B-mode imaging, and combined imaging

Deformation measurements can be derived both from TDI data and B-mode data. Until recently, the predominant method has involved TDI, and most reported studies are based on this method. Improvements in two-dimensional (2-D) image resolution and post-processing algorithms have enabled speckle tracking in B-mode images. TDI and strain rate imaging (SRI) are limited to assessment along the ultrasound beam, but speckle tracking can in addition assess deformation perpendicular to the beam.

### Tissue Doppler imaging

The high temporal resolution of TDI permits quantitation of brief events, such as iso-volumetric contraction, and it enables cardiac events to be timed accurately. However, this high frame rate is achieved at the cost of spatial resolution. Analysis based on tissue Doppler is dependent on B-mode for identifying the location of the cardiac structures. The restriction of accurate analysis to velocities along the ultrasound beam makes the technique angle-dependent, as well as restricting tracking to a single dimension.

### Speckle tracking

This new technique has been implemented in commercial software such as the 2D strain software package, part of Echo PAC (GE Medical Systems, Horten, Norway) and Imaging (Siemens Medical Solutions, California, USA). Speckle tracking involves following the speckle pattern from frame to frame. Strain is derived through the relative displacement between two kernel regions by following the changes during several frames. However, if the frame rate is too low, large changes in the interference pattern are present from frame to frame and tracking will be poorer compared to higher frame rates. On the other hand, if the frame rate is too high, the spatial resolution will be poorer, making the speckles harder to recognize and follow. The advantage of these methods relative to TDI are that

they are angle-independent and allow the possibility of tracking in two dimensions (hence, the software package is denoted “2D strain”). On the other hand, their accuracy is dependent upon B-mode image quality and frame rate. The automated measurement of strain by speckle tracking has been validated by ultrasonomicrometry [4]. Commercially available software for the analysis of the 2D strain has been described as having the potential of becoming a standard for real-time automatic echocardiographic assessment of cardiac function (Figure 24.2) [3]. However, the current implementation of 2D strain software package is not automatic but automated. The operator defines the endocardium at end-systole by placing two markers at the annular ring and one marker in the apex. Then AVC is defined manually, using the electrocardiogram (ECG). Tracking is then performed automatically, but the position of the endocardial line can be manipulated if the tracking quality is insufficient. Two additional lines are produced by the software – a middle line identifying the myocardium and the middle area of interest and an outer line that can be manipulated over the epicardium (but free of the pericardium) by the operator changing the width of the region of interest. This procedure takes approximately 35 sec per view. The software indicates if the B-mode frame rate is too low or if the tracking quality is insufficient.

Tracking of radiofrequency (RF) data can also be used for 2-D strain echocardiography and has been

evaluated in an experimental work by Langeland et al. [7]. The method is based on finding the velocity vectors by tracking patterns in the RF image between consecutive frames. Anatomic tracking is performed automatically after first manually defining the endocardial and epicardial borders of the region of interest in the beginning of systole.

Velocity vector imaging has also been introduced recently. This technique has been applied to not only the left but also the right ventricle (Figure 24.3) [6].

### Combination of tissue Doppler imaging and speckle tracking

The commercially available systems are based on either TDI or B-mode, which have unique advantages as well as disadvantages. The combination of both modalities allows their strengths to be combined (Table 24.1). TDI can provide the high temporal resolution necessary for accurate timing of the cardiac events and for quantification of cardiac events requiring high frame rate, as well as more accurate measurements of displacement along the ultrasound beam. Speckle tracking allows tracking and measurement of deformation in more than one direction.

### Automated deformation analysis system

Functional analysis of the left ventricle requires knowledge of the location of the myocardium.

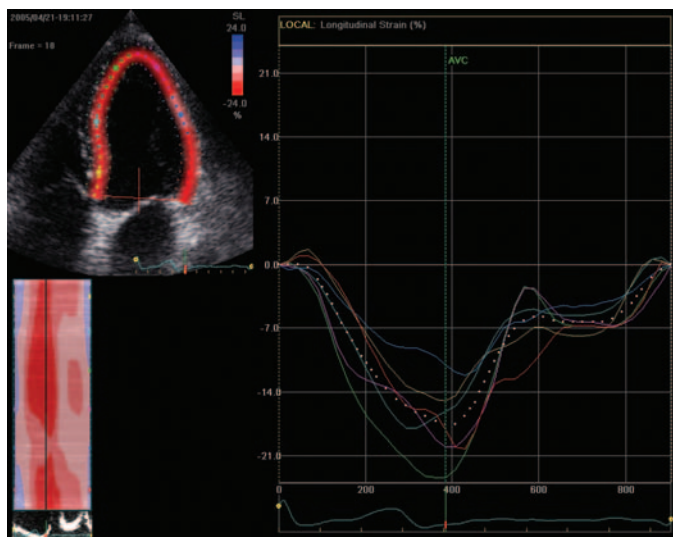


**Figure 24.2** The 2D strain software package is illustrated in a healthy volunteer in an apical four-chamber view. The top left image shows a tracked curve at end-systole with the inner points representing the endocardial line, the midpoints the myocardium, and the outer points the epicardial line. Strain curves are illustrated to the right, and a curved anatomical strain M-mode is shown in the lower left image.

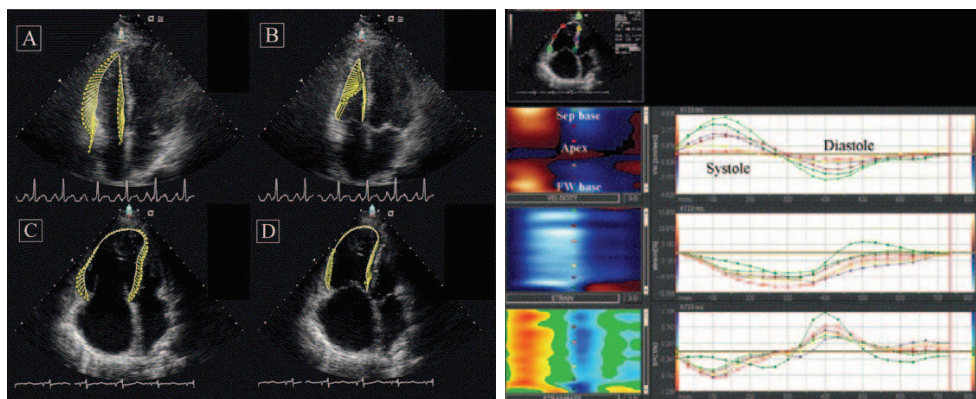


**Figure 24.3** Velocity vector imaging is illustrated in a right ventricle. After manually drawing the endocardial border in one frame, the endocardial border is then automatically tracked throughout the cardiac cycle. The vectors indicate the direction of the motion and the amplitude of the velocity. A and B represent a healthy individual, and C and

D show a patient with severe pulmonary hypertension. The right column images show velocity, strain, and strain rate curves to the right and curved anatomical M-modes to the left. (From Pirat et al. [6].)

**Table 24.1** Methods using speckle tracking and/or TDI with automatic/automated technique.

Author	Number/ category	Method/longitudinal, circumferential, radial	Reference	Feasibility	Intra- and interobserver reproducibility
Becker et al. [2]	64/MI	Speckle/circ, rad	MRI	88% (rad strain)	4.4%/7.3% (rad strain)
Cho [8]	30/known or suspected CD	Speckle/cir, rad, long TDI/ rad, long	MRI	87% (TDI) 90% (speckle), 11%/21% (long TDI), 16%/23% (rad TDI)	8%/15% (long speckle), 18%/22% (rad speckle), 18%/17% (circ speckle)
Ingul et al. [5]	60/normal + MI	Speckle + TDI/ long, rad	Coronary angiography	81%(strain rate)/ 80%(strain)	15%/15% coefficient of variation
Ingul et al. [8]	198/DSE	Speckle + TDI/ long, rad	Coronary angiography	86%(strain rate)/ 79%(strain)	10%/16% coefficient of variation
Ingul et al. [9]	614/DSE	Speckle + TDI/ long, rad	Survival	93%(strain rate)/ 87%(strain)	
Amundsen et al. [4]	9 dogs ischemia/ 11 subjects	Speckle/ long, rad	Sonomicrometry/ MRI	85%/90% (strain)	5.2%/8.6% (strain)
Leitman et al. [3]	20 MI/10 normal	Speckle/ long, rad	Coronary angiography	86%	5%/10%
Pirat et al. [6]	58 PAH/ 19 normal	Speckle/VVI		82%/76%	4.7±4.7% (strain)/ 0.51±0.41 sec <sup>-1</sup> (strain rate)
Langeland et al. [7]	5 sheep	Speckle	Sonomicrometry	90%	Correlation coefficient 0.72 radial/0.8 longitudinal strain

MI, myocardial infarction; DSE, dobutamine stress echocardiography; PAH, pulmonary arterial hypertension; VVI, velocity vector imaging; rad, radial; long, longitudinal; circ, circumferential.

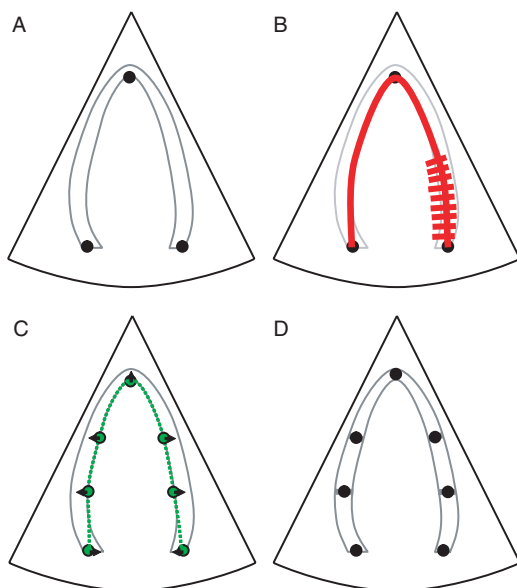


**Figure 24.4** Ultrasound sector with apical view of left ventricle illustrating the initial steps of an automated analysis method. (A) Automatic detection of the landmarks defining the atrioventricular plane and the apex. (B) A generic ventricle-shaped initial contour is adapted to the detected points, and search lines for endocardial detection are placed over the contour. (C) The length of the detected endocardial contour is divided into six segments. The seven segment border markers are then pushed slightly to be positioned in the myocardium. (D) The segment border markers defined at one frame (end-diastole) can be tracked to get the location of the segment borders during the cardiac cycle.

To automate the analysis of cardiac ultrasound images, both the location of cardiac structures and information concerning the temporal relation between the images and the cardiac events are needed. In the Trondheim Autostrain method [5], this knowledge is gained by first locating the positions of the apex and the two landmarks defining the atrioventricular plane (Figure 24.4A). This is achieved by an automatic method that uses TDI velocities and scores candidate landmarks based on gray-scale intensity, velocity profiles, and depth [11]. Having found the apex and the two atrioventricular landmarks, a simple initial generically shaped contour is fitted to these three points. This contour will then very roughly approximate the endocardium. Then, search lines are placed over the contour (Figure 24.4B). Candidate points representing the endocardial border along the search lines are

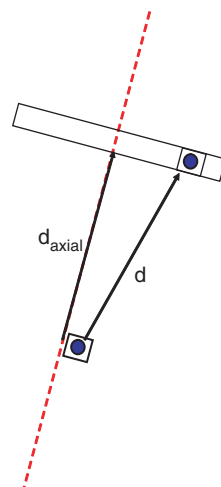


**Figure 24.5** Tracking using the combination of TDI and speckle tracking. A pattern is displaced a distance ( $d$ ) between two consequent frames. With TDI, the axial component ( $d_{\text{axial}}$ ) of the displacement can be estimated. Using the estimated axial displacement, a limited search area for the lateral displacement can be positioned at the axial depth determined by TDI, thus speeding up the speckle tracking. To increase robustness, this process can be repeated with several neighboring kernels at the position of the pattern, and the resulting displacement vectors averaged.

found using an active contour model with a scoring function expressing the strength of candidate gradients from cavity to myocardium [12–14]. After identifying points at each search line, spline fitting is used to produce an endocardial contour (Figure 24.4B). The length of the endocardial contour is then divided into six equal-length segments and the seven points needed for defining the segments are relocated slightly to be 3 mm into the myocardium (Figure 24.4C). Thus, six segments in the myocardium are detected automatically in the end-diastolic frame of the ultrasound recording (Figure 24.4D).

The entire process, including landmark detection, endocardial detection, and segment border marker placement, is automatic and can be applied to all three standard apical views. The process does not always produce perfectly detected landmarks and a perfect endocardial contour, but this is not critical as the goal of the process is to automatically place the segment border markers. After the segment border markers are placed, the locations can be manually adjusted.

Having determined the segment border markers in end-diastole, tracking can be used to find the location of the markers in all frames of the cardiac cycle. In the Trondheim method [5], a combination of TDI and speckle tracking is used; axial tracking using TDI and lateral tracking using a sum of absolute differences speckle tracking algorithm [5]. TDI tracking of a marker at a given frame simply consists of calculating the displacement (in axial direction) of that marker from the velocity at that location. B-mode intensity-based speckle tracking is performed in the lateral direction (Figure 24.5). To avoid drift, the tracking algorithm is applied both forward and backward through the cardiac cycle, and the results are averaged.

The results of tracking are visualized in the ultrasound sector as markers moving during the cardiac cycle. By visual assessment, the users can then discard or relocate and re-track markers with bad tracking.

Although the described landmark detection method is TDI-dependent, manually setting the seven segment border markers with speckle tracking in both directions allows dynamic positioning of segment border markers to be achieved without TDI [4]. Based on this information concerning the segment markers, we tried four methods for strain and strain rate calculation to investigate the strengths and weaknesses of the different methods.

### Static velocity gradient method

First, the geometric mid-point of each segment is located in the end-diastolic frame. The closest TDI beam to this point is then selected, and velocities from a predefined distance in both directions along this beam are extracted for each frame in the cardiac cycle (Video clip 27 ). The difference between the extracted velocities is then divided by the predefined geometrical distance, thus calculating strain rate. Strain is calculated by temporal integration and Lagrangian correction of strain rate (Figure 24.6) [16,17].

### Dynamic velocity gradient method

The position of the mid-point of each segment is located in all frames in the recording using the described tracking scheme. Then for all frames and segments, the closest TDI beam is located and strain and strain rate is calculated as in the

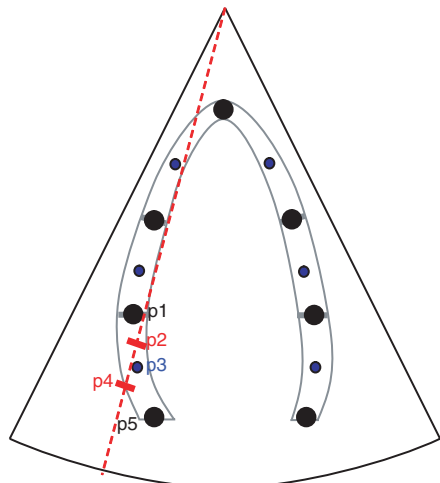


**Figure 24.6** Ultrasound sector with apical view of the left ventricle illustrating differences between methods for calculating strain and strain rate. In the static velocity gradient and the dynamic velocity gradient methods, the closest TDI beam to the middle point (p3) of the segment is located, and velocities from two points along this beam (p2 and p4) are then extracted and used for strain rate calculations. In the static velocity gradient method, the middle point (p3) is static for all frames, whereas in the dynamic velocity gradient method, the middle point (p3) is at a new location for each frame. In the segment length methods, strain is calculated based on the dynamic positions of the segment border points (p1 and p5).

static velocity gradient method (Figure 24.6; Video clip 28 ).

### Segment length method using tissue Doppler imaging for tracking

The positions of all segment border markers are located during all frames (Video clip 29 ). For each pair of segment border points and each adjacent pair of frames, strain is calculated from the variation in segment length ( $L$ ) in relation to starting length ( $L_0$ ), so strain is derived from the equation  $(L - L_0)/L_0$ . Strain rate is calculated as the temporal derivative of strain with Eulerian correction (Figure 24.6) [16,17].

### Segment length method without using tissue Doppler imaging

This method works as the previous method, but segment length variation is tracked by speckle tracking only (Figure 24.6; Video clip 30 ).

Before automated analysis of the calculated strain and strain rate curves can be performed, the timing of cardiac events, especially AVC, must be determined.

### Automatic timing of cardiac events

The major cardiac events (ejection and filling with consequent valve closure and opening) determine the movement of cardiac tissue. Therefore, extracted curves for displacement, velocity, strain, and strain rate from ultrasound recordings can, to varying degrees, be used for timing of cardiac events.

The four left ventricular events related to the left ventricular valves divide the cardiac cycle into its main phases. AVO and AVC are particularly needed to be able to determine several parameters related to ejection and shortening. The simplest approaches for timing AVC are the use of spectral Doppler of the blood flow through the aortic valve, or parasternal M-mode of the aortic valve [8]. Several other methods have been used, including those using TDI and color M-mode [18–20], detection of the T-wave in ECG, phonocardiography of the second heart sound, and empirical regression relations based on heart rate calculated from ECG [21]. In some of these modalities, the timing of AVC is extracted from a separate recording and cardiac cycle than the recording where the timing of AVC is needed for analysis. Such approaches are not optimal, as the heart rate varies from cycle to cycle, even at rest [22].

With high framerate TDI recorded from the apical position, the timing of AVC can be determined manually in all standard views (two-, three-, and four-chamber) [19,23]. The detection of AVC is based on a short oscillation in the base of the left ventricle, provoked by AVC [24]. During closure, the basal tissue of the ventricle is moving away from the apex but stops with a slight “bounce” at the time of AVC. This event results in a shift from negative to positive velocities and also a positive acceleration peak (Figure 24.7).

Methods for automatically estimating the timing of AVC using TDI have been discussed by Aase et al. [21]. These automatic methods all rely on an automatic curve analyzer first identifying other events of the cardiac cycle (E-wave and mitral valve opening) and, thereafter, searching for AVC as the highest acceleration within a temporal

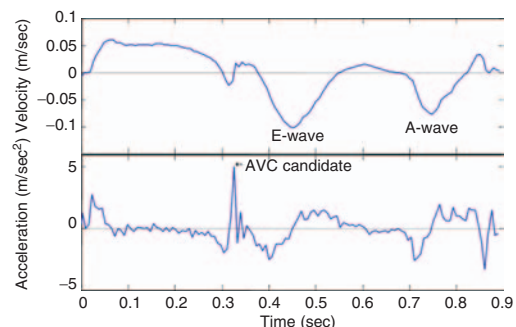


**Figure 24.7** AVC can be detected as the peak positive acceleration in velocity/time curves extracted from the base of the left ventricle in the apical views.

search interval. Additionally, the methods rely on mechanisms for limiting the spatial area from which the velocity/time curves are extracted, such that the influence of mitral valve movement on the data is limited. The temporal resolution of the velocity/time curves is sufficient for AVC detection with TDI [21]. If sufficient B-mode frame rate is provided and speckle tracking-based velocities are generated, such curves can probably also be used for AVC detection.

In the Trondheim Auto Strain method, the timing of AVO was automatically detected from peak acceleration in a search interval between 15 and 120 msec from the QRS complex using the same curves as used for timing of AVC. However, both the timing of AVO and AVC can be manually adjusted by the user with respect to the velocity, ECG, and strain and strain rate curves (when calculated).

The combination of a strain/strain rate curve with reasonable quality with knowledge of AVC and AVO allows several SRI parameters, such as peak systolic strain rate, time to end of shortening, post-systolic shortening, peak systolic strain, end-systolic strain, and time-to-peak systolic strain rate, to be identified automatically and placed on the curves. For analysis of the iso-volumetric relaxation and isovolumetric relaxation phases, mitral valve opening and mitral valve closure are also needed.

### Clinical use of an automated method

The automated analysis of strain and strain rate has been shown to be a clinically promising tool

for the assessment of wall motion at rest and stress echocardiography.

One of the greatest potential benefits of the automated application is the ability to quantify wall motion changes with stress echocardiography and, thereby, develop an objective and rapid test of the functional significance of coronary artery disease (CAD). Clinical studies using TDI, speckle tracking, or a combination have been published over the past few years. In 197 patients referred for dobutamine stress echocardiography with clinically suspected CAD, 137 of whom had undergone coronary angiography [9], the number of analyzable segments at peak was highest for the manual method with 98%, followed by 84% for the speckle tracking method, and finally 80% for the TDI/speckle tracking method. Peak systolic strain rate and end-systolic found to be the optimal variables strain were for both automated TDI and speckle tracking methods to distinguish between CAD and no CAD. For peak systolic strain rate, the combined TDI/speckle tracking technique gave an overall sensitivity of 89%, specificity of 93%, and accuracy of 90%. The speckle tracking technique gave an overall sensitivity of 84%, specificity of 92%, and accuracy of 87%. Conventional wall motion score was, in comparison, significantly less sensitive (75%), but the specificity of 81% and accuracy of 77% were not significantly different from those of strain rate.

There have been three comparative studies between manual and automated analysis of strain and strain rate [3,5,8]. The first study compared 30 patients with acute myocardial infarction and 30 subjects with a normal left ventricle [5]. Echopac PC (GE Vingmed) was used for the manual analysis of strain and strain rate. The automated method was feasible, but with 12% fewer segments analyzable. The reproducibility was highest for the automated speckle tracking method. The second study included 20 patients with myocardial infarction, 10 healthy subjects, and 10 patients for comparing the 2D strain software package with manual TDI [3]. Among the segments that were suitable for wall motion analysis, 85% of the segments could be adequately tracked by the automated software. The correlation between the 2D strain software package and TDI was better for strain ( $r = 0.74$ ) than for strain rate ( $r = 0.52$ ). The third comparative study evaluated 30 patients with known or suspected

ischemic heart disease with manual method and the 2D strain software package, validated by magnetic resonance imaging (MRI) [8]. They found radial 2D strain to be accurate and feasible to quantify regional function compared to TDI. Another study using automated speckle tracking and MRI tagging as reference compared seven patients with myocardial infarction and four healthy volunteers [4]. The 95% limits of agreement were -9% to 8% and the correlation for strain was good ( $r = 0.87$ ).

We have also applied the automated method to predict outcome in patients undergoing dobutamine stress echocardiography with known or suspected CAD [10]. In this study of 646 patients with an average follow-up time of 5.2 years, automated SRI analysis of dobutamine stress echocardiography response gave independent and incremental information to standard wall motion score index. Segmental peak systolic strain rate had better predictive value than strain.

Automated velocity vector imaging was tested in a study of right ventricular function, including 48 patients and 19 age-matched controls. The optimal cutoff value for determining pulmonary artery systolic pressure  $>50$  mm Hg using receiver operating characteristic curves was a strain rate of  $-1.7 \text{ sec}^{-1}$  with a sensitivity of 80% and a specificity of 78% [6].

## Future automated analysis systems

Research and development in ultrasound technology is likely to permit a higher acquisition rate than is currently available for both B-mode and TDI images. One promising technology to deliver this increase in data rate is the use of multiple parallel receive beams [5,26]. Increased data rate can provide either increased temporal resolution, or improved lateral resolution, or a combination of both.

Automated analysis of such data would be facilitated by including features for automatically detecting artefacts – both those related to the methods used for high data rate imaging [7] and artefacts related to reverberations. If the analysis system could automatically detect the areas of the ultrasound sector with low quality data, the user could be made aware that further processing of such data would give uncertain results.

In the near future, the increased data rate will probably improve the data sets used for 2-D strain and strain rate analysis. With even further increases in data rate, 3-D recordings with sufficient temporal and lateral resolution for strain and strain rate calculation may emerge. To calculate strain and strain rate in all directions, 3-D speckle tracking may be used [8]. The problem of features moving out of plane in 2-D speckle tracking can be avoided by using 3-D speckle tracking. A 3-D ultrasound recording will provide the possibility of analyzing all six walls using one recording. Analysis can be done on both long-axis and short-axis projections. Three-dimensional cardiac ultrasound will possibly speed up acquisition and provide more information than current 2-D recordings.

An automated analysis system for 3-D will provide some means of detecting and segmenting the myocardium (endocardium and epicardium) as well as a means for detecting the main cardiac events. Myocardial detection might be built on automated methods used for ventricular volume detection. As with the 2-D system, a 3-D system will also have to illustrate the tracking and preferably the calculated parameters for the user to evaluate.

## Conclusion

The development of an automated strain and strain rate method for analyzing echocardiography and stress echocardiography has been shown to be feasible, time-saving, and more accurate than conventional wall motion scoring. The automated methods define the region of interest, and objective traces are obtained as there is no possibility of searching for a suitable curve. However, the feasibility is lower than for manual analysis. Strain and strain rate assessment by the automated method has been shown to increase accuracy compared to wall motion score for dobutamine stress echocardiography and to be a stronger predictor for the prognosis of all cause mortality.

The automated methods have so far been used only by experts. The critical next phase will be to move them to a non-expert environment.

## References

1. Ingul C. Quantification of regional myocardial function by strain rate and strain for evaluation of coronary artery disease. [Doctoral thesis]. Trondheim: NTNU; 2006; 163:22.

- 2 Becker M, Bilke E, Kühl H, et al. Analysis of myocardial deformation based on pixel tracking in two dimensional echocardiographic images enables quantitative assessment of regional left ventricular function. *Heart* 2006; **92**: 1102–8.
- 3 Leitman M, Lysyansky P, Sidenko S, et al. Two-dimensional strain – a novel software for real-time quantitative echocardiographic assessment of myocardial function. *J Am Soc Echocardiogr* 2004; **17**: 1021–9.
- 4 Amundsen BH, Helle-Valle T, Edvardsen T, et al. Noninvasive myocardial strain measurement by speckle tracking echocardiography: validation against sonomicrometry and tagged magnetic resonance imaging. *J Am Coll Cardiol* 2006; **47**: 789–93.
- 5 Ingul C, Torp H, Aase SA, Berg S, Stoylen A, Slordahl SA. Automated analysis of strain rate and strain: feasibility and clinical implications. *J Am Soc Echocardiogr* 2005; **18**: 411–8.
- 6 Pirat B, McCulloch ML, Zoghbi WA. Evaluation of global and regional right ventricular systolic function in patients with pulmonary hypertension using a novel speckle tracking method. *Am J Cardiol* 2006; **98**: 699–704.
- 7 Langeland S, D'hooge J, Wouters PF, et al. Experimental validation of a new ultrasound method for the simultaneous assessment of radial and longitudinal myocardial deformation independent of insonation angle. *Circulation* 2005; **112**: 2157–62.
- 8 Cho GY, Chan J, Leano R, et al. Comparison of two-dimensional and tissue velocity based strain and validation with harmonic phase magnetic resonance imaging. *Am J Cardiol* 2006; **97**(11): 1661–6.
- 9 Ingul C, Stoylen A, Slordahl S, et al. Automated analysis of myocardial deformation at dobutamine stress echocardiography: an angiographic validation. *J Am Coll Cardiol* 2007; **49**:1651–9.
- 10 Bjork Ingual C, Rozis E, Slordahl SA, et al. Incremental value of strain rate imaging to well motion analysis for prediction of outcome in patients undergoing dobutamine stress echocardiography. *Circulation* 2007; **115**: 1252–9.
- 11 Torp A, Rabben S, Stoylen A, et al. *Automatic detection and tracking of left ventricular landmarks in echocardiography*. Proceedings of the IEEE Ultrasonics Symposium; 2004; Aug 23–27; Montreal, Canada; 2004. p. 474–7.
- 12 Kass M, Witkin A, Terzopoulos D. Snakes: active contour models. *Int J Comput Vision* 1987; **1**: 321–31.
- 13 Olstad B, Torp A. Encoding of a priori information in active contour models. *IEEE Trans Pattern Anal Mach Intell* 1996; **18**: 863–72.

- 14 Rabben SI, Torp AH, Støylen A, Slørdahl S, Bjørnstad K, Haugen BO, et al. Semiautomatic contour detection in ultrasound M-mode images. *Ultrasound Med Biol* 2000; **26**: 287–96.
- 15 Bohs L, Trahey G. A novel method for angle independent ultrasonic imaging of blood flow and tissue motion. *IEEE Trans Biomed Eng* 1991; **38**: 280–6.
- 16 Heimdal A. *Doppler based ultrasound imaging methods for noninvasive assessment of tissue viability* [Doctoral thesis]. Trondheim: NTNU; 1999; **77**: p. 51–3.
- 17 Støylen A. *Strain rate imaging of the left ventricle by ultrasound. Feasibility, clinical validation and physiological aspects* [Doctoral thesis]. Trondheim: Bjørum AS; 2001. pp. 64–9.
- 18 Weidemann F, Kowalski M, D'hooge J, Bijnens B, Sutherland GR. Doppler myocardial imaging. A new tool to assess regional inhomogeneity in cardiac function. *Basic Res Cardiol* 2001; **96**: 595–605.
- 19 Voigt JU, Lindenmeier G, Exner B, et al. Incidence and characteristics of segmental postsystolic longitudinal shortening in normal, acutely ischemic, and scarred myocardium. *J Am Soc Echocardiogr* 2003; **16**: 415–23.
- 20 Jamal F, Kukulski T, Strotmann J, et al. Quantification of the spectrum of changes in regional myocardial function during acute ischemia in closed chest pigs: an ultrasonic strain rate and strain study. *J Am Soc Echocardiogr* 2001; **14**: 874–84.
- 21 Aase S, Støylen A, Ingul CB, Frigstad S, Torp H. Automatic timing of aortic valve closure in apical tissue Doppler images. *Ultrasound Med Biol* 2006; **32**: 19–27.
- 22 Støylen A, Wisloff U, Slørdahl S. Left ventricular mechanics during exercise: a Doppler and tissue Doppler study. *Eur J Echocardiogr* 2003; **4**: 286–91.
- 23 Støylen A, Malm S, Aase S, Sagberg E. Aortic valve closure can be timed by tissue Doppler. *Eur J Echocardiogr* 2004; **5 Suppl 1**: 159.
- 24 Kupari M. Aortic valve closure and cardiac vibrations in the genesis of the second heart sound. *Am J Cardiol* 1983; **52**: 152–4.
- 25 Shattuck D, Weinshenker M, Smith S, Ramm O. Explososcan: A parallel processing technique for high speed ultrasound imaging with linear phased arrays. *J Acoust Soc Am* 1984; **75**: 1273–1282.
- 26 Hergum T, Bjåstad T, Kristoffersen K, Torp H. Parallel beamforming using synthetic transmit beams. *IEEE Trans Ultrason Ferroelectr Freq Control* 2007; **54**(2): 271–280.
- 27 Bjåstad T, Aase S, Torp H. The impact of aberration on high frame rate cardiac B-mode imaging. *IEEE Trans Ultrason Ferroelectr Freq Control* 2007; **54**: 32–41.
- 28 Meunier J. Tissue motion assessment from 3-D echographic speckle tracking. *Phys Med Biol* 1998; **43**: 1241–54.

# Use of tissue characterization in relation to arterial function

Brian A. Haluska and James E. Sharman

## Background: significance of arterial function for cardiologists

In recent years, there has been increasing recognition of the importance of arterial function to the heart [1,2]. In both experimental and clinical studies, elevations in left ventricular (LV) afterload have been shown to directly impair myocardial relaxation and increase end-diastolic left ventricular pressure [3,4]. Indeed, chronically elevated afterload is one of the major contributory factors to the eventual development of diastolic heart failure [5]. However, the traditional method for estimating afterload by measuring blood pressure at the upper arm fails to take into account individual differences in the amplification of systolic blood pressure (and, therefore, also pulse pressure) that occurs between the ascending aorta (true afterload) and the brachial artery (estimated afterload) [6]. This disparity occurs due to the nature of pressure waveform travel in the arterial system, which is influenced by ejection duration [7], but is primarily determined by the structure and function of the arteries distal to the heart [8].

## Wave reflection and ventricular-vascular interaction

With each cardiac contraction, a pressure pulse is generated, which travels distally from the large elastic arteries of low resistance, progressively through smaller, stiffer, muscular arteries of higher resistance. Although there is some dissipation of the pressure wave, a proportion is reflected back toward the heart and interacts with outgoing pressure

wavelets [9]. The main sites of wave reflection are thought to be the high resistance arterioles [10], as well as the branching points of major vessels [11]. The magnitude and timing of the reflected pressure wave has been shown to affect the rate of left ventricular relaxation [12]. In the case of optimal ventricular–vascular interaction (Figure 25.1, dashed line), the reflected wave arrives at the aortic root after aortic valve closure, and serves to boost diastolic pressure and subendocardial perfusion without increasing left ventricular afterload or impairing diastolic function [9,13]. Conversely, with advancing age and diseases that stiffen the large central arteries [14], the transmission time of the outgoing and reflected pressure wave is reduced, resulting in an early return to the heart of the reflected wave (Figure 25.1, solid line). This finding increases late systolic pressure, and the myocardium must pump against increased load; relaxation time is prolonged [3,12] and, over time, left atrial volume and [15] left ventricular mass [16–18] may increase.

Due to wide individual variance in factors that affect arterial wave reflection (e.g., age, height, aortic stiffness, peripheral vascular tone, heart rate) patients with the same (or similar) brachial blood pressure may have radically different central (ascending aortic) systolic blood pressure and pulse pressure [19]. Under resting conditions, the difference in systolic blood pressure between the heart and upper arm may be as little as 2 mm Hg or as high as 33 mm Hg [20], but the magnitude of pressure difference cannot be discerned through traditional cuff blood pressure measures. This fact must be of prime interest to the cardiologist because *independent of brachial blood pressure*, central indices of systolic

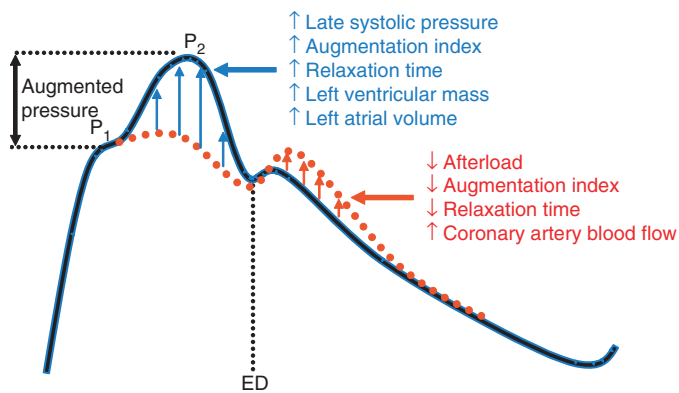


**Figure 25.1** Example of ascending aortic pressure waveforms in which early wave reflection is increased (solid line) or decreased (dashed line). The first systolic shoulder ( $P_1$ ) corresponds to peak aortic flow, whereas  $P_2$  is central systolic blood pressure. Augmentation index is the percentage contribution of the augmented pressure to the overall central pulse pressure and is a marker of wave reflection. ED, ejection duration.

stress or wave reflection (i.e., ascending aortic pulse pressure, augmented pressure, augmentation index) predict left ventricular structure [21,22], the extent of coronary artery disease [23], and the risk of cardiovascular events (death, myocardial infarction, and restenosis) in patients undergoing percutaneous coronary intervention [24]. Furthermore, central pulse pressure and the degree of wave reflection independently predict all-cause and cardiovascular mortality in high-risk renal patients [25,26].

### Effect of drugs on central and brachial blood pressure

One of the main aims of antihypertensive medication is to reduce left ventricular afterload and improve function. Due to variation in pharmacological mechanisms of action, different vasoactive drug classes may have differential effects on the central and peripheral waveforms. In short-term studies (i.e., acute effect to 6 weeks intervention), the following drugs were shown to have a greater central, compared to brachial, blood pressure lowering effect: glyceryl trinitrate (sublingual [27] or patch [28] delivery), angiotensin converting enzyme inhibitors (perindopril, enalapril [29], lisinopril [30]), calcium channel blockers (felodipine, amlodipine [29]), and the angiotensin receptor blocker eprosartan [31]. The diuretic hydrochlorthiazide has been shown to have a similar pressure lowering effect at the upper arm and central arteries [29], whereas amlodipine appears to be the most efficacious drug for lowering wave reflection (augmentation index) and central systolic blood pressure [29,30]. On the other hand, the beta blockers atenolol and

bisoprolol have an unfavorable central effect by increasing augmented pressure [29–31], as well as elevating plasma brain natriuretic peptide [30,31], indicating increased cardiac strain. Finally, despite similar changes in brachial blood pressure, an atenolol-based antihypertensive regimen was shown to be less effective at reducing central blood pressure compared to amlodipine-based therapy, and central blood pressure was a stronger predictor of clinical events in 2,199 patients followed up for up to 4 years in the Conduit Artery Function Evaluation (CAFÉ) study [32]. Altogether, these data confirm the inadequacy of traditional clinic blood pressure measures for assessing patient risk and determining the effect of treatment.

### Current techniques for assessment of arterial stiffness and the pulse contour

Arterial stiffness is inversely related to arterial distensibility and is determined by vascular function (i.e., vascular smooth muscle tone) as well as by the structure of the vessel wall (i.e., elastin and collagen content) [33]. A variety of commercially available devices may be used to assess local, regional, or systemic arterial stiffness and wave reflections. A summary of techniques is presented in Table 25.1. Some of these methods require expensive equipment and technical expertise (i.e., magnetic resonance imaging), whereas others have less dependency on user skills (i.e., Complior). Carotid to femoral pulse-wave velocity (the speed of pressure wave travel along the aorta, aortic pulse-wave velocity) is considered to

**Table 25.1** Devices for recording arterial stiffness and wave reflections adapted from Reference 34.

<i>Measurement and device</i>	<i>Methods</i>	<i>Recording site</i>
<b>Local stiffness</b>		
Wall Track®	Echotacking	All superficial arteries
NIUS®	Echotacking	Radial artery
Artlab®	Echotacking	All superficial arteries
Vascular ultrasound systems	Echotacking	All superficial arteries
Magnetic resonance imaging (MRI)	Cine-MRI	Aorta
<b>Regional stiffness</b>		
Complior®	Mechanotransducer	All devices measure carotid to femoral, carotid to radial and femoral to tibialis anterior pulse-wave velocities.
SphygmoCor®	Applanation tonometry	
Wall Track®	Echotacking	
Artlab®	Echotacking	
Ultrasound systems	Doppler probes	
<b>Systemic stiffness</b>		
Area method	Diastolic decay	—
HDI PW CR-2000®	Modified Windkessel	—
SV/PP	Stroke volume and pulse pressure	—
<b>Wave reflections</b>		
SphygmoCor®	Applanation tonometry	All superficial arteries
Pulse Trace®	Photoplethysmography	Finger
Omron Healthcare HEM-9000AI®	Applanation tonometry	Radial artery

be the gold standard and most clinically relevant measure of *regional* artery stiffness [34]. This finding is because of the independent value of aortic pulse-wave velocity for predicting cardiovascular mortality [35–41] and highlights the important buffering role of this arterial segment [42]. In contrast, there are no studies demonstrating the prognostic worth of pulse-wave velocity in the upper (carotid to radial) or lower limb (femoral to tibialis anterior) arterial segments. SphygmoCor (AtCor Medical, Sydney, Australia) is the only commercial system that measures ascending aortic blood pressure and wave reflection (augmentation index; Figure 25.1). To achieve this reading, radial pressure waveforms are recorded by applanation tonometry using a pencil-like high-fidelity transducer (SPT-301, Millar Instruments). A validated generalized transfer function [43–45] is used to synthesize the ascending aortic waveform from the ensemble averaged radial waveform. This procedure enables improved patient care by providing potentially helpful insight on the “true” loading at the heart, rather than reliance on brachial measures alone [46]. The usefulness of this finding is empha-

sized in Figure 25.2, where pressure waveforms were recorded in two men with similar brachial blood pressure using the SphygmoCor system. Note that the patients’ radial waveform morphology, central pressure, and wave reflection are markedly different, suggesting that the approach to antihypertensive therapy between individuals may be quite different, despite similar brachial blood pressures. If need be, the untransformed radial augmentation index may also be used as a surrogate of central wave reflection, because there is strong agreement between the two measures [47]. Alternatively, central pressures and wave reflection can be reliably estimated from tonometric recordings at the common carotid artery [48].

### **Limitations: importance of standardizing measurements**

Brachial artery cuff blood pressure has been in clinical use for over 100 years, and despite accumulating evidence supporting a role for central blood pressure and wave reflection, there is a general lack of enthusiasm for clinicians to take on widespread use of this technology. This reluctance may

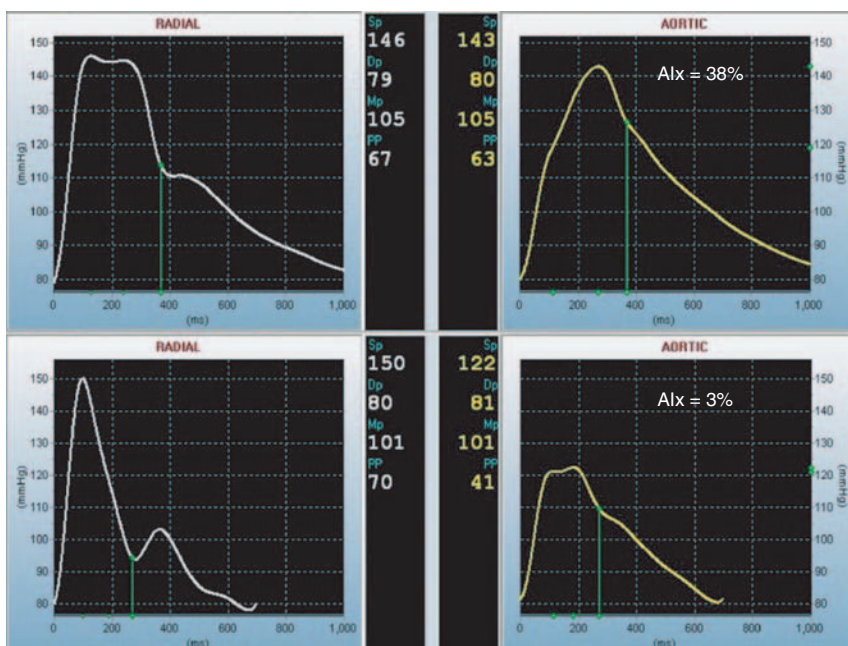


**Figure 25.2** Radial and synthesized ascending aortic pressure waveforms from two middle-aged men with similar brachial blood pressure (146/79 mm Hg vs. 150/80 mm Hg; mean of two readings; left column), but significantly different central systolic blood pressure (143 mm Hg vs. 122 mm Hg; right column), pulse pressure (63 mm Hg vs.

41 mm Hg), and augmentation index (Alx; 38% versus 3%). The top panels show low pressure amplification and high central relative to brachial systolic blood pressure, whereas the bottom panels show high pressure amplification and low relative central systolic blood pressure.

be related to a deficit of studies indicating its use as a management tool for physicians. The applanation tonometry technique also requires some expertise in recording and interpreting waveforms. Nonetheless, the field is moving toward acceptance of newer arterial measures [49], although it is unclear as to how these will be incorporated into clinical practice. To be clinically useful and robust for repeated measures, it should be appreciated that arterial stiffness and wave reflection are pressure dependent, both increasing with rises in mean arterial pressure. Therefore, testing conditions and procedures need to be standardized so that the chance of error arising from factors either intrinsic or extrinsic to the patient (i.e., nervousness, noise, or temperature) may be lessened or avoided. Recommendations for the standardization of patient and methodological conditions are presented in Table 25.2 (for comprehensive reviews of the clinical application of arterial stiffness, see references 33,34,50).

### Assessment of arterial compliance

Total arterial compliance, which is a measure of the stiffness of the arterial system, has been shown to be closely linked to both systolic and diastolic heart function. Arterial compliance is reduced with age, vascular disease, and hypertension [51–53] and is linked with the sequelae of these disorders. Reduction of vessel elasticity leads to an increment of afterload on the heart, which in turn leads to left ventricular hypertrophy [54]. Lower arterial compliance is closely related to an increase in pulse pressure, and increased pulse pressure is a determinant of cardiovascular risk and mortality [55,56]. A stiffer vascular system also leads to lower diastolic pressure, resulting in a decreased coronary perfusion pressure [57].

Several different methods have been used in the past to estimate total arterial compliance. Current methods are generally based on the two-element

**Table 25.2** Recommendations on standard clinic protocol for haemodynamic assessment adapted from previous evidence and expert consensus [33,34,51,52].

Possible confounders	Recommendation
<b>Patient factors</b>	
Smoking	Patient to refrain for ≥3 hr
Drinking	Patient to refrain from alcohol for ≥10 hours and caffeinated drinks for ≥3 hr
Eating	Patient to be postabsorptive (advise a light meal ~3 hr before assessment)
Exercise	Avoid strenuous exercise on the day of testing
Diurnal variation (time of the day)	For repeated measures, conduct at a similar time
Speaking, sleeping	Patients should neither speak nor sleep during testing
Position	Position (supine, seated) should be noted. Supine position preferred
Cardiac arrhythmia	Be aware of possible disturbance
<b>Environmental factors</b>	
White coat effect	If suspected, perform repeated measurements within one visit or in additional visits to detect it
Background noise	Conduct test in a quiet room. Operator not to talk to patient during measurement
Room temperature	Control temperature to 22 ± 1°C

Windkessel model introduced by Otto Frank in 1899 [58]. In the Windkessel model, the entire arterial tree is modeled as an elastic chamber with a constant compliance ( $C = dV/dP$ ,  $V$  = systemic blood volume, and  $P$  = pressure) and resistance ( $R$ ) representing total resistance. The equations governing this theory in the frequency and time domain are:

$$Z_{in} = \frac{R}{1+jwRC} \text{ and } \frac{dP}{dt} + \frac{P}{RC} = \frac{Q}{C}$$

where  $w = 2\pi f$ ,  $f$  being frequency,  $t$  is time,  $Z_{in}$  is the input impedance, and  $Q$  is the flow.

The *stroke volume–pulse pressure method* is a simple index that is a ratio of the stroke volume of the heart, calculated from two-dimensional (2-D) echo, and the pulse pressure (systolic–diastolic pressure). It is not generally accepted as a calculation or estimation of  $C$  but rather a crude index of normal/abnormal compliance. The *area method* uses an integral variation of the Windkessel equations and calculates compliance as:

$$RC = \int_{t_1}^{t_2} \frac{P dt}{(P_1 - P_2)}$$

where  $P_1$  and  $P_2$  are diastolic pressure at times  $t_1$  and  $t_2$ , respectively. Using this equation, the value for compliance can be found when the value for

resistance is known. For steady states,  $R$  is calculated as mean pressure over mean flow. This equation is only valid when local pressure is zero, so that it can only be applied to the ascending aortic wave form in diastole, because for normally functioning heart valves, diastolic flow is zero [58]. The *pulse–pressure method* proposed by Stergiopoulos et al. [58] is based on the fact that only the features of aortic flow and pulse pressure will be similar in a true arterial system and the two-element Windkessel model. It finds the value for  $C$  that gives the best fit between the measured pulse pressure and the one predicted by the Windkessel model. In this method, instantaneous aortic flow is calculated as the product of the left ventricular outflow tract (LVOT) area and the pulsed Doppler velocity in the LVOT, both obtained with echocardiography and simultaneously acquired with applanation tonometry.

Several studies have shown a correlation between arterial compliance and the presence of significant CAD [59–61], as might be expected from their attribution to common cardiovascular risk factors. In addition, arterial compliance may be an important contributor to the provocation of ischemia at stress testing, and an association has been documented with reduced exercise capacity and the presence of a lower ischemic threshold [62–64].

Total or systemic arterial compliance reflects compliance in the entire arterial tree; that is, the elastic large arteries and the muscular peripheral arteries. Pulse-wave velocity, as described earlier, has been shown to be a good measure arterial compliance and is obtained from applanation tonometry. Measures of local arterial function reflect the displacement or distensibility in relation to pressure at a certain point and are more a reflection of local arterial behavior rather than functional performance. Other methods such as M-mode and echo tracking have also been used to obtain measures of local arterial stiffness and elasticity.

### Assessment of arterial elasticity

As discussed above, increased arterial stiffness is an important determinant of increased systolic and pulse pressure, which are important determinants of the risk of cardiovascular disease [65]. However, although the measurement of arterial stiffness might be used to characterize arterial health [66,67], the many different approaches to its measurement attests to its difficulty. The most widely used approach has been the evaluation of arterial waveforms, obtained by applanation tonometry of compressible arteries (usually the radial), and the use of a transfer function to generate a central pressure waveform [68,69]. However, even more than potential problems imposed by the use of important transfer functions [70], the adoption of this technique has been adversely impacted by lack of familiarity with tonometry and the need to obtain specialized equipment. Echo tracking, with exported radiofrequency (RF) data, which measures the distensibility of large arteries, usually the common carotid, has also been used with success but requires dedicated hardware, software, and training to use [71–76].

Selzer et al. [74] described the use of echo tracking to obtain the classic measures of local arterial elasticity:

- Peterson's Elastic Modulus =  $PP/[(D_{max} - D_{min})/D_{min}]$  or  $(PP/DD)$
- Beta stiffness index =  $(P_s/P_d)/DD$
- Arterial distensibility =  $100\% * [(D_{2max} - D_{2min}/D_{2min})]/PP$
- Local arterial compliance =  $(D_{2max} - D_{2min})/PP$   
where PP is pulse pressure, Ps is systolic blood pressure, Pd is diastolic blood pressure; Dmax

is maximum artery diameter, Dmin is minimum artery diameter, and DD is  $(D_{max} - D_{min})/D_{min}$ .

M-mode echocardiography has been used in several previous studies to measure intimal-medial thickness (IMT) and arterial distensibility, and the coefficients of variation for this technique are in the range of 10%. The major limitation of M-mode measurement is the inability to distinguish the media-adventitia interface. Low signal to noise ratio and angle dependency are also pitfalls with M-mode echo. Other imaging studies of arterial displacement have also shown rather high variation both between and within observers [74–77]. Some of these imaging techniques based on M-mode such as echo tracking also require specialized equipment (Figure 25.3).

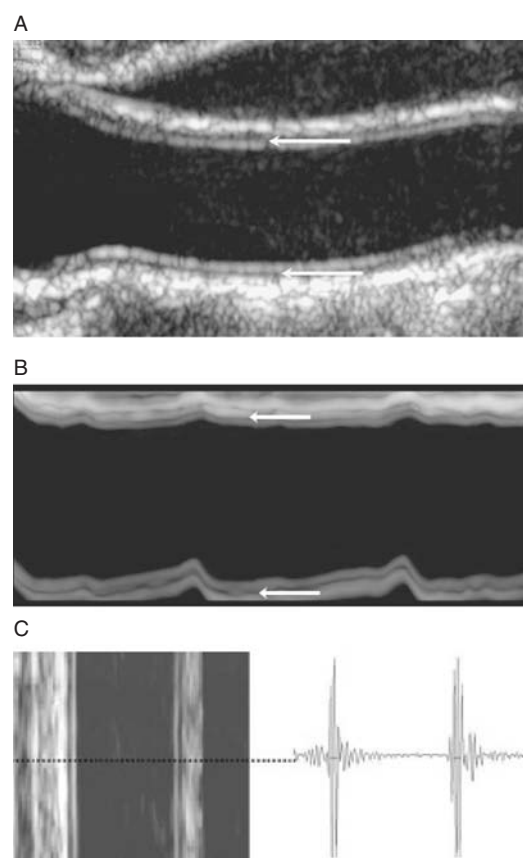


**Figure 25.3** Longitudinal scans of the common carotid artery immediately below the bifurcation using 2-D B-mode (A), M-mode (B), and echo tracking (C). White arrows denote M lines in anterior and posterior walls.

## Application of tissue Doppler to arterial function

Doppler echocardiography is used traditionally to evaluate the velocity and direction of blood flow in the heart and vessels. Recent technical developments allowed reduction of the wall filters and scale, thus, permitting the evaluation of low-velocity, high-amplitude signals, as described in previous chapters. Color tissue Doppler imaging (TDI) can be used to examine the large arteries of the body as well. The velocities derived from the smooth muscle layer as the artery expands in systole and contracts in diastole may give a measure of arterial compliance. An automated method of analyzing this velocity data could provide the newest and simplest method of determining arterial compliance.

The incorporation of measurement of vascular stiffness with measurement of carotid IMT could solve issues of both familiarity and availability. However, previous imaging studies have failed to produce a robust technique for assessing both arterial elasticity and IMT using M-mode, RF signals, impedance, or other techniques. Doppler echocardiography on the other hand, used traditionally to evaluate the velocity and direction of blood flow in the heart and vessels, can be used to evaluate low-velocity, high-amplitude signals that come from tissue by reduction of the wall filters and scale. The use of color TDI permits rapid, simultaneous visualization of multiple structures in a single view. To date however, the main cardiovascular application of this technique has been in myocardial evaluation.

Acquisition of images using TDI of a large artery is simple and feasible and can be incorporated in the normal cardiac or vascular examination. To date, color TDI has not been widely implemented on vascular imaging probes. Using such equipment, however, the carotid arteries may be scanned longitudinally in the anterior, lateral, and posterior aspects 2–10 cm below the bifurcation, and digital cine-loops are acquired for offline analysis. The image is optimized for TDI using the smallest possible region of interest (ROI) box to achieve the highest frame rate, which was usually between 160 and 220 frames/sec, and then 2-D and color Doppler settings are also customized for extraction of vessel displacement. For 2-D imaging, the dynamic range is 150 dB, the 2-D option is set to

penetration, persistence is set at low, and frame rate is set at maximum. For the color TDI, the gain was set at 100%, with a pulse repetition frequency > 200 Hz. Care should be taken not to include any discrete plaques in the TDI measurements. Loops of 3–5 cardiac cycles with TDI are usually then acquired digitally for offline analysis (Figure 25.4).

The TDI images are analyzed offline using custom-written software (AWM v1.05, Philips Medical Systems, Bothell, WA), which extracts the velocity information for the ROI area over the cardiac cycle and, with a processing algorithm, generates values for vessel wall displacement (in microns) over time. These data can then be saved and exported in numerical format for analysis (Figure 25.5). As the TDI technique is based on tissue Doppler rather than B-mode imaging, it is relatively independent of gray-scale image quality.

## Tissue Doppler estimation of arterial distensibility

Carotid TDI may be used to determine a distensibility coefficient, which is “corrected” for blood

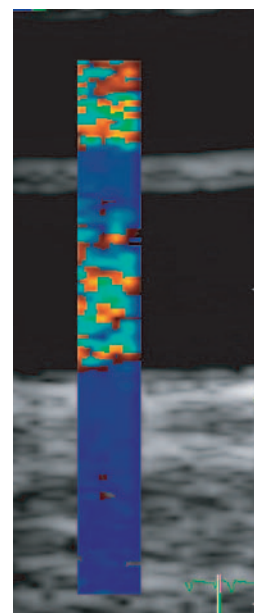


**Figure 25.4** Longitudinal B-mode ultrasound of the common carotid artery with tissue Doppler optimization. High-velocity (aliased) signal can be seen in the vessel lumen (center) and jugular vein (above), whereas the tissue velocities are seen as low-velocity (blue).

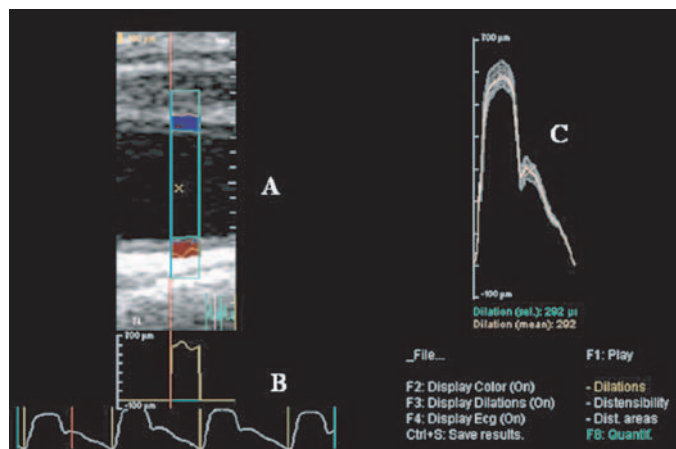


**Figure 25.5** AWM processing window with carotid TDI displacement curves. Color TDI displacement for the cardiac cycles is seen at top left (A), raw displacement curves bottom left (B), and the mean displacement for the cardiac cycles on the right (C). These data can then be exported numerically for analysis.

pressure measured using a standard sphygmomanometer on the right brachial artery, after the patient has been allowed to rest 5–10 min. The B-mode digital cine-loops are measured off line (HDI Lab v1.91d, Philips Medical Systems, Bothell, WA) at end-systole and end-diastole to obtain maximal and minimal dimensions. Measurements are made from the anterior M-line to the lumen–endothelial interface in the posterior wall (Figure 25.3). The distensibility coefficient is determined using the equation:

$$2 * ((\text{net displacement}/\text{diameter})/\text{PP})$$

where net displacement is maximum minus minimum displacement (in microns) and PP is pulse pressure. Distensibility coefficient has been reported in the past by either M-mode or B-mode echo using echo tracking techniques but the use of TDI may make it more robust because of its user interface.

Ramnarine et al. were the first to TDI and arterial wall motion analysis (AWM) clinically in a pilot study published in 2004 [78]. These investigators studied a group of patients with and without varying degrees of carotid disease and reported on the correlation of vessel displacement with severity of disease and its ability to characterize plaques. They concluded that there was poor correlation between AWM and plaque severity and that AWM had limitations in its ability to distinguish vulnerable plaques and characterize atheroma. However, in other studies using AWM to assess *arterial elasticity* rather than *atheroma*, the TDI technique appears to be more robust.

### Calibration of TDI displacement curves

Several approaches have been taken to compare TDI and AWM analysis with other techniques in assessing arterial elasticity in normal subjects and in patients with varying degrees of clinical and subclinical cardiovascular disease. The first was to “calibrate” the TDI displacement curves for blood pressure using a transfer function similar to the one used to derive central pressure from brachial pressure using applanation tonometry, effectively turning displacement (in microns) into pressure (in mmHg). Applanation tonometry (Millar SPT-301 Mikro-Tip transducer, Millar Instruments, Houston, TX) was performed on the right carotid artery in all patients. Blood pressure was measured using a standard sphygmomanometer on the right brachial artery, after the patient had been allowed to rest 5–10 min. Calibration of the tonometric waveform was performed by assuming equivalence of mean  $[(2 \times \text{DBP} + \text{SBP})/3]$  and diastolic brachial cuff pressure. TDI images of the right carotid artery were acquired and analyzed using the method described above. Both the extracted TDI displacement curves and the tonometric curves were then imported into a custom written MatLab program (SAMTDI, Carlier 2004) for analysis, and once calibrated, a comparison was done between the waveforms (Figure 25.6). Carotid distension waves (in microns) derived from the TDI recordings were transformed into approximated pulse pressure curves (in millimeters of mercury), based on the observation that the mean blood pressure is constant throughout the large artery tree, as well as the

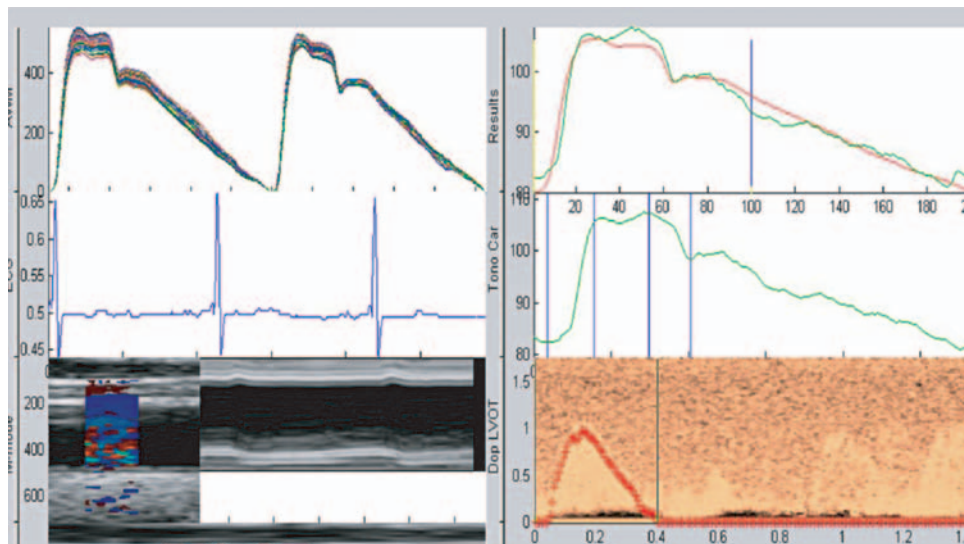


**Figure 25.6** Analysis window for comparison of tonometry and TDI showing the extracted displacement curves (A), ECG for timing (B), raw TDI and M-mode of the carotid artery (C), the tonometric data (D), pulsed aortic Doppler

(E), and once calibrated, a comparison of the tonometric and TDI curves (F). For comparison, the TDI curves were calibrated using the same mean and diastolic blood pressure data from the tonometry.

diastolic pressure [79]. The tonometric recordings were calibrated setting the average integrated curve equal to the mean blood pressure, with the minimum diastolic tonometric value set equal to the diastolic blood pressure. Once the distension curves were calibrated by the above method, there were no significant differences in systolic central pressures between tonometry and calibrated TDI. Thus, TDI may provide a simple index of arterial elasticity or simplify the estimation of central pressure used to calculate total arterial compliance. However, there are some potential technical problems that can limit the ability of calibrated TDI displacement to assess central pressure. For example, failure to use a sufficiently high pulse repetition frequency causes aliasing of the velocity signals, and excessive motion of the carotid artery may lead to failure of the edge detection mechanism.

### Comparison between TDI displacement and other markers of distensibility

A distensibility coefficient derived from pressure corrected TDI displacement curves has also been

compared with measures obtained by applanation tonometry and with other classic measures of systemic and local arterial elasticity. Our preliminary data show a good correlation between TDI displacement and previously described methods of determining arterial elasticity and stiffness such as Peterson's elastic modulus and local arterial compliance. The correlation was less between TDI displacement and markers of systemic compliance including TAC. Interestingly, the relationship between TAC and pulse pressure and TDI displacement and pulse pressure was almost identical, with similar regression coefficients. Subgroup analysis showed that as cardiovascular risk increased TDI displacement became less, with significant differences between all groups. The same analysis comparing Peterson's elastic modulus, local arterial compliance, and TAC between the groups showed similar trends, but with larger standard deviations for the groups and hence, fewer differences between the groups.

Ultrasonic imaging of the carotid arteries is widely used and very feasible and derivation of a carotid TDI-based distensibility coefficient may simplify the assessment of arterial elasticity.

Potentially, patients referred for carotid imaging for measurement of IMT could also have TDI displacement measured as part of their examination.

## Future directions

To date, studies have not been performed comparing TDI displacement with measures obtained using systems such as SphygmoCor (AtCor, Sydney, Australia) for pulse-wave analysis or comparing distensibility coefficient derived by TDI with that derived by echo tracking using either B-mode or M-mode imaging. The use of TDI displacement to serially follow-up patients after interventions such as blood pressure control, lipid control, and exercise intervention has also not been explored. Hopefully, more studies will show that the use of TDI displacement in the clinical setting is simple, feasible, and reproducible and can be used to follow-up patients with and without cardiovascular disease.

## References

- 1 Fathi R, Marwick TH. Noninvasive tests of vascular function and structure: why and how to perform them. *Am Heart J* 2001; **141**: 694–703.
- 2 Haluska BA, Fathi R, Jeffriess L, Leano R, Carlier SG, Marwick TH. Noninvasive tests for arterial structure, function, and compliance: do they identify risk or diagnose disease? *J Am Soc Echocardiogr* 2004; **17**: 195–202.
- 3 Leite-Moreira AF, Correia-Pinto J, Gillebert TC. Afterload induced changes in myocardial relaxation: a mechanism for diastolic dysfunction. *Cardiovasc Res* 1999; **43**: 344–53.
- 4 Kawaguchi M, Hay I, Fetis B, Kass DA. Combined ventricular systolic and arterial stiffening in patients with heart failure and preserved ejection fraction: implications for systolic and diastolic reserve limitations. *Circulation* 2003; **107**: 714–20.
- 5 Chen HH, Lainchbury JG, Senni M, Bailey KR, Redfield MM. Diastolic heart failure in the community: clinical profile, natural history, therapy, and impact of proposed diagnostic criteria. *J Card Fail* 2002; **8**: 279–87.
- 6 O'Rourke MF. From theory into practice: arterial haemodynamics in clinical hypertension. *J Hypertens* 2002; **20**: 1901–15.
- 7 O'Rourke MF. Influence of ventricular ejection on the relationship between central aortic and brachial pressure pulse in man. *Cardiovasc Res* 1970; **4**: 291–300.
- 8 Westerhof N, O'Rourke MF. Haemodynamic basis for the development of left ventricular failure in systolic hypertension and for its logical therapy. *J Hypertens* 1995; **13**: 943–52.
- 9 O'Rourke MF, Kelly RP. Wave reflection in the systemic circulation and its implications in ventricular function. *J Hypertens* 1993; **11**: 327–37.
- 10 O'Rourke MF. Vascular impedance in studies of arterial and cardiac function. *Physiol Rev* 1982; **62**: 570–623.
- 11 Latham RD, Westerhof N, Sipkema P, Rubal BJ, Reuderink P, Murgo JP. Regional wave travel and reflections along the human aorta: a study with six simultaneous micromanometric pressures. *Circulation* 1985; **72**: 1257–69.
- 12 Yano M, Kohno M, Kobayashi S, et al. Influence of timing and magnitude of arterial wave reflection on left ventricular relaxation. *Am J Physiol Heart Circ Physiol* 2001; **280**: H1846–52.
- 13 Buckberg GD, Fixler DE, Archie JP, Hoffman JI. Experimental subendocardial ischemia in dogs with normal coronary arteries. *Circ Res* 1972; **30**: 67–81.
- 14 Safar ME. Systolic blood pressure, pulse pressure and arterial stiffness as cardiovascular risk factors. *Curr Opin Nephrol Hypertens* 2001; **10**: 257–61.
- 15 Abhayaratna WP, Barnes ME, O'Rourke MF, et al. Relation of arterial stiffness to left ventricular diastolic function and cardiovascular risk prediction in patients > or = 65 years of age. *Am J Cardiol* 2006; **98**: 1387–92.
- 16 Saba PS, Roman MJ, Pini R, Spitzer M, Ganau A, Devereux RB. Relation of arterial pressure waveform to left ventricular and carotid anatomy in normotensive subjects. *J Am Coll Cardiol* 1993; **22**: 1873–80.
- 17 Gates PE, Tanaka H, Graves J, Seals DR. Left ventricular structure and diastolic function with human ageing: relation to habitual exercise and arterial stiffness. *Eur Heart J* 2003; **24**: 2213–20.
- 18 Roman MJ, Pickering TG, Schwartz JE, Pini R, Devereux RB. Relation of arterial structure and function to left ventricular geometric patterns in hypertensive adults. *J Am Coll Cardiol* 1996; **28**: 751–6.
- 19 Karamanoglu M, O'Rourke MF, Avolio AP, Kelly RP. An analysis of the relationship between central aortic and peripheral upper limb pressure waves in man. *Eur Heart J* 1993; **14**: 160–7.
- 20 Sharman JE, Holland DJ, Marwick TH. Who are the people that would benefit most from central blood pressure monitoring? *J Hypertens* 2006; **24(S6)**: S171.
- 21 Marchais SJ, Guerin AP, Pannier BM, Levy BI, Safar ME, London GM. Wave reflections and cardiac hypertrophy in chronic uremia. Influence of body size. *Hypertension* 1993; **22**: 876–83.
- 22 Sharman JE, Fang ZY, Haluska B, Stowasser M, Prins JB, Marwick TH. Left ventricular mass in patients with

- type 2 diabetes mellitus is independently associated with central but not peripheral pulse pressure. *Diabetes Care* 2005; **28**: 937–9.
- 23 Weber T, Auer J, O'Rourke MF, et al. Arterial stiffness, wave reflections, and the risk of coronary artery disease. *Circulation* 2004; **109**: 184–9.
  - 24 Weber T, Auer J, O'Rourke MF, Kvas E, et al. Increased arterial wave reflections predict severe cardiovascular events in patients undergoing percutaneous coronary interventions. *Eur Heart J* 2005; **26**: 2657–63.
  - 25 London GM, Blacher J, Pannier B, Guerin AP, Marchais SJ, Safar ME. Arterial wave reflections and survival in end-stage renal failure. *Hypertension* 2001; **38**: 434–8.
  - 26 Safar ME, Blacher J, Pannier B, et al. Central pulse pressure and mortality in end-stage renal disease. *Hypertension* 2002; **39**: 735–8.
  - 27 Kelly RP, Gibbs HH, O'Rourke MF, et al. Nitroglycerin has more favourable effects on left ventricular afterload than apparent from measurement of pressure in a peripheral artery. *Eur Heart J* 1990; **11**: 138–44.
  - 28 Jiang XJ, O'Rourke MF, Jin WQ, et al. Quantification of glyceryl trinitrate effect through analysis of the synthesised ascending aortic pressure waveform. *Heart* 2002; **88**: 143–8.
  - 29 Morgan T, Lauri J, Bertram D, Anderson A. Effect of different antihypertensive drug classes on central aortic pressure. *Am J Hypertens* 2004; **17**: 118–23.
  - 30 Deary AJ, Schumann AL, Murfet H, Haydock S, Foo RS, Brown MJ. Influence of drugs and gender on the arterial pulse wave and natriuretic peptide secretion in untreated patients with essential hypertension. *Clin Sci (Lond)* 2002; **103**: 493–9.
  - 31 Dhakam Z, McEnery CM, Yasmin, Cockcroft JR, Brown MJ, Wilkinson IB. Atenolol and Eprosartan: differential effects on central blood pressure and aortic pulse wave velocity. *Am J Hypertens* 2006; **19**: 214–9.
  - 32 The CAFE Investigators, for the Anglo-Scandinavian Cardiac Outcomes Trial (ASCOT) Investigators, CAFE Steering Committee and Writing Committee, Williams B, Lacy PS, Thom SM, et al. Differential impact of blood pressure-lowering drugs on central aortic pressure and clinical outcomes: principal results of the conduit artery function evaluation (CAFE) study. *Circulation* 2006; **113**: 1213–25.
  - 33 Van Bortel LM, Duprez D, Starmans-Kool MJ, et al. Clinical applications of arterial stiffness, Task Force III: recommendations for user procedures. *Am J Hypertens* 2002; **15**: 445–52.
  - 34 Laurent S, Cockcroft J, Van Bortel L, et al. Expert consensus document on arterial stiffness: methodological issues and clinical applications. *Eur Heart J* 2006; **27**: 2588–605.
  - 35 Sutton-Tyrrell K, Najjar SS, Boudreau RM, et al. Elevated aortic pulse wave velocity, a marker of arterial stiffness, predicts cardiovascular events in well-functioning older adults. *Circulation* 2005; **111**: 3384–90.
  - 36 Shokawa T, Imazu M, Yamamoto H, et al. Pulse wave velocity predicts cardiovascular mortality: findings from the Hawaii-Los Angeles–Hiroshima study. *Circ J* 2005; **69**: 259–64.
  - 37 Meaume S, Benetos A, Henry OF, Rudnicki A, Safar ME. Aortic pulse wave velocity predicts cardiovascular mortality in subjects >70 years of age. *Arterioscler Thromb Vasc Biol* 2001; **21**: 2046–50.
  - 38 Laurent S, Katsahian S, Fassot C, et al. Aortic stiffness is an independent predictor of fatal stroke in essential hypertension. *Stroke* 2003; **34**: 1203–6.
  - 39 Laurent S, Boutouyrie P, Asmar R, et al. Aortic stiffness is an independent predictor of all-cause and cardiovascular mortality in hypertensive patients. *Hypertension* 2001; **37**: 1236–41.
  - 40 Cruickshank K, Riste L, Anderson SG, Wright JS, Dunn G, Gosling RG. Aortic pulse-wave velocity and its relationship to mortality in diabetes and glucose intolerance: an integrated index of vascular function? *Circulation* 2002; **106**: 2085–90.
  - 41 Blacher J, Guerin AP, Pannier B, Marchais SJ, Safar ME, London GM. Impact of aortic stiffness on survival in end-stage renal disease. *Circulation* 1999; **99**: 2434–9.
  - 42 Nichols WW, O'Rourke MF. *McDonald's blood flow in arteries: theoretical, experimental and clinical principles*. 5th ed. London: Hodder Arnold; 2005.
  - 43 Pauca AL, O'Rourke MF, Kon ND. Prospective evaluation of a method for estimating ascending aortic pressure from the radial artery pressure waveform. *Hypertension* 2001; **38**: 932–7.
  - 44 Chen CH, Nevo E, Fetis B, et al. Estimation of central aortic pressure waveform by mathematical transformation of radial tonometry pressure. Validation of generalized transfer function. *Circulation* 1997; **95**: 1827–36.
  - 45 Sharman JE, Lim R, Qasem AM, et al. Validation of a generalized transfer function to noninvasively derive central blood pressure during exercise. *Hypertension* 2006; **47**: 1203–8.
  - 46 Izzo J, Joseph L. Pulse contour analysis and augmentation index: it's time to move beyond cuff blood pressure measurement. *Am J Hypertens* 2005; **18 Suppl 1**: 1–2.
  - 47 Millasseau SC, Patel SJ, Redwood SR, Ritter JM, Chowienczyk PJ. Pressure wave reflection assessed from the peripheral pulse: is a transfer function necessary? *Hypertension* 2003; **41**: 1016–20.

- 48 Chen CH, Ting CT, Nussbacher A, et al. Validation of carotid artery tonometry as a means of estimating augmentation index of ascending aortic pressure. *Hypertension* 1996; **27**: 168–75.
- 49 Pickering TG. New ways of measuring blood pressure. *Am J Hypertens* 2006; **19**: 988–90.
- 50 O'Rourke MF, Staessen JA, Vlachopoulos C, Duprez D, Plante GE. Clinical applications of arterial stiffness: definitions and reference values. *Am J Hypertens* 2002; **15**: 426–44.
- 51 London GM, Pannier B, Guerin AP, Marchais SJ, Safar ME, Cuche JL. Cardiac hypertrophy, aortic compliance, peripheral resistance, and wave reflection in end-stage renal disease. Comparative effects of ACE inhibition and calcium channel blockade. *Circulation* 1994; **90**: 2786–96.
- 52 McVeigh GE, Bratteli CW, Morgan DJ, et al. Age-related abnormalities in arterial compliance identified by pressure pulse contour analysis: aging and arterial compliance. *Hypertension* 1999; **33**: 1392–8.
- 53 Safar ME, London GM. Arterial and venous compliance in sustained essential hypertension. *Hypertension* 1987; **10**: 133–9.
- 54 Rajkumar C, Cameron JD, Christopidis N, Jennings GL, Dart AM. Reduced systemic arterial compliance is associated with left ventricular hypertrophy and diastolic dysfunction in older people. *Am Geriatr Soc* 1997; **45**: 803–8.
- 55 Benetos A, Safar M, Rudnichi A, Smulyan H, Richard JL, Ducimetiere P, Guize L. Pulse pressure: a predictor of long-term cardiovascular mortality in a French male population. *Hypertension* 1997; **30**: 1410–5.
- 56 Franklin SS, Khan SA, Wong ND, Larson MG, Levy D. Is pulse pressure useful in predicting risk for coronary heart disease? The Framingham heart study. *Circulation* 1999; **100**: 354–60.
- 57 Kass DA, Saeki A, Tunin RS, Recchia FA. Adverse influence of systemic vascular stiffening on cardiac dysfunction and adaptation to acute coronary occlusion. *Circulation* 1996; **93**: 1533–41.
- 58 Stergiopoulos N, Meister JJ, Westerhof N. Evaluation of methods for estimation of total arterial compliance. *Am J Physiol* 1995; **268**: H1540–8.
- 59 Gatzka CD, Cameron JD, Kingwell BA, Dart AM. Relation between coronary artery disease, aortic stiffness, and left ventricular structure in a population sample. *Hypertension* 1998; **32**: 575–8.
- 60 Herrington DM, Kesler K, Reiber JC, et al. Arterial compliance adds to conventional risk factors for prediction of angiographic coronary artery disease. *Am Heart J* 2003; **146**: 662–7.
- 61 Syeda B, Gottschauner-Wolf M, Denk S, Pichler P, Khorsand A, Glogar D. Arterial compliance: a diagnostic marker for atherosclerotic plaque burden? *Am J Hypertens* 2003; **16**(Pt 1): 356–62.
- 62 Kingwell BA. Large artery stiffness: implications for exercise capacity and cardiovascular risk. *Clin Exp Pharmacol Physiol* 2002; **29**: 214–7.
- 63 Kingwell BA, Waddell TK, Medley TL, Cameron JD, Dart AM. Large artery stiffness predicts ischemic threshold in patients with coronary artery disease. *J Am Coll Cardiol* 2002; **40**: 773–9.
- 64 Haluska BA, Matthys K, Fathi R, Rozis E, Carlier SG, Marwick TH. Influence of arterial compliance on presence and extent of ischaemia during stress echocardiography. *Heart* 2006; **92**: 40–3.
- 65 Sesso HD, Meir J, Stampfer BR, et al. Systolic and diastolic blood pressure, pulse pressure and mean arterial pressure as predictors of cardiovascular disease risk in men. *Hypertension* 2000; **36**: 801–7.
- 66 Cameron JD, Gatzka CD, Kingwell, BA. Assessment of large artery function. *Coron Artery Dis* 2002; **13**: 405–13.
- 67 O'Rourke M, Staessen J. Clinical applications of arterial stiffness: definitions and reference values. *Am J Hypertens* 2002; **15**: 426–44.
- 68 O'Rourke MF, Pauca A, Jiang X-J. Pulse wave analysis. *Br J Clin Pharmacol* 2001; **51**: 507–22.
- 69 Chen CH, Nevo E, Fetis B, et al. Estimation of central aortic pressure waveform by mathematical transformation of radial tonometry pressure. Validation of generalized transfer function. *Circulation* 1997; **95**: 1827–36.
- 70 Segers P, Carlier SG, Pasquet A, et al. Individualizing the aorto-radial pressure transfer function: feasibility of a model-based approach. *Am J Physiol Heart Circ Physiol* 2000; **279**: H542–49.
- 71 Van Bortel LM, Balkstein EJ, van der Heijden-Spek JJ, et al. Non-invasive assessment of local arterial pulse pressure: comparison of applanation tonometry and echo-tracking. *J Hypertens* 2001; **19**: 1037–44.
- 72 Brands PJ, Hoeks AP, Willigers J, Willekes C, Reneman RS. An integrated system for the non-invasive assessment of vessel wall and hemodynamic properties of large arteries by means of ultrasound. *Eur J Ultrasound* 1999; **9**: 257–66.
- 73 Meinders JM, Hoeks AP. Simultaneous assessment of diameter and pressure waveforms in the carotid artery. *Ultrasound Med Biol* 2004; **30**: 147–54.
- 74 Selzer RH, Mack WJ, Lee PL, Kwong-Fu H, Hodis HN. Improved common carotid elasticity and intima-media thickness measurements from computer analysis of sequential ultrasound frames. *Atherosclerosis* 2001; **154**: 185–93.
- 75 Arnett DK, Chambliss LE, Kim H, Evans GW, Riley W. Variability in ultrasonic measurements of arterial

- stiffness in the Atherosclerosis Risk in Communities study. *Ultrasound Med Biol* 1999; **25**: 175–80.
- 76 Gamble G, Zorn J, Sanders G, MacMahon S, Sharpe N. Estimation of arterial stiffness, compliance, and distensibility from M-mode ultrasound measurements of the common carotid artery. *Stroke* 1994; **25**: 11–16.
- 77 Pannier BM, Avolio AP, Hoeks A, Mancia G, Takazawa K. Methods and devices for measuring arterial compliance in humans. *Am J Hypertens* 2002; **15**: 743–53.
- 78 Ramnarine KV, Hartshorne T, Sensier Y, et al. Tissue Doppler imaging of carotid plaque wall motion: a pilot study. *Cardiovasc Ultrasound* 2003; **1**: 17.
- 79 Nichols WW, O'Rourke M. *McDonald's blood flow in arteries. Theoretical, experimental and clinical principles*. 4th ed. London: Arnold; 1998. p. 453–76.

# Future applications of speckle tracking echocardiography

Jing Ping Sun

## Introduction

In recent years, quantitative ultrasound tools have been developed, based on leading-edge technologies such as tissue velocity imaging (TVI), tissue tracking, strain, and strain rate imaging, as well as tissue synchronization imaging. These well-established Doppler-based techniques [1–5] provide precise, quantitative measurement of regional wall motion and function, while adding new parametric imaging displays. Applications include studies of regional function, stress echocardiography, diastolic function analysis, cardiomyopathy, cardiac resynchronization imaging, and more. However, Doppler-based techniques are limited due to the angle dependence of the signal. As a result, certain myocardial areas are excluded. For example, the apex in the apical views, as well as large portions of the myocardium in the parasternal views and especially the short-axis views.

Until now, only magnetic resonance imaging (MRI) could provide full, two-dimensional (2-D) motion analysis through tracking of magnetic tags [6,7]. However, MRI is not widely available for clinical use because it is expensive and time consuming. Other limitations include relatively low spatial (~2–5 mm) and temporal resolution (at best ~30 msec) of the magnetic tags, difficulties in analyzing the entire cardiac cycle due to the short persistence of the tagging, and its inability to analyze beat-to-beat variability.

## Introducing speckle tracking (two-dimensional strain): tagged echocardiography

### Advanced research applications for quantitative echocardiography

Speckle tracking is a unique, advanced research tool in quantitative echocardiography and includes the

latest breakthroughs in strain and strain rate imaging. It is based on similar principles that are used with tagged MRI. One of the main differences is that, instead of using external, short-lived magnetic tags, 2-D strain uses inherent features (natural acoustic markers) for frame-to-frame tracking of the myocardial tissue.

In addition to providing 2-D motion analysis similar to MRI tagging, 2-D strain offers the same favorable properties as other echocardiographic techniques: high spatial and temporal resolution, wide availability, affordability and safety. 2-D strain is a natural extension of 1-D motion analysis provided by TVI. When tissue Doppler data are available through TVI scans, 2-D strain complements that of TVI to increase sensitivity. This benefit is especially useful in cases of high fixed-pattern noise interference (extremely high clutter). The 2-D strain technique applies our experience with pathophysiology and clinical applications from tissue Doppler and tagged MRI studies.

## Two-dimensional strain: measuring myocardial deformation by natural acoustic tagging

Two-dimensional strain is a unique imaging mode that allows objective analysis of the complete myocardial motion throughout the entire heart cycle. Similar in concept to MRI tagging, 2-D strain analyzes motion by tracking tags in the ultrasonic image in two dimensions. These natural acoustic markers are used in a way similar to the magnetic tags in MRI. As with tagged MRI, the tags are short-lived; one cannot expect the natural acoustic markers to persist throughout the entire cardiac cycle, mainly due to their movement in and out of the imaging plane. However, unlike MRI in which

the entire tagging fades out and limits the analysis time to only part of the heart cycle, ultrasound's new acoustic markers keep coming in as some of the previous markers fade out.

Myocardial motion and velocities are then analyzed by calculating frame-to-frame changes. The 2-D strain mode is also a natural extension of 1-D motion analysis, which is based solely on Doppler techniques. It is, however, based on regular 2-D gray-scale imaging, or a combination of gray-scale and Doppler data (TVI).

Similar to 1-D Doppler, myocardial motion is characterized in terms of tissue velocity and tissue deformation parameters, such as strain and strain rate. One of the main advantages of this technique is that it allows the region of interest (ROI) to be automatically tracked in the myocardium. This ability excludes spurious signals from the intra-cavity blood pool and provides additional information on myocardial motion, shortening the postprocessing workload compared to methods requiring manual tracking (e.g., tissue Doppler), and enhancing its day-to-day clinical practicality.

However, 2-D strain is image quality-dependent. That is why the application is limited to raw data images, whose outstanding image quality for all types of patients allows for meaningful analysis in nearly 90% of the segments [8]. The two main issues that adversely affect 2-D strain for difficult patients include clutter and "speckle noise." Under these circumstances, the 2-D strain algorithm optimally trades off resolution to gain noise reduction.

Another new important feature of 2-D strain is a built-in quality assurance tool that automatically evaluates the reliability of the results. The key focus of 2-D strain is to improve tracking on difficult patients, minimizing the tracking of "well-developed speckles" and looking instead for larger and/or brighter structures in the image, which usually result from structures in the myocardium that are large relative to the system resolution. The motion of these structures in the image represents the motion of the corresponding objects within the myocardium. Furthermore, the motion of these objects will be relatively smooth in time. The temporal and spatial smoothness of the myocardial motion, as well as the cross-correlation of the corresponding images between successive frames, form the basis for the automatic tracking scoring system.

This system is mainly based on the cross-correlation between corresponding areas in successive frames, as well as on the variability of velocities in small-tissue areas. In the case of high clutter noise, the system automatically avoids tracking speckles, focusing instead on larger tissue structures for tracking, making the tracking more robust than the traditional "speckle tracking."

### **Parametric imaging**

One of the major achievements in 2-D strain is the ability to include the entire myocardium for quantitative evaluation. Coupling this advantage with the previously validated and published indices of TVI, 2-D strain offers new tools for a more comprehensive analysis. For example, in cases where TVI Doppler has been applied, 2-D strain can also be applied to increase the sensitivity. Beyond obvious indices, such as peak strain, end-systolic strain, or peak strain rate, and so on, which have been tested in a variety of clinical applications [9–13] more sophisticated and less obvious indices have been proposed and evaluated clinically using TVI. Kukulski et al. [9,14] proposed the postsystolic strain index (PSI) for the identification of acutely ischemic myocardium. Abraham et al. [15] proposed time-to-zero strain rate (which is equivalent to time-to-peak strain) as an index for detection of ischemia during dobutamine stress echocardiography. In addition to the automatic ROI tracking feature, 2-D strain instantly allows the computation of almost any desired index at all myocardial points simultaneously, even without requiring patients to hold their breath as with tagged MRI.

Presentation of the results at all myocardial points throughout the entire heart cycle could be a problem because of the huge amount of data involved. The solution to this problem is to display the results graphically as a "parametric image." In this type of presentation, a color map is assigned to the desired index, which is then displayed as an overlay on the anatomic image. Examples of longitudinal parametric images (from apical views) are provided below.

### **Built-in quality assurance**

The myocardium is divided into six segments: basal septal, mid-septal, apical septal, apical lateral, mid-lateral, and basal lateral, closely following

Automated Software Engineering convention. Built-in automatic validation and verification are essential for a reliable diagnosis. The 2-D strain algorithm automatically evaluates the tracking quality at each myocardial location over time and provides a score that represents the quality of the tracking. The user can additionally validate the score by visual comparison of the tracking (position represented as red dots in the image) to the actual motion of the tissue. In Figure 26.1, the ROI is automatically divided into six segments. The software automatically evaluates tracking quality in each segment and provides a score ranging from 1 (excellent) to 3 (unacceptable) (Figure 26.2; Video clip 31 .

**Longitudinal velocity (cm/sec):** The left ventricular (LV) longitudinal segmental velocity curve in a young and an old normal subject showing the E/A ratio changes with age (Figure 26.3A and B).

**Longitudinal strain rate (1/sec):** The LV longitudinal segmental strain rate curves of normal young and old subjects show that the E/A ratio changes with age (Figure 26.4a and b). Furthermore, compared with a normal subject, the longitudinal segmental strain rate is not synchronized during the systolic and diastolic period in a patient with LV hypertrophy, a finding demonstrated well by M-mode and tracing curves (Figures 25.5A and B and 25.6; Video clip 32 .

**Longitudinal displacement (mm):** The LV longitudinal displacement is each segment displaced distance during systole, which provides us an objective tool to estimate segmental systolic function. The moving distance is decreased from basal to apical

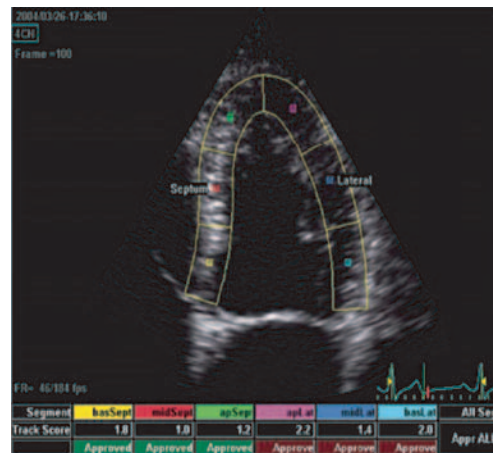


**Figure 26.1** Automatic-tracking quality scoring in an apical 4 chamber view of the left ventricle. The myocardium is divided into six segments: basal septal, mid septal, apical septal, apical lateral, mid lateral and basal lateral, closely following ASE convention.



**Figure 26.2** Longitudinal strain (%) from apical 4-chamber view in a normal subject. See also Video clip 31 .

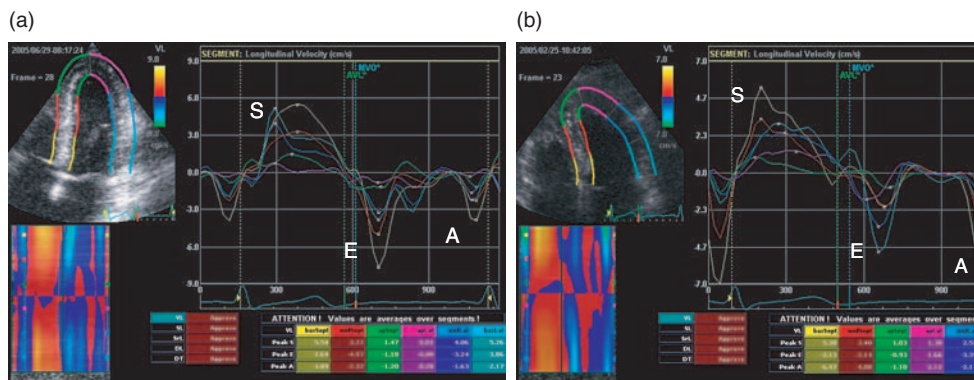


**Figure 26.3** (A) Normal velocity, female, 28 years old (E/A > 1). (B) Normal velocity, female, 60 years old (E/A < 1).

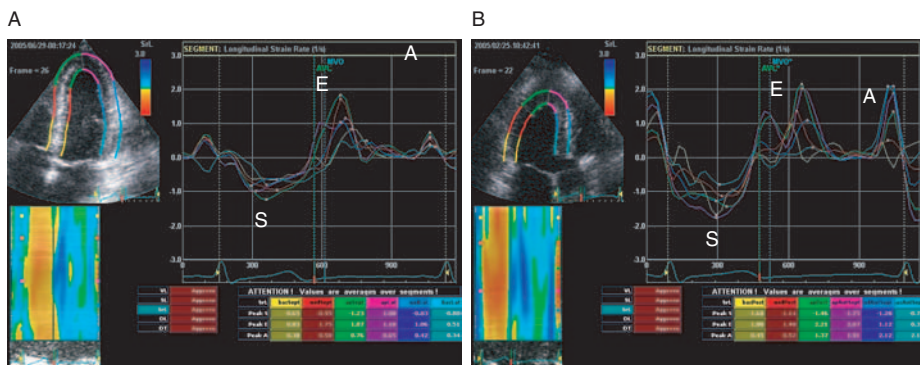


Figure 26.4 (A) Normal strain rate, female, 28 years old ( $E/A < 1$ ). (B) Normal strain rate, female, 60 years old ( $E/A=1$ ).

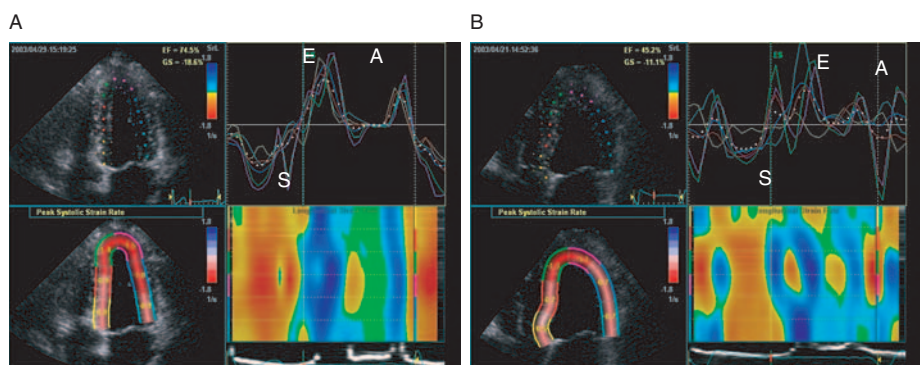


Figure 26.5 (A) Normal strain rate. (B) Pathological strain rate in a patient with LV hypertrophy.

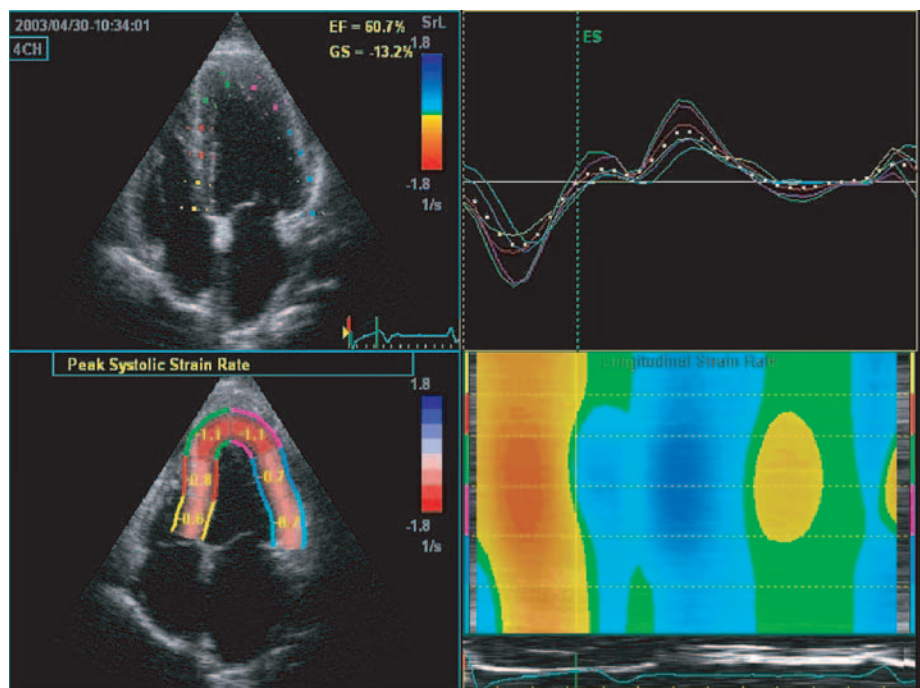


Figure 26.6 Longitudinal strain rate (1/sec) in a normal subject. See also Video clip 32

segments in normal subject (Figure 26.7). We can obtain the bull's eye graphic to demonstrate the segmental displacement by analyzing two-, three-, and four-chamber views automatically. The pattern of segmental displacement in normal, myocardial infarction in left anterior descending coronary artery (LAD), left circumflex coronary artery (LCX), and right coronary artery (RCA) territories are shown in Figure 26.8A–D.

**Transverse displacement (mm):** The amplitude and direction (inward/outward) of the wall motion (transverse displacement) have long been recognized as important markers of ischemia, and are, in fact, some of the most common motion attributes used in “eyeballing” to evaluate function. An automatic tissue tracking feature also facilitates the automatic position tracking of the central line along the myocardium on a frame-by-frame basis. This results are an accurate, objective method to quantify excursion, measuring the local amount and direction of the inward/outward motion of the cardiac wall during systole.

This index is similar to the edge detection-based method [16], except that, in 2-D strain, the computation is based on tissue tracking combined with tissue Doppler, which we believe to be more robust, as

edges are much more image quality-dependent and tend to disappear in some of the frames. Similar to “tissue tracking,” this index represents a time integral of the velocity and is, therefore, expected to be robust and relatively immune to noise.

The peak segmental transverse displacement amplitude is higher and occurs at the same time (synchronous) of end-systole from tracing curve and M-mode in a normal subject (Figure 26.9a). The displacement amplitude is lower and does not occur at the same time (asynchronous) in a patient with LV hypertrophy (Figure 26.9b).

**Peak longitudinal strain (%):** The LV global and segmental amplitude of peak longitudinal strain can be measured and represents the LV global and segmental systolic function. In this example, the peak longitudinal systolic strain value is high and synchronized from the M-mode and tracing curves in a normal subject (Figures 25.2 and 25.10a), but the value is very low and asynchronous in a patient with dilated cardiomyopathy (Figures 25.10b, 25.11, and 25.12; Video clips 33–35 ).

The author performed a study in which the global strain was measured in 49 patients with cardiomyopathies of different etiologies and 44 normal subjects. The results indicated the global strain

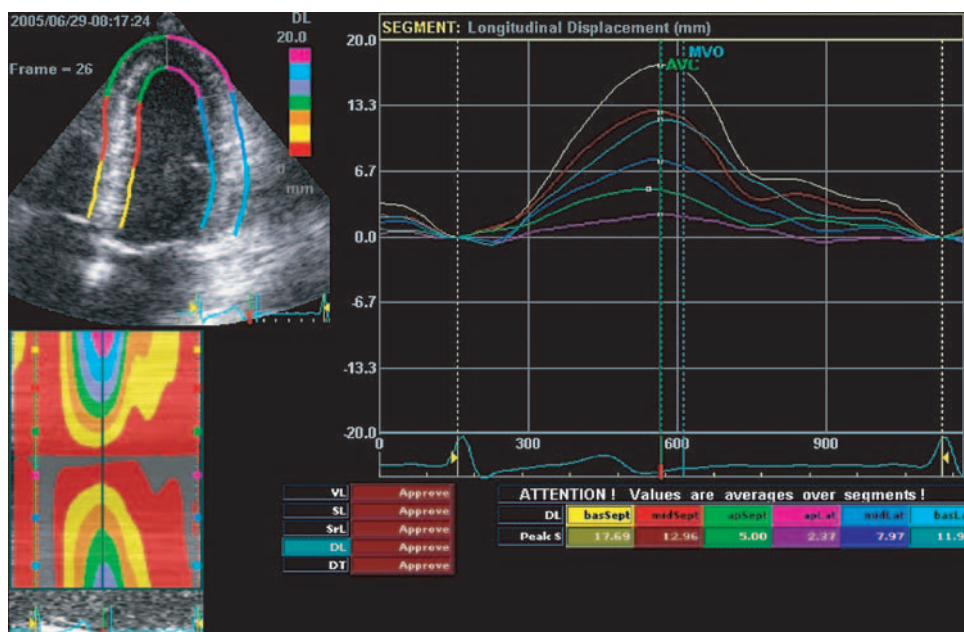
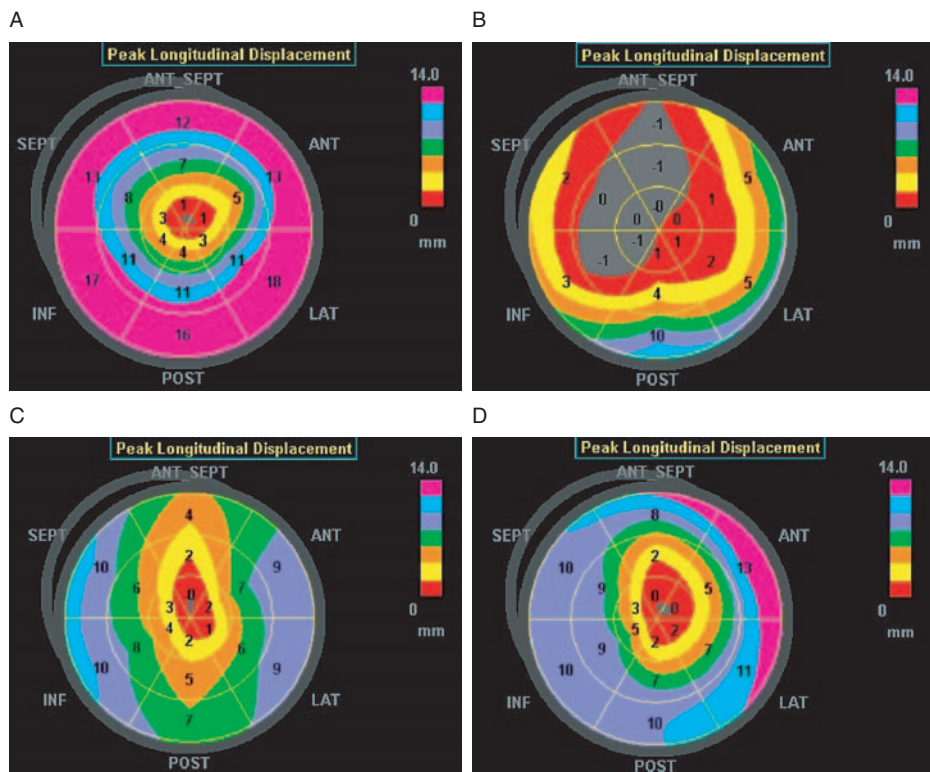
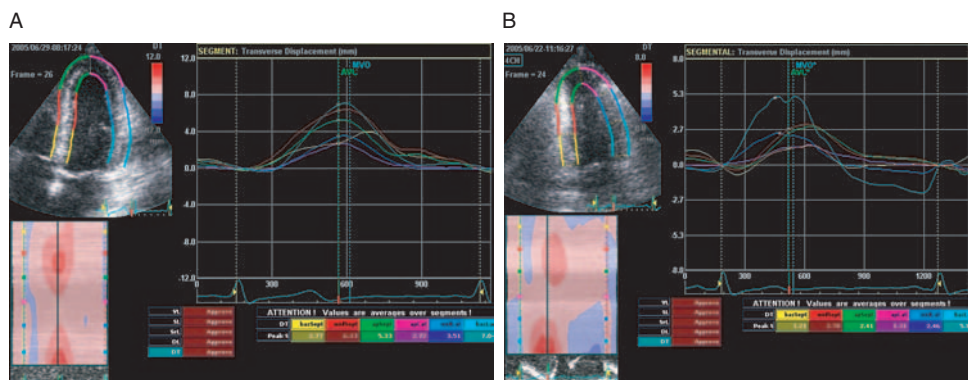


Figure 26.7 Longitudinal displacement in a normal subject.



**Figure 26.8** (A) Normal. (B) LAD territory infarction. (C) LCX territory infarction. (D) RCA territory infarction.



**Figure 26.9** (A) Transverse displacement in a normal subject. (B) Transverse displacement in a patient with LV hypertrophy.

was >15% in normal subjects; all the patients with cardiomyopathic disease had <15%, except patients with secondary LV hypertrophy due to hypertension (Figure 26.13).

The time-to-peak systolic strain also can be used as an index of synchrony of myocardial contraction. This is clearly shown in Figure 26.14;

A is normal, B is a myocardial infarction in the LAD, C is in the LCX, and D in the RCA territory. The example of a heart failure case with cardiac resynchronization therapy (CRT) before (A) and after (B) CRT on is shown in Figure 26.15.

Regional delay in the onset of myocardial motion is an important marker of ischemia, in addition

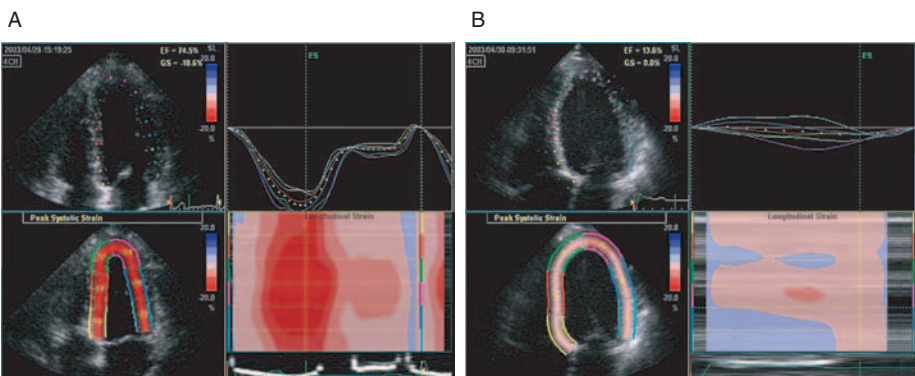


**Figure 26.10** (A) Longitudinal strain in a normal subject. (B) Longitudinal strain in a patient with dilated cardiomyopathy. See also Video clip 33

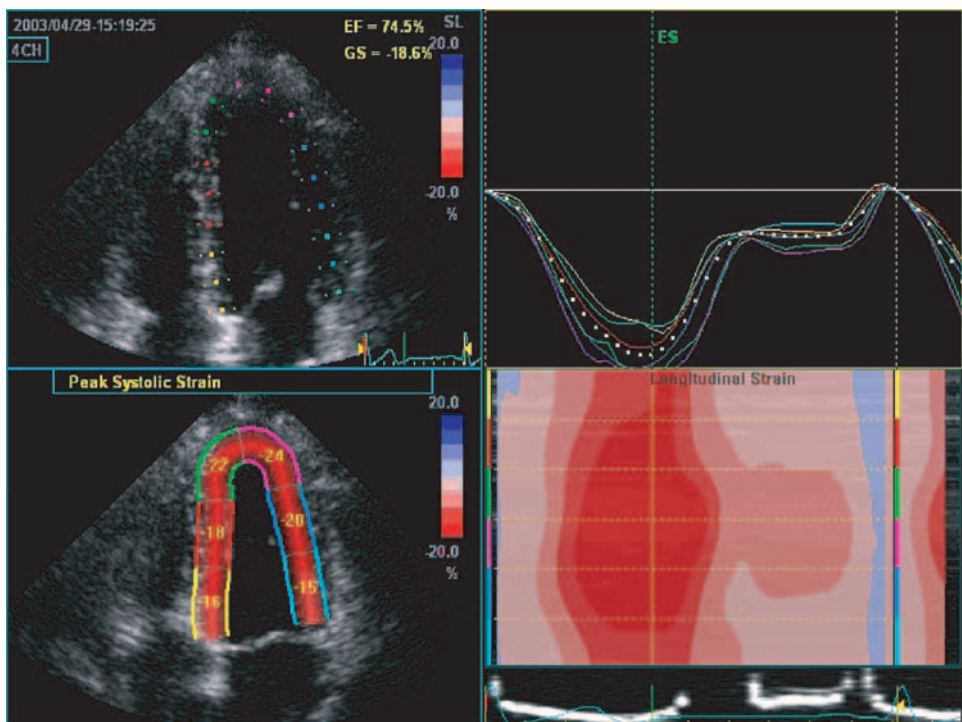


**Figure 26.11** Longitudinal strain from apical 4-chamber view in a normal subject. See also Video clip 34

to regional wall thickening and thinning characteristics, and the amplitude and direction of the wall motion. This regional delay has been shown to precede changes in regional myocardial systolic amplitude of motion [17], and the visual detection of small differences in regional asynchrony is poor [18]. An interesting regional myocardial parameter based on timing, with respect to electrocardiography, was successfully applied from animal models

to clinically demonstrate regional asynchrony in the presence of resting and induced ischemia [15,19,20]. The time from the R-wave on electrocardiography, to transition from regional systole to early diastolic lengthening (TR), was attenuated with acute ischemia. Normally, the mean TR of the mid-segments was shorter than in the apical or basal segments. During dobutamine stress, the normally detected TR change from baseline

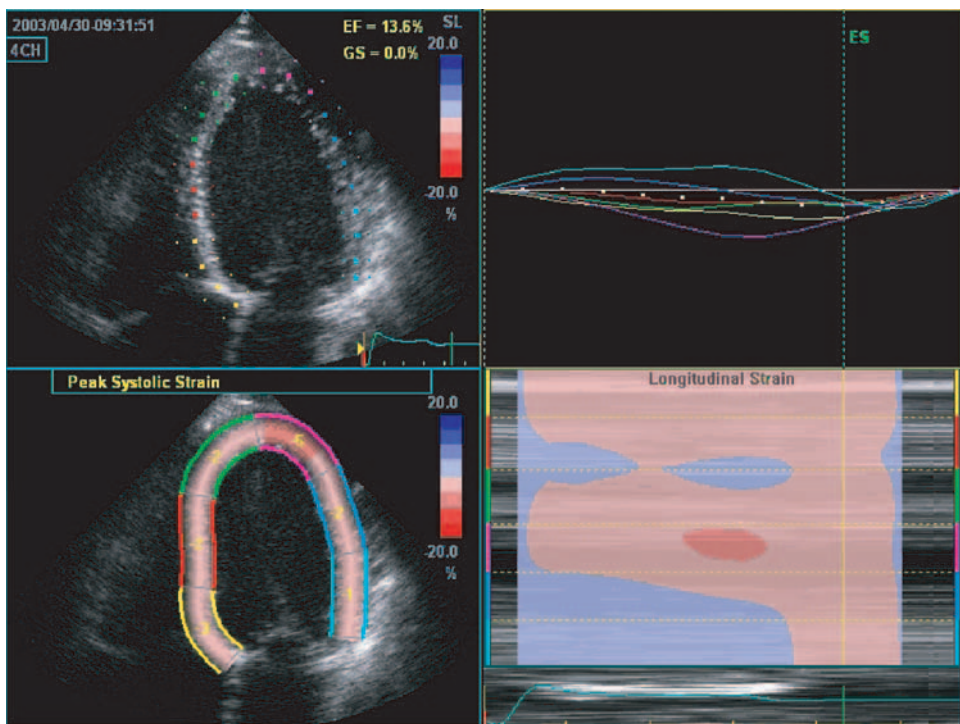


Figure 26.12 Longitudinal strain (%) in a patient with dilated cardiomyopathy. See also Video clip 35

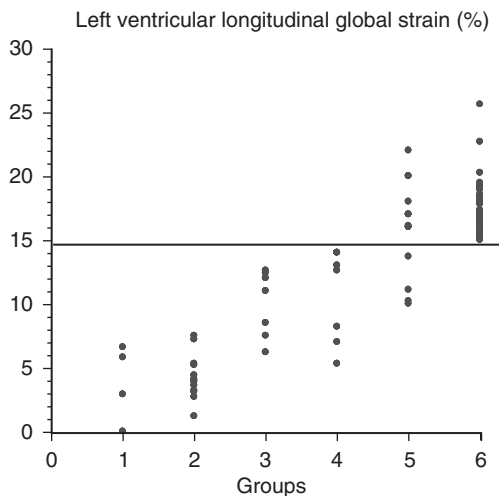


Figure 26.13 Comparison of LV longitudinal strain in normal and different pathological hearts. Group 1: Amyloid Cardiomyopathy ( $n = 4$ ), Group 2: Congestive heart failure ( $n = 13$ ), Group 3: Coronary artery disease with cardiac infarction ( $n = 8$ ), Group 4: Hypertrophic cardiomyopathy ( $n = 8$ ), Group 5: Hypertrophy due to hypertension ( $n = 16$ ), and Group 6: normal ( $n = 44$ ). Group 6 vs. Group 1,2,3,4,  $P < 0.0001$ ; Group 6 vs. Group 5,  $P = 0.1$ . The left ventricular global strain was lower than 15% in patients with all of cardialmyopathy.

was blunted in ischemic segments. In a TVI-based study, Abraham et al. showed a change of >20% in TR patients identified ischemia during dobutamine stress, with a sensitivity of 92% and a specificity of 75% [15]. The method has since been restricted to zones accessible with TVI, due to Doppler limitations. The 2-D strain could potentially extend the utility of the method, and allow a comprehensive study of the entire myocardium in apical views (to which TVI is usually applied), as well as in short-axis views.

Post-systolic compression (PSC) is an abnormality in the onset of early relaxation. Although the underlying mechanism of PSC has not been completely elucidated, experimental animal models suggest that PSC is also a marker for the potential recovery of function after reperfusion [21]. A timely onset of diastolic relaxation requires the uptake of cytoplasmic calcium by the sarcoplasmic reticulum, which is an energy-demanding process. Alteration of this active process is an established predictor of myocardial dysfunction at the level of the myocyte metabolism [22–24]. At the tissue

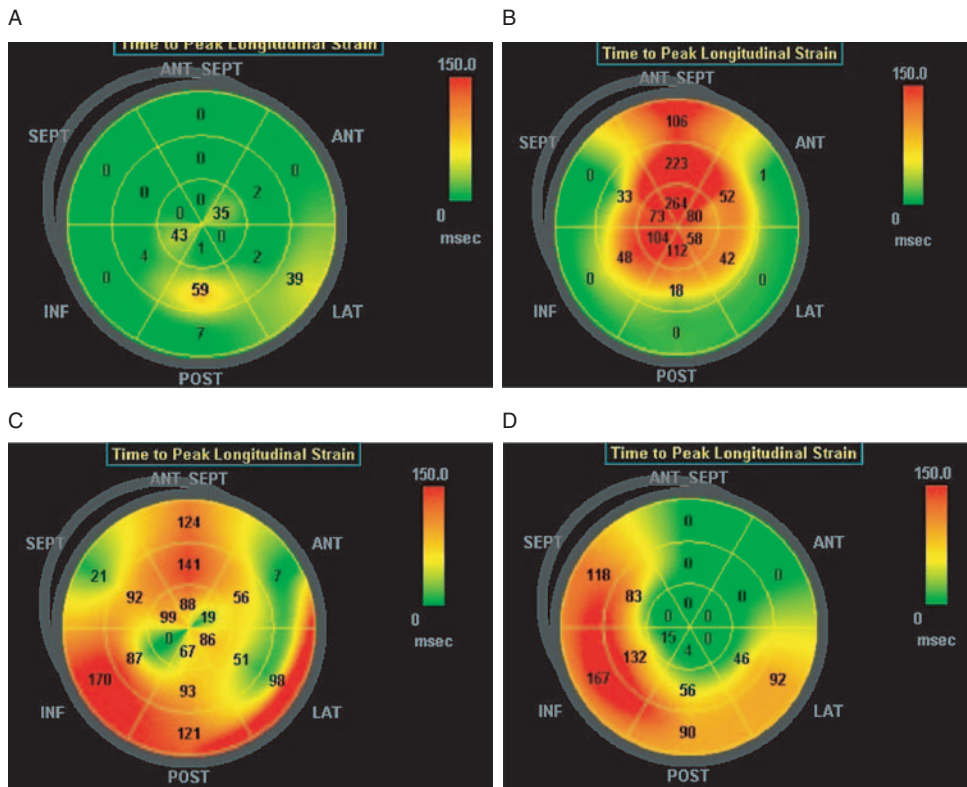


Figure 26.14 (A) Normal. (B) LAD Territory Infarction. (C) LCX Territory Infarction. (D) RCA Territory Infarction.

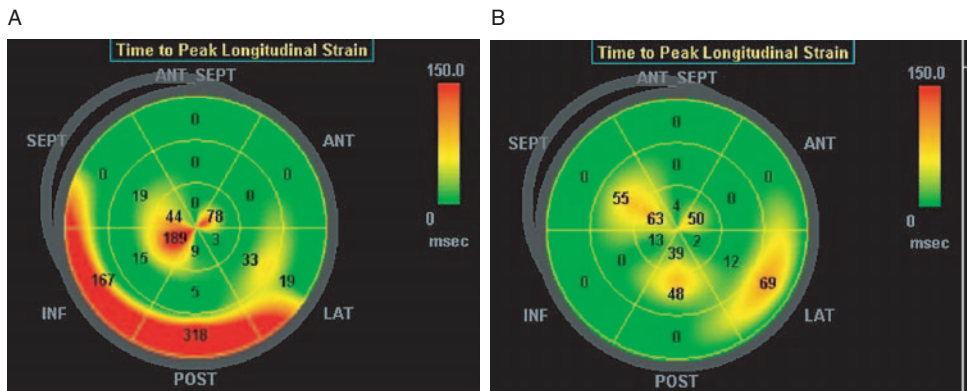


Figure 26.15 The time to peak strain was delay at basal inferior and posterior wall when CRT off (A) in a patient with heart failure treated with bi-pacing therapy; the time to peak strain were synchronized after CRT on (B).

level, regional myocardial asynchrony characterizes these diastolic functional abnormalities, which are known to occur during acute ischemia, even in the absence of changes in systolic function [25,26]. Therefore, quantitative temporal and spatial assessment of PSC could be an early measurable

indicator of ischemic yet viable myocardium. Kukulski et al. [9,14] have defined the PSI as a marker that combines systolic and early diastolic deformation values as a quantitative measure of PSC. ( $\text{PSI} = [\text{E}_{\text{PEAK}} - \text{E}_{\text{SYS}}]/\text{E}_{\text{PEAK}}$ ). They found that PSI had a sensitivity of 95% and a specificity of 89%

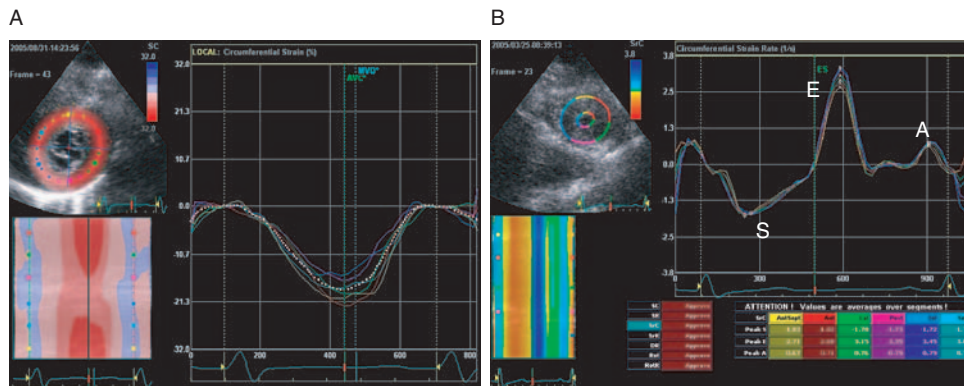


Figure 26.16 Circumferential strain (%), A) and circumferential strain rate (1/sec), B) from a normal subject.

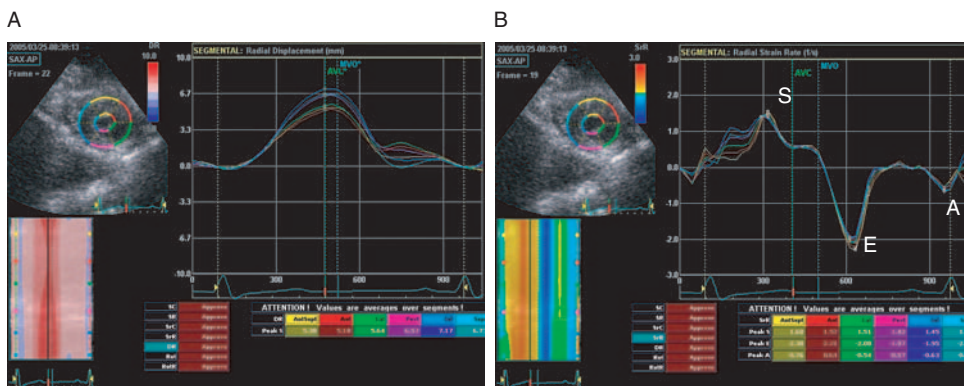


Figure 26.17 Radial strain (%), A) and radial strain rate (1/sec), B) from a normal subject.

in the identification of acutely ischemic segments during coronary occlusion. Voigt et al. [26,27] have shown that this index defines stress-induced ischemia in DSE with a sensitivity and specificity of 86% and 89%, respectively, compared to perfusion scintigraphy as a “gold standard.”

Examples of radial and circumferential parametric images (from short-axis views) are provided.

**Circumferential strain (%) and circumferential strain rate (1/sec):** The examples are from a normal subject (Figure 26.16a and b).

**Radial strain (%) and radial strain rate (1/sec):** The examples are from a normal subject (Figure 26.17a and b).

**Radial displacement (mm):** The example of peak radial displacement is synchronized from the M-mode and the traced curve in a normal subject (Figure 26.18a). The radial displacements of mid inferior and posterior segments were very

low in a patient with coronary artery disease (Figure 26.18b inferior–posterior infarction)

The author performed an experiment using animal models [28]. Seven pigs, body weight 22–25 kg, were subjected to myocardial infarction by occlusion of the LAD and followed up for 8 weeks. Regional radial and circumferential deformations were quantified noninvasively by ultrasonic strain-rate imaging before LAD occlusion, immediately at LAD occlusion, and 4, 6, and 8 weeks after LAD occlusion. Strain-based left ventricular torsion was assessed at the same time points. The radial and circumferential strains as well as radial displacement were decreased significantly in the LAD-territory areas due to myocardial ischemia and infarction. There were no significant changes in both radial and circumferential strains as well as radial displacement in the areas of adjacent and remote zones over time (see Table 26.1, Figure 26.19a and b). These findings demonstrate

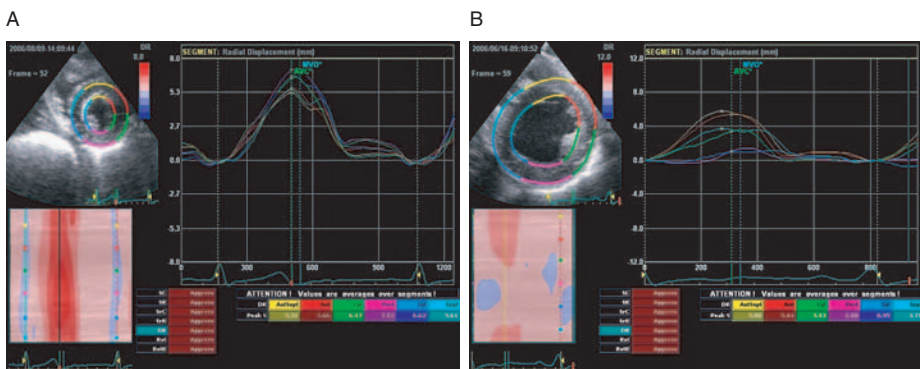


**Figure 26.18** Radial displacement (mm) in a normal subject (A) and in a patient with inferior and posterior infarction (B).

**Table 26.1** Seven pigs were subjected to myocardial infarction (MI) by occlusion of the left anterior descending coronary artery (LAD) and followed up for 8 weeks.

	Circumferential Strain (%)			Radial Strain (%)			Radial Displacement (cm)		
	RCA	LAD	LCX	RCA	LAD	LCX	RCA	LAD	LCX
Baseline	15±3	13±3	11±4	34±17	31±16	44±24	3.9±1.3	2.9±0.8	4.3±1.2
AMI	12±4	7±2**	9±3	32±16	12±7**	27±12	4±1.4	1.4±0.6**	2.9±0.8*
4 weeks	13±4	7±2**	11±2	20±11	17±4*	25±16	3.6±1.6	1.8±0.7*	4.2±1.3
6 weeks	15±3	6±2**	13±6	33±10	14±4*	33±7	1.3±1.3	1.7±0.4**	5±2
8 weeks	13±3	6±1.6**	10±5	21±13	13±6*	25±11	3.4±1.9	1.3±1*	3.4±1.9

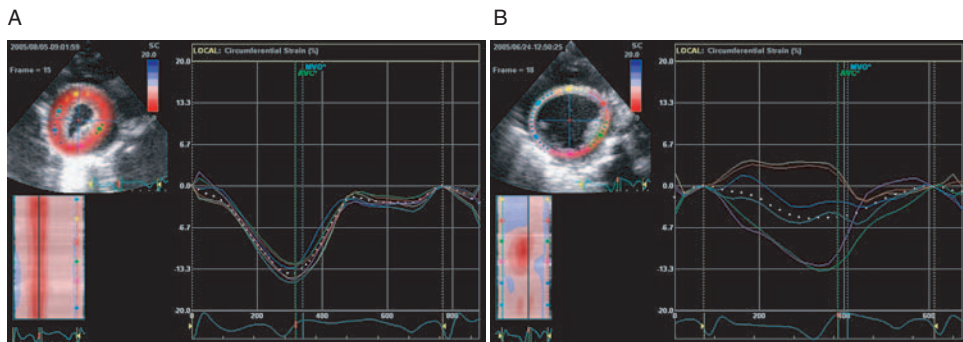


**Figure 26.19** Circumferential strain (%) baseline (A) compared with MI (B) anterior and anteroseptal segments were significantly decreased.

that speckle-tracking using tissue Doppler strain imaging may be suitable for noninvasive quantification of left ventricular segmental function in ischemic heart disease.

#### Rotation (degrees) and Rotation Rate (degrees/sec):

Cardiac contraction is very complex in nature, and involves twisting and untwisting of the helically wrapped myocardial fibers during contraction and relaxation. The 2-D strain is a natural

tool for measuring torsion, which is defined as the difference in rotation of the apical and basal short-axis LV planes. The ability of 2-D strain to process short-axis views in real time is key to its ability to measure torsion.

Oblique views of the muscle surface combined with the new 2-D strain method provide an improved delineation of torsion and twist in a heart muscle model [29]. During the cardiac cycle, there

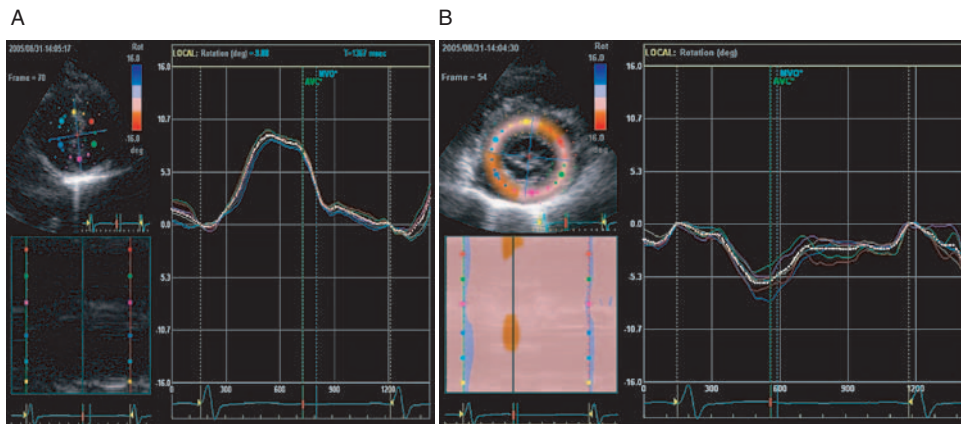


Figure 26.20 (A) Rotation (deg) of apical level in a normal subject. (B) Rotation (deg) of mitral level in a normal subject.

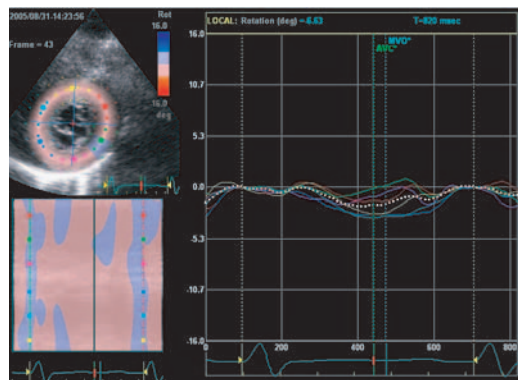


Figure 26.21 Rotation at mitral level from a patient with dilated cardiomyopathy.

is a systolic twist and an early diastolic untwist of the LV about its long axis because of oppositely directed apical and basal rotations. As viewed from the LV apex, systolic apical rotation is counterclockwise and basal rotation, clockwise (Figure 26.20A and B). The systolic rotation is significantly lower in a patient with dilated cardiomyopathy (Figure 26.21). An example of rotation rates from the mitral and apical levels in a normal subject are shown in Figure 26.22A and B. The rotation and rotation rates from a patient with dilated cardiomyopathy are significantly lower than in a normal subject (Figure 26.23A and B).

The 2-D strain technique has been tested and validated both technically and clinically [30–36]. This new technique should be used widely in clinical practice and research.

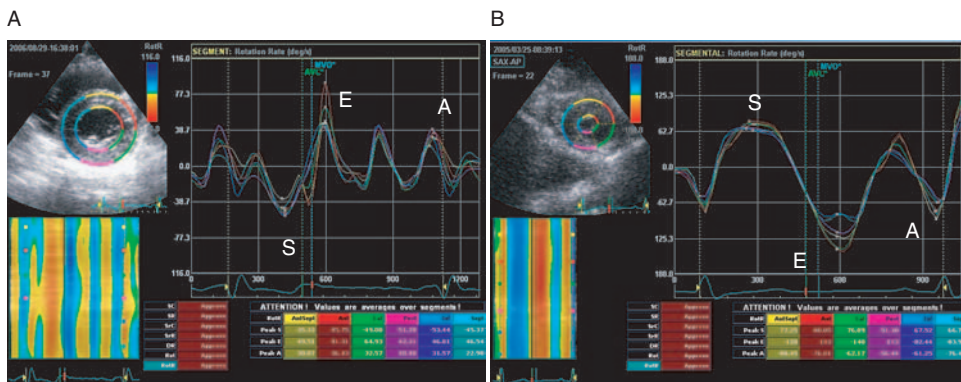
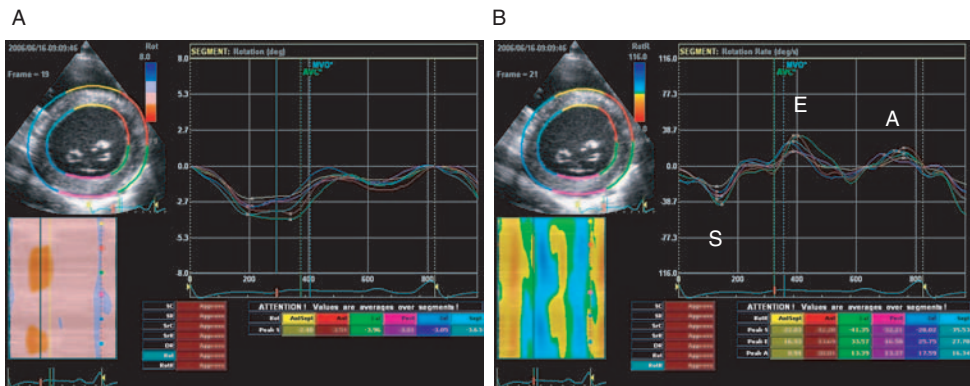


Figure 26.22 (A) Rotation Rate (deg/s) from mitral level. (B) Rotation Rate (deg/s) from apical level.



**Figure 26.23** (A) Rotation (deg) from mitral level in a patient with cardiomyopathy. (B) Rotation rate (deg/s) from mitral level in a patient with cardiomyopathy.

## References

- Sutherland GR, Di Salvo G, Claus P, D'hooge J, Bijnens B. Strain and strain rate imaging: a new clinical approach to quantifying regional myocardial function. *J Am Soc Echocardiogr* 2004; **17**: 788–802.
- Voigt JU, Flachskampf FA. Strain and strain rate: new and clinically relevant echo parameters of regional myocardial function. *Z Kardiol* 2004; **93**: 249–58.
- Yip G, Abraham T, Belohlavek M, Khandheria BK. Clinical applications of strain rate imaging. *J Am Soc Echocardiogr* 2003; **16**: 1334–42.
- Pislariu C, Abraham TP, Belohlavek M. Strain and strain rate echocardiography. *Curr Opin Cardiol* 2002; **17**: 443–54.
- D'hooge J, Heimdal A, Jamal F, et al. Regional strain and strain rate measurements by cardiac ultrasound: principles, implementation and limitations. *Eur J Echocardiogr* 2000; **1**: 154–70.
- Castillo E, Lima JA, Bluemke DA. Regional myocardial function: advances in MR imaging and analysis. *Radiographics* 2003; **23 Spec No**: S127–40.
- Moore CC, McVeigh ER, Zerhouni EA. Quantitative tagged magnetic resonance imaging of the normal human left ventricle. *Top Magn Reson Imaging* 2000; **11**: 359–71.
- Notomi Y, Setser RM, Shiota T, et al. Assessment of left ventricular torsional deformation by Doppler tissue imaging: A validation study using tagged magnetic resonance imaging. *Circulation* 2005; **111**: 1141–7.
- Kukulski T, Jamal F, Herborts L, et al. Identification of acutely ischemic myocardium using ultrasonic strain measurements. A clinical study in patients undergoing coronary angioplasty. *J Am Coll Cardiol* 2003; **41**: 810–9.
- Davidavicius G, Kowalski M, Williams RI, D'hooge J, Di Salvo G, Pierre-Justin G, et al. Can regional strain and strain rate measurement be performed during both dobutamine and exercise echocardiography, and do regional deformation responses differ with different forms of stress testing. *J Am Soc Echocardiogr* 2003; **16**: 299–308.
- Jamal F, Kukulski T, Sutherland GR, et al. Can changes in systolic longitudinal deformation quantify regional myocardial function after acute infarction? An ultrasonic strain rate and strain study? *J Am Soc Echocardiogr* 2002; **15**: 23–30.
- Voigt JU, Arnold MF, Karlsson M, et al. Assessment of regional longitudinal myocardial strain rate derived from Doppler myocardial imaging indexes in normal and infarcted myocardium. *J Am Soc Echocardiogr* 2000; **13**: 588–98.
- Hoffmann R, Altio E, Nowak B, et al. Strain rate measurement by Doppler echocardiography allows improved assessment of myocardial viability in patients with depressed left ventricular function. *J Am Coll Cardiol* 2002; **39**: 443–9.
- Kukulski T, Jamal F, D'Hooge J, Bijnens B, Scheerder ID, Sutherland GR. Acute changes in systolic and diastolic events during clinical coronary angioplasty: a comparison of regional velocity, strain rate, and strain measurement. *J Am Soc Echocardiogr* 2002; **15**: 1–12.
- Abraham TP, Belohlavek M, Thomson HL, et al. Time to onset of regional relaxation: feasibility, variability and utility of a novel index of regional myocardial function by strain rate imaging. *J Am Coll Cardiol* 2002; **39**: 1531–7.
- Mor-Avi VV, Godoy IE, Lang RM. Color kinesis: new technique or just another display of acoustic quantification? *Echocardiography* 1999; **16**: 95–103.
- Kvitting JP, Wigstrom L, Strotman JM, Sutherland GR. How accurate is visual assessment of synchronicity in myocardial motion? An in vitro study with

- computer-simulated regional delay in myocardial motion: clinical implications for rest and stress echocardiography studies. *J Am Soc Echocardiogr* 1999; **12**: 698–705.
- 18 Pislaru C, Belohlavek M, Bae RY, Abraham TP, Greenleaf JF, Seward JB. Regional asynchrony during acute myocardial ischemia quantified by strain rate imaging. *J Am Coll Cardiol* 2001; **37**: 1141–8.
- 19 Belohlavek M, Pislaru C, Bae RY, Greenleaf JF, Seward JB. Real-time strain rate echocardiographic imaging: temporal and spatial analysis of systolic compression in acutely ischemic myocardium. *J Am Soc Echocardiogr* 2001; **14**: 360–9.
- 20 Brown M, Morris R, Takayama M, White H. Post-systolic shortening: a marker of potential for early recovery of acutely ischemic myocardium in the dog. *Cardiovasc Res* 1987; **21**: 703–16.
- 21 Ehring T, Heusch G. Left ventricular asynchrony: an indicator of regional myocardial dysfunction. *Am Heart J* 1990; **120**: 1047–57.
- 22 Tian R, Ingwall JS. Energetic basis for reduced contractile reserve in isolated rat hearts. *Am J Physiol* 1996; **270** (Pt 2): H1207–16.
- 23 Lamb HJ, Beyerbach HP, van der Laarseb A, et al. diastolic dysfunction in hypertensive heart disease is associated with altered myocardial metabolism. *Circulation* 1999; **4**: 99: 2261–7.
- 24 Kolev N, Zimpfer M. Impact of ischemia on diastolic function: clinical relevance and recent Doppler echocardiographic insights. *Eur J Anaesthesiol* 1995; **12**: 123–6.
- 25 Kondo H, Masuyama T, Ishihara K, et al. Digital subtraction high-frame-rate echocardiography in detecting delayed onset of regional left ventricular relaxation in ischemic heart disease. *Circulation* 1995; **91**: 304–12.
- 26 Voigt JU, Exner B, Schmiedehausen K, et al. Strain-rate imaging during dobutamine stress echocardiography provides objective evidence of inducible ischemia. *Circulation* 2003; **107**: 2120–6.
- 27 Voigt JU, Lindenmeier G, Exner B, et al. Incidence and characteristics of segmental post-systolic longitudinal shortening in normal, acutely ischemic, and scarred myocardium. *J Am Soc Echocardiogr* 2003; **16**: 415–23.
- 28 Sun JP, Niu J, Chou D et al. Alterations of regional myocardial function in a swine model of myocardial infarction assessed by echocardiographic 2-D strain imaging. *J Am Soc Echocardiogr* (in press).
- 29 Ashraf M, Li XK, Young MT, et al. Delineation of cardiac twist by a sonographically based 2-dimensional strain analysis method: an in vitro validation study. *J Ultrasound Med* 2006; **25**: 1193–8.
- 30 Notomi Y, Lysyansky PM, Setser RM, et al. Measurement of ventricular torsion by 2D ultrasound speckle tracking imaging. *J Am Coll Cardiol* 2005; **45**: 2034–41.
- 31 Modesto K, Cauduro S, Dispenzieri A, et al. *A novel two-dimensional strain imaging modality closely correlates with tissue Doppler derived strain measurements*. ASE-04. 19th IEEE International Conference Automated Software Engineering; 2004 Sep 20–24; Linz, Austria.
- 32 Gilman G, Khandheria BK, Hagen ME, Abraham TP, Seward JB, Belohlavek M. Strain rate and strain: a step-by-step approach to image and data acquisition [review]. *J Am Soc Echocardiogr* 2004; **17**: 1011–20.
- 33 Yip G, Abraham T, Belohlavek M, Khandheria BK. Clinical applications of strain rate imaging [review]. *J Am Soc Echocardiogr* 2003; **16**: 1334–42.
- 34 Sutherland GR, Di Salvo G, Claus P, D'hooge J, Bijnens B. Strain and strain rate imaging: a new clinical approach to quantifying regional myocardial function [review]. *Am Soc Echocardiogr* 2004; **17**: 788–802.
- 35 Notomi Y, Martin-Miklovic MG, Oryszak SJ, et al. Enhanced ventricular untwisting during exercise: a mechanistic manifestation of elastic recoil described by Doppler tissue imaging. *Circulation* 2006; **113**: 2524–33.
- 36 Notomi Y, Srinath G, Shiota T, et al. Maturational and adaptive modulation of left ventricular torsional biomechanics: Doppler tissue imaging observation from infancy to adulthood. *Circulation* 2006; **113**: 2534–41.

# Index

Note: Page numbers in **bold** refer to tables, and in *italic* refer to figures.

- ACE inhibitors 289  
acoustic tagging 301–2  
acromegaly 216–17, 217  
advanced glycation end-products 190  
amlodipine 289  
amyloidosis 234–5, 235  
angle dependence 12–14, 13  
annulus paradoxus 202, 203  
aortic regurgitation 229  
aortic stenosis 229–30  
arterial compliance 291–3  
    area method 292  
    pulse-pressure method 292  
    stroke volume-pulse pressure method 292  
    Windkessel model 292  
arterial distensibility 293  
    markers of 296–7  
    tissue Doppler imaging 294–6, 295, 296  
arterial elasticity 293, 293  
arterial function 288–300  
    central and brachial blood pressure 289  
    compliance 291–3  
    distensibility  
        markers of 296–7  
        tissue Doppler imaging 294–6, 295, 296  
    elasticity 293, 293  
    pulse contour 289–90, **290**, 291  
    standardization of measurements 290–1, **292**  
    stiffness 289–90, **290**, 291  
    tissue Doppler imaging 294, 294  
    ventricular-vascular interaction 288–9, 289  
    wave reflection 288–9, 289  
arterial stiffness 289–90, **290**, 291  
atenolol 289  
atrial fibrillation 259–60  
    left ventricular filling pressure 61–8, 67  
atrial function 255–64  
    haemodynamics 255  
    left atrial function *see* left atrial function  
atrial myocardial performance 257–8, 257  
atrial pacing 75  
atrial pump 258–9, 259  
atrial septal defect 261  
atrioventricular rings 81  
augmentation index 289  
averaging 14–15, 14  
  
beta stiffness index 293  
bisoprolol 289  
block-matching 21  
brachial blood pressure, drug effects 289  
brain natriuretic peptide 90  
B-type natriuretic peptide 191  
  
calcium channel blockers 289  
cardiac catheterization 55  
cardiac cycle 36–41, 37–41  
    electrical and mechanical events 37  
    timing of events 278–9, 279, 283–4, 284  
cardiac hypercontractility 211–12  
cardiac magnetic resonance imaging 30–1, 31  
cardiac resynchronization therapy 96, 111–24  
    displacement imaging 118, 120  
    dynamic cardiac dyssynchrony 123–4  
    heart failure with normal QRS interval 118–23  
    mechanisms of benefit 112  
    prediction of responders 112–13  
    speckle tracking 118, 121  
    strain imaging 116–18  
    strain rate imaging 118, 119  
    tissue synchronization imaging 116  
    tissue velocity imaging 114–16  
cardiomyopathy  
    diabetic 185  
    dilated 58  
    infiltrative 182  
    restrictive 198–208  
cardioversion 259–60  
central blood pressure, drug effects 289  
children, left ventricular twist 273–4

- circumferential strain 268, 309, 310  
 color coding 39  
 color Doppler myocardial imaging 209, 210  
 color M-mode flow propagation velocity 59–61, 61  
   diastolic heart failure 94  
 color tissue velocity imaging 4–5, 5, 103, 105  
   M-mode 105  
 constrictive pericarditis 198–208  
   mitral annulus 199–202, 200, 201, 203  
   myocardial velocity gradient 204  
     strain rate imaging 204–5, 205  
 contractile reserve 223, 229  
 conventional (engineering) strain 7–8  
 coronary angiogram 150  
 coronary artery disease  
   automated strain/strain rate 285  
   diabetes mellitus 191  
     stress echocardiography 156–7, 156, 157  
 coronary artery occlusion 134  
 curved anatomical M-mode 6, 6
- deformation imaging  
   automated analysis 280–3, 282, 283  
     dynamic velocity gradient method 283  
     segment length method 283  
     static velocity gradient method 283, 283  
 Doppler-based 144  
 myocardial viability 143  
 speckle tracking-based 144  
 diabetes mellitus 185–97  
   biochemical detection of myocardial dysfunction 191–2  
   development of heart failure 186  
   diastolic dysfunction 186  
   insulin resistance 189–91  
     coronary artery disease/impaired myocardial microperfusion 191  
       hyperglycemia 190–1, 190  
   intervention 192  
   long-axis function 193  
   myocardial imaging 186–7, 187  
   obesity 192–3  
   pathophysiology 187–9  
     hypertension 187–8, 188  
     left ventricular hypertrophy and myocardial fibrosis 188–9, 189  
   systolic dysfunction 186  
 diabetic cardiomyopathy 185  
 diastolic dyssynchronous 102  
   indices of 105–6  
 diastolic filling period 95  
 diastolic function  
   exercise-induced changes 72–4, 73, 74  
   valvular heart disease 225
- diastolic functional reserve 74  
 diastolic heart failure 89–101  
 Doppler echocardiographic indices 91–6, **92**  
   color M-mode flow propagation velocity 94  
   dynamic diastology 95  
   left atrial size 93–4  
   mitral inflow and annulus velocity 95–6  
   preload alteration 92  
   pulmonary venous Doppler velocities 92–3, 93  
   tissue Doppler echocardiography 94–5, 95  
   dyssynchrony 109–10  
   echocardiography in 90–1, 91  
   left ventricular dyssynchrony 96–7  
   need for assessment 89–90, **90**  
   diastolic relaxation 168–9, 169  
   dilated cardiomyopathy 58  
   displacement imaging 6–7, 7, 103, 106  
     cardiac resynchronization therapy 118, 120  
   dobutamine stress 75  
   radial deformation **166**  
   strain rate imaging 168  
     *see also* stress echocardiography  
 Doppler echocardiography *see* tissue Doppler echocardiography  
 Doppler equation 3  
 Doppler strain 28–30, 28  
   strain vs velocity 29  
   strain wave morphology 29–30, 30  
   validation 28–9, 29  
     *see also* strain; strain rate  
 Doppler tissue displacement 48–9  
 Doppler tissue imaging *see* tissue Doppler imaging  
 drift 14, 14  
 drift compensation 14, 14  
 dynamic cardiac dyssynchrony 123–4  
 dynamic diastology 95  
 dyssynchrony 102–27  
   assessment 102–8  
     speckle tracking 107–8  
     tissue velocity imaging 102, 105–7  
   cardiac resynchronization therapy 111–24  
     displacement imaging 118, 120  
     dynamic cardiac dyssynchrony 123–4  
     heart failure with normal QRS interval 118–23  
     mechanisms of benefit 112  
     prediction of responders 112–13  
     speckle tracking 118, 121  
     strain imaging 116–18, 119  
     strain rate imaging 118  
     tissue synchronization imaging 116  
     tissue velocity imaging 114–16  
   diastolic 102, 105–6  
   diastolic heart failure 109–10  
   interventricular 102

- intraventricular 102
- left ventricular hypertrophy 110
- prognostic implications 110–11
- right ventricular pacing-induced systolic 110
- systolic 102, 103–4, 105
- Systolic Dyssynchrony Index 124–5
- systolic heart failure 108–9
  
- echocardiography 42, 43
  - diastolic heart failure 90–1, 91
  - left ventricular filling pressure 55–61
  - myocardial viability 141–2
  - speckle *see* speckle tracking
  - strain *see* strain; strain rate
  - stress *see* stress echocardiography
  - three-dimensional 224, 226
  - tissue Doppler *see* tissue Doppler imaging
  - two-dimensional 43
- ejection fraction 55
  - left ventricular 81
- elastic model 22
- electromechanical coupling 259
- enalapril 289
- endocrine disorders 209–22
  - growth hormone deficiency 217
  - growth hormone excess 216–17, 217
  - hyperaldosteronism 217–19, 218
  - subclinical hyperthyroidism 211–12, 212, 213
  - subclinical hypothyroidism 210, 212–16, 214, 215
- eprosartan 289
- exercise effects 75–6
  - diastolic function 72–4, 73, 74
  - mitral annulus velocity 74
  - mitral inflow 74
- exercise intolerance 74
- experimental models
  - systolic heart failure 81, 82–6
  - ventricular torsion 274–6, 275, 275
  
- Fabry's disease 237–9, 238, 239
- felodipine 289
- 18F-fluorodeoxyglucose PET 167–8
- flow propagation velocity 59–61, 61, 94
- Fourier transform 4
- Friedreich's ataxia 236–7, 236, 237
  
- glyceryl trinitrate 289
- gray-scale tracking 21
- gray value conservation 21
- growth hormone deficiency 217
- growth hormone excess 216–17, 217
  
- heart failure
  - diabetes mellitus 186
  - diastolic *see* diastolic heart failure
  - left ventricular filling pressure 55
  - normal ejection fraction 89, 90
  - normal QRS interval 118–23
  - systolic *see* systolic heart failure
  - heart rate 36
  - hydrochlorothiazide 289
  - hyperaldosteronism 217–19, 218
  - hyperglycemia 190–1, 190
  - hypertension 187–8, 188
  - hypertensive heart disease 175–84
    - tissue Doppler echocardiography 177–81, 178, 179
    - clinical utility 181–2, 182
  - two-dimensional and conventional spectral Doppler 175–7, 177
- hyperthyroidism. subclinical 211–12, 212, 213
- hypothyroidism. subclinical 210, 212–16, 214, 215
  
- infants, enhanced ventricular torsion 274–6, 275, 275
- infiltrative cardiomyopathies 182
- insulin resistance 189–91
  - coronary artery disease/impaired myocardial microperfusion 191
  - hyperglycemia 190–1, 190
  - see also* diabetes mellitus
- integrated backscatter 209, 210
- interventricular septum
  - M-mode echocardiography 198
  - tissue Doppler echocardiography 202–4, 203
- ischemic heart disease 260
- isovolumic contraction 36
- isovolumic relaxation 36
- isovolumic relaxation time 56–7, 57
  
- kernel 21
  
- late diastolic wave 258, 258
- late systolic wave 258, 258
- left atrial appendage 256–7
  - myocardial performance 258, 258
- left atrial function 255–61
  - atrial fibrillation and cardioversion 259–60
  - atrial septal defect 261
  - Doppler echocardiographic indices 256–7
  - echocardiography 256
  - health subjects 258–9, 259
  - ischemic heart disease 260
  - mitral regurgitation 261
  - mitral stenosis 260–1
  - pressure-volume relationship 255–6
  - tissue Doppler imaging 257–8, 257, 258
- left atrial pressure 55, 58, 65
- left atrial size 256

- left atrial volume 56  
   diastolic heart failure 93–4
- left ventricular dysfunction 141
- left ventricular dyssynchrony 96–7
- left ventricular ejection fraction 81
- left ventricular end-diastolic pressure 55
- left ventricular filling pressure 55  
   during recovery 76–7, 76, 77
- echocardiography 55–61  
   increased 63  
   stress effects 72–8  
   systolic heart failure 84–5  
   tissue velocity imaging 61–8, 67
- left ventricular function, aging effects 49–50
- left ventricular hypertrophy 175–6  
   diabetes mellitus 186, 188–9, 189  
   dyssynchrony 110
- left ventricular relaxation 65
- left ventricular volume 224
- lisinopril 289
- longitudinal displacement 303, 305, 305, 306
- longitudinal strain rate 268, 303, 303, 304
- longitudinal velocity 303
- magnetic resonance imaging  
   cardiac 30–1, 31  
   myocardial viability 149
- matrix metalloproteinases 179
- median filtering 22
- mitral annulus  
   annulus paradoxus 202, 203  
   tissue Doppler echocardiography 199–202, 200, 201, 203  
   tissue velocity 206  
   mitral annulus velocity 61–5, 62–5, 73  
     at rest 77  
     exercise effects 74  
     and inflow 95–6  
   mitral inflow 56–8, 57, 58, 73  
     and annulus velocity 95–6  
     at rest 77  
     exercise effects 74  
     pulsed-wave Doppler 58  
   mitral inflow velocity 206  
   mitral regurgitation 57, 85, 225–8, 226, 227, 228  
     left atrial function 261  
   mitral stenosis 64, 228  
     left atrial function 260–1  
   mitral venous flow 60
- M-mode echocardiography  
   constrictive pericarditis 198  
   curved anatomical 6, 6  
   systolic heart failure 83
- muscular dystrophy 239–40
- myocardial boundaries 22
- myocardial deformation 228–9
- myocardial displacement  
   by age group 47  
   and strain 45–7, 47, 48
- myocardial fibrosis in diabetes mellitus 188–9, 189
- myocardial hibernation 141
- myocardial infarction 166–8, 167, 168  
   experimental studies 137–9  
   radial strain profiles 167  
   *see also* myocardial ischemia
- myocardial ischemia 150, 162–71  
   acute 163–4, 164  
   chronic 164–6, 165, 166  
   diastolic mechanics 168–9, 169  
   experimental studies 131–40  
     acute ischemia 135–7  
     myocardial infarction 137–9  
     strain rate parameters 132–5  
     tissue velocity imaging 132–5  
   future directions 169–70  
   tissue velocity imaging 155
- myocardial microperfusion in diabetes mellitus 191
- myocardial strain imaging 39–41  
   two-dimensional 23–4
- myocardial strain rate 44–5, 49
- myocardial stunning 131, 141, 165, 166
- myocardial velocity 48–9
- myocardial velocity gradient *see* velocity gradient
- myocardial velocity imaging 22–3, 23
- myocardial viability assessment 141–9  
   clinical importance 141  
   deformation imaging  
     Doppler-based 144  
     speckle tracking-based 144  
   deformation responses 143  
   echocardiographic techniques 141–2  
   stress echocardiography 157–8, 158, 158  
   velocity responses 142–3  
   wall motion score 147
- myotonic dystrophy 239–40
- natural strain 7–8, 9
- noise reduction, averaging 14–15, 14
- Nyquist velocity 3–4
- obesity 192–3
- optical flow method 21
- parametric imaging 302
- peak longitudinal strain 305–10, 307–9
- peak systolic velocity 83–4, 84  
   dobutamine stress  
     age 153

- hemodynamics and ventricular volume 154  
 perindopril 289  
 PET *see* positron emission tomography  
 Peterson's Elastic Modulus 293  
 positron emission tomography 167–8  
 postejection relaxation period 136–7  
 postsystolic thickening 132  
 pre-ejection contraction period 135–6  
 preload alteration 92  
 pressure-volume relationship, left atrium 255–6  
 pressure overload 224, 225  
 pulmonary capillary wedge pressure 55, 75  
 pulmonary congestion 72  
 pulmonary venous Doppler velocities 92–3, 93  
 pulmonary venous flow 58–9, 59, 60  
 pulse contour 289–90, 290, 291  
 pulsed tissue velocity imaging 103, 105  
 pulsed-wave Doppler 3  
     constrictive pericarditis 199  
     pulsed-wave tissue velocity imaging 4, 4  
     pulse repetition frequency 3  
  
 radial deformation 166  
 radial displacement 310–11, 311, 311  
 radial strain 310, 310  
 radiofrequency 19  
 tracking 21  
 region of interest 5, 5  
 restrictive cardiomyopathy 198–208  
     mitral annulus 199–202, 200, 201, 203  
     myocardial velocity gradient 204  
     strain rate imaging 204–5, 205  
 restrictive filling pattern 57  
 reverberation artifacts 11–12, 11, 12  
 right atrial pressure 245–6, 246  
 right ventricular dyssynchrony 248–9  
 right ventricular function 243–52  
     speckle tracking 249  
     strain/strain rate imaging 246–9, 247, 249  
     tissue Doppler imaging 244–6, 244–6  
 right ventricular pacing-induced systolic  
     dyssynchrony 110  
 rotation 311–13, 312, 313  
 rotation rate 311–13, 312, 313  
  
 sarcoidosis 235–6  
 scattering sites 18  
 scatter reflections 18  
 segmental diastolic strain rate 46  
 segmental diastolic velocity  
     early 44  
     late 45  
 segmental systolic strain rate 45  
 segmental systolic velocity 43  
  
     and age 44  
     segmentation, automatic 278–9, 279  
     shear strain 8  
     signal quality 11–15  
         angle dependence 12–14, 13  
         drift and drift compensation 14, 14  
         noise reduction by averaging 14–15, 14  
         reverberation artifacts 11–12, 11, 12  
     sinus tachycardia 64, 65  
     sonomicrometry 28–30, 28, 29, 30  
     speckle motion 19, 20  
     speckle pattern 17, 18  
         conservation of 19–20  
         physical origin of 18–19, 18, 19  
     speckle tracking 17–25, 163  
         advanced research applications 301  
         approaches to 20–1  
         cardiac resynchronization therapy 118, 121  
         dyssynchrony assessment 107–8  
         myocardial viability 144  
         natural acoustic tagging 301–2  
         parametric imaging 302  
         principle of 17–18, 18  
         quality assurance 302–13, 303–13  
         radiofrequency vs gray-scale tracking 21  
         right ventricular function 249  
         strain measurement  
             automated 279–80, 280, 281  
             three-dimensional 269–70, 270  
             two-dimensional 268–9, 269, 269, 301–2  
         systolic dyssynchrony 104  
         two-dimensional  
             strain measurement 268–9, 269, 269  
             ventricular torsion 274  
         validation studies 31–2, 33  
         velocity vector field  
             postprocessing 22–4, 23  
             regularization of 21–2  
             resolution of 22  
 Steinert's disease 239–40  
 strain  
     automated 278–87  
     benefits of 278–9, 279  
     clinical use 284–5  
     data acquisition 279–80, 280, 281, 281  
     deformation analysis system 280–3, 282, 283  
     future developments 285–6  
     timing of cardiac events 283–4, 284  
     circumferential 268  
     conventional (engineering) 7–8  
     longitudinal 268  
     natural 7–8, 9  
     peak longitudinal 305–10, 307–9  
     shear 8

- strain (*Cont'd*)
- three-dimensional measurement 267–70
  - clinical uses 266–7
  - limitations and solutions 267
  - possible uses 266–7
  - reconstruction 266–7, 266
  - speckle tracking 268–70, 269, **269**, 270
  - tissue Doppler imaging 268, 268
  - transmural 268
  - see also* strain imaging
- strain imaging 7–9, 49, 96–7, 106–7, 162–3, 163
- cardiac magnetic resonance imaging 30–1, 31
  - cardiac resynchronization therapy 116–18
  - definition 7–8
  - Doppler 28–30, 28, 29, 30
  - myocardial ischemia 164
  - myocardial viability 149
  - right ventricular function 246–9, 247, 249
  - systolic dyssynchrony 103
  - systolic heart failure 86
  - two- or three-dimensional 8, 8
  - ultrasound estimation 9–11, 9, 10, 11
  - see also* strain rate imaging
- strain rate
- automated 278–87
  - benefits of 278–9, 279
  - clinical use 284–5
  - data acquisition 279–80, 280, 281, **281**
  - deformation analysis system 280–3, 282, 283
  - future developments 285–6
  - timing of cardiac events 283–4, 284
- longitudinal 268, 303, 303, 304
- segmental diastolic 46
- segmental systolic 45
- transmural 268
- strain rate imaging 7–9, 39, 107
- cardiac resynchronization therapy 118, 119
  - color coding 39
  - constrictive pericarditis 204–5, 205
  - definition 8–9
  - diabetes mellitus 189
  - dobutamine stress 168
  - integration of 11, 11
  - myocardial ischemia 132–5
  - myocardial viability 147, 148
  - restrictive cardiomyopathy 204–5, 205
  - right ventricular function 246–9, 247, 249
  - systolic dyssynchrony 104
  - systolic heart failure 86
  - ultrasound estimation 9–11, 10
  - and velocity gradient 9–11, 9, 10
  - see also* strain imaging
- strain wave morphology 29–30, 30
- stress echocardiography 150–61
- accuracy 150–1
- false-positive and false-negative 151
- limitations of 151–2
- peak systolic velocity
- age 153
  - hemodynamics and ventricular volume 154
- tissue velocity imaging 152–9
- clinical application 155–9
  - detection of coronary artery disease 156–7, 156, 157
  - detection of myocardial viability 157–8, **158**
  - feasibility and variability 155–6
  - imaging considerations 152–3
  - limitations 159, **159**
  - prognostic data 158, 158
  - response to ischemia 156
  - stress response determinants 153
  - technical considerations 152
  - what to measure 153–5
- stress effects 72–8
- hemodynamic validation 76
  - nonphysiologic stress
  - dobutamine 75
  - exercise 75–6
  - pacing 75
- systemic diseases 233–42
- amyloidosis 234–5, 235
  - cardiac function assessment 233–4
  - Fabry's disease 237–9, 238, 239
  - Friedreich's ataxia 236–7, 236, 237
  - imaging perspectives 240
  - muscular dystrophy 239–40
  - sarcoidosis 235–6
- systolic dyssynchrony 102
- assessment 103–4
  - indices of 105
- Systolic Dyssynchrony Index 124–5
- systolic filling fraction 59
- systolic heart failure 81–8
- diagnosis 85–6, **85**, **85**
  - dyssynchrony 108–9
  - experimental models 81, 82–6
  - left ventricular filling pressure 84–5
  - mitral regurgitation 85
  - M-mode measurements 83
  - peak systolic velocity 83–4, 84
  - regional systolic and long-axis function 81–2
  - strain and strain rate 86
  - tricuspid annular velocity 85
- systolic strain rate
- Fabry's disease 238
  - Friedreich's ataxia 237
- time-traces 5–6
- timing, automated 278–9, 279, 283–4, 284

- TIMPs 179  
 tissue Doppler echocardiography *see* tissue Doppler imaging  
 tissue Doppler imaging 26–8, 27, 38, **43**, 162–3  
   arterial function 294, 294  
   automated deformation analysis 283  
   cardiac resynchronization therapy 114–16  
   color 103, 105  
   color M-mode 105  
   diabetes mellitus 187  
   diagnosis of heart failure 85–6, 85, **85**  
   diastolic heart failure 94–5, 95  
   dyssynchrony 102, 105–7  
   hypertensive heart disease 177–82, 178, 179, 181, **181**  
   interventricular septum 202–4, 203  
   left atrial function 256–8, 257, 258  
   left ventricular filling pressure 61–8, 67  
   mitral annulus 199–202, 200, 201, 203  
   mitral regurgitation 226–7, 227  
   myocardial ischemia 132–5  
   myocardial viability 147  
   normal range 36–51  
   peak systolic velocity 83–4, 84  
   pulsed 103  
   right ventricular function 244–6, 244–6  
   strain measurement 268, 268  
     automated 279  
   *see also* echocardiography; tissue velocity imaging  
 tissue synchronization imaging 107, 116  
   systolic dyssynchrony 104  
 tissue tracking 6, 7, 103, 278–9, 279  
 tissue velocity imaging 3–5  
   color coding 4–5, 5, 39  
   displacement imaging 6–7, 7  
   pulsed-wave 4, 4  
   quantitative analysis 5–6  
     curved anatomical M-mode 6, 6  
     time-traces 5–6  
 stress echocardiography 152–9  
   clinical application 155–9  
   detection of coronary artery disease 156–7,  
 156, 157  
   detection of myocardial viability 157–8, **158**  
   feasibility and variability 155–6  
   imaging considerations 152–3  
   limitations 159, **159**  
   prognostic data 158, 158  
 response to ischemia 156  
 stress response determinants 153  
 technical considerations 152  
 what to measure 153–5  
 tracking *see* tissue tracking  
 transcatheter occlusion 261  
 transmural strain 268  
 transmural strain rate 268  
 transverse displacement 305, 306  
 tricuspid annular velocity 85  
 valvular heart disease 223–32  
   aortic regurgitation 229  
   aortic stenosis 229–30  
   chronic pressure overload 224, 225  
   chronic volume overload 224–5  
   diastolic function 225  
   mitral regurgitation 225–8, 226, 227, 228  
   mitral stenosis 228  
 velocity 29  
 velocity gradient 9–11, 9, 10, 204  
   constrictive pericarditis 204  
   dynamic 283  
   Friedreich's ataxia 236  
   restrictive cardiomyopathy 204  
   static 283, 283  
 velocity vector field  
   postprocessing 22–4, 23  
   two-dimensional myocardial strain imaging 23–4  
   *two-dimensional myocardial velocity imaging*  
 22–3, 23  
   regularization of 21–2  
   resolution of 22  
 ventricular torsion 273–7  
   effects of aging 274  
   enhanced in infancy and middle-aged adults 274–6,  
 275, 275  
   experimental models 274–6, 275, **275**  
   maturing left ventricular twist 273–4  
 ventricular-vascular interaction 288–9, 289  
 videodensitometry 209, 210  
 volume overload 224–5  
 wall motion score 147  
 wave reflection 288–9, 289  
 weighted smoothing 22  
 Windkessel model 292





